# Molecular Loops – Mating Cyclophanes and Macrocycles

**Inauguraldissertation**

zur

Erlangung der Würde eines Doktors der Philosophie

vorgelegt der
Philosophisch-Naturwissenschaftlichen Fakultät
Der Universität Basel

von

**Kevin Julian Weiland**
aus
Deutschland

Basel 2019

Genehmigt von der Philosophisch-Naturwissenschaftlichen Fakultät

auf Antrag von

Prof. Dr. Marcel Mayor

Prof. Dr. Christof Sparr

Basel, den 16.10.2018

Prof. Dr. Martin Spiess (Dekan)

Rebecca und meiner Familie

In theory there is no difference between theory and practice; in practice there is.

Yogi Berra

**Acknowledgements**

I am deeply grateful to my supervisor Prof. Dr. Marcel Mayor for confidence in my work and for giving me the opportunity to complete my dissertation in his research group. I am deeply indebted to you for the excellent intellectual support, for the mentorship and for your guidance throughout the last years. I also want to thank you for advertising my various products with our collaborators and letting me independently develop our various projects. Lastly, our common taste in excellent music is something I treasure.

I thank Prof. Dr. Christof Sparr and Prof. Dr. Peter Bäuerle for the co-examination of this thesis.

Furthermore, Prof. Dr. Konrad Tiefenbacher is acknowledged for chairing the exam.

Collaborative work on nanotechnology is only possible with the best partners. For their collaborative effort, the endless discussions and especially for the excellent working atmosphere I would like to thank all co-authors of the following publications. This work would not have been possible without Dr. Almudena Gallego, Thomas Brandl, and Dr. Tomáš Šolomek. I further thank PD Dr. Daniel Häussinger and his students for their expert help with various NMR analyses. Dr. Markus Neuburger and Dr. Alessandro Prescimone are thanked for X-ray analyses.

I thank our collaborators at the TU Delft/EMPA, Davide Stefani, Chunwei Hsu, Dr. Mickael Perrin and Prof. Dr. Herre van der Zant for single molecule measurements and for hosting me at their institute. Maxim Skripnik and Prof. Dr. Fabian Pauly at the University of Konstanz/ Okinawa Institute of Science and Technology are thanked for providing theoretical background to our work.

Dr. Francesco Tassinari and Prof. Dr. Ron Naaman are thanked for hosting me at the Weizmann Institute of Science and for electrochemical measurements.

I am grateful for having been a student in the Marie-Curie ITN “MOLESCO”, which was organized by Prof. Dr. Martin Bryce. It really was a pleasure to spend time with all the members of the network and I thank them all for the discussions and the inspiring time we had together.

Moreover, I thank all the former and present members of the Mayor research group for their valuable discussions and the constant fun we had together. Furthermore, all students who spent time working with me are acknowledged. Pascal, Lukas, Kenan, Linda, Lorenzo, Patrick, Florian and Ksenia are thanked for the excellent atmosphere we had in lab 08.

I want to express my gratitude to my friends outside the lab, who have always cheered me up and moreover always made me feel at home. I thank you wholeheartedly, I greatly value your friendship. I thank the runners, the cyclists and all the members of the Therwil Flyers who made it easy to relax and clear my mind.

I thank my family for their continuous support and for being there without question, anytime, anyplace. Especially my parents Georgette and Anton, as well as my brother and sister Steven and Jacqueline are thanked for loving and supporting me constantly.

Finally, I thank Rebecca for not only moving to Basel with me but also for her love and patience during all our years together.

## Preface

This thesis is the translation of a conceptual idea that was born years before its realization. In the autumn 2014 at a conference on molecular electronics at the University of Konstanz the discussion about single molecule transport experiments reveled around an intriguing question:

Is there a chemical design, where it is possible to distinguish between different electronic transport pathways within one molecule?

This thesis approaches the envisaged molecular design through various publications, they are ordered such that the final structure is approached after elucidating a suitable macrocyclic structure, followed by stabilized helically chiral macrocycles, and a test system with the conductive backbone of the desired molecule. Finally, the initially planned molecule is presented.

The elucidation of the size of the macrocycle was published in *Helvetica Chimica Acta*, where optical investigations and the dynamic behavior of the parent macrocycle are included.[1] Having found a suitable macrocycle, a tetrasubstituted [2.2]paracyclophane was published in the *Journal of the American Chemical Society*, where the detailed synthesis, chiroptical studies and the dynamic behavior of the molecule, as well as theoretical studies, are presented.[1] Finally, single molecule conductance measurements and theoretical investigations of a molecular rod, which is the backbone of the envisaged macrocycle, have been published in *Nano Letters*. The last chapter then gives the synthesis of the original target compound of this thesis. The supplementary information for all chapters is given in the same order at the end of this thesis for the reader's convenience.

Preceding these three manuscripts, the reader will find a review entitled *"Beyond Simple Substitution Patterns – Symmetrically Tetrasubstituted [2.2]Paracyclophanes as 3D Functional Materials*" which has been published in the *European Journal of Organic Chemistry*.[1] It gives a systematic overview over the three main approaches towards symmetrically tetrasubstituted [2.2]paracyclophanes – including the substitution pattern that found application in this thesis. It integrates the topic of this thesis into the wider world of molecules that are based on [2.2]paracyclophanes with four symmetrical substituents.

Kevin Weiland
Basel, September 2018
Amended for print: Basel, October 2019

[1] The publications were originally included in the state of evolved drafts. They have been published in the meantime and are consequently integrated as such in the print edition.

**Table of Contents**

## Overview of the Thesis

Molecular electronics is nowadays a mature research field and the measurement of conductance through single molecules by means of the mechanically controlled break junction (MCBJ) technique is performed on many classes of molecules.[1,2] In order to fabricate devices based on the charge transport pathway through single molecules, it is of crucial importance to understand the exact properties of the metal molecule metal junction. In contrast to conductivity through single molecules, π-π stacking between molecular wires is strong enough to provide weak through-space coupling and thereby conductance.[3,4] Within this thesis, a concept is proposed which can be useful in answering the underlying question to this problem: when two conductance pathways are possible, like through-bond or through-space conductance, is there a way to distinguish between them? A conductive molecule to study this problem must be designed in such a way that through-bond and through-space transport are possible at the same time. Since both conductance pathways cannot be distinguished in an experimental set up, a further design requirement is that at least one of the pathways can be monitored in an alternative measure.

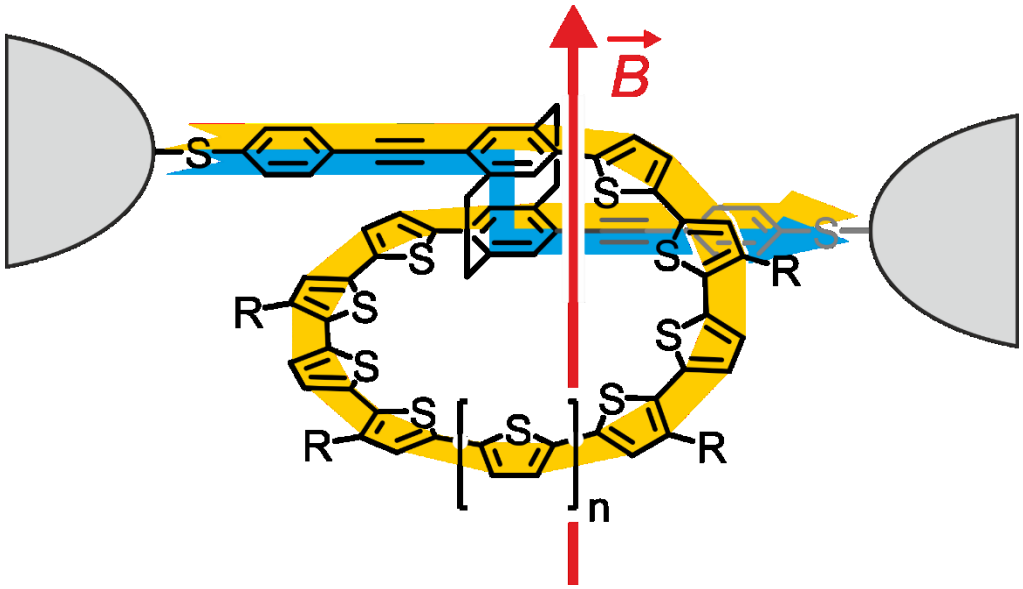


**Figure 1.** Visualization of both possible conductance pathways for the anchored helical molecule in a MCBJ.

The goal of this thesis is to develop a molecular design to answer the illustrated problem. In order to investigate such a problem, the following conceptual idea is proposed: A rod-like structure with pseudo-para connectivity on [2.2]paracyclophane is further modified in such a way that a second through-bond conductance pathway is introduced by means of an oligothiophenic macrocycle.
Charge carriers that pass through the molecule have two options. Either they tunnel through space (blue color, figure 1) or they follow the π-conjugated pathway through the oligothiophene (yellow color, figure 1). Most likely, the applied current will profit from both pathways and the observed conductivity will be a

complex mixture of both. However, only the red pathway follows a helical structure and is thereby sensitive to an applied magnetic field.

This thesis contains the approach towards this structure. The stepwise approach to find a suitable macrocyclic structure as well as the chiroptical and dynamic properties of a system that is slightly different than the proposed target structure are described within the ensuing manuscripts. Furthermore, a molecule to investigate the through-space conductance is presented. Throughout the course of this thesis the unique properties of [2.2]paracyclophane are utilized to synthesize materials with extraordinary properties which arise from the three-dimensional structure of the hydrocarbon. The investigations on this special class of materials was presented to the scientific community in two communications and one full paper, as well as a review. However, the main goal of this work has not been reported yet and is thus presented in this thesis. On the following pages the general concept of the work will be elucidated to the interested reader.

## I. Symmetrically Tetrasubstituted [2.2]Paracyclophanes – an Emerging Class of 3D Functional Materials (2019, Review, published in the European Journal of Organic Chemistry)

[2.2]Paracyclophane is the prototypical layered hydrocarbon with its benzene rings in a face to face orientation.[5,6] This unique property leads to unusual characteristic properties, such as through space conjugation,[7,8] pseudo-*geminal* electrophilic aromatic substitutions,[9] and appealing thermal isomerization properties.[10] Chemists routinely exploited these properties and over the last decades many novel materials have been developed. These materials mainly rely on mono- or disubstituted [2.2]paracyclophane and are described in detail in the literature.[11–13] A rather novel approach is the exploration of [2.2]paracyclophane with four substituents. Literature elaborating on these molecules is to our knowledge not available. A probable reason for this is that the known tetrasubstituted [2.2]paracyclophanes were employed for various applications, without a clear link between the substance classes.

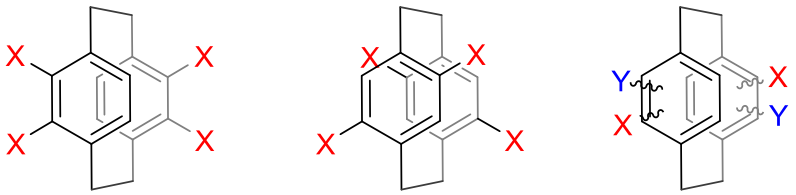


**Figure 2.** The three symmetrically tetrasubstituted [2.2]paracyclophanes which are discussed in the review. Within this work bis-(ps-*meta*)-*ortho* and bis-(ps-*meta*)-*para* homo-tetrasubstitution as well as symmetrically tetrasubstituted [2.2]paracyclophanes with heterosubstituents are described.

We therefore aim to structure the existing substitution patterns and survey the excellent materials that were developed. The work is summarized in the review "Symmetrically Tetrasubstituted [2.2]Paracyclophanes – an Emerging Class of 3D Functional Materials" (**2019**) which is published in the *European Journal of Organic Chemistry*. This review article was prepared together with Dr. Almudena Gallego. A

general assessment reveals three classes of symmetrically tetrasubstituted [2.2]paracyclophanes. The first class consists of molecules in the bis-(ps-*meta*)-*ortho*-substitution pattern. These molecules were used as bis-aryne equivalents,[14–16] as extended through-space conjugated acenes,[17,18] to elucidate through space conjugation properties,[19–21] and to construct strained alkanes through photochemical reactions.[22] The second class are the bis-(ps-*meta*)-*para* tetrasubstituted [2.2]paracyclophanes. The racemic products were used for the investigation on through space electronic conjugation,[23–25] as hole-transporting materials,[26,27] as materials for phane-property investigations,[28] and to construct hydrogen-bonded chiral helices.[29] We further survey the development on enantiopure helically chiral bis-(ps-*meta*)-*para* [2.2.]paracyclophanes. Chiral molecules based on this pattern in propeller,[30–32] X-,[33–35] and helix-shape are known.[36] The third class consists of symmetrically tetrasubstituted [2.2]paracyclophanes with heterosubstituents. Examples of such materials were used in catalyst development,[37] as precursors for [2.2.2.2] (1,2,4,5)cyclophane,[38] and as photo switches[39]. Helically chiral molecules based on this pattern are known[40] and directing effects in the syntheses of symmetrically hetero-tetrasubstituted were surveyed.[41] It is this last class of materials that serves as inspiration for the design of helically chiral macrocycles wrapped around [2.2]paracyclophane.

## II. A Chiral Macrocyclic Oligothiophene with Broken Conjugation – Rapid Racemization through Internal Rotation (2019, Full Paper, published in Helvetica Chimica Acta)

Helically chiral molecules based on symmetrically tetrasubstituted [2.2]paracyclophane are known and were presented in the preceding review, the helical chirality of the structures results in all cases from the intrinsically chiral substitution pattern of the [2.2]paracyclophane.[33,36,42,43]In other words, while all hitherto known molecules are cleverly designed and have esthetically pleasing structures, it is a question of separating the enantiomers in the initial stages of the syntheses, the chiral properties depend on the substitution pattern of the [2.2]paracyclophane. Furthermore, it is difficult to introduce variety in the molecules, only the building blocks in close proximity to the central cyclophane are affected by the chiral environment.[34,43] The chiroptical effects in such molecules thus result only from the rigid conformation of the central building block, chiroptical signals are weak from chromophores that are placed away from the [2.2]paracyclophane. We became interested in introducing helical chirality through a three-dimensional building block, which is not intrinsically chiral.

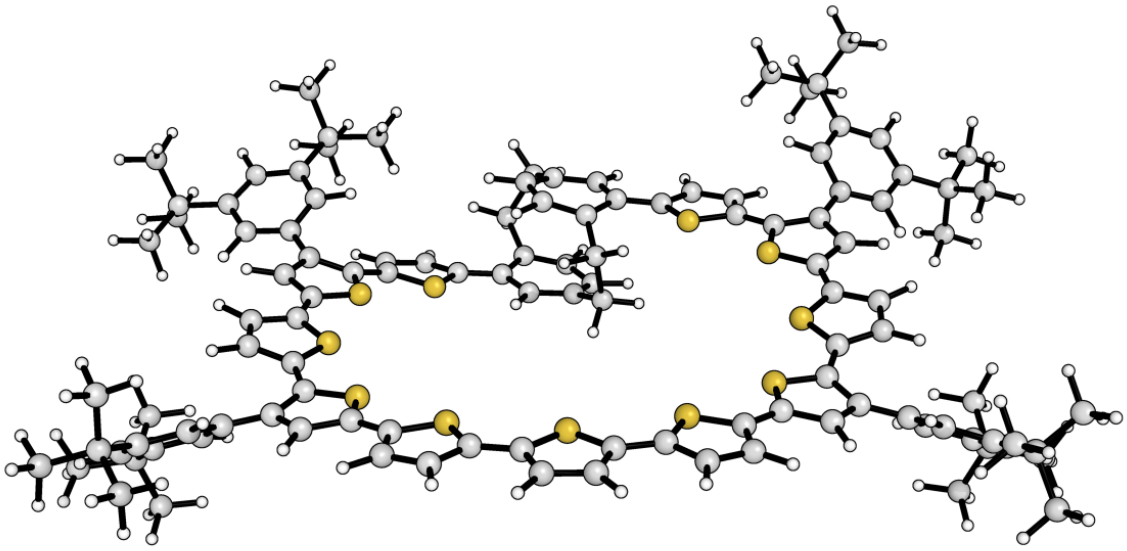

**Figure 3.** Target molecule for the *Helvetica Chimica Acta* publication. The disubstituted [2.2]paracyclophane was synthesized for optical and dynamic investigations. No further substituents on the cyclophane allow for unhindered rotation of the hydrocarbon on the NMR timescale at room temperature.

The chemical synthesis towards the presented target structure of this thesis starts with the structural investigation to find a suitable oligothiophenic macrocycle. For this reason, a disubstituted [2.2]paracyclophane was designed and synthesized. We presented the results of this work in a full paper which is published in *Helvetica Chimica Acta* (**2019**) entitled "A Chiral Macrocyclic Oligothiophene with Broken Conjugation – Rapid Racemization through Internal Rotation". The author of this thesis synthesized and characterized the target molecule and performed the optical characterization of the macrocycle, as well as its precursors. The master students Natalia Münch and Wanja Gschwind performed 2D-NMR analysis, PD Dr. Daniel Häussinger recorded and analyzed variable temperature (VT) $^{1}$H-NMR spectra. This work emphasizes the step-by-step assembly of the oligothiophenic macrocycle by repetitive halogenation and palladium catalyzed cross-coupling chemistry. A large solubilizing group was implemented, showing the importance of aggregation-preventing building blocks, which were essential in all wet-chemistry steps throughout the entire synthesis. The macrocyclization which was employed to close the macrocycle revealed that the undecathiophene was one of the smallest possible target structures, as the major product was the twofold closed dimer of the desired ring. Finally, UV/Vis- and emission spectroscopy allowed us to elucidate the change in conjugation through the newly established macrocycle with respect to only through-space conjugation, which was prevalent before the macrocycle was implemented. We subjected the molecule to VT-NMR experiments to gain insight into the free energy of enantiomerization of the chiral macrocycle and discovered that the enantiomerization proceeds rapidly on the timescale of the NMR experiment at room temperature, consequently confirming the need for large substituents which are essential for stabilized helicity under ambient conditions.

**III. Mechanical Stabilization of Helical Chirality in a Macrocyclic Oligothiophene (2019, Article, published in the Journal of the American Chemical Society)**

To further the synthetic progress towards the target structure of this thesis, the helical molecule presented in the preceding publication was modified such that the helical chirality could be retained through bulky substituents.

Helical chirality is an intriguing design concept in natural structures, as well as in chemistry.[44–46] From a chemist's perspective, the resulting properties and the structural beauty of such molecules are sufficient as a reason to elaborate on and design such motifs. Having surveyed the various substitution patterns which are laid out in the preceding review, we decided to develop a strategy to produce such a structure based on the bis(ps-*para*)*para* substitution pattern where one pair of substituents connects to the macrocycle, while the other pair prevents rotations of the [2.2]paracyclophane.[41] An oligothiophenic chain was chosen as target structure for the macrocycle as such structures are known for their excellent properties.[47,48]

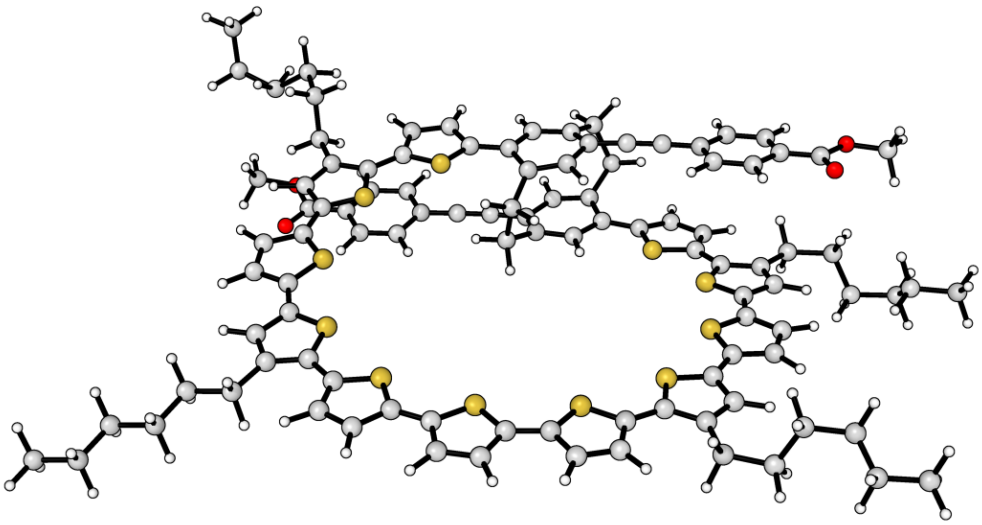

**Figure 4.** Target molecule for the *Journal of the American Chemical Society* publication showing a helically chiral oligothiophene wrapped around a pseudo-*para* substituted [2.2]paracyclophane. The helical chirality of the molecule is stabilized through large substituents which enable the isolation and characterization of a novel type of helically chiral tetrasubstituted [2.2]paracyclophane.

Our manuscript which is published in the *Journal of the American Chemical Society* is entitled "Mechanical Stabilization of Helical Chirality in a Macrocyclic Oligothiophene". It is the synthetically most meaningful work of this thesis. We present therein a novel design concept to stabilize helicity. To demonstrate the viability of the work, a chiral macrocyclic oligothiophene was synthesized and investigated in detail. A macrocyclic oligothiophene is introduced in a pseudo-para motif on [2.2]paracyclophane. This structure is already chiral, however the cyclophane can rotate freely and the chirality is not retained. Therefore, a second set of substituents is needed to prevent the rotation of the macrocycle around the cyclophane. A linear ethynyl methyl benzoate is introduced which is able to effectively hinder the rotation and thus retains the chirality. The helical molecule was synthesized through

a series of functional-group transformations and cross-coupling chemistry. The macrocycle was formed through a high dilution coupling strategy. The synthesis and characterization as well as all optical investigations were performed by the author of this thesis, the separation of the enantiomers by means of HPLC was performed by Thomas Brandl. The master student Kenneth Atz and PD Dr. Daniel Häussinger performed 2D NMR experiments and assigned the resonances for all macrocyclic structures in this work. Dr. Alessandro Prescimone performed X-Ray spectroscopy, while Dr. Tomáš Šolomek performed DFT calculations. The isolation of pure enantiomers by HPLC on a chiral stationary phase and ECD spectroscopy allowed the characterization of the target structure as well as the assignment of the absolute configuration by DFT calculations. We found racemization which proceeds with a half-life of minutes at room temperature. Variable temperature HPLC analysis on a chiral stationary phase and high-temperature EXSY spectroscopy gave access to the thermodynamic parameters of the enantiomerization. A pathway for the racemization was obtained from semi-empirical and DFT calculations, the ethynyl methyl benzoate is moved through the macrocycle like a thread through the eye of a needle. The enantiomerization pathway proceeds through rotations around single bonds, as well as deformations of the molecule in a pathway like Mislow's Euclidian rubber glove.[49,50] The results from this work were more than encouraging and allowed us to focus on a substructure of the target molecule of this thesis to further understand the properties of single molecules with only through-space conductance pathways.

**IV. Large conductance variations in a mechanosensitive single-molecule junction (2018, Communication, Nano Letters)**

Besides working on macrocyclic oligothiophenes bound to [2.2]paracyclophane, smaller molecules based on the same hydrocarbon still remain an active field of research.[8,51] For example, electronic transport through single molecules derived from oligophenylethynyl-structures has not yet been investigated. While derivatives of [2.2]paracyclophane were already investigated in conductance measurements, this was thus far only performed in monolayers where the control over the number of molecules and the precise configuration in the junction was poor.[7,51]

We were also able to elucidate the electronic transport through single [2.2]paracyclophane molecules by means of the MCBJ technique. The single-molecule measurements were performed at TU Delft (Prof. Dr. Herre van der Zant), while the equally impressive theoretical background to the obtained data was provided at University of Konstanz/Okinawa Institute of Science and Technology (Prof. Dr. Fabian Pauly).

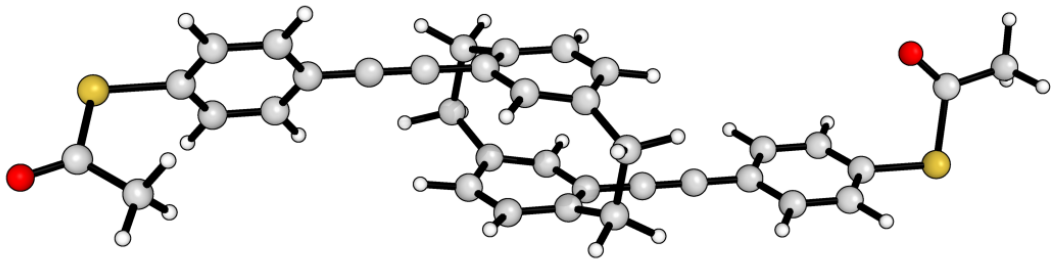

**Figure 5.** Target molecule for the *Nano Letters* publication; a molecular rod with spring-like behavior. The pseudo-*para* substitution pattern directs the mechanical manipulation induced through the electrodes in the MCBJ onto the [2.2]para-cyclophane.

The resulting manuscript "Large conductance variations in a mechanosensitive single-molecule junction" was published in *Nano Letters* (**2018**) and includes extensive experimental data as well as computational results. Davide Stefani, Chunwei Hsu, and Dr. Mickael Perrin built the experimental setup and performed the physical measurements of the molecules. Maxim Skripnik performed the DFT calculations and analysis, while the author of this thesis synthesized and characterized the molecule which was specifically designed to transmit motion of the nanoelectrodes onto the central [2.2]paracyclophane. The conductance through these individual pseudo-*para* disubstituted [2.2]paracyclophane derivatives was studied by two different methods. Initially, fast-breaking measurements were performed by increasing the distance of two gold nanoelectrodes while statistically trapping a molecule between the electrodes and measuring the conductance through the molecule.[2,52] Secondly, the same molecule was subjected to self-breaking measurements where the working principle relies on nanoelectrodes which form from a notched wire that self-breaks due to surface tension.[53] We found different behaviors of the compound towards applied motion on the electrodes. During the fast-breaking measurements, we observed jumps in the conductance traces which could be confirmed by DFT calculations as jumping of the anchoring group on the gold nanoelectrode due to strain-release of the molecule. The self-breaking measurements with periodic alterations of the electrode distance revealed more complex behavior. DFT calculations reveal deconstructive interference in the frontier orbitals of the molecule in its relaxed state, which is periodically relieved through small distance alterations. We believe this information to be of general interest for MCBJ measurements as it shows dynamic effects of the anchoring group on the electrode. This could apply to many flexible molecular structures. The investigation of this molecule will furthermore serve as a test-system for the molecule which will be proposed in the outlook of this thesis.

## V. Conclusion: A Tetrasubstituted Helically Chiral Macrocycle with Anchoring Groups for Gold Electrodes

The last chapter of this thesis details the synthesis of the original target structure of this work. The elucidation of the rotationally hindered macrocycle presented in *Angewandte Chemie* provided an intermediate from which the desired molecule could be achieved in one step.

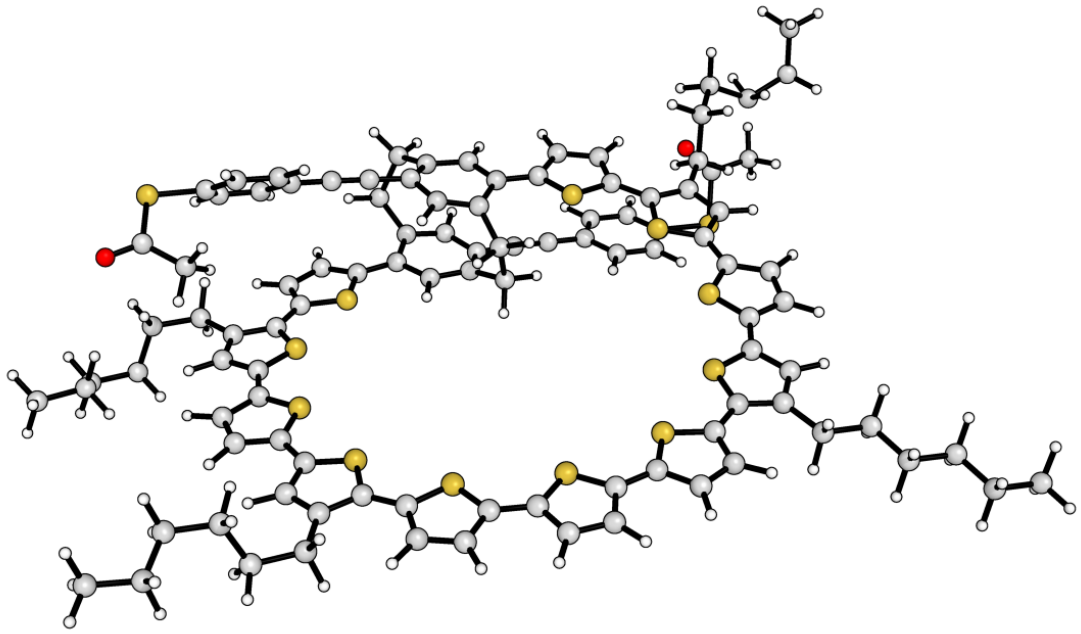

**Figure 6.** The target molecule of this thesis.

The molecule was synthesized but was found to be unstable and decomposed in various purification techniques. Therefore, only high-resolution mass spectrometry allowed to prove the successful synthesis.
In order to achieve the desired structure, two main improvements need to be addressed. The stability of the molecule should be significantly enhanced, therefore the introduction of a different anchoring group like a methyl thioether or a pyridine is recommended. Secondly the weak chiroptical response of the parent compound should be improved. The helix in the investigated species is flexible, a more rigid structure is recommended. This would bring about the advantage of enhanced chiroptical effects and would allow to design similar materials for circular polarized luminescence.

Overall, the knowledge acquired during our research allowed us to share our detailed investigations with the scientific community. Chiral macrocyclic oligothiophenes, and more generally, compounds based on highly substituted [2.2]paracyclophane are promising candidates for fundamental studies and we expect many more such studies to appear in the literature.

[1] G.-P. Zhang, Z. Xie, Y. Song, G.-C. Hu, C.-K. Wang, *Top. Curr. Chem.* **2017**, *375*, 85.

[2] S. van der Molen, R. Naaman, E. Scheer, J. Neaton, A. Nitzan, D. Natelson, N. Tao, H. van der Zant, M. Mayor, M. Ruben, M. Reed, M. Calame, *Nat. Nanotechnol.* **2013**, *8*, 385–389.

[3] S. Wu, M. T. González, R. Huber, S. Grunder, M. Mayor, C. Schönenberger, M. Calame, *Nat. Nanotechnol.* **2008**, *3*, 569–574.

[4] R. Frisenda, V. A. E. C. Janssen, F. C. Grozema, H. S. J. van der Zant, N. Renaud, *Nat. Chem.* **2016**, *8*, 1099–1104.

[5] C. J. Brown, A. C. Farthing, *Nature* **1949**, *164*, 915–916.

[6] D. J. Cram, H. Steinberg, *J. Am. Chem. Soc.* **1951**, *73*, 5691–5704.

[7] D. S. Seferos, S. A. Trammell, G. C. Bazan, J. G. Kushmerick, *Proc. Natl. Acad. Sci.* **2005**, *102*, 8821–8825.

[8] S. T. Schneebeli, M. Kamenetska, Z. Cheng, R. Skouta, R. A. Friesner, L. Venkataraman, R. Breslow, *J. Am. Chem. Soc.* **2011**, *133*, 2136–2139.

[9] H. J. Reich, D. J. Cram, *J. Am. Chem. Soc.* **1968**, *90*, 1365–1367.

[10] H. J. Reich, D. J. Cram, *J. Am. Chem. Soc.* **1969**, *91*, 3517–3526.

[11] O. R. P. David, *Tetrahedron* **2012**, *68*, 8977–8993.

[12] A. A. Aly, A. B. Brown, *Tetrahedron* **2009**, *65*, 8055–8089.

[13] H. Hopf, *Angew. Chem. Int. Ed.* **2008**, *47*, 9808–9812.

[14] B. König, B. Knieriem, A. D. Meijere, *Chem. Ber.* **1993**, *126*, 1643–1650.

[15] B. König, B. Knieriem, K. Rauch, A. D. Meijere, *Chem. Ber.* **1993**, *126*, 2531–2534.

[16] H. J. Reich, D. J. Cram, *J. Am. Chem. Soc.* **1969**, *91*, 3527–3533.

[17] R. Bula, M. Fingerle, A. Ruff, B. Speiser, C. Maichle-Mössmer, H. F. Bettinger, *Angew. Chem. Int. Ed.* **2013**, *52*, 11647–11650.

[18] H. F. Bettinger, R. Einholz, A. Göttler, M. Junge, M.-S. Sättele, A. Schnepf, C. Schrenk, S. Schundelmeier, B. Speiser, *Org. Chem. Front.* **2017**, *4*, 853–860.

[19] Y. Asano, A. Muranaka, A. Fukasawa, T. Hatano, M. Uchiyama, N. Kobayashi, *J. Am. Chem. Soc.* **2007**, *129*, 4516–4517.

[20] M. Leung, M. B. Viswanath, P.-T. Chou, S.-C. Pu, H.-C. Lin, B.-Y. Jin, *J. Org. Chem.* **2005**, *70*, 3560–3568.

[21] A. R. Wartini, H. A. Staab, F. A. Neugebauer, *Eur. J. Org. Chem.* **1998**, *1998*, 1161–1170.

[22] R. Gleiter, K. Staub, H. Irngartinger, T. Oeser, *J. Org. Chem.* **1997**, *62*, 7644–7649.

[23] G. C. Bazan, *J. Org. Chem.* **2007**, *72*, 8615–8635.

[24] G. P. Bartholomew, G. C. Bazan, *J. Am. Chem. Soc.* **2002**, *124*, 5183–5196.

[25] G. P. Bartholomew, M. Rumi, S. J. K. Pond, J. W. Perry, S. Tretiak, G. C. Bazan, *J. Am. Chem. Soc.* **2004**, *126*, 11529–11542.

[26] S. Park, J. H. Heo, C. H. Cheon, H. Kim, S. H. Im, H. J. Son, *J. Mater. Chem. A* **2015**, *3*, 24215–24220.

[27] S. Park, J. H. Heo, J. H. Yun, T. S. Jung, K. Kwak, M. J. Ko, C. H. Cheon, J. Y. Kim, S. H. Im, H. J. Son, *Chem. Sci.* **2016**, *7*, 5517–5522.

[28] H. Hinrichs, A. J. Boydston, P. G. Jones, K. Hess, R. Herges, M. M. Haley, H. Hopf, *Chem. - Eur. J.* **2006**, *12*, 7103–7115.

[29] D. E. Fagnani, M. J. Meese, K. A. Abboud, R. K. Castellano, *Angew. Chem. Int. Ed.* **2016**, *55*, 10726–10731.

[30] Y. Morisaki, M. Gon, T. Sasamori, N. Tokitoh, Y. Chujo, *J. Am. Chem. Soc.* **2014**, *136*, 3350–3353.

[31] M. Gon, Y. Morisaki, Y. Chujo, *J. Mater. Chem. C* **2015**, *3*, 521–529.

[32] M. Gon, H. Kozuka, Y. Morisaki, Y. Chujo, *Asian J. Org. Chem.* **2016**, *5*, 353–359.

[33] M. Gon, Y. Morisaki, R. Sawada, Y. Chujo, *Chem. - Eur. J.* **2016**, *22*, 2291–2298.

[34] M. Gon, Y. Morisaki, Y. Chujo, *Eur. J. Org. Chem.* **2015**, *2015*, 7756–7762.

[35] M. Gon, R. Sawada, Y. Morisaki, Y. Chujo, *Macromolecules* **2017**, *50*, 1790–1802.
[36] M. Gon, Y. Morisaki, Y. Chujo, *Chem. Commun.* **2017**, *53*, 8304–8307.
[37] D. C. Braddock, I. D. MacGilp, B. G. Perry, *Adv. Synth. Catal.* **2004**, *346*, 1117–1130.
[38] R. Gray, V. Boekelheide, *J. Am. Chem. Soc.* **1979**, *101*, 2128–2136.
[39] K. Mutoh, Y. Nakagawa, A. Sakamoto, Y. Kobayashi, J. Abe, *J. Am. Chem. Soc.* **2015**, *137*, 5674–5677.
[40] Y. Morisaki, R. Sawada, M. Gon, Y. Chujo, *Chem. - Asian J.* **2016**, *11*, 2524–2527.
[41] N. V. Vorontsova, V. I. Rozenberg, E. V. Sergeeva, E. V. Vorontsov, Z. A. Starikova, K. A. Lyssenko, H. Hopf, *Chem. - Eur. J.* **2008**, *14*, 4600–4617.
[42] Y. Morisaki, M. Gon, T. Sasamori, N. Tokitoh, Y. Chujo, *J. Am. Chem. Soc.* **2014**, *136*, 3350–3353.
[43] Y. Morisaki, R. Sawada, M. Gon, Y. Chujo, *Chem. - Asian J.* **2016**, *11*, 2524–2527.
[44] J. D. WATSON, F. H. C. CRICK, *Nature* **1953**, *171*, 737.
[45] M. Rickhaus, M. Mayor, M. Juríček, *Chem. Soc. Rev.* **2016**, *45*, 1542–1556.
[46] M. Rickhaus, M. Mayor, M. Juríček, *Chem. Soc. Rev.* **2017**, *46*, 1643–1660.
[47] J. Krömer, I. Rios-Carreras, G. Fuhrmann, C. Musch, M. Wunderlin, T. Debaerdemaeker, E. Mena-Osteritz, P. Bäuerle, *Angew. Chem. Int. Ed.* **2000**, *39*, 3481–3486.
[48] A. Mishra, C.-Q. Ma, P. Bäuerle, *Chem. Rev.* **2009**, *109*, 1141–1276.
[49] E. Flapan, *When Topology Meets Chemistry: A Topological Look at Molecular Chirality* **2000** Cambridge University Press ; Mathematical Association of America, Cambridge ; New York : Washington, DC.
[50] J.-C. Chambron, J.-P. Sauvage, K. Mislow, A. De Cian, J. Fischer, *Chem. - Eur. J.* **2001**, *7*, 4085–4096.
[51] M. Carlotti, A. Kovalchuk, T. Wächter, X. Qiu, M. Zharnikov, R. C. Chiechi, *Nat. Commun.* **2016**, *7*, 13904.
[52] S. V. Aradhya, L. Venkataraman, *Nat. Nanotechnol.* **2013**, *8*, 399–410.
[53] M. Tsutsui, K. Shoji, M. Taniguchi, T. Kawai, *Nano Lett.* **2008**, *8*, 345–349.

EurJOC
European Journal of Organic Chemistry

A Journal of
ChemPubSoc Europe

20/2019
www.eurjoc.org

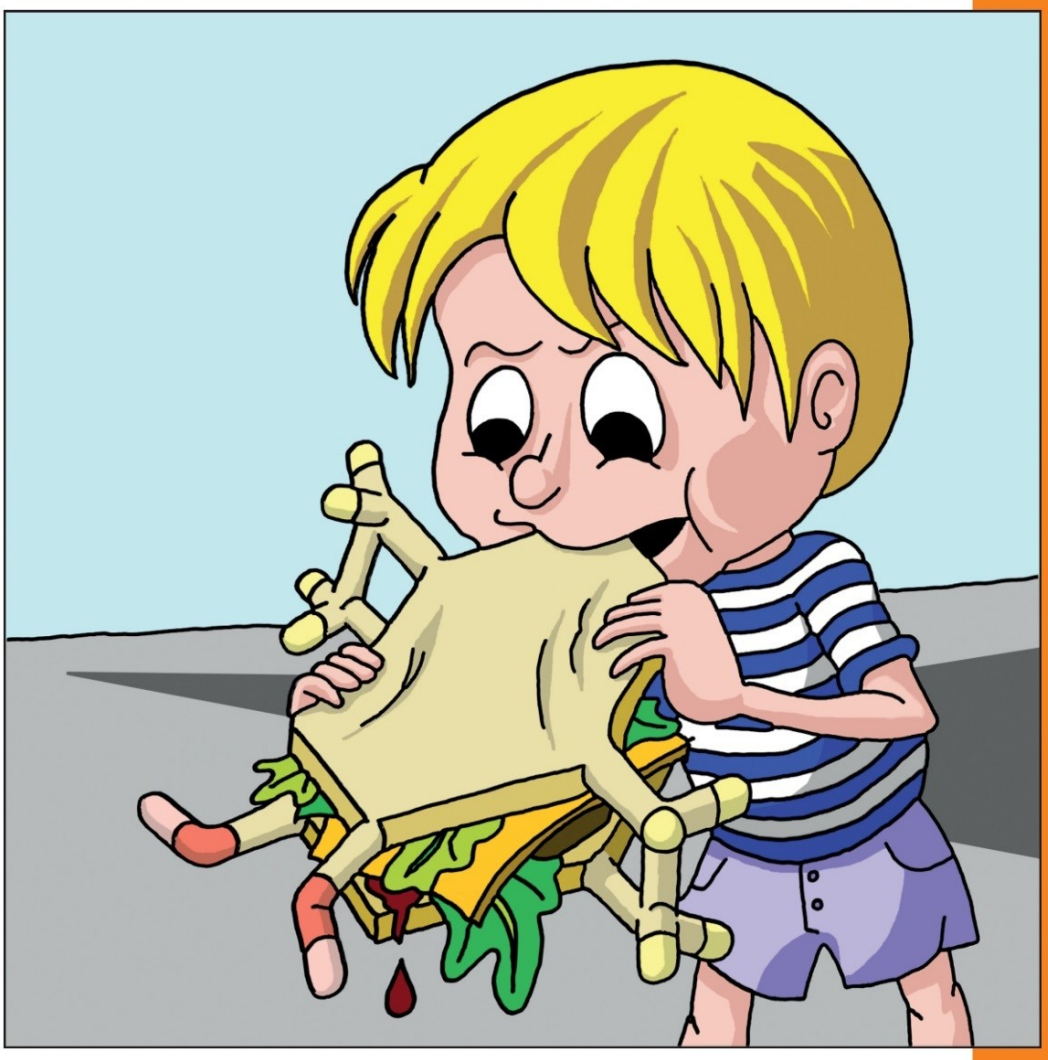

**Front Cover**

*Marcel Mayor et al.*
Beyond Simple Substitution Patterns – Symmetrically Tetrasubstituted [2.2] Paracyclophanes as 3D Functional Materials

Supported by
ACES Asian Chemical Editorial Society

WILEY-VCH

ChemPubSoc Europe

DOI: 10.1002/ejoc.201900061

EurJOC European Journal of Organic Chemistry

Minireview

Functionalized Cyclophanes | *Very Important Paper* |

VIP

# Beyond Simple Substitution Patterns – Symmetrically Tetrasubstituted [2.2]Paracyclophanes as 3D Functional Materials

Kevin J. Weiland,[a] Almudena Gallego,[a] and Marcel Mayor*[a,b,c]

**Abstract:** [2.2]Paracyclophane is the prototypical layered hydrocarbon and has been essential for investigations of through-space electronic interactions. Over the last years more examples of tetrasubstituted derivatives have been reported. This minireview discusses the synthetic approaches towards various substitution patterns and provides a survey over different approaches used to achieve and derivatize symmetric tetrasubstitution. The first two sections of this work present homo-tetrasubstituted derivatives, while the third section gives insight into symmetrically hetero-tetrasubstituted analogues. These approaches are briefly discussed, the resulting structures are presented in detail, and their specific properties resulting from the incorporation of [2.2]paracyclophane are elucidated.

## 1. Introduction

In 1949, *Farthing* and *Brown* isolated [2.2]paracyclophane (PC, **1**) as by-product from low-pressure pyrolysis of *para*-xylene.[1] This prototypical layered molecule was for the first time successfully synthesized through an intramolecular macrocyclization only two years later by *Cram* and *Steinberg*, who also demonstrated the transannular electronic communication of the benzene rings by means of UV/Vis spectroscopy.[2] *Cram* and *Reich* were further able to elucidate the chemistry of PC, where they found remarkable transannular effects and unique behavior, for example in thermal isomerization of substituted isomers and in directing effects, which can dominate the direction of the electrophilic aromatic substitution on PC derivatives.[3–5] Nowadays, the focus has shifted away from the chemical modification of PC and its application in asymmetric catalysis, and materials chemistry is now in the foreground.[6–8] The extraordinary configuration of the molecule displays a face-to-face arrangement of a two slightly-bent aromatic rings, with short inter-ring distances between 2.83 and 3.09 Å. It allows an effective transannular charge transfer between the benzene rings, leading to unique applications of PC derivatives in optoelectronics, non-linear optics, chemical vapor deposition or photoluminescent conjugated polymers.[2,7,9] Until recently, most of these materials were based on mono- or disubstituted PCs due to their well-known chemistry.[10] Higher substituted PCs were barely isolated,[11,12] although the formation of symmetrical tetrasubstituted PCs was reported by the elimination of sulfur for appropriately substituted 2,11-dithia[3.3]paracyclophanes in low yields.[13,14] Nowadays, dedicated chemists achieve the efficient synthesis and modification of symmetrical tetrasubstituted CPs, which have led to the design of a variety of complex

[a] *Department of Chemistry, University of Basel, St. Johanns Ring 19, 4056 Basel, Switzerland*
*E-mail: marcel.mayor@unibas.ch*
*https:/www.chemie.unibas.ch/~mayor/*
[b] *Karlsruhe Institute of Technology (KIT), P.O. Box 3640, 76021 Karlsruhe, Germany*
[c] *Lehn Institute of Functional Materials, School of Chemistry, Sun Yat-Sen University, Guangzhou 510275, China*
*ORCID(s) from the author(s) for this article is/are available on the WWW under https://doi.org/10.1002/ejoc.201900061.*

*(From left to the right) Kevin Weiland studied chemistry at the Ludwig Maximilian University of Munich and received his M. Sc. in 2013. He then moved to the University of Basel where he completed his doctorate in 2018 under the supervision of Professor Marcel Mayor on the subject of tailor-made three-dimensional molecules for organic electronics.*

*Almudena Gallego received her PhD in 2012 from the University of Madrid under the supervision of Professor Félix Zamora, where she investigated new coordination polymers showing electrical conductivity for its application as nanomaterials. After a one-year postdoc supervised by Professor Tomás Torres at University of Madrid, she joined the group of Professor Marcel Mayor in 2013 as a postdoctoral researcher, where she leads different projects with focus on nanoelectronics.*

*Marcel Mayor received his PhD in 1995 from the University of Bern under the supervision of Rolf Scheffold and Lorenz Walder. After working with Jean-Marie Lehn at the University Louis Pasteur in Strasbourg (France) and at the Collège de France in Paris (France), he founded his own research group in the Institute of Nanotechnology (INT) at the Karlsruhe Institute of Technology (KIT, Germany) in 1998. In 2004 he became Professor of Chemistry at the Department of Chemistry of the University of Basel (Switzerland), and in 2011 he became adjunct Professor of Chemistry of School of Chemistry of the Sun Yat-Sen University in Guangzhou (China). His current research interests are supramolecular chemistry, molecular electronics, nanoscale architectures, functional and hybrid materials.*

 

ChemPubSoc Europe
EurJOC European Journal of Organic Chemistry
Minireview

and interesting molecules based on these building blocks, with promising applications.

In this minireview we provide an overview over tetrasubstituted PC scaffolds (Scheme 1). We will discuss the different synthetic strategies, as well describing the most remarkable optical and electronic properties. Here, we will show that tetrasubstituted PCs can be easily achieved in a statistical approach. We will further present advances made towards chiral resolution of planar chiral tetrasubstituted PCs. We will demonstrate that symmetrically tetrasubstituted PCs serve as key building blocks that are used to investigate transannular charge transfer and optoelectronical properties. Furthermore, we will present examples, where chiroptical effects are introduced through helically chiral tetrasubstituted PCs.

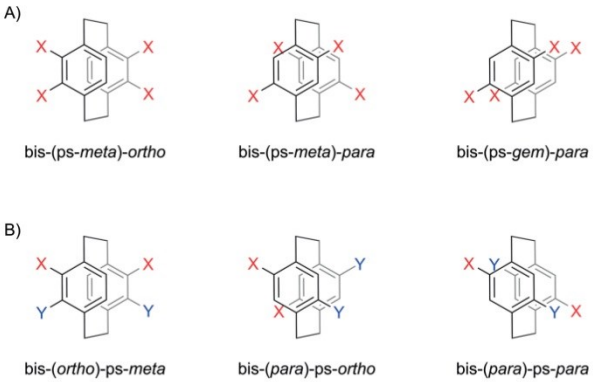


Scheme 1. Overview of some symmetric fourfold homo-substituted (A) and hetero-substituted (B) PC patterns discussed in this mini-review. The nomenclature used is based on the suggestion of *Hopf* and co-workers,[7] labelling the spatial relation between substituents attached to opposed phenyl rings with the prefix "ps" for "pseudo".

The review is organized by the molecules structures and not from a chronological perspective. It is divided in 3 sections. The first two describe molecules whose design and structure are based on tetrasubstituted PCs with identical substituents in positions 4, 5, 12, 13 and 4, 7, 12, 15 (bis(ps-*meta*)-*ortho* and bis(ps-*meta*)-*para* isomers respectively), and the third one focuses on tetrasubstituted PCs derivatives with unequal substituents. While there are different nomenclatures found in literature, we rely on the one introduced by Hopf and co-workers.[7]

## 2. Bis(ps-*meta*)-*ortho*-homo-tetrasubstituted [2.2]paracyclophanes

In 1969 *Cram* and *Reich* reported on the reaction of PC with an excess of bromine, which leads to two main tetrabrominated products, compound **2** and **3**.[5] They were able to isolate both compounds by means of column chromatography and further derivatize both compounds (see Scheme 2, A).

In 1992, *de Meijere* and co-workers demonstrated that the treatment of PC with liquid bromine and catalytic amounts of iodine over seven days at room temperature leads to two structural isomers of homo-symmetrically tetrasubstituted PC.[15]

The isomers could be separated on the basis of their different solubility in dichloromethane. The isomers **2** and **3** are often used as precursors of functionalized homo-tetrasubstituted PCs with either a bis(ps-*meta*)-*ortho* or a bis(ps-*meta*)-*para* substitution pattern, respectively. This chapter will discuss the bis(ps-*meta*)-*ortho* arrangement, the discussion of the bis-(ps-*meta*)-*para* configuration is given in the next chapter. An alternative synthetic approach has been reported for bis-(ps-*meta*)-*ortho* homo-tertasubstituted PCs,[16] which can be obtained directly by a one-step *Diels-Alder* cyclization using acetylene precursors decorated with electron withdrawing groups (Scheme 2, B). A variety of symmetrically functionalized PC derivatives was obtained by this strategy, and some of the exposed electron withdrawing groups could be further modified.[16]

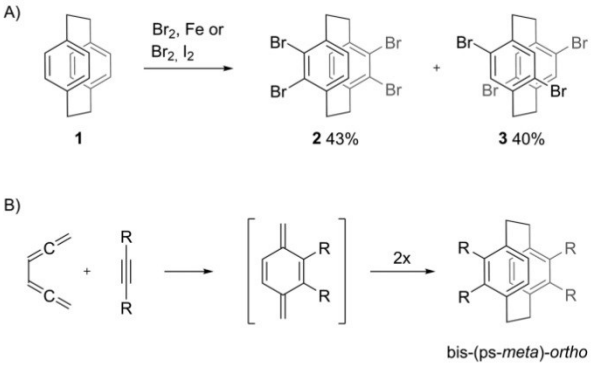


Scheme 2. A) Synthesis of bromine precursors of bis(ps-*meta*)-*ortho* and bis(ps-*meta*)-*para* homo-tetrasubstituted PCs, **2** and **3**, respectively. Yields reported from *de Meijere* and co-workers.[15] B) Alternative approach to bis-(ps-*meta*)-*ortho* PCs obtained by direct *Diels-Alder* cyclization (R = electron withdrawing e.g. $CO_2CH_3$, $CO_2C_2H_5$, $CO_2H$, CN, $CF_3$).

In 1992, *de Meijere* and co-workers, isolated compounds **2** and **3** on large scale by exploiting their different solubility. The authors report on one derivative obtained from **2**, where they achieved a fourfold *Heck* coupling with styrene. The obtained chromophore shows intense blue-green fluorescence when exposed to daylight. Following up on their seminal work on homo-tetrasubstituted PC, *de Meijere* and co-workers developed a strategy, where **2** was employed as an aryne equivalent.[17] Both *Cram* and *Reich*,[5] as well as *de Meijere* and co-workers found, that **2** can be used as a bis-aryne equivalent upon treatment with two equivalents of *n*-butyllithium (*n*BuLi).

When the aryne is generated in the presence of furan *syn,syn*-**4** and *anti,syn*-**4** are obtained in 12 and 15 % yield, respectively, while the *anti,anti*-isomer was not observed (Scheme 3). Further reductive deoxygenation with low-valent titanium leads to **5.** The authors successfully applied the same strategy to the reaction of the bis aryne with cyclopentadiene. The ratio of regioisomers for the synthesis of *syn,syn*-**6** and *anti,syn*-**6** is the same as for **4**. When reacting **2** with 2,5-diphenylisobenzofuran, **7** could be obtained in higher yields, but could only be deoxygenated with in situ generated trimethylsilyl iodide.

Interestingly, after treating **2** with one equivalent of *n*BuLi and trapping of the intermediate with a half-equivalent of [2.2]furanophane, stair-like molecule **8** could be obtained,

 

ChemPubSoc Europe
EurJOC European Journal of Organic Chemistry
Minireview

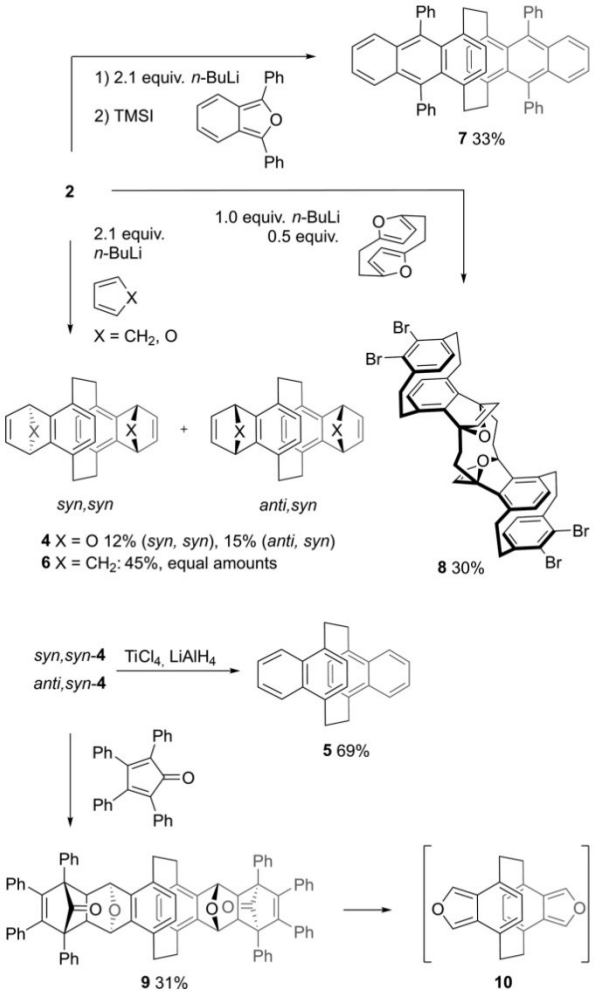


Scheme 3. Scope of the reactivity of **2** under aryne-forming conditions.[5,17,18] Only one stereoisomer of **9** is shown.

where the deoxygenation was unsuccessful, due to steric hindrance of the cyclic ethers. When *syn,syn*-**4** and *anti,syn*-**4** where refluxed with tetraphenylcyclopentadienone in benzene, the *Diels-Alder* adduct **9** was obtained as a mixture of four stereoisomers.[18]

Further heating of **9** led to a retro-*Diels-Alder* reaction, to give reactive intermediate **10**, which could not be isolated but only be confirmed through mass spectrometry. Trapping of **10** with *p*-benzoquinone led to the twofold *Diels-Alder* addition product in an undetermined mixture of regioisomers.

Based on the mixture of regioisomers of **4**, Bettinger and co-workers reported on a covalently coupled pentacene dimer.[19]

*Diels-Alder* addition of **4** and anthraquinone gives tetraketone **11**, which could be deoxygenated and reacted with lithium triisopropylsilylacetylide (Scheme 4). Subsequent reduction leads to pentaceneophane **12**. Comparison of the absorption spectra of **12** with the one obtained from 6,13-bis(triisopropylsilylethynyl)pentacene revealed a red shift of the p-band of 20 nm, which the authors attribute to through-space coupling of the pentacene units of **12**. In a similar approach *Bettinger* and co-workers furthered the understanding of through-space coupled *anti*-[2.2](1,4)acenophanes by following the same strategy to form tetracenophane **13**.[20] The regioisomeric mixture of **4** is reacted under *Diels-Alder* conditions with 1,4-naphtaquinone in the presence of 3,6-di(2-pyridyl)-1,2,4,5-tetrazine, followed by basic deoxygenation and addition of lithium triisopropylsilylacetylide. The investigation of the absorption spectra reveals a general red shift of the spectrum of **13** when compared with its non-phane analogue. The through-space coupling of the tetracene dimers is more pronounced than the coupling of the pentacene dimers reported above, the red shift of the tetraceneophane of 26 nm is larger, compared to the red shift of **12**.

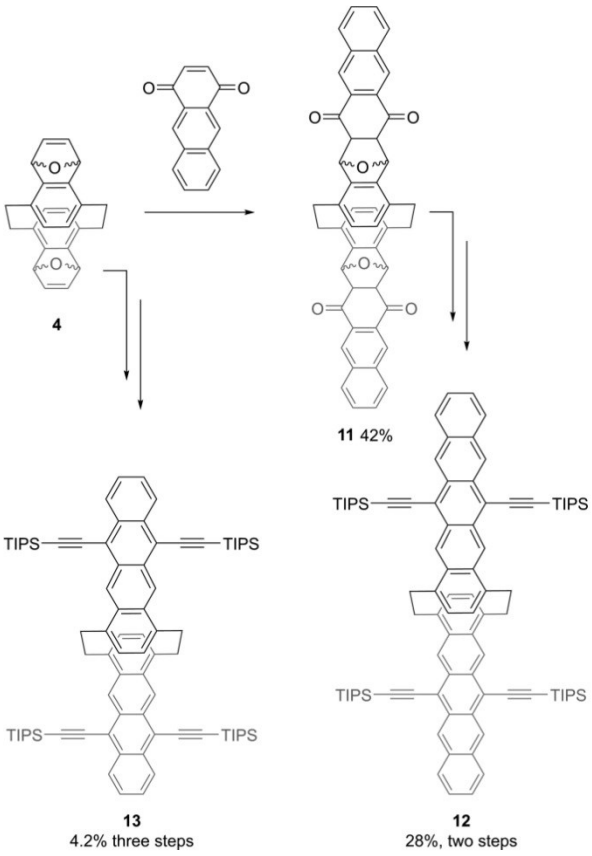


Scheme 4. Synthesis of pentacenophane **12** and tetracenophane **13**. *Diels-Alder* reaction of **4** followed by basic dehydration and addition of lithium triisopropylsilylacetylide gives pentaceneophane **12**.[19] Compound **13** was achieved following a similar pathway.[20]

In 2007, *Kobayashi* and co-workers reported on a phthalocyanine dimer (Scheme 5), which is coupled through a central PC building block, also derived from compound **2**.[21]

The authors found that cyanation of **2** proceeds in good yields and were subsequently able to generate both the mono- and dimeric phthalocyanines **15** and **16** in one step under typical conditions for phthalocyanine synthesis. The tetranitrile precursor **14** can also be obtained by the *Diels-Alder* based strategy

 

ChemPubSoc Europe
EurJOC European Journal of Organic Chemistry
Minireview

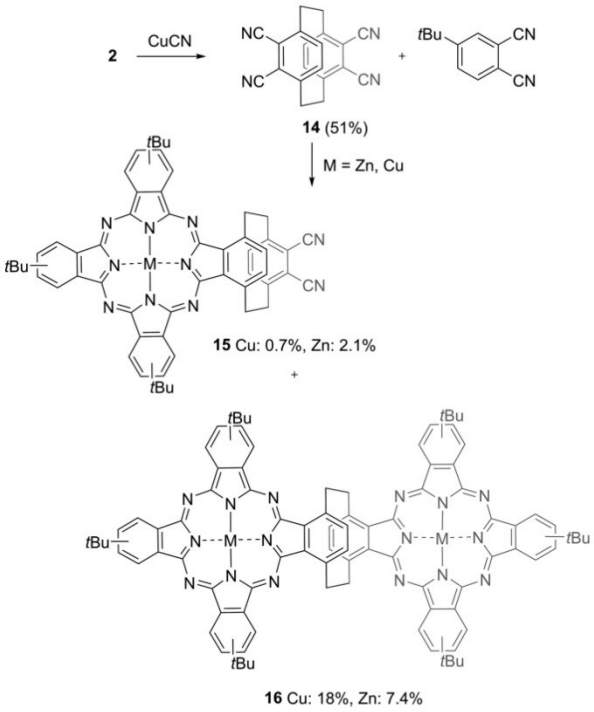


Scheme 5. Synthesis of phthalocyanine-monomer **15** and -dimer **16**.[21]

(see Scheme 2 B) from 1,2,4,5-hexatetraene and dicyanoacetylene.[16] Optical investigations of Zn-**15** and Zn-**16** and comparison with non-PC-substituted zinc-tetra-(tertbutyl)-phthalocyanine revealed a significant redshift of the absorption bands. Both absorption bands are split when compared to the non-PC containing analogue, hinting to substantial electronic communication through the PC-building block.

The electronic communication was further confirmed through DFT calculations, where it was shown that the electronic coupling of one phthalocyanine subunit through the PC is a substantial factor for the shape of the absorption spectrum and the splitting of the absorption band.

In 2004, *Jin* and co-workers reported on the synthesis of *anti*-[2.2](1,4)biphenyleneophane.[22] In an elegant synthetic sequence (Scheme 6), they were able to prepare biphenylene **18** and investigate the optical and electrochemical properties.

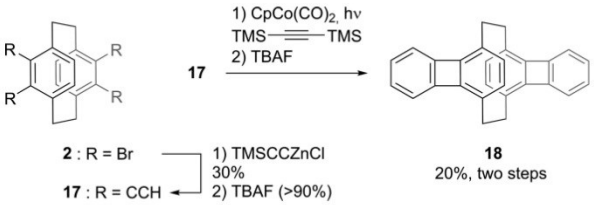


Scheme 6. Synthesis of *anti*-[2.2](1,4)biphenyleneophane **18**.[22]

The authors successfully grew single crystals suitable for X-ray analysis of **18** and found the inner benzene rings to be bent in a boat-like conformation, while the outer rings were unaffected by the strain of the cyclophane. The C=C and C–C bonds of the benzene ring in the PC subunit differ by length in 0.062 Å while the carbon-carbon bonds of the outer benzene rings differ in length by 0.045 Å. The PC thus resembles more the electronic structure of cyclohexatriene, while the outer benzene rings are of aromatic nature. When the authors investigated the absorption spectra and compared them with the one of biphenylene, they found a considerable red shift, which they assign to phane-contributions to the delocalization of the frontier orbitals. Two irreversible single-electron oxidations separated by 180 mV were observed during the electrochemical investigation of **18**, documenting the electrostatic repulsion between both biphenylene subunits.

Another interesting class of molecules was reported in 1997 by *Gleiter* and co-workers, forming dibenzoequinenes based on bis(ps-*meta*)-*ortho*-homo tetrasubstituted PCs (Scheme 7).[23] Some of the starting materials were not prepared from the tetrabromo compound **2** but by reaction of 1,2,4,5-hexatetraene with suitable internal acetylenes, as reported by *Hopf* and co-workers.[16] While the synthesis of such building blocks is only briefly mentioned in this minireview (Scheme 2 B), it remains an important access to symmetrically substituted PCs. Subsequent modifications provided the desired substitution pattern after the synthesis of the PC core of the respective molecules.

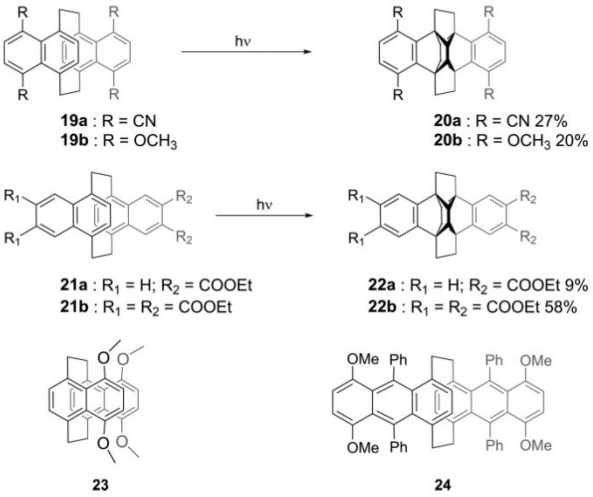


Scheme 7. Scope of the substitution pattern of substituted dibenzoequinene,[23] and tetramethoxy PC derivatives **23** and **24** by *Neugebauer* and co-workers which were compared with **19b**.[24]

In order to achieve the asymmetrically substituted derivative **21a**, a [3.3]selenophane was generated, from which selene was released by UV-irradiation. The four [2.2]naphthalenophanes were then irradiated in benzene at a wavelength of 350 nm yielding the corresponding dibenzoequinenes in yields from 9–58 %. The solid-state structure of **20a** showed considerable deviations from the optimized angle of 90° for the four membered rings (92.7–83.4°). The average bond length of the four membered rings was 1.579 Å, which is longer than the average bond length of cyclobutane compounds (1.554 Å). These differences in bond lengths and angles are accounted for by the

 

ChemPubSoc Europe

EurJOC European Journal of Organic Chemistry
Minireview

ethano bridges over the four membered rings, which also introduce strong folding in the five-membered rings.

*Neugebauer* and co-workers utilized bis(ps-meta)-ortho CP derivatives to investigate the transannular delocalization in radical cations.[24] To achieve this, they synthesized and studied three species of PCs, **19b**, **23** and **24** by means of EPR and ENDOR spectroscopy. *Syn*-[2.2]naphthalenophane **23** was obtained as a by-product following the synthesis of **19b**. The synthesis of *anti*-[2.2]anthracenophane **24** was performed similarly to the synthesis of **7**. To compare the electronic delocalization of the series of cyclophanes, they were oxidized and were subjected to EPR and ENDOR spectroscopy. The naphthalenophanes showed a high degree of electronic conjugation through the PC building block, which was determined through the small splitting of the aromatic hydrogen atoms directly on the PC in the ENDOR spectrum. The ENDOR spectrum for **24** showed that electron transfer between the two electrophores is slow on the EPR time-scale, while there is still substantial spin population within the PC.

## 3. Bis(ps-*meta*)-*para*-homo-tetrasubstituted [2.2]paracyclophanes

The substitution pattern discussed above is achiral since **2** has an inversion center. Also obtained in the synthesis of **2** is bis-(ps-*meta*)-*para* tetrabrominated PC, **3,** which is planar chiral. The compound described here can either be obtained by subjecting the crude to chromatography,[5] or by exploiting the difference in solubility of **2** and **3** in dichloromethane.[15]

*Cram* and *Reich* initially were able to prove the substitution pattern of **3** by reacting it with *n*BuLi and dimethyl sulfate, yielding compound **25** (Scheme 8).[5] *De Meijere* and co-workers addressed **3** with transition metal catalyzed cross-coupling conditions and provided a series of tetraolefin-substituted PC derivatives **26** through fourfold palladium catalyzed *Heck* reactions with **3**.[15] Depending on the styrene derivative employed, yields up to 70 % were obtained. The scope of palladium catalyzed coupling reactions was complemented by engaging **3** in a *Sonogashira*-coupling protocol with phenylacetylene giving **28** in good yields. Nickel catalyzed transformation of **3** with phenylmagensium bromide gave **27** in low yields. When the absorption spectra of the star-shaped molecules were compared with their linear oligophenylvinyl (OPV) and oligophenylethynyl (OPE) analogues, a bathochromic shift of the PC-based molecules was found for all cases. The synthetic accessibility and its easy engagement in cross coupling reactions made **3** a popular parent structure for model compounds investigating through space cross-conjugation.

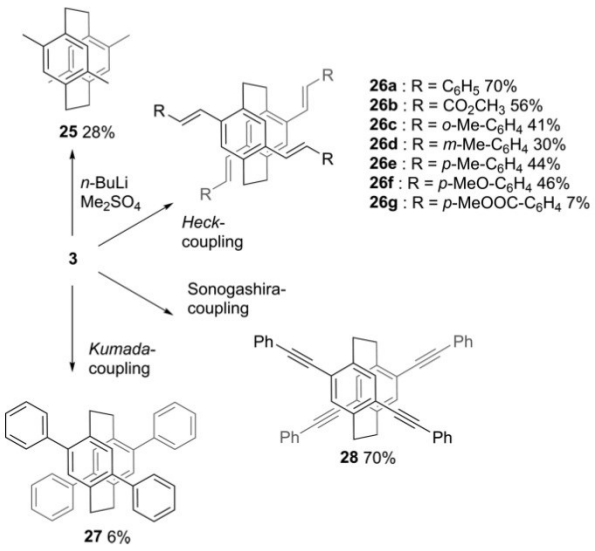


Scheme 8. Synthesis and derivatization of **3** by lithiation and trapping, as well as Pd-catalyzed coupling chemistry.[5,15]

An example of such model compounds for the study of PC mediated through-space conjugation are the PC connected OPV structures **29** and **30** (Scheme 9). The compounds were synthesized by *Bazan* and co-workers employing a fourfold *Heck* reaction[25] comparable with the approach of *de Meijere* and co-workers. The compounds were isolated in low yields, which was rationalized by limited solubility of the intermediates in the reaction. Comparison of the absorption spectra of **29** and **30** revealed similar absorption properties. The authors further concluded that excitations were delocalized across the entire molecules, which they describe as strong mixing of the "phane" and the antenna (chromophore) states within the respective molecule. This was contrasting symmetrically disubstituted distyryl-PCs, where the absorption of the molecules occurs via the stilbene fragments, and therefore the absorption spectra are similar to those of the constitutional monomers.[26]

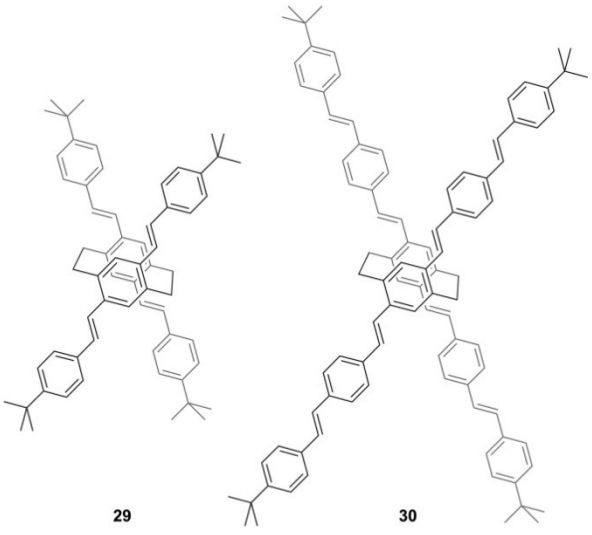


Scheme 9. Symmetrically tetrasubstituted OPV based chromophores by *Bazan* and co-workers.[25]

Shortly after, *Bazan* and *Bartholomew* published on donor-acceptor tetrasubstituted PC based chromophores.[27] Based on the previous experience of the group concerning the poor solubility and general challenges in the handling of tetrasubstituted PCs, they designed a more selective pathway involving the

 

ChemPubSoc Europe
EurJOC European Journal of Organic Chemistry
Minireview

*Horner-Emmons* coupling precursor **33** (Scheme 10). The initial synthesis proceeded through a sonication driven bromomethylation of **1**, from which both **31** and **32** were obtained. After separation of the two regioisomers, **31** was converted to **33** in excellent yields. Subsequent *Horner-Emmons* reactions give chromophores **34**, **35**, and **36**. Compounds **35** and **36** were obtained by reaction of **33** with one or two equivalents of 4-dihexylaminobenzaldehyde and subsequent isolation of the desired precursor, enabling the formation of the target compounds upon treatment with 4-nitrobenzaldehyde.

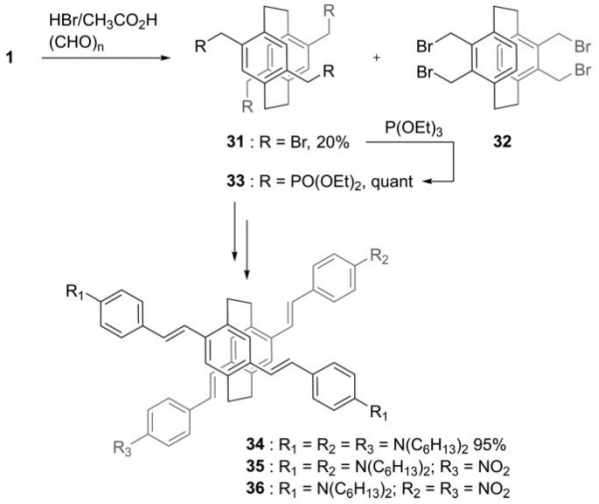


Scheme 10. Bromomethylation of **1** followed by preparation of the *Horner-Emmons* precursor **33** and synthesis of the tetraamine **34**. Asymmetric chromophores **35** and **36**, which are obtained in a statistical approach from **33**.[27]

This strategy to tetrasubstituted PCs with different styrene substituents based on **33** faced severe limitations and thus, the authors developed an alternative synthetic access to this class of model compounds. The fourfold substituted push-pull CP chromophores **39**, **40** and **41** were assembled using this site-selective strategy (Scheme 11). The approach is based on the transformation of bromines of **3** into aldehydes by a bromine lithium exchange followed by addition of *N*,*N*-dimethylformamide (DMF).

The extent of lithiation of the tetrabromide **3** was controlled by the equivalents of the reagent. Upon addition of two equivalents of *n*BuLi, exclusively the two regioisomers **38a** and **38b** with a formyl group attached at each phenyl ring of the CP were obtained after treatment with DMF.

Monoformyl-compound **37** first was subjected to *Heck* coupling conditions with *para*-dihexylaminostyrene and after isolation of the intermediate, exposed to *Horner-Emmons* conditions using 4-nitrophenylmethanephosphonate to yield the asymmetric chromophore **39**. The two diformylated regioisomers **38a** and **38b** were first isolated by high-performance liquid chromatography (HPLC) before the same strategy as applied for **37** provided the push-pull target PC structures **40** and **41**.

Investigation of the optical properties of compounds **35**, **36** and **39** revealed that the relaxation of the internal conversion

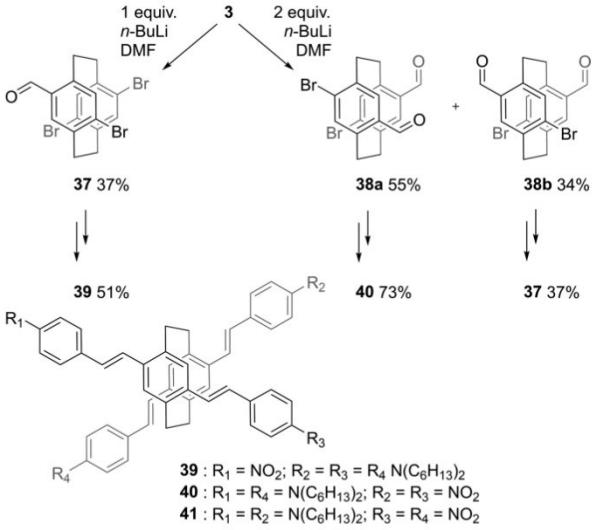


Scheme 11. Synthetic access to donor acceptor tetrasubstituted PCs.[27]

from $S_2$ to $S_1$ was not complete, and emission from $S_2$ was observed. For **34**, **40**, and **41** delocalization through the entire molecule was observed. *Bazan* and co-workers further elaborated on the charge delocalization throughout similarly tetrasubstituted charged PCs where the molecules were either tetraammonium salts or tetrasulfonate salts of X-shaped styryl chromophores.[28] The molecules were prepared from their common intermediate **33**. The authors reported that the through-space state, created by electron exchange across the PC core, is susceptible to solvent polarity. The solvatochromic behavior of such molecules is dominated by the charge transfer component of the distyrylbenzene chromophore. Notably, based on elongated OPV structures of **34** efficient materials for two-photon absorption (TPA) applications were synthesized also from precursor **33**.[29] These materials have a TPA cross section which has about twice the size of the individual monomer, and the excited states are further fully delocalized throughout the entire molecule. Comparison of linear absorption and TPA revealed that the trough-space conjugation affected one- or two-electron absorption differently. Absorption spectroscopy for the X-shaped molecules reveals a characteristic *Davydov* splitting of the monomer band into two components. In contrast TPA gives no such splitting as the contributions of each monomer of the X-shaped molecules are additive.

The electron delocalization through a homo-tetrasubstituted PC was also employed for the assembly of an efficient hole-transporting material in a perovskite based solar cell by *Son* and co-workers (Scheme 12).[30,31] The hole transporting material **42** was fabricated through a tetrafold *Suzuki* reaction starting from **3**. It was incorporated into the hole transporting layer of a perovskite solar cell, were the rigid geometry of **42** allowed for 3D directional transport pathways, resulting in increased charge carrier mobility. The device achieved a solar cell efficiency of 17.9 %, whereas the efficiency of the solar cell, where **43** was employed as hole transporting material was 16.4 % The higher efficiency for the device made with **42** was attributed to its

 

ChemPubSoc Europe
EurJOC European Journal of Organic Chemistry
Minireview

greater capacity for efficient charge transfer from the perovskite layer to the hole transporting material.

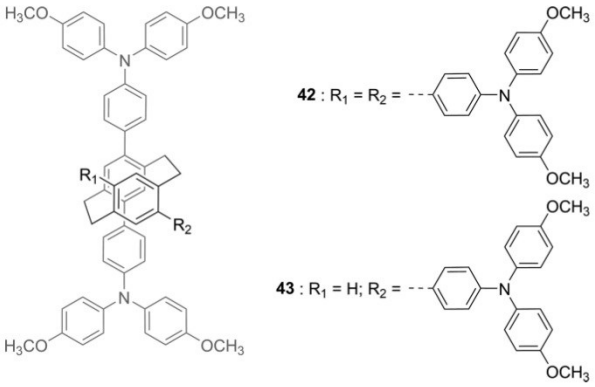


Scheme 12. Hole transporting materials **42** and **43**.[30,31]

A fascinating approach to incorporate racemic homo tetrasubstituted PC into chiral functional materials was presented by *Castellano* and co-workers in 2016.[32] They synthesized bis-(ps-*meta*)-*para* substituted tetraamide **45** in which the amides allow for efficient intra- and intermolecular hydrogen bonding. The molecules form well-defined 1D columns, in which the racemic molecules are separated such that the monomers in a particular column have the same chirality (Scheme 13).

Analysis of the crystal data revealed intramolecular aryl-aryl distances of 3.1 Å, and intermolecular distances of 3.8 Å. The intra- and intermolecular H-bonding distances were 2.81 Å and 2.77 Å, respectively. A pronounced shift of the amide-proton by 0.6 ppm upon increasing the concentration enabled to observe the association behavior by $^1$H-NMR experiments. The supramolecular growth of the arrangement was analyzed by DOSY-NMR. As macroscopic feature, the increased viscosity of the solution already at mM concentrations upon altering the solvent to apolar media is described.

As already discussed in the introduction, compound **3** is chiral and it is obtained as a racemic mixture in all reported syntheses.[5,15] An elegant method making gram scale quantities of a fourfold substituted pure PC enantiomer available was reported by *Chujo* and co-workers.[33] The synthetic strategy (Scheme 14) is based on the conversion of one of the four bromines into a hydroxyl group, which is subsequently engaged in the ester formation with (–)-(1*S*,4*R*)-camphanoyl chloride (Cam-Cl) yielding the pair of diastereomers ($S_p$,1*S*,4*R*)-**46a** and ($R_p$,1*S*,4*R*)-**46b**, which were separated by flash column chromatography and further purified by recrystallization giving both with a diastereomeric ratio better than 99.5 %. The absolute configuration of the diastereomers was determined by single crystal analysis.

Hydrolysis of the diastereomer ($S_p$,1*S*,4*R*)-**46a** followed by treatment with trifluoromethanesulfonic anhydride provided the enantiopure PC derivative ($S_p$)-**47** with three bromine and one triflate substituents. Optimized reaction conditions enabled to address the bromines selectively over the triflate in a *Sonogashira–Hagihara* cross-coupling reaction, providing the trialkyne PC ($S_p$)-**48** in very good yields. The selectivity of the

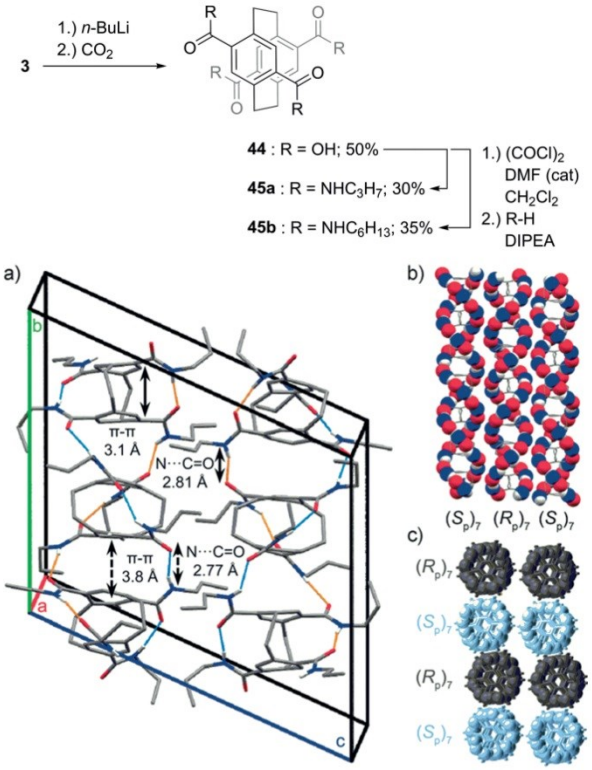


Scheme 13. Synthesis of tetraamide **45** and crystal structure (R = propyl), reprinted from *Castellano* and co-workers.[32] a) Unit cell containing each enantiomorphic asymmetric unit, b) side view of extended PC stacks, c) packing diagram showing different stacks from a top down view. Reproduced with permission from ref.[32]. Copyright 2016 WILEY.

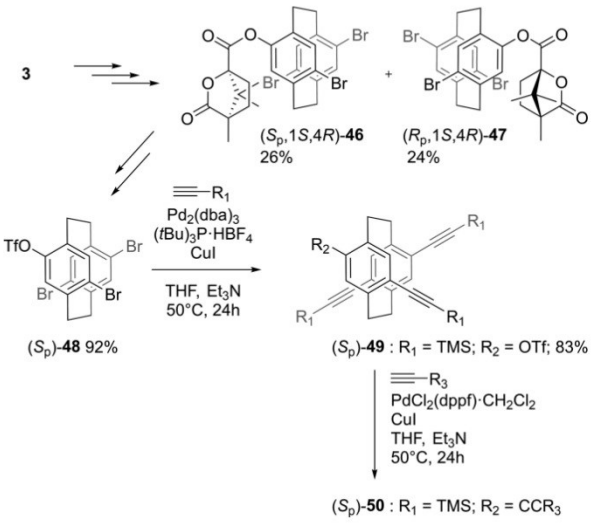


Scheme 14. Synthetic strategy for the chiral resolution of bis(ps-*meta*)-*para* tetrasubstituted PC.[33]

catalytic system allowed *Morisaki* and co-workers to introduce asymmetric tetrasubstituted X-shaped compounds based on tetraalkyne substituted PC derivatives.[34]

 

ChemPubSoc Europe
EurJOC European Journal of Organic Chemistry
Minireview

The protocol further lead to the first enantioselective synthesis of the trimethylsilyl (TMS)-protected tetraalkyne ($S_p$)-**50**. Further modification of **50** resulted in the chiral propeller shaped molecule ($S_p$)-**51** (Scheme 15).[33] The similar PC scaffold **52** was already reported by *Hopf* and co-workers, albeit not enantioselectively.[35] Electron delocalization was investigated by absorption spectroscopy and delocalization through the central PC unit was mainly found for the propeller shaped **52**, while model compounds like e.g. the constitutional isomer **53** did not display comparable extents of delocalization.

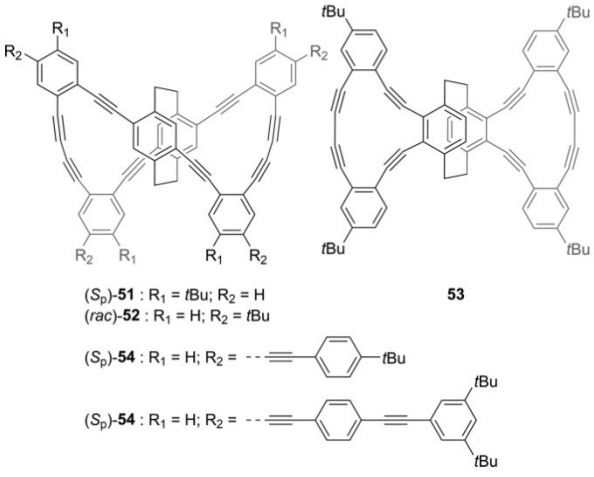


Scheme 15. Propeller shaped molecules ($S_p$)-**51** by *Chujo* and co-workers[33] and (*rac*)-**52** by Hopf and co-workers.[35] Constitutional isomer **53** which was used by *Hopf* and co-workers to elucidate cross conjugation properties. Compounds **54** and **55**, which were used to investigate chiroptical properties of extended propellers by *Chujo* and co-workers.[36]

*Chujo* and co-workers investigated the chiroptical properties of compound **51**. They found intense signals in the electronic circular dicroism (ECD) spectra for both enantiomers, which they attributed to the fixed and rigid geometry of **51**.

A qualitatively similar chiroptical behavior was observed for a derivative of the described compound where the outer benzene rings were replaced by naphthalenes.[36] When the optical properties of **52** were compared with the ones observed for compounds **54** and **55**, *Chujo* and co-workers observed intense chiroptical properties for all investigated species.[37] The key parameters describing the chiroptical properties are the dissymmetry factor of absorbance ($g_{abs} = 2(\Delta\varepsilon/\varepsilon)$) and the circular polarized luminescence (CPL) dissymmetry factor ($g_{lum} = 2(I_{left} - I_{right})/(I_{left} + I_{right})$. For $g_{abs}$ the extinction coefficient of the molecule is compared with the circular dichroism due to electronic transitions (ECD), and for $g_{lum}$ the polarized luminescence intensities of left and right CPL ($I_{left}$ and $I_{right}$ respectively) are compared. For both enantiomers of **52** the values for $g_{abs}$ and $g_{lum}$ were exceptionally high at $1.0 \pm 0.1 \times 10^{-2}$, and the minor differences in the respective values were interpreted as indication of only small structural changes between ground and excited states. This hypothesis was further supported by the absence of temperature- or solvent-induced change in the UV, ECD and CPL spectra. The peripheral oligophenylethylene (OPE) decorated derivatives **54** and **55** have localized excited states on their OPE arms, while molecule **52** has its excited state localized on the central cyclophane. Of particular interest was the comparison of the chiroptical properties of the propeller shaped molecules with their precursors with a not yet fixed propeller structure. Considerable larger molar ellipticities and CPL dissymmetry factors were observed for the propellers. These intense chiroptical properties are discussed as emerging from the rigid propeller shaped secondary structure of the molecules, which was maintained in the excited state. The $g_{abs}$ and $g_{lum}$ for **54** and **55** were in the same range as for **52**.

To further explore the potential of X-shaped conjugated structures with a central PC subunit, the same group attached dendrons via *Sonogshira*-type chemistry at the four alkynes of the enantiopure tetraalkyne **56**.[38]

The authors present the series of dendrimers **57**. The aromatic branches act as light harvesting antennas and inhibit aggregation induced quenching of the excited state. The series of dendrimers have strong CPL both in solution and in thin films, as evidenced by their high $g_{abs}$ and $g_{lum}$ values around $10^{-3}$, recorded for the four members of **57** in solution, as well as in thin films.

*Chujo* and co-workers further reported optically active PC compounds to study the influence of aggregation on emission properties.[39] They prepared enantiopure samples of compound **26a** (R = phenyl) from **47**, together with an analogue comprising an extended peripheral π-system. For both model compounds $g_{abs}$ and $g_{lum}$ values of ca. $10^{-3}$ were recorded, which are of comparable dimensions as the ones observed for the series of dendrimers **57**. Interestingly, the chiroptical features of these compounds displayed temperature dependence with decreasing polarized luminescence with increased temperature. The same authors further elaborated on aggregation studies of X-shaped molecules **58** and **59** exposing mesogenic substituents of various dimension.[40] The chiroptical properties of these model compounds were investigated in solution as well as in thin films obtained by drop-casting and spin coating. Different aggregates were observed depending on the film preparation. In particular, the dissymmetry factors changed their sign depending on the film deposition technique. Simulation of the stacking behavior of the molecules in each deposition technique supported the observed behavior. Transmission electron microscopy even displayed fiber formation for the enantiopure CP **59**. Annealing of the films of **58** and **59** triggered their transformation into the thermodynamically most stable aggregates.

The series of CP model compounds reported by *Chujo* and co-workers was further complemented by the enantiopure tetra-aryl decorated X-shaped structures **28**, **60** and **61**.[41] Intense chiroptical effects were found (characteristic $g_{abs}$ and $g_{lum}$ values are ca. $10^{-3}$) for these compounds emerging from the rigid confirmation of the X-shaped center of the molecule. Interestingly, the chirality of the central CP subunit was not communicated to the peripheral anthracene units of **61**, as it displayed substantial *Cotton* effects only in the region where the core of the molecule contributed to the ECD-spectrum.

Another recent example of an X-shaped PC derivative synthesized as pure enantiomer is **62** (Scheme 16), acting as model

 

ChemPubSoc Europe

EurJOC European Journal of Organic Chemistry
Minireview

compound for two terminally methoxy functionalized OPE rods with stacked central phenyl units. The chiroptical properties of X-shaped **62** were compared with its V-shaped structural isomer **63** (Scheme 16), with stacking terminal phenyl subunits.[42] Also **63** was synthesized as pure enantiomer and the access of pure enantiomers of the PC building block will be discussed in the following chapter 4 (**80** in Scheme 19). Comparison of the CPL features of the X- and V-shaped model compounds **62** and **63** displayed opposite CPL signs with respect to the chirality of their CP subunit. The authors thus identified the spatial orientation of both OPE rods as more important for their chiroptical properties than their absolute configuration.[42]

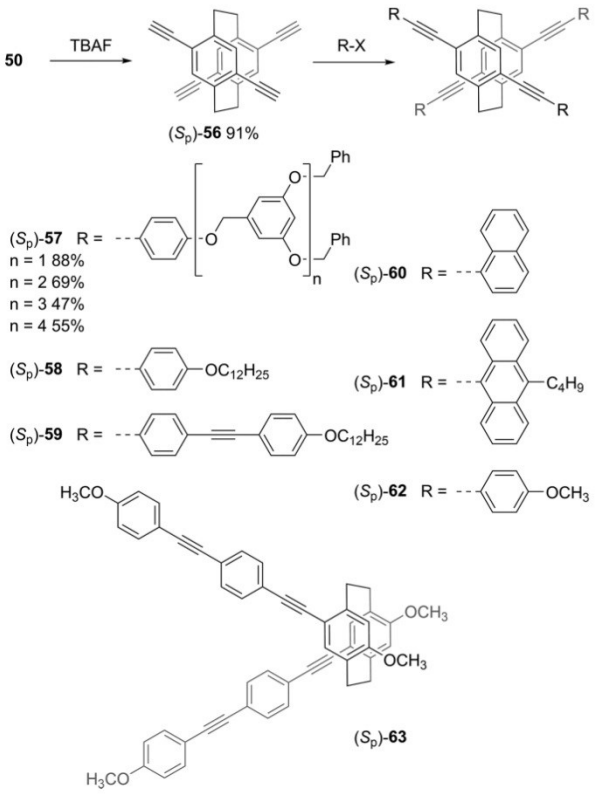


Scheme 16. Synthesis of the series of chiral CP comprising dendrimers **57**[38] and the X-shaped molecules **58** and **59** for aggregation studies,[39] the extended model compounds **60** and **61**, which were analyzed as CPL emitters,[40] and the V-shaped model compound **63**.[42]

*Morisaki* and *Chujo* recently summarized their attempts to control optical features of model compounds with CP controlled intramolecular π-stacking.[43]

An appealing approach to vary chiroptical properties is the introduction of binding sites at the periphery of **56** giving access to higher order structure through metal coordination.[44] For the purpose enantiopure **56** was decorated with pyridiyl-substituents providing the X-shaped multidentate ligands **64** and **66**. The synthesis is shown in Scheme 17. The intramolecular coordination of silver ions by pyridine nitrogens rigidifies the secondary structure of both dinuclear complexes **65** and **67**. The change of the degree of freedom in vicinity of the pyridyl groups is low for the silver ion coordination of **64** giving **65**. Consequently, the chiroptical properties are qualitatively hardly affected. While the maximum absorption is red-shifted, the intensity of the *Cotton* effects in the ECD spectrum remains almost the same upon coordination. The situation is different for the extended structure **66**, which is more rigidified upon coordination of silver-cations yielding in **67**. While the absorption spectrum is only slightly affected by the transition from **66** to **67**, the *Cotton* effects in the ECD spectra are tripled in intensity. Interestingly, the coordination of silver quenches the circular polarized luminescence for **67** selectively. The authors suggest two competing second order structures as potential explanation with the silver ions not exclusively coordinating to the pyridyl nitrogens but also interacting with the π-system of the molecule.

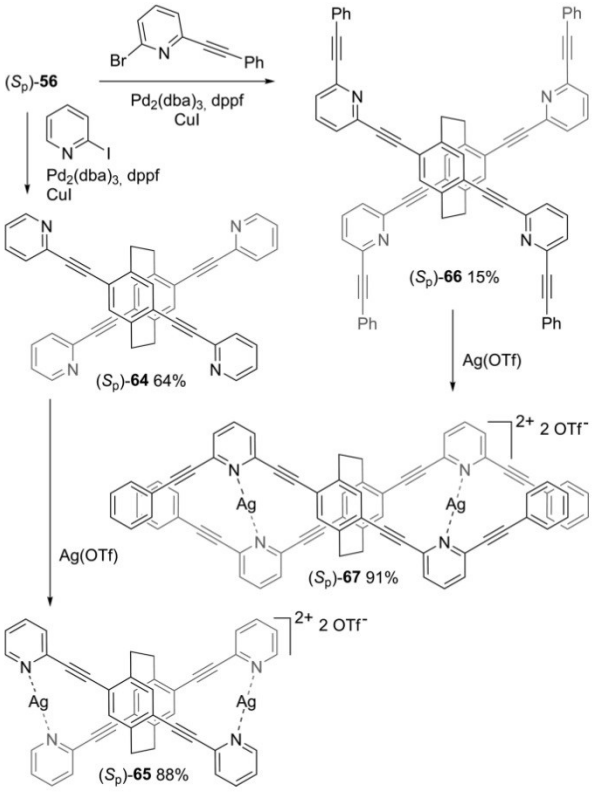


Scheme 17. Synthesis of the tetra-pyridyl ligands **64** and **66**, together with their dinuclear Ag(I)-coordination compounds **65** and **67**.[44]

## 4. Symmetrically Tetrasubstituted PCs with Heterosubstituents: PC Design through Regioselective Electrophilic Aromatic Substitution

In the preceding chapter, we have seen the amazing potential of synthetic strategies providing precise control over more than one type of substituents. Until 2008, the number of symmetrically tetrasubstituted PC derivatives mainly relied on synthetic

 

ChemPubSoc Europe
EurJOC European Journal of Organic Chemistry
Minireview

approaches displayed before, also commonly employed was the *Hoffmann* 1,6-elimination to synthesize the parent hydrocarbon, as well as symmetrically higher substituted analogues. *Hopf* and co-workers elucidated in a seminal publication the double electrophilic substitution of suitable disubstituted PCs.[7] Until this point, only isolated examples of regioselective disubstitution were known, which are summarized in Scheme 18.

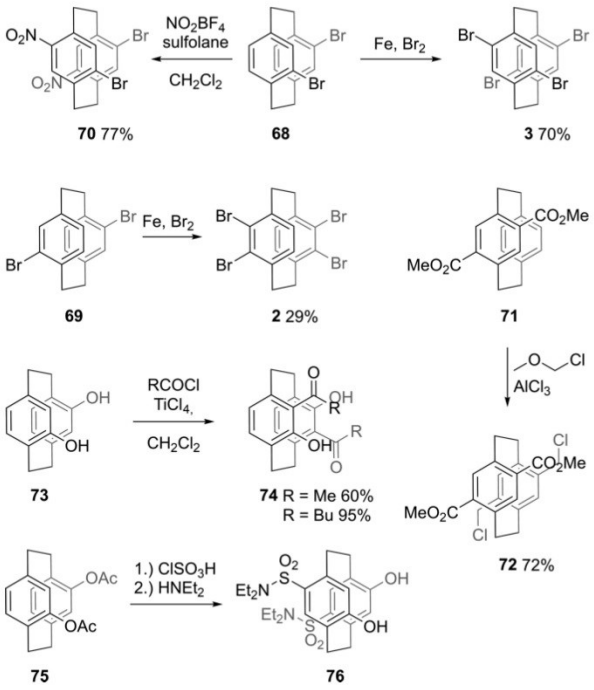


Scheme 18. Overview over the double electrophilic substitution prior to the work of *Hopf* and co-workers. The reactions to form **2** and **3** were elucidated by *Cram* and *Reich*.[5] Compounds **70**, **74**, and **76** were elucidated by *Braddock* and co-workers.[45] Compound **72** was prepared by *Gray* and *Boekelheide*.[46]

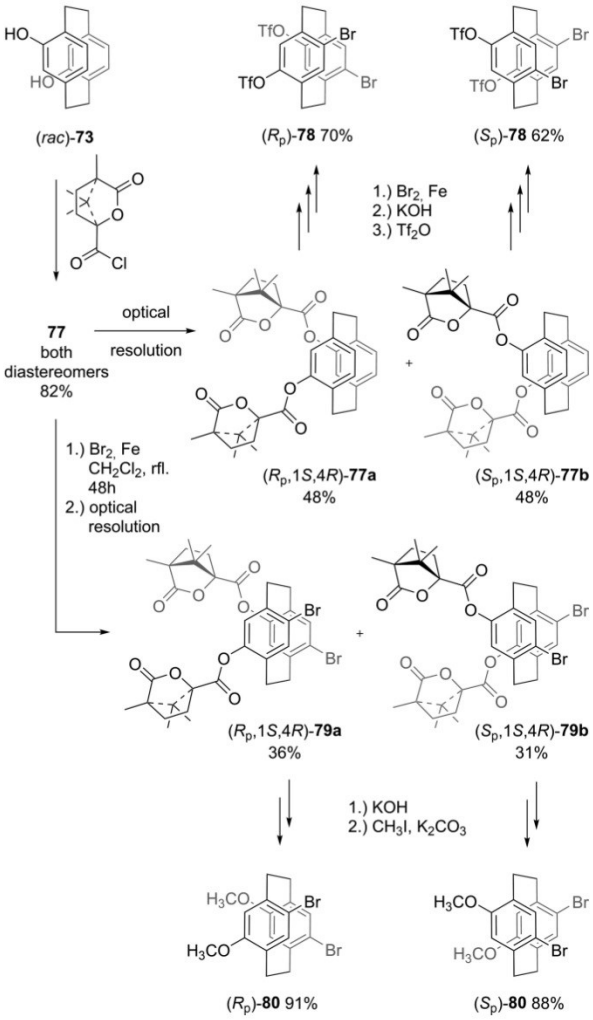


Scheme 19. Optical resolution and transformation of diastereomers **77**[47] and **79**.[42]

In their synthesis of a hydrogen-bonding chiral organocatalyst, *Braddock* and co-workers found that the dinitration of **68** proceeds *para* selectively, as did the chorosulfination of diacetate **75**. The diacylation of diol **73** proceeded in the *ortho* position regioselectively.[45] *Gray* and *Boekelheide* found the chloromethylation of diester **71** to proceed pseudo-*gem* regioselectively, when they elaborated on the synthesis of [2.2.2.2](1,2,4,5)cyclophane.[46]

An interesting access to planar chiral [2.2]paracyclophanes, based on the twofold electrophilic substitution of purified samples of the diester **77**,[47] was reported by *Chujo* and co-workers in 2016 (Scheme 19). With a very similar approach as already applied by the authors before,[33] the diol **73**[48] was treated with camphanoyl chloride to yield the pair of diastereomers ($R_p$,1*S*,4*R*)-**77a** and ($S_p$,1*S*,4*R*)-**77b** which were separated by chromatography on silica gel. Each diastereomer was obtained in 48 % yield with a diastereomeric excess larger than 99.5 %.

Having the isolated diastereomers in hand, the authors further converted them into the symmetrically tetrasubstituted enantiomers ($R_p$)-**78** and ($S_p$)-**78**. The diesters ($R_p$,1*S*,4*R*)-**77a** and ($S_p$,1*S*,4*R*)-**77b** were regioselectively dibrominated, and after saponification, both phenolic OH-groups were converted to triflates providing the enantiopure building blocks ($R_p$)-**78** and ($S_p$)-**78**.

A variation of the optical resolution procedure giving access to the enantiopure building blocks ($R_p$)-**80** and ($S_p$)-**80** has been reported recently by the same group.[42] The pairs of diastereomers **77** was first doubly brominated and subsequently separated by crystallization and silica gel chromatography, making both diastereomers ($R_p$,1*S*,4*R*)-**79a** and ($S_p$,1*S*,4*R*)-**79b** available in gram scale. Removal of the chiral auxiliary followed by methylation of the liberated phenol groups provided both enantiomers ($R_p$)-**80** and ($S_p$)-**80** in excellent yields. Subsequent substitution of the bromine via Sonogashira cross-coupling reactions gave the enantiopure samples of the V-shaped model compound **63**.

 

ChemPubSoc Europe

EurJOC European Journal of Organic Chemistry
Minireview

Careful selection of the catalytic system enabled to address exclusively the bromide substituents of ($R_p$)-**78** in a *Sonogashira–Hagihara* cross-coupling reaction with TMS acetylene, providing the enantiopure di-TMS-alkyne decorated CP ($R_p$)-**81** in good yields (Scheme 20). In a second *Sonogashira–Hagihara* reaction the conditions were optimized to substitute the triflates with triisopropylsilylacetylene. Thus ($R_p$)-**81** was converted into the CP derivative ($R_p$)-**82**, exposing two pairs of differently protected alkyne groups. Selective deprotection of the TMS protecting group of ($R_p$)-**82** gave the building block required for the assembly of the helical structure ($R_p$,$R_p$)-**83**, with a handedness emerging from the planar chiral CP subunit.

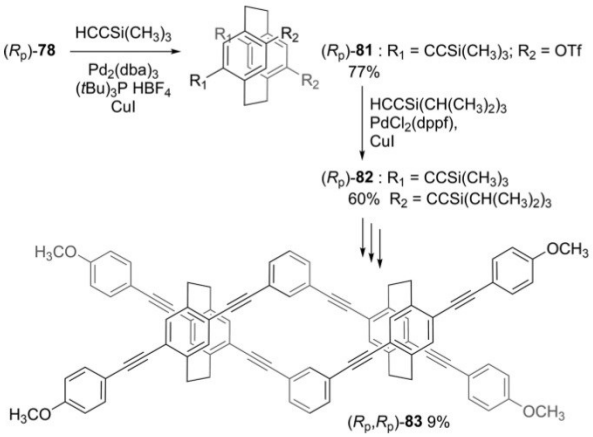


Scheme 20. Synthesis of the planar chiral building block **82**, enabling the assembly of the one-handed helix **83**.[47]

Investigation of **83** by UV/Vis spectroscopy displayed π-conjugation throughout the entire molecule and ECD of enantiopure samples showed intense chiroptical properties with comparable values ($g_{abs}$ and $g_{lum}$) as found for the chiral dendrimers **57**. The same group reported the isolation of the bis(*para*)-ps-*ortho* regioisomers of **78**, which were isolated by column chromatography.[49]

*Abe* and co-workers reported the synthesis of the PC bridged bis(imidazole dimer) **86**, with a central tetrasubstituted PC subunit (Scheme 21).[50] The structure displayed interesting photochromic properties with promising potential as multiphoton gated optical materials: Upon absorption of the first photon by **86**, the short-lived biradical species **86**(BR) is formed, which transforms back to **86** within a few ms. Upon absorption of a second photon by **86**(BR) however, the tetraradical **86**(TR) is formed which undergoes quickly a photochromic reaction to the long-liver quinoid form **86**(Q). Interestingly, the transformation could be performed by incoherent continuous-wave irradiation, pointing at the high efficiency of the processes involved in the transformation. The synthesis of **86** used the symmetrically tetrasubstituted PC **72** as starting point, which was converted into the PC-tetracarbaldehyde **84** in a few steps. Treatment with benzil and ammonium acetate in acetic acid provided the fourfold (4,5-diphenyl-1H-imidazol-2-yl)substituted PC **85**, which was oxidized with lead dioxide to **86**.

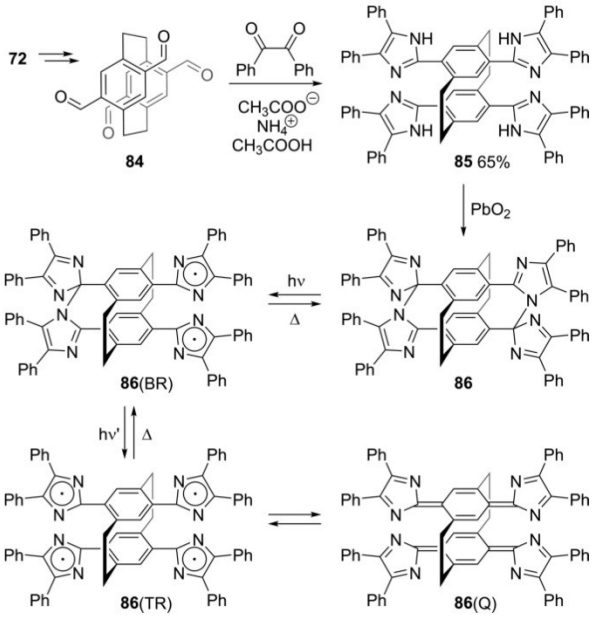


Scheme 21. Synthesis of the PC-bridged tetraimidazole model compound **86** and its two-photon-gated photochemical transformation.[50]

*Hopf* and co-workers elaborated on the regioselective double electrophilic substitution of symmetrically disubstituted PCs[7] and their findings are summarized in Scheme 22. Both diols **87**

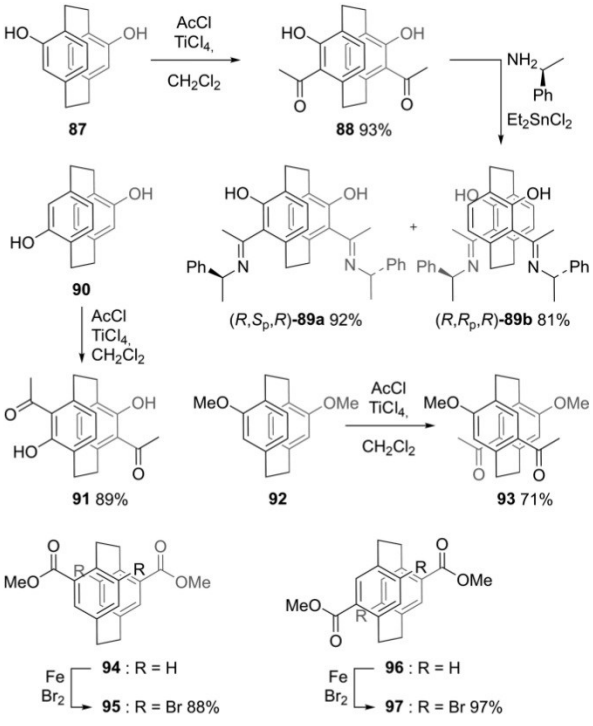


Scheme 22. Scope of the double regioselective electrophilic substitution on symmetrically disubstituted PCs by *Hopf* and co-workers.[7]

ChemPubSoc Europe
EurJOC European Journal of Organic Chemistry
Minireview

and **90** were acylated regioselectively in the *ortho* position with acetyl chloride giving the diketones **88** and **91**. The racemic diketone **88** was converted into the pair of diastereomeric bisimines ($R,S_p,R$)-**89a** and ($R,R_p,R$)-**89b**, which were separated by conventional column chromatography. The catalytic activity and selectivity of both diastereoisomers **89** in the asymmetric additions of diethylzinc to benzaldehyde was investigated. The reaction proceeded with an enantiomeric excess (*ee*) of 76 % with ($R,S_p,R$)-**89a** as catalyst, and an *ee* of 36 % using ($R,R_p,R$)-**89b**. Interestingly, the addition of benzoyl chloride to **87** gave a mixture of products. Next, Hopf and co-workers investigated the double electrophilic substitution of acetyl chloride on PC methyether **92**. The double *para*-acylated compound **93** was formed in reasonable yields as the major product of the reaction. They further elaborated on the double electrophilic substitution of the PC di-methyl esters **94** and **96**. For both compounds, exclusively pseudo-*gem* dibromination was found, providing the symmetric fourfold decorated PCs **95** and **97** in very good yields. With respect to compound **97** the authors concluded with the visionary statement: "We believe this compound to be a prominent precursor of a wide range of novel [2.2]paracyclophane derivatives obtainable by further chemical transformations of its bromine atoms and/or of its ester groups."

Very recently, we were able to make a first contribution verifying the expressed belief of *Hopf* and co-workers. The fourfold substituted PC **97** was the ideal building block to introduce a step into a macrocyclic oligothiophene. The introduction of a PC-subunit into the framework of the macrocycle results in a helical chiral architecture. While for that purpose a twofold functionalized PC like **69** would be enough,[51] only a fourfold substituted PC like **97** enables the decoration with bulky substituents slowing down the racemization process to a level enabling the isolation of the helical chiral enantiomers. As first model compound the macrocycle **98** exposing two *para*-(methoxycarbony)phenylethynyl substituents (Scheme 23) stabilizing both enantiomers to a level, enabling their isolation was assembled.[52]

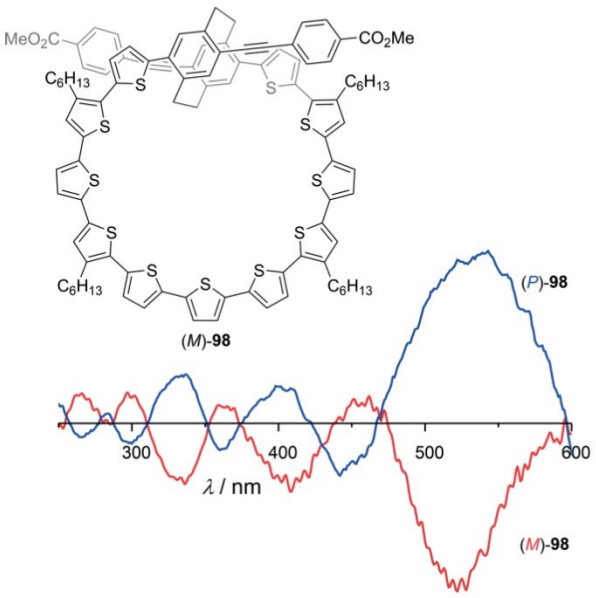


Scheme 23. *Top*: Helically chiral macrocycle **98**, assembled from the diester **97**. For clarity exclusively one enantiomer ((*M*)-**98**) is displayed. *Bottom*: ECD spectra of both enantiomers (*M*)-**98** (red) and (*P*)-**98** (blue).[52]

The synthesis of **98** was based on **97**, the two bromine substituents allowed the integration into the macrocycle by *Suzuki* cross-coupling reactions, while the two methyl ester substituents were reduced to aldehydes and subsequently converted to alkynes by a *Corey-Fuchs* reaction sequence. The two enantiomers were separated by high-performance chromatography on a chiral stationary phase and displayed weak *Cotton* effects pointing at the high flexibility of the helical chiral structure. The structure racemizes at room temperature with a half-life time of a few minutes. The racemization process requires the penetration of one *para*-(methoxycarbony)phenylethynyl substituent through the macrocycle and was confirmed by modeling using semiempirical calculations.

## 5. Conclusion

Symmetrically tetrasubstituted [2.2]paracyclophanes are compounds of great value in many fields of chemical materials research. The first substitution pattern, based on achiral bis(ps-*meta*)-*ortho* homotetrasubstitution has provided layered aromatic compounds, which are important building blocks in the investigation of transannular communication. The most prominent approach to advanced structures in this class is the double aryne forming reaction, which is then reacted with suitable electrophiles. The second class of materials, with the largest number of synthetic approaches, is based on bis(ps-*meta*)-*para*-homotetrasubstituion. These materials were incorporated into functional devices and were also used to understand transannular chromophore interactions. Bis(ps-*meta*)-*para*-homotetrasubstitution gives access to planar chiral molecules, enantioselective syntheses of such structures, and the corresponding chiroptical studies of compounds in X-, propeller- and helix-shapes were described herein. The third class of materials relies on regioselective double electrophilic aromatic heterosubstitution, and only few such examples are known. These materials however also provide access to a new synthetic route to symmetrically substituted PCs, and a first example of functional materials based on such compounds is described.

Overall, this minireview highlights the current synthetic routes and functional materials based on symmetrically tetrasubstituted PCs, an appealing family of aromatic compounds with unique properties based on the special 3D geometry of PC. Even 70 years after the discovery of the parent hydrocarbon, PC based materials are a promising class of organic compounds with excellent structural and optical features.

## Acknowledgments

Financial support by the Swiss National Science Foundation (grant no. 200020-178808), and the European Union's Horizon 2020 Research and Innovation Program "QuIET" (grant no.

 

ChemPubSoc Europe

EurJOC European Journal of Organic Chemistry
Minireview

767187) is gratefully acknowledged. M. M. acknowledges support by the 111 project (90002-18011002).

**Keywords:** [2.2]Paracyclophanes · Layered compounds · π-Stacking · Cross-conjugation · Chirality

[1] C. J. Brown, A. C. Farthing, *Nature* **1949**, *164*, 915–916.
[2] D. J. Cram, H. Steinberg, *J. Am. Chem. Soc.* **1951**, *73*, 5691–5704.
[3] H. J. Reich, D. J. Cram, *J. Am. Chem. Soc.* **1968**, *90*, 1365–1367.
[4] H. J. Reich, D. J. Cram, *J. Am. Chem. Soc.* **1969**, *91*, 3517–3526.
[5] H. J. Reich, D. J. Cram, *J. Am. Chem. Soc.* **1969**, *91*, 3527–3533.
[6] H. Hopf, *Angew. Chem. Int. Ed.* **2008**, *47*, 9808–9812; *Angew. Chem.* **2008**, *120*, 9954.
[7] N. V. Vorontsova, V. I. Rozenberg, E. V. Sergeeva, E. V. Vorontsov, Z. A. Starikova, K. A. Lyssenko, H. Hopf, *Chem. Eur. J.* **2008**, *14*, 4600–4617. references 3–7, herein.
[8] J. L. Zafra, A. Molina Ontoria, P. Mayorga Burrezo, M. Peña-Alvarez, M. Samoc, J. Szeremeta, F. J. Ramírez, M. D. Lovander, C. J. Droske, T. M. Pappenfus, et al., *J. Am. Chem. Soc.* **2017**, *139*, 3095–3105.
[9] A. Marrocchi, I. Tomasi, L. Vaccaro, *Isr. J. Chem.* **2012**, *52*, 41–52.
[10] O. R. P. David, *Tetrahedron* **2012**, *68*, 8977–8993.
[11] A. A. Aly, A. B. Brown, *Tetrahedron* **2009**, *65*, 8055–8089.
[12] R. Gleiter, H. Hopf (Eds.), *Modern Cyclophane Chemistry:* Wiley-VCH Verlag GmbH & Co. KGaA, Weinheim, Germany, **2004**.
[13] H. A. Staab, H. Haffner, *Chem. Ber.* **1977**, *110*, 3358–3365.
[14] H. A. Staab, V. Taglieber, *Chem. Ber.* **1977**, *110*, 3366–3376.
[15] B. König, B. Knieriem, A. D. Meijere, *Chem. Ber.* **1993**, *126*, 1643–1650.
[16] H. Hopf, F. T. Lenich, *Chem. Ber.* **1974**, *107*, 1891–1902.
[17] B. König, B. Knieriem, K. Rauch, A. D. Meijere, *Chem. Ber.* **1993**, *126*, 2531–2534.
[18] B. König, S. Ramm, P. Bubenitschek, P. G. Jones, H. Hopf, B. Knieriem, A. D. Meijere, *Chem. Ber.* **1994**, *127*, 2263–2266.
[19] R. Bula, M. Fingerle, A. Ruff, B. Speiser, C. Maichle-Mössmer, H. F. Bettinger, *Angew. Chem. Int. Ed.* **2013**, *52*, 11647–11650; *Angew. Chem.* **2013**, *125*, 11861.
[20] H. F. Bettinger, R. Einholz, A. Göttler, M. Junge, M.-S. Sättele, A. Schnepf, C. Schrenk, S. Schundelmeier, B. Speiser, *Org. Chem. Front.* **2017**, *4*, 853–860.
[21] Y. Asano, A. Muranaka, A. Fukasawa, T. Hatano, M. Uchiyama, N. Kobayashi, *J. Am. Chem. Soc.* **2007**, *129*, 4516–4517.
[22] M. Leung, M. B. Viswanath, P.-T. Chou, S.-C. Pu, H.-C. Lin, B.-Y. Jin, *J. Org. Chem.* **2005**, *70*, 3560–3568.
[23] R. Gleiter, K. Staub, H. Irngartinger, T. Oeser, *J. Org. Chem.* **1997**, *62*, 7644–7649.
[24] A. R. Wartini, H. A. Staab, F. A. Neugebauer, *Eur. J. Org. Chem.* **1998**, *1998*, 1161–1170.
[25] G. P. Bartholomew, G. C. Bazan, *Acc. Chem. Res.* **2001**, *34*, 30–39.
[26] G. C. Bazan, *J. Org. Chem.* **2007**, *72*, 8615–8635.
[27] G. P. Bartholomew, G. C. Bazan, *J. Am. Chem. Soc.* **2002**, *124*, 5183–5196.
[28] J. W. Hong, H. Y. Woo, B. Liu, G. C. Bazan, *J. Am. Chem. Soc.* **2005**, *127*, 7435–7443.
[29] G. P. Bartholomew, M. Rumi, S. J. K. Pond, J. W. Perry, S. Tretiak, G. C. Bazan, *J. Am. Chem. Soc.* **2004**, *126*, 11529–11542.
[30] S. Park, J. H. Heo, C. H. Cheon, H. Kim, S. H. Im, H. J. Son, *J. Mater. Chem. A* **2015**, *3*, 24215–24220.
[31] S. Park, J. H. Heo, J. H. Yun, T. S. Jung, K. Kwak, M. J. Ko, C. H. Cheon, J. Y. Kim, S. H. Im, H. J. Son, *Chem. Sci.* **2016**, *7*, 5517–5522.
[32] D. E. Fagnani, M. J. Meese, K. A. Abboud, R. K. Castellano, *Angew. Chem. Int. Ed.* **2016**, *55*, 10726–10731; *Angew. Chem.* **2016**, *128*, 10884.
[33] Y. Morisaki, M. Gon, T. Sasamori, N. Tokitoh, Y. Chujo, *J. Am. Chem. Soc.* **2014**, *136*, 3350–3353.
[34] Y. Sasai, H. Tsuchida, T. Kakuta, T. Ogoshi, Y. Morisaki, *Mater. Chem. Front.* **2018**, *2*, 791–795.
[35] H. Hinrichs, A. J. Boydston, P. G. Jones, K. Hess, R. Herges, M. M. Haley, H. Hopf, *Chem. Eur. J.* **2006**, *12*, 7103–7115.
[36] M. Gon, H. Kozuka, Y. Morisaki, Y. Chujo, *Asian J. Org. Chem.* **2016**, *5*, 353–359.
[37] M. Gon, Y. Morisaki, Y. Chujo, *J. Mater. Chem. C* **2015**, *3*, 521–529.
[38] M. Gon, Y. Morisaki, R. Sawada, Y. Chujo, *Chem. Eur. J.* **2016**, *22*, 2291–2298.
[39] M. Gon, Y. Morisaki, Y. Chujo, *Chem. Eur. J.* **2017**, *23*, 6323–6329.
[40] M. Gon, R. Sawada, Y. Morisaki, Y. Chujo, *Macromolecules* **2017**, *50*, 1790–1802.
[41] M. Gon, Y. Morisaki, Y. Chujo, *Eur. J. Org. Chem.* **2015**, *2015*, 7756–7762.
[42] K. Kikuchi, J. Nakamura, Y. Nagata, H. Tsuchida, T. Kakuta, T. Ogoshi, Y. Morisaki, *Chem. Asian J.* **2019**, *14*, https://doi.org/10.1002/asia.201801741.
[43] Y. Morisaki, Y. Chujo, *Bull. Chem. Soc. Jpn.* **2019**, *92*, 265–274.
[44] M. Gon, Y. Morisaki, Y. Chujo, *Chem. Commun.* **2017**, *53*, 8304–8307.
[45] D. C. Braddock, I. D. MacGilp, B. G. Perry, *Adv. Synth. Catal.* **2004**, *346*, 1117–1130.
[46] R. Gray, V. Boekelheide, *J. Am. Chem. Soc.* **1979**, *101*, 2128–2136.
[47] Y. Morisaki, R. Sawada, M. Gon, Y. Chujo, *Chem. Asian J.* **2016**, *11*, 2524–2527.
[48] G. Meyer-Eppler, E. Vogelsang, C. Benkhäuser, A. Schneider, G. Schnakenburg, A. Lützen, *Eur. J. Org. Chem.* **2013**, 4523–4532.
[49] R. Sawada, M. Gon, J. Nakamura, Y. Morisaki, Y. Chujo, *Chirality* **2018**, *30*, 1109–1114.
[50] K. Mutoh, Y. Nakagawa, A. Sakamoto, Y. Kobayashi, J. Abe, *J. Am. Chem. Soc.* **2015**, *137*, 5674–5677.
[51] K. J. Weiland, N. Münch, W. Gschwind, D. Häussinger, M. Mayor, *Helv. Chim. Acta* **2018**, *101*, e1800205.
[52] K. J. Weiland, T. Brandl, K. Atz, A. Prescimone, D. Häussinger, T. Šolomek, M. Mayor, *J. Am. Chem. Soc.* **2019**, *141*, 2104–2110.

Received: January 11, 2019

 

## About the Project

In this thesis, a concept is proposed which can be useful to further understand the precise properties of a metal molecule metal junction and might bring forward the understanding of through-bond versus through-space conductance. The goal of this thesis is the synthesis of the proposed molecule which must consist of structural subunits that allows for both conductance pathways at the same time while also allowing that both pathways can be observed independently.

As outlined in the preceding review, [2.2]paracyclophane is a versatile building block which has been applied for tailor-made applications in organic materials research. Three different substitution patterns were discussed: I) the bis-(ps-*meta*)-*ortho* tetrasubstitution pattern, II) the bis-(ps-*meta*)-*para* tetrasubstitution pattern, and III) symmetrically hetero tetrasubstituted derivatives. The third class is especially intriguing for bis-disubstituted approaches. This substitution pattern would allow to introduce a rod-like structure with *pseudo*-para connectivity [2.2]paracyclophane which could further be modified in such a way that a second through-bond conductance pathway is introduced by means of an oligothiophenic macrocycle. The conductance through the macrocycle should proceed in a helical structure and should be susceptible to an external magnetic field which would allow to distinguish the through-bond from the through-space conductance.

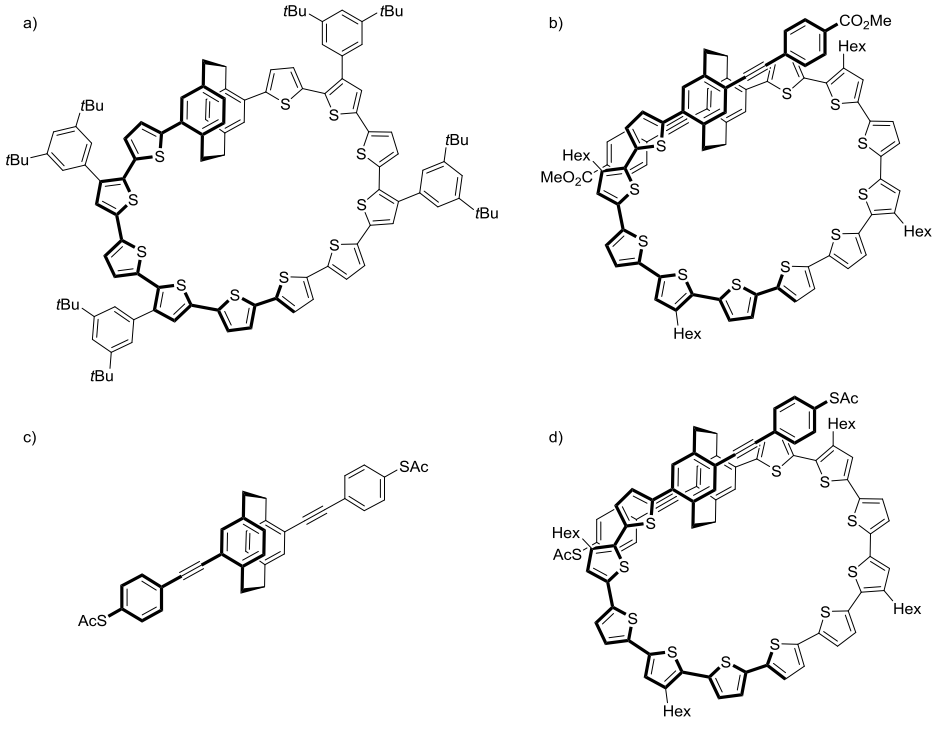


**Figure 1.** Overview of the target molecules presented in this thesis. (a) The oligothiophenic macrocycle which was used to identify a suitable ring-size for the desired target structure. b) The rotationally hindered macrocycle whose chiroptical and dynamic properties were investigated. c) The molecular wire whose conductance was investigated. d) The ultimate target structure of this thesis.

The synthesis of a helically chiral macrocycle, the stabilization of such a macrocycle by means of bulky substituents; and a molecular wire with through-space conductance properties are presented in the

ensuing manuscripts. The detailed synthesis, the structural dynamics, chiroptic properties of the described molecules lead to the realization of the ultimate target molecule of this thesis in the last chapter.

DOI: 10.1002/hlca.201800205

FULL PAPER

HELVETICA chimica acta

# A Chiral Macrocyclic Oligothiophene with Broken Conjugation – Rapid Racemization through Internal Rotation

Kevin J. Weiland,[a] Nathalia Münch,[a] Wanja Gschwind,[a] Daniel Häussinger,[a] and Marcel Mayor*[a, b, c]

[a] Department of Chemistry, University of Basel, St. Johanns-Ring 19, 4056 Basel, Switzerland, e-mail: marcel.mayor@unibas.ch

[b] Institute for Nanotechnology (INT), Karlsruhe Institute of Technology (KIT), P. O. Box 3640, 76021 Karlsruhe, Germany

[c] Lehn Institute of Functional Materials, School of Chemistry, Sun Yat-Sen University, Guangzhou 510275, P. R. China

Dedication to Prof. *François Diederich* on the occasion of his retirement celebration.

A macrocyclic oligothiophene with an integrated *pseudo-para* substituted [2.2]paracyclophane has been achieved. The synthetic sequence relies on alternating steps of halogenation- and *Suzuki*-coupling conditions. By employing a modified *Eglinton* reaction under high dilution conditions, the macrocycle is closed and the obtained diacetylene is efficiently transferred to the corresponding thiophene. The molecule is fully characterized and its dynamic racemization is analyzed by variable temperature NMR experiments. The racemization barrier hints with 38 kJ/mol at rapid enantiomerization at room temperature by *Mislow*'s '*Euclidian* rubber glove' enantiomerization process. Macrocycle formation results in red-shifted absorption and emission spectra, hinting at increased conjugation through the oligothiophene *versus* the trough space conjugation through the [2.2]paracyclophane.

**Keywords:** cyclophanes, oligothiophenes, macrocycles, helical chirality.

## Introduction

The ongoing miniaturization of electronic components approaches the nanometer scale, and novel concepts to fabricate objects in this range are a topic of high interest. One of the fabrication principles can be the bottom-up synthesis of molecules, profiting from the impressive achievements reported in the synthetic and macromolecular community. This assembly of tailor-made macromolecules from small reactive building blocks is approaching the nanoscale form the opposed direction than the scaling down of bulk materials in conventional inorganic silicon-based technology[1] and promising new research directions develop at the interface between both approaches.

Over the past decades, conjugated macrocycles have attracted high interest due to both, their structural integrity offering well-defined shapes and diameters, and their role as model compounds for infinitely conjugated $\pi$-systems.[2][3] Furthermore their physical and chemical features like their optical, electrochemical, and encapsulation properties moved into the focus of interest.[4–7] A synthetic milestone in the field of conjugated aromatic compounds was the synthesis and investigation of kekulene by the young *François Diederich* in the labs of *Heinz Staab*.[8][9]

Various molecular motifs have been reported as subunits of conjugated macrocyclic compounds, like *e.g.* pyridines, benzenes, acetylenes, as well as five-membered aromatic heterocycles, like furans and thiophenes.[10][11] We reported the assembly and investigation of a variety of macrocycles consisting of aromatic subunits in the past, among others structures

Supporting information for this article is available on the WWW under https://doi.org/10.1002/hlca.201800205

Helv. Chim. Acta **2019**, *102*, e1800205

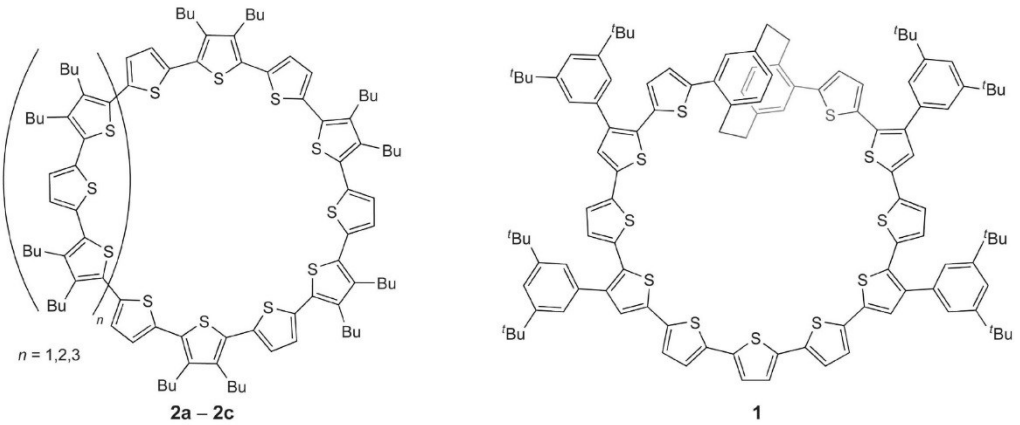


**Figure 1.** Series of oligothiophene macrocycles **2a**–**2c** (left side) developed by *Bäuerle et al.* as basis for the design of the target structure **1** (right side). The eleven thiophene subunits of the macrocycle are separated by a step due to the *pseudo-para* substituted PC subunit (top) which disturbs the conjugation. The four peripheral bis-3,5-(*tert*-butyl)phenyl substituents provide the solubility required for wet chemical processing.

comprising functional subunits like redox chromophores[12][13] or optically addressable azo-benzenes,[14] macrocycles designed as single molecule switches[15–17] or with pronounced $\pi$-stacking features,[18][19] and giant macrocycles as model compounds for persistent ring currents.[20] More recently, our focus moved to axial chiral systems like bicyclic 'Geländer'-type structures[21] or the macrocyclization of the ligands assembled in a M(II) terpyridine complex resulting in a helical macrocycle with an arrangement resembling a propeller.[22]

Cyclo[*n*]thiophenes are an interesting class of conjugated macrocycles; they are model compounds for polythiophenes, with well-defined self-assembling and electronic features.[23] Initially, the synthesis of macrocyclic oligothiophenes was performed by reacting on both sides ethynyl-terminated ter- and quinquethiophenes under oxidative acetylene coupling conditions in the presence of a copper catalyst.[3] The resulting diethynyl linkers in the macrocycles were converted to thiophenes with sodium sulfide to form the corresponding cyclo[*n*]thiophenes. In this way, a library of macrocycles was obtained, where the smallest member of the series contained twelve thiophenes. In a later approach, strained oligothiophenic macrocycles were assembled, where only one diacetylene was formed oxidatively.[24] *Bäuerle* and coworkers also reported on catenanes, where the synthesis of the target structure was achieved through complexation of platinum followed by reductive elimination to obtain the corresponding catenanes, comprising the diethynyl link in their oligothiophene macrocycles.[25]

The here presented structure is inspired by a split-ring resonator (SRR). This is the smallest possible realization of a circuit comprising a coil and a capacitor and thus displays interesting interactions with electromagnetic fields of suitable wavelength.[26] As an example, a negative refractive index at microwave frequencies was reported for a large array of equally micrometer sized metallic SRRs.[27][28]

The design of molecule **1** (*Figure 1*) combines the conjugated periphery of an oligothiophene macrocycle with the conjugation altering *pseudo-para* [2.2]-paracyclophane (PC). Using again the inspiring picture of a SRR, the macrocycle consisting of 2,5-interlinked thiophenes represent the 'ring', while the PC acts as the 'split'. A particular appealing feature from the molecular design perspective is the helical chirality introduced by the step-like PC in the macrocycle, which might result in intriguing structural and chiroptical properties.[29]

The step in the macrocycle is realized due to the 3D-structure of *pseudo-para* [2.2]paracyclophane (PC).[30] It has attracted considerable attention due to the face-to-face orientation of its benzene rings, which are considerably closer than twice their individual *van-der-Waals* radii (typical ring distance: 3.09 Å), resulting in unusual optical, electronical, and through-space charge-delocalization properties.[31–34] For example the comparison of annulene-PC hybrids with their benzannulene analogues displays typically a bathochromic shift in their absorption spectra, indicating an electronic conjugation throughout the PC building block.[35] Also, electrochemical investigations of di-

 

Helv. Chim. Acta **2019**, *102*, e1800205

thienyl-substituted PC point at electronic coupling, as the oxidation wave is separated documenting the interdependence of both redox chromophores.[34][36] Self-assembled molecular rods comprising a central PC unit displayed very comparable electronic transport features compared with their benzene analogues, such that the limited control over the number of molecules in the crossed-wire junctions did not allow to trace the origin of the observed subtle variations.[32] Very recent single molecule experiments with molecular rods comprising a central PC subunit in a mechanically controlled break junction experiment even displayed mechanically triggered quantum interference in the junctions transport behavior.[37]

Symmetrical disubstitution of PC leads to four different regioisomers.[38] *Pseudo-para* and *geminal* disubstitution leads to derivatives that are achiral due to internal symmetry elements.[39] However, *pseudo-ortho* and *meta* disubstitution leads to chiral products, separation of enantiomers of PCs with different substitution pattern have been accomplished.[40] Notably, *pseudo-ortho* disubstituted PC derivatives were incorporated in chiral thiophene-PC macrocycles, which showed pronounced chiroptical behavior.[41]

Here we report a novel approach making the *pseudo-para* disubstituted PC chiral by integrating it into the macrocyclic structure **1**. In compound **1**, the macrocycle is complemented by eleven 2,5-diyl-thiophene subunits, which are introduced pair-wise in a sequential synthetic strategy at both ends of the open oligomer in order to identify the number of thiophene subunits required for a successful macrocyclization. In addition, four bis-3,5-(*tert*-butyl)phenyl substituents provide the solubility in organic solvents required to enable wet chemical processing of both, the precursors and the target structure. The unique integration of the PC substitution pattern in the macrocyclic structure **1** leads, to the best of our knowledge, to the first chiral *pseudo-para* symmetrically disubstituted PC, as the introduction of the macrocycle leads to decreased symmetry. Interesting is the enantiomerization of **1**, which due to its 3D PC building block follows *Mislow*'s '*Euclidean* rubber glove' mechanism.[42][43] In other words, the molecule becomes its mirror image by rotations around single bonds without ever adapting a flat achiral conformation. The enantiomerization mechanism thus resembles the inversion of the chirality of a rubber glove, which is achieved by the complex movement of turning the glove inside out.

In this article, the stepwise assembly of the macrocycle **1** is reported together with its full characterization. The molecular dynamics of **1** are investigated by variable temperature NMR (VT-NMR) experiments shining light on its unique racemization behavior. The extent of electronic conjugation through macrocycle **1** and its precursors is qualitatively investigated by UV-Vis absorption and emission spectroscopy.

## Results and Discussion

The synthesis of a complex structure as macrocycle **1** requires repetitive synthetic steps; mainly alternating halogenation and Pd-catalyzed C–C coupling reactions. The linear and sequential synthetic strategy for macrocycle **1** (*Scheme 1*) involves a late stage macrocyclization and formation of a thiophene from the corresponding diacetylene, based on the linear protected intermediate **3**. Precedence for this strategy exists, as the cyclization of alkyne substituted oligothiophenes under oxidative acetylene coupling conditions[44] was employed by *Bäuerle et al.* for the synthesis of phenanthroline-containing cyclic oligothiophenes of similar ring diameters.[24] Based on this concept, chiral carbon-rich macrocycles were also obtained in the labs of *François Diederich*, who produced alleno-acetylenic macrocycles with outstanding chiroptical properties.[45][46] The open-ring intermediate **3** is divided into two building blocks **4** and **5** which can be coupled in a *Sonogashira* reaction. This linear synthetic strategy allows for a step-by-step buildup of structure **4** through a series of halogenation and *Suzuki* coupling reactions without the need of excessive protecting-group strategies. Subunit **4** was assembled from highly functionalized building blocks **6**, **7**, and **8** in a repetitive halogenation, Pd-catalyzed coupling chemistry sequence. Building blocks **7** and **8** were introduced to achieve reasonable solubility for all relevant intermediates during the course of the synthesis. While building blocks **6** and **8** are already literature-known, a strategy to form **7** had to be developed.[36][47]

The synthesis of building block **7** (*Scheme 2*), that is introduced to increase the solubility, started from commercially available 3-bromothiophene (**9**) and literature-known 2-(3,5-di-*tert*-butylphenyl)-4,4,5,5-tetramethyl-1,3,2-dioxaborolane (**10**).[48] The *Suzuki* coupling of both compounds afforded **11** in 88% yield and multigram amounts of **11** could be isolated after purification by silica gel chromatography. Next, compound **11** was reacted with one equivalent of *N*-bromosuccinimide (NBS) to selectively afford **12**. Excess of NBS lead to bromination also in the 5-

Helv. Chim. Acta **2019**, *102*, e1800205

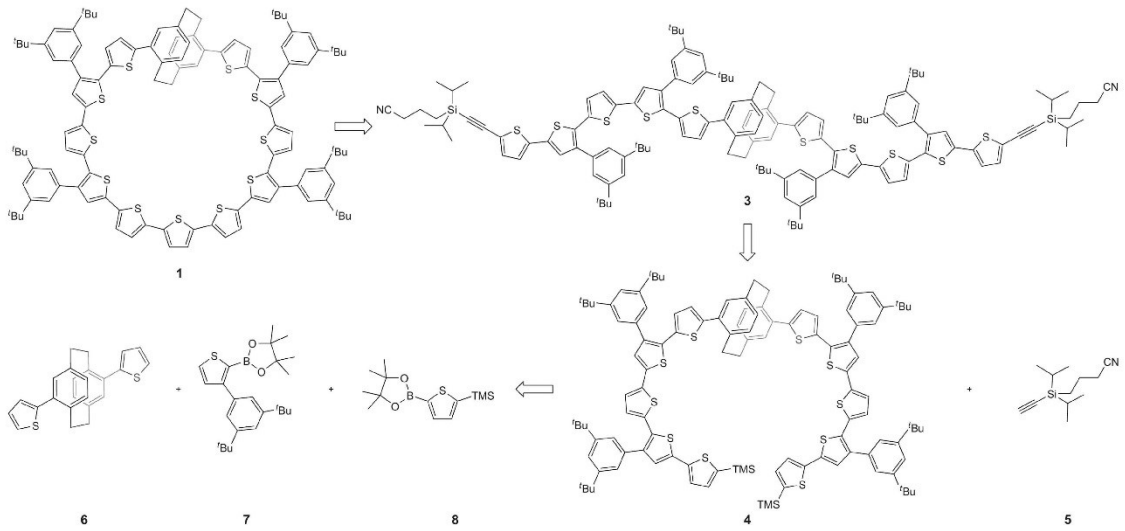

**Scheme 1.** Synthetic strategy for the assembly of racemic macrocycle **1**.

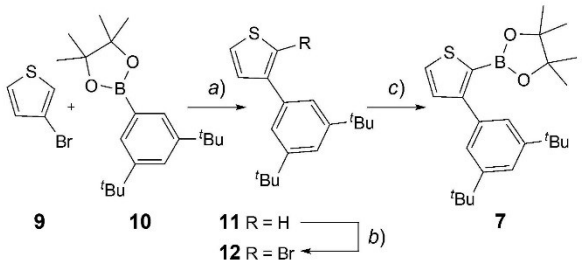

**Scheme 2.** Synthesis of building block **7**. Reagents and conditions: *a*) $Pd(PPh_3)_4$, $Na_2CO_3$, DMF, $H_2O$, 120 °C, 2 h, 88%. *b*) NBS, $CHCl_3$, AcOH, 40 °C, 1 h, 77%. *c*) n-BuLi, 2-isopropoxy-4,4,5,5-tetramethyl-1,3,2-dioxaborolane, THF, −78 °C to room temp., 20 h, 90%.

position of the thiophene. Compound **12** was, after isolation by column chromatography (CC) in 77% yield, reacted with n-butyllithium (n-BuLi) and 2-isopropoxy-4,4,5,5-tetramethyl-1,3,2-dioxaborolane to yield compound **7**. During the course of the lithiation it is crucial that the temperature is kept at −78 °C, as at higher temperatures, deprotonation of **12** at the 5-position was observed, leading to the corresponding 2-bromo-5-pinacolboronato thiophene after work up. After addition of 2-isopropoxy-4,4,5,5-tetramethyl-1,3,2-dioxaborolane and aqueous workup, **7** was isolated without purification in 90% yield as a yellow solid.

Having solubilizing building block **7** in hand, our focus moved towards the assembly of precursor **6** (*Scheme 3*). While its synthesis is already literature known, we aimed to develop a higher yielding procedure than the one published previously. *Collard et al.* reported a procedure relying on a *Stille* coupling which was efficient yet difficult to purify.[36] More recently, a procedure developed by *Martin et al.* was reported which utilized *Suzuki* coupling conditions, however working with 5-alkyl-thiophene boronic acids.[34] Therefore, a procedure utilizing *Kumada* reaction conditions as developed by *Rozenberg et al.* was adapted.[49] Commercially available 2-thienyl magnesium bromide (**13**) was added dropwise to a suspension of *pseudo-para*-dibromo-PC (**14**) and Pd(dppf)$Cl_2$ in tetrahydrofuran (THF). After heating to 60 °C for two h, building block **6** started to precipitate from the mixture. Following aqueous workup and removal of the solvent, compound **6** could be isolated by washing the crude product with cyclohexane and cooled dichloromethane. Compound **6** was isolated in a yield of 87% as a white solid.

Subsequently, compound **6** was dibrominated with NBS in dimethylformamide (DMF), and after aqueous workup and filtration through a plug of *Celite*, **15** was obtained as a white solid. Compound **15** could only be dissolved in substantial amounts of toluene after heating the suspension to 60 °C. Thus, compounds **15** and **7** were reacted in a *Suzuki* reaction with Pd-PEPPSI-IPr$^{TM}$ (PEPPSI: pyridine-enhanced precatalyst preparation stabilization and initiation, IPr: isopropyl) and $K_2CO_3$ in methanol (MeOH) and toluene in a procedure adapted from *Nilsson et al.*[50] The reaction proceeded over the course of 15 minutes and

 

Helv. Chim. Acta **2019**, *102*, e1800205

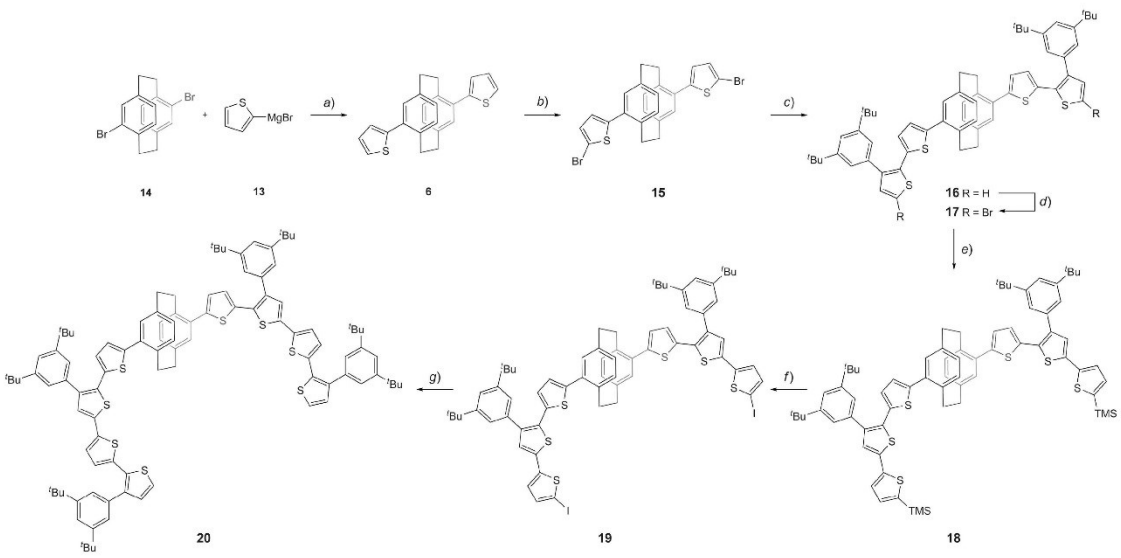


**Scheme 3.** Synthesis of fragment **20**. Reagents and conditions: *a*) $Pd(dppf)Cl_2$, THF, 60 °C, 2 h, 87 %. *b*) NBS, $CHCl_3$, DMF, room temp., 20 h, 91 %. *c*) **7**, Pd-PEPPSI-IPr$^{TM}$, $K_2CO_3$, toluene, MeOH, 70 °C, 15 min, 95 %. *d*) NBS, DMF, room temp., 20 h, 92 %. *e*) **8**, Pd-PEPPSI-IPr$^{TM}$, $K_2CO_3$, toluene, MeOH, 70 °C, 20 min, 82 %. *f*) NIS, $CHCl_3$, AcOH, room temp., 1.5 h, 99 %. *g*) **7**, Pd-PEPPSI-IPr$^{TM}$, $K_2CO_3$, toluene, MeOH, 70 °C, 30 min, 83 %.

compound **16** was obtained after CC in excellent yield as an off-white solid. To elongate the chain of thiophenes, compound **16** was brominated with NBS in DMF under exclusion of light. Aqueous work up and CC provided compound **17** as a yellow solid in 92 % yield. Initial attempts to react **17** with thienyl boronic acid led to the hexathiophenic building block of very limited solubility that prevented its separation from the byproducts of the synthesis. Therefore, **17** was reacted in a Pd-PEPPSI-IPr$^{TM}$ catalyzed *Suzuki* reaction with trimethyl[5-(4,4,5,5-tetramethyl-1,3,2-dioxaborolan-2-yl)thien-2-yl)silane (**8**) to ensure improved solubility due to the presence of TMS groups, that can be easily transferred to an iodine with *N*-iodosuccinimide (NIS).[47]

After reacting **17** and **8** in a Pd-PEPPSI-IPr$^{TM}$ catalyzed *Suzuki* reaction for 20 minutes, **18** could be isolated after aqueous workup and CC as a yellow amorphous solid. Next, compound **18** was readily interconverted to compound **19** by dissolving it in a 1 : 1 mixture of chloroform and acetic acid and treatment with NIS. During the reaction, compound **19** precipitated from the solution, but it was soluble enough to be purified by CC and was then isolated in quantitative yield as a yellow wax. Subsequently, compound **19** was reacted with building block **7** with Pd-PEPPSI-IPr$^{TM}$ and $K_2CO_3$ in toluene and MeOH. After a reaction time of 30 minutes, followed by aqueous work up, **20** was isolated in good yield of 83 % after CC as a yellow amorphous solid.

Compound **20** was dibrominated with NBS in $CHCl_3$ under the exclusion of light (*Scheme 4*). After letting the mixture react for 20 h, aqueous workup and CC lead to compound **21** in excellent yield as a yellow amorphous solid. Subsequently, compound **21** was reacted with building block **8** under the established *Suzuki* coupling conditions. Chromatography over silica gel and automated gel permeation chromatography (GPC) lead to the isolation of compound **4** in 72 % yield. Unfortunately, all attempts to convert the TMS functionality of **4** to the corresponding dibromide or -iodide lead to a complex product mixture, which, according to their MALDI-ToF MS analyses, also contained mono- and trihalogenated species besides the desired material. Attempts to isolate the desired compound from those mixtures, either by silica gel chromatography or GPC were unsuccessful. Therefore, the mixture of bromides was directly reacted with CPDIPS acetylene in a *Sonogashira* reaction. The use of the polar protecting group introduced by *Höger et al.* lead to facile isolation of the desired protected diyne **3** by silica gel chromatography in toluene in 63 % yield over two subsequent steps.[51] Deprotection of **3** to diyne **22** with tetrabutylammonium fluoride in THF proceeded in excellent yield.

 

Helv. Chim. Acta **2019**, *102*, e1800205

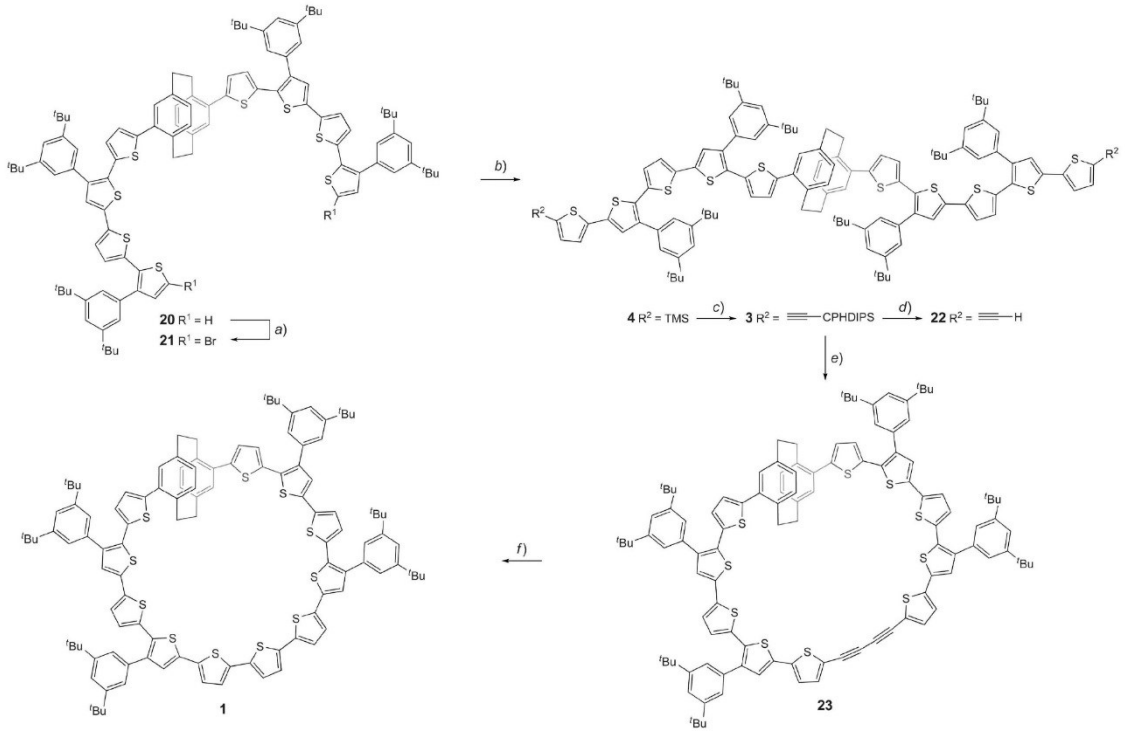


**Scheme 4.** Synthesis of target molecule **1**. Reagents and conditions: *a*) NBS, $CHCl_3$, room temp., 20 h, 90%. *b*) **8**, Pd-PEPPSI-IPr$^{TM}$, $K_2CO_3$, toluene, MeOH, 70 °C, 30 min, 72%. *c*) NBS, $CHCl_3$, AcOH, room temp., 15 min; then CPDIPS acetylene, $Pd(PPh_3)_4$, CuI, toluene, diisopropylamine, 100 °C, 20 h, 63% (two steps). *d*) TBAF, THF, room temp., 20 h, 97%. *e*) CuCl, $Cu(OAc)_2$, pyridine, room temp., 48 h, 33%. *f*) $Na_2S \cdot 9\,H_2O$, DMF, 2-methoxyethanol, 120 °C, 1.5 h, quant.

The macrocyclization of **22** to **23** was achieved through a modified *Eglinton* coupling as published by *Scott et al.*[52] To facilitate selective formation of **23**, a 0.55 mM solution of **22** in pyridine was added by a syringe pump over the course of 48 h to a solution of 15 equivalents CuCl and 21 equivalents $Cu(OAc)_2$ in 60 mL of pyridine. After aqueous workup, CC and size exclusion chromatography (*BioBeads*, *SX-3*) in toluene, the key intermediate **23** was isolated as a red amorphous solid in 33% yield. We also observed the twofold closed cyclic dimer of **22**, which was removed easily by size exclusion chromatography. It is noteworthy that the macrocyclization of a similar molecule with eight thiophenes instead of ten exclusively resulted in the formation of its twofold closed dimer. The final cyclization step to form the target compound **1** was performed using a procedure of *Bäuerle et al.*, where **23** was reacted with $Na_2S \cdot 9\,H_2O$ in a 1:1 mixture of DMF and 2-methoxyethanol.[25] To our delight, MALDI-TOF analysis of the mixture after 1.5 h of reaction showed only the mass of the target compound **1**. After acidic workup to remove excess reagent and solvent and subsequent purification by CC, target compound **1** was isolated as a red amorphous solid in quantitative yield.

The identity of macrocycle **1** was fully corroborated by $^1$H- and $^{13}$C-NMR, as well as by 2D-NMR spectroscopy, which enabled us to fully assign the observed resonances to the corresponding proton and carbon atoms. All recorded spectra of **1** are available in the *Supporting Information* (*SI*); its $^1$H-NMR spectrum recorded at 600 MHz is displayed in *Figure 2* to demonstrate both purity and identity of the isolated target structure. The elemental formula of **1** was confirmed by high-resolution matrix-assisted laser desorption/ionization time-of-flight mass spectrometry (HR-MALDI-TOF-MS, displayed in *Figure S57* in the *SI*). The signal observed for **1** showed an isotopic pattern matching the one expected for its elemental composition ($M^+$, $C_{116}H_{116}S_{11}^+$).

The macrocyclization of **22** to **23** yields the product as a racemic mixture. Both enantiomers for macrocycles **23** and **1** can readily interconvert through a concerted rotation around the C–C bonds between

 

Helv. Chim. Acta **2019**, *102*, e1800205

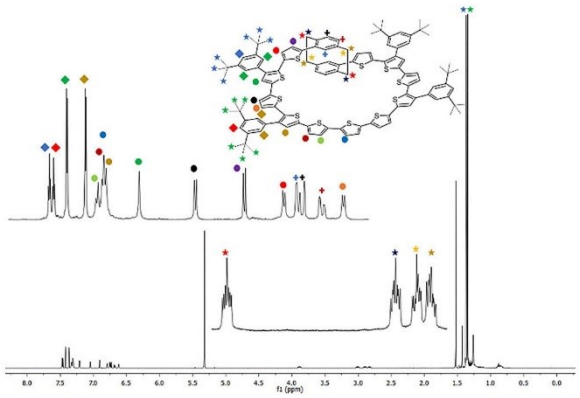

**Figure 2.** $^1$H-NMR spectrum of macrocycle **1** in $CD_2Cl_2$ at room temperature. Inlet: aromatic (top) and benzylic (bottom) protons of **1**.

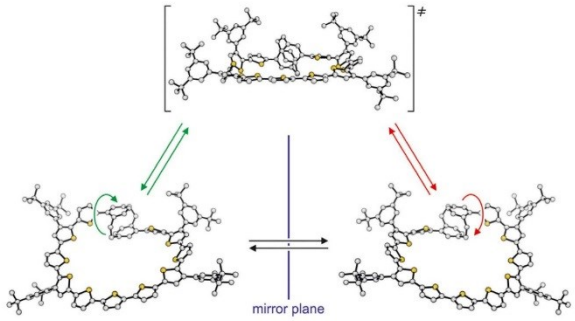


**Figure 3.** Graphical representation of both enantiomers of macrocycle **1** together with a transition state of the enantiomerization process. Rotation around the bonds between the oligothiophene-belt and the [2.2]paracyclophane interconverts one enantiomer into the other.

the benzene rings of the PC and the thiophene building blocks on each adjacent side (see *Figure 3*). We investigated the racemization dynamics for macrocycle **1**. The rotation proceeds rapidly at room temperature, separation of the enantiomers by means of HPLC on a chiral stationary phase was not possible. It is worth to note that the racemization does not proceed through an achiral transition state, unlike in the cases of helicenes, twistacenes, or banister-like molecules because the *pseudo-para* substituted PC does not allow for a symmetry element along the reaction coordinate that renders the transition state to be achiral.[53][54]

To further investigate the dynamics of the racemization, **1** was subjected to VT-NMR experiments in $CD_2Cl_2$. The most instructive picture of the dynamics is obtained when the resonances of the four $CH_2$-groups of the PC unit are analyzed at different temperatures. For the static, chiral structure of **1**, these eight protons are all magnetically inequivalent, and, hence, eight resonances are expected. At room temperature, however, only four distinct complex *multiplet*s are observed in the range between 2.5 and 4.0 ppm. This clearly demonstrates racemization kinetics that is fast on the $^1$H-NMR time scale. Depending on the concentration of the sample, the resonances appear as sharp resolved signals (*c.f. Figure 2*) or, at higher concentration, stacking of the extended aromatic ring systems leads to broadening which is not related to a dynamic process originating in the racemization. When the temperature was lowered to 218 K, severe line broadening occurred, and after coalescence at approximately 213 K, a splitting into eight, partially overlapping signals was observed indicating slow interconversion of the enantiomers by the rubber glove mechanism (see *Figure 4*). The activation barrier

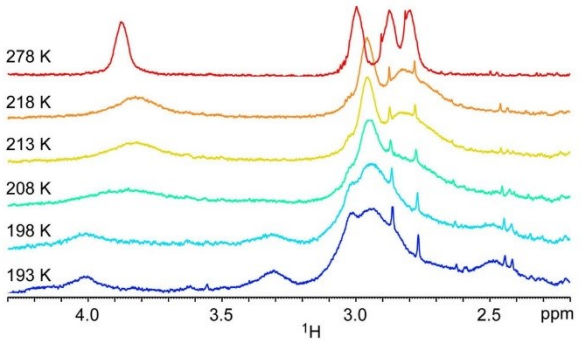


**Figure 4.** VT-NMR spectra of the resonances, corresponding to the benzylic protons of **1**.

for the racemization was determined from the shift difference of 417 Hz for H–C(41)/H–C(41a) and the coalescence temperature (213 K) to be 38 kJ mol$^{-1}$. The barrier for racemization is considerably lower than the barrier for similar ferrocene-based macrocycles with smaller ring sizes.[55] Further cooling of the sample to 183 K revealed a second dynamic process that is most likely related to rotational restrictions in the di-*tert*-butylphenyl units.

To investigate the change in through-space *versus* through-bond conjugation by the introduced macrocycle, the optoelectronical properties of macrocycles **23** and **1** were investigated by UV/Vis absorption and emission spectroscopy and compared to linear building block **22** (*Figure 5*). The terminal alkyne substituted oligothiophene with a central PC subunit **22** has its

 

Helv. Chim. Acta **2019**, *102*, e1800205

absorption maximum at 438 nm. After macrocyclization, the absorption maxima of **23** and **1** are hypsochromically shifted with respect to **22**. The absorption maximum of **23** is found at 413 nm and the absorption maximum of **1** is at 420 nm. Both absorption spectra of the macrocyclic compounds display additional shoulders, one is found around 450 nm, which is more pronounced in the case of **23**, the other appears at wavelengths higher than 500 nm. The comparison of the absorption spectrum of **22** with reported electronic data from linear oligothiophenes points at through-space conjugation in the central PC subunit. Penta- and heptathiophenic oligomers have absorption maxima at 386 and 409 nm, respectively.[56] The absorption maximum of **22**, consisting of two pentathiophenes interlinked by PC, is at 438 nm. The bathochromic shift compared to the reported oligothiophenes confirms the through-space conjugation in the central PC subunit, as already reported for similar compounds.[34–36] Macrocyclic thiophenes of a given size have absorption maxima that correspond in energy to the absorption maxima of linear oligothiophenes of approximately half the number of thiophene subunits.[56] The hypsochromic shift of the absorption maxima of the macrocycles **23** and **1** compared to linear **22** was thus not surprising. Also, the rather small values of 25 nm and 18 nm of the recorded shifts for **23** and **1** respectively can be rationalized by the through-space conjugation in the central PC unit of the linear precursor **22**. Compared with an oligomer of comparable length consisting exclusively of 2,5-interlinked thiophenes, the through-space conjugation is less effective than the delocalization in a thiophene, resulting in a larger separation of the frontier orbitals. The bathochromic shift of 7 nm of the absorption maximum of **1** compared to the signal of macrocycle **23** points at the increased delocalization through the $sp^2$ carbon atoms of the 2,5-diyl-thiophene linker in **1** (through-bond conjugation) compared with the sp centers of the diacetylene connection in **23**.

The emission spectra of all three samples **22**, **23**, and **1** have an intense maximum with a more or less pronounced shoulder at about 648–649 nm in common. While the maximum of the emission of **22** is at 537 with a *Stokes*' shift of 99 nm, the one of **23** is at 573 nm with a *Stokes*' shift of 160 nm and the emission maximum of **1** is at 588 nm with a *Stokes*' shift of 168 nm. Again, a bathochromic shift with increasing conjugation in the macromolecules' subunits is observed in the order of the emission signals.

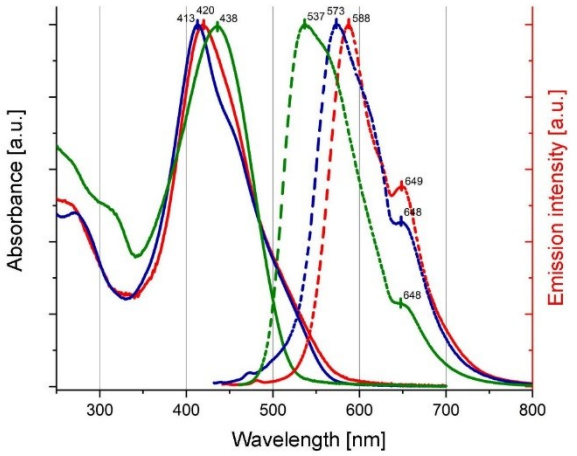


**Figure 5.** Absorption spectra of **22** (green line), **23** (blue line), and **1** (red line) and emission spectra (dotted lines of corresponding color). All spectra were recorded in dichloromethane at room temperature. The emission spectra were exited at 438 nm (**22**), 413 nm (**23**), and 420 nm (**1**).

Initial attempts to measure the HOMO-LUMO gap electrochemically failed due to irreversible behavior of **1** in the cyclic voltammetry experiment. As approximations of the HOMO-LUMO gaps, the electronic transitions between the vibrational ground states of the absorption and emission spectra were compared. For the linear precursor **22**, the absorption and emission bands intersect at 500 nm, corresponding to a transition energy of 2.48 eV. The intersection is bathochromically shifted to 528 nm (2.35 eV) for the cyclized **23** and shifts further to 542 nm (2.29 eV) upon replacing the diacetylene linkage with a thiophene subunit in **1**. The decrease of transition energies further corroborates the trend of increasing conjugation in the subunits of the investigated series.

## Conclusions

We present an efficient synthesis of chiral macrocycle **1** and its full characterization by $^{1}$H-, $^{13}$C- and 2D-NMR spectroscopy as well as high resolution mass spectrometry. Suitable precursors to incorporate PC as a key building block to break the conjugation of the macrocycle were designed and synthesized. The assembly of the achiral linear precursors is based on Pd-catalyzed coupling chemistry combined with halogenation sequences of the corresponding thiophenes. A linear synthetic strategy allowed to determine the required length of the precursor for a successful

 

Helv. Chim. Acta **2019**, *102*, e1800205

macrocyclization. The ring closing as key step of the synthesis provided the target molecule in reasonable yields, considering both its size and structural flexibility. The macrocyclization yielded a racemic mixture that could not be resolved due to the low racemization barrier at room temperature. The racemization barrier was investigated with VT-NMR experiments and was found to be 38 kJ mol$^{-1}$, indicating unhindered rotation of the central PC unit *versus* the oligothiophenic chain at room temperature. Investigation of the optical properties of the obtained macrocycles and comparison with the open-ring precursor allowed to determine the change of electronic features upon macrocyclization. All spectra of the macrocycles were considerably red-shifted compared to the open-ring precursor. We obtained rare insights into the through-space *versus* through-bond conjugation through the comparison of the considerable lowered transition energies between vibrational ground states.

In summary, two unique conjugated macrocycles have been prepared and investigated, elucidating the influence of a prochiral building block with broken conjugation on structural and electronical properties.

We are currently advancing the concept of helical chiral oligothiophene macrocycles comprising a PC subunit by designing model compounds of increased stability due to sterically hindered enantiomerization processes.

## Experimental Section

### *General*

Instruments, materials and methods are described in detail in the *Supporting Information.*

### *Previously Described Compounds*

4,16-Dibromo[2.2]paracyclophane, trimethyl[5-(4,4,5,5-tetramethyl-1,3,2-dioxaborolan-2-yl)thiophen-2-yl]-silane, 2-(3,5-di-*tert*-butylphenyl)-4,4,5,5-tetramethyl-1,3,2-dioxaborolane, and CPDIPS-acetylene were prepared according to reported procedures.[47][48][51][57]

### *Experimental*

**3-(3,5-Di-*tert*-butylphenyl)thiophene** (**11**): 2-(3,5-Di-*tert*-butylphenyl)-4,4,5,5-tetramethyl-1,3,2-dioxaborolane[48] (**10**; 12.9 g, 40.7 mmol, 1.05 equiv.), 3-bromothiophene (**9**; 3.64 mL, 38.8 mmol, 1.00 equiv.), $Na_2CO_3$ (20.5 g, 194 mmol, 5.00 equiv.), and $Pd(PPh_3)_4$ (1.12 g, 970 μmol, 2.5 mol-%) were suspended in a mixture of DMF (54 mL) and $H_2O$ (6 mL). The mixture was degassed by bubbling a stream of argon through the solution and was heated to 120 °C for 2 h. The mixture was allowed to reach room temperature, toluene was added, and the organic phase was washed with 2M HCl and dried over $MgSO_4$. The solvent was removed under reduced pressure and the crude was purified by column chromatography (pentane), yielding **11** as a colorless oil (9.35 g, 34.3 mmol, 88%). $^1$H-NMR (250 MHz, $CD_2Cl_2$): 7.47–7.38 (*m*, 6 H); 1.37 (*s*, 18 H). $^{13}$C-NMR (101 MHz, $CD_2Cl_2$): 151.88; 135.76; 127.89; 127.29; 126.52; 122.00; 121.49; 120.56; 35.39; 31.79. EI-MS (70 eV): 272.20 (48.90), 257.20 (100), 57.10 (73.16). HR-EI-MS: 272.1598 ($C_{18}H_{24}S^+$, $M^+$; calc. 272.1599).

**2-Bromo-3-(3,5-di-*tert*-butylphenyl)thiophene** (**12**): 3-(3,5-Di-*tert*-butylphenyl)thiophene (**11**; 9.33 g, 34.3 mmol, 1.00 equiv.) was dissolved in $CHCl_3$ (100 mL) and AcOH (100 mL). To this was added, under exclusion of light, NBS (6.11 g, 34.3 mmol, 1.00 equiv.), and the mixture was heated to 40 °C for 1 h. The mixture was allowed to reach room temperature, $CH_2Cl_2$ was added, and the mixture was neutralized with sat. aq. $NaHCO_3$. It was dried over $MgSO_4$, and the solvent was removed *in vacuo*. The crude was purified by column chromatography (cyclohexane), yielding **12** as a colorless oil (9.27 g, 26.4 mmol, 77%). $^1$H-NMR (400 MHz, $CD_2Cl_2$): 7.45 (*t*, $^4J$ = 1.8, 1 H); 7.41 (*d*, $^4J$ = 1.8, 2 H); 7.35 (*d*, $^3J$ = 5.6, 1 H); 7.08 (*d*, $^3J$ = 5.6, 1 H); 1.37 (*s*, 18 H). $^{13}$C-NMR (101 MHz, $CD_2Cl_2$): 151.48; 142.81; 134.60; 129.88; 126.45; 123.63; 122.27; 108.62; 35.45; 31.77. EI-MS (70 eV): 352.20 (28.89), 350.15 (28.84), 337.15 (75.23), 335.15 (72.64), 57.10 (100). Anal. calc. for $C_{18}H_{23}BrS$ (351.34): C 61.53, H 6.60; found: C 61.65, H 6.87.

**2-[3-(3,5-Di-*tert*-butylphenyl)thiophen-2-yl]-4,4,5,5-tetramethyl-1,3,2-dioxaborolane** (**7**): 2-Bromo-3-(3,5-di-*tert*-butylphenyl)thiophene (**12**; 3.45 g, 9.83 mmol, 1.0 equiv.) was dissolved in THF (60 mL) and was degassed with argon. The mixture was cooled to −78 °C and n-BuLi (1.6 M in hexane, 6.14 mL, 9.83 mmol, 1.0 equiv.) was added dropwise. The mixture was stirred for 2 h, and 4,4,5,5-tetramethyl-2-(propan-2-yloxy)-1,3,2-dioxaborolane (2.21 mL, 10.8 mmol, 1.10 equiv.) was added dropwise. The mixture was allowed to reach room temperature, and 2M HCl was added. The crude was taken up in toluene and filtered through a plug of *Celite*. The solvent was removed, and compound **7** was obtained as brown oil, which solidified upon standing (3.51 g, 8.86 mmol, 90%). M.p.: 69–71 °C. $^1$H-NMR (400 MHz, $CDCl_3$): 7.60

Helv. Chim. Acta **2019**, *102*, e1800205

(*d*, $^3J$=4.8, 1 H); 7.47 (*d*, $^4J$=1.8, 2 H); 7.40 (*t*, $^4J$=1.8, 1 H); 7.31 (*d*, $^3J$=4.8, 1 H); 1.39 (*s*, 18 H); 1.31 (*s*, 12 H). $^{13}$C-NMR (101 MHz, $CDCl_3$): 153.02; 149.96; 136.33; 131.64; 131.36; 123.82; 121.37; 83.99; 35.05; 31.69; 24.94; the carbon, to which the boron is bound is not observed. HR-EI-MS: 398.2452 ($C_{24}H_{35}BO_2S^+$, $M^+$; calc. 398.2451).

**4,16-Dithienyl[2.2]paracyclophane (=2,2′-Tricyclo[8.2.2.2$^{4,7}$]hexadeca-1(12),4,6,10,13,15-hexaene-5,11-diyldithiophene**; **6**): 4,16-Dibromo[2.2]paracyclophane (=5,11-dibromotricyclo[8.2.2.2$^{4,7}$]hexadeca-1(12),4,6,10,13,15-hexaene, **14**; 4.58 g, 12.5 mmol, 1.0 equiv.) and Pd(dppf)$Cl_2$ (229 mg, 313 μmol, 2.5 mol-%) were suspended in THF (100 mL) and degassed with argon. To this was added thienyl magnesium bromide (**13**; 1.0M in THF, 50.0 mL, 50.0 mmol, 4.0 equiv.), and the mixture was heated to 60 °C for 2 h. The mixture was allowed to reach room temperature and sat. aq. $NH_4Cl$ was added. The organic phase was diluted with $CH_2Cl_2$ and was washed with 2M HCl. The solvent was removed under reduced pressure, and the crude was washed with cyclohexane and cold $CH_2Cl_2$ and dried. Compound **6** was obtained as white solid (4.06 g, 10.9 mmol, 87%). The analytical data agreed with the values reported in literature.[36] $^1$H-NMR (400 MHz, $CDCl_3$): 7.39 (*dd*, $^3J$=4.9, $^4J$=1.4, 2 H); 7.16–7.11 (*m*, 4 H); 6.74 (*dd*, $^3J$=7.8, $^4J$=2.0, 2 H); 6.66 (*d*, $^4J$=2.0, 2 H); 6.59 (*d*, $^3J$=7.8, 2 H); 3.77–3.69 (*m*, 2 H); 3.01–2.85 (*m*, 4 H). $^{13}$C-NMR (101 MHz, $CD_2Cl_2$): 144.35; 140.26; 137.35; 135.08; 135.05; 133.66; 129.77; 127.74; 126.13; 125.38; 34.54; 34.17. EI-MS (70 eV): 373.20 (13.43), 372.25 (48.76), 187.10 (100), 185.10 (68.51), 171.10 (48.12), 141.15 (24.68), 115.15 (14.17).

**4,16-Di-(5-bromothienyl)[2.2]paracyclophane (=2,2′-Tricyclo[8.2.2.2$^{4,7}$]hexadeca-1(12),4,6,10,13,15-hexaene-5,11-diylbis(5-bromothiophene)**; **15**): 4,16-Dithienyl[2.2]paracyclophane (**6**; 4.06 g, 10.9 mmol, 1.00 equiv.) was suspended in $CHCl_3$ (75 mL) and DMF (75 mL), and under exclusion of light, NBS (3.98 g, 22.3 mmol, 2.05 equiv.) was added. The reaction was allowed to proceed for 20 h, and then, 2M HCl was added. The organic layer was washed with 2M HCl and dried over $MgSO_4$. The solvent was removed under reduced pressure; the crude was taken up in toluene and filtered through a plug of *Celite*. Compound **15** was obtained as white solid after solvent removal (5.23 g, 9.86 mmol, 91%). M.p.: 240–242 °C. $^1$H-NMR (400 MHz, $CDCl_3$): 7.09 (*d*, $^3J$=3.8, 2 H); 6.86 (*d*, $^3J$=3.8, 2 H); 6.74 (*dd*, $^3J$=7.8, $^4J$=2.0, 2 H); 6.57–6.53 (*m*, 4 H); 3.72–3.64 (*m*, 2 H); 3.00–2.86 (*m*, 6 H). $^{13}$C-NMR (101 MHz, $CDCl_3$): 145.83; 140.36; 137.30; 135.13; 134.40; 133.39; 130.64; 130.06; 126.39; 111.80; 34.47; 34.03. HR-EI-MS: 527.9216 ($C_{24}H_{18}Br_2S_2^+$, $M^+$; calc. 527.9217).

**4,16-Di-(3′-(3,5-di-*tert*-butylphenyl))-[2,2′-bithien]-5-yl-[2.2]paracyclophane (=5,5′-Tricyclo[8.2.2.2$^{4,7}$]hexadeca-1(12),4,6,10,13,15-hexaene-5,11-diylbis[3′-(3,5-di-*tert*-butylphenyl)-2,2′-bithiophene]**; **16**): 4,16-Di-(5-bromothienyl)[2.2]paracyclophane (**15**; 340 mg, 640 μmol, 1.00 equiv.), boronic ester **7** (770 mg, 1.93 mmol, 3.00 equiv.), and $K_2CO_3$ (532 mg, 3.85 mmol, 6.00 equiv.) were suspended in toluene (10 mL) and MeOH (10 mL). The mixture was degassed with argon, and Pd-PEPPSI-IPr$^{TM}$ (22.2 mg, 32.1 μmol, 5 mol-%) was added. The mixture was placed in a preheated oil bath and stirred at 70 °C for 15 min. The mixture was allowed to reach room temperature, and the organic layer was washed with 2 M HCl and dried over $MgSO_4$. The solvent was removed under reduced pressure. The crude was purified by column chromatography (cyclohexane/$CH_2Cl_2$ 4:1) and compound **16** was obtained as off-white solid (557 mg, 610 μmol, 95%). M.p.: >250 °C. $^1$H-NMR (400 MHz, $CD_2Cl_2$): 7.44 (*t*, $^4J$=1.9, 2 H); 7.34 (*d*, $^3J$=5.2, 2 H); 7.32 (*d*, $^4J$=1.8, 4 H); 7.16 (*d*, $^3J$=5.2, 2 H); 7.00 (*d*, $^3J$=3.7, 2 H); 6.93 (*d*, $^3J$=3.7, 2 H); 6.61 (*dd*, $^3J$=7.8, $^4J$=1.9, 2 H); 6.51 (*d*, $^4J$=1.9, 2 H); 6.43 (*d*, $^3J$=7.8, 2 H); 3.69–3.60 (*m*, 2 H); 2.92–2.78 (*m*, 6 H); 1.33 (*s*, 36 H). $^{13}$C-NMR (101 MHz, $CD_2Cl_2$): 151.47; 144.82; 140.77; 140.69; 137.69; 136.65; 135.89; 135.48; 135.22; 133.65; 132.11; 131.21; 130.17; 127.64; 126.66; 124.40; 124.29; 121.92; 35.40; 34.77; 34.48; 31.80. HR-MALDI-TOF-MS (DCTB): 912.3882 ($C_{60}H_{64}S_4^+$, $M^+$; calc. 912.3891).

**4,16-Di-(5′-bromo-3′-(3,5-di-*tert*-butylphenyl))-[2,2′-bithien]-5-yl-[2.2]paracyclophane (=5,5′-Tricyclo[8.2.2.2$^{4,7}$]hexadeca-1(12),4,6,10,13,15-hexaene-5,11-diylbis[5′-bromo-3′-(3,5-di-*tert*-butylphenyl)-2,2′-bithiophene]**; **17**): Tetrathiophene **16** (400 mg, 440 μmol, 1.00 equiv.) was dissolved in DMF (25 mL), and to this was added in the dark NBS (160 mg, 900 μmol, 2.05 equiv.). The mixture was stirred at room temperature for 20 h, and toluene was added to the mixture. The organic layer was washed with 2M HCl and dried over $MgSO_4$. The solvent was removed under reduced pressure, and the crude product was purified by column chromatography ($CH_2Cl_2$/cyclohexane 1:9). Compound **17** was isolated as yellow solid (432 mg, 400 μmol, 92%). M.p.: 250–252 °C. $^1$H-NMR (400 MHz, $CD_2Cl_2$): 7.44 (*t*, $^4J$=1.9, 2 H);

 

Helv. Chim. Acta **2019**, *102*, e1800205

7.27 (*d*, $^4J$ = 1.9, 4 H); 7.14 (*s*, 2 H); 6.98 (*d*, $^3J$ = 3.8, 2 H); 6.92 (*d*, $^3J$ = 3.8, 2 H); 6.58 (*dd*, $^3J$ = 7.8, $^4J$ = 1.9, 2 H); 6.48 (*d*, $^4J$ = 1.9, 2 H); 6.40 (*d*, $^3J$ = 7.8, 2 H); 3.65–3.57 (*m*, 2 H); 2.91–2.78 (*m*, 6 H); 1.32 (*s*, 36 H). $^{13}$C-NMR (101 MHz, $CD_2Cl_2$): 151.64; 145.36; 141.13; 140.70; 137.72; 135.48; 135.05; 134.82; 133.86; 133.65; 133.56; 131.92; 130.26; 127.99; 126.67; 124.17; 122.36; 110.97; 35.41; 34.75; 34.43; 31.77. HR-MALDI-TOF-MS (DCTB): 1068.2095 ($C_{60}H_{62}Br_2S_4^+$, $M^+$; calc. 1068.2101).

**4,16-Di-(3′-(3,5-di-*tert*-butylphenyl))-5″-trimethylsilyl-[2,2′:5′,2″-terthien]-5-yl-[2.2]paracyclophane (={Tricyclo[8.2.2.2$^{4,7}$]hexadeca-1(12),4,6,10,13,15-hexaene-5,11-diylbis[4′-(3,5-di-*tert*-butylphenyl)-2,2′:5′,2″-terthiene-5″,5-diyl]}bis(trimethylsilane); 18**): Dibromide **17** (800 mg, 750 µmol, 1.00 equiv.), boronic ester **8** (845 mg, 2.99 mmol, 4.00 equiv.), and $K_2CO_3$ (619 mg, 4.48 mmol, 6.00 equiv.) were suspended in toluene (25 mL) and MeOH (25 mL). The mixture was degassed with argon, and Pd-PEPPSI-IPr$^{TM}$ (25.9 mg, 37.4 µmol, 5 mol-%) was added. The mixture was placed in a preheated oil bath and the mixture was stirred at 70 °C for 20 min. The mixture was allowed to reach room temperature, and the organic layer was washed with 2M HCl and dried over $MgSO_4$, and the solvent was removed under reduced pressure. The crude was purified by column chromatography (cyclohexane/$CH_2Cl_2$ 9:1), and **18** was obtained as yellow wax (744 mg, 610 µmol, 82%). $^1$H-NMR (400 MHz, $CD_2Cl_2$): 7.27 (*t*, $^4J$ = 1.9, 2 H); 7.14 (*d*, $^4J$ = 1.9, 4 H); 7.12 (*d*, $^3J$ = 3.5, 2 H); 7.03 (*s*, 2 H); 7.00 (*d*, $^3J$ = 3.5, 2 H); 6.82 (*d*, $^3J$ = 3.8, 2 H); 6.72 (*d*, $^3J$ = 3.8, 2 H); 6.39 (*dd*, $^3J$ = 7.8, $^4J$ = 1.9, 2 H); 6.29 (*d*, $^4J$ = 1.9, 2 H); 6.21 (*d*, $^3J$ = 7.8, 2 H); 3.48–3.38 (*m*, 12 H); 2.71–2.60 (*m*, 6 H); 1.14 (*s*, 36 H); 0.15 (*s*, 18 H). $^{13}$C-NMR (101 MHz, $CD_2Cl_2$): 151.63; 144.83; 142.34; 141.37; 141.00; 140.68; 137.70; 136.37; 135.70; 135.53; 135.49; 135.17; 133.65; 131.13; 130.20; 127.79; 127.77; 127.42; 126.70; 125.69; 124.27; 122.23; 35.44; 34.75; 34.51; 31.82; 0.12. HR-MALDI-TOF-MS (DCTB): 1220.4422 ($C_{74}H_{84}S_6Si_2^+$, $M^+$; calc. 1220.4436).

**4,16-Di-(3′-(3,5-di-*tert*-butylphenyl))-5″-iodo-[2,2′:5′,2″-terthien]-5-yl-[2.2]paracyclophane (=5,5′-Tricyclo[8.2.2.2$^{4,7}$]hexadeca-1(12),4,6,10,13,15-hexaene-5,11-diylbis[3′-(3,5-di-*tert*-butylphenyl)-5″-iodo-2,2′:5′,2″-terthiophene]; 19**): TMS-thienyl derivative **18** (752 mg, 620 µmol, 1.00 equiv.) was dissolved in $CHCl_3$ (50 mL) and AcOH (50 mL). After degassing the mixture with argon, NIS (314 mg, 1.35 mmol, 2.20 equiv.) was added in one portion. It was stirred at room temperature for 1.5 h, and to the crude was added sat. aq. $NaHCO_3$. The organic layer was washed with sat. aq. $NaHCO_3$ and brine and was dried over $MgSO_4$. The solvent was removed under reduced pressure, and the crude was purified by column chromatography (cyclohexane/$CH_2Cl_2$ 4:1). Compound **19** was obtained as yellow wax (812 mg, 610 µmol, 99%). $^1$H-NMR (500 MHz, $CD_2Cl_2$): 7.48 (*t*, $^4J$ = 1.8, 2 H); 7.33 (*d*, $^4J$ = 1.8, 4 H); 7.23 (*d*, $^3J$ = 3.7, 2 H); 7.18 (*s*, 2 H); 7.03 (*d*, $^3J$ = 3.7, 2 H); 6.95 (*d*, $^3J$ = 3.8, 2 H); 6.92 (*d*, $^3J$ = 3.8, 2 H); 6.59 (*dd*, $^3J$ = 7.8, $^4J$ = 1.9, 2 H); 6.49 (*d*, $^4J$ = 1.9, 2 H); 6.41 (*d*, $^3J$ = 7.8, 2 H); 3.66–3.61 (*m*, 2 H); 2.90–2.77 (*m*, 6 H); 1.35 (*s*, 36 H). $^{13}$C-NMR (126 MHz, $CD_2Cl_2$): 151.10; 144.46; 142.86; 140.74; 140.09; 138.00; 137.12; 135.47; 134.91; 134.90; 134.53; 133.57; 133.07; 131.12; 129.64; 127.62; 127.01; 126.13; 125.21; 123.67; 121.76; 72.07; 34.86; 34.16; 33.92; 31.24. HR-MALDI-TOF-MS (DCTB): 1328.1570 ($C_{68}H_{62}I_2S_6^+$, $M^+$; calc. 1328.1578).

**4,16-Di-(3′,3‴-bis(3,5-di-*tert*-butylphenyl))-[2,2′:5′,2″:5″,2‴quarterthien]-5-yl-[2.2]paracyclophane (=5,5′-Tricyclo[8.2.2.2$^{4,7}$]hexadeca-1(12),4,6,10,13,15-hexaene-5,11-diylbis[3′,3‴-bis(3,5-di-*tert*-butylphenyl)-2,2′:5′,2″:5″,2‴-quaterthiophene]; 20**): Diiodo compound **19** (800 mg, 620 µmol, 1.00 equiv.), boronic ester **7** (982 mg, 2.46 mmol, 4.00 equiv.), and $K_2CO_3$ (511 mg, 3.70 mmol, 6.00 equiv.) were suspended in toluene (30 mL) and MeOH (30 mL). The mixture was degassed with argon, and Pd-PEPPSI-IPr$^{TM}$ (42.6 mg, 61.6 µmol, 5 mol-%) was added. The mixture was placed in a preheated oil bath, and the mixture was stirred at 70 °C for 30 min. The mixture was allowed to reach room temperature, and the organic layer was washed with 2M HCl and dried over $MgSO_4$, and the solvent was removed under reduced pressure. The crude was purified by column chromatography (cyclohexane/$CH_2Cl_2$ 4:1) and **20** was obtained as yellow wax (827 mg, 511 µmol, 83%). $^1$H-NMR (500 MHz, $CD_2Cl_2$): 7.52 (*t*, $^4J$ = 1.8, 2 H); 7.48 (*t*, $^4J$ = 1.8, 2 H); 7.38–7.34 (*m*, 10 H); 7.20 (*d*, $^3J$ = 5.2, 2 H); 7.12–7.10 (*m*, 4 H); 7.06 (*d*, $^3J$ = 3.8, 2 H); 7.04 (*d*, $^3J$ = 3.8, 2 H); 6.97 (*d*, $^3J$ = 3.8, 2 H); 6.65 (*dd*, $^3J$ = 7.8, $^4J$ = 1.9, 2 H); 6.54 (*d*, $^4J$ = 1.9, 2 H); 6.46 (*d*, $^3J$ = 7.8, 2 H); 3.67–3.62 (*m*, 2 H); 2.96–2.82 (*m*, 6 H); 1.39 (*s*, 36 H); 1.38 (*s*, 36 H). $^{13}$C-NMR (126 MHz, $CD_2Cl_2$): 151.62; 151.43; 144.88; 141.31; 141.01; 140.68; 137.70; 137.27; 136.28; 136.11; 135.58; 135.48; 135.45; 135.29; 135.15; 133.65; 131.47; 131.32; 131.07; 130.20; 127.98; 127.51; 127.49; 126.72; 124.71; 124.35; 124.30; 124.22; 122.23; 121.99; 35.44; 35.40; 34.75; 34.51; 31.82; 31.76. HR-MALDI-TOF-MS (DCTB): 1616.6526 ($C_{104}H_{112}S_8^+$, $M^+$; calc. 1616.6530).

Helv. Chim. Acta **2019**, *102*, e1800205

**4,16-Di-(5‴-bromo-3′,3‴-bis(3,5-di-*tert*-butylphenyl))-[2,2′:5′,2″:5″,2‴quarterthien]-5-yl-[2.2]paracyclophane (=5,5′-Tricyclo[8.2.2.2$^{4,7}$]hexadeca-1(12),4,6,10,13,15-hexaene-5,11-diylbis[5‴-bromo-3′,3‴-bis(3,5-di-*tert*-butylphenyl)-2,2′:5′,2″:5″,2‴-quaterthiophene]; 21**): Octathiophene **20** (385 mg, 240 μmol, 1.00 equiv.) was dissolved in $CHCl_3$ (70 mL), and to this was added in the dark NBS (84.7 mg, 480 μmol, 2.00 equiv.). The mixture was stirred at room temperature for 20 h. The organic layer was washed with 2M HCl and dried over $MgSO_4$. The solvent was removed under reduced pressure, and the crude product was purified by column chromatography ($CH_2Cl_2$/cyclohexane 1:9). Compound **21** was isolated as yellow wax (381 mg, 210 μmol, 90%). $^1$H-NMR (400 MHz, $CD_2Cl_2$): 7.46 (*t*, $^4J$=1.8, 2 H); 7.43 (*t*, $^4J$=1.8, 2 H); 7.30 (*d*, $^4J$=1.8, 4 H); 7.25 (*d*, $^4J$=1.8, 4 H); 7.12 (*s*, 2 H); 7.09–7.08 (*m*, 4 H); 7.00 (*d*, $^3J$=3.7, 2 H); 6.96 (*d*, $^3J$ =3.8, 2 H); 6.91 (*d*, $^3J$=3.7, 2 H); 6.58 (*dd*, $^3J$=7.8, $^4J$=1.9, 2 H); 6.48 (*d*, $^4J$=1.9, 2 H); 6.40 (*d*, $^3J$=7.8, 2 H); 3.66–3.60 (*m*, 2 H); 2.90–2.74 (*m*, 6 H); 1.33 (*s*, 36 H); 1.31 (*s*, 36 H). $^{13}$C-NMR (101 MHz, $CD_2Cl_2$): 151.64; 151.60; 144.94; 141.36; 141.33; 140.67; 137.85; 137.69; 136.20; 135.51; 135.47; 135.12; 135.00; 134.70; 134.37; 133.94; 133.63; 132.86; 131.31; 130.20; 128.33; 127.70; 127.52; 126.72; 124.25; 124.21; 124.20; 122.42; 122.26; 111.30; 35.43; 35.41; 34.74; 34.50; 31.80; 31.71. HR-MALDI-TOF-MS (DCTB): 1772.4743 ($C_{104}H_{110}Br_2S_8^+$, $M^+$; calc. 1772.4740).

**4,16-Di-(3′,3‴-bis(3,5-di-*tert*-butylphenyl))-5‴′-trimethylsilyl-[2,2′:5′,2″:5″,2‴:5‴,2‴′qinquethien]-5-yl-[2.2]paracyclophane (={Tricyclo-[8.2.2.2$^{4,7}$]hexadeca-1(12),4,6,10,13,15-hexaene-5,11-diylbis[4′,4‴-bis(3,5-di-*tert*-butylphenyl)-2,2′:5′,2″:5″,2‴:5‴,2‴′-quinquethiene-5‴′,5-diyl]}-bis(trimethylsilane); 4**): Dibromide **21** (160 mg, 90.0 μmol, 1.00 equiv.), boronic ester **8** (153 mg, 540 μmol, 6.00 equiv.), and $K_2CO_3$ (74.8 mg, 540 μmol, 6.00 equiv.) were suspended in toluene (10 mL) and MeOH (10 mL). The mixture was degassed with argon, and Pd-PEPPSI-IPr$^{TM}$ (6.15 mg, 9.02 μmol, 10 mol-%) was added. The mixture was placed in a preheated oil bath and stirred at 70 °C for 30 min. The mixture was allowed to reach room temperature, and the organic layer was washed with 2M HCl. It was dried over $MgSO_4$, and the solvent was removed under reduced pressure. The crude was purified by column chromatography (cyclohexane/$CH_2Cl_2$ 4:1) as well as GPC. Compound **4** was obtained as yellow wax (125 mg, 65.0 μmol, 72%). $^1$H-NMR (500 MHz, $CD_2Cl_2$): 7.46 (*t*, $^4J$=1.8, 2 H); 7.45 (*t*, $^4J$=1.8, 2 H); 7.32–7.30 (*m*, 10 H); 7.21 (*s*, 2 H); 7.20 (*d*, $^3J$=3.5, 2 H); 7.10–7.08 (*m*, 4 H); 7.01–6.99 (*m*, 4 H); 6.92 (*d*, $^3J$=3.7, 2 H); 6.59 (*dd*, $^3J$=7.8, $^4J$=1.9, 2 H); 6.49 (*d*, $^4J$=1.9, 2 H); 6.41 (*d*, $^3J$=7.8, 2 H); 3.66–3.61 (*m*, 2 H); 2.90–2.77 (*m*, 6 H); 1.34–1.33 (*m*, 72 H); 0.35 (*s*, 18 H). $^{13}$C-NMR (126 MHz, $CD_2Cl_2$): 151.61; 151.56; 142.16; 142.15; 141.59; 141.58; 141.31; 141.14; 140.67; 137.69; 137.22; 137.21; 136.25; 135.82; 135.74; 135.53; 135.52; 135.46; 135.22; 135.12; 133.63; 130.40; 130.19; 127.83; 127.71; 127.51; 127.49; 126.71; 125.80; 124.29; 124.28; 124.20; 122.28; 122.23; 35.43; 35.42; 34.73; 34.49; 31.80; 31.75; 0.10. HR-MALDI-TOF-MS (DCTB): 1924.7068 ($C_{118}H_{132}S_{10}Si_2^+$, $M^+$; calc. 1924.7075).

**4,16-Di-((3′,3‴-bis(3,5-di-*tert*-butylphenyl))-5‴′-((3-cyanopropyl)diisopropyl)silylethynyl-[2,2′:5′,2″:5″,2‴:5‴,2‴′qinquethien]-5-yl)-[2.2]paracyclophane (=4,4′-[Tricyclo[8.2.2.2$^{4,7}$]hexadeca-1(12),4,6,10,13,15-hexaene-5,11-diylbis{[4′,4‴-bis(3,5-di-*tert*-butylphenyl)-2,2′:5′,2″:5″,2‴:5‴,2‴′-quinquethiene-5‴′,5-diyl]ethyne-2,1-diyl[di(propan-2-yl)silanediyl]}]dibutanenitrile; 3**): Decathiophene **4** (125 mg, 65.0 μmol, 1.00 equiv.) was suspended in $CHCl_3$ (5 mL) and AcOH (5 mL) and degassed with argon. NBS (24.3 mg, 137 μmol, 2.10 equiv.) was added in one portion, and the mixture was stirred at room temperature for 15 min. The crude was poured into sat. aq. $NaHCO_3$, and the organic layer was washed with brine. The solvent was removed under reduced pressure, and the crude was passed through a plug of silica gel in toluene. After removal of the solvent, the crude was dissolved in toluene (5 mL) and diisopropylamine (2 mL). To this was added CPDIPS acetylene (27.3 mg, 131 μmol, 3.00 equiv.), and the mixture was degassed with argon. $Pd(PPh_3)_4$ (2.53 mg, 2.20 μmol, 5.0 mol-%) and CuI (0.21 mg, 1.10 μmol, 2.5 mol-%) were added to the mixture, and it was heated to 100 °C for 20 h. After completion of the reaction, the mixture was diluted with toluene, and the organic layer was washed with 2 M HCl and dried over $MgSO_4$; the solvent was removed under reduced pressure. The crude was purified by column chromatography in toluene and **3** was obtained as orange wax (92.6 mg, 43.8 μmol, 63%). $^1$H-NMR (400 MHz, $CD_2Cl_2$): 7.48–7.46 (*m*, 4 H); 7.32 (*d*, $^4J$=1.8, 8 H); 7.22 (*s*, 2 H); 7.20 (*d*, $^3J$=3.8, 2 H); 7.12 (*d*, $^3J$=3.8, 2 H); 7.10–7.09 (*m*, 4 H); 7.02–7.00 (*m*, 4 H); 6.92 (*d*, $^3J$=3.8, 2 H); 6.60 (*dd*, $^3J$=7.8, $^4J$=1.9, 2 H); 6.49 (*d*, $^4J$=1.9, 2 H); 6.41 (*d*, $^3J$=7.8, 2 H); 3.67–3.61 (*m*, 2 H); 2.92–2.77 (*m*, 6 H); 2.44 (*t*, *J*=7.0, 4 H); 1.91–1.81 (*m*, 4 H); 1.35 (*s*, 72 H); 1.12–1.09 (*m*, 24 H); 0.89–0.83 (*m*, 4 H). $^{13}$C-NMR (101 MHz, $CD_2Cl_2$): 151.66; 151.64;

Helv. Chim. Acta **2019**, *102*, e1800205

144.94; 141.66; 141.35; 140.68; 138.95; 137.70; 137.54; 136.23; 135.54; 135.49; 135.43; 135.14; 135.02; 134.75; 134.41; 133.65; 131.36; 131.24; 130.21; 128.47; 127.94; 127.61; 127.53; 126.73; 124.30; 124.21; 124.16; 122.50; 122.44; 122.265; 122.258; 120.30; 100.36; 96.66; 35.46; 35.44; 34.75; 34.51; 31.82; 31.77; 30.28; 21.86; 21.27; 18.55; 18.32; 12.32; 10.15; two aliphatic carbon signals do not correspond to a signal from compound **A**. HR-MALDI-TOF-MS (DCTB): 2190.8816 ($C_{136}H_{154}N_2S_{10}Si_2^+$, $M^+$; calc. 2190.8858).

**4,16-Di-((3′,3‴-bis(3,5-di-*tert*-butylphenyl))-5‴′-ethynyl-[2,2′:5′,2″:5″,2‴:5‴,2‴′qinquethien]-5-yl)-[2.2]paracyclophane (=5,5′-Tricyclo[8.2.2.2$^{4,7}$]hexadeca-1(12),4,6,10,13,15-hexaene-5,11-diylbis[3′,3‴-bis(3,5-di-*tert*-butylphenyl)-5‴′-ethynyl-2,2′:5′,2″:5″,2‴:5‴,2‴′-quinquethiophene]]; 22)**: Compound **3** (150 mg, 70.0 μmol, 1.00 equiv.) was dissolved in wetted THF (25 mL). The mixture was degassed with argon, and TBAF (1.0M in THF, 0.21 mL, 210 μmol, 3.00 equiv.) was added dropwise. The mixture was stirred at room temperature for 20 h and then diluted with toluene. The organic layer was washed with brine and dried over $MgSO_4$. After column chromatography (cyclohexane/$CH_2Cl_2$ 4:1), **22** was received as orange wax (124 mg, 68.0 μmol, 97%). $^1$H-NMR (400 MHz, $CD_2Cl_2$): 7.47–7.45 (*m*, 4 H); 7.31 (*d*, $J$=1.8, 8 H); 7.23 (*d*, $^3J$=3.9, 2 H); 7.22 (*s*, 2 H); 7.12 (*d*, $^3J$=3.8, 2 H); 7.10–7.08 (*m*, 4 H); 7.01–7.00 (*m*, 4 H); 6.92 (*d*, $^3J$=3.8, 2 H); 6.59 (*dd*, $^3J$=7.8, $^4J$=1.9, 2 H); 6.49 (*d*, $^4J$=1.9, 2 H); 6.40 (*d*, $^3J$=7.8, 2 H); 3.66–3.60 (*m*, 2 H); 3.50 (*s*, 2 H); 2.91–2.76 (*m*, 6 H); 1.35–1.33 (*m*, 72 H). $^{13}$C-NMR (101 MHz, $CD_2Cl_2$): 151.47; 151.45; 144.74; 141.98; 141.45; 140.48; 138.96; 137.50; 137.35; 136.03; 135.33; 135.21; 134.93; 134.81; 134.55; 134.39; 133.44; 133.07; 131.25; 131.04; 130.03; 128.37; 128.33; 127.74; 127.42; 127.33; 126.53; 124.09; 124.00; 123.91; 122.25; 122.06; 121.19; 120.85; 82.83; 76.95; 35.25; 35.24; 34.55; 34.31; 31.61; 31.56. HR-MALDI-TOF-MS (DCTB): 1828.6274 ($C_{116}H_{116}S_{10}^+$, $M^+$; calc. 1828.6284).

*Macrocycle* **23**: Diyne **22** (60.0 mg, 32.8 μmol, 1.00 equiv.) was dissolved in pyridine (60 mL) and degassed with argon. CuCl (48.7 mg, 490 μmol, 15.0 equiv.) and $Cu(OAc)_2$ (125 mg, 690 μmol, 21.0 equiv.) were dissolved in pyridine (60 mL) and degassed with argon. The solution of diyne **22** was added dropwise through a syringe pump over the course of 48 h. After completed addition, the crude was diluted with toluene, and 2M HCl was added. The organic layer was washed with 2M HCl and brine, and the solvent was removed under reduced pressure. The crude was filtered through a plug of *Celite* and purified by size exclusion chromatography (*BioBeads SX-3*, toluene) and column chromatography (pentane/$CH_2Cl_2$ 4:1). Compound **23** was obtained as red wax (19.8 mg, 10.8 μmol, 33%). $^1$H-NMR (600 MHz, $CD_2Cl_2$): 7.47–7.40 (*m*, 4 H); 7.40 (*d*, $^4J$=1.8, 4 H); 7.37 (*d*, $^4J$=1.8, 4 H); 7.29 (*s*, 2 H); 7.25 (*d*, $^3J$=3.8, 2 H); 7.22–7.21 (*m*, 4 H); 7.05 (*d*, $^3J$=3.8, 2 H); 6.90 (*d*, $^3J$=3.7, 2 H); 6.76 (*d*, $^3J$=3.7, 2 H); 6.73–6.72 (*m*, 2 H); 6.69–6.68 (*m*, 4 H); 6.66 (*d*, $^3J$=3.9, 2 H); 3.90–3.86 (*m*, 2 H); 3.04–2.98 (*m*, 6 H); 1.36 (*s*, 36 H); 1.35 (*s*, 36 H). $^{13}$C-NMR (151 MHz, $CD_2Cl_2$): 151.66; 151.50; 143.75; 141.07; 141.03; 140.82; 140.52; 136.89; 136.26; 135.68; 135.65; 135.48; 135.40; 134.78; 134.75; 134.16; 134.13; 133.05; 131.66; 131.14; 129.99; 129.98; 128.18; 126.91; 126.47; 126.27; 125.24; 123.87; 123.77; 123.69; 123.07; 122.16; 121.98; 121.01; 80.05; 78.62; 35.29; 35.28; 34.93; 34.85; 31.59; 31.58. HR-MALDI-TOF-MS (DCTB): 1826.6110 ($C_{116}H_{114}S_{10}^+$, $M^+$; calc. 1826.6128).

*Macrocycle* **1**: Macrocycle **23** (4.00 mg, 2.19 μmol, 1.00 equiv.) was suspended in DMF (2 mL) and 2-methoxyethanol (2 mL). It was degassed with argon and $Na_2S \cdot 9\,H_2O$ (5.26 mg, 21.9 μmol, 10.0 equiv.) was added to the mixture. The mixture was placed in a preheated oil bath and was stirred for 1.5 h at 120 °C. It was allowed to reach room temperature, and then was diluted with toluene and washed with 2M HCl, repeatedly. The solvent was removed under reduced pressure, and the crude was purified by column chromatography (pentane/$CH_2Cl_2$ 4:1). Compound **1** was obtained as red wax (4.00 mg, 2.18 μmol, 99%). $^1$H-NMR (600 MHz, $CD_2Cl_2$; for atom numbering, see *Figure 6*): 7.47 (*t*, $^4J$=1.9, 2 H, H-28/H-28a); 7.46 (*t*, $^4J$=1.8, 2 H, H-14/H-14a); 7.42 (*d*, $^4J$=1.9, 4 H, H-26/H-26a); 7.37 (*d*, $^4J$=1.8, 4 H, H-12/H-12a); 7.34–7.30 (*m*, 8 H, H-1/H-1a, H-4/H-4a, H-5/H-5a, H-8/H-8a); 7.21 (*s*, 2 H, H-22/H-22a); 7.05 (*d*, $^3J$=3.8, 2 H, H-19/H-19a); 6.90 (*d*, $^3J$=3.7, 2 H, H-33/H-33a); 6.79 (*d*, $^3J$=3.7, 2 H, H-32/H-32a); 6.76–6.72 (*m*, 4H, H-36/H-36a, H-39/H-39a); 6.68 (*dd*, $^3J$=7.9, $^4J$=1.8, 2 H, H-40/H-40a); 6.62 (*d*, $^3J$=3.9, 2 H, H-18/H-18a); 3.91–3.86 (*m*, 2 H, H-41/H-41a); 3.03–2.98 (*m*, 2 H, H-41/H-41a); 2.92–2.88 (*m*, 2 H, H-42/H-42a); 2.85–2.80 (*m*, 2 H, H-42/H-42a); 1.37 (*s*, 36 H, H-30/H-30a); 1.35 (*s*, 36 H, H-16/H-16a). $^{13}$C-NMR (151 MHz, $CD_2Cl_2$): 151.77 (2 C, C-13/ C-13a); 151.64 (2 C, C-27/C-27a); 143.90 (2 C, C-34/C-34a); 143.75, (2 C, C-37/C37a); 141.43 (2 C, C-9/C-9a); 140.47 (2 C, C-23/C-23a); 138.00 (2 C, C-38/C-38a); 137.19 (2 C, C-31/C-31a); 136.58 (2 C, C-2/C-2a); 136.55 (2 C, C-7/C-7a); 136.45 (2 C, C-3/C-3a); 136.23 (2 C, C-20/C-20a or C-21/C-21a); 135.88 (2 C, C-17/C-17a); 135.68 (2 C, C-24/C-24a);

Helv. Chim. Acta **2019**, *102*, e1800205

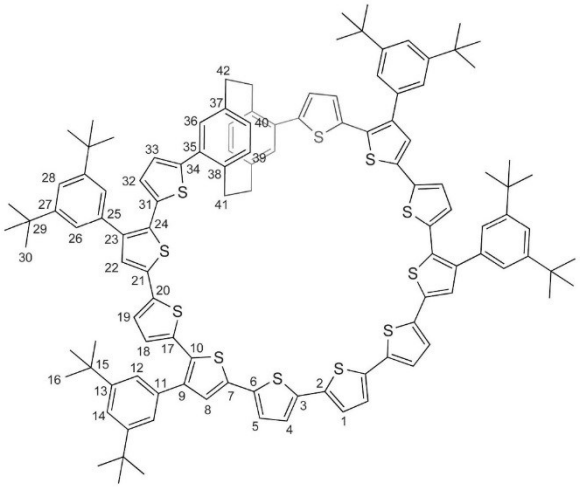

**Figure 6.** Atom numbering scheme for macrocycle **1**.

135.54 (2 C, C-39/C-39a); 135.40 (2 C, C-11/C-11a); 135.16 (2 C, C-6/C-6a); 135.15 (2 C, C-36/C-36a); 134.97 (2 C, C-20/C-20a or C-21/C-21a); 134.92 (2 C, C-35/C-35a); 131.14 (2 C, C-25/C-25a); 130.70 (2 C, C-10/C-10a); 130.09 (2 C, C-40/C-40a); 128.02 (2 C, C-8/C-8a); 126.94 (2 C, C-22/C-22a); 126.79 (2 C, C-18/C-18a); 126.24 (2 C, C-33/C-33a); 125.18 (2 C, C-5/C-5a); 125.16 (2 C, C-1/C-1a); 125.01 (2 C, C-4/C-4a); 124.87 (2 C, C-32/C-32a); 124.03 (2 C, C-19/C-19a); 123.93 (2 C, C-12/C-12a); 123.91 (2 C, C-26/C-26a); 122.17 (4 C, C-28/C-28a and C-14/C-14a); 35.46 (2 C, C-29/C-29a); 35.43 (2 C, C-15/C-15a); 35.29 (2 C, C-41/C-41a); 35.16 (2 C, C-42/C-42a); 31.76 (2 C, C-30/C-30a); 31.75 (2 C, C-16/C-16a). HR-MALDI-TOF-MS (DCTB): 1860.5977 ($C_{116}H_{116}S_{11}^{+}$, $M^{+}$; calc. 1860.6005).

## Acknowledgements

We would like to thank the Mass Spectrometry team in the Molecular and Biomolecular Analysis service at ETH Zurich for their expert help in providing high-resolution measurements of the synthesized compounds. We acknowledge financial support by the *European FP7-ITN MOLESCO* (project no. 606728), the *Swiss National Science Foundation* (SNF, grant no. 200020-178808), and the Swiss Nanoscience Institute (SNI).

## Author Contribution Statement

*K. J. W.* performed the synthesis and characterization of all materials and co-wrote the manuscript. *D. H.*, *N. M.*, and *W. G.* performed NMR analyses of the macrocyclic compounds. *M. M.* supervised the work and wrote the manuscript. All authors commented on the manuscript.

## References

[1] J. D. Meindl, Q. Chen, J. A. Davis 'Limits on Silicon Nanoelectronics for Terascale Integration', *Science* **2001**, *293*, 2044–2049.
[2] S. Höger, 'Shape-Persistent Macrocycles: From Molecules to Materials', *Chem. Eur. J.* **2004**, *10*, 1320–1329.
[3] J. Krömer, I. Rios-Carreras, G. Fuhrmann, C. Musch, M. Wunderlin, T. Debaerdemaeker, E. Mena-Osteritz, P. Bäuerle, 'Synthesis of the First Fully $\alpha$-Conjugated Macrocyclic Oligothiophenes: Cyclo[*n*]Thiophenes with Tunable Cavities in the Nanometer Regime', *Angew. Chem. Int. Ed.* **2000**, *39*, 3481–3486.
[4] L. Favereau, A. Cnossen, J. B. Kelber, J. Q. Gong, R. M. Oetterli, J. Cremers, L. M. Herz, H. L. Anderson, 'Six-Coordinate Zinc Porphyrins for Template-Directed Synthesis of Spiro-Fused Nanorings', *J. Am. Chem. Soc.* **2015**, *137*, 14256–14259.
[5] M. S. Inkpen, S. Scheerer, M. Linseis, A. J. P. White, R. F. Winter, T. Albrecht, N. J. Long, ‚Oligomeric Ferrocene Rings', *Nat. Chem.* **2016**, *8*, 825–830.
[6] H. Shimizu, J. D. Cojal González, M. Hasegawa, T. Nishinaga, T. Haque, M. Takase, H. Otani, J. P. Rabe, M. Iyoda, 'Synthesis, Structures, and Photophysical Properties of $\pi$-Expanded Oligothiophene 8-mers and Their Saturn-Like $C_{60}$ Complexes', *J. Am. Chem. Soc.* **2015**, *137*, 3877–3885.
[7] E. A. Meyer, R. K. Castellano, F. Diederich, 'Interactions with Aromatic Rings in Chemical and Biological Recognition', *Angew. Chem. Int. Ed.* **2003**, *42*, 1210–1250.
[8] H. A. Staab, F. Diederich, 'Cycloarenes, a New Class of Aromatic Compounds, I. Synthesis of Kekulene', *Chem. Ber.* **1983**, *116*, 3487–3503.
[9] C. Krieger, F. Diederich, D. Schweitzer, H. A. Staab, 'Molecular Structure and Spectroscopic Properties of Kekulene', *Angew. Chem. Int. Ed. Engl.* **1979**, *18*, 699–701.
[10] H. Omachi, Y. Segawa, K. Itami, 'Synthesis of Cycloparaphenylenes and Related Carbon Nanorings: A Step toward the Controlled Synthesis of Carbon Nanotubes', *Acc. Chem. Res.* **2012**, *45*, 1378–1389.
[11] M. Iyoda, J. Yamakawa, M. J. Rahman, 'Conjugated Macrocycles: Concepts and Applications', *Angew. Chem. Int. Ed.* **2011**, *50*, 10522–10553.
[12] V. Hoffmann, L. Le Pleux, D. Häussinger, O. T. Unke, A. Prescimone, M. Mayor, 'Deltoid versus Rhomboid: Controlling the Shape of Bis-ferrocene Macrocycles by the Bulkiness of the Substituents', *Organometallics* **2017**, *36*, 858–866.
[13] M. Mayor, J.-M. Lehn, 'Reducible Nanosize Macrocycles', *J. Am. Chem. Soc.* **1999**, *121*, 11231–11232.

 

Helv. Chim. Acta **2019**, *102*, e1800205


[14] M. Müri, K. C. Schuermann, L. De Cola, M. Mayor, 'Shape-Switchable Azo-Macrocycles', *Eur. J. Org. Chem.* **2009**, *15*, 2562–2575.

[15] A. Błaszczyk, M. Chadim, C. von Hänisch, M. Mayor, 'Synthesis of Macrocyclic Molecular Rods as Potential Electronic Devices', *Eur. J. Org. Chem.* **2006**, *17*, 3809–3825.

[16] N. Weibel, A. Mishchenko, T. Wandlowski, M. Neuburger, Y. Leroux, M. Mayor, 'Catechol-Based Macrocyclic Rods: En Route to Redox-Active Molecular Switches', *Eur. J. Org. Chem.* **2009**, *35*, 6140–6150.

[17] L. Le Pleux, E. Kapatsina, J. Hildesheim, D. Häussinger, M. Mayor, 'A Molecular Turnstile as an *E*-Field-Triggered Single-Molecule Switch: Concept and Synthesis', *Eur. J. Org. Chem.* **2017**, *22*, 3165–3178.

[18] L. Shu, M. Mayor, 'Shape-Persistent Macrocycle with a Self-Complementary Recognition Pattern Based on Diacetylene-Linked Alternating Hexylbenzene and Perfluorobenzene Rings', *Chem. Commun.* **2006**, 4134–4136.

[19] L. Shu, M. Müri, R. Krupke, M. Mayor, 'Shape-Persistent Macrocycles Comprising Perfluorinated Benzene Subunits: Synthesis, Aggregation Behaviour and Unexpected μ-Rod Formation', *Org. Biomol. Chem.* **2009**, *7*, 1081–1092.

[20] M. Mayor, C. Didschies, 'A Giant Conjugated Molecular Ring', *Angew. Chem. Int. Ed.* **2003**, *42*, 3176–3179.

[21] R. Mannancherry, M. Rickhaus, D. Häussinger, A. Prescimone, M. Mayor, 'Molecular Dynamic Staircases: All-Carbon Axial Chiral "Geländer" Structures', *Chem. Sci.* **2018**, *9*, 5758–5766.

[22] T. Brandl, V. Hoffmann, A. Pannwitz, D. Häussinger, M. Neuburger, O. Fuhr, S. Bernhard, O. S. Wenger, M. Mayor, 'Chiral Macrocyclic Terpyridine Complexes', *Chem. Sci.* **2018**, *9*, 3837–3843.

[23] M. Iyoda, H. Shimizu, 'Multifunctional π-Expanded Oligothiophene Macrocycles', *Chem. Soc. Rev.* **2015**, *44*, 6411–6424.

[24] P. Bäuerle, M. Ammann, M. Wilde, G. Götz, E. Mena-Osteritz, A. Rang, C. A. Schalley, 'Oligothiophene-Based Catenanes: Synthesis and Electronic Properties of a Novel Conjugated Topological Structure', *Angew. Chem. Int. Ed.* **2007**, *46*, 363–368.

[25] G. Götz, X. Zhu, A. Mishra, J.-L. Segura, E. Mena-Osteritz, P. Bäuerle, 'π-Conjugated [2]Catenanes Based on Oligothiophenes and Phenanthrolines: Efficient Synthesis and Electronic Properties', *Chem. Eur. J.* **2015**, *21*, 7193–7210.

[26] R. A. Shelby, D. R. Smith, S. Schultz, 'Experimental Verification of a Negative Index of Refraction', *Science* **2001**, *292*, 77–79.

[27] Y. Shen, H.-Y. Ko, Q. Ai, S.-M. Peng, B.-Y. Jin, 'Molecular Split-Ring Resonators Based on Metal String Complexes', *J. Phys. Chem. C* **2014**, *118*, 3766–3773.

[28] M. W. Klein, C. Enkrich, M. Wegener, C. M. Soukoulis, S. Linden, 'Single-Slit Split-Ring Resonators at Optical Frequencies: Limits of Size Scaling', *Opt. Lett.* **2006**, *31*, 1259–1261.

[29] Y. Morisaki, M. Gon, T. Sasamori, N. Tokitoh, Y. Chujo, 'Planar Chiral Tetrasubstituted [2.2]Paracyclophane: Optical Resolution and Functionalization', *J. Am. Chem. Soc.* **2014**, *136*, 3350–3353.

[30] C. J. Brown, A. C. Farthing, 'Preparation and Structure of Di-*p*-Xylylene', *Nature* **1949**, *164*, 915–916.

[31] M. Gon, Y. Morisaki, Y. Chujo, 'Optically Active Cyclic Compounds Based on Planar Chiral [2.2]Paracyclophane: Extension of the Conjugated Systems and Chiroptical Properties', *J. Mater. Chem. C* **2015**, *3*, 521–529.

[32] D. S. Seferos, S. A. Trammell, G. C. Bazan, J. G. Kushmerick, 'Probing π-Coupling in Molecular Junctions', *Proc. Natl. Acad. Sci. USA* **2005**, *102*, 8821–8825.

[33] M. Wielopolski, A. Molina-Ontoria, C. Schubert, J. T. Margraf, E. Krokos, J. Kirschner, A. Gouloumis, T. Clark, D. M. Guldi, N. Martín, 'Blending Through-Space and Through-Bond π–π-Coupling in [2,2']-Paracyclophane-Oligophenylenevinylene Molecular Wires', *J. Am. Chem. Soc.* **2013**, *135*, 10372–10381.

[34] J. L. Zafra, A. Molina Ontoria, P. Mayorga Burrezo, M. Peña-Alvarez, M. Samoc, J. Szeremeta, F. J. Ramírez, M. D. Lovander, C. J. Droske, T. M. Pappenfus, L. Echegoyen, J. T. López Navarrete, N. Martin, J. Casado, 'Fingerprints of Through-Bond and Through-Space Exciton and Charge π-Electron Delocalization in Linearly Extended [2.2]Paracyclophanes', *J. Am. Chem. Soc.* **2017**, *139*, 3095–3105.

[35] H. Hinrichs, A. J. Boydston, P. G. Jones, K. Hess, R. Herges, M. M. Haley, H. Hopf, 'Phane Properties of [2.2]Paracyclophane/Dehydrobenzoannulene Hybrids', *Chem. Eur. J.* **2006**, *12*, 7103–7115.

[36] F. Salhi, B. Lee, C. Metz, L. A. Bottomley, D. M. Collard, 'Influence of π-Stacking on the Redox Properties of Oligothiophenes: (α-Alkyloligo-Thienyl)Para[2.2]Cyclophanes', *Org. Lett.* **2002**, *4*, 3195–3198.

[37] D. Stefani, K. J. Weiland, M. Skripnik, C. Hsu, M. L. Perrin, M. Mayor, F. Pauly, H. S. J. van der Zant, 'Large Conductance Variations in a Mechanosensitive Single-Molecule Junction', *Nano Lett.* **2018**, *18*, 5981–5988.

[38] H. J. Reich, D. J. Cram, 'Macro Rings. XXXVII. Multiple Electrophilic Substitution Reactions of [2.2]Paracyclophanes and Interconversions of Polysubstituted Derivatives', *J. Am. Chem. Soc.* **1969**, *91*, 3527–3533.

[39] L. Bondarenko, I. Dix, H. Hinrichs, H. Hopf, 'Cyclophanes. Part LII: Ethynyl[2.2]paracyclophanes – New Building Blocks for Molecular Scaffolding', *Synthesis* **2004**, 2751–2759.

[40] G. Meyer-Eppler, R. Sure, A. Schneider, G. Schnakenburg, S. Grimme, A. Lützen, 'Synthesis, Chiral Resolution, and Absolute Configuration of Dissymmetric 4,15-Difunctionalized [2.2]Paracyclophanes', *J. Org. Chem.* **2014**, *79*, 6679–6687.

[41] M. Hasegawa, K. Kobayakawa, H. Matsuzawa, T. Nishinaga, T. Hirose, K. Sako, Y. Mazaki, 'Macrocyclic Oligothiophene with Stereogenic [2.2]Paracyclophane Scaffolds: Chiroptical Properties from π-Transannular Interactions', *Chem. Eur. J.* **2017**, *23*, 3267–3271.

[42] E. Flapan, 'When Topology Meets Chemistry: A Topological Look at Molecular Chirality', Cambridge University Press, Mathematical Association of America, Cambridge, New York, Washington, DC, 2000.

[43] J.-C. Chambron, J.-P. Sauvage, K. Mislow, A. De Cian, J. Fischer, 'A [2]Catenane and a [2]Rotaxane as Prototypes of Topological and Euclidean Molecular "Rubber Gloves."', *Chem. Eur. J.* **2001**, *7*, 4085–4096.

[44] P. Siemsen, R. C. Livingston, F. Diederich, 'Acetylenic Coupling: A Powerful Tool in Molecular Construction', *Angew. Chem. Int. Ed.* **2000**, *39*, 2632–2657.


 

Helv. Chim. Acta **2019**, *102*, e1800205

[45] S. Odermatt, J. L. Alonso-Gómez, P. Seiler, M. M. Cid, F. Diederich, 'Shape-Persistent Chiral Alleno-Acetylenic Macrocycles and Cyclophanes by Acetylenic Scaffolding with 1,3-Diethynylallenes', *Angew. Chem. Int. Ed.* **2005**, *44*, 5074–5078.

[46] J. L. Alonso-Gómez, P. Rivera-Fuentes, N. Harada, N. Berova, F. Diederich, 'An Enantiomerically Pure Alleno-Acetylenic Macrocycle: Synthesis and Rationalization of Its Outstanding Chiroptical Response', *Angew. Chem. Int. Ed.* **2009**, *48*, 5545–5548.

[47] Y. Wang, J. Song, L. Xu, Y. Kan, J. Shi, H. Wang, 'Synthesis and Characterization of Cyclooctatetrathiophenes with Different Connection Sequences', *J. Org. Chem.* **2014**, *79*, 2255–2262.

[48] D. Thirion, C. Poriel, R. Métivier, J. Rault-Berthelot, F. Barrière, O. Jeannin, 'Violet-to-Blue Tunable Emission of Aryl-Substituted Dispirofluorene-Indenofluorene Isomers by Conformationally-Controllable Intramolecular Excimer Formation', *Chem. Eur. J.* **2011**, *17*, 10272–10287.

[49] V. I. Rozenberg, E. V. Sergeeva, V. G. Kharitonov, N. V. Vorontsova, E. V. Vorontsov, V. V. Mikul'shina, 'Synthesis of Novel Mono- and Diaryl-Substituted [2.2]Paracyclophanes', *Russ. Chem. Bull.* **1994**, *43*, 1018–1023.

[50] T. Klingstedt, A. Åslund, R. A. Simon, L. B. G. Johansson, J. J. Mason, S. Nyström, P. Hammarström, K. P. R. Nilsson, *Org. Biomol. Chem.* **2011**, *9*, 8356–8370.

[51] G. Gaefke, S. Höger, '[(3-Cyanopropyl)diisopropylsilyl]-acetylene, a More Stable Analogue of [(3-Cyanopropyl)-dimethylsilyl]acetylene', *Synthesis* **2008**, 2155–2157.

[52] L. T. Scott, M. J. Cooney, C. Otte, C. Puls, T. Haumann, R. Boese, A. B. Smith III, P. J. Carroll, A. de Meijere, 'Enhancement of Through-Space and Through-Bond .Pi.-Orbital Interactions. Syntheses and Properties of Permethylated and Perspirocyclopropanated Cyclotetradeca-1,3,6,9,12-pentayne', *J. Am. Chem. Soc.* **1994**, *116*, 10275–10283.

[53] M. Rickhaus, M. Mayor, M. Juríček, 'Strain-Induced Helical Chirality in Polyaromatic Systems', *Chem. Soc. Rev.* **2016**, *45*, 1542–1556.

[54] M. Rickhaus, M. Mayor, M. Juríček, 'Chirality in Curved Polyaromatic Systems', *Chem. Soc. Rev.* **2017**, *46*, 1643–1660.

[55] M. Stępień, I. Simkowa, L. Latos-Grażyński, 'Helical Porphyrinoids: Incorporation of Ferrocene Subunits into Macrocyclic Structures', *Eur. J. Org. Chem.* **2008**, *15*, 2601–2611.

[56] M. Bednarz, P. Reineker, E. Mena-Osteritz, P. Bäuerle, 'Optical Absorption Spectra of Linear and Cyclic Thiophenes – Selection Rules Manifestation', *J. Lumin.* **2004**, *110*, 225–231.

[57] N. V. Vorontsova, V. I. Rozenberg, E. V. Sergeeva, E. V. Vorontsov, Z. A. Starikova, K. A. Lyssenko, H. Hopf, 'Symmetrically Tetrasubstituted [2.2]Paracyclophanes: Their Systematization and Regioselective Synthesis of Several Types of Bis-Bifunctional Derivatives by Double Electrophilic Substitution', *Chem. Eur. J.* **2008**, *14*, 4600–4617.

*Received October 20, 2018*
*Accepted November 27, 2018*

 

JACS JOURNAL OF THE AMERICAN CHEMICAL SOCIETY
Article
Cite This: J. Am. Chem. Soc. 2019, 141, 2104−2110
pubs.acs.org/JACS

# Mechanical Stabilization of Helical Chirality in a Macrocyclic Oligothiophene

Kevin J. Weiland,[†] Thomas Brandl,[†] Kenneth Atz,[†] Alessandro Prescimone,[†] Daniel Häussinger,[†] Tomáš Šolomek,[†] and Marcel Mayor*[,†,‡,§]

[†]Department of Chemistry, University of Basel, St. Johanns-Ring 19, 4056 Basel, Switzerland
[‡]Institute for Nanotechnology (INT), Karlsruhe Institute of Technology (KIT), P.O. Box 3640, 76021 Karlsruhe, Germany
[§]Lehn Institute of Functional Materials, School of Chemistry, Sun Yat-Sen University, Guangzhou 510274, China

Supporting Information

**ABSTRACT:** We introduce a design principle to stabilize helically chiral structures from an achiral tetrasubstituted [2.2]paracyclophane by integrating it into a macrocycle. The [2.2]paracyclophane introduces a three-dimensional perturbation into a nearly planar macrocyclic oligothiophene. The resulting helical structure is stabilized by two bulky substituents installed on the [2.2]paracyclophane unit. The increased enantiomerization barrier enabled the separation of both enantiomers. The synthesis of the target helical macrocycle **1** involves a sequence of halogenation and cross-coupling steps and a high-dilution strategy to close the macrocycle. Substituents tuning the energy of the enantiomerization process can be introduced in the last steps of the synthesis. The chiral target compound **1** was fully characterized by NMR spectroscopy and mass spectrometry. The absolute configurations of the isolated enantiomers were assigned by comparing the data of circular dichroism spectroscopy with TD-DFT calculations. The enantiomerization dynamics was studied by dynamic HPLC and variable-temperature 2D exchange spectroscopy and supported by quantum-chemical calculations.

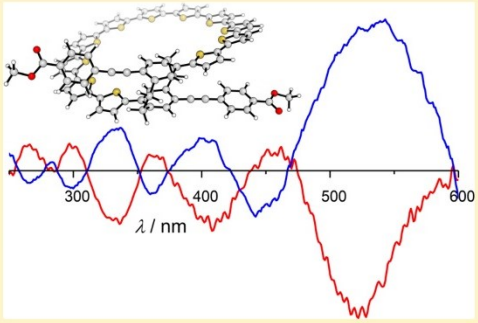


## INTRODUCTION

Helically chiral aromatic molecules,[1−3] besides their esthetic beauty, often possess interesting chiroptical properties such as intense circular dichroism or spin-selective electron transport.[4−6] Apart from ubiquitous helicenes, [2.2]paracyclophane (PC)[7,8] represents an interesting building block to form helical structures because tetrasubstituted PCs, prepared initially by Hopf and co-workers, are chiral. For instance, Chujo and co-workers demonstrated the synthesis of enantiopure doubly helical macrocycles and discovered their intense chiroptical effects,[9,10] which were concluded to arise from the rigid geometry of the propeller-shaped molecules.

Our interest in "loop-shaped" helically chiral model compounds arises from their potential physical properties in single-molecule junctions. To investigate the suitability of the PC synthon, an achiral PC derivative was recently analyzed in a single-molecule junction displaying mechanically triggered conductance variations.[11] As the next step, we decided to investigate the PC building block as a helicity-inducing subunit in macrocycle **2b** (Figure 1). We found the helically chiral molecule to enantiomerize rapidly in solution and therefore decided to stabilize the helical chirality by mechanically hindering the racemization through strategic installation of bulky substituents.[12]

Disconnection of a C−C bond between two thiophenes in a planar oligothiophene macrocycle (Figure 1a,b) and attaching each of the termini to the pseudo-*para*-position of the top and the bottom benzene ring in PC, respectively, introduces a step in the macrocyclic ring from which the helicity of the resulting PC macrocycle emanates (Figure 1c,d). The oligothiophene macrocycle **2b** (Figure 1d) comprising a pseudo-*para* PC step was first assembled sequentially to determine the number of thiophene subunits required to close the macrocycle.[12] Such chiral macrocycles follow an enantiomerization process described first by Kurt Mislow as "Euclidean rubber glove".[13−15] This means that during the entire enantiomerization process the object remains chiral and achiral arrangements cannot be adopted without breaking a bond. The process resembles the transformation of a right-handed rubber glove into a left-handed one by turning it inside out. In the case of **2b**, spontaneous enantiomerization was observed at room temperature due to rotation of the PC subunit around the single bonds integrating it into the oligothiophene macrocycle.[12]

Introduction of bulky rod-like arms with a bis(*para*)-pseudo-*para* orientation[16] to the PC (Figure 1e,f) should gear its free

Received: November 8, 2018
Published: January 11, 2019





DOI: 10.1021/jacs.8b11797
J. Am. Chem. Soc. 2019, 141, 2104−2110

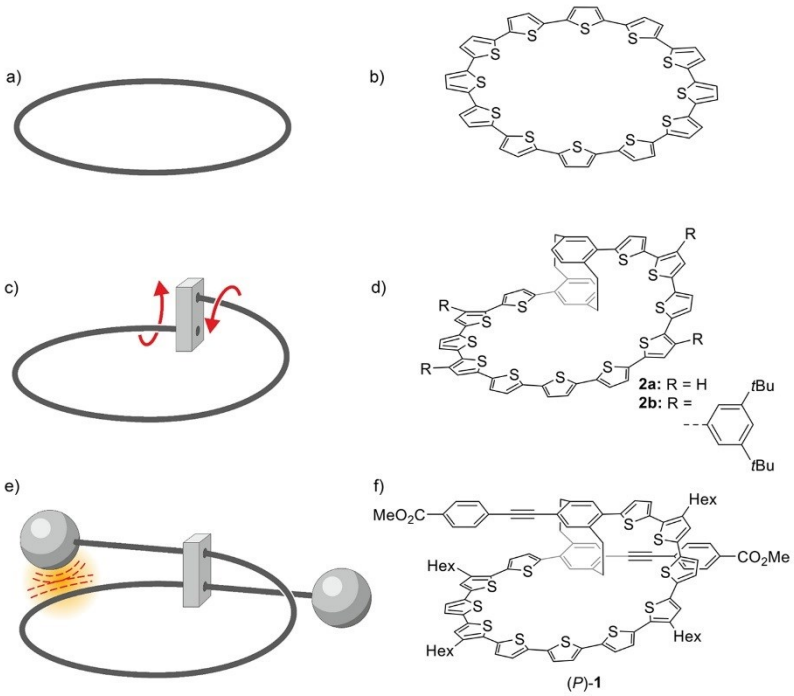


**Figure 1.** Development of the design of the mechanically stabilized helical chiral PC macrocycle **1**. Starting from the planar ring (a) represented by cyclo[12]thiophene (b), the introduction of a step results in a helical chiral object (c) as in the oligothiophene macrocycle **2** comprising a PC subunit (d). Additional decoration of the PC subunit with bulky substituents hinders its enantiomerization by rotation of the PC subunit as sketched in (e). The concept is realized with the macrocyclic model compound **1** reported here (f).

rotation and thereby allow the separation of the enantiomers. To estimate the dimensions of the target structure **1**, the geometry of one enantiomer, based on the smallest unstrained cyclo[12]thiophene with one thiophene unit replaced by the substituted PC, was optimized by density functional theory (DFT) and is depicted as Figure S1.[17,18] The calculated distance between the carboxylic oxygen atoms is ~21 Å, while the largest distance between two sulfur atoms in the macrocycle is ~13.5 Å (figure S1). For the enantiomerization to occur, one of the *para*-ethynyl methylbenzoates must pass through the ring of the macrocycle, like a thread through the eye of a needle. We employed a similar strategy in the synthesis of a molecular turnstyle, where a size mismatch of a push–pull rod and a conjugated macrocyclic ring was used to stabilize atropisomers through hindered rotation.[19]

## ■ RESULTS AND DISCUSSION

The synthesis (Scheme 1) of target macrocycle **1** started from the literature-known dimethyl 7,13-dibromo[2.2]-paracyclophane-4,16-dicarboxylate and trimethyl(5-(4,4,5,5-tetramethyl-1,3,2-dioxaborolan-2-yl)thiophen-2-yl)silane (**3**), which were coupled under Suzuki–Miyaura conditions.[16,20] Conversion of the trimethylsilyl group in **4** to bromine proceeded in high yield but had to be performed in dimethylformamide at 70 °C since the obtained building block **5** was poorly soluble in other common solvents. Subsequently, **5** was reacted under Pd-PEPPSI$^{TM}$-IPr catalysis with 3-hexylthiophene-2-boronic acid pinacol ester, yielding tetrathiophene **6**. Suitable crystals for single-crystal X-ray analysis of **6** (Figure S18) were obtained from a dichloromethane (DCM) ethanol mixture. The methyl esters of **6** were then reduced with diisobutylaluminum hydride (DIBAL-H) and subsequently oxidized with Bobitt's salt to give dialdehyde **7**. It was necessary to control the amount of DIBAL-H precisely, because more than four equivalents of the reagent led to complex product mixtures. Halogenation of **7** leads to a poorly soluble intermediate, which was directly reacted with **3** under Pd-PEPPSI-IPr catalysis to give hexathiophene **8**. Conversion of the TMS groups of **8** to the corresponding dibromide yielded **9** in excellent yield. Next, building block **12** was assembled from triisopropyl(thiophene-2-ylethynyl)silane, which was converted to pinacolboronic ester **10**. Suzuki–Miyaura coupling afforded intermediate **11**, which was converted to pinacolboronic ester **12**. Another Suzuki–Miyaura reaction of **12** and **9** afforded decathiophene **13**, which was first deprotected with tetrabutylammonium fluoride and subjected directly to modified Eglinton coupling conditions. Macrocycle **14** was obtained in an excellent yield of 85% and was reacted with $Na_2S$ to give undecathiophene macrocycle **15**, which contains all 11 thiophene units of the target compound **1**. The rod-like arms were installed by treating **15** with the Corey–Fuchs reaction sequence,[21] converting the dialdehyde into the diacetylene, which was directly subjected to Sonogashira–Hagihara coupling conditions with 4-iodomethylbenzoate to yield the target molecule **1**, which was purified by recycling gel permeation chromatography in chloroform after aqueous workup. Compound **1** showed prolonged stability to air and light as a solid. It was characterized by $^1$H NMR, as well as 2D NMR and UV/vis spectroscopy, and high-resolution MALDI-TOF spectrometry (see the Supporting Information). Notably, the $^1$H NMR spectrum showed two separate resonances of the two methyl



DOI: 10.1021/jacs.8b11797
J. Am. Chem. Soc. 2019, 141, 2104–2110

**Scheme 1. Synthesis of Target Compound 1**[a]

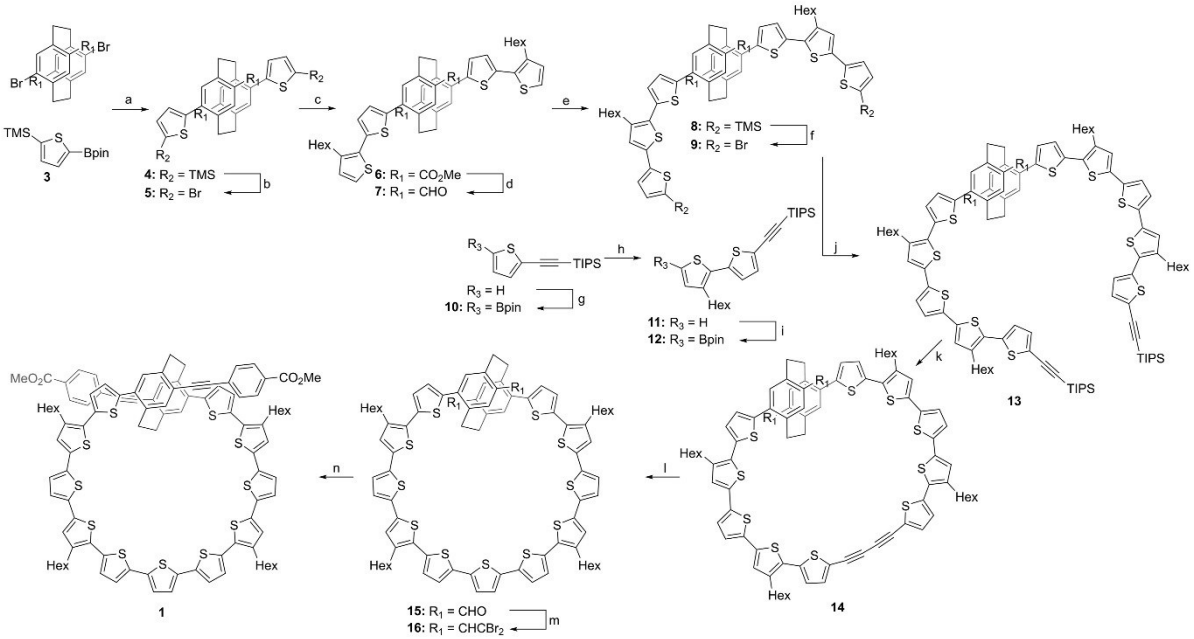


[a]Reaction conditions: (a) **3**, $Pd(dppf)Cl_2$, $K_3PO_4$, toluene/$H_2O$, 10:1, 2 h, 110 °C, 83%; (b) NBS, DMF, 70 °C, 18 h, 93%; (c) 3-hexylthiophene-2-boronic acid pinacol ester, Pd-PEPPSI™-IPr, $K_2CO_3$, toluene/MeOH, 1:1, 70 °C, 20 min, 81%; (d) 1. DIBAL-H, THF, 0 °C, 3 h; 2. Bobitt's salt, silica gel, $CH_2Cl_2$, rt, 18 h, 79%; (e) 1. NBS, $CHCl_3$, rt, 18 h; 2. **3**, Pd-PEPPSI™-IPr, $K_2CO_3$, toluene/MeOH, 1:1, 70 °C, 30 min, 89%; (f) NBS, AcOH/$CHCl_3$, 1:1, rt, 16 h, 99%; (g) *n*-BuLi, 2-isopropoxy-4,4,5,5-tetramethyl-1,3,2-dioxaborolane, THF, −78 °C to rt, 18 h, 99%; (h) 2-bromo-3-hexylthiophene, Pd-PEPPSI™-IPr, $K_2CO_3$, toluene/MeOH, 1:1, 70 °C, 20 min, 51%; (i) *n*-BuLi, THF, 2-isopropoxy-4,4,5,5-tetramethyl-1,3,2-dioxaborolane, −78 °C to rt, 18 h, 97%; (j) Pd-PEPPSI™-IPr, $K_2CO_3$, toluene/MeOH, 1:1, 70 °C, 30 min, 72%; (k) 1. TBAF, $THF_{aq}$, 16 h; 2. CuCl, $Cu(OAc)_2$, pyridine, 80 °C, 40 h (syringe pump), 85%; (l) $Na_2S{\cdot}9\,H_2O$, DMF/2-methoxyethanol, 1:1, 122 °C, 2 h, 94%; (m) $CBr_4$, $PPh_3$, $CH_2Cl_2$, 0 °C, 1 h, 80%; (n) 1. LDA, THF, 0 °C to rt; 2. methyl-4-iodobenzoate, $Pd(PPh_3)_4$, CuI, THF, diisopropylamine, 55 °C, 2 h, 18%.

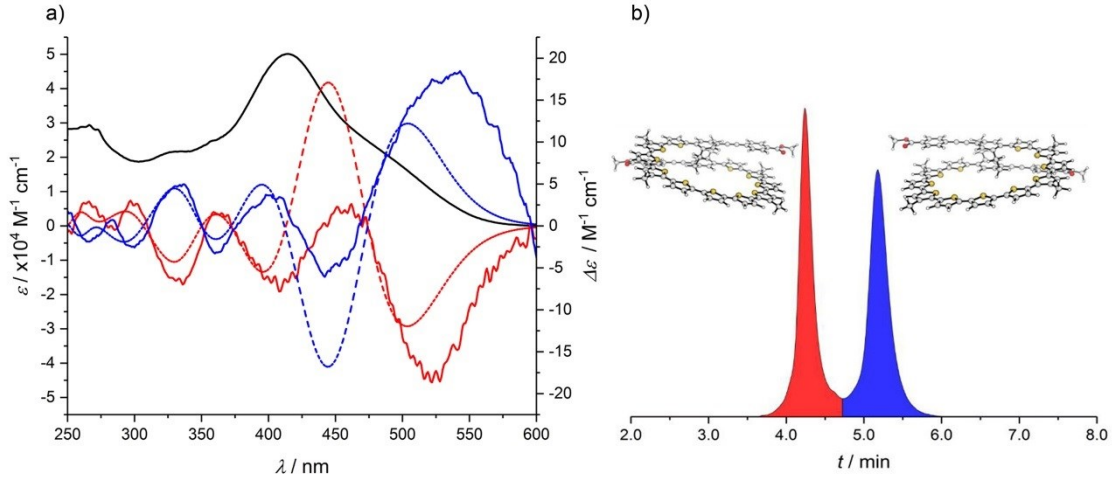


**Figure 2.** (a) UV/vis spectrum (black line) of a DCM solution of **1**, experimental (solid lines; recorded at 10 °C in *n*-hexane/EtOAc, 4:1) and calculated (dashed lines) ECD spectra of (*M*)-**1** (red) and (*P*)-**1** (blue). (b) Representative elution profile from the VT HPLC experiment (298 K column temperature, detected at 409 nm): (*M*)-**1** (red area) and (*P*)-**1** (blue area). The model shows the absolute configuration (the hexyl chains are replaced with methyl groups for clarity).

esters, indicating that the enantiomerization is slow on the time scale of the NMR experiment. The isotopic pattern recorded in the MALDI-TOF mass spectrometry experiment matched the elemental composition of **1** ($[M]^+$ $C_{104}H_{98}O_4S_{11}$).

The enantiomers of **1** were separated by HPLC on a chiral stationary phase (Chiralpak IG, eluent ethyl acetate/*n*-hexane, 1:4, 1.0 mL $min^{-1}$, column oven: $T$ = 18 °C). The isolated fractions of enantiomers displayed identical MALDI-TOF mass



DOI: 10.1021/jacs.8b11797
J. Am. Chem. Soc. 2019, 141, 2104−2110

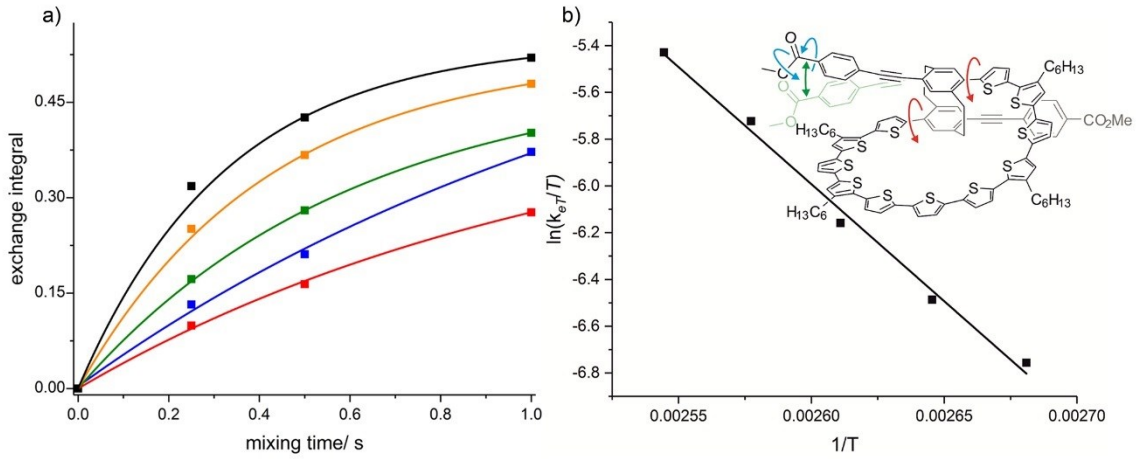


**Figure 3.** (a) Exchange integral against mixing time in the VT EXSY experiment (red: 373 K, blue: 378 K, green: 383 K, orange: 388 K, black: 393 K). (b) Eyring plot from data obtained from the VT EXSY experiment. Linear fit to the data provides the enthalpy ($\Delta H_e^{\ddagger}$ = 83 kJ mol$^{-1}$) and the entropy ($\Delta S_e^{\ddagger}$ = −31 J mol$^{-1}$ K$^{-1}$) for the racemization process. The arrows indicate specific geometric changes obtained from calculations (red: PC rotation, green: arm bending, blue: methoxy or carboxylate rotations).

spectra and mirror images of their electronic circular dichroism (ECD) spectra with a set of Cotton effects at 265, 283, 298, 333, 364, 408, 457, and 536 nm (Figure 2a). The Cotton effects are of low intensity compared with, for example, those observed for doubly helical PC macrocycles of Chujo and co-workers,[22,23] which probably reflects the high flexibility of the PC unit in the oligothiophene macrocycle. It should be noted that despite all precautions (see Experimental Section) a partial racemization of the samples could occur during the course of the ECD measurements. The absolute configuration of the enantiomers was revealed by simulation of the ECD spectra with TD-DFT calculations (see Supporting Information (SI)), which allowed assigning the *M*- and the *P*-configuration to the first and the second eluted fraction, respectively, in the chiral HPLC separation (Figure 2b).[24,25]

Reinjection of an initially pure enantiomer of **1** stored at room temperature (rt) for several minutes already displayed the appearance of the other enantiomer, pointing at racemization at rt in spite of the length of the rod-like arms which were mounted to hinder the PC rotation. Thus, the enantiomerization behavior of **1** was investigated by means of dynamic variable-temperature (VT) HPLC on a chiral stationary phase. The elution profiles of **1** in the temperature range from 293 to 328 K in steps of 5 K (eluent ethyl acetate/*n*-hexane, 2:3) were recorded and analyzed (see SI) with the DCXplorer[26] and the dHPLC Y2K[27,28] software packages. We found the half-life of enantiomerization is only $t_{1/2}^{298\ K}$ = 15.9 ± 0.5 min at 298 K with the activation free energy calculated as $\Delta G^{\ddagger}_{298\ K} \approx$ 91 kJ mol$^{-1}$ by both programs. The VT HPLC experiments further allowed for constructing an Eyring plot to dissect the free energy barrier into the corresponding enthalpy ($\Delta H_e^{\ddagger} \approx$ 37−42 kJ mol$^{-1}$) and entropy ($\Delta S_e^{\ddagger} <$ −160 J mol$^{-1}$ K$^{-1}$) contributions. The values determined for $\Delta H_e^{\ddagger}$ and $\Delta S_e^{\ddagger}$ are striking because they suggest that the PC rotation is to a large extent controlled by a vast entropic penalty. Considering the size of the macrocycle **1** and the length and the stiffness of the methyl 4-ethynylbenzoate arms, the $\Delta H_e^{\ddagger}$ values appear to be intriguingly low. The preexponential factor log($A$) ≈ 5 ($E_a$ ≈ 45 kJ mol$^{-1}$) for enantiomerization of **1**, which is a unimolecular process, obtained from Arrhenius analysis suggests that the temperature dependence of the rate constant obtained from the elution profile analysis may be inaccurate. Indeed, it has been described previously that the elution profile analysis from dynamic VT HPLC experiments provides accurate values of activation free energy but tends to overestimate the entropy contribution when compared to alternative methods such as dynamic ECD, VT NMR spectroscopies, or quantum-chemical calculations.[29] Possibly, the heterogeneous nature of the HPLC experiment, where equilibria of the analyte with the chiral stationary phase are involved, results in enthalpy−entropy compensation affecting the individual activation parameters. As alternative access to these values, a 1,1,2,2-tetrachloroethane-$d_2$ solution of racemic **1** was studied by VT 2D exchange spectroscopy (EXSY) in a temperature range of 373−393 K in steps of 5 K (see Figure 3a and SI) to determine the rate constants. Indeed, in agreement with our expectation, an enthalpy-dominated racemization process was monitored with $\Delta H_e^{\ddagger}$ = 83 kJ mol$^{-1}$ and $\Delta S_e^{\ddagger}$ = −31 J mol$^{-1}$ K$^{-1}$ obtained from the corresponding Eyring plot (Figure 3b). The activation free energy at 298 K, however, was with $\Delta G^{\ddagger}_{298\ K}$ = 92.4 kJ mol$^{-1}$ comparable with the value obtained by the dynamic VT HPLC experiments.

We performed quantum-chemical calculations to get a deeper insight into the enantiomerization mechanism. The size and the flexible nature of macrocycle **1**[30] coerced us to use a combination of semiempirical and DFT calculations (see SI for detailed description) at the PM6 and B3LYP level of theory, respectively. First, we performed a PM6 relaxed potential energy surface scan (PES scan) for **1** along the dihedral angle $\alpha$, which is defined as the angle between the planes of the PC benzene rings and those of the two adjacent thiophene units to mimic the PC rotation.[31] Note that clockwise and anticlockwise PC rotations are not equivalent because **1** is chiral. In any case, we discovered a few possible enantiomerization pathways that all require (i) a considerable turn of the PC from its energy minimum geometry, (ii) bending of the *para*-ethynyl methylbenzoate arm, and, unexpectedly, (iii) a rotation of either (a) the methyl carboxylate by ∼180° or (b) the methoxy group from its more stable *s-cis* to *s-trans* conformation. The latter processes (iii-a,b) decrease the steric repulsion between



DOI: 10.1021/jacs.8b11797
J. Am. Chem. Soc. 2019, 141, 2104−2110

the methyl carboxylate and the thiophene macrocycle and are inevitable to complete the full PC turn required for enantiomerization. All our attempts to find a transition state for the enantiomerization of (*M*)- or (*P*)-**1** failed. We found that the energy range of the region of the PM6 PES where we observed the arm to successfully thread through the macrocycle during the constrained optimization was ~94−103 kJ mol$^{-1}$ (Figures S16 and S17). This energy range represents, neglecting the heat capacities, the upper boundary of the activation enthalpy, and it is in far better agreement with the VT EXSY experimental data than with that obtained from the VT HPLC. Additional evidence can be obtained by considering the energy cost of each of the processes (i−iii) separately assuming their additivity. This allowed us to use the higher level B3LYP calculations (see SI for details) to obtain the PC rotation profile (Figure S12) for the parent PC macrocycle **2a** (Figure 1d). Again, an identical dihedral angle $\alpha$ for the two thiophene units was assumed. The calculated activation energy of ~35 kJ mol$^{-1}$ (at 0 K) for the PC rotation is in very good agreement with the VT NMR activation free energy determined for **2b** ($\Delta G^{\ddagger}_{298\ K}$ = 38 kJ mol$^{-1}$).[12]

Constraining the valence and dihedral angles of the bent acetylene unit in the *para*-ethynyl methylbenzoate arm from the PM6 PES scan while relaxing all other internal coordinates provided (Figure S13b) a penalty of ~26 kJ mol$^{-1}$ for process (ii). Finally, rotation (iii-a) and (iii-b) in *para*-ethynyl methylbenzoate was computed[32−34] to require an activation energy of ~21 and ~28 kJ mol$^{-1}$, respectively. Addition of the individual contributions (i−iii) provides a semiquantitative estimate for the enantiomerization enthalpy of ~82−89 kJ mol$^{-1}$, in very good agreement with our VT EXSY experiments data, suggesting that the enantiomerization of **1** is predominantly controlled by enthalpy.

## CONCLUSION

In summary, we designed and synthesized a helically chiral oligothiophene macrocycle, the chirality of which emerges from the incorporated [2.2]paracyclophane. The fast enantiomerization is prevented by employing bulky rod-like arms on the central [2.2]paracyclophane unit, which allowed resolving and characterizing the chiroptical properties of individual enantiomers by ECD spectroscopy and DFT calculations. The dynamic variable-temperature HPLC and 2D exchange spectroscopy permitted us to obtain the activation free energy for the enantiomerization process, and the latter method gave reliable values of activation enthalpy and entropy further supported by quantum-chemical calculations. Our calculations also revealed the individual internal rotations and structural deformations necessary for the enantiomerization of the helically chiral macrocycle to occur and confirmed thereby also that it follows Mislow's "Euclidian rubber glove" mechanism.

## EXPERIMENTAL SECTION

**Synthesis and Characterization.** Experimental procedures and characterization data for all new compounds described in this work are compiled in the Supporting Information. All commercially available compounds were purchased from Sigma-Aldrich, Acros, Apollo Scientific, Alfa Aesar, and Fluorochem and used without further purification. All reactions with reagents that are easily oxidized or hydrolyzed were performed under argon using Schlenk techniques with anhydrous solvents in glassware, which was dried prior to use. The NMR experiments were performed at 400, 500, or 600 MHz proton frequencies. The instruments were equipped with a direct-observe 5 mm BBFO smart probe (400 and 600 MHz), an indirect-detection 5 mm BBI probe (500 MHz), or a five-channel cryogenic 5 mm QCI probe (600 MHz). All probes were equipped with actively shielded z-gradients (10 A). The chemical shifts are reported in ppm relative to tetramethylsilane or referenced to the residual solvent peak, and the *J* values are given in Hz (±0.1 Hz). The HPLC separation of the enantiomers of **1** was performed on an HPLC instrument equipped with a diode array UV−vis detector ($\lambda$ = 200−600 nm). The used column for separation on the chiral stationary phase was a Chiralpak IG, 5 $\mu$m, 4.6 × 250 mm, Daicel Chemical Industries Ltd. The samples for CD spectra were eluted in *n*-hexane/EtOAc, 4:1, and the VT-HPLC studies were performed in *n*-hexane/EtOAc, 2:1, flow rate 1.0 mL min$^{-1}$. The CD spectra were measured in a precooled 1 cm quartz glass cuvette directly after chiral HPLC at 283 K. All EXSY NMR experiments were performed on a Bruker Avance III NMR spectrometer operating at 600.13 MHz proton frequency. The instrument was equipped with an indirect 5 mm BBI probe with z-gradient. The experiments were performed between 373 and 393 K, and the temperature was calibrated using a glycerol standard showing an accuracy within ±0.2 K. Temperature equilibration was achieved after 20 min, and only then were the EXSY experiments performed. The mixing times were set to 1000, 500, or 250 ms, and the total experiment varied between 68 and 94 min. Manual integration of the EXSY cross-peaks, normalized with the diagonal peaks, yielded the rate constants, which were determined applying the initial rate approximation. Eyring analysis of these rates yielded the enthalpic and entropic contributions to the activation energy.

**DFT Calculations.** The Gaussian 09 (release D01) program suite was used in all calculations.[35] The potential energy surface scans were performed at either semiempirical PM6 or B3LYP/6-31G(d) level of theories. The full gas phase geometry optimizations were done with the B3LYP functional and 6-31G(d) basis set, and the character of the stationary point reached was confirmed by a subsequent frequency calculation. The zero-point vibrational energy correction obtained this way was used unscaled. The electronic circular dichroism spectra were obtained at the CAM-B3LYP/cc-pVDZ level of theory calculating the first 75 electronic transitions. The velocity form of the rotatory strength was used. Empirical vibrational broadening for the electronic transitions was assumed (0.16 eV), and the position of the absorption bands was empirically shifted by +20 nm to match the energy of the first electronic transition. The ECD spectra were simulated in SpecDis (v1.71).[36]

## ASSOCIATED CONTENT

### Supporting Information

The Supporting Information is available free of charge on the ACS Publications website at DOI: 10.1021/jacs.8b11797.

Synthetic procedures and analytical data for all new compounds, HPLC, CD, results of DFT calculations, and $^{1}$H and $^{13}$C NMR and HRMS spectra (PDF)
Crystallographic data (CIF)

## AUTHOR INFORMATION


### Corresponding Author

*marcel.mayor@unibas.ch

### ORCID

Daniel Häussinger: 0000-0002-4798-0072
Tomáš Šolomek: 0000-0003-0013-4116
Marcel Mayor: 0000-0002-8094-7813


### Notes

The authors declare no competing financial interest.

## ACKNOWLEDGMENTS

Dedicated to Prof. Heinz Langhals on the occasion of his 70th birthday. We acknowledge financial support by the European



DOI: 10.1021/jacs.8b11797
J. Am. Chem. Soc. 2019, 141, 2104−2110

FP7-ITN MOLESCO (project no. 606728), the Swiss National Science Foundation (SNF, grant no. 200020-178808 (M.M.) and PZ00P2_174175 (T.Š.)), and the Swiss Nanoscience Institute (SNI). M.M. acknowledges support by the 111 project (90002-18011002). We would like to thank the Mass Spectrometry team in the Molecular and Biomolecular Analysis service at ETH Zurich for their expert help in providing high-resolution measurements of the synthesized compounds. We thank Marco Pierini (University of Rome, Italy) for dHPLC Y2K calculations and Oliver Trapp (University of Munich, Germany) for providing DCXplorer. The SciCore cluster at the University of Basel is acknowledged for the computational resources.

## ■ REFERENCES

(1) Rickhaus, M.; Mayor, M.; Juríček, M. Strain-Induced Helical Chirality in Polyaromatic Systems. *Chem. Soc. Rev.* **2016**, *45*, 1542−1556.
(2) Berezhnaia, V.; Roy, M.; Vanthuyne, N.; Villa, M.; Naubron, J.-V.; Rodriguez, J.; Coquerel, Y.; Gingras, M. Chiral Nanographene Propeller Embedding Six Enantiomerically Stable [5]Helicene Units. *J. Am. Chem. Soc.* **2017**, *139*, 18508−18511.
(3) Fujikawa, T.; Preda, D. V.; Segawa, Y.; Itami, K.; Scott, L. T. Corannulene−Helicene Hybrids: Chiral π-Systems Comprising Both Bowl and Helical Motifs. *Org. Lett.* **2016**, *18*, 3992−3995.
(4) Schuster, N. J.; Paley, D. W.; Jockusch, S.; Ng, F.; Steigerwald, M. L.; Nuckolls, C. Electron Delocalization in Perylene Diimide Helicenes. *Angew. Chem., Int. Ed.* **2016**, *55*, 13519−13523.
(5) Gohler, B.; Hamelbeck, V.; Markus, T. Z.; Kettner, M.; Hanne, G. F.; Vager, Z.; Naaman, R.; Zacharias, H. Spin Selectivity in Electron Transmission Through Self-Assembled Monolayers of Double-Stranded DNA. *Science* **2011**, *331*, 894−897.
(6) Iyoda, M.; Yamakawa, J.; Rahman, M. J. Conjugated Macrocycles: Concepts and Applications. *Angew. Chem., Int. Ed.* **2011**, *50*, 10522−10553.
(7) Brown, C. J.; Farthing, A. C. Preparation and Structure of Di-p-Xylylene. *Nature* **1949**, *164*, 915−916.
(8) Cram, D. J.; Steinberg, H. Macro Rings. I. Preparation and Spectra of the Paracyclophanes. *J. Am. Chem. Soc.* **1951**, *73*, 5691−5704.
(9) Hinrichs, H.; Boydston, A. J.; Jones, P. G.; Hess, K.; Herges, R.; Haley, M. M.; Hopf, H. Phane Properties of [2.2]Paracyclophane/Dehydrobenzoannulene Hybrids. *Chem. - Eur. J.* **2006**, *12*, 7103−7115.
(10) Morisaki, Y.; Gon, M.; Sasamori, T.; Tokitoh, N.; Chujo, Y. Planar Chiral Tetrasubstituted [2.2]Paracyclophane: Optical Resolution and Functionalization. *J. Am. Chem. Soc.* **2014**, *136*, 3350−3353.
(11) Stefani, D.; Weiland, K. J.; Skripnik, M.; Hsu, C.; Perrin, M. L.; Mayor, M.; Pauly, F.; van der Zant, H. S. J. Large Conductance Variations in a Mechanosensitive Single-Molecule Junction. *Nano Lett.* **2018**, *18*, 5981−5988.
(12) Weiland, K. J.; Münch, N.; Gschwind, W.; Häussinger, D.; Mayor, M. A Chiral Macrocyclic Oligothiophene with Broken Conjugation - Rapid Racemization through Internal Rotation. *Helv. Chim. Acta* **2019**, *101*, No. e1800205.
(13) Flapan, E. *When Topology Meets Chemistry: A Topological Look at Molecular Chirality; Outlooks*; Cambridge University Press; Mathematical Association of America: Cambridge; New York; Washington, DC, 2000.
(14) Chambron, J.-C.; Sauvage, J.-P.; Mislow, K.; De Cian, A.; Fischer, J. A [2]Catenane and a [2]Rotaxane as Prototypes of Topological and Euclidean Molecular "Rubber Gloves. *Chem. - Eur. J.* **2001**, *7*, 4085−4096.
(15) Mislow, K. Limitations of the Symmetry Criteria for Optical Inactivity and Resolvability. *Science* **1954**, *120*, 232−233.
(16) Vorontsova, N. V.; Rozenberg, V. I.; Sergeeva, E. V.; Vorontsov, E. V.; Starikova, Z. A.; Lyssenko, K. A.; Hopf, H. Symmetrically Tetrasubstituted [2.2]Paracyclophanes: Their Systematization and Regioselective Synthesis of Several Types of Bis-Bifunctional Derivatives by Double Electrophilic Substitution. *Chem. - Eur. J.* **2008**, *14*, 4600−4617.
(17) Krömer, J.; Rios-Carreras, I.; Fuhrmann, G.; Musch, C.; Wunderlin, M.; Debaerdemaeker, T.; Mena-Osteritz, E.; Bäuerle, P. Synthesis of the First Fully α-Conjugated Macrocyclic Oligothiophenes: Cyclo[n]Thiophenes with Tunable Cavities in the Nanometer Regime. *Angew. Chem., Int. Ed.* **2000**, *39*, 3481−3486.
(18) Mishra, A.; Ma, C.-Q.; Bäuerle, P. Functional Oligothiophenes: Molecular Design for Multidimensional Nanoarchitectures and Their Applications. *Chem. Rev.* **2009**, *109*, 1141−1276.
(19) Le Pleux, L.; Kapatsina, E.; Hildesheim, J.; Häussinger, D.; Mayor, M. A Molecular Turnstile as an *E* -Field-Triggered Single-Molecule Switch: Concept and Synthesis: A Molecular Turnstile as an *E* -Field-Triggered Single-Molecule Switch: Concept and Synthesis. *Eur. J. Org. Chem.* **2017**, *2017*, 3165−3178.
(20) Thirion, D.; Poriel, C.; Métivier, R.; Rault-Berthelot, J.; Barrière, F.; Jeannin, O. Violet-to-Blue Tunable Emission of Aryl-Substituted Dispirofluorene-Indenofluorene Isomers by Conformationally-Controllable Intramolecular Excimer Formation. *Chem. - Eur. J.* **2011**, *17*, 10272−10287.
(21) Corey, E. J.; Fuchs, P. L. A. Synthetic Method for Formyl -> Ethynyl Conversion. *Tetrahedron Lett.* **1972**, *13*, 3769−3772.
(22) Morisaki, Y.; Kawakami, N.; Shibata, S.; Chujo, Y. Through-Space Conjugated Molecular Wire Comprising Three π-Electron Systems. *Chem. - Asian J.* **2014**, *9*, 2891−2895.
(23) Gon, M.; Morisaki, Y.; Sawada, R.; Chujo, Y. Synthesis of Optically Active, X-Shaped, Conjugated Compounds and Dendrimers Based on Planar Chiral [2.2]Paracyclophane, Leading to Highly Emissive Circularly Polarized Luminescence. *Chem. - Eur. J.* **2016**, *22*, 2291−2298.
(24) Yanai, T.; Tew, D. P.; Handy, N. C. A New Hybrid Exchange−Correlation Functional Using the Coulomb-Attenuating Method (CAM-B3LYP). *Chem. Phys. Lett.* **2004**, *393*, 51−57.
(25) Bruhn, T.; Schaumlöffel, A.; Hemberger, Y.; Bringmann, G. SpecDis: Quantifying the Comparison of Calculated and Experimental Electronic Circular Dichroism Spectra: UV AND ECD EVALUATION WITH SPECDIS. *Chirality* **2013**, *25*, 243−249.
(26) Trapp, O. A Novel Software Tool for High Throughput Measurements of Interconversion Barriers: DCXplorer☆. *J. Chromatogr. B: Anal. Technol. Biomed. Life Sci.* **2008**, *875*, 42−47.
(27) D'Acquarica, I.; Gasparrini, F.; Pierini, M.; Villani, C.; Zappia, G. Dynamic HPLC on Chiral Stationary Phases: A Powerful Tool for the Investigation of Stereomutation Processes. *J. Sep. Sci.* **2006**, *29*, 1508−1516.
(28) Rizzo, S.; Benincori, T.; Bonometti, V.; Cirilli, R.; Mussini, P. R.; Pierini, M.; Pilati, T.; Sannicolò, F. Steric and Electronic Effects on the Configurational Stability of Residual Chiral Phosphorus-Centered Three-Bladed Propellers: Tris-Aryl Phosphanes. *Chem. - Eur. J.* **2013**, *19*, 182−194.
(29) Bihlmeier, A.; Rotzler, J.; Rickhaus, M.; Mayor, M.; Klopper, W. Activation Enthalpies and Entropies of the Atropisomerization of Substituted Butyl-Bridged Biphenyls. *Phys. Chem. Chem. Phys.* **2015**, *17*, 11165−11173.
(30) Even with the solubilizing hexyl chains reduced to methyl groups or hydrogen atoms.
(31) Although the dihedral angles between the plane of each of the thiophene units and the plane of the top or the bottom benzene ring of the PC, respectively, are not necessarily identical, a single variable α had to be used to simulate the PC rotation to avoid rotation of the thiophene unit when a single dihedral angle was constrained, while the other was relaxed in the optimization.
(32) The B3LYP PES calculations for both rotations overestimate the activation energy of each process. Therefore, both were corrected by the difference of the activation barrier obtained from the PES calculated for methyl benzoate and methyl formate at the same level



DOI: 10.1021/jacs.8b11797
J. Am. Chem. Soc. 2019, 141, 2104−2110

of theory and the experimental values reported in the literature (refs 33 and 34).

(33) Bailey, J.; North, A. M. Ultrasonic Relaxation in Some Alkyl Esters. *Trans. Faraday Soc.* **1968**, *64*, 1499.

(34) Pawar, D. M.; Wilson, K. K.; Noe, E. A. Barrier to Rotation about the Phenyl−Carbonyl Carbon Bond of Methyl Benzoate by Dynamic NMR Spectroscopy and Ab Initio Molecular Orbital Calculations. *J. Org. Chem.* **2000**, *65*, 1552−1553.

(35) Frisch, M. J.; Trucks, G. W.; Schlegel, H. B.; Scuseria, G. E.; Robb, M. A.; Cheeseman, J. R.; Scalmani, G.; Barone, V.; Petersson, G. A.; Nakatsuji, H.; Li, X.; Caricato, M.; Marenich, A. V.; Bloino, J.; Janesko, B. G.; Gomperts, R.; Mennucci, B.; Hratchian, H. P.; Ortiz, J. V.; Izmaylov, A. F.; Sonnenberg, J. L.; Williams-Young, D.; Ding, F.; Lipparini, F.; Egidi, F.; Goings, J.; Peng, B.; Petrone, A.; Henderson, T.; Ranasinghe, D.; Zakrzewski, V. G.; Gao, J.; Rega, N.; Zheng, G.; Liang, W.; Hada, M.; Ehara, M.; Toyota, K.; Fukuda, R.; Hasegawa, J.; Ishida, M.; Nakajima, T.; Honda, Y.; Kitao, O.; Nakai, H.; Vreven, T.; Throssell, K.; Montgomery, J. A., Jr.; Peralta, J. E.; Ogliaro, F.; Bearpark, M. J.; Heyd, J. J.; Brothers, E. N.; Kudin, K. N.; Staroverov, V. N.; Keith, T. A.; Kobayashi, R.; Normand, J.; Raghavachari, K.; Rendell, A. P.; Burant, J. C.; Iyengar, S. S.; Tomasi, J.; Cossi, M.; Millam, J. M.; Klene, M.; Adamo, C.; Cammi, R.; Ochterski, J. W.; Martin, R. L.; Morokuma, K.; Farkas, O.; Foresman, J. B.; Fox, D. J. *Gaussian 09*, Revision D.01; Gaussian, Inc.: Wallingford, CT, 2009.

(36) Bruhn, T.; Schaumlöffel, A.; Hemberger, Y.; Bringmann, G. SpecDis: Quantifying the Comparison of Calculated and Experimental Electronic Circular Dichroism Spectra. *Chirality* **2013**, *25*, 243−249.



DOI: 10.1021/jacs.8b11797
*J. Am. Chem. Soc.* 2019, 141, 2104−2110

NANO LETTERS
Letter
Cite This: Nano Lett. 2018, 18, 5981−5988
pubs.acs.org/NanoLett

# Large Conductance Variations in a Mechanosensitive Single-Molecule Junction

Davide Stefani,[†] Kevin J. Weiland,[‡] Maxim Skripnik,[§,∥] Chunwei Hsu,[†] Mickael L. Perrin,[†,⊥] Marcel Mayor,[*,‡,#,▽] Fabian Pauly,[*,§,∥] and Herre S. J. van der Zant[*,†]

[†]Kavli Institute of Nanoscience, Delft University of Technology, 2600 GA Delft, The Netherlands
[‡]Department of Chemistry, University of Basel, 4056 Basel, Switzerland
[§]Okinawa Institute of Science and Technology Graduate University, Onna-son, Okinawa 904-0395, Japan
[∥]Department of Physics, University of Konstanz, 78457 Konstanz, Germany
[⊥]Transport at Nanoscale Interfaces Laboratory, Empa, Swiss Federal Laboratories for Materials Science and Technology, 8600 Dübendorf, Switzerland
[#]Karlsruhe Institute of Technology (KIT), P.O. Box 3640, 76021 Karlsruhe, Germany
[▽]Lehn Institute of Functional Materials, School of Chemistry, Sun Yat-Sen University, Guangzhou 510275, China

*Supporting Information*

**ABSTRACT:** An appealing feature of molecular electronics is the possibility of inducing changes in the orbital structure through external stimuli. This can provide functionality on the single-molecule level that can be employed for sensing or switching purposes if the associated conductance changes are sizable upon application of the stimuli. Here, we show that the room-temperature conductance of a spring-like molecule can be mechanically controlled up to an order of magnitude by compressing or elongating it. Quantum-chemistry calculations indicate that the large conductance variations are the result of destructive quantum interference effects between the frontier orbitals that can be lifted by applying either compressive or tensile strain to the molecule. When periodically modulating the electrode separation, a conductance modulation at double the driving frequency is observed, providing a direct proof for the presence of quantum interference. Furthermore, oscillations in the conductance occur when the stress built up in the molecule is high enough to allow the anchoring groups to move along the surface in a stick−slip-like fashion. The mechanical control of quantum interference effects results in the largest-gauge factor reported for single-molecule devices up to now, which may open the door for applications in, e.g., a nanoscale mechanosensitive sensing device that is functional at room temperature.

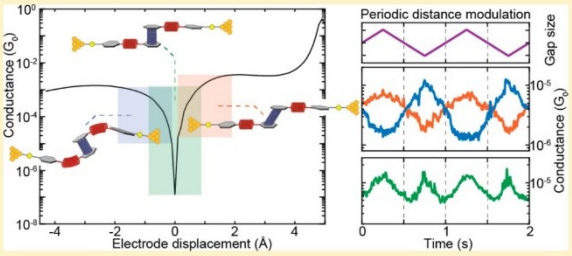


**KEYWORDS:** *Quantum interference, mechanically controlled break-junctions, single-molecule, nanoscale transport, molecular electronics, density functional theory*

In recent years, studies on single-molecule junctions have rapidly become a mature research field.[1,2] The combination of the structural diversity accessible by synthetic chemistry with the continuously improving skills of experimental and theoretical physics enabled the exploration of individual molecules as the tiniest functional building blocks for electronic circuits and sensors.[3,4] The steady refinement of the break-junction technique also allowed to study correlations between mechanical manipulations and transport features at the single-molecule level in a systematic way.[5] Examples include binary switching through mechanical control of the metal−molecule contact geometry[6] or through stereoelectronic effects,[7] mechanical-stress-sensitive redox chromophores,[8] and coordination compounds that show spin-state switching under mechanical stress.[9] Furthermore, the sensitivity of the technique makes it possible to observe intermolecular behaviors such as $\pi$-stacking,[10,11] and more recently, the interdependence of conductance and frontier orbitals involved in the $\pi$-stacking[12,13] could be directly demonstrated.[14]

Particularly interesting are destructive quantum interference effects leading to a strong suppression of electron transmission at specific energies, which make them an ideal feature for applications in, e.g., thermo-[15] or voltage-dependent switching.[16] Their manipulation has been reported by external means including solid-state[17] or electrochemical gating,[18] humidity,[19] and the sliding of $\pi$-stacked molecules relative to each other.[14] Deliberate manipulation of the latter, however, remains elusive as it requires strict temperature conditions and is based on

**Received:** July 10, 2018
**Revised:** August 14, 2018
**Published:** August 22, 2018





DOI: 10.1021/acs.nanolett.8b02810
Nano Lett. 2018, 18, 5981−5988

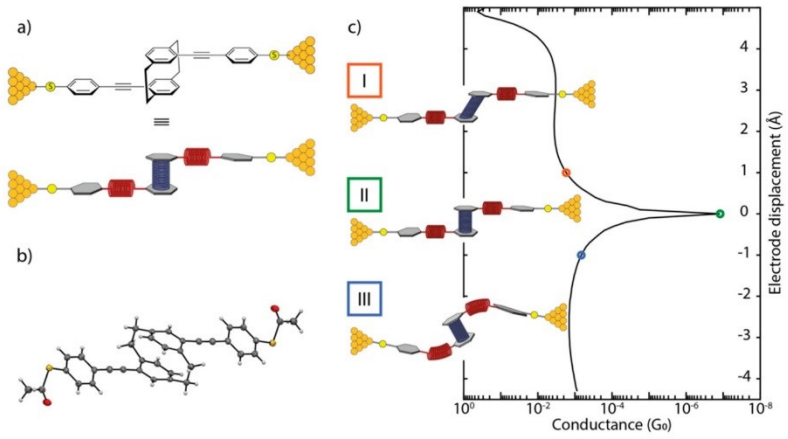


**Figure 1.** (a) Schematic illustration of the break-junction experiment of the OPE-linked PC molecule trapped between nanoelectrodes (top panel), together with a presentation displaying, as springs, the combinations of mechanosensitive structures in the molecular design (bottom drawing in this panel). (b) Solid-state molecular structure determined by single-crystal X-ray analysis. (c) Possible behavior of the molecule under applied force: (I) elongation of the molecule under pulling force of the electrodes, (II) junction with the molecule in its relaxed configuration, and (III) compression results in a shortening of the overall junction length. The simulated conductance (in units of the conductance quantum $G_0 = 2e^2/h$) as a function of the applied mechanical stress is displayed as the drawn line; the three cases (I–III) are indicated by the colored circles.

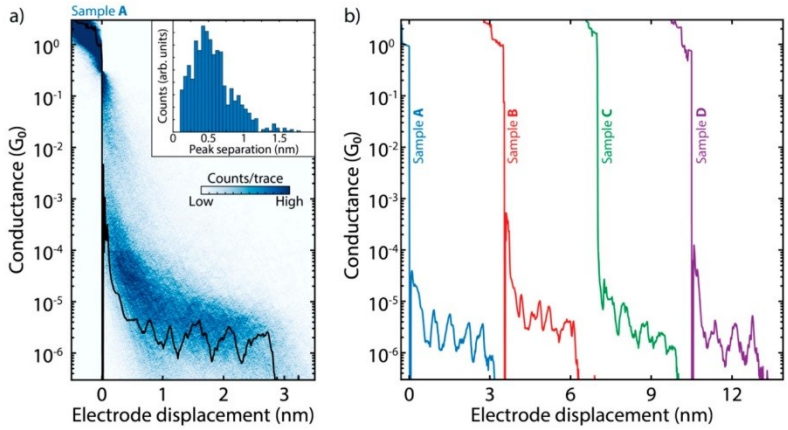


**Figure 2.** (a) Two-dimensional histogram built from 3000 consecutive breaking traces collected after deposition of the solution containing the molecule displayed in Figure 1. The applied bias is 100 mV, and the electrode speed is 4.0 nm/s. A single breaking trace (black line) has been overlaid as an example. The inset shows the peak-separation distribution. (b) Examples of breaking traces, showing oscillations in conductance as a function of displacement. The traces are taken from four different samples and are offset in the *x*-axis for clarity. The first trace comes from sample A, shown in panel a; samples B–D are presented in Figures S6–S9 alongside more examples of breaking traces.

intermolecular interactions. In particular, the intermolecular character requires the coincidental presence of two molecules inside the junction. For this reason, approaches that intramolecularly imitate intermolecular $\pi$-stacking move into the focus of interest. Along these lines, the [2.2]paracyclophane (PC) compound is highly appealing.[20] First described by Farthing et al. in 1949, it consists of two stacked benzene rings that are mechanically stabilized by two nonconjugated linkers.[21] Integrated as central unit of an oligo-phenylene-ethynylene (OPE) rod with terminal binding groups to gold electrodes (Figure 1), we show here that using a mechanically controlled break junction (MCBJ) the $\pi$-stacking (and, therefore, the conductance) can be modulated by exerting a mechanical shear force to it. Simulations based on density functional theory (DFT) reveal a sensitive correlation between electrode displacement and molecular conductance, which is interpreted in terms of quantum interference effects between the frontier orbitals.

**Results.** The employed molecule and the conceptual idea behind the mechanical conductance manipulation are displayed in Figure 1. The molecule consists of a motif in which two ethynylphenylthiols are bound to PC in such a way that the connection resembles a para substitution in benzene.[22,23] The thiol groups are connected in the para position of the outer benzene rings with respect to the PC building block, directing the current path through the PC and offering considerable mechanical stability between gold electrodes.[24] The molecular motif and substitution pattern allow for flexibility by stretching of the PC; the ethynylphenylthiol building block, however, only offers limited movement upon application of a pulling force on the molecule (Figure 1c). High-pressure solid state absorption experiments on PC



DOI: 10.1021/acs.nanolett.8b02810
*Nano Lett.* 2018, 18, 5981–5988

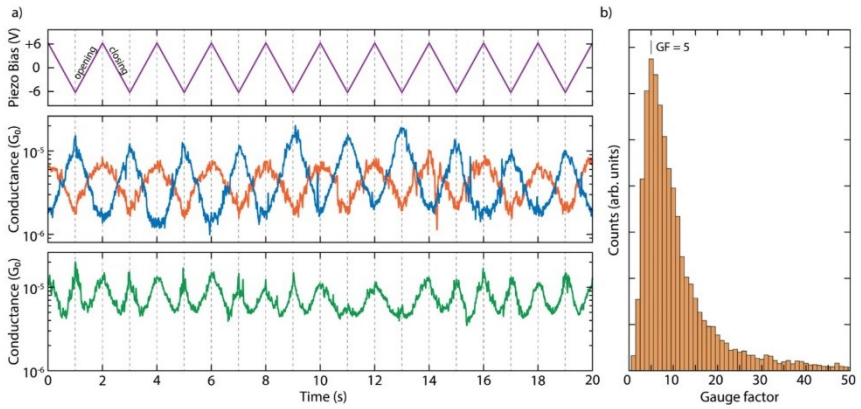


**Figure 3.** (a) Examples of distance-modulation traces (sample B). The blue, orange, and green lines (middle and bottom panel) represent three different conductance measurements, whereas the purple line (top panel) represents the voltage applied to the piezoelectric stack. The applied piezo voltage translates into a peak-to-peak distance of 5.0 Å, and a positive voltage corresponds to a larger electrode distance. The total modulation time is 120 s at a frequency of 0.5 Hz. The conductance responds to the electrode-separation modulation either in-phase (orange), in antiphase (blue), or with double the modulation frequency (green). An example of a full measurement, extending over 120 s, is shown in Figures S17 and S19. (b) Distribution of absolute values of gauge factors obtained from 123 selected traces of the distance-modulation measurements performed on sample B. The number in the figure corresponds to the peak value of the distribution.

derivatives show shortened distances between [25] When the thiol groups are moved apart, the applied tensile force is relayed to the central PC unit along the axis connecting the anchoring groups (Figure S4). Our DFT calculations show that the alkynes are more susceptible to compressive motions, whereas the PC subunit only stretches after these are fully extended. It is noteworthy that electrical transport studies through monolayers consisting of the proposed molecular rods and similar PC-containing subunits have been reported.[23,26] However, the limited control over the number of molecules inside the junction made the interpretation of the results challenging.

**Single-Molecule Experiments.** The target molecule was synthesized by adapting literature-known procedures;[27,28] its structure was unambiguously verified by single-crystal X-ray analysis (Figure 1b). Details of the synthetic protocols are provided in the Supporting Information, together with the analytical data corroborating its identity, which is in agreement with the data already reported.[23] The molecular conductance was investigated using the MCBJ technique under ambient conditions. In this technique, atomically sharp electrodes are formed in a lithographically defined gold wire and repeatedly opened and closed with sub-nanometer accuracy. The measurement of the conductance as the electrodes are continuously moved further apart constitutes a so-called breaking trace. Further details about the MCBJ setup and the measuring technique have been described elsewhere.[29,30]

Fast-breaking measurements were performed to characterize the conductance of the OPE-linked PC molecules.[31] The two-dimensional histogram in Figure 2a shows the distribution of conductance versus electrode displacement. Fitting a log-normal distribution to the one-dimensional histogram constructed from the same data (Figure S5a) reveals that the most-probable conductance value is $3.7 \times 10^{-6}$ $G_0$, where $G_0 = 2e^2/h$ is the quantum of conductance. Interestingly, inspection of individual traces shows the appearance of pronounced oscillations in the conductance as the electrodes are pulled from one another, as illustrated in Figure 2b for four different samples. These oscillations are found in a large fraction of the molecular traces (40%) and have an amplitude up to an order of magnitude. The inset of Figure 2a presents a histogram of the spacing of the individual peaks, showing a periodicity of about 0.5 nm (see Supporting Information section II-1 for more details). Note that such oscillations are absent in the control measurements without the molecule (Figure S10).

To investigate in more detail the dependence of the molecular conductance on the electrode displacement, we performed conductance measurements with modulated electrode spacing.[32] In this experiment, the MCBJ was initially stretched to a few-atoms width (about 3 $G_0$) and allowed to self-break by its surface tension to form atomically sharp electrodes.[33] Next, the electrodes were separated by a distance equal to the length of the molecule to recognize, by evaluating the conductance, whether the trapping of a molecule occurred: if the conductance is found to be larger than $10^{-6}$ $G_0$, a molecule is presumably connected between the two electrodes, and a triangular wave is applied to the piezoelectric stack that controls the electrode positions (Figure 3a). Note that a higher voltage on the piezoelectric stack corresponds to a larger electrode separation. Hundreds of such so-called distance-modulation traces are collected and from them a conductance histogram is built, similar to that obtained for fast-breaking measurements. Fitting a log-normal distribution to this histogram yields a peak at $2.7 \times 10^{-6}$ $G_0$, a value close to that found for fast-breaking measurements (Figure S5b). Thus, molecular traces in this measurement appear at approximately the same conductance values as found for the fast-breaking measurements and have a long lifetime, consistently surviving for the entire modulation time of 120 s.

As illustrated in Figures 3a and S12−S16, as the gap size increases, the conductance can either increase or decrease. In the former case, we define the conductance changes to be in phase with the gap size modulation (orange curve in Figure 3a). In the latter, it is the other way around: the conductance change is in antiphase with the gap-size modulation (blue curve in Figure 3a). About 32% of the molecular traces show in-phase conductance variations, 28% appear to respond in antiphase, and about 40% show a mixture of both or a more-



DOI: 10.1021/acs.nanolett.8b02810
Nano Lett. 2018, 18, 5981−5988

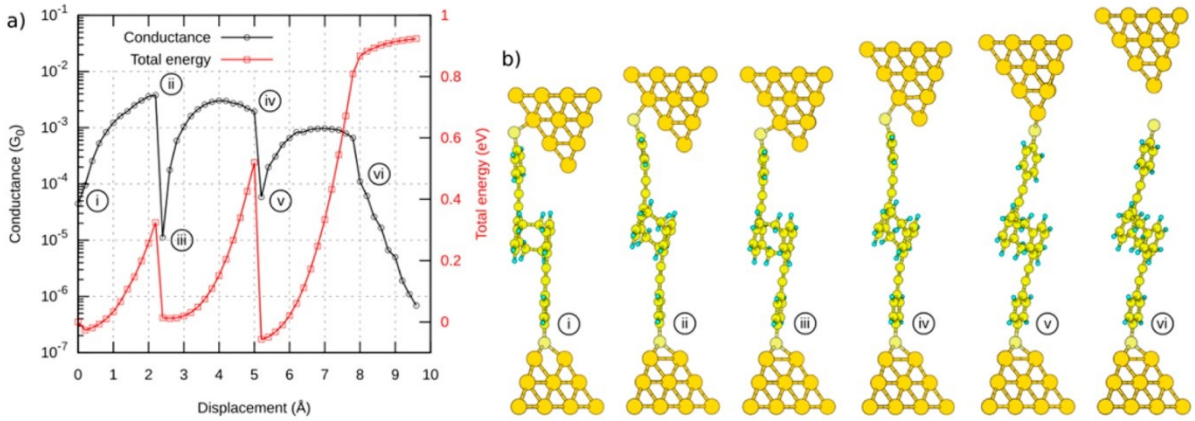


**Figure 4.** (a) Calculated conductance and total energy of the system during gap opening. (b) Selection of snapshots illustrating the stick−slip motion. A video of the simulated stick−slip motion can be found in the Supporting Information.

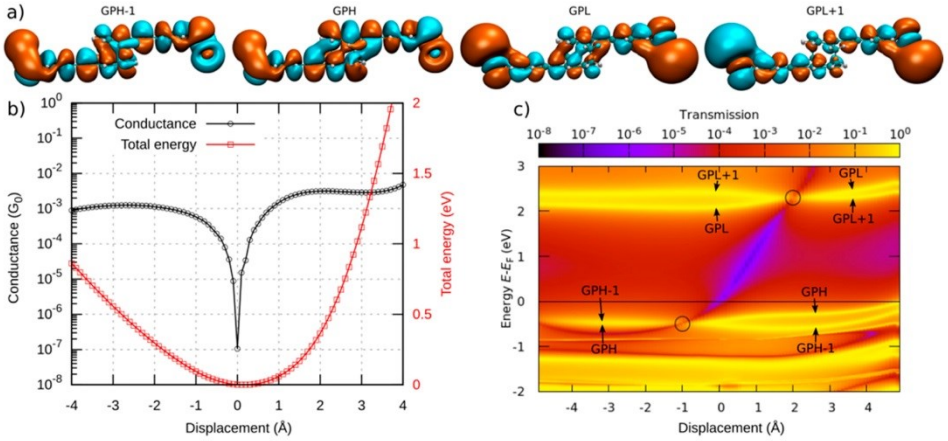


**Figure 5.** (a) Frontier orbitals of the molecule. The orbitals are either symmetric (GPH and GPL) or antisymmetric (GPH−1 and GPL+1) with respect to the center of the molecule. The frontier orbitals are shown in the gas phase for clarity (with the sulfur atoms "terminated" with one gold atom each) because they do not change significantly when the gold leads are attached to the molecule. (b) Conductance (horizontal black line in panel c) and total energy. (c) Transmission map of the molecule between two leads from DFT calculations. The horizontal yellow traces in the map arise from orbitals that can be related to the gas-phase frontier orbitals. An anti-resonance is observed between the frontier orbital traces. It shifts in energy as the displacement is varied. The positions at which the pairs of GPH−1 and GPH and of GPL and GPL+1 degenerate are marked with circles.

complex response (Figures S13−S17). Most of the conductance traces show these conductance variations at the same frequency as the driving modulation (Figure S18); however, surprisingly, many (31%) respond at double the driving frequency. The green curve in Figure 3a is an example of this.

**Theoretical Calculations.** To shed more light on these experimental observations, DFT-based calculations were carried out. For the evaluation of the conductance, we used a proprietary framework.[34] To start, we place the molecule between two pyramidal gold leads, as shown in Figure 4b. The upper electrode exhibits an atomically sharp tip, while the tip atom is removed for the lower one. By the placement of a terminal sulfur atom of the molecule at the hollow site of the lower pyramid, it binds to three gold atoms. Compared to the sulfur−gold bonding at the top lead, the stronger bonding of the sulfur atom to the hollow site ensures a stable mechanical connection, and the sulfur atom at the upper electrode starts sliding down the gold facets as the contact is being stretched.

The total energy and conductance of this system show pronounced jumps at certain displacements during the gap opening. The snapshots at these displacements are shown in Figure 4b and reveal the expected movement of the sulfur atom. The displacement between snapshots iii and v (just after the sulfur atom jumped to the next gold atom) amounts to 2.8 Å, which is close to the gold−gold bond length of 2.89 Å in the simulated leads. The molecule in snapshots i, iii, and v is close to its relaxed gas-phase configuration (discussed below) and exhibits a low conductance. Upon further stretching, the conductance rises until it eventually levels off and reaches a local maximum at snapshots ii and iv. At this point, the sulfur anchor slips onto the next gold atom, thus releasing the mechanical tension in the molecule and restoring the conductance to a low value (panels iii and v). After the sulfur atom has reached the last gold atom of the upper lead, it finally loses its connection: the junction breaks and the molecule snaps back, as shown in snapshot vi. Thus, distancing of the



DOI: 10.1021/acs.nanolett.8b02810
Nano Lett. 2018, 18, 5981−5988

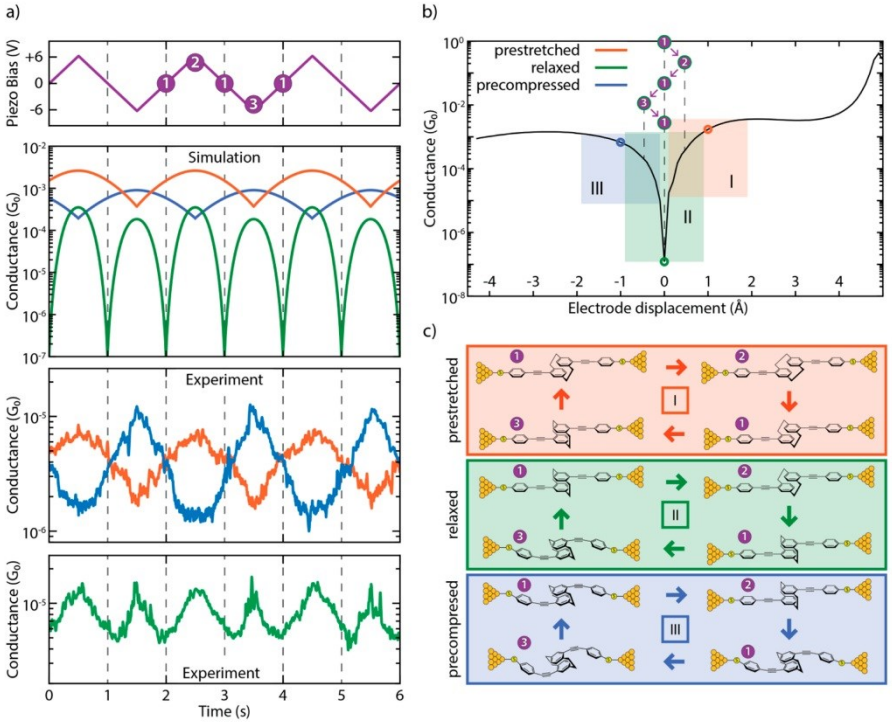


**Figure 6.** (a, top panels) Simulation of conductance traces (second panel) when the electrode displacement is periodically modulated (top panel) for three different trapping configurations: pre-stretched (orange), relaxed (green), and pre-compressed (blue). Centers of oscillation at +1, 0, and −1 Å, respectively; amplitude of 0.5 Å. (a, bottom panels) Zoomed-in panel showing the experimental distance-modulation traces presented in Figure 3. (b) Calculated conductance vs electrode displacement. The blue, green, and orange areas (I, II, and III, respectively) show the portion of the curve spanned in the case of different starting positions (pre-compressed, relaxed, and pre-stretched, represented by circles in the same colors). The numbers in the purple circles represent the position of the electrodes along the oscillation period in the case of a relaxed trapping configuration. (c) Schematics of the molecular configurations along a period of electrode distance modulation. Different starting configurations are represented with different colors: pre-stretched in orange, relaxed in green, and pre-compressed in blue. White numbers in purple circles represent the position of the electrodes along the oscillation period. Note that the molecular compression and elongation in the simulation is 0.5 Å, a value smaller than the gap-size variation in the experiment. This can be rationalized by the elastic response of the sulfur−gold connections and of the gold atoms in the electrodes themselves.

electrodes leads to a stick−slip-like motion of the molecule along the surface of one of the electrodes.

In a detailed analysis of the displacement-dependent conductance, we study the molecule between two hollow leads, in which each sulfur binds to three gold atoms of the respective lead. This allows us to concentrate on the deformations of the actual molecule: the rigid bonding of the hollow−hollow configuration ensures that the lead displacement is directly passed to the molecule, minimizing deformations of the lead-molecule bonds. Starting from the configuration with minimal energy, corresponding to a molecule close to its relaxed state in the gas phase, the leads are either separated farther apart (positive displacement) or brought closer together (negative displacement), thereby stretching or compressing the molecule. The resulting conductance shows a pronounced dip at a well-determined displacement, which we define here as zero (see Figure 5b). The conductance rapidly increases when the molecule is either stretched or compressed from this position. The deformation in the stretched molecule is mainly identified with the shifting of the stacked benzene rings.

By evaluating the transmission in an energy range between −2 and +3 eV around the Fermi energy $E_F$ for each displacement step, we obtain the transmission map in Figure 5c. It reveals a transmission valley (purple diagonal line) between the traces related to the molecular frontier orbitals (yellow horizontal lines). The conductance dip in Figure 5b can be traced back to the intersection of the transmission valley and the Fermi energy. In other words, the energy position of the dip can be tuned by the lead separation. In the following, we present the underlying mechanism based on quantum interference of the molecular frontier orbitals.

A closer look at Figure 5c reveals HOMO and LUMO pairs that arise from the HOMO and LUMO states of the OPE units and are typically slightly split by the weak coupling through the PC core. To distinguish the character of the HOMO−1, HOMO, LUMO, and LUMO+1, we relate them to the frontier orbitals in the gas phase. For this purpose, we introduce the abbreviations GPH−1 to GPL+1, where GPH and GPL denote the gas-phase HOMO and LUMO, respectively. The orbitals are either symmetric (GPH and GPL) or anti-symmetric (GPH−1 and GPL+1) with respect to the center of the molecule. The crucial aspect is now that the energy of the frontier orbitals depends on the displacement. The states within HOMO and LUMO pairs, GPH−1 and GPH as well as GPL and GPL+1, eventually change their energetic order in



DOI: 10.1021/acs.nanolett.8b02810
Nano Lett. 2018, 18, 5981−5988

the studied displacement window between around −4 to +4 Å. The displacements of the degeneracy points, at which these reversals take place, differ for the occupied and unoccupied states. They are located at $d$ = −1.0 and +2.0 Å, respectively, as marked by circles in Figure 5c. According to the theory of quantum interference[12,35] the orbital symmetry leads to a pronounced destructive interference feature in the HOMO−LUMO gap between displacements from −1.0 to +2.0 Å when the HOMO and LUMO pairs are ordered as in the gas phase. Outside of this displacement window, the molecular orbital pairs GPH−1 and GPH or GPL and GPL+1 rearrange in energy, thereby lifting the condition for destructive interference. Indeed, we can reproduce the main features of the conductance map by considering the displacement-dependent energies of the four frontier orbitals and their symmetries, as corroborated further in section III of the Supporting Information.

**Discussion and Concluding Remarks.** With the insights provided by the DFT calculations, the pronounced conductance oscillations can be explained through quantum interference of frontier orbitals in combination with the molecule acting as a spring when subject to mechanical deformations. Its relaxed conformation corresponds to the situation in which the anti-resonance originating from destructive interference of the HOMO and LUMO is in the vicinity of the Fermi energy, yielding a low-conductance state. By stretching or compressing the molecule, the anti-resonance is moved away from the Fermi energy, which leads to an increase of the conductance. The experimentally observed oscillations in conductance during continuous opening of the junction (Figure 2b) can then be associated with the stick−slip motion of the anchoring sulfur atoms on the gold surface, as this process releases the built-up mechanical strain in a semi-periodic fashion. Ab initio molecular-dynamics calculations at room temperature predict that Au−Au bonds should break instead of the Au−S bonds.[36] However, if a gold adatom attached to a sulfur anchor was dragged along the gold electrode instead of the S itself, this would not lead to a qualitative change of the stick−slip picture.

The different behaviors (in-phase, antiphase, and frequency doubling) observed in the distance-modulation measurements (simulation: second panel in Figure 6a; experiment: bottom two panels in Figure 6a) can be attributed to variations in the initial molecular configuration at the beginning of the modulation. Traces that are in phase with the gap modulation are related to molecules that are pre-stretched in the starting configuration (orange panel in Figure 6c and the "pre-stretched" video in the Supporting Information). The starting point is at positive displacement and the oscillation takes place at the right lobe of the conductance curve (orange area in Figure 6b): an increase in electrode displacement corresponds to a higher conductance (and a decrease to a lower conductance). Along a similar line, traces in antiphase with the gap modulation can be related to molecules that are pre-compressed in the starting configuration (blue panel in Figure 6c and the "pre-compressed" video in the Supporting Information) and therefore correspond to oscillations at the left lobe of the conductance curve (blue area in Figure 6b). Traces with a doubled frequency (such as the green trace in Figure 6a and the "relaxed" video in the Supporting Information) are related to molecules that are close to the relaxed gas-phase geometry, in which the Fermi energy of the leads is aligned with the position of the interference dip (green panel, Figure 6c). In this case, the conductance dip is crossed two times during each piezo-modulation period, therefore doubling the frequency of the measured conductance, as can be seen by following the purple steps in Figure 6b. The appearance of the doubled frequency is thus a direct proof of the existence of the destructive interference dip. Importantly, the ability to mechanically tune the position of this dip to be located at the Fermi energy can be exploited in future studies and applications of quantum interference effects.

We note that the conductance variations as a function of displacement can be used to estimate the gauge factor, characterizing the piezoresistive response of the molecular spring. The gauge factor is defined as the relative conductance change divided by displacement normalized to the molecular length (see Figure 3b and Supporting Information section II-4 for more details). We find gauge factors exhibiting a wide distribution with a peak located at $GF$ = 5 and a tail at higher values, reaching up to 40 orders of magnitude larger than those that have been reported on single DNA molecules.[37] We expect that thermally occupied ring rotations of the OPE rods at room temperature will reduce the electronic coupling in the molecule and the electron delocalization and, hence, the conductance. Besides the known shortcomings of DFT with regard to the description of level alignments,[38] this could explain part of the over-estimation of the theoretically predicted conductance values in our static DFT geometries. In addition, longitudinal vibrations, as well as thermal fluctuations, will lead to gap-size modulations and an effective averaging over a range of junction configurations. Such vibrationally induced decoherence effects will wash out the interference-induced conductance minimum.[39] Therefore, a precise control of the temperature may turn out to be crucial in the optimization of gauge factors, and the molecule studied here appears to be an ideal candidate with which to investigate quantum interference effects at lower temperatures and to quantify if decoherence limits the room-temperature performance.[39−41] To achieve even-higher gauge factors, it would also be interesting to explore different chemical designs based on the mechanical manipulation principle of quantum interference.

**Methods.** *MCBJ Experiments.* For MCBJ experiments, a thin (<100 nm) gold wire is lithographically fabricated and suspended on a flexible substrate. Atomically sharp electrodes are formed when rupturing the wire in a three-point bending configuration. After the breaking of the wire, the electrodes can be fused together again by reducing the mechanical force used to bend the substrate. This opening and closing of the gap can be controlled with sub-nanometer accuracy on the position of the electrodes. Further details about the MCBJ setup and the measuring technique have been described elsewhere.[29,30] The molecule was dissolved in dichloromethane, and the solution was drop-cast on the MCBJ sample after the characterization of the bare device (Figure S10). All measurements were performed in air at room temperature after the evaporation of the solvent. Concentrations of 9 $\mu$M (samples A and B), 90 $\mu$M (sample C), and 900 $\mu$M (sample D) have been used, but no significant dependence on the concentration has been observed.

*Fast-Breaking Measurements.* Fast-breaking measurements were performed by applying a bias of 100 mV and using a constant pulling speed of the electrodes of 4.0 nm/s. The conductance is recorded until it falls below the noise level, which is about $5{\cdot}10^{-7}$ $G_0$ in our setup. At this point the



DOI: 10.1021/acs.nanolett.8b02810
Nano Lett. 2018, 18, 5981−5988

electrodes are fused back and a new trace is recorded. A total of 3000 such traces were recorded for samples A–C and 5000 for sample D. Further information on the technique can be found in Frisenda et al.[31]

*Distance-Modulation Measurements.* In these measurements, the electrode spacing was modulated to periodically increase and decrease.[32] The MCBJ was initially stretched to a few-atom width (3 $G_0$) and allowed to self-break by its surface tension to form atomically sharp electrodes. Then, the electrodes were separated by 1.75 nm, which is approximately the estimated length of the unstretched molecule. At this point, a 0.5 Hz triangular wave was applied to the piezoelectric stack that controls the electrode positions with a peak-to-peak gap size variation of 5.0 Å (Figure 3) or 2.5 Å (Figure S12), depending on the amplitude of the applied piezo voltage. Note that a higher voltage on the piezoelectric corresponds to a larger electrode separation.

The initial opening of the junction allows us to recognize if trapping of a molecule occurs because, for a displacement of 1.75 nm, the tunnelling conductance in the absence of a molecule is below the noise level of our setup. The modulation was kept for 120 s, after which the junction was stretched until the noise level was reached and fused back again to start a new cycle. It should be noted that the initial configuration in a distance-modulation experiment cannot be controlled.

*Simulations.* DFT calculations were carried out with TURBOMOLE.[42] We used the def-SVP basis set and the PBE functional.[43,44] During structural relaxations the total energy was converged to $10^{-6}$ au and the maximum norm of the Cartesian gradient to $10^{-3}$ au. The electronic transmission was evaluated with a proprietary cluster-based framework. The procedure includes the separation of the system into semi-infinite leads and a central part, which contains the molecule and parts of the electrodes. The energy-dependent transmission function is expressed in terms of non-equilibrium Green's functions (NEGFs) of the leads and the central part. The bulk parameters of the leads were extracted from a cluster of 1415 gold atoms. Further details on the method can be found in Pauly et al.[34]

## ■ ASSOCIATED CONTENT

### Supporting Information

The Supporting Information is available free of charge on the ACS Publications website at DOI: 10.1021/acs.nanolett.8b02810.

Details on the synthesis and characterization of the molecules, crystal data and structure refinement, additional fast-breaking and distance-modulation measurements, statistical analysis, and the transport calculations (PDF)

A movie showing a simulation of the stick-slip motion (MPG)

A movie showing a simulation of a distance-modulation trace with a molecule pre-stretched in the starting configuration (MPG)

A movie showing a simulation of a distance-modulation trace with a molecule pre-compressed in the starting configuration (MPG)

A movie showing a simulation of a distance-modulation trace with a molecule relaxed in the starting configuration (MPG)

## ■ AUTHOR INFORMATION


### Corresponding Authors

*E-mail: marcel.mayor@unibas.ch (chemistry matters).
*E-mail: fabian.pauly@oist.jp (theoretical calculations).
*E-mail: h.s.j.vanderzant@tudelft.nl (experiments).

### ORCID

Davide Stefani: 0000-0002-9406-9265
Marcel Mayor: 0000-0002-8094-7813
Fabian Pauly: 0000-0001-8017-2379


### Author Contributions

D.S., K.J.W., and M.S. contributed equally. D.S., C.H., K.J.W., M.M.m and H.S.J.Z. conceived of and designed the experiment. M.L.P. assembled the MCBJ setup. M.L.P., D.S., and C.H. wrote the software used for the experiments. D.S. and C.H. performed the break-junction experiments and the data analysis. K.J.W. and M.M. provided and characterized the molecule. M.S. and F.P. performed transport calculations. All authors wrote the manuscript.

### Notes

The authors declare no competing financial interest.

## ■ ACKNOWLEDGMENTS

The authors in Basel and Delft acknowledge financial support by the European FP7-ITN MOLESCO (project no. 606728) and the H2020 FET QuIET (project no. 767187). The work at the University of Basel was also supported by the Swiss National Science Foundation (SNF, grant no. 200020-178808) and the Swiss Nanoscience Institute (SNI); the work at TU Delft was supported by the EU through an advanced ERC grant (Mols@Mols). M.S. and F.P. acknowledge funding through the Collaborative Research Centre (SFB) 767 of the German Research Foundation (DFG) as well as computational resources provided by the state of Baden-Württemberg through bwHPC and the DFG through grant no. INST 40/467-1 FUGG. Device fabrication was done at the Kavli Nanolab at Delft. D.S. thanks Riccardo Frisenda for fruitful discussions. K.J.W. thanks Markus Neuburger for single-crystal X-ray analysis.

## ■ REFERENCES


(1) van der Molen, S.; Naaman, R.; Scheer, E.; Neaton, J.; Nitzan, A.; Natelson, D.; Tao, N.; van der Zant, H.; Mayor, M.; Ruben, M.; Reed, M.; Calame, M. *Nat. Nanotechnol.* **2013**, *8*, 385–389.
(2) Aradhya, S.; Venkataraman, L. *Nat. Nanotechnol.* **2013**, *8*, 399–410.
(3) Sun, L.; Diaz-Fernandez, Y.; Gschneidtner, T.; Westerlund, F.; Lara-Avila, S.; Moth-Poulsen, K. *Chem. Soc. Rev.* **2014**, *43*, 7378–7411.
(4) Xiang, D.; Wang, X.; Jia, C.; Lee, T.; Guo, X. *Chem. Rev.* **2016**, *116*, 4318–4440.
(5) Wang, L.; Wang, L.; Zhang, L.; Xiang, D. *Top. Curr. Chem.* **2017**, *375*, 85.
(6) Quek, S.; Kamenetska, M.; Steigerwald, M.; Choi, H.; Louie, S.; Hybertsen, M.; Neaton, J.; Venkataraman, L. *Nat. Nanotechnol.* **2009**, *4*, 230–234.
(7) Su, T.; Li, H.; Steigerwald, M.; Venkataraman, L.; Nuckolls, C. *Nat. Chem.* **2015**, *7*, 215–220.
(8) Li, Y.; Haworth, N.; Xiang, L.; Ciampi, S.; Coote, M.; Tao, N. *J. Am. Chem. Soc.* **2017**, *139*, 14699–14706.
(9) Frisenda, R.; Harzmann, G.; Celis Gil, J.; Thijssen, J.; Mayor, M.; van der Zant, H. *Nano Lett.* **2016**, *16*, 4733–4737.
(10) Wu, S.; González, M.; Huber, R.; Grunder, S.; Mayor, M.; Schönenberger, C.; Calame, M. *Nat. Nanotechnol.* **2008**, *3*, 569–574.




DOI: 10.1021/acs.nanolett.8b02810
*Nano Lett.* 2018, 18, 5981–5988

(11) Schneebeli, S.; Kamenetska, M.; Cheng, Z.; Skouta, R.; Friesner, R.; Venkataraman, L.; Breslow, R. *J. Am. Chem. Soc.* **2011**, *133*, 2136−2139.
(12) Nozaki, D.; Lücke, A.; Schmidt, W. *J. Phys. Chem. Lett.* **2017**, *8*, 727−732.
(13) Solomon, G.; Vura-Weis, J.; Herrmann, C.; Wasielewski, M.; Ratner, M. *J. Phys. Chem. B* **2010**, *114*, 14735−14744.
(14) Frisenda, R.; Janssen, V.; Grozema, F.; van der Zant, H.; Renaud, N. *Nat. Chem.* **2016**, *8*, 1099−1104.
(15) Lambert, C. *Chem. Soc. Rev.* **2015**, *44*, 875−888.
(16) Schwarz, F.; Kastlunger, G.; Lissel, F.; Egler-Lucas, C.; Semenov, S.; Venkatesan, K.; Berke, H.; Stadler, R.; Lörtscher, E. *Nat. Nanotechnol.* **2016**, *11*, 170−176.
(17) Koole, M.; Thijssen, J.; Valkenier, H.; Hummelen, J.; van der Zant, H. *Nano Lett.* **2015**, *15*, 5569−5573.
(18) Darwish, N.; Díez-Pérez, I.; Da Silva, P.; Tao, N.; Gooding, J.; Paddon-Row, M. *Angew. Chem., Int. Ed.* **2012**, *51*, 3203−3206.
(19) Atesci, H.; Kaliginedi, V.; Celis Gil, J.; Ozawa, H.; Thijssen, J.; Broekmann, P.; Haga, M.; van der Molen, S. *Nat. Nanotechnol.* **2018**, *13*, 117−121.
(20) Li, X.; Staykov, A.; Yoshizawa, K. *Bull. Chem. Soc. Jpn.* **2012**, *85*, 181−188.
(21) Brown, C.; Farthing, A. *Nature* **1949**, *164*, 915−916.
(22) Vorontsova, N.; Rozenberg, V.; Sergeeva, E.; Vorontsov, E.; Starikova, Z.; Lyssenko, K. A.; Hopf, H. *Chem. - Eur. J.* **2008**, *14*, 4600−4617.
(23) Carlotti, M.; Kovalchuk, A.; Wächter, T.; Qiu, X.; Zharnikov, M.; Chiechi, R. *Nat. Commun.* **2016**, *7*, 13904.
(24) Häkkinen, H. *Nat. Chem.* **2012**, *4*, 443−455.
(25) Zafra, J.; Molina Ontoria, A.; Mayorga Burrezo, P.; Peña-Alvarez, M.; Samoc, M.; Szeremeta, J.; Ramírez, F.; Lovander, M.; Droske, C.; Pappenfus, T.; Echegoyen, L.; López Navarrete, J.; Martin, N.; Casado, J. *J. Am. Chem. Soc.* **2017**, *139*, 3095−3105.
(26) Seferos, D.; Trammell, S.; Bazan, G.; Kushmerick, J. *Proc. Natl. Acad. Sci. U. S. A.* **2005**, *102*, 8821−8825.
(27) Bondarenko, L.; Dix, I.; Hinrichs, H.; Hopf, H. *Synthesis* **2004**, *2004*, 2751−2759.
(28) Shi, Z.; Wang, L.; Wang, H.; Cao, X.; Zhang, H. *Org. Lett.* **2007**, *9*, 595−598.
(29) Martin, C.; Ding, D.; van der Zant, H.; van Ruitenbeek, J. *New J. Phys.* **2008**, *10*, 065008.
(30) Martin, C.; Smit, R.; van Egmond, R.; van der Zant, H.; van Ruitenbeek, J. *Rev. Sci. Instrum.* **2011**, *82*, 053907.
(31) Frisenda, R.; Perrin, M.; Valkenier, H.; Hummelen, J.; van der Zant, H. *Phys. Status Solidi B* **2013**, *250*, 2431−2436.
(32) Xia, J.; Diez-Perez, I.; Tao, N. *Nano Lett.* **2008**, *8*, 1960−1964.
(33) Tsutsui, M.; Shoji, K.; Taniguchi, M.; Kawai, T. *Nano Lett.* **2008**, *8*, 345−349.
(34) Pauly, F.; Viljas, J.; Huniar, U.; Häfner, M.; Wohlthat, S.; Bürkle, M.; Cuevas, J.; Schön, G. *New J. Phys.* **2008**, *10*, 125019.
(35) Yoshizawa, K.; Tada, T.; Staykov, A. *J. Am. Chem. Soc.* **2008**, *130*, 9406−9413.
(36) Krüger, D.; Fuchs, H.; Rousseau, R.; Marx, D.; Parrinello, M. *Phys. Rev. Lett.* **2002**, *89*, 186402.
(37) Bruot, C.; Palma, J.; Xiang, L.; Mujica, V.; Ratner, M.; Tao, N. *Nat. Commun.* **2015**, *6*, 8032.
(38) Quek, S.; Venkataraman, L.; Choi, H.; Louie, S.; Hybertsen, M.; Neaton, J. *Nano Lett.* **2007**, *7*, 3477−3482.
(39) Ballmann, S.; Härtle, R.; Coto, P.; Elbing, M.; Mayor, M.; Bryce, M.; Thoss, M.; Weber, H. *Phys. Rev. Lett.* **2012**, *109*, 056801.
(40) Selzer, Y.; Cabassi, M.; Mayer, T.; Allara, D. *Nanotechnology* **2004**, *15*, 483−488.
(41) Kamenetska, M.; Widawsky, J.; Dell'Angela, M.; Frei, M.; Venkataraman, L. *J. Chem. Phys.* **2017**, *146*, 092311.
(42) Ahlrichs, R.; Bär, M.; Häser, M.; Horn, H.; Kölmel, C. *Chem. Phys. Lett.* **1989**, *162*, 165−169.
(43) Schäfer, A.; Horn, H.; Ahlrichs, R. *J. Chem. Phys.* **1992**, *97*, 2571−2577.
(44) Perdew, J.; Burke, K.; Ernzerhof, M. *Phys. Rev. Lett.* **1996**, *77*, 3865−3868.



DOI: 10.1021/acs.nanolett.8b02810
*Nano Lett.* 2018, 18, 5981−5988

## A Tetrasubstituted Helically Chiral Macrocycle with Anchoring Groups for Gold Electrodes

As demonstrated in this thesis, it is possible to substitute a symmetrically disubstituted pseudo-*para*-[2.2]paracyclophane in such a way that helical chirality is formed. The helical chirality was further stabilized through large substituents which could prevent fast racemization at room temperature and allowed for separation and characterization of the enantiomers. After an elaborate synthesis, the structure was elucidated by conventional analysis, including separation of the enantiomers by HPLC on a chiral stationary phase. Chiroptical spectroscopy allowed for the assignment of the absolute configuration as confirmed through DFT calculations. According to variable temperature EXSY spectroscopy and HPLC analysis, the free energy of racemization was around 91 kJ $mol^{-1}$. The racemization of both species proceeds through Mislow's Euclidean rubber glove enantiomerization mechanism. The investigation of a disubstituted [2.2]paracyclophane with the same ring size had its free energy of racemization at 38 kJ $mol^{-1}$ as was determined by variable temperature NMR experiments.
Furthermore, a molecular wire comprising a pseudo-*para* disubstituted [2.2]paracyclophane was investigated through mechanically controlled break-junction experiments; it was observed that the conductance through the molecule is susceptible to applied compressive or tensile strain. When the electrode distance was elongated rapidly periodic jumps in the conductance traces were observed. DFT calculations allowed to assign these jumps to the anchoring group which moved from gold atom to gold atom in order to release tensile strain on the molecule. Subjecting the molecule to self-breaking measurements revealed complex conductance behavior upon periodic alteration of the electrode distance. The preconfiguration of the molecule determined the periodicity with which the conductance changed. According to DFT analysis, the relaxed molecule low conductance due to destructive interference. By applying stress or strain on the molecule through moving of the electrodes the interference could be lifted and the conductance increased.

Within the synthesis of the tetrasubstituted [2.2]paracyclophane, an advanced intermediate was developed from which the ultimate target molecule of this thesis was accessible in one step.

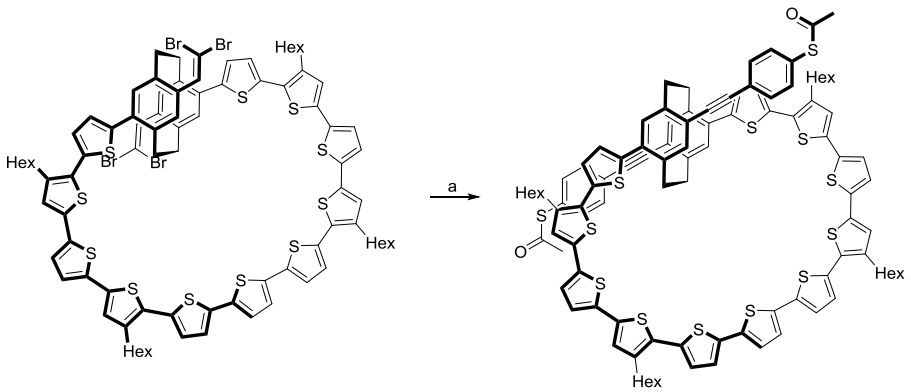


**Figure 1:** Synthesis of the target structure for the investigation on competing conductance pathways. a) 1. LDA, THF, room temperature, 30 min; 2. $Pd(PPh_3)_4$, CuI, THF, diisopropylamine, 55 °C, 2 h.

Molecule **16** from the *Journal of the American Chemical Society* publication was thus reacted with lithium disopropylamide and after completion of the reaction as determined by MALDI-TOF analysis, the crude was reacted with 4-acetylthioiodobenzene in a *Sonogashira-Hagihara* reaction. After aqueous extraction, an isotopic pattern matching the one expected for its elemental composition was observed ($[M]^+$ $C_{104}H_{96}O_2S_{13}$). The compound showed poor stability both in solution and in various purification techniques, it decomposed rapidly on silicon dioxide as well as when subjected to high performance liquid chromatography both on normal- and chiral stationary phase in various solvents. Purification by size-exclusion chromatography (BioBeads, SX-1 in toluene or BioBeads SX-3 in toluene or dichloromethane) or recycling gel-permeation chromatography in chloroform led to unspecific decomposition products with molecular masses reaching up to 6000 *m/z* according to MALDI-TOF analysis. The small structural difference between the target molecule of this chapter and the target molecule in the *Journal of the American Chemical Society* publication seems to suggest that the thioacetate anchoring group substantially affects the stability of the molecule.

## Outlook

With the obtained knowledge, the project can now be developed in many directions. The following prospects seem especially appealing:

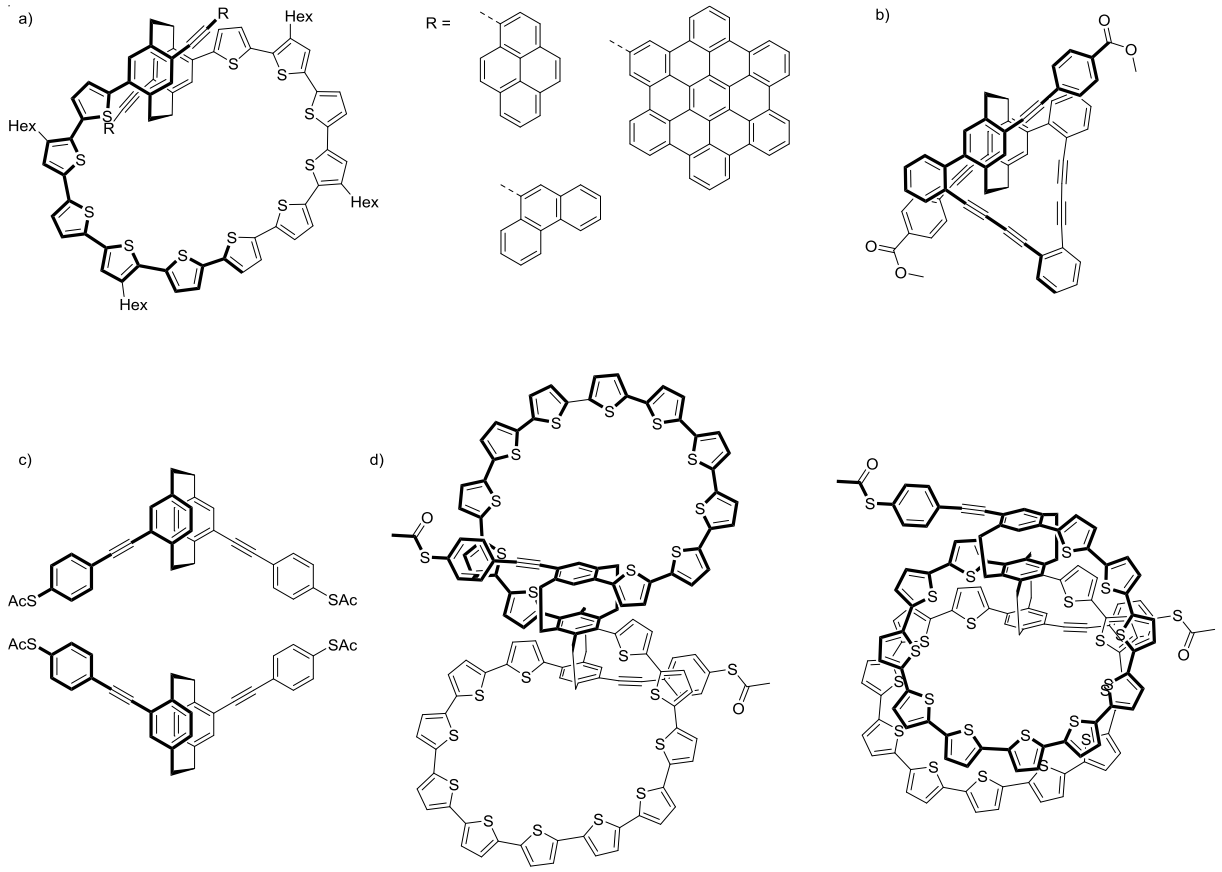


1)

**Figure 2:** Future prospects: a) Changing of the bulky group, which was used to hinder the racemization could be realized through large aromatic building blocks. b) One possible smaller macrocycle which has a more rigid macrocycle around the [2.2]paracyclophane for enhanced chiroptical properties. c) Both enantiomers of a structural isomer of the investigated molecular wire from the *Nano Letters* publication; both enantiomers are shown. d) Two possible conformations of an extended helical structure.

Concerning the work presented in the *Journal of the American Chemical Society* publication, larger substituents on the tetrasubstituted [2.2]paracyclophane should hinder the racemization in such a way that configurationally stable enantiomers could be isolated. Some possible structures are presented in figure 2(a). A more rigid macrocycle instead of the oligothiophenic chain should result in a stable secondary structure, thereby enhancing the chiroptical properties in the ground and excited state. One possible structure is presented in figure 2(b) where the oligothiophenic macrocycle is replaced by *ortho*-disubstituted benzene rings. Such a pattern would be advantageous to realize a substantially smaller macrocycle than the one which is presented within this thesis.

2) Spin-dependent electron transport through organic molecules is an active field of research since selective transport of a single electron spin could find application in many advanced technologies. An appealing molecule for such a measurement would be a structural isomer of the molecule utilized in the

*Nano Letters* publication. Pseudo-*meta* symmetrically disubstituted [2.2] paracyclophane is chiral and cannot racemize without breaking a covalent bond. Both enantiomers of the proposed molecule are presented in figure 2(c).

3) A suitable anchoring group should be employed for the synthesis of a helically chiral macrocycle which can be connected to gold electrodes. An appealing functional group could be pyridine which is connected para with respect to the nitrogen atom.

4) Lastly, the pair of molecules in figure 2(d) could serve as an extension to the work presented in this chapter. If both individual helices of one of the molecules have the same helicity the helical magnetic field should be twice as large as the one for the structure presented above. If the individual helices have their helicity in opposite direction, the magnetic response of this molecule should be zero.

# Supporting Information
# A Chiral Macrocyclic Thiophene with Broken Conjugation – Rapid Racemization through Internal Rotation

Kevin J. Weiland, Nathalia Münch, Wanja Gschwind, Daniel Häussinger, Marcel Mayor

## General Information

### *Reagents and Solvents*

All commercially available compounds were purchased from Sigma-Aldrich, Acros, Apollo Scientific, Alfa Aesar and Fluorochem and used without further purification. Anhydrous solvents were purchased from Sigma-Aldrich and stored over molecular sieves (4 Å). Column chromatography was performed on silica gel P60 (40-63 µm) from Silicycle$^{TM}$, the solvents were technical grade. TLC was performed with silica gel 60 F254 aluminium sheets with a thickness of 0.25 mm purchased from Merck.

### *Synthesis*

All reactions with reagents that are easily oxidized or hydrolyzed were performed under Argon using Schlenk techniques with anhydrous solvents in glassware, which was dried prior to use.

### *Analytics and Instruments*

Recycling gel permeation chromatography (GPC) was performed on a Shimadzu Prominence System equipped with SDV preparative columns from Polymer Standards Service (two Showdex columns in series, 20 x 600 mm each, exclusion limit: 30000 g/mol) with chloroform as solvent. NMR experiments were performed on Bruker Avance III NMR spectrometers operating at 250, 400, 500 or 600 MHz proton frequencies. The instruments were equipped with a direct-observe 5 mm BBFO smart probe (250, 400 and 600 MHz), an indirect-detection 5 mm BBI probe (500 MHz), or a five-channel cryogenic 5 mm QCI probe (600 MHz). All probes were equipped with actively shielded z-gradients (10 A). The chemical shifts are reported in ppm relative to tetramethylsilane or referenced to residual solvent peak and the *J* values are given in Hz (±0.1 Hz). Standard Bruker pulse sequences were used, and the data was processed on Topspin 3.2 (Bruker) using twofold zero-filling in the indirect dimension for all 2D experiments. GC-MS was performed on a Shimadzu GC-MS-2020- SE instrument equipped with a Zebron 5 MS Inferno column, with a temperature range of up to 350 °C. MALDI-TOF mass spectra were recorded on a Bruker MicroFlex LRF spectrometer using *trans*-2-[3-(4-*tert*-Butylphenyl)-2-methyl-propenylidene]malono-nitrile (DCTB) as a matrix. High resolution mass spectra (HRMS) were measured on a Bruker solariX spectrometer with a MALDI source and a Micromass (Waters) AutoSpec Ultima – EI-Sector-MS. Elemental analyses were recorded at room temperature on an Elementar Vario Micro Cube instrument. Melting points were measured on a *Büchi M-565* melting point apparatus and are uncorrected. UV/Vis absorption spectra were

recorded at 20 °C on a Jasco V-770 Spectrophotometer. Emission spectra were recorded with a Horiba Jobin-Yvon FluoroMax 4 fluorimeter.

## 3-(3,5-di-*tert*-butylphenyl)thiophene (2)

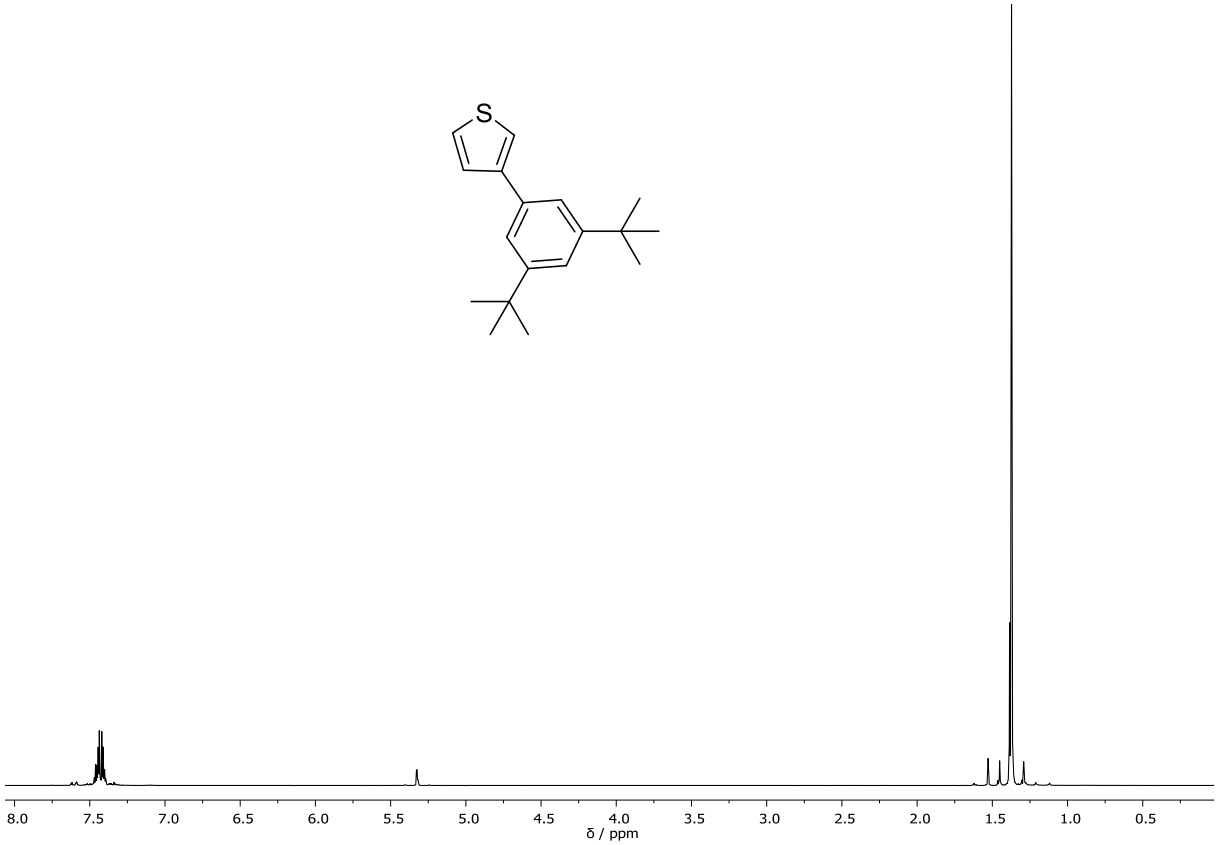


**Figure S1:** $^{1}H$ NMR spectrum (250 MHz, $CD_2Cl_2$) of compound **2**.

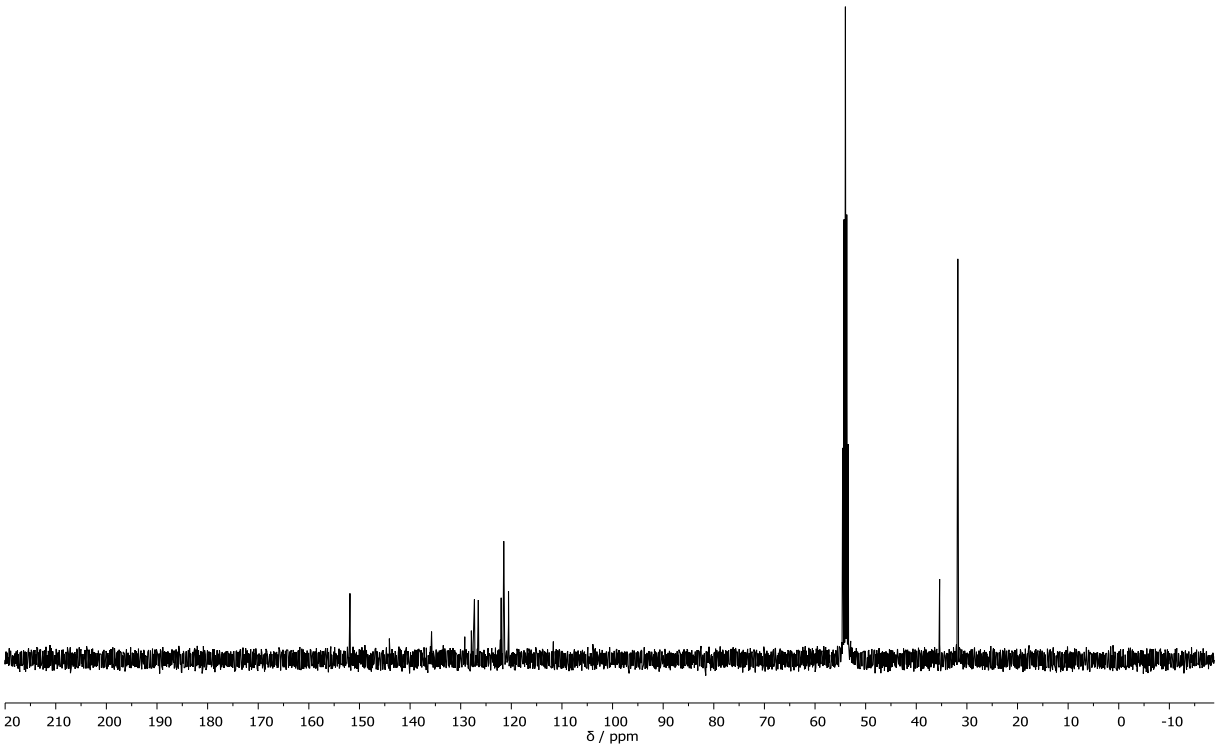


**Figure S2:** $^{13}C$ NMR spectrum (101 MHz, $CD_2Cl_2$) of compound **2**.

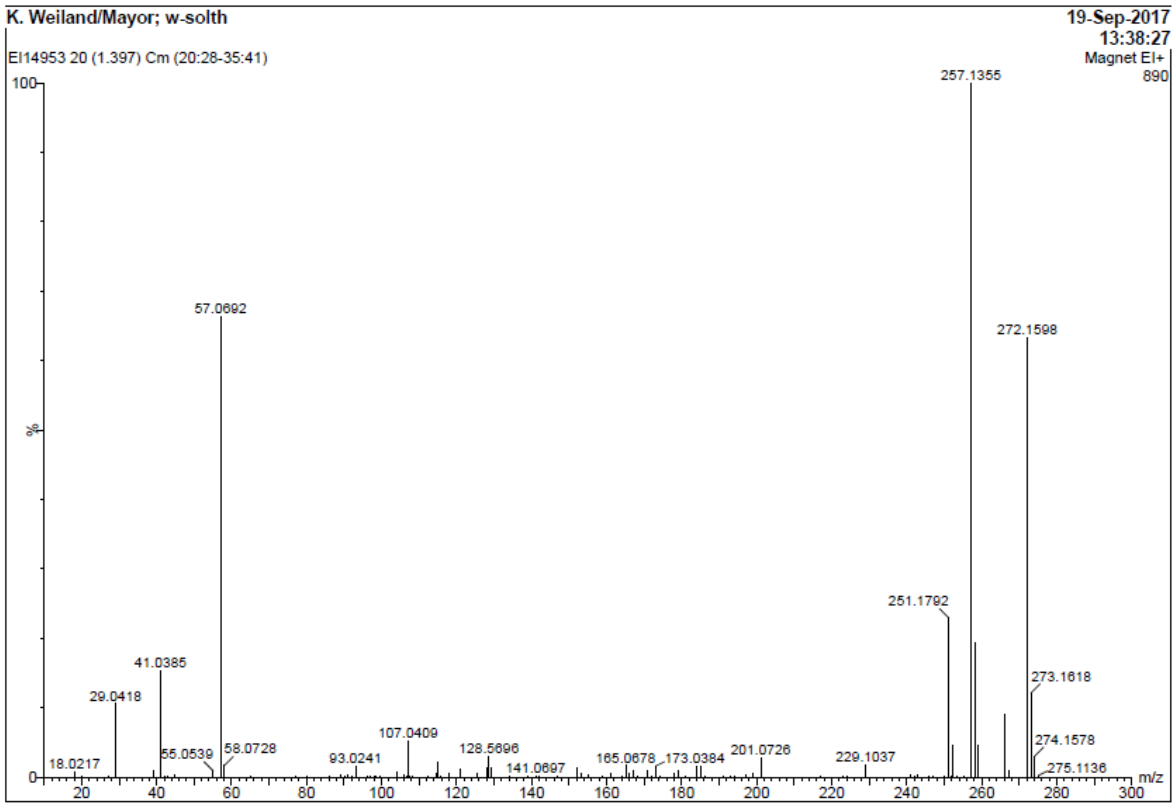


K. Weiland/Mayor; w-solth — 19-Sep-2017 13:38:27 — EI14953 20 (1.397) Cm (20:28-35:41) — Magnet EI+

| No | Mass | Inten | %BPI | %TIC | No | Mass | Inten | %BPI | %TIC | No | Mass | Inten | %BPI | %TIC |
|---|---|---|---|---|---|---|---|---|---|---|---|---|---|---|
| 1: | 18.0217 | 7.00e0 | 0.79 | 0.21 | 74: | 217.0833 | 1.00e0 | 0.11 | 0.03 | | | | | |
| 2: | 20.0151 | 1.00e0 | 0.11 | 0.03 | 75: | 223.1416 | 1.00e0 | 0.11 | 0.03 | | | | | |
| 3: | 27.0269 | 1.00e0 | 0.11 | 0.03 | 76: | 224.1491 | 1.00e0 | 0.11 | 0.03 | | | | | |
| 4: | 29.0418 | 9.40e1 | 10.56 | 2.76 | 77: | 229.1037 | 1.60e1 | 1.80 | 0.47 | | | | | |
| 5: | 39.0229 | 9.00e0 | 1.01 | 0.26 | 78: | 241.1021 | 3.00e0 | 0.34 | 0.09 | | | | | |
| 6: | 41.0385 | 1.37e2 | 15.39 | 4.02 | 79: | 242.1066 | 1.00e0 | 0.11 | 0.03 | | | | | |
| 7: | 42.0422 | 1.00e0 | 0.11 | 0.03 | 80: | 242.9783 | 3.00e0 | 0.34 | 0.09 | | | | | |
| 8: | 43.0535 | 1.00e0 | 0.11 | 0.03 | 81: | 246.0008 | 1.00e0 | 0.11 | 0.03 | | | | | |
| 9: | 44.9782 | 3.00e0 | 0.34 | 0.09 | 82: | 247.0003 | 2.00e0 | 0.22 | 0.06 | | | | | |
| 10: | 55.0539 | 8.00e0 | 0.90 | 0.23 | 83: | 249.9932 | 1.00e0 | 0.11 | 0.03 | | | | | |
| 11: | 57.0692 | 5.91e2 | 66.40 | 17.35 | 84: | 251.1792 | 2.04e2 | 22.92 | 5.99 | | | | | |
| 12: | 58.0728 | 1.50e1 | 1.69 | 0.44 | 85: | 251.7579 | 1.00e0 | 0.11 | 0.03 | | | | | |
| 13: | 66.0377 | 1.00e0 | 0.11 | 0.03 | 86: | 252.1818 | 4.00e1 | 4.49 | 1.17 | | | | | |
| 14: | 77.0373 | 2.00e0 | 0.22 | 0.06 | 87: | 253.1877 | 1.00e0 | 0.11 | 0.03 | | | | | |
| 15: | 80.0154 | 1.00e0 | 0.11 | 0.03 | 88: | 255.1219 | 1.00e0 | 0.11 | 0.03 | | | | | |
| 16: | 86.0162 | 1.00e0 | 0.11 | 0.03 | 89: | 257.1355 | 8.90e2 | 100.00 | 26.12 | | | | | |
| 17: | 89.0395 | 3.00e0 | 0.34 | 0.09 | 90: | 258.1390 | 1.73e2 | 19.44 | 5.08 | | | | | |
| 18: | 90.0482 | 2.00e0 | 0.22 | 0.06 | 91: | 259.1328 | 4.10e1 | 4.61 | 1.20 | | | | | |
| 19: | 91.0531 | 3.00e0 | 0.34 | 0.09 | 92: | 266.2032 | 8.00e1 | 8.99 | 2.35 | | | | | |
| 20: | 92.0173 | 1.00e0 | 0.11 | 0.03 | 93: | 267.2039 | 9.00e0 | 1.01 | 0.26 | | | | | |
| 21: | 93.0241 | 1.40e1 | 1.57 | 0.41 | 94: | 272.1598 | 5.64e2 | 63.37 | 16.55 | | | | | |
| 22: | 96.0452 | 1.00e0 | 0.11 | 0.03 | 95: | 272.2810 | 1.00e0 | 0.11 | 0.03 | | | | | |
| 23: | 97.0109 | 2.00e0 | 0.22 | 0.06 | 96: | 273.1618 | 1.08e2 | 12.13 | 3.17 | | | | | |
| 24: | 98.0132 | 2.00e0 | 0.22 | 0.06 | 97: | 274.1578 | 2.70e1 | 3.03 | 0.79 | | | | | |
| 25: | 98.5203 | 1.00e0 | 0.11 | 0.03 | 98: | 275.1136 | 2.00e0 | 0.22 | 0.06 | | | | | |
| 26: | 99.5275 | 1.00e0 | 0.11 | 0.03 | | | | | | | | | | |
| 27: | 104.0628 | 7.00e0 | 0.79 | 0.21 | | | | | | | | | | |
| 28: | 106.0304 | 3.00e0 | 0.34 | 0.09 | | | | | | | | | | |
| 29: | 106.5364 | 1.00e0 | 0.11 | 0.03 | | | | | | | | | | |
| 30: | 107.0409 | 4.60e1 | 5.17 | 1.35 | | | | | | | | | | |
| 31: | 107.5449 | 2.00e0 | 0.22 | 0.06 | | | | | | | | | | |
| 32: | 108.0345 | 1.00e0 | 0.11 | 0.03 | | | | | | | | | | |
| 33: | 112.1456 | 1.00e0 | 0.11 | 0.03 | | | | | | | | | | |
| 34: | 114.5542 | 4.00e0 | 0.45 | 0.12 | | | | | | | | | | |
| 35: | 115.0534 | 1.90e1 | 2.13 | 0.56 | | | | | | | | | | |
| 36: | 115.5591 | 1.00e0 | 0.11 | 0.03 | | | | | | | | | | |
| 37: | 118.0775 | 4.00e0 | 0.45 | 0.12 | | | | | | | | | | |
| 38: | 121.0564 | 1.00e1 | 1.12 | 0.29 | | | | | | | | | | |
| 39: | 126.5891 | 4.00e0 | 0.45 | 0.12 | | | | | | | | | | |
| 40: | 128.0605 | 1.20e1 | 1.35 | 0.35 | | | | | | | | | | |
| 41: | 128.5696 | 2.70e1 | 3.03 | 0.79 | | | | | | | | | | |
| 42: | 129.0697 | 1.20e1 | 1.35 | 0.35 | | | | | | | | | | |
| 43: | 134.0186 | 1.00e0 | 0.11 | 0.03 | | | | | | | | | | |
| 44: | 139.0507 | 1.00e0 | 0.11 | 0.03 | | | | | | | | | | |
| 45: | 141.0697 | 2.00e0 | 0.22 | 0.06 | | | | | | | | | | |
| 46: | 142.0743 | 1.00e0 | 0.11 | 0.03 | | | | | | | | | | |
| 47: | 147.0308 | 1.00e0 | 0.11 | 0.03 | | | | | | | | | | |
| 48: | 152.0619 | 1.10e1 | 1.24 | 0.32 | | | | | | | | | | |
| 49: | 153.0678 | 4.00e0 | 0.45 | 0.12 | | | | | | | | | | |
| 50: | 155.0836 | 3.00e0 | 0.34 | 0.09 | | | | | | | | | | |
| 51: | 159.0213 | 1.00e0 | 0.11 | 0.03 | | | | | | | | | | |
| 52: | 161.0399 | 4.00e0 | 0.45 | 0.12 | | | | | | | | | | |
| 53: | 164.0573 | 1.00e0 | 0.11 | 0.03 | | | | | | | | | | |
| 54: | 165.0678 | 1.50e1 | 1.69 | 0.44 | | | | | | | | | | |
| 55: | 166.0728 | 4.00e0 | 0.45 | 0.12 | | | | | | | | | | |
| 56: | 167.0840 | 8.00e0 | 0.90 | 0.23 | | | | | | | | | | |
| 57: | 168.0901 | 1.00e0 | 0.11 | 0.03 | | | | | | | | | | |
| 58: | 171.0246 | 9.00e0 | 1.01 | 0.26 | | | | | | | | | | |
| 59: | 172.0338 | 1.00e0 | 0.11 | 0.03 | | | | | | | | | | |
| 60: | 173.0384 | 1.40e1 | 1.57 | 0.41 | | | | | | | | | | |
| 61: | 174.0440 | 2.00e0 | 0.22 | 0.06 | | | | | | | | | | |
| 62: | 178.0794 | 4.00e0 | 0.45 | 0.12 | | | | | | | | | | |
| 63: | 179.0844 | 8.00e0 | 0.90 | 0.23 | | | | | | | | | | |
| 64: | 181.1003 | 1.00e0 | 0.11 | 0.03 | | | | | | | | | | |
| 65: | 184.0323 | 1.30e1 | 1.46 | 0.38 | | | | | | | | | | |
| 66: | 185.0389 | 1.40e1 | 1.57 | 0.41 | | | | | | | | | | |
| 67: | 186.0472 | 1.00e0 | 0.11 | 0.03 | | | | | | | | | | |
| 68: | 191.0853 | 1.00e0 | 0.11 | 0.03 | | | | | | | | | | |
| 69: | 193.1012 | 2.00e0 | 0.22 | 0.06 | | | | | | | | | | |
| 70: | 194.0950 | 2.00e0 | 0.22 | 0.06 | | | | | | | | | | |
| 71: | 197.0391 | 3.00e0 | 0.34 | 0.09 | | | | | | | | | | |
| 72: | 199.0570 | 5.00e0 | 0.56 | 0.15 | | | | | | | | | | |
| 73: | 201.0726 | 2.50e1 | 2.81 | 0.73 | | | | | | | | | | |

**Figure S3:** High resolution EI spectrum for compound **2**.

## 2-bromo-3-(3,5-di-*tert*-butylphenyl)thiophene (3)

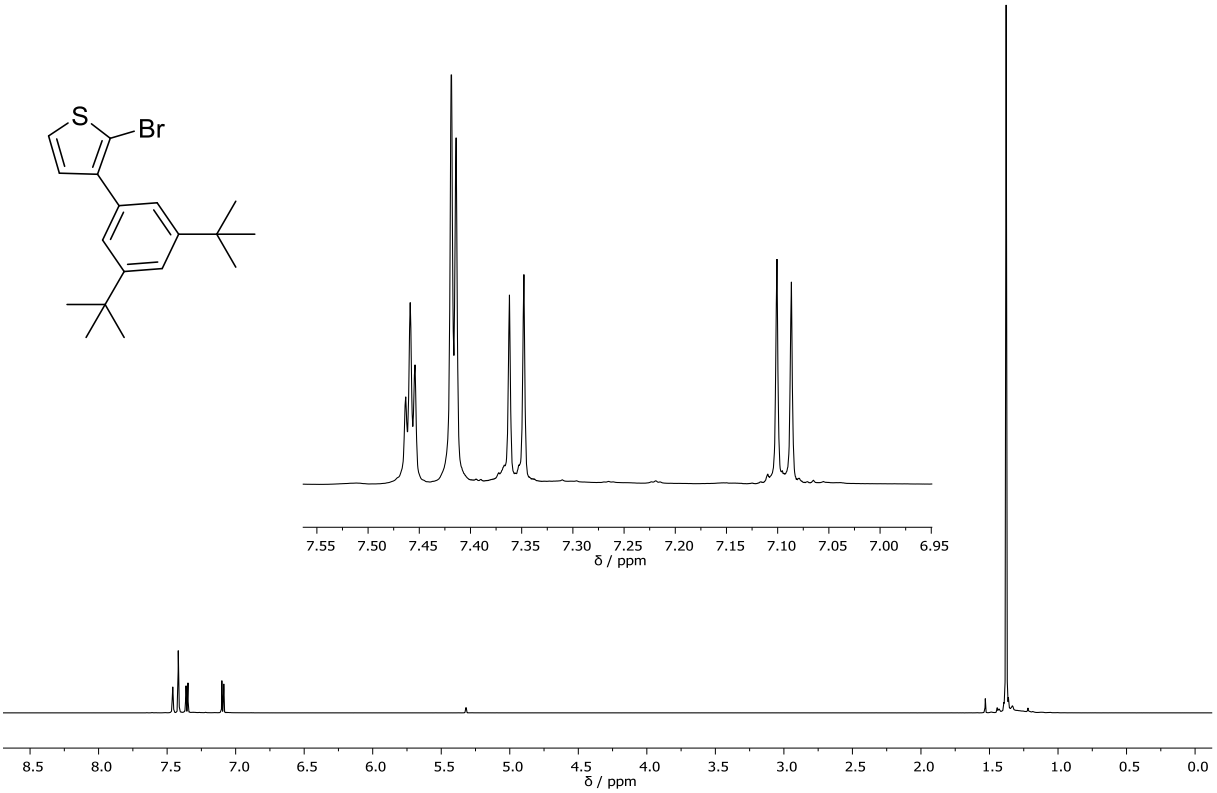


**Figure S4:** $^{1}H$ NMR spectrum (400 MHz, $CD_2Cl_2$) of compound **3**.

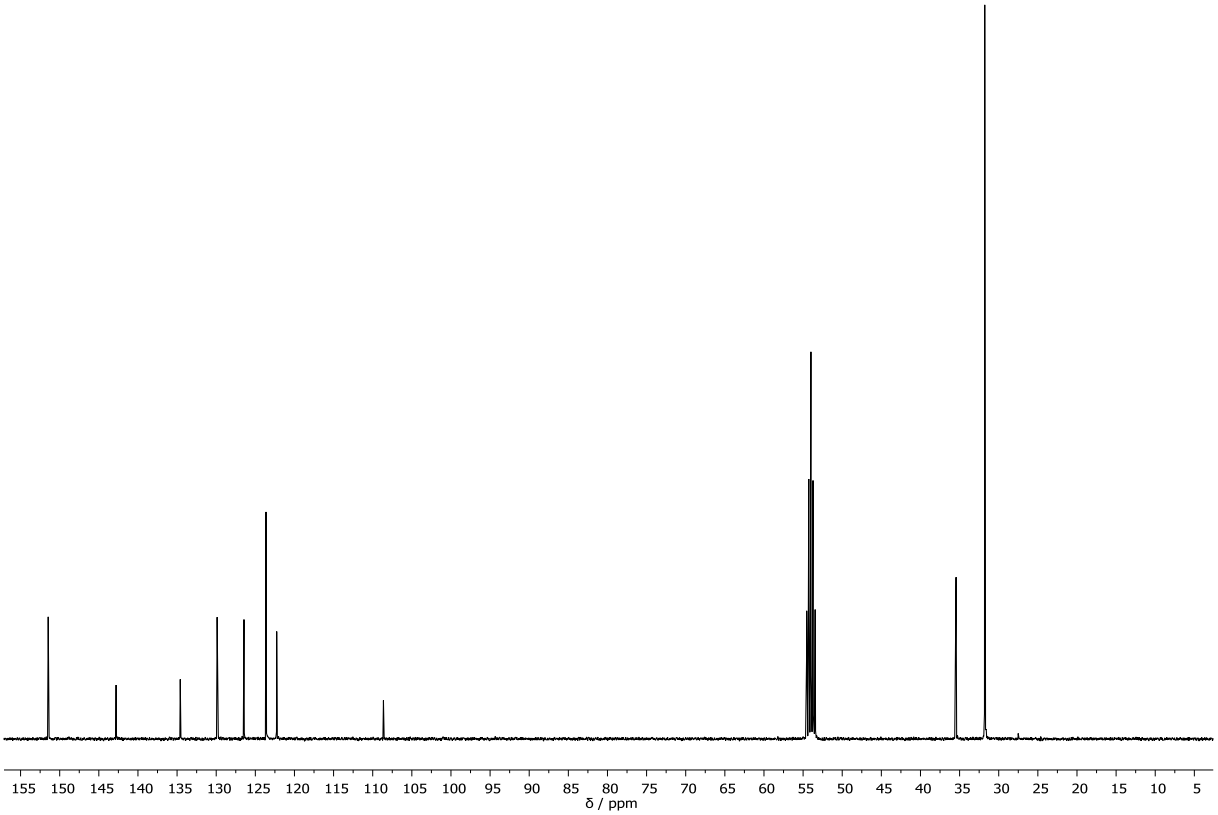


**Figure S5:** $^{13}C$ NMR spectrum (101 MHz, $CD_2Cl_2$) of compound **3**.

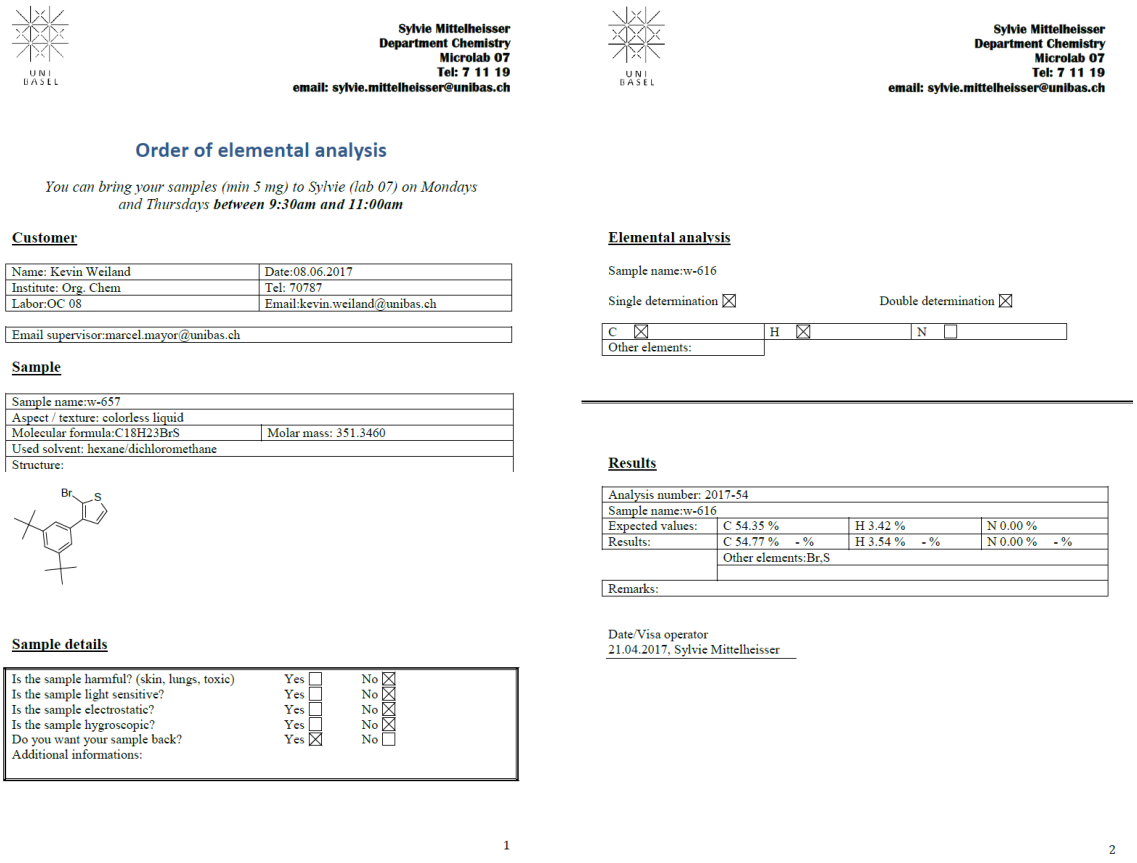

**Sylvie Mittelheisser**
**Department Chemistry**
**Microlab 07**
**Tel: 7 11 19**
**email: sylvie.mittelheisser@unibas.ch**

## Order of elemental analysis

*You can bring your samples (min 5 mg) to Sylvie (lab 07) on Mondays and Thursdays **between 9:30am and 11:00am***

**Customer**

| | |
|---|---|
| Name: Kevin Weiland | Date:08.06.2017 |
| Institute: Org. Chem | Tel: 70787 |
| Labor:OC 08 | Email:kevin.weiland@unibas.ch |

Email supervisor:marcel.mayor@unibas.ch

**Sample**

| | |
|---|---|
| Sample name:w-657 | |
| Aspect / texture: colorless liquid | |
| Molecular formula:C18H23BrS | Molar mass: 351.3460 |
| Used solvent: hexane/dichloromethane | |
| Structure: | |

**Sample details**

| | | |
|---|---|---|
| Is the sample harmful? (skin, lungs, toxic) | Yes ☐ | No ☒ |
| Is the sample light sensitive? | Yes ☐ | No ☒ |
| Is the sample electrostatic? | Yes ☐ | No ☒ |
| Is the sample hygroscopic? | Yes ☐ | No ☒ |
| Do you want your sample back? | Yes ☒ | No ☐ |
| Additional informations: | | |

1

**Sylvie Mittelheisser**
**Department Chemistry**
**Microlab 07**
**Tel: 7 11 19**
**email: sylvie.mittelheisser@unibas.ch**

**Elemental analysis**

Sample name:w-616

Single determination ☒ Double determination ☒

| | | |
|---|---|---|
| C ☒ | H ☒ | N ☐ |
| Other elements: | | |

**Results**

| | | | |
|---|---|---|---|
| Analysis number: 2017-54 | | | |
| Sample name:w-616 | | | |
| Expected values: | C 54.35 % | H 3.42 % | N 0.00 % |
| Results: | C 54.77 % - % | H 3.54 % - % | N 0.00 % - % |
| | Other elements:Br,S | | |
| Remarks: | | | |

Date/Visa operator
21.04.2017, Sylvie Mittelheisser

2

**Figure S6:** Elemental analysis result for compound **3**.

## 2-(3-(3,5-di-tert-butylphenyl)thiophen-2-yl)-4,4,5,5-tetramethyl-1,3,2-dioxaborolane (E)

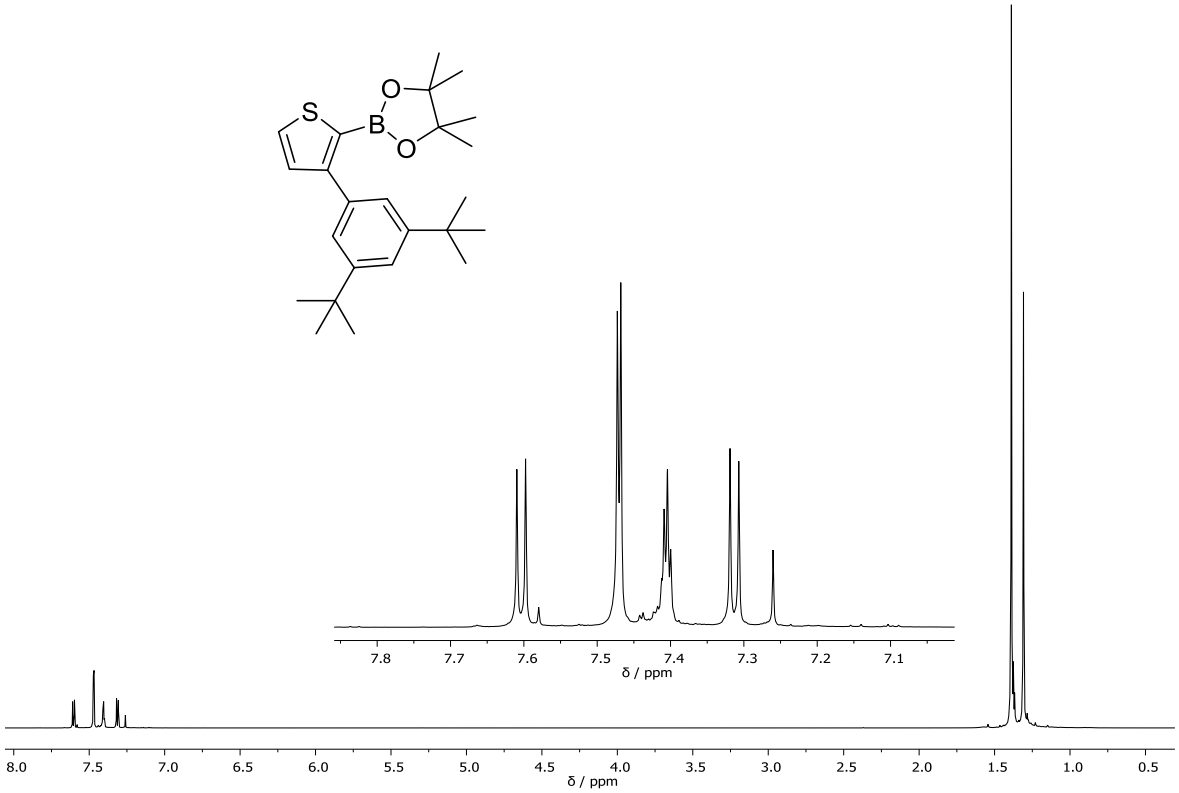


**Figure S7:** $^{1}H$ NMR spectrum (400 MHz, $CDCl_3$) of compound **E**.

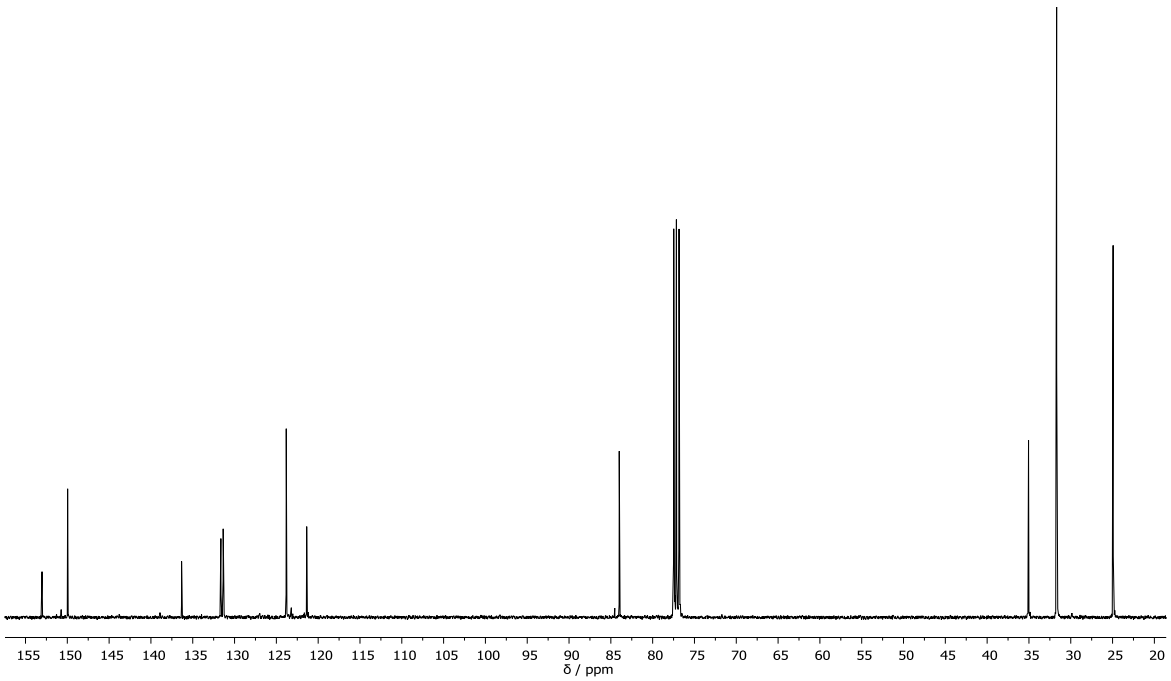


**Figure S8:** $^{13}C$ NMR spectrum (101 MHz, $CDCl_3$) of compound **E**.

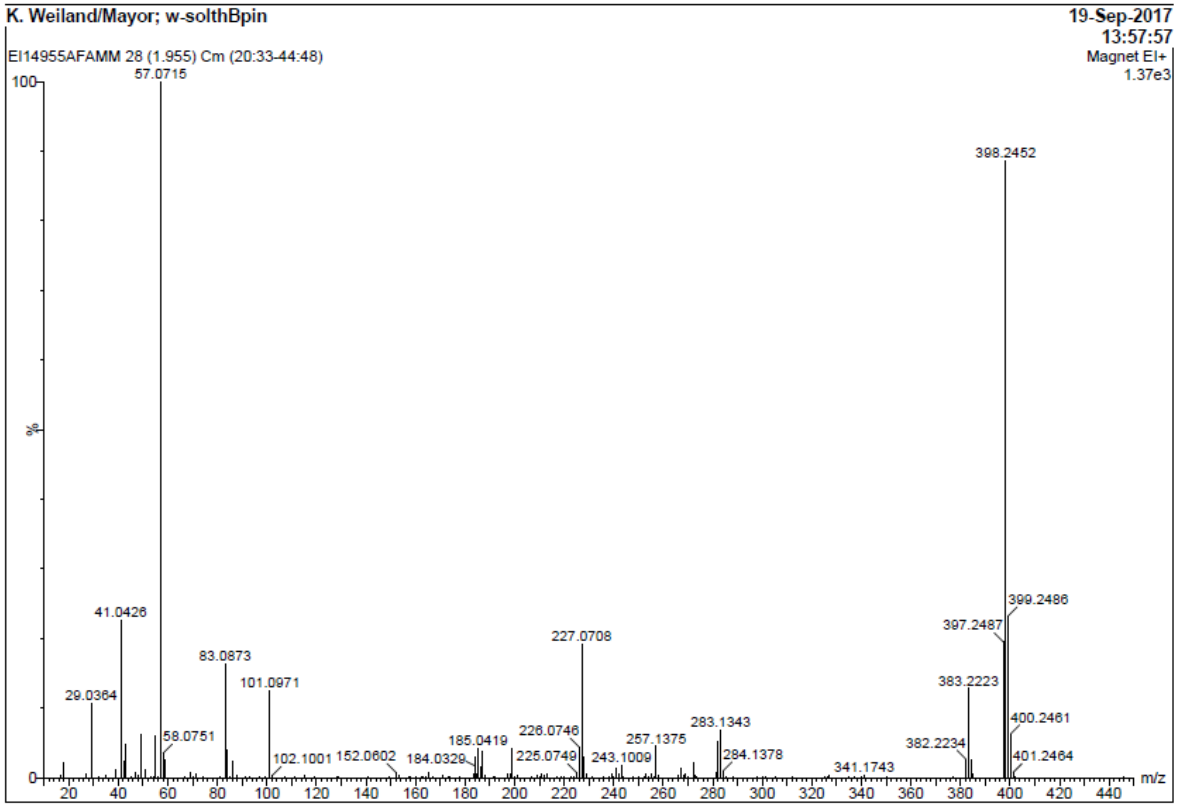


K. Weiland/Mayor; w-solthBpin — 19-Sep-2017 13:57:57

EI14955AFAMM 28 (1.955) Cm (20:33-44:48) — Magnet EI+

| No | Mass | Inten | %BPI | %TIC | No | Mass | Inten | %BPI | %TIC | No | Mass | Inten | %BPI | %TIC |
|---|---|---|---|---|---|---|---|---|---|---|---|---|---|---|
| 1: | 16.9554 | 4.00e0 | 0.29 | 0.06 | 74: | 188.0431 | 4.00e0 | 0.29 | 0.06 | 147: | 327.1602 | 4.00e0 | 0.29 | 0.06 |
| 2: | 17.9668 | 2.80e1 | 2.05 | 0.45 | 75: | 191.6101 | 1.00e0 | 0.07 | 0.02 | 148: | 335.0505 | 2.00e0 | 0.15 | 0.03 |
| 3: | 27.0142 | 8.00e0 | 0.58 | 0.13 | 76: | 192.0944 | 1.00e0 | 0.07 | 0.02 | 149: | 337.0354 | 1.00e0 | 0.07 | 0.02 |
| 4: | 29.0364 | 1.47e2 | 10.74 | 2.34 | 77: | 197.0412 | 6.00e0 | 0.44 | 0.10 | 150: | 340.1747 | 3.00e0 | 0.22 | 0.05 |
| 5: | 31.9893 | 1.00e0 | 0.07 | 0.02 | 78: | 198.0441 | 8.00e0 | 0.58 | 0.13 | 151: | 341.1743 | 5.00e0 | 0.37 | 0.08 |
| 6: | 34.9704 | 4.00e0 | 0.29 | 0.06 | 79: | 199.0482 | 5.80e1 | 4.24 | 0.92 | 152: | 350.0709 | 1.00e0 | 0.07 | 0.02 |
| 7: | 39.0266 | 1.50e1 | 1.10 | 0.24 | 80: | 200.0563 | 2.00e0 | 0.15 | 0.03 | 153: | 376.9830 | 1.00e0 | 0.07 | 0.02 |
| 8: | 40.9718 | 2.00e0 | 0.15 | 0.03 | 81: | 201.0700 | 4.00e0 | 0.29 | 0.06 | 154: | 382.2234 | 3.60e1 | 2.63 | 0.57 |
| 9: | 41.0426 | 3.10e2 | 22.64 | 4.93 | 82: | 207.0459 | 1.00e0 | 0.07 | 0.02 | 155: | 383.2223 | 1.75e2 | 12.78 | 2.78 |
| 10: | 42.0493 | 3.30e1 | 2.41 | 0.52 | 83: | 209.0527 | 4.00e0 | 0.29 | 0.06 | 156: | 384.2255 | 3.60e1 | 2.63 | 0.57 |
| 11: | 43.0214 | 6.60e1 | 4.82 | 1.05 | 84: | 210.0372 | 2.00e0 | 0.15 | 0.03 | 157: | 385.2227 | 6.00e0 | 0.44 | 0.10 |
| 12: | 43.0578 | 6.30e1 | 4.60 | 1.00 | 85: | 210.1338 | 1.00e0 | 0.07 | 0.02 | 158: | 397.2487 | 2.67e2 | 19.50 | 4.25 |
| 13: | 45.0376 | 1.00e0 | 0.07 | 0.02 | 86: | 211.0503 | 8.00e0 | 0.58 | 0.13 | 159: | 398.2452 | 1.21e3 | 88.68 | 19.31 |
| 14: | 46.9702 | 9.00e0 | 0.66 | 0.14 | 87: | 211.0807 | 1.00e0 | 0.07 | 0.02 | 160: | 399.2486 | 3.18e2 | 23.23 | 5.06 |
| 15: | 47.9772 | 4.00e0 | 0.29 | 0.06 | 88: | 212.0533 | 5.00e0 | 0.37 | 0.08 | 161: | 400.2461 | 8.60e1 | 6.28 | 1.37 |
| 16: | 48.9841 | 8.50e1 | 6.21 | 1.35 | 89: | 213.0559 | 8.00e0 | 0.58 | 0.13 | 162: | 401.2464 | 1.00e1 | 0.73 | 0.16 |
| 17: | 50.9818 | 1.60e1 | 1.17 | 0.25 | 90: | 217.1638 | 1.00e0 | 0.07 | 0.02 | 163: | 402.2511 | 1.00e0 | 0.07 | 0.02 |
| 18: | 53.0402 | 1.00e0 | 0.07 | 0.02 | 91: | 219.0419 | 1.00e0 | 0.07 | 0.02 | 164: | 445.9545 | 1.00e0 | 0.07 | 0.02 |
| 19: | 54.0262 | 1.00e0 | 0.07 | 0.02 | 92: | 220.1053 | 1.00e0 | 0.07 | 0.02 | | | | | |
| 20: | 55.0557 | 8.30e1 | 6.06 | 1.32 | 93: | 223.0391 | 2.00e0 | 0.15 | 0.03 | | | | | |
| 21: | 56.0645 | 2.00e0 | 0.15 | 0.03 | 94: | 224.0588 | 2.00e0 | 0.15 | 0.03 | | | | | |
| 22: | 57.0715 | 1.37e3 | 100.00 | 21.77 | 95: | 225.0749 | 9.00e0 | 0.66 | 0.14 | | | | | |
| 23: | 58.0427 | 5.00e0 | 0.37 | 0.08 | 96: | 226.0746 | 6.00e1 | 4.38 | 0.95 | | | | | |
| 24: | 58.0751 | 4.80e1 | 3.51 | 0.76 | 97: | 227.0708 | 2.63e2 | 19.21 | 4.18 | | | | | |
| 25: | 59.0497 | 3.60e1 | 2.63 | 0.57 | 98: | 227.1830 | 1.00e0 | 0.07 | 0.02 | | | | | |
| 26: | 67.0544 | 3.00e0 | 0.22 | 0.05 | 99: | 228.0746 | 4.00e1 | 2.92 | 0.64 | | | | | |
| 27: | 69.0675 | 1.10e1 | 0.80 | 0.17 | 100: | 228.8602 | 1.00e0 | 0.07 | 0.02 | | | | | |
| 28: | 70.0803 | 1.00e0 | 0.07 | 0.02 | 101: | 229.0657 | 8.00e0 | 0.58 | 0.13 | | | | | |
| 29: | 71.0837 | 7.00e0 | 0.51 | 0.11 | 102: | 231.0777 | 1.00e0 | 0.07 | 0.02 | | | | | |
| 30: | 73.9933 | 1.00e0 | 0.07 | 0.02 | 103: | 236.0809 | 1.00e0 | 0.07 | 0.02 | | | | | |
| 31: | 81.0729 | 1.00e0 | 0.07 | 0.02 | 104: | 238.0536 | 1.00e0 | 0.07 | 0.02 | | | | | |
| 32: | 83.0873 | 2.23e2 | 16.29 | 3.55 | 105: | 239.0743 | 7.00e0 | 0.51 | 0.11 | | | | | |
| 33: | 83.9547 | 5.50e1 | 4.02 | 0.87 | 106: | 240.0856 | 2.00e0 | 0.15 | 0.03 | | | | | |
| 34: | 84.0911 | 9.00e0 | 0.66 | 0.14 | 107: | 241.0885 | 1.80e1 | 1.31 | 0.29 | | | | | |
| 35: | 84.9581 | 1.00e0 | 0.07 | 0.02 | 108: | 242.0960 | 7.00e0 | 0.51 | 0.11 | | | | | |
| 36: | 85.9524 | 3.20e1 | 2.34 | 0.51 | 109: | 243.1009 | 2.50e1 | 1.83 | 0.40 | | | | | |
| 37: | 87.9492 | 4.00e0 | 0.29 | 0.06 | 110: | 243.9882 | 1.00e0 | 0.07 | 0.02 | | | | | |
| 38: | 91.0565 | 1.00e0 | 0.07 | 0.02 | 111: | 248.0762 | 1.00e0 | 0.07 | 0.02 | | | | | |
| 39: | 93.0276 | 1.00e0 | 0.07 | 0.02 | 112: | 250.0017 | 1.00e0 | 0.07 | 0.02 | | | | | |
| 40: | 97.1042 | 1.00e0 | 0.07 | 0.02 | 113: | 250.0754 | 1.00e0 | 0.07 | 0.02 | | | | | |
| 41: | 99.0813 | 2.00e0 | 0.15 | 0.03 | 114: | 252.0752 | 2.00e0 | 0.15 | 0.03 | | | | | |
| 42: | 101.0971 | 1.72e2 | 12.56 | 2.74 | 115: | 253.0848 | 6.00e0 | 0.44 | 0.10 | | | | | |
| 43: | 102.1001 | 4.00e0 | 0.29 | 0.06 | 116: | 254.0636 | 1.00e0 | 0.07 | 0.02 | | | | | |
| 44: | 107.0410 | 1.00e0 | 0.07 | 0.02 | 117: | 255.1080 | 8.00e0 | 0.58 | 0.13 | | | | | |
| 45: | 111.0646 | 1.00e0 | 0.07 | 0.02 | 118: | 256.0947 | 1.00e0 | 0.07 | 0.02 | | | | | |
| 46: | 114.9973 | 1.00e0 | 0.07 | 0.02 | 119: | 257.1375 | 6.20e1 | 4.53 | 0.99 | | | | | |
| 47: | 115.0552 | 4.00e0 | 0.29 | 0.06 | 120: | 258.1395 | 5.00e0 | 0.37 | 0.08 | | | | | |
| 48: | 119.0867 | 2.00e0 | 0.15 | 0.03 | 121: | 266.1307 | 4.00e0 | 0.29 | 0.06 | | | | | |
| 49: | 126.0620 | 3.00e0 | 0.22 | 0.05 | 122: | 267.0992 | 8.00e0 | 0.58 | 0.13 | | | | | |
| 50: | 129.0690 | 2.00e0 | 0.15 | 0.03 | 123: | 267.1383 | 1.70e1 | 1.24 | 0.27 | | | | | |
| 51: | 141.0639 | 1.00e0 | 0.07 | 0.02 | 124: | 268.1227 | 4.00e0 | 0.29 | 0.06 | | | | | |
| 52: | 149.0659 | 1.00e0 | 0.07 | 0.02 | 125: | 268.1487 | 1.00e0 | 0.07 | 0.02 | | | | | |
| 53: | 152.0602 | 1.00e1 | 0.73 | 0.16 | 126: | 269.1168 | 7.00e0 | 0.51 | 0.11 | | | | | |
| 54: | 153.0681 | 4.00e0 | 0.29 | 0.06 | 127: | 270.1365 | 1.00e0 | 0.07 | 0.02 | | | | | |
| 55: | 157.0868 | 1.00e0 | 0.07 | 0.02 | 128: | 272.1590 | 2.80e1 | 2.05 | 0.45 | | | | | |
| 56: | 158.0020 | 1.00e0 | 0.07 | 0.02 | 129: | 273.1275 | 5.00e0 | 0.37 | 0.08 | | | | | |
| 57: | 160.0247 | 1.00e0 | 0.07 | 0.02 | 130: | 273.1643 | 2.00e0 | 0.15 | 0.03 | | | | | |
| 58: | 162.5713 | 1.00e0 | 0.07 | 0.02 | 131: | 281.1623 | 1.00e1 | 0.73 | 0.16 | | | | | |
| 59: | 163.0766 | 1.00e0 | 0.07 | 0.02 | 132: | 282.1230 | 3.00e0 | 0.22 | 0.05 | | | | | |
| 60: | 164.0865 | 1.00e0 | 0.07 | 0.02 | 133: | 282.1564 | 7.20e1 | 5.26 | 1.15 | | | | | |
| 61: | 165.0694 | 9.00e0 | 0.66 | 0.14 | 134: | 283.1343 | 9.30e1 | 6.79 | 1.48 | | | | | |
| 62: | 167.0856 | 3.00e0 | 0.22 | 0.05 | 135: | 283.1659 | 7.00e0 | 0.51 | 0.11 | | | | | |
| 63: | 171.0251 | 5.00e0 | 0.37 | 0.08 | 136: | 284.1378 | 1.30e1 | 0.95 | 0.21 | | | | | |
| 64: | 173.0421 | 2.00e0 | 0.15 | 0.03 | 137: | 285.1246 | 1.00e0 | 0.07 | 0.02 | | | | | |
| 65: | 173.9909 | 1.00e0 | 0.07 | 0.02 | 138: | 288.0971 | 1.00e0 | 0.07 | 0.02 | | | | | |
| 66: | 178.0778 | 1.00e0 | 0.07 | 0.02 | 139: | 288.1591 | 2.00e0 | 0.15 | 0.03 | | | | | |
| 67: | 183.6034 | 8.00e0 | 0.58 | 0.13 | 140: | 298.1529 | 3.00e0 | 0.22 | 0.05 | | | | | |
| 68: | 184.0329 | 2.30e1 | 1.68 | 0.37 | 141: | 300.1788 | 1.00e0 | 0.07 | 0.02 | | | | | |
| 69: | 184.1005 | 4.10e1 | 2.99 | 0.65 | 142: | 301.1496 | 1.00e0 | 0.07 | 0.02 | | | | | |
| 70: | 184.6015 | 6.00e0 | 0.44 | 0.10 | 143: | 305.0483 | 1.00e0 | 0.07 | 0.02 | | | | | |
| 71: | 185.0419 | 5.80e1 | 4.24 | 0.92 | 144: | 312.1698 | 1.00e0 | 0.07 | 0.02 | | | | | |
| 72: | 186.0399 | 2.10e1 | 1.53 | 0.33 | 145: | 325.1763 | 2.00e0 | 0.15 | 0.03 | | | | | |
| 73: | 187.0392 | 5.10e1 | 3.73 | 0.81 | 146: | 326.1950 | 1.00e0 | 0.07 | 0.02 | | | | | |

**Figure S9:** High resolution EI spectrum for compound **E**.

## 4,16-dithienyl[2.2]paracyclophane (D)

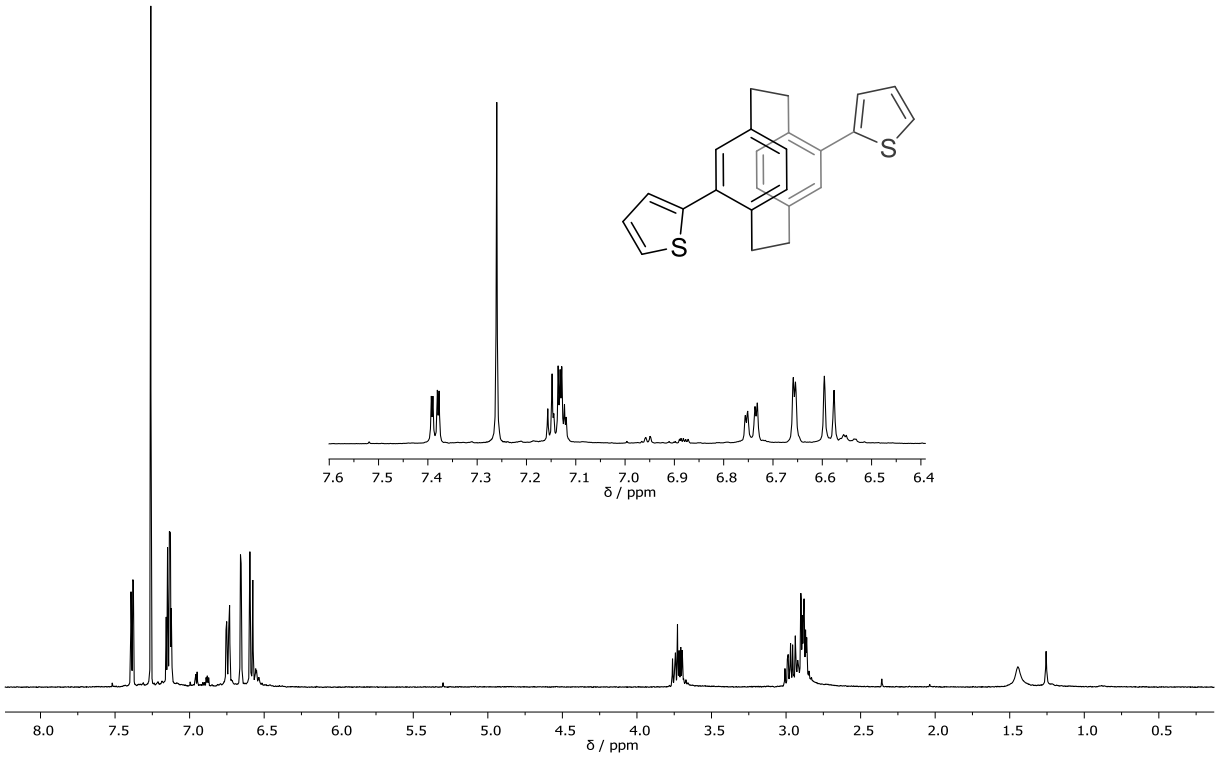


**Figure S10:** $^{1}H$ NMR spectrum (400 MHz, $CDCl_3$) of compound **D**.

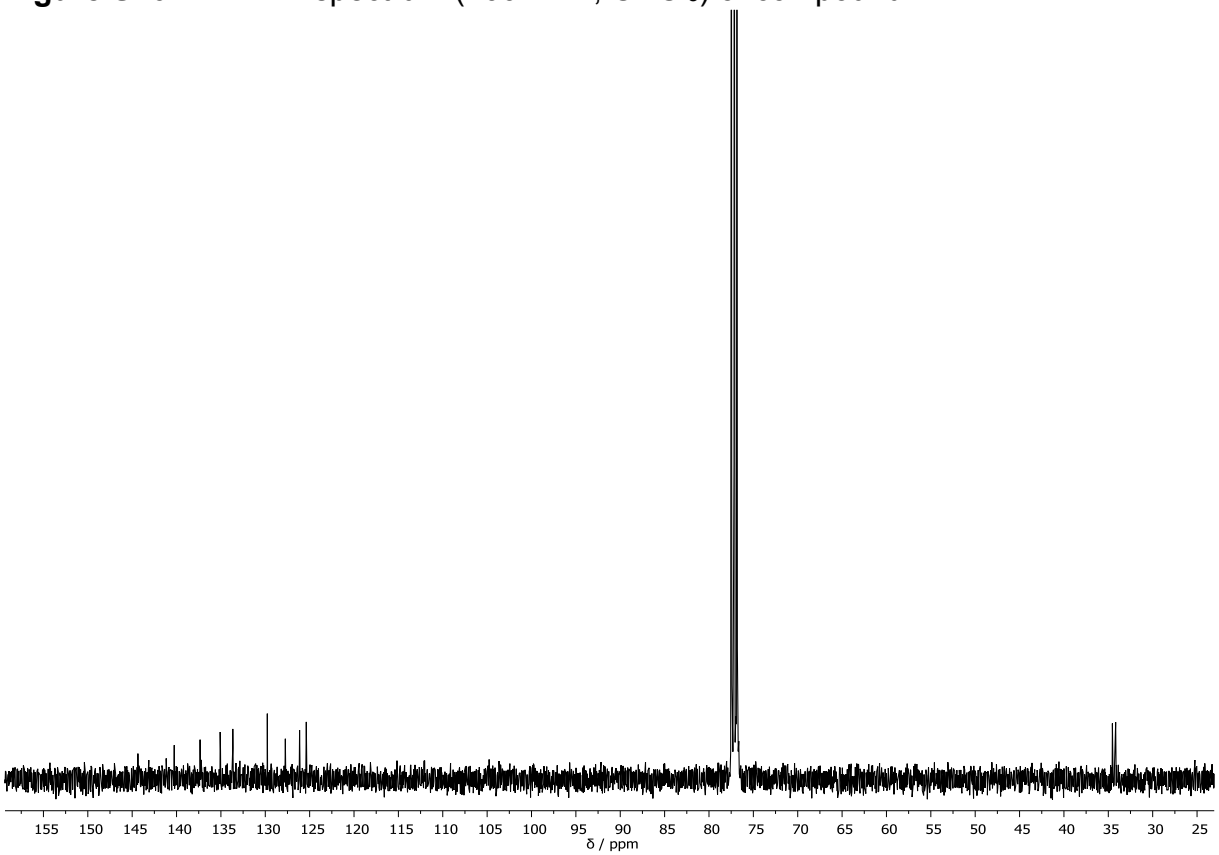


**Figure S11:** $^{13}C$ NMR spectrum (101 MHz, $CDCl_3$) of compound **D**.

## 4,16-di-(5-bromothienyl)[2.2]paracyclophane (4)

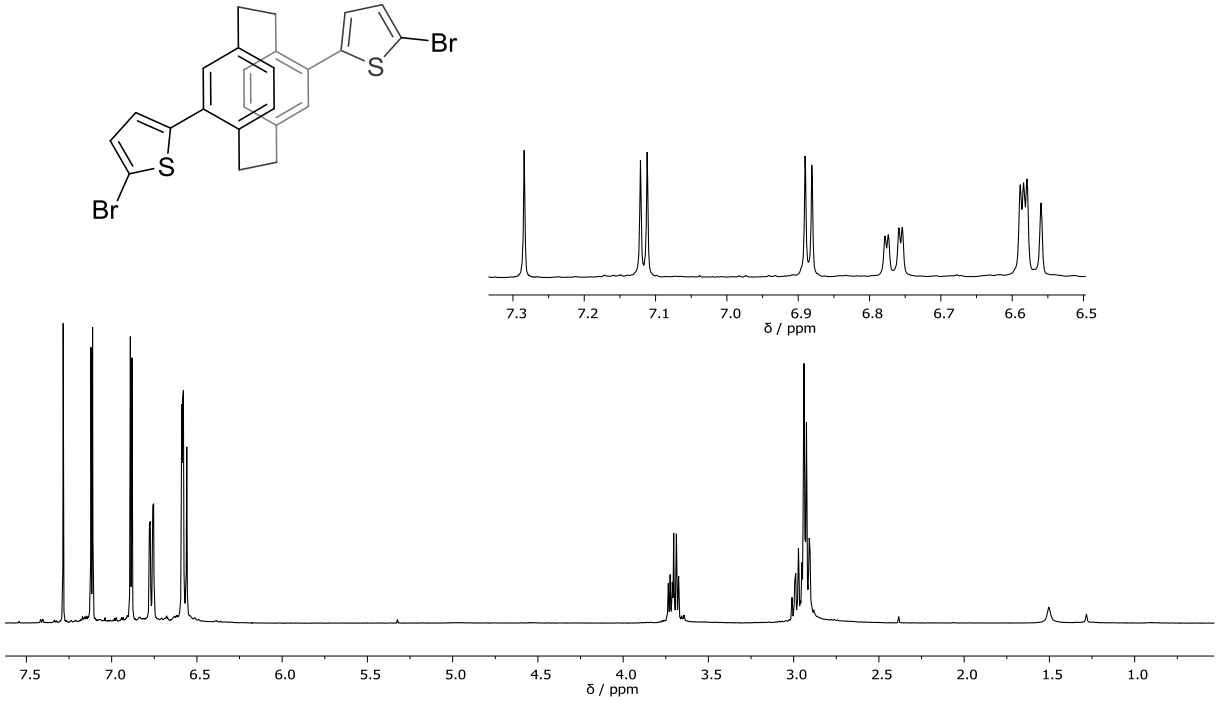


**Figure S12:** $^{1}H$ NMR spectrum (400 MHz, $CDCl_3$) of compound **4**.

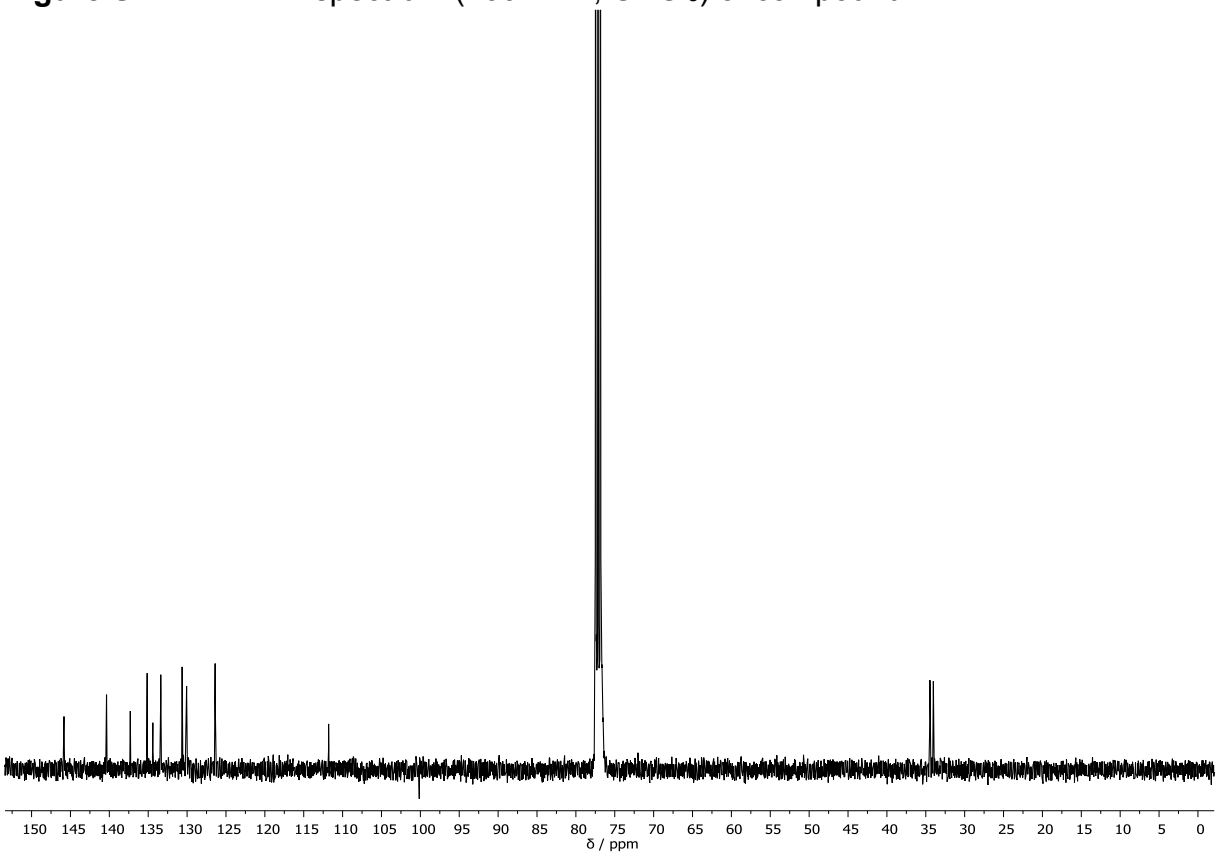


**Figure S13:** $^{13}C$ NMR spectrum (101 MHz, $CDCl_3$) of compound **4**.

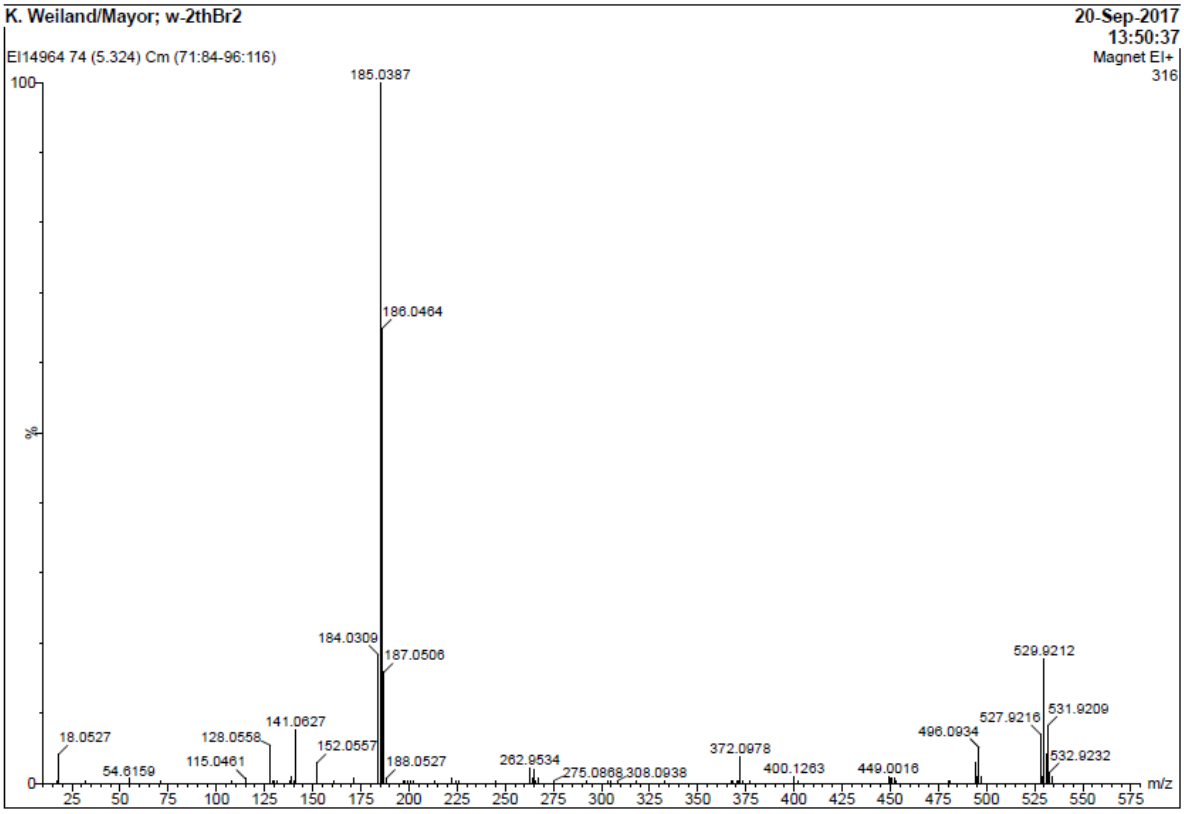


K. Weiland/Mayor; w-2thBr2 — 20-Sep-2017 13:50:37

EI14964 74 (5.324) Cm (71:84-96:116) — Magnet EI+

| No | Mass | Inten | %BPI | %TIC | No | Mass | Inten | %BPI | %TIC | No | Mass | Inten | %BPI | %TIC |
|---|---|---|---|---|---|---|---|---|---|---|---|---|---|---|
| 1: | 17.0468 | 1.00e0 | 0.32 | 0.11 | 74: | 530.9236 | 1.30e1 | 4.11 | 1.37 | | | | | |
| 2: | 18.0527 | 1.30e1 | 4.11 | 1.37 | 75: | 531.8781 | 1.00e0 | 0.32 | 0.11 | | | | | |
| 3: | 32.0108 | 1.00e0 | 0.32 | 0.11 | 76: | 531.9209 | 2.60e1 | 8.23 | 2.73 | | | | | |
| 4: | 54.6159 | 2.00e0 | 0.63 | 0.21 | 77: | 532.9232 | 5.00e0 | 1.58 | 0.53 | | | | | |
| 5: | 71.0891 | 1.00e0 | 0.32 | 0.11 | 78: | 533.9152 | 3.00e0 | 0.95 | 0.32 | | | | | |
| 6: | 108.0433 | 1.00e0 | 0.32 | 0.11 | | | | | | | | | | |
| 7: | 115.0461 | 2.00e0 | 0.63 | 0.21 | | | | | | | | | | |
| 8: | 128.0558 | 1.70e1 | 5.38 | 1.79 | | | | | | | | | | |
| 9: | 129.0604 | 1.00e0 | 0.32 | 0.11 | | | | | | | | | | |
| 10: | 130.2655 | 1.00e0 | 0.32 | 0.11 | | | | | | | | | | |
| 11: | 131.5349 | 1.00e0 | 0.32 | 0.11 | | | | | | | | | | |
| 12: | 138.0357 | 1.00e0 | 0.32 | 0.11 | | | | | | | | | | |
| 13: | 139.0497 | 3.00e0 | 0.95 | 0.32 | | | | | | | | | | |
| 14: | 140.0289 | 1.00e0 | 0.32 | 0.11 | | | | | | | | | | |
| 15: | 140.6981 | 1.00e0 | 0.32 | 0.11 | | | | | | | | | | |
| 16: | 141.0627 | 2.40e1 | 7.59 | 2.52 | | | | | | | | | | |
| 17: | 152.0557 | 9.00e0 | 2.85 | 0.95 | | | | | | | | | | |
| 18: | 161.0428 | 1.00e0 | 0.32 | 0.11 | | | | | | | | | | |
| 19: | 171.0240 | 2.00e0 | 0.63 | 0.21 | | | | | | | | | | |
| 20: | 171.5250 | 1.00e0 | 0.32 | 0.11 | | | | | | | | | | |
| 21: | 184.0309 | 5.80e1 | 18.35 | 6.09 | | | | | | | | | | |
| 22: | 185.0387 | 3.16e2 | 100.00 | 33.19 | | | | | | | | | | |
| 23: | 186.0464 | 2.05e2 | 64.87 | 21.53 | | | | | | | | | | |
| 24: | 187.0506 | 5.00e1 | 15.82 | 5.25 | | | | | | | | | | |
| 25: | 188.0527 | 2.00e0 | 0.63 | 0.21 | | | | | | | | | | |
| 26: | 197.0328 | 1.00e0 | 0.32 | 0.11 | | | | | | | | | | |
| 27: | 198.0509 | 1.00e0 | 0.32 | 0.11 | | | | | | | | | | |
| 28: | 199.0495 | 1.00e0 | 0.32 | 0.11 | | | | | | | | | | |
| 29: | 200.5657 | 1.00e0 | 0.32 | 0.11 | | | | | | | | | | |
| 30: | 201.0709 | 1.00e0 | 0.32 | 0.11 | | | | | | | | | | |
| 31: | 202.0676 | 1.00e0 | 0.32 | 0.11 | | | | | | | | | | |
| 32: | 212.9737 | 1.00e0 | 0.32 | 0.11 | | | | | | | | | | |
| 33: | 222.4891 | 2.00e0 | 0.63 | 0.21 | | | | | | | | | | |
| 34: | 224.4946 | 1.00e0 | 0.32 | 0.11 | | | | | | | | | | |
| 35: | 226.0809 | 1.00e0 | 0.32 | 0.11 | | | | | | | | | | |
| 36: | 244.9927 | 1.00e0 | 0.32 | 0.11 | | | | | | | | | | |
| 37: | 262.9534 | 7.00e0 | 2.22 | 0.74 | | | | | | | | | | |
| 38: | 263.9485 | 2.00e0 | 0.63 | 0.21 | | | | | | | | | | |
| 39: | 264.4613 | 1.00e0 | 0.32 | 0.11 | | | | | | | | | | |
| 40: | 264.9452 | 6.00e0 | 1.90 | 0.63 | | | | | | | | | | |
| 41: | 265.4582 | 1.00e0 | 0.32 | 0.11 | | | | | | | | | | |
| 42: | 265.9565 | 1.00e0 | 0.32 | 0.11 | | | | | | | | | | |
| 43: | 266.9585 | 2.00e0 | 0.63 | 0.21 | | | | | | | | | | |
| 44: | 275.0868 | 1.00e0 | 0.32 | 0.11 | | | | | | | | | | |
| 45: | 292.0744 | 1.00e0 | 0.32 | 0.11 | | | | | | | | | | |
| 46: | 303.1192 | 1.00e0 | 0.32 | 0.11 | | | | | | | | | | |
| 47: | 304.9984 | 1.00e0 | 0.32 | 0.11 | | | | | | | | | | |
| 48: | 308.0938 | 1.00e0 | 0.32 | 0.11 | | | | | | | | | | |
| 49: | 318.0905 | 1.00e0 | 0.32 | 0.11 | | | | | | | | | | |
| 50: | 333.0757 | 1.00e0 | 0.32 | 0.11 | | | | | | | | | | |
| 51: | 367.3940 | 1.00e0 | 0.32 | 0.11 | | | | | | | | | | |
| 52: | 368.0650 | 1.00e0 | 0.32 | 0.11 | | | | | | | | | | |
| 53: | 370.0885 | 1.00e0 | 0.32 | 0.11 | | | | | | | | | | |
| 54: | 371.0940 | 1.00e0 | 0.32 | 0.11 | | | | | | | | | | |
| 55: | 372.0978 | 1.20e1 | 3.80 | 1.26 | | | | | | | | | | |
| 56: | 373.1017 | 1.00e0 | 0.32 | 0.11 | | | | | | | | | | |
| 57: | 376.9761 | 1.00e0 | 0.32 | 0.11 | | | | | | | | | | |
| 58: | 400.1263 | 3.00e0 | 0.95 | 0.32 | | | | | | | | | | |
| 59: | 402.1346 | 1.00e0 | 0.32 | 0.11 | | | | | | | | | | |
| 60: | 449.0016 | 3.00e0 | 0.95 | 0.32 | | | | | | | | | | |
| 61: | 450.0160 | 2.00e0 | 0.63 | 0.21 | | | | | | | | | | |
| 62: | 451.0043 | 2.00e0 | 0.63 | 0.21 | | | | | | | | | | |
| 63: | 452.0166 | 2.00e0 | 0.63 | 0.21 | | | | | | | | | | |
| 64: | 452.9828 | 1.00e0 | 0.32 | 0.11 | | | | | | | | | | |
| 65: | 479.9601 | 1.00e0 | 0.32 | 0.11 | | | | | | | | | | |
| 66: | 480.9716 | 1.00e0 | 0.32 | 0.11 | | | | | | | | | | |
| 67: | 494.0956 | 9.00e0 | 2.85 | 0.95 | | | | | | | | | | |
| 68: | 495.0995 | 3.00e0 | 0.95 | 0.32 | | | | | | | | | | |
| 69: | 496.0934 | 1.60e1 | 5.06 | 1.68 | | | | | | | | | | |
| 70: | 497.0956 | 3.00e0 | 0.95 | 0.32 | | | | | | | | | | |
| 71: | 527.9216 | 2.20e1 | 6.96 | 2.31 | | | | | | | | | | |
| 72: | 528.9195 | 3.00e0 | 0.95 | 0.32 | | | | | | | | | | |
| 73: | 529.9212 | 5.60e1 | 17.72 | 5.88 | | | | | | | | | | |

**Figure S14:** High resolution EI spectrum for compound **4**.

## Compound 5

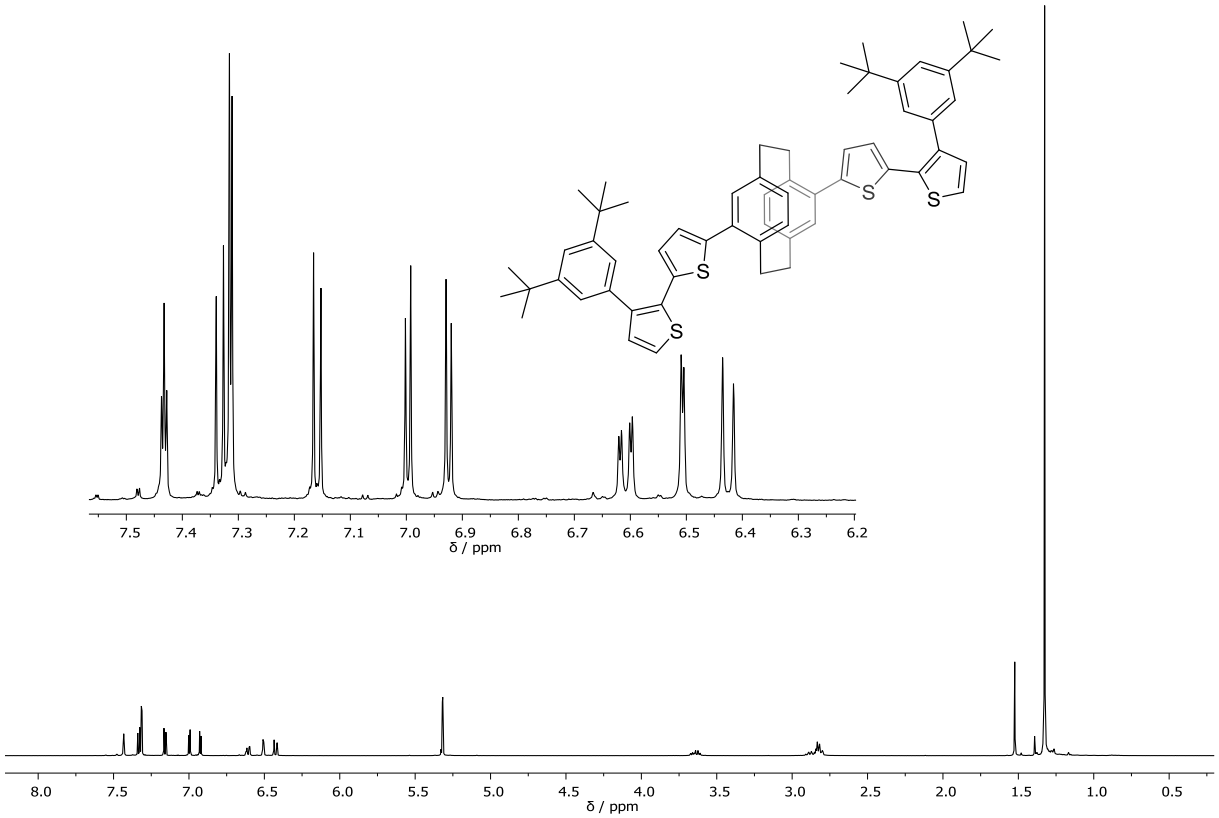


**Figure S15:** $^{1}H$ NMR spectrum (400 MHz, $CD_2Cl_2$) of compound **5**.

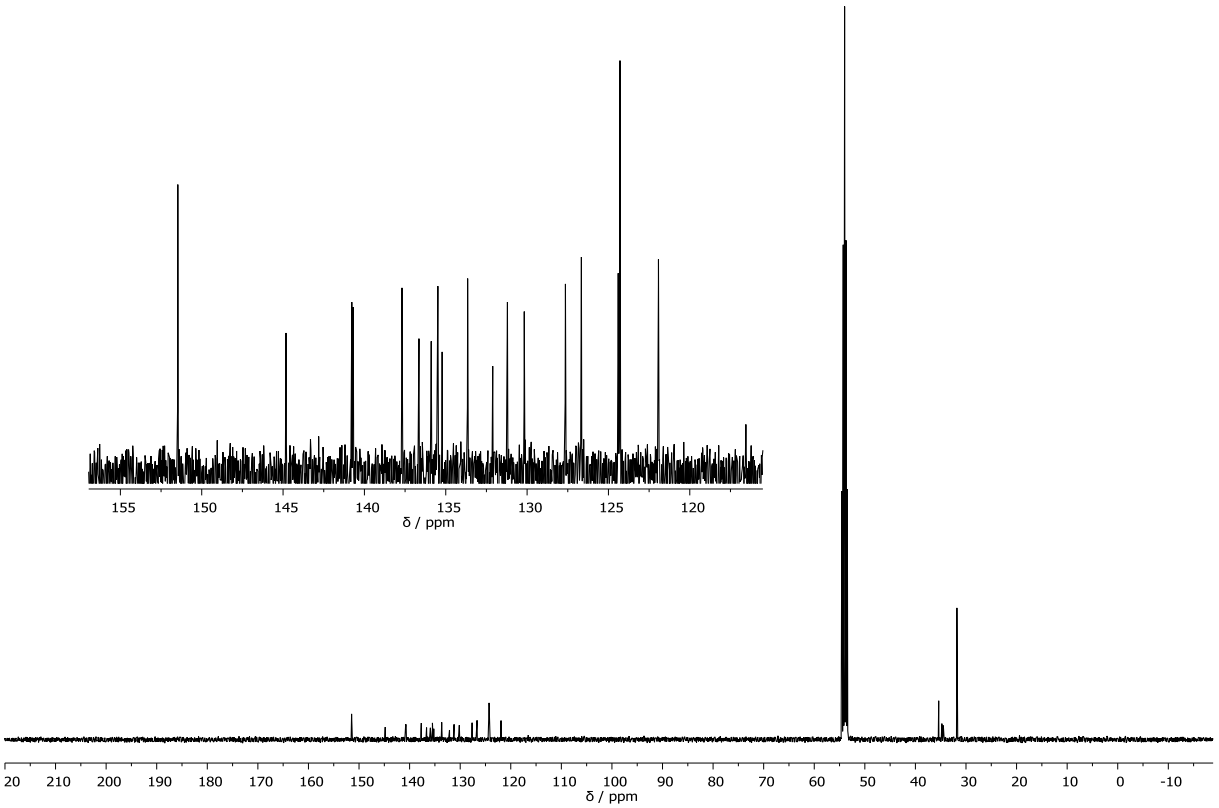


**Figure S16:** $^{13}C$ NMR spectrum (101 MHz, $CD_2Cl_2$) of compound **5**

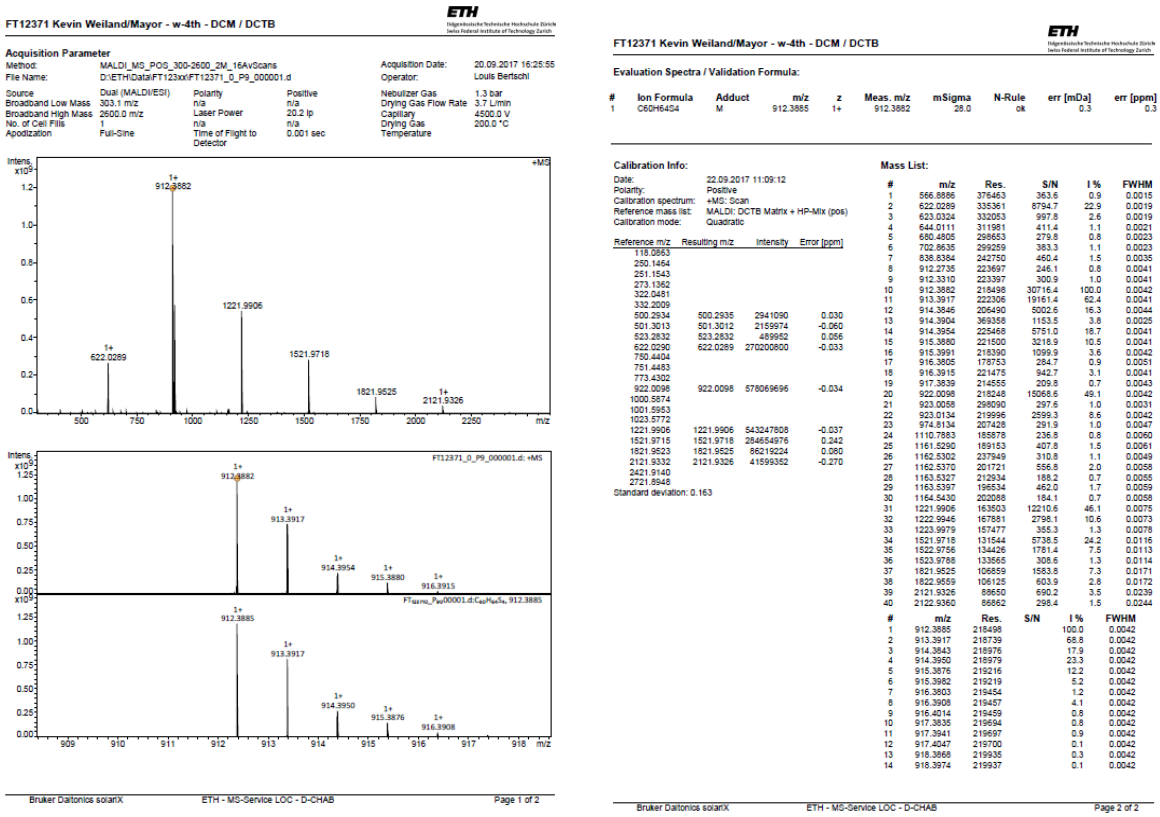

FT12371 Kevin Weiland/Mayor - w-4th - DCM / DCTB

ETH Eidgenössische Technische Hochschule Zürich Swiss Federal Institute of Technology Zurich

**Acquisition Parameter**

| | | | | | |
|---|---|---|---|---|---|
| Method: | MALDI_MS_POS_300-2600_2M_16Av0cans | | | Acquisition Date: | 20.09.2017 16:25:55 |
| File Name: | D:\ETH\Data\FT123xx\FT12371_0_P9_000001.d | | | Operator: | Louis Bertschi |
| Source | Dual (MALDI/ESI) | Polarity | Positive | Nebulizer Gas | 1.3 bar |
| Broadband Low Mass | 303.1 m/z | n/a | n/a | Drying Gas Flow Rate | 3.7 L/min |
| Broadband High Mass | 2600.0 m/z | Laser Power | 20.2 lp | Capillary | 4500.0 V |
| No. of Cell Fills | 1 | n/a | n/a | Drying Gas | 200.0 °C |
| Apodization | Full-Sine | Time of Flight to Detector | 0.001 sec | Temperature | |



Bruker Daltonics solarix ETH - MS-Service LOC - D-CHAB Page 1 of 2

FT12371 Kevin Weiland/Mayor - w-4th - DCM / DCTB

ETH Eidgenössische Technische Hochschule Zürich Swiss Federal Institute of Technology Zurich

**Evaluation Spectra / Validation Formula:**

| # | Ion Formula | Adduct | m/z | z | Meas. m/z | mSigma | N-Rule | err [mDa] | err [ppm] |
|---|---|---|---|---|---|---|---|---|---|
| 1 | C60H64S4 | M | 912.3885 | 1+ | 912.3882 | 28.0 | ok | 0.3 | 0.3 |

**Calibration Info:**

| | |
|---|---|
| Date: | 22.09.2017 11:09:12 |
| Polarity: | Positive |
| Calibration spectrum: | +MS: Scan |
| Reference mass list: | MALDI: DCTB Matrix + HP-Mix (pos) |
| Calibration mode: | Quadratic |

| Reference m/z | Resulting m/z | Intensity | Error [ppm] |
|---|---|---|---|
| 118.0863 | | | |
| 250.1464 | | | |
| 251.1543 | | | |
| 273.1362 | | | |
| 322.0481 | | | |
| 332.2009 | | | |
| 500.2934 | 500.2935 | 2941090 | 0.030 |
| 501.3013 | 501.3012 | 2159974 | -0.060 |
| 523.2832 | 523.2832 | 489952 | 0.056 |
| 622.0290 | 622.0289 | 270200600 | -0.033 |
| 750.4404 | | | |
| 751.4483 | | | |
| 773.4302 | | | |
| 922.0098 | 922.0098 | 578069696 | -0.034 |
| 1000.5874 | | | |
| 1001.5953 | | | |
| 1023.5772 | | | |
| 1221.9906 | 1221.9906 | 543247808 | -0.037 |
| 1521.9715 | 1521.9718 | 284654976 | 0.242 |
| 1821.9523 | 1821.9525 | 86219224 | 0.080 |
| 2121.9332 | 2121.9326 | 41599352 | -0.270 |
| 2421.9140 | | | |
| 2721.8948 | | | |

Standard deviation: 0.163

**Mass List:**

| # | m/z | Res. | S/N | I % | FWHM |
|---|---|---|---|---|---|
| 1 | 566.8886 | 376463 | 363.6 | 0.9 | 0.0015 |
| 2 | 622.0289 | 335361 | 8794.7 | 22.9 | 0.0019 |
| 3 | 623.0324 | 332053 | 997.8 | 2.6 | 0.0019 |
| 4 | 644.0111 | 311981 | 411.4 | 1.1 | 0.0021 |
| 5 | 680.4805 | 298653 | 279.8 | 0.8 | 0.0023 |
| 6 | 702.8635 | 299259 | 383.3 | 1.1 | 0.0023 |
| 7 | 838.8384 | 242750 | 460.4 | 1.5 | 0.0035 |
| 8 | 912.2735 | 223697 | 246.1 | 0.8 | 0.0041 |
| 9 | 912.3310 | 223397 | 300.9 | 1.0 | 0.0041 |
| 10 | 912.3882 | 218498 | 30716.4 | 100.0 | 0.0042 |
| 11 | 913.3917 | 222306 | 19161.4 | 62.4 | 0.0041 |
| 12 | 914.3846 | 206490 | 5002.6 | 16.3 | 0.0044 |
| 13 | 914.3904 | 369358 | 1153.5 | 3.8 | 0.0025 |
| 14 | 914.3954 | 225468 | 5751.0 | 18.7 | 0.0041 |
| 15 | 915.3880 | 221500 | 3218.9 | 10.5 | 0.0041 |
| 16 | 915.3991 | 218390 | 1099.9 | 3.6 | 0.0042 |
| 17 | 916.3805 | 178753 | 284.7 | 0.9 | 0.0051 |
| 18 | 916.3915 | 221475 | 942.7 | 3.1 | 0.0041 |
| 19 | 917.3839 | 214555 | 209.8 | 0.7 | 0.0043 |
| 20 | 922.0098 | 218248 | 15068.6 | 49.1 | 0.0042 |
| 21 | 923.0058 | 298090 | 297.6 | 1.0 | 0.0031 |
| 22 | 923.0134 | 219996 | 2599.3 | 8.6 | 0.0042 |
| 23 | 974.8134 | 207428 | 291.9 | 1.0 | 0.0047 |
| 24 | 1110.7883 | 185878 | 236.8 | 0.8 | 0.0060 |
| 25 | 1161.5290 | 189153 | 407.8 | 1.5 | 0.0061 |
| 26 | 1162.5302 | 237949 | 310.8 | 1.1 | 0.0049 |
| 27 | 1162.5370 | 201721 | 556.8 | 2.0 | 0.0058 |
| 28 | 1163.5327 | 212934 | 188.2 | 0.7 | 0.0055 |
| 29 | 1163.5397 | 196534 | 462.0 | 1.7 | 0.0059 |
| 30 | 1164.5430 | 202088 | 184.1 | 0.7 | 0.0058 |
| 31 | 1221.9906 | 163503 | 12210.6 | 46.1 | 0.0075 |
| 32 | 1222.9946 | 167881 | 2798.1 | 10.6 | 0.0073 |
| 33 | 1223.9979 | 157477 | 355.3 | 1.3 | 0.0078 |
| 34 | 1521.9718 | 131544 | 5738.5 | 24.2 | 0.0116 |
| 35 | 1522.9756 | 134426 | 1781.4 | 7.5 | 0.0113 |
| 36 | 1523.9788 | 133565 | 308.6 | 1.3 | 0.0114 |
| 37 | 1821.9525 | 106859 | 1583.8 | 7.3 | 0.0171 |
| 38 | 1822.9559 | 106125 | 603.9 | 2.8 | 0.0172 |
| 39 | 2121.9326 | 88650 | 690.2 | 3.5 | 0.0239 |
| 40 | 2122.9360 | 86862 | 298.4 | 1.5 | 0.0244 |

| # | m/z | Res. | S/N | I % | FWHM |
|---|---|---|---|---|---|
| 1 | 912.3885 | 218498 | | 100.0 | 0.0042 |
| 2 | 913.3917 | 218739 | | 68.8 | 0.0042 |
| 3 | 914.3843 | 218976 | | 17.9 | 0.0042 |
| 4 | 914.3950 | 218979 | | 23.3 | 0.0042 |
| 5 | 915.3876 | 219216 | | 12.2 | 0.0042 |
| 6 | 915.3982 | 219219 | | 5.2 | 0.0042 |
| 7 | 916.3803 | 219454 | | 1.2 | 0.0042 |
| 8 | 916.3908 | 219457 | | 4.1 | 0.0042 |
| 9 | 916.4014 | 219459 | | 0.8 | 0.0042 |
| 10 | 917.3835 | 219694 | | 0.8 | 0.0042 |
| 11 | 917.3941 | 219697 | | 0.9 | 0.0042 |
| 12 | 917.4047 | 219700 | | 0.1 | 0.0042 |
| 13 | 918.3868 | 219935 | | 0.3 | 0.0042 |
| 14 | 918.3974 | 219937 | | 0.1 | 0.0042 |

Bruker Daltonics solarix ETH - MS-Service LOC - D-CHAB Page 2 of 2

**Figure S17:** High resolution MALDI ToF spectrum for compound **5**.

## Compound 6

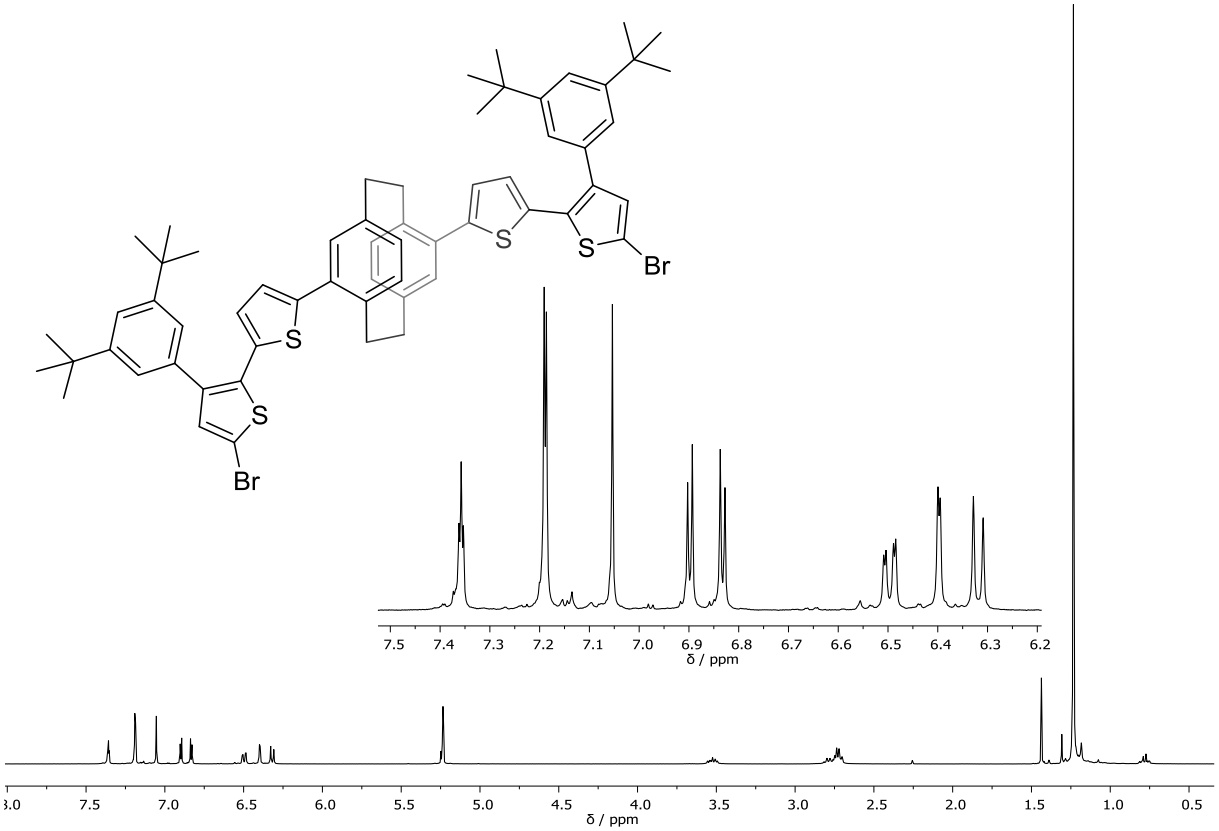


**Figure S19:** $^{1}H$ NMR spectrum (400 MHz, $CD_2Cl_2$) of compound **6**.

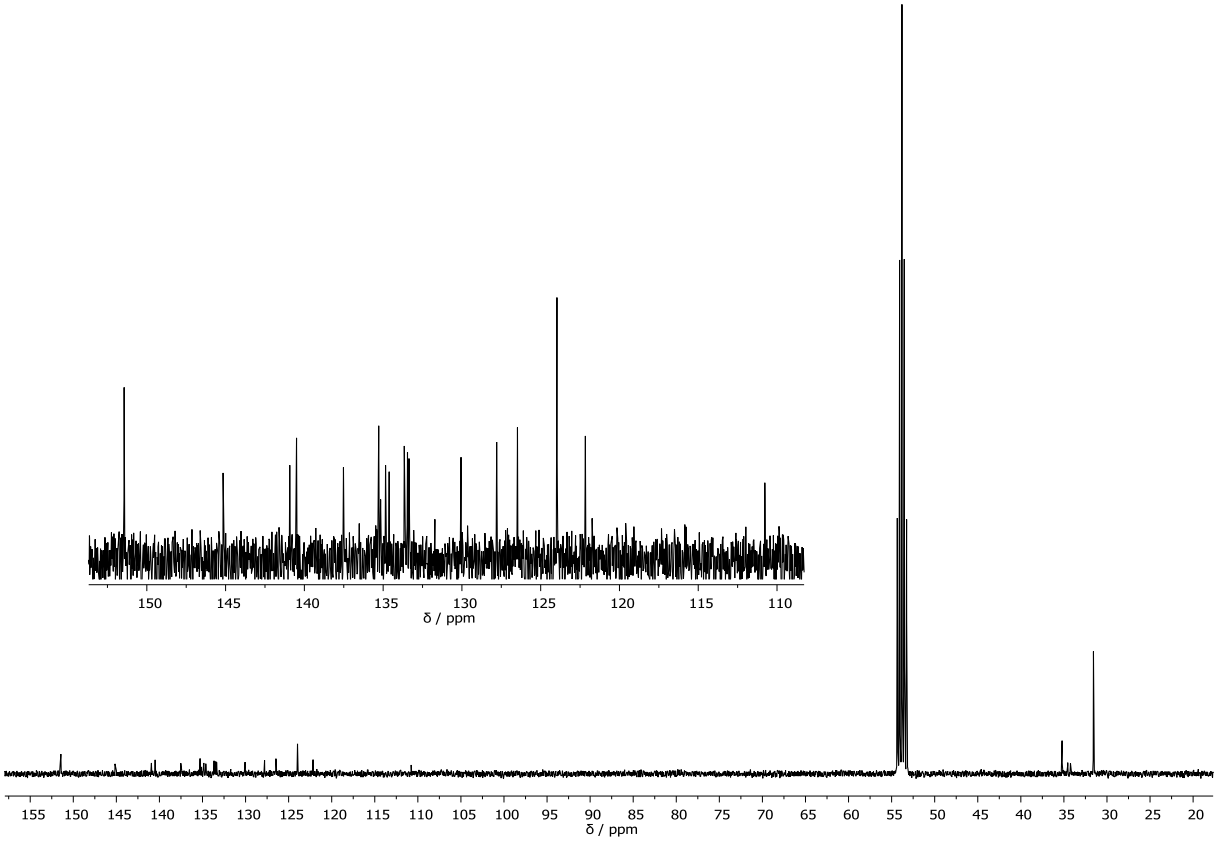


**Figure S20:** $^{13}C$ NMR spectrum (101 MHz, $CD_2Cl_2$) of compound **6**.

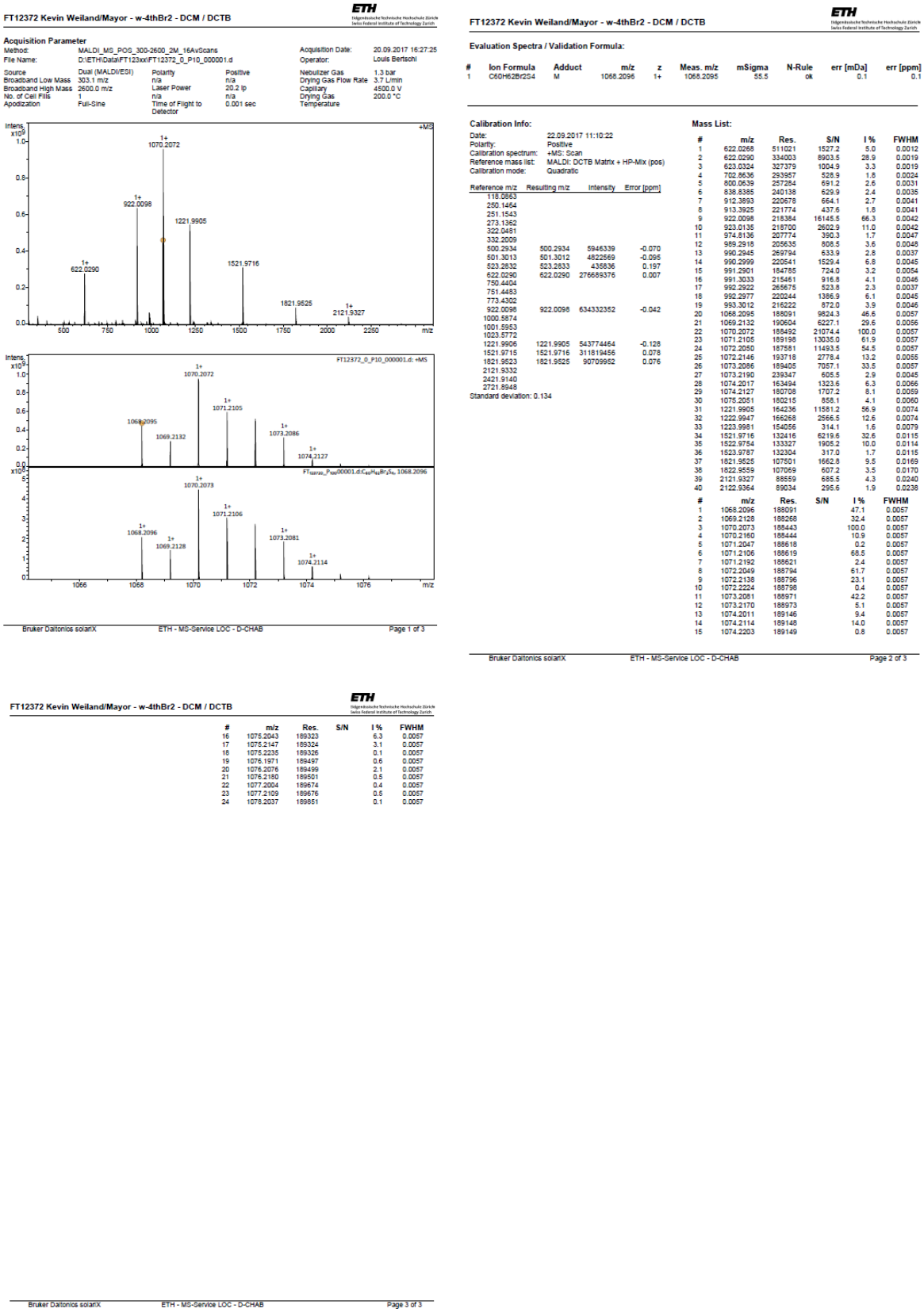

FT12372 Kevin Weiland/Mayor - w-4thBr2 - DCM / DCTB

ETH Eidgenössische Technische Hochschule Zürich Swiss Federal Institute of Technology Zurich

**Acquisition Parameter**

| | | | | | |
|---|---|---|---|---|---|
| Method: | MALDI_MS_POS_300-2600_2M_16Avgscans | | | Acquisition Date: | 20.09.2017 16:27:25 |
| File Name: | D:\ETH\Data\FT123xx\FT12372_0_P10_000001.d | | | Operator: | Louis Bertschi |
| Source | Dual (MALDI/ESI) | Polarity | Positive | Nebulizer Gas | 1.3 bar |
| Broadband Low Mass | 303.1 m/z | n/a | n/a | Drying Gas Flow Rate | 3.7 L/min |
| Broadband High Mass | 2600.0 m/z | Laser Power | 20.2 lp | Capillary | 4500.0 V |
| No. of Cell Fills | 1 | n/a | n/a | Drying Gas Temperature | 200.0 °C |
| Apodization | Full-Sine | Time of Flight to Detector | 0.001 sec | | |



Bruker Daltonics solariX ETH - MS-Service LOC - D-CHAB Page 1 of 3

FT12372 Kevin Weiland/Mayor - w-4thBr2 - DCM / DCTB

ETH Eidgenössische Technische Hochschule Zürich Swiss Federal Institute of Technology Zurich

**Evaluation Spectra / Validation Formula:**

| # | Ion Formula | Adduct | m/z | z | Meas. m/z | mSigma | N-Rule | err [mDa] | err [ppm] |
|---|---|---|---|---|---|---|---|---|---|
| 1 | C60H62Br2S4 | M | 1068.2096 | 1+ | 1068.2095 | 55.5 | ok | 0.1 | 0.1 |

**Calibration Info:**

| | |
|---|---|
| Date: | 22.09.2017 11:10:22 |
| Polarity: | Positive |
| Calibration spectrum: | +MS: Scan |
| Reference mass list: | MALDI: DCTB Matrix + HP-Mix (pos) |
| Calibration mode: | Quadratic |

| Reference m/z | Resulting m/z | Intensity | Error [ppm] |
|---|---|---|---|
| 118.0863 | | | |
| 250.1464 | | | |
| 251.1543 | | | |
| 273.1362 | | | |
| 322.0481 | | | |
| 332.2009 | | | |
| 500.2934 | 500.2934 | 5946339 | -0.070 |
| 501.3013 | 501.3012 | 4822569 | -0.095 |
| 523.2832 | 523.2833 | 435836 | 0.197 |
| 622.0290 | 622.0290 | 276689376 | 0.007 |
| 750.4404 | | | |
| 751.4483 | | | |
| 773.4302 | | | |
| 922.0098 | 922.0098 | 634332352 | -0.042 |
| 1000.5874 | | | |
| 1001.5953 | | | |
| 1023.5772 | | | |
| 1221.9906 | 1221.9905 | 543774464 | -0.128 |
| 1521.9715 | 1521.9716 | 311819456 | 0.078 |
| 1821.9523 | 1821.9525 | 90709952 | 0.076 |
| 2121.9332 | | | |
| 2421.9140 | | | |
| 2721.8948 | | | |

Standard deviation: 0.134

**Mass List:**

| # | m/z | Res. | S/N | I % | FWHM |
|---|---|---|---|---|---|
| 1 | 622.0268 | 511021 | 1527.2 | 5.0 | 0.0012 |
| 2 | 622.0290 | 334003 | 8903.5 | 28.9 | 0.0019 |
| 3 | 623.0324 | 327379 | 1004.9 | 3.3 | 0.0019 |
| 4 | 702.8636 | 293957 | 528.9 | 1.8 | 0.0024 |
| 5 | 800.0639 | 257284 | 691.2 | 2.6 | 0.0031 |
| 6 | 836.8385 | 240138 | 629.9 | 2.4 | 0.0035 |
| 7 | 912.3893 | 220678 | 664.1 | 2.7 | 0.0041 |
| 8 | 913.3925 | 221774 | 437.6 | 1.8 | 0.0041 |
| 9 | 922.0098 | 218364 | 16145.5 | 66.3 | 0.0042 |
| 10 | 923.0135 | 218700 | 2602.9 | 11.0 | 0.0042 |
| 11 | 974.8136 | 207774 | 390.3 | 1.7 | 0.0047 |
| 12 | 989.2918 | 205635 | 808.5 | 3.6 | 0.0048 |
| 13 | 990.2945 | 269794 | 633.9 | 2.8 | 0.0037 |
| 14 | 990.2999 | 220541 | 1529.4 | 6.8 | 0.0045 |
| 15 | 991.2901 | 184785 | 724.0 | 3.2 | 0.0054 |
| 16 | 991.3033 | 215461 | 916.8 | 4.1 | 0.0046 |
| 17 | 992.2922 | 265675 | 523.8 | 2.3 | 0.0037 |
| 18 | 992.2977 | 220244 | 1366.9 | 6.1 | 0.0045 |
| 19 | 993.3012 | 216222 | 872.0 | 3.9 | 0.0046 |
| 20 | 1068.2095 | 188091 | 9824.3 | 46.6 | 0.0057 |
| 21 | 1069.2132 | 190604 | 6227.1 | 29.6 | 0.0056 |
| 22 | 1070.2072 | 188492 | 21074.4 | 100.0 | 0.0057 |
| 23 | 1071.2105 | 189198 | 13035.0 | 61.9 | 0.0057 |
| 24 | 1072.2050 | 187581 | 11493.5 | 54.5 | 0.0057 |
| 25 | 1072.2146 | 193718 | 2778.4 | 13.2 | 0.0055 |
| 26 | 1073.2086 | 189405 | 7057.1 | 33.5 | 0.0057 |
| 27 | 1073.2190 | 239347 | 605.5 | 2.9 | 0.0045 |
| 28 | 1074.2017 | 163494 | 1323.6 | 6.3 | 0.0066 |
| 29 | 1074.2127 | 180708 | 1707.2 | 8.1 | 0.0059 |
| 30 | 1075.2051 | 180215 | 858.1 | 4.1 | 0.0060 |
| 31 | 1221.9905 | 164236 | 11581.2 | 56.9 | 0.0074 |
| 32 | 1222.9947 | 166268 | 2566.5 | 12.6 | 0.0074 |
| 33 | 1223.9981 | 154056 | 314.1 | 1.6 | 0.0079 |
| 34 | 1521.9716 | 132416 | 6219.6 | 32.6 | 0.0115 |
| 35 | 1522.9754 | 133327 | 1905.2 | 10.0 | 0.0114 |
| 36 | 1523.9787 | 132304 | 317.0 | 1.7 | 0.0115 |
| 37 | 1821.9525 | 107501 | 1662.8 | 9.5 | 0.0169 |
| 38 | 1822.9559 | 107069 | 607.2 | 3.5 | 0.0170 |
| 39 | 2121.9327 | 88559 | 685.5 | 4.3 | 0.0240 |
| 40 | 2122.9364 | 89034 | 295.6 | 1.9 | 0.0238 |

| # | m/z | Res. | S/N | I % | FWHM |
|---|---|---|---|---|---|
| 1 | 1068.2096 | 188091 | | 47.1 | 0.0057 |
| 2 | 1069.2128 | 188268 | | 32.4 | 0.0057 |
| 3 | 1070.2073 | 188443 | | 100.0 | 0.0057 |
| 4 | 1070.2160 | 188444 | | 10.9 | 0.0057 |
| 5 | 1071.2047 | 188618 | | 0.2 | 0.0057 |
| 6 | 1071.2106 | 188619 | | 68.5 | 0.0057 |
| 7 | 1071.2192 | 188621 | | 2.4 | 0.0057 |
| 8 | 1072.2049 | 188794 | | 61.7 | 0.0057 |
| 9 | 1072.2138 | 188796 | | 23.1 | 0.0057 |
| 10 | 1072.2224 | 188798 | | 0.4 | 0.0057 |
| 11 | 1073.2081 | 188971 | | 42.2 | 0.0057 |
| 12 | 1073.2170 | 188973 | | 5.1 | 0.0057 |
| 13 | 1074.2011 | 189146 | | 9.4 | 0.0057 |
| 14 | 1074.2114 | 189148 | | 14.0 | 0.0057 |
| 15 | 1074.2203 | 189149 | | 0.8 | 0.0057 |

Bruker Daltonics solariX ETH - MS-Service LOC - D-CHAB Page 2 of 3

FT12372 Kevin Weiland/Mayor - w-4thBr2 - DCM / DCTB

ETH Eidgenössische Technische Hochschule Zürich Swiss Federal Institute of Technology Zurich

| # | m/z | Res. | S/N | I % | FWHM |
|---|---|---|---|---|---|
| 16 | 1075.2043 | 189323 | | 6.3 | 0.0057 |
| 17 | 1075.2147 | 189324 | | 3.1 | 0.0057 |
| 18 | 1075.2235 | 189326 | | 0.1 | 0.0057 |
| 19 | 1076.1971 | 189497 | | 0.6 | 0.0057 |
| 20 | 1076.2076 | 189499 | | 2.1 | 0.0057 |
| 21 | 1076.2180 | 189501 | | 0.5 | 0.0057 |
| 22 | 1077.2004 | 189674 | | 0.4 | 0.0057 |
| 23 | 1077.2109 | 189676 | | 0.5 | 0.0057 |
| 24 | 1078.2037 | 189851 | | 0.1 | 0.0057 |

Bruker Daltonics solariX ETH - MS-Service LOC - D-CHAB Page 3 of 3

**Figure S21:** High resolution MALDI ToF spectrum for compound **6**.

## Compound 7

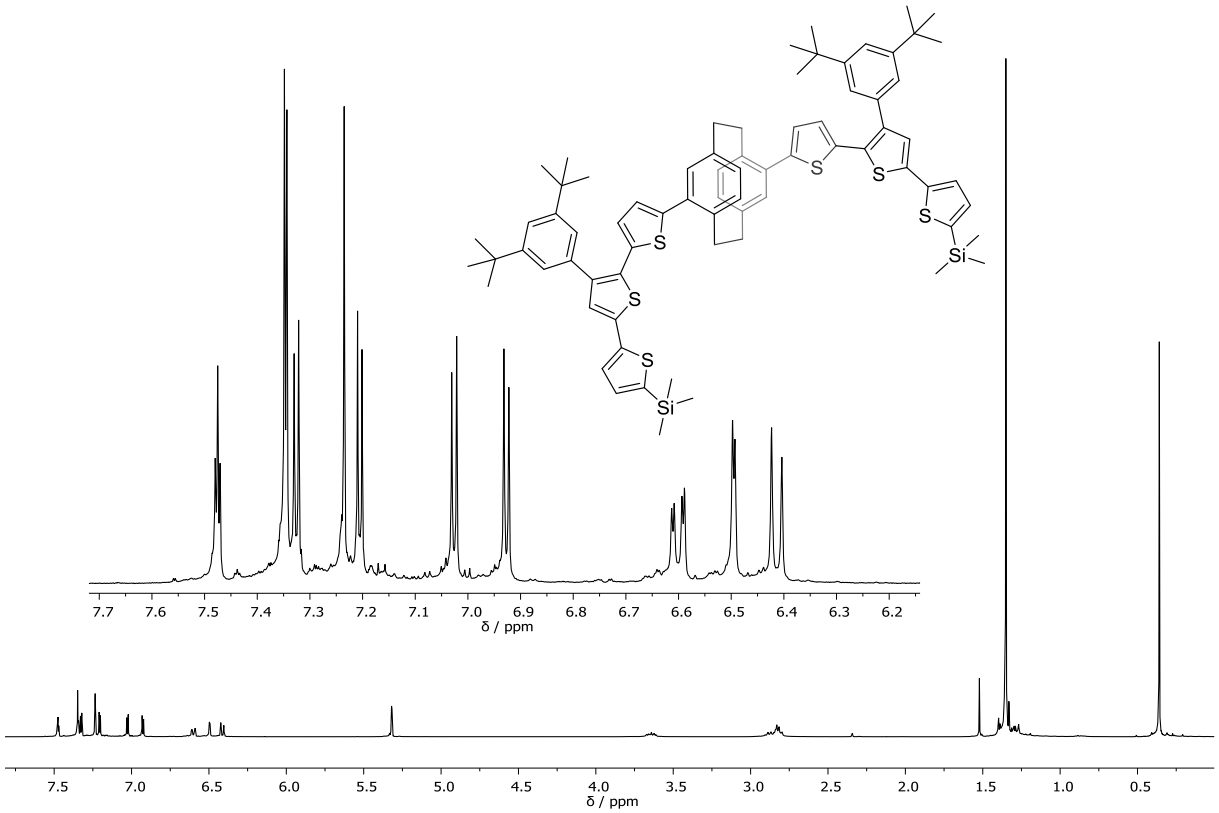


**Figure S22:** $^{1}H$ NMR spectrum (400 MHz, $CD_2Cl_2$) of compound **7**.

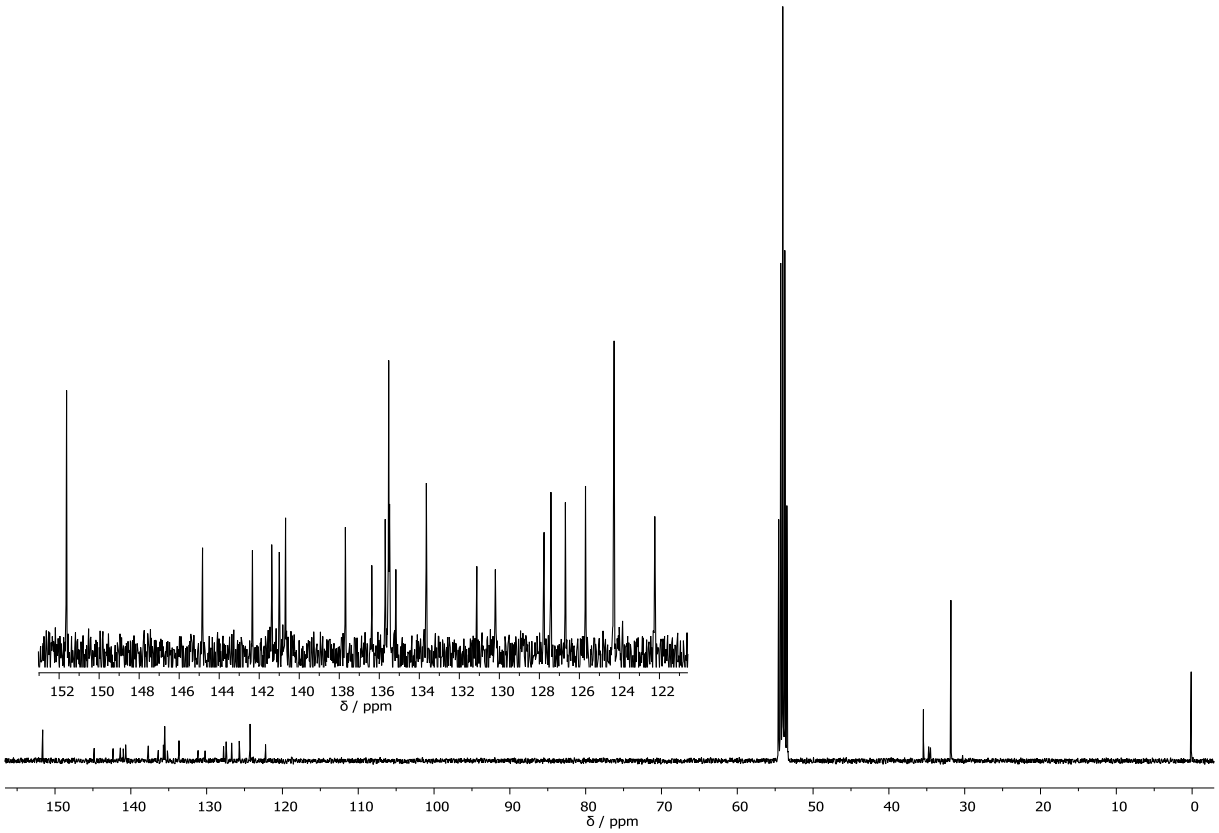


**Figure S23:** $^{13}C$ NMR spectrum (101 MHz, $CD_2Cl_2$) of compound **7**.

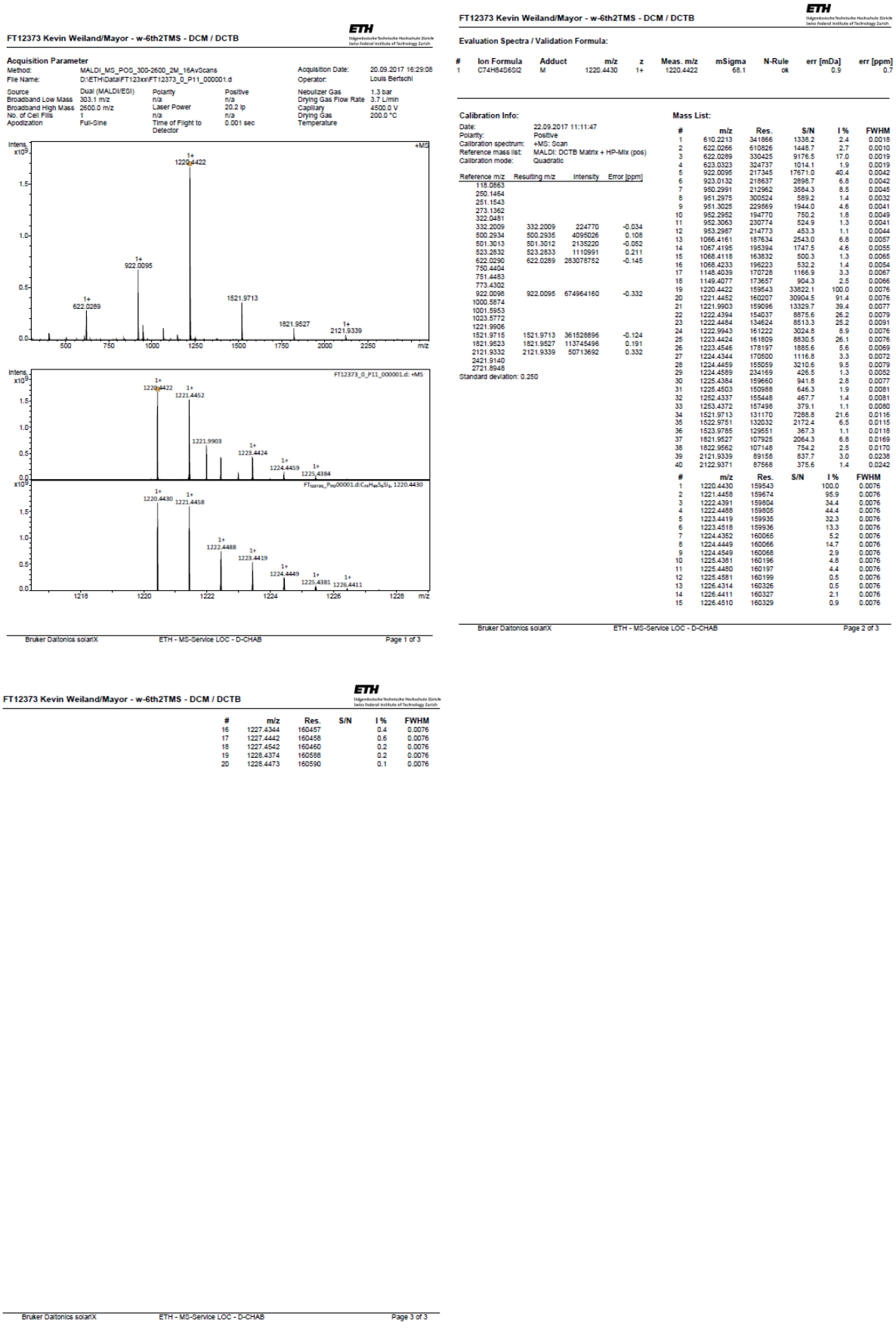

FT12373 Kevin Weiland/Mayor - w-6th2TMS - DCM / DCTB

ETH Eidgenössische Technische Hochschule Zürich Swiss Federal Institute of Technology Zurich

**Acquisition Parameter**

| | | | | | |
|---|---|---|---|---|---|
| Method: | MALDI_MS_POS_300-2600_2M_16AvScans | | | Acquisition Date: | 20.09.2017 16:29:08 |
| File Name: | D:\ETH\Data\FT123xx\FT12373_0_P11_000001.d | | | Operator: | Louis Bertschi |
| Source | Dual (MALDI/ESI) | Polarity | Positive | Nebulizer Gas | 1.3 bar |
| Broadband Low Mass | 303.1 m/z | n/a | n/a | Drying Gas Flow Rate | 3.7 L/min |
| Broadband High Mass | 2600.0 m/z | Laser Power | 20.2 lp | Capillary | 4500.0 V |
| No. of Cell Fills | 1 | n/a | n/a | Drying Gas Temperature | 200.0 °C |
| Apodization | Full-Sine | Time of Flight to Detector | 0.001 sec | | |



Bruker Daltonics solariX | ETH - MS-Service LOC - D-CHAB | Page 1 of 3

FT12373 Kevin Weiland/Mayor - w-6th2TMS - DCM / DCTB

ETH Eidgenössische Technische Hochschule Zürich Swiss Federal Institute of Technology Zurich

**Evaluation Spectra / Validation Formula:**

| # | Ion Formula | Adduct | m/z | z | Meas. m/z | mSigma | N-Rule | err [mDa] | err [ppm] |
|---|---|---|---|---|---|---|---|---|---|
| 1 | C74H84S6Si2 | M | 1220.4430 | 1+ | 1220.4422 | 68.1 | ok | 0.9 | 0.7 |

**Calibration Info:**

| | |
|---|---|
| Date: | 22.09.2017 11:11:47 |
| Polarity: | Positive |
| Calibration spectrum: | +MS: Scan |
| Reference mass list: | MALDI: DCTB Matrix + HP-Mix (pos) |
| Calibration mode: | Quadratic |

| Reference m/z | Resulting m/z | Intensity | Error [ppm] |
|---|---|---|---|
| 118.0863 | | | |
| 250.1464 | | | |
| 251.1543 | | | |
| 273.1362 | | | |
| 322.0481 | | | |
| 332.2009 | 332.2009 | 224770 | -0.034 |
| 500.2934 | 500.2935 | 4095026 | 0.108 |
| 501.3013 | 501.3012 | 2135220 | -0.052 |
| 523.2832 | 523.2833 | 1110991 | 0.211 |
| 622.0290 | 622.0289 | 283078752 | -0.145 |
| 750.4404 | | | |
| 751.4483 | | | |
| 773.4302 | | | |
| 922.0098 | 922.0095 | 674964160 | -0.332 |
| 1000.5874 | | | |
| 1001.5953 | | | |
| 1023.5772 | | | |
| 1221.9906 | | | |
| 1521.9715 | 1521.9713 | 361528896 | -0.124 |
| 1821.9523 | 1821.9527 | 113745496 | 0.191 |
| 2121.9332 | 2121.9339 | 50713692 | 0.332 |
| 2421.9140 | | | |
| 2721.8948 | | | |

Standard deviation: 0.250

**Mass List:**

| # | m/z | Res. | S/N | I % | FWHM |
|---|---|---|---|---|---|
| 1 | 610.2213 | 341866 | 1338.2 | 2.4 | 0.0018 |
| 2 | 622.0266 | 610826 | 1448.7 | 2.7 | 0.0010 |
| 3 | 622.0289 | 330425 | 9176.5 | 17.0 | 0.0019 |
| 4 | 623.0323 | 324737 | 1014.1 | 1.9 | 0.0019 |
| 5 | 922.0095 | 217345 | 17671.0 | 40.4 | 0.0042 |
| 6 | 923.0132 | 218637 | 2898.7 | 6.8 | 0.0042 |
| 7 | 950.2991 | 212962 | 3584.3 | 8.5 | 0.0045 |
| 8 | 951.2975 | 300524 | 589.2 | 1.4 | 0.0032 |
| 9 | 951.3025 | 229569 | 1944.0 | 4.6 | 0.0041 |
| 10 | 952.2952 | 194770 | 750.2 | 1.8 | 0.0049 |
| 11 | 952.3063 | 230774 | 524.9 | 1.3 | 0.0041 |
| 12 | 953.2987 | 214773 | 453.3 | 1.1 | 0.0044 |
| 13 | 1066.4161 | 187634 | 2543.0 | 6.8 | 0.0057 |
| 14 | 1067.4195 | 195394 | 1747.5 | 4.6 | 0.0055 |
| 15 | 1068.4118 | 163832 | 500.3 | 1.3 | 0.0065 |
| 16 | 1068.4233 | 196223 | 532.2 | 1.4 | 0.0054 |
| 17 | 1148.4039 | 170728 | 1166.9 | 3.3 | 0.0067 |
| 18 | 1149.4077 | 173657 | 904.3 | 2.5 | 0.0066 |
| 19 | 1220.4422 | 159543 | 33822.1 | 100.0 | 0.0076 |
| 20 | 1221.4452 | 160207 | 30904.5 | 91.4 | 0.0076 |
| 21 | 1221.9903 | 159096 | 13329.7 | 39.4 | 0.0077 |
| 22 | 1222.4394 | 154037 | 8875.6 | 26.2 | 0.0079 |
| 23 | 1222.4484 | 134624 | 8513.3 | 25.2 | 0.0091 |
| 24 | 1222.9943 | 161222 | 3024.8 | 8.9 | 0.0076 |
| 25 | 1223.4424 | 161809 | 8830.5 | 26.1 | 0.0076 |
| 26 | 1223.4546 | 178197 | 1885.6 | 5.6 | 0.0069 |
| 27 | 1224.4344 | 170500 | 1116.8 | 3.3 | 0.0072 |
| 28 | 1224.4459 | 155059 | 3210.6 | 9.5 | 0.0079 |
| 29 | 1224.4589 | 234169 | 426.5 | 1.3 | 0.0052 |
| 30 | 1225.4384 | 159660 | 941.8 | 2.8 | 0.0077 |
| 31 | 1225.4503 | 150988 | 646.3 | 1.9 | 0.0081 |
| 32 | 1252.4337 | 155448 | 467.7 | 1.4 | 0.0081 |
| 33 | 1253.4372 | 157498 | 379.1 | 1.1 | 0.0080 |
| 34 | 1521.9713 | 131170 | 7288.8 | 21.6 | 0.0116 |
| 35 | 1522.9751 | 132032 | 2172.4 | 6.5 | 0.0115 |
| 36 | 1523.9785 | 129551 | 367.3 | 1.1 | 0.0118 |
| 37 | 1821.9527 | 107925 | 2064.3 | 6.8 | 0.0169 |
| 38 | 1822.9562 | 107148 | 754.2 | 2.5 | 0.0170 |
| 39 | 2121.9339 | 89158 | 837.7 | 3.0 | 0.0238 |
| 40 | 2122.9371 | 87568 | 375.6 | 1.4 | 0.0242 |

| # | m/z | Res. | S/N | I % | FWHM |
|---|---|---|---|---|---|
| 1 | 1220.4430 | 159543 | | 100.0 | 0.0076 |
| 2 | 1221.4458 | 159674 | | 95.9 | 0.0076 |
| 3 | 1222.4391 | 159804 | | 34.4 | 0.0076 |
| 4 | 1222.4486 | 159805 | | 44.4 | 0.0076 |
| 5 | 1223.4419 | 159935 | | 32.3 | 0.0076 |
| 6 | 1223.4518 | 159936 | | 13.3 | 0.0076 |
| 7 | 1224.4352 | 160065 | | 5.2 | 0.0076 |
| 8 | 1224.4449 | 160066 | | 14.7 | 0.0076 |
| 9 | 1224.4549 | 160068 | | 2.9 | 0.0076 |
| 10 | 1225.4381 | 160196 | | 4.8 | 0.0076 |
| 11 | 1225.4480 | 160197 | | 4.4 | 0.0076 |
| 12 | 1225.4581 | 160199 | | 0.5 | 0.0076 |
| 13 | 1226.4314 | 160326 | | 0.5 | 0.0076 |
| 14 | 1226.4411 | 160327 | | 2.1 | 0.0076 |
| 15 | 1226.4510 | 160329 | | 0.9 | 0.0076 |

Bruker Daltonics solariX | ETH - MS-Service LOC - D-CHAB | Page 2 of 3

FT12373 Kevin Weiland/Mayor - w-6th2TMS - DCM / DCTB

ETH Eidgenössische Technische Hochschule Zürich Swiss Federal Institute of Technology Zurich

| # | m/z | Res. | S/N | I % | FWHM |
|---|---|---|---|---|---|
| 16 | 1227.4344 | 160457 | | 0.4 | 0.0076 |
| 17 | 1227.4442 | 160458 | | 0.6 | 0.0076 |
| 18 | 1227.4542 | 160460 | | 0.2 | 0.0076 |
| 19 | 1228.4374 | 160588 | | 0.2 | 0.0076 |
| 20 | 1228.4473 | 160590 | | 0.1 | 0.0076 |

Bruker Daltonics solariX | ETH - MS-Service LOC - D-CHAB | Page 3 of 3

**Figure S24:** High resolution MALDI ToF spectrum for compound **7**.

## Compound 8

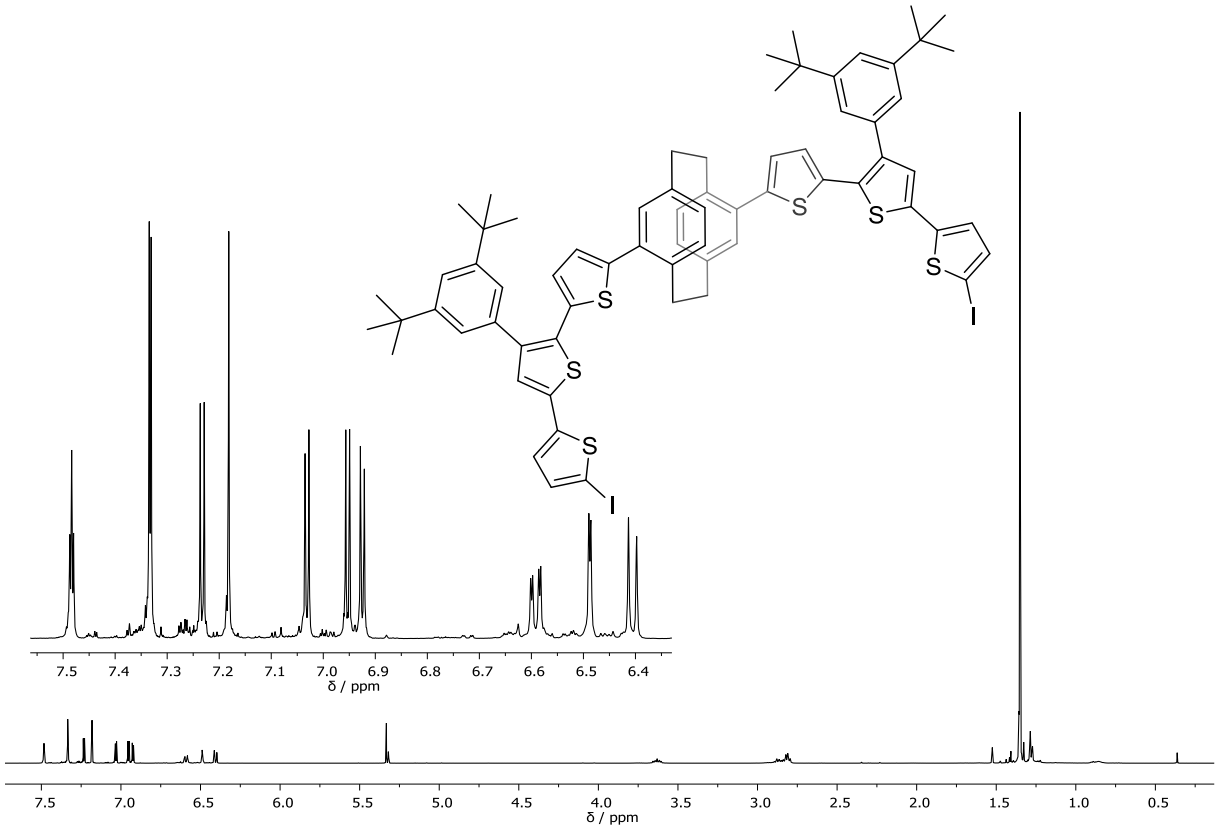


**Figure S25:** $^{1}H$ NMR spectrum (500 MHz, $CD_2Cl_2$) of compound **8**.

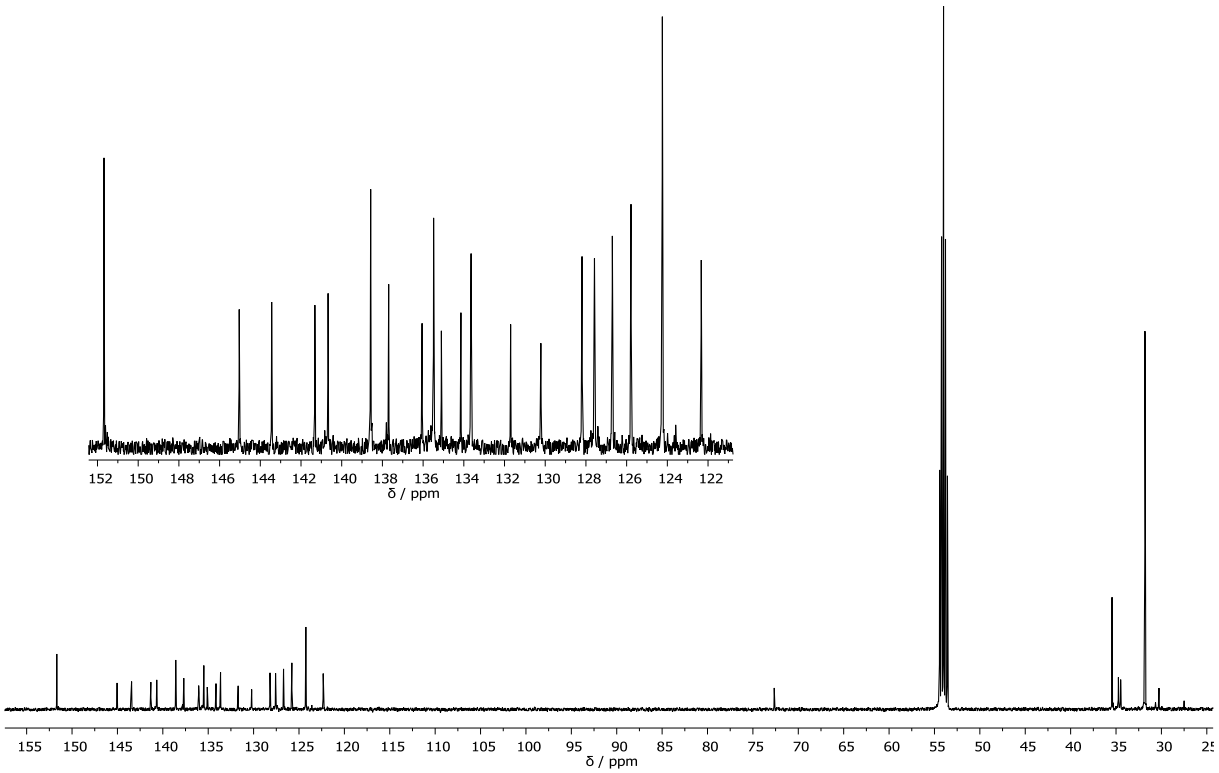


**Figure S26:** $^{13}C$ NMR spectrum (126 MHz, $CD_2Cl_2$) of compound **8**.

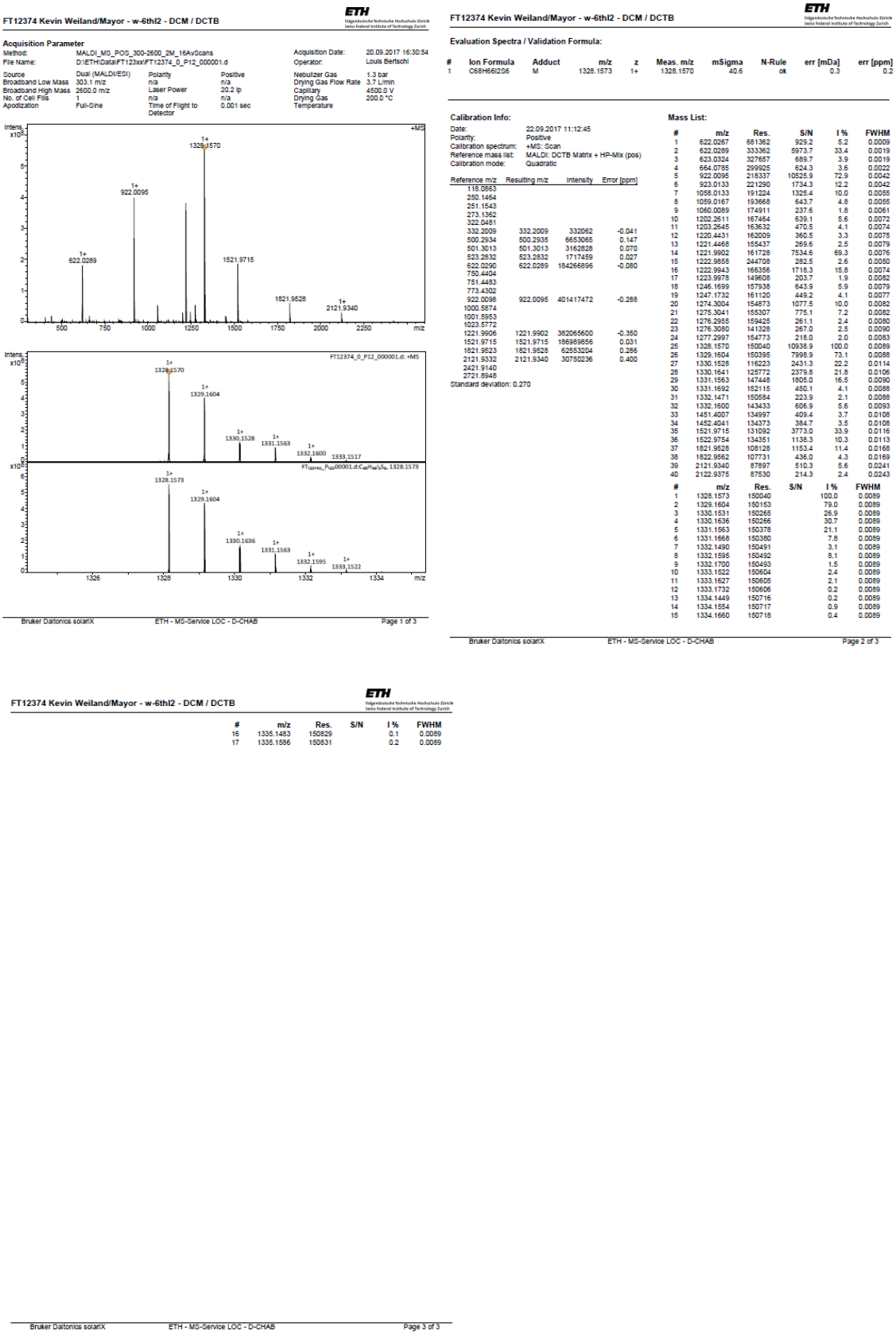

FT12374 Kevin Weiland/Mayor - w-6thl2 - DCM / DCTB

ETH Eidgenössische Technische Hochschule Zürich Swiss Federal Institute of Technology Zurich

**Acquisition Parameter**

| | | | | | |
|---|---|---|---|---|---|
| Method: | MALDI_MS_POS_300-2600_2M_16Av5cans | | | Acquisition Date: | 20.09.2017 16:30:54 |
| File Name: | D:\ETHCadal\FT123xx\FT12374_0_P12_000001.d | | | Operator: | Louis Bertschi |
| Source | Dual (MALDI/ESI) | Polarity | Positive | Nebulizer Gas | 1.3 bar |
| Broadband Low Mass | 303.1 m/z | n/a | n/a | Drying Gas Flow Rate | 3.7 L/min |
| Broadband High Mass | 2600.0 m/z | Laser Power | 20.2 lp | Capillary | 4500.0 V |
| No. of Cell Fills | 1 | n/a | n/a | Drying Gas | 200.0 °C |
| Apodization | Full-Sine | Time of Flight to Detector | 0.001 sec | Temperature | |



Bruker Daltonics solariX — ETH - MS-Service LOC - D-CHAB — Page 1 of 3

FT12374 Kevin Weiland/Mayor - w-6thl2 - DCM / DCTB

ETH Eidgenössische Technische Hochschule Zürich Swiss Federal Institute of Technology Zurich

**Evaluation Spectra / Validation Formula:**

| # | Ion Formula | Adduct | m/z | z | Meas. m/z | mSigma | N-Rule | err [mDa] | err [ppm] |
|---|---|---|---|---|---|---|---|---|---|
| 1 | C68H66I2S6 | M | 1328.1573 | 1+ | 1328.1570 | 40.6 | ok | 0.3 | 0.2 |

**Calibration Info:**

| | |
|---|---|
| Date: | 22.09.2017 11:12:45 |
| Polarity: | Positive |
| Calibration spectrum: | +MS: Scan |
| Reference mass list: | MALDI: DCTB Matrix + HP-Mix (pos) |
| Calibration mode: | Quadratic |

| Reference m/z | Resulting m/z | Intensity | Error [ppm] |
|---|---|---|---|
| 118.0863 | | | |
| 250.1464 | | | |
| 251.1543 | | | |
| 273.1362 | | | |
| 322.0481 | | | |
| 332.2009 | 332.2009 | 332062 | -0.041 |
| 500.2934 | 500.2935 | 6653065 | 0.147 |
| 501.3013 | 501.3013 | 3162828 | 0.070 |
| 523.2832 | 523.2832 | 1717459 | 0.027 |
| 622.0290 | 622.0289 | 184266896 | -0.080 |
| 750.4404 | | | |
| 751.4483 | | | |
| 773.4302 | | | |
| 922.0096 | 922.0095 | 401417472 | -0.288 |
| 1000.5874 | | | |
| 1001.5953 | | | |
| 1023.5772 | | | |
| 1221.9906 | 1221.9902 | 382065600 | -0.350 |
| 1521.9715 | 1521.9715 | 186989656 | 0.031 |
| 1821.9623 | 1821.9528 | 62553204 | 0.286 |
| 2121.9332 | 2121.9340 | 30750236 | 0.400 |
| 2421.9140 | | | |
| 2721.8948 | | | |

Standard deviation: 0.270

**Mass List:**

| # | m/z | Res. | S/N | I % | FWHM |
|---|---|---|---|---|---|
| 1 | 622.0267 | 681362 | 929.2 | 5.2 | 0.0009 |
| 2 | 622.0289 | 333362 | 5973.7 | 33.4 | 0.0019 |
| 3 | 623.0324 | 327657 | 689.7 | 3.9 | 0.0019 |
| 4 | 664.0785 | 299925 | 624.3 | 3.6 | 0.0022 |
| 5 | 922.0095 | 218337 | 10525.9 | 72.9 | 0.0042 |
| 6 | 923.0133 | 221290 | 1734.3 | 12.2 | 0.0042 |
| 7 | 1058.0133 | 191224 | 1325.4 | 10.0 | 0.0055 |
| 8 | 1059.0167 | 193668 | 643.7 | 4.8 | 0.0055 |
| 9 | 1060.0089 | 174911 | 237.6 | 1.8 | 0.0061 |
| 10 | 1202.2611 | 167464 | 639.1 | 5.6 | 0.0072 |
| 11 | 1203.2645 | 163632 | 470.5 | 4.1 | 0.0074 |
| 12 | 1220.4431 | 162009 | 360.5 | 3.3 | 0.0075 |
| 13 | 1221.4468 | 155437 | 269.6 | 2.5 | 0.0079 |
| 14 | 1221.9902 | 161728 | 7534.6 | 69.3 | 0.0076 |
| 15 | 1222.9858 | 244708 | 282.5 | 2.6 | 0.0050 |
| 16 | 1222.9943 | 166356 | 1718.3 | 15.8 | 0.0074 |
| 17 | 1223.9978 | 149608 | 203.7 | 1.9 | 0.0082 |
| 18 | 1246.1699 | 157938 | 643.9 | 5.9 | 0.0079 |
| 19 | 1247.1732 | 161120 | 449.2 | 4.1 | 0.0077 |
| 20 | 1274.3004 | 154873 | 1077.5 | 10.0 | 0.0082 |
| 21 | 1275.3041 | 155307 | 775.1 | 7.2 | 0.0082 |
| 22 | 1276.2955 | 159425 | 261.1 | 2.4 | 0.0080 |
| 23 | 1276.3080 | 141328 | 267.0 | 2.5 | 0.0090 |
| 24 | 1277.2997 | 154773 | 218.0 | 2.0 | 0.0083 |
| 25 | 1328.1570 | 150040 | 10938.9 | 100.0 | 0.0089 |
| 26 | 1329.1604 | 150395 | 7998.9 | 73.1 | 0.0088 |
| 27 | 1330.1528 | 116223 | 2431.3 | 22.2 | 0.0114 |
| 28 | 1330.1641 | 125772 | 2379.8 | 21.8 | 0.0106 |
| 29 | 1331.1563 | 147448 | 1805.0 | 16.5 | 0.0090 |
| 30 | 1331.1692 | 152115 | 450.1 | 4.1 | 0.0088 |
| 31 | 1332.1471 | 150584 | 223.9 | 2.1 | 0.0088 |
| 32 | 1332.1600 | 143433 | 606.9 | 5.6 | 0.0093 |
| 33 | 1451.4007 | 134997 | 409.4 | 3.7 | 0.0108 |
| 34 | 1452.4041 | 134373 | 384.7 | 3.5 | 0.0108 |
| 35 | 1521.9715 | 131092 | 3773.0 | 33.9 | 0.0116 |
| 36 | 1522.9754 | 134351 | 1138.3 | 10.3 | 0.0113 |
| 37 | 1821.9528 | 108128 | 1153.4 | 11.4 | 0.0168 |
| 38 | 1822.9562 | 107731 | 436.0 | 4.3 | 0.0169 |
| 39 | 2121.9340 | 87897 | 510.3 | 5.6 | 0.0241 |
| 40 | 2122.9375 | 87530 | 214.3 | 2.4 | 0.0243 |

| # | m/z | Res. | S/N | I % | FWHM |
|---|---|---|---|---|---|
| 1 | 1328.1573 | 150040 | | 100.0 | 0.0089 |
| 2 | 1329.1604 | 150153 | | 79.0 | 0.0089 |
| 3 | 1330.1531 | 150265 | | 26.9 | 0.0089 |
| 4 | 1330.1636 | 150266 | | 30.7 | 0.0089 |
| 5 | 1331.1563 | 150378 | | 21.1 | 0.0089 |
| 6 | 1331.1668 | 150380 | | 7.8 | 0.0089 |
| 7 | 1332.1490 | 150491 | | 3.1 | 0.0089 |
| 8 | 1332.1595 | 150492 | | 8.1 | 0.0089 |
| 9 | 1332.1700 | 150493 | | 1.5 | 0.0089 |
| 10 | 1333.1522 | 150604 | | 2.4 | 0.0089 |
| 11 | 1333.1627 | 150605 | | 2.1 | 0.0089 |
| 12 | 1333.1732 | 150606 | | 0.2 | 0.0089 |
| 13 | 1334.1449 | 150716 | | 0.2 | 0.0089 |
| 14 | 1334.1554 | 150717 | | 0.9 | 0.0089 |
| 15 | 1334.1660 | 150718 | | 0.4 | 0.0089 |

Bruker Daltonics solariX — ETH - MS-Service LOC - D-CHAB — Page 2 of 3

FT12374 Kevin Weiland/Mayor - w-6thl2 - DCM / DCTB

ETH Eidgenössische Technische Hochschule Zürich Swiss Federal Institute of Technology Zurich

| # | m/z | Res. | S/N | I % | FWHM |
|---|---|---|---|---|---|
| 16 | 1335.1483 | 150829 | | 0.1 | 0.0089 |
| 17 | 1335.1586 | 150831 | | 0.2 | 0.0089 |

Bruker Daltonics solariX — ETH - MS-Service LOC - D-CHAB — Page 3 of 3

**Figure S27:** High resolution MALDI ToF spectrum for compound **8**.

## Compound 9

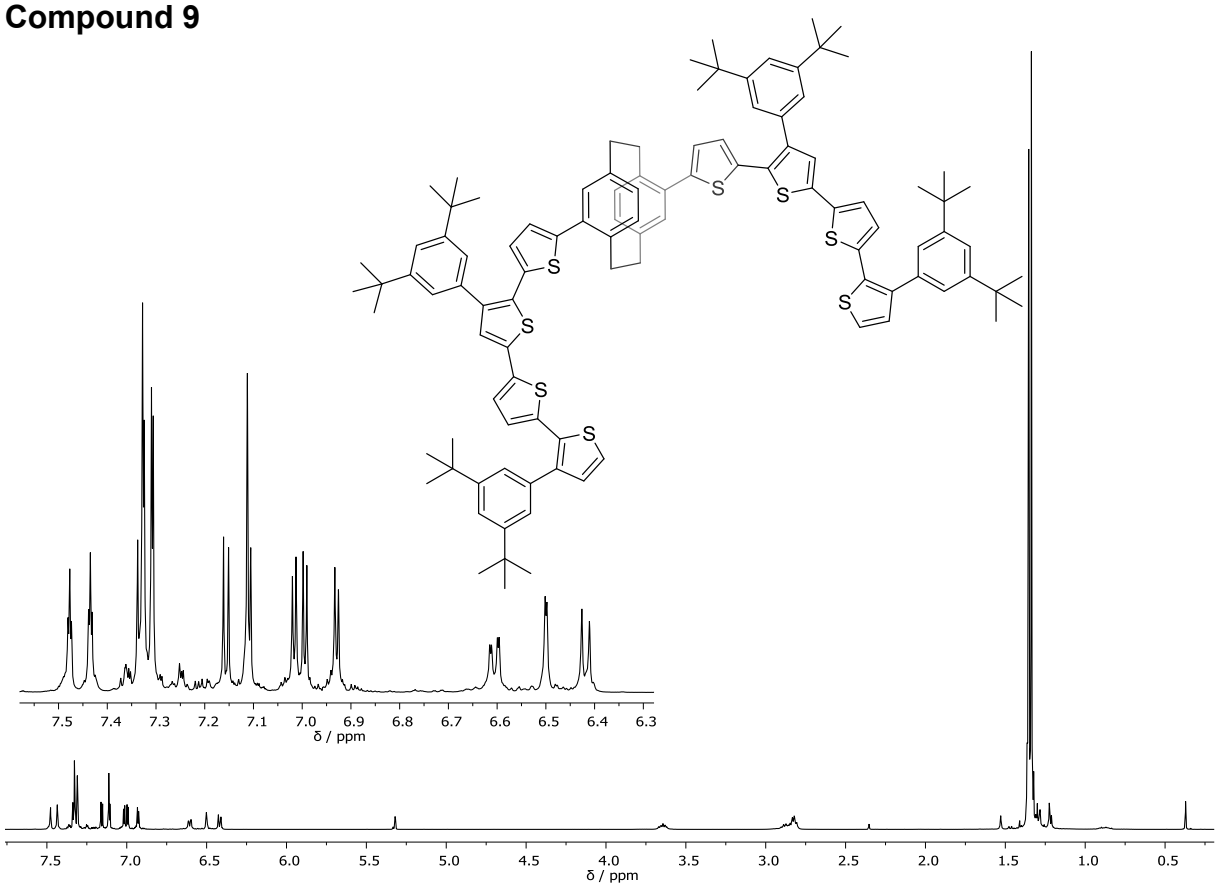


**Figure S28:** $^{1}H$ NMR spectrum (500 MHz, $CD_2Cl_2$) of compound **9**.

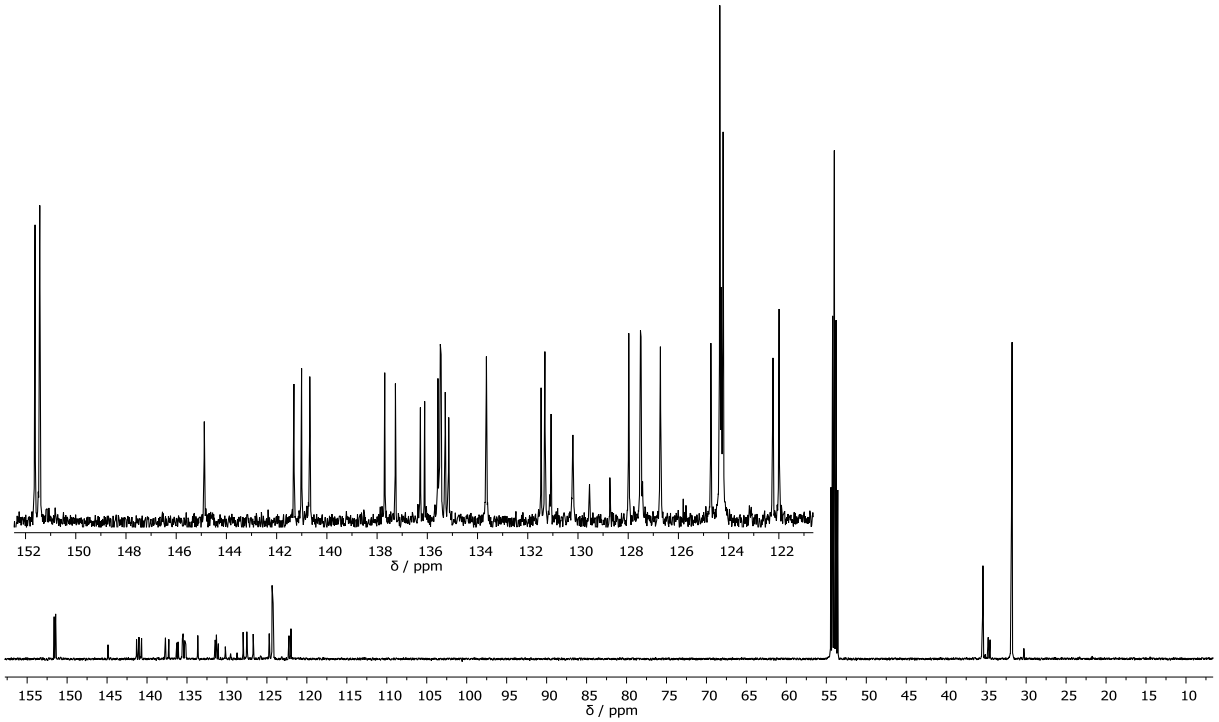


**Figure S29:** $^{13}C$ NMR spectrum (126 MHz, $CD_2Cl_2$) of compound **9**.

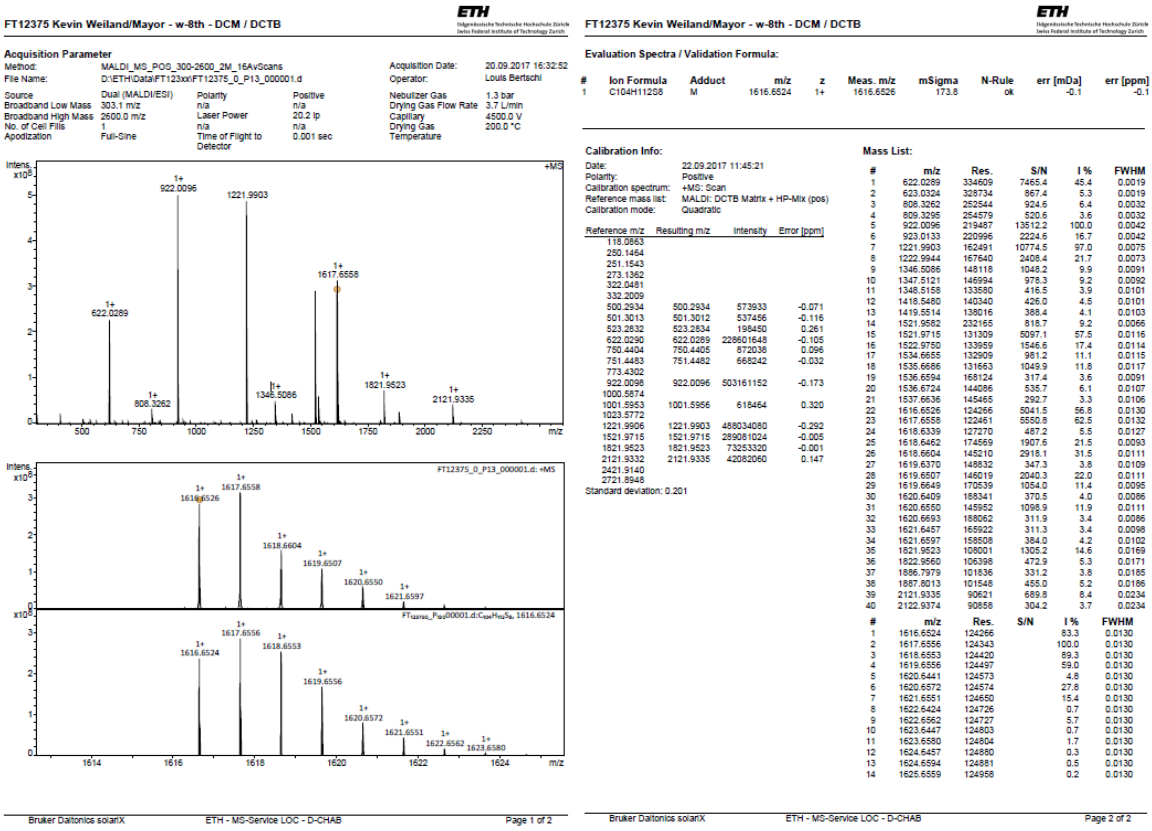

FT12375 Kevin Weiland/Mayor - w-8th - DCM / DCTB

Acquisition Parameter

| | | | | | |
|---|---|---|---|---|---|
| Method: | MALDI_MS_POS_300-2600_2M_16Av0cans | | | Acquisition Date: | 20.09.2017 16:32:52 |
| File Name: | D:\ETH\Data\FT123xxx\FT12375_0_P13_000001.d | | | Operator: | Louis Bertschi |
| Source | Dual (MALDI/ESI) | Polarity | Positive | Nebulizer Gas | 1.3 bar |
| Broadband Low Mass | 303.1 m/z | n/a | n/a | Drying Gas Flow Rate | 3.7 L/min |
| Broadband High Mass | 2600.0 m/z | Laser Power | 20.2 lp | Capillary | 4500.0 V |
| No. of Cell Fills | 1 | n/a | n/a | Drying Gas | 200.0 °C |
| Apodization | Full-Sine | Time of Flight to Detector | 0.001 sec | Temperature | |



Bruker Daltonics solariX | ETH - MS-Service LOC - D-CHAB | Page 1 of 2

FT12375 Kevin Weiland/Mayor - w-8th - DCM / DCTB

Evaluation Spectra / Validation Formula:

| # | Ion Formula | Adduct | m/z | z | Meas. m/z | mSigma | N-Rule | err [mDa] | err [ppm] |
|---|---|---|---|---|---|---|---|---|---|
| 1 | C104H112S8 | M | 1616.6524 | 1+ | 1616.6526 | 173.8 | ok | -0.1 | -0.1 |

Calibration Info:

| | |
|---|---|
| Date: | 22.09.2017 11:45:21 |
| Polarity: | Positive |
| Calibration spectrum: | +MS: Scan |
| Reference mass list: | MALDI: DCTB Matrix + HP-Mix (pos) |
| Calibration mode: | Quadratic |

| Reference m/z | Resulting m/z | Intensity | Error [ppm] |
|---|---|---|---|
| 118.0863 | | | |
| 260.1464 | | | |
| 261.1543 | | | |
| 273.1362 | | | |
| 322.0481 | | | |
| 332.2009 | | | |
| 500.2934 | 500.2934 | 573933 | -0.071 |
| 501.3013 | 501.3012 | 537456 | -0.116 |
| 523.2832 | 523.2834 | 198450 | 0.261 |
| 622.0290 | 622.0289 | 228601648 | -0.105 |
| 750.4404 | 750.4405 | 872038 | 0.096 |
| 751.4483 | 751.4482 | 668242 | -0.032 |
| 773.4302 | | | |
| 922.0098 | 922.0096 | 503161152 | -0.173 |
| 1000.5874 | | | |
| 1001.5953 | 1001.5956 | 618464 | 0.320 |
| 1023.5772 | | | |
| 1221.9906 | 1221.9903 | 488034080 | -0.292 |
| 1521.9715 | 1521.9715 | 289081024 | -0.005 |
| 1821.9523 | 1821.9523 | 73253320 | -0.001 |
| 2121.9332 | 2121.9335 | 42082060 | 0.147 |
| 2421.9140 | | | |
| 2721.8948 | | | |

Standard deviation: 0.201

Mass List:

| # | m/z | Res. | S/N | I % | FWHM |
|---|---|---|---|---|---|
| 1 | 622.0289 | 334609 | 7465.4 | 45.4 | 0.0019 |
| 2 | 623.0324 | 328734 | 867.4 | 5.3 | 0.0019 |
| 3 | 808.3262 | 252544 | 924.6 | 6.4 | 0.0032 |
| 4 | 809.3295 | 254579 | 520.6 | 3.6 | 0.0032 |
| 5 | 922.0096 | 219487 | 13512.2 | 100.0 | 0.0042 |
| 6 | 923.0133 | 220996 | 2224.6 | 16.7 | 0.0042 |
| 7 | 1221.9903 | 162491 | 10774.5 | 97.0 | 0.0075 |
| 8 | 1222.9944 | 167640 | 2408.4 | 21.7 | 0.0073 |
| 9 | 1346.5086 | 148118 | 1048.2 | 9.9 | 0.0091 |
| 10 | 1347.5121 | 146994 | 978.3 | 9.2 | 0.0092 |
| 11 | 1348.5158 | 133580 | 416.5 | 3.9 | 0.0101 |
| 12 | 1418.5480 | 140340 | 426.0 | 4.5 | 0.0101 |
| 13 | 1419.5514 | 138016 | 388.4 | 4.1 | 0.0103 |
| 14 | 1521.9582 | 232165 | 818.7 | 9.2 | 0.0066 |
| 15 | 1521.9715 | 131309 | 5097.1 | 57.5 | 0.0116 |
| 16 | 1522.9750 | 133959 | 1546.6 | 17.4 | 0.0114 |
| 17 | 1534.6655 | 132909 | 981.2 | 11.1 | 0.0115 |
| 18 | 1535.6686 | 131663 | 1049.9 | 11.8 | 0.0117 |
| 19 | 1536.6594 | 168124 | 317.4 | 3.6 | 0.0091 |
| 20 | 1536.6724 | 144086 | 535.7 | 6.1 | 0.0107 |
| 21 | 1537.6636 | 145465 | 292.7 | 3.3 | 0.0106 |
| 22 | 1616.6526 | 124266 | 5041.5 | 56.8 | 0.0130 |
| 23 | 1617.6558 | 122461 | 5550.8 | 62.5 | 0.0132 |
| 24 | 1618.6339 | 127270 | 467.2 | 5.5 | 0.0127 |
| 25 | 1618.6462 | 174569 | 1907.6 | 21.5 | 0.0093 |
| 26 | 1618.6604 | 145210 | 2918.1 | 31.5 | 0.0111 |
| 27 | 1619.6370 | 148832 | 347.3 | 3.8 | 0.0109 |
| 28 | 1619.6507 | 146019 | 2040.3 | 22.0 | 0.0111 |
| 29 | 1619.6649 | 170539 | 1054.0 | 11.4 | 0.0095 |
| 30 | 1620.6409 | 188341 | 370.5 | 4.0 | 0.0086 |
| 31 | 1620.6550 | 145952 | 1098.9 | 11.9 | 0.0111 |
| 32 | 1620.6693 | 188062 | 311.9 | 3.4 | 0.0086 |
| 33 | 1621.6457 | 165922 | 311.3 | 3.4 | 0.0098 |
| 34 | 1621.6597 | 158508 | 384.0 | 4.2 | 0.0102 |
| 35 | 1821.9523 | 108001 | 1305.2 | 14.6 | 0.0169 |
| 36 | 1822.9560 | 106398 | 472.9 | 5.3 | 0.0171 |
| 37 | 1886.7979 | 101836 | 331.2 | 3.8 | 0.0185 |
| 38 | 1887.8013 | 101548 | 455.0 | 5.2 | 0.0186 |
| 39 | 2121.9335 | 90621 | 689.8 | 8.4 | 0.0234 |
| 40 | 2122.9374 | 90858 | 304.2 | 3.7 | 0.0234 |

| # | m/z | Res. | S/N | I % | FWHM |
|---|---|---|---|---|---|
| 1 | 1616.6524 | 124266 | | 83.3 | 0.0130 |
| 2 | 1617.6556 | 124343 | | 100.0 | 0.0130 |
| 3 | 1618.6553 | 124420 | | 89.3 | 0.0130 |
| 4 | 1619.6556 | 124497 | | 59.0 | 0.0130 |
| 5 | 1620.6441 | 124573 | | 4.8 | 0.0130 |
| 6 | 1620.6572 | 124574 | | 27.8 | 0.0130 |
| 7 | 1621.6551 | 124650 | | 15.4 | 0.0130 |
| 8 | 1622.6424 | 124726 | | 0.7 | 0.0130 |
| 9 | 1622.6562 | 124727 | | 5.7 | 0.0130 |
| 10 | 1623.6447 | 124803 | | 0.7 | 0.0130 |
| 11 | 1623.6580 | 124804 | | 1.7 | 0.0130 |
| 12 | 1624.6457 | 124880 | | 0.3 | 0.0130 |
| 13 | 1624.6594 | 124881 | | 0.5 | 0.0130 |
| 14 | 1625.6559 | 124958 | | 0.2 | 0.0130 |

Bruker Daltonics solariX | ETH - MS-Service LOC - D-CHAB | Page 2 of 2

**Figure S30:** High resolution MALDI ToF spectrum for compound **9**.

**Compound 10**

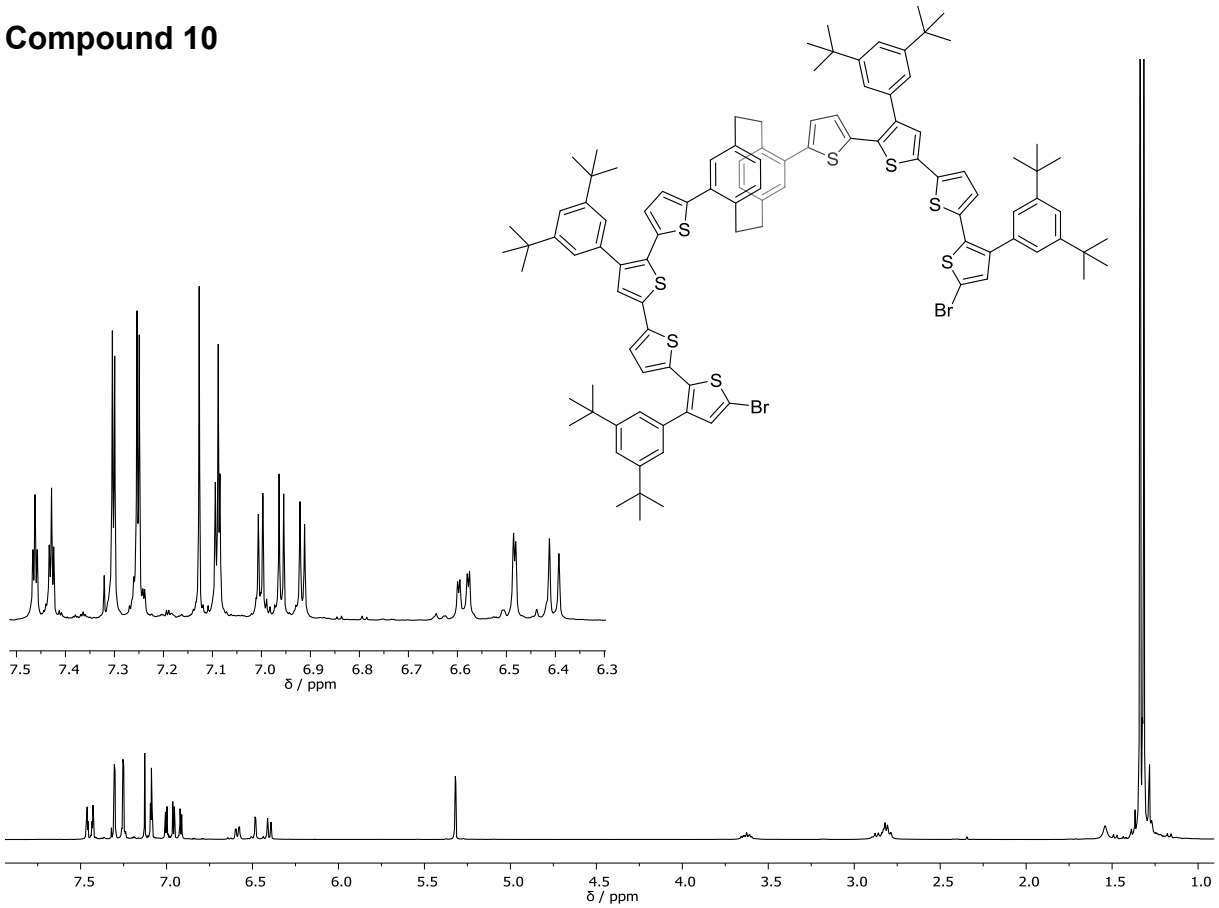


**Figure S31:** $^{1}H$ NMR spectrum (400 MHz, $CD_2Cl_2$) of compound **10**.

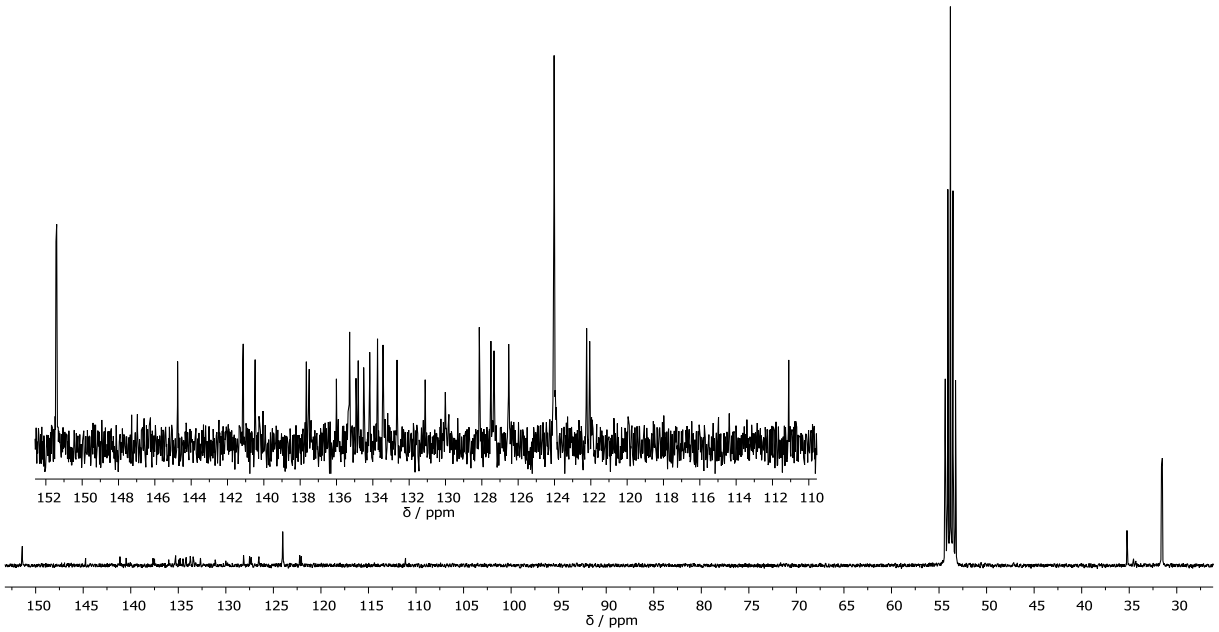


**Figure S32:** $^{13}C$ NMR spectrum (101 MHz, $CD_2Cl_2$) of compound **10**.

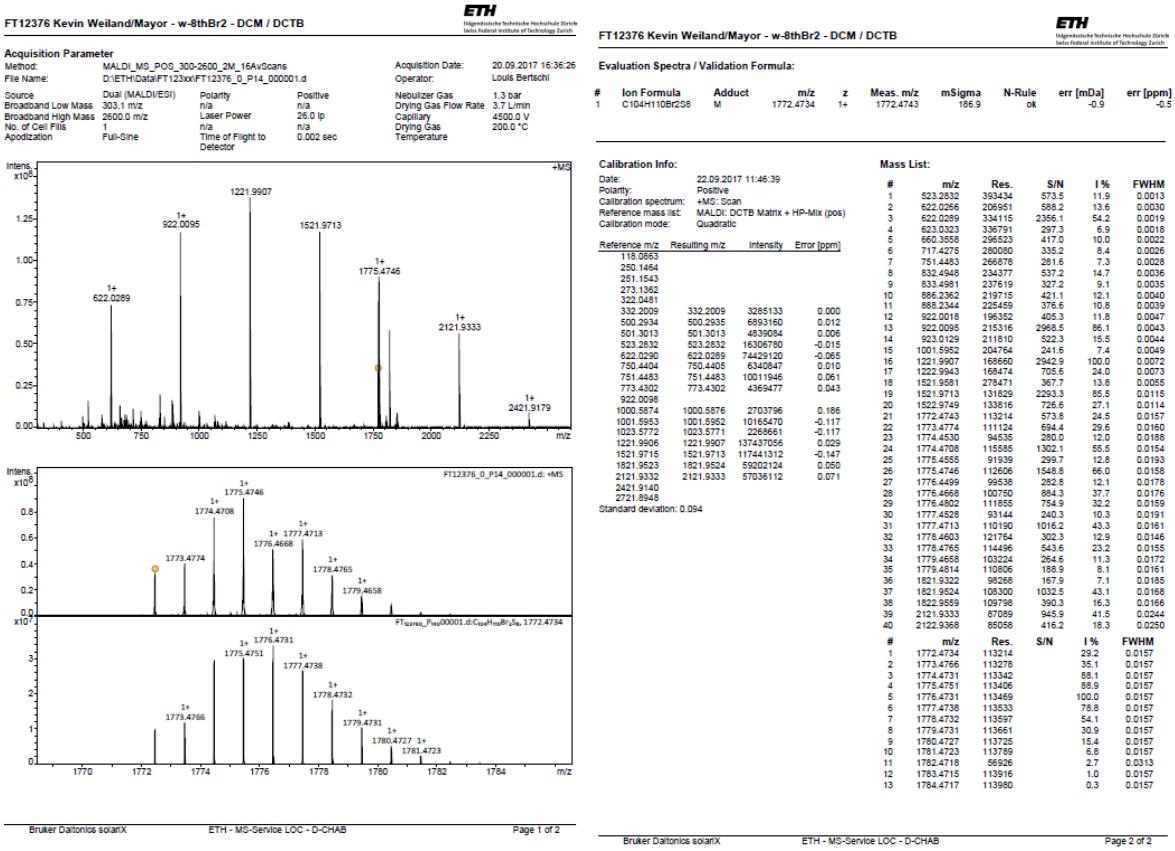

FT12376 Kevin Weiland/Mayor - w-8thBr2 - DCM / DCTB

ETH Eidgenössische Technische Hochschule Zürich Swiss Federal Institute of Technology Zurich

**Acquisition Parameter**

| | | | | | |
|---|---|---|---|---|---|
| Method: | MALDI_MS_POS_300-2600_2M_16AvScans | | | Acquisition Date: | 20.09.2017 16:36:26 |
| File Name: | D:\ETH\Data\FT123xx\FT12376_0_P14_000001.d | | | Operator: | Louis Bertschi |
| Source | Dual (MALDI/ESI) | Polarity | Positive | Nebulizer Gas | 1.3 bar |
| Broadband Low Mass | 303.1 m/z | n/a | n/a | Drying Gas Flow Rate | 3.7 L/min |
| Broadband High Mass | 2600.0 m/z | Laser Power | 26.0 lp | Capillary | 4500.0 V |
| No. of Cell Fills | 1 | n/a | n/a | Drying Gas | 200.0 °C |
| Apodization | Full-Sine | Time of Flight to Detector | 0.002 sec | Temperature | |



Bruker Daltonics solariX | ETH - MS-Service LOC - D-CHAB | Page 1 of 2

FT12376 Kevin Weiland/Mayor - w-8thBr2 - DCM / DCTB

ETH Eidgenössische Technische Hochschule Zürich Swiss Federal Institute of Technology Zurich

**Evaluation Spectra / Validation Formula:**

| # | Ion Formula | Adduct | m/z | z | Meas. m/z | mSigma | N-Rule | err [mDa] | err [ppm] |
|---|---|---|---|---|---|---|---|---|---|
| 1 | C104H110Br2S8 | M | 1772.4734 | 1+ | 1772.4743 | 186.9 | ok | -0.9 | -0.5 |

**Calibration Info:**

Date: 22.09.2017 11:46:39
Polarity: Positive
Calibration spectrum: +MG: Sican
Reference mass list: MALDI: DCTB Matrix + HP-Mix (pos)
Calibration mode: Quadratic

| Reference m/z | Resulting m/z | Intensity | Error [ppm] |
|---|---|---|---|
| 118.0863 | | | |
| 250.1464 | | | |
| 251.1543 | | | |
| 273.1362 | | | |
| 322.0481 | | | |
| 332.2009 | 332.2009 | 3285133 | 0.000 |
| 500.2934 | 500.2935 | 6893160 | 0.012 |
| 501.3013 | 501.3013 | 4839084 | 0.006 |
| 523.2832 | 523.2832 | 16306780 | -0.015 |
| 622.0290 | 622.0289 | 74429120 | -0.065 |
| 750.4404 | 750.4405 | 6340847 | 0.010 |
| 751.4483 | 751.4483 | 10011946 | 0.061 |
| 773.4302 | 773.4302 | 4369477 | 0.043 |
| 922.0098 | | | |
| 1000.5874 | 1000.5876 | 2703796 | 0.186 |
| 1001.5953 | 1001.5952 | 10165470 | -0.117 |
| 1023.5772 | 1023.5771 | 2268661 | -0.117 |
| 1221.9906 | 1221.9907 | 137437056 | 0.029 |
| 1521.9715 | 1521.9713 | 117441312 | -0.147 |
| 1821.9523 | 1821.9524 | 59202124 | 0.050 |
| 2121.9332 | 2121.9333 | 57036112 | 0.071 |
| 2421.9140 | | | |
| 2721.8948 | | | |

Standard deviation: 0.094

**Mass List:**

| # | m/z | Res. | S/N | I % | FWHM |
|---|---|---|---|---|---|
| 1 | 523.2832 | 393434 | 573.5 | 11.9 | 0.0013 |
| 2 | 622.0266 | 206951 | 588.2 | 13.6 | 0.0030 |
| 3 | 622.0289 | 334115 | 2356.1 | 54.2 | 0.0019 |
| 4 | 623.0323 | 336791 | 297.3 | 6.9 | 0.0018 |
| 5 | 660.3558 | 296523 | 417.0 | 10.0 | 0.0022 |
| 6 | 717.4275 | 280080 | 335.2 | 8.4 | 0.0026 |
| 7 | 751.4483 | 266878 | 281.6 | 7.3 | 0.0028 |
| 8 | 832.4948 | 234377 | 537.2 | 14.7 | 0.0036 |
| 9 | 833.4981 | 237619 | 327.2 | 9.1 | 0.0035 |
| 10 | 886.2362 | 219715 | 421.1 | 12.1 | 0.0040 |
| 11 | 888.2344 | 225459 | 376.6 | 10.8 | 0.0039 |
| 12 | 922.0018 | 196362 | 405.3 | 11.8 | 0.0047 |
| 13 | 922.0095 | 215316 | 2968.5 | 86.1 | 0.0043 |
| 14 | 923.0129 | 211610 | 522.3 | 15.5 | 0.0044 |
| 15 | 1001.5952 | 204764 | 241.5 | 7.4 | 0.0049 |
| 16 | 1221.9907 | 168660 | 2942.9 | 100.0 | 0.0072 |
| 17 | 1222.9943 | 168474 | 705.6 | 24.0 | 0.0073 |
| 18 | 1521.9681 | 278471 | 367.7 | 13.8 | 0.0055 |
| 19 | 1521.9713 | 131629 | 2293.3 | 86.5 | 0.0115 |
| 20 | 1522.9749 | 133816 | 726.6 | 27.1 | 0.0114 |
| 21 | 1772.4743 | 113214 | 573.8 | 24.5 | 0.0157 |
| 22 | 1773.4774 | 111124 | 694.4 | 29.6 | 0.0160 |
| 23 | 1774.4530 | 94535 | 280.0 | 12.0 | 0.0188 |
| 24 | 1774.4708 | 115585 | 1302.1 | 55.5 | 0.0154 |
| 25 | 1775.4555 | 91939 | 299.7 | 12.8 | 0.0193 |
| 26 | 1775.4746 | 112606 | 1548.8 | 66.0 | 0.0158 |
| 27 | 1776.4499 | 99538 | 282.8 | 12.1 | 0.0178 |
| 28 | 1776.4668 | 100750 | 884.3 | 37.7 | 0.0176 |
| 29 | 1776.4802 | 111855 | 754.9 | 32.2 | 0.0159 |
| 30 | 1777.4528 | 93144 | 240.3 | 10.3 | 0.0191 |
| 31 | 1777.4713 | 110190 | 1016.2 | 43.3 | 0.0161 |
| 32 | 1778.4603 | 121764 | 302.3 | 12.9 | 0.0146 |
| 33 | 1778.4765 | 114496 | 543.6 | 23.2 | 0.0155 |
| 34 | 1779.4658 | 103224 | 264.6 | 11.3 | 0.0172 |
| 35 | 1779.4814 | 110806 | 188.9 | 8.1 | 0.0161 |
| 36 | 1821.9322 | 98268 | 167.9 | 7.1 | 0.0185 |
| 37 | 1821.9524 | 108300 | 1032.5 | 43.1 | 0.0168 |
| 38 | 1822.9559 | 109798 | 390.3 | 16.3 | 0.0166 |
| 39 | 2121.9333 | 87089 | 945.9 | 41.5 | 0.0244 |
| 40 | 2122.9368 | 85058 | 416.2 | 18.3 | 0.0250 |

| # | m/z | Res. | S/N | I % | FWHM |
|---|---|---|---|---|---|
| 1 | 1772.4734 | 113214 | | 29.2 | 0.0157 |
| 2 | 1773.4766 | 113278 | | 35.1 | 0.0157 |
| 3 | 1774.4731 | 113342 | | 88.1 | 0.0157 |
| 4 | 1775.4751 | 113406 | | 88.9 | 0.0157 |
| 5 | 1776.4731 | 113469 | | 100.0 | 0.0157 |
| 6 | 1777.4738 | 113533 | | 78.8 | 0.0157 |
| 7 | 1778.4732 | 113597 | | 54.1 | 0.0157 |
| 8 | 1779.4731 | 113661 | | 30.9 | 0.0157 |
| 9 | 1780.4727 | 113725 | | 15.4 | 0.0157 |
| 10 | 1781.4723 | 113789 | | 6.8 | 0.0157 |
| 11 | 1782.4718 | 56926 | | 2.7 | 0.0313 |
| 12 | 1783.4715 | 113916 | | 1.0 | 0.0157 |
| 13 | 1784.4717 | 113980 | | 0.3 | 0.0157 |

Bruker Daltonics solariX | ETH - MS-Service LOC - D-CHAB | Page 2 of 2

**Figure S33:** High resolution MALDI ToF spectrum for compound **10**.

## Compound B

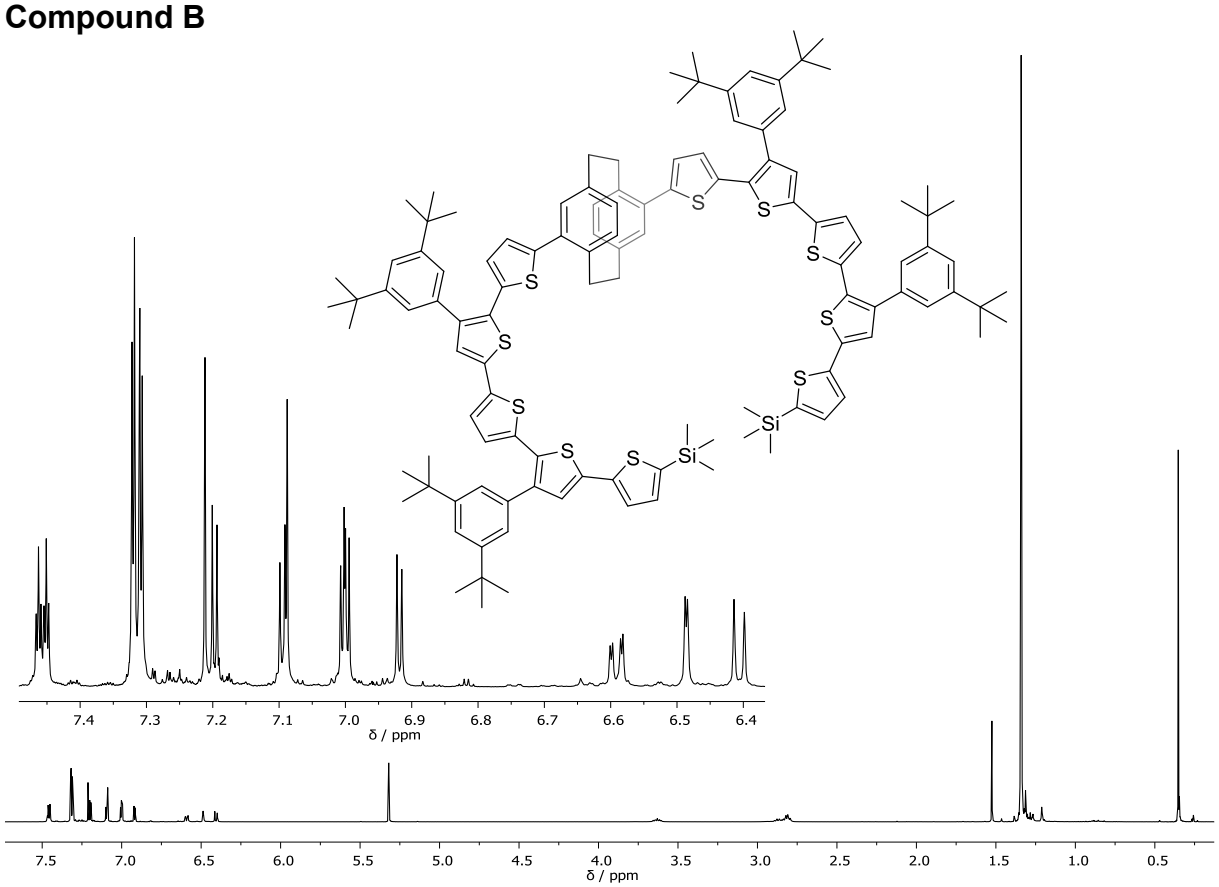


**Figure S34:** $^{1}H$ NMR spectrum (500 MHz, $CD_2Cl_2$) of compound **B**.

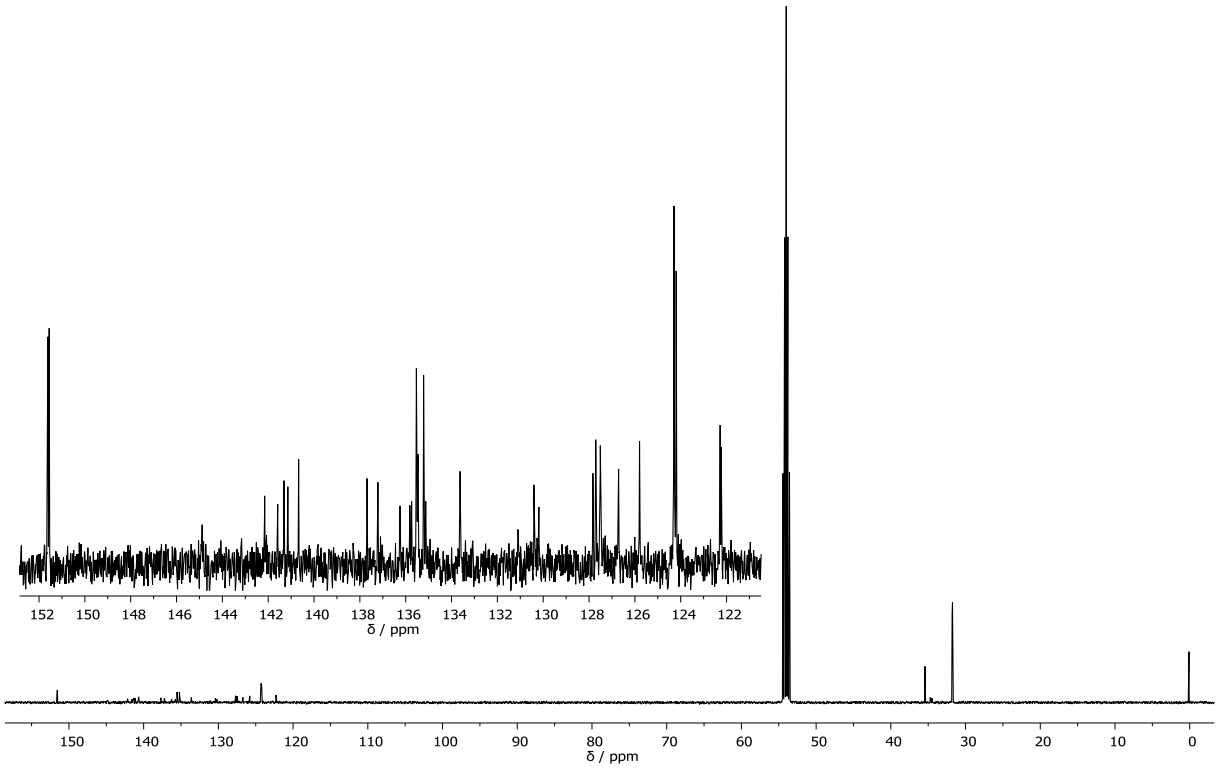


**Figure S35:** $^{13}C$ NMR spectrum (126 MHz, $CD_2Cl_2$) of compound **B**.

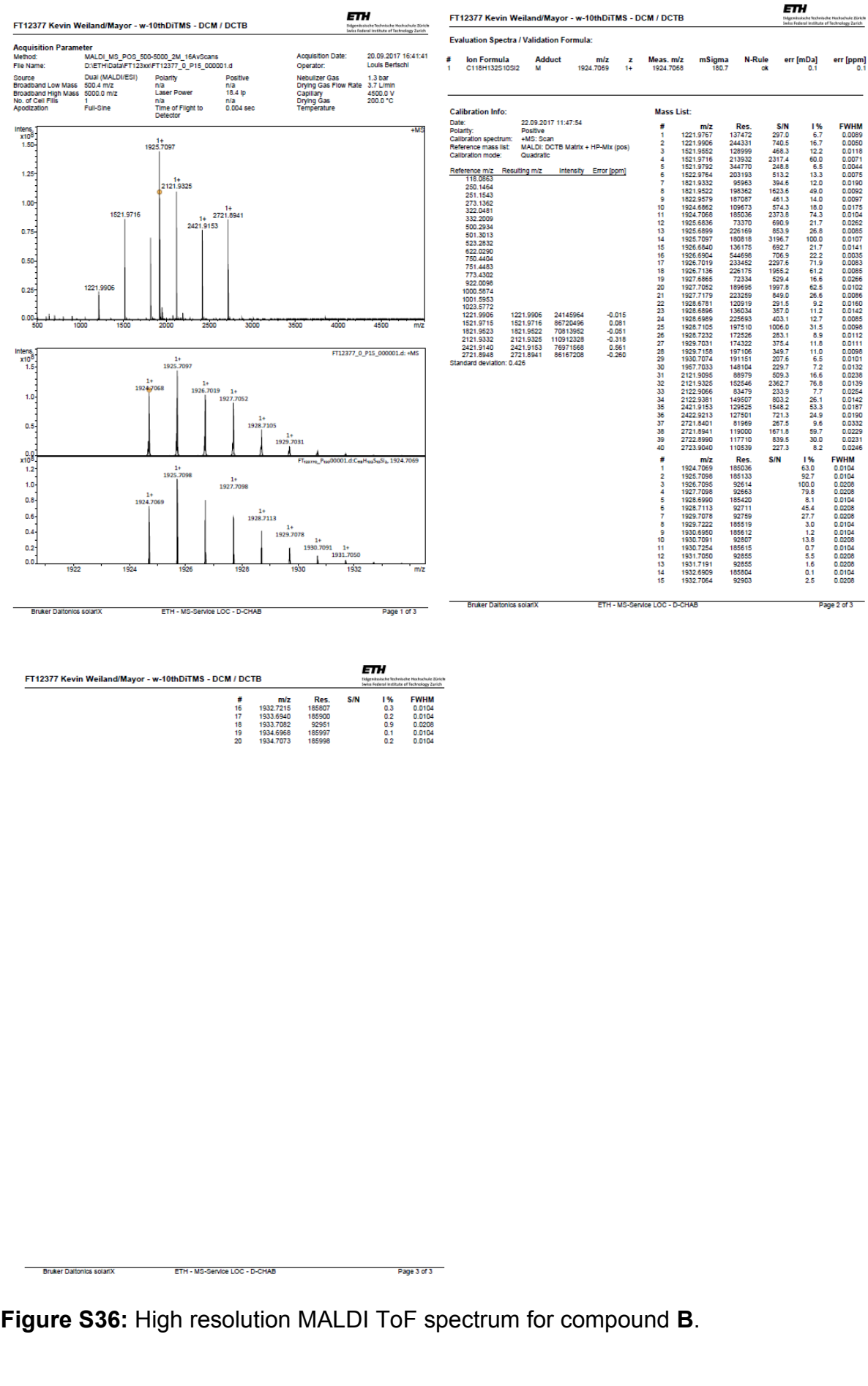

FT12377 Kevin Weiland/Mayor - w-10thDiTMS - DCM / DCTB

ETH Eidgenössische Technische Hochschule Zürich Swiss Federal Institute of Technology Zurich

**Acquisition Parameter**

| | | | | | |
|---|---|---|---|---|---|
| Method: | MALDI_MS_POS_500-5000_2M_16AvScans | | | Acquisition Date: | 20.09.2017 16:41:41 |
| File Name: | D:\ETH\Data\FT123xx\FT12377_0_P15_000001.d | | | Operator: | Louis Bertschi |
| Source | Dual (MALDI/ESI) | Polarity | Positive | Nebulizer Gas | 1.3 bar |
| Broadband Low Mass | 500.4 m/z | n/a | n/a | Drying Gas Flow Rate | 3.7 L/min |
| Broadband High Mass | 5000.0 m/z | Laser Power | 18.4 lp | Capillary | 4500.0 V |
| No. of Cell Fills | 1 | n/a | n/a | Drying Gas Temperature | 200.0 °C |
| Apodization | Full-Sine | Time of Flight to Detector | 0.004 sec | | |



Bruker Daltonics solariX ETH - MS-Service LOC - D-CHAB Page 1 of 3

FT12377 Kevin Weiland/Mayor - w-10thDiTMS - DCM / DCTB

ETH Eidgenössische Technische Hochschule Zürich Swiss Federal Institute of Technology Zurich

**Evaluation Spectra / Validation Formula:**

| # | Ion Formula | Adduct | m/z | z | Meas. m/z | mSigma | N-Rule | err [mDa] | err [ppm] |
|---|---|---|---|---|---|---|---|---|---|
| 1 | C118H132S10SI2 | M | 1924.7069 | 1+ | 1924.7068 | 180.7 | ok | 0.1 | 0.1 |

**Calibration Info:**

| | |
|---|---|
| Date: | 22.09.2017 11:47:54 |
| Polarity: | Positive |
| Calibration spectrum: | +MS: Scan |
| Reference mass list: | MALDI: DCTB Matrix + HP-Mix (pos) |
| Calibration mode: | Quadratic |

| Reference m/z | Resulting m/z | Intensity | Error [ppm] |
|---|---|---|---|
| 118.0863 | | | |
| 250.1464 | | | |
| 251.1543 | | | |
| 273.1362 | | | |
| 322.0481 | | | |
| 332.2009 | | | |
| 500.2934 | | | |
| 501.3013 | | | |
| 523.2832 | | | |
| 622.0290 | | | |
| 750.4404 | | | |
| 751.4483 | | | |
| 773.4302 | | | |
| 922.0098 | | | |
| 1000.5874 | | | |
| 1001.5953 | | | |
| 1023.5772 | | | |
| 1221.9906 | 1221.9906 | 24145964 | -0.015 |
| 1521.9715 | 1521.9716 | 86720496 | 0.081 |
| 1821.9523 | 1821.9522 | 70813952 | -0.051 |
| 2121.9332 | 2121.9325 | 110912328 | -0.316 |
| 2421.9140 | 2421.9153 | 76971568 | 0.561 |
| 2721.8948 | 2721.8941 | 86167208 | -0.260 |

Standard deviation: 0.426

**Mass List:**

| # | m/z | Res. | S/N | I % | FWHM |
|---|---|---|---|---|---|
| 1 | 1221.9767 | 137472 | 297.0 | 6.7 | 0.0089 |
| 2 | 1221.9906 | 244331 | 740.5 | 16.7 | 0.0050 |
| 3 | 1521.9552 | 128999 | 468.3 | 12.2 | 0.0118 |
| 4 | 1521.9716 | 213932 | 2317.4 | 60.0 | 0.0071 |
| 5 | 1521.9792 | 344770 | 248.8 | 6.5 | 0.0044 |
| 6 | 1522.9764 | 203193 | 513.2 | 13.3 | 0.0075 |
| 7 | 1821.9332 | 95963 | 394.6 | 12.0 | 0.0190 |
| 8 | 1821.9522 | 198362 | 1623.6 | 49.0 | 0.0092 |
| 9 | 1822.9579 | 187087 | 461.3 | 14.0 | 0.0097 |
| 10 | 1924.6862 | 109673 | 574.3 | 18.0 | 0.0175 |
| 11 | 1924.7068 | 185036 | 2373.8 | 74.3 | 0.0104 |
| 12 | 1925.6836 | 73370 | 690.9 | 21.7 | 0.0262 |
| 13 | 1925.6899 | 226169 | 853.9 | 26.8 | 0.0085 |
| 14 | 1925.7097 | 180818 | 3196.7 | 100.0 | 0.0107 |
| 15 | 1926.6840 | 136175 | 692.7 | 21.7 | 0.0141 |
| 16 | 1926.6904 | 544698 | 706.9 | 22.2 | 0.0035 |
| 17 | 1926.7019 | 233452 | 2297.6 | 71.9 | 0.0083 |
| 18 | 1926.7136 | 226175 | 1955.2 | 61.2 | 0.0085 |
| 19 | 1927.6865 | 72334 | 529.4 | 16.6 | 0.0266 |
| 20 | 1927.7052 | 189695 | 1997.8 | 62.5 | 0.0102 |
| 21 | 1927.7179 | 223259 | 849.0 | 26.6 | 0.0086 |
| 22 | 1928.6781 | 120919 | 291.5 | 9.2 | 0.0160 |
| 23 | 1928.6896 | 136034 | 357.0 | 11.2 | 0.0142 |
| 24 | 1928.6989 | 225693 | 403.1 | 12.7 | 0.0085 |
| 25 | 1928.7105 | 197510 | 1006.0 | 31.5 | 0.0098 |
| 26 | 1928.7232 | 172526 | 283.1 | 8.9 | 0.0112 |
| 27 | 1929.7031 | 174322 | 375.4 | 11.8 | 0.0111 |
| 28 | 1929.7158 | 197106 | 349.7 | 11.0 | 0.0098 |
| 29 | 1930.7074 | 191151 | 207.6 | 6.5 | 0.0101 |
| 30 | 1957.7033 | 148104 | 229.7 | 7.2 | 0.0132 |
| 31 | 2121.9095 | 88979 | 509.3 | 16.6 | 0.0238 |
| 32 | 2121.9325 | 152546 | 2362.7 | 76.8 | 0.0139 |
| 33 | 2122.9066 | 83479 | 233.9 | 7.7 | 0.0254 |
| 34 | 2122.9381 | 149507 | 803.2 | 26.1 | 0.0142 |
| 35 | 2421.9153 | 129525 | 1548.2 | 53.3 | 0.0187 |
| 36 | 2422.9213 | 127501 | 721.3 | 24.9 | 0.0190 |
| 37 | 2721.8401 | 81969 | 267.5 | 9.6 | 0.0332 |
| 38 | 2721.8941 | 119000 | 1671.8 | 59.7 | 0.0229 |
| 39 | 2722.8990 | 117710 | 839.5 | 30.0 | 0.0231 |
| 40 | 2723.9040 | 110539 | 227.3 | 8.2 | 0.0246 |

| # | m/z | Res. | S/N | I % | FWHM |
|---|---|---|---|---|---|
| 1 | 1924.7069 | 185036 | | 63.0 | 0.0104 |
| 2 | 1925.7098 | 185133 | | 92.7 | 0.0104 |
| 3 | 1926.7095 | 92614 | | 100.0 | 0.0208 |
| 4 | 1927.7098 | 92663 | | 79.8 | 0.0208 |
| 5 | 1928.6990 | 185420 | | 8.1 | 0.0104 |
| 6 | 1928.7113 | 92711 | | 45.4 | 0.0208 |
| 7 | 1929.7078 | 92759 | | 27.7 | 0.0208 |
| 8 | 1929.7222 | 185519 | | 3.0 | 0.0104 |
| 9 | 1930.6950 | 185612 | | 1.2 | 0.0104 |
| 10 | 1930.7091 | 92807 | | 13.8 | 0.0208 |
| 11 | 1930.7254 | 185615 | | 0.7 | 0.0104 |
| 12 | 1931.7050 | 92855 | | 5.5 | 0.0208 |
| 13 | 1931.7191 | 92855 | | 1.6 | 0.0208 |
| 14 | 1932.6909 | 185804 | | 0.1 | 0.0104 |
| 15 | 1932.7064 | 92903 | | 2.5 | 0.0208 |

Bruker Daltonics solariX ETH - MS-Service LOC - D-CHAB Page 2 of 3

FT12377 Kevin Weiland/Mayor - w-10thDiTMS - DCM / DCTB

ETH Eidgenössische Technische Hochschule Zürich Swiss Federal Institute of Technology Zurich

| # | m/z | Res. | S/N | I % | FWHM |
|---|---|---|---|---|---|
| 16 | 1932.7215 | 185807 | | 0.3 | 0.0104 |
| 17 | 1933.6940 | 185900 | | 0.2 | 0.0104 |
| 18 | 1933.7082 | 92951 | | 0.9 | 0.0208 |
| 19 | 1934.6966 | 185997 | | 0.1 | 0.0104 |
| 20 | 1934.7073 | 185998 | | 0.2 | 0.0104 |

Bruker Daltonics solariX ETH - MS-Service LOC - D-CHAB Page 3 of 3

**Figure S36:** High resolution MALDI ToF spectrum for compound **B**.

## Compound A

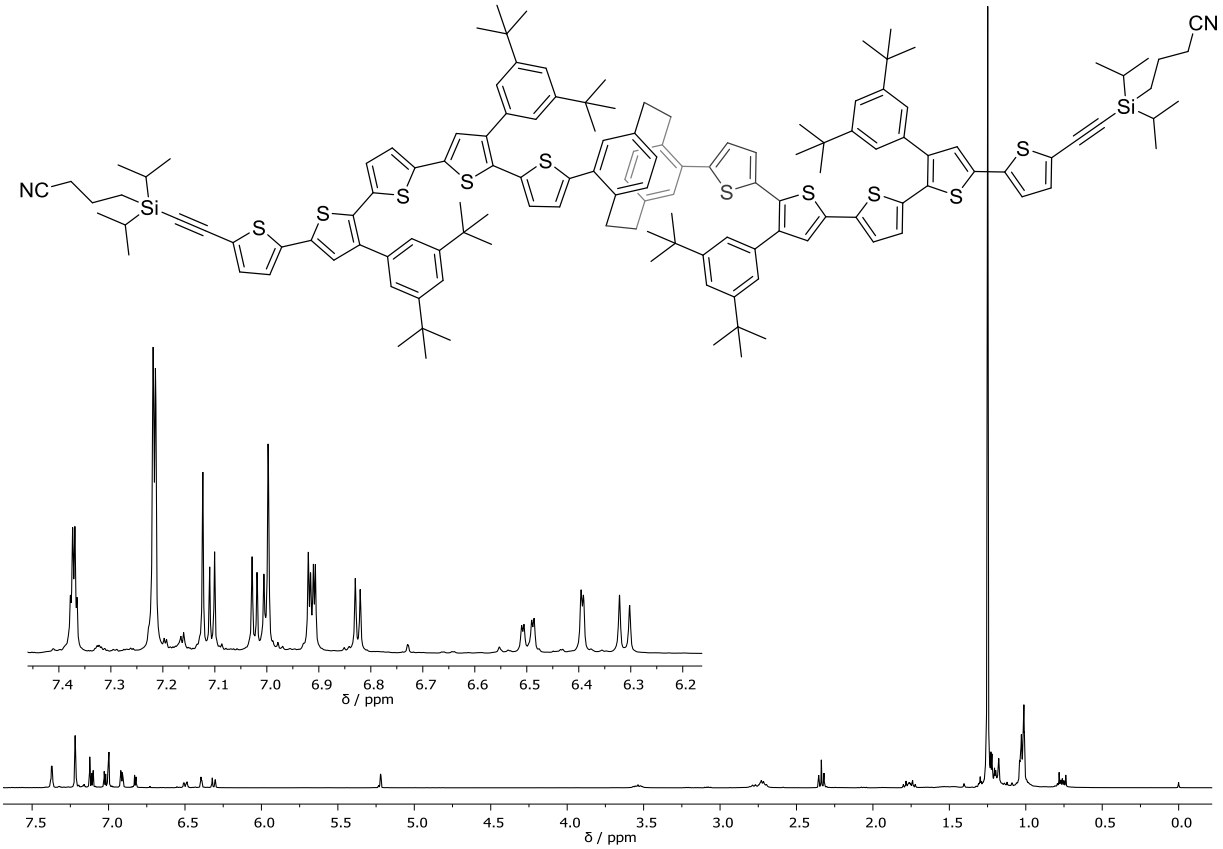


**Figure S37:** $^{1}H$ NMR spectrum (400 MHz, $CD_2Cl_2$) of compound **A**.

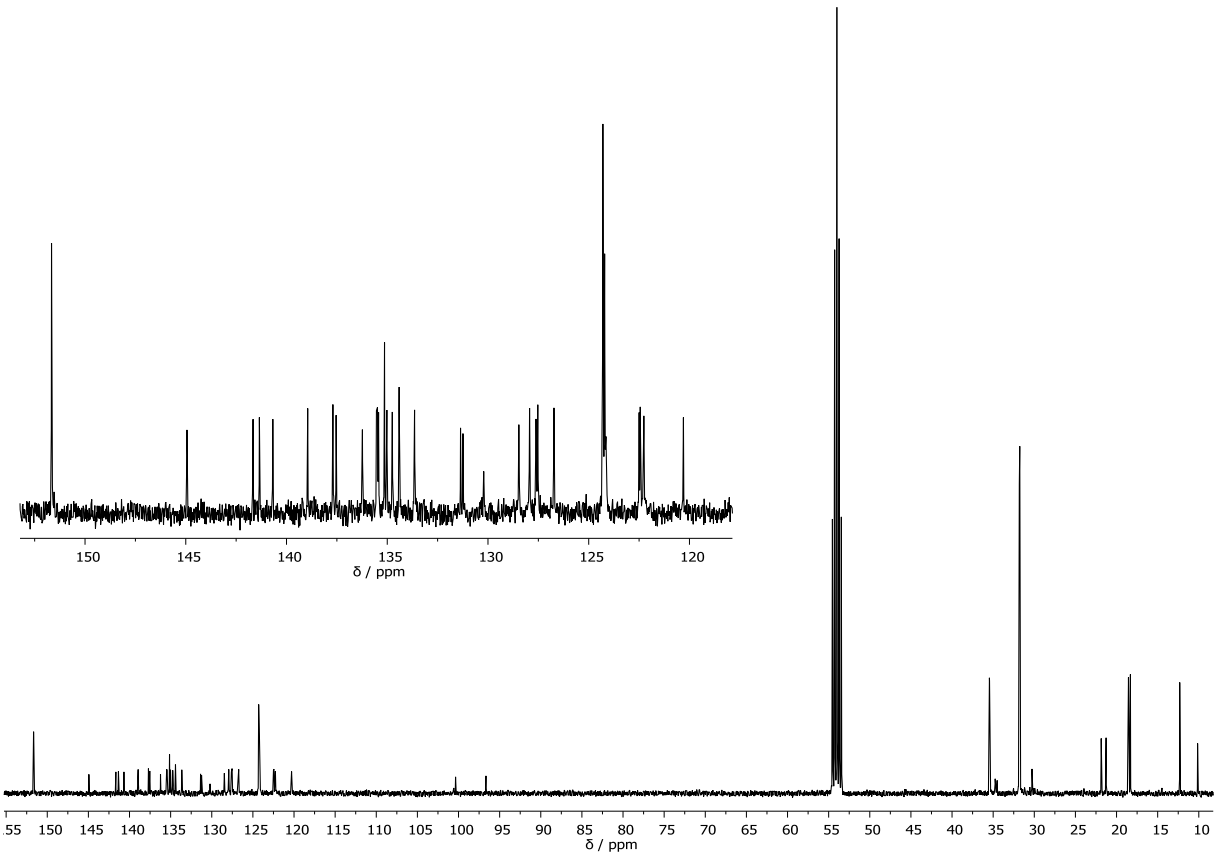


**Figure S38:** $^{13}C$ NMR spectrum (101 MHz, $CD_2Cl_2$) of compound **A**.

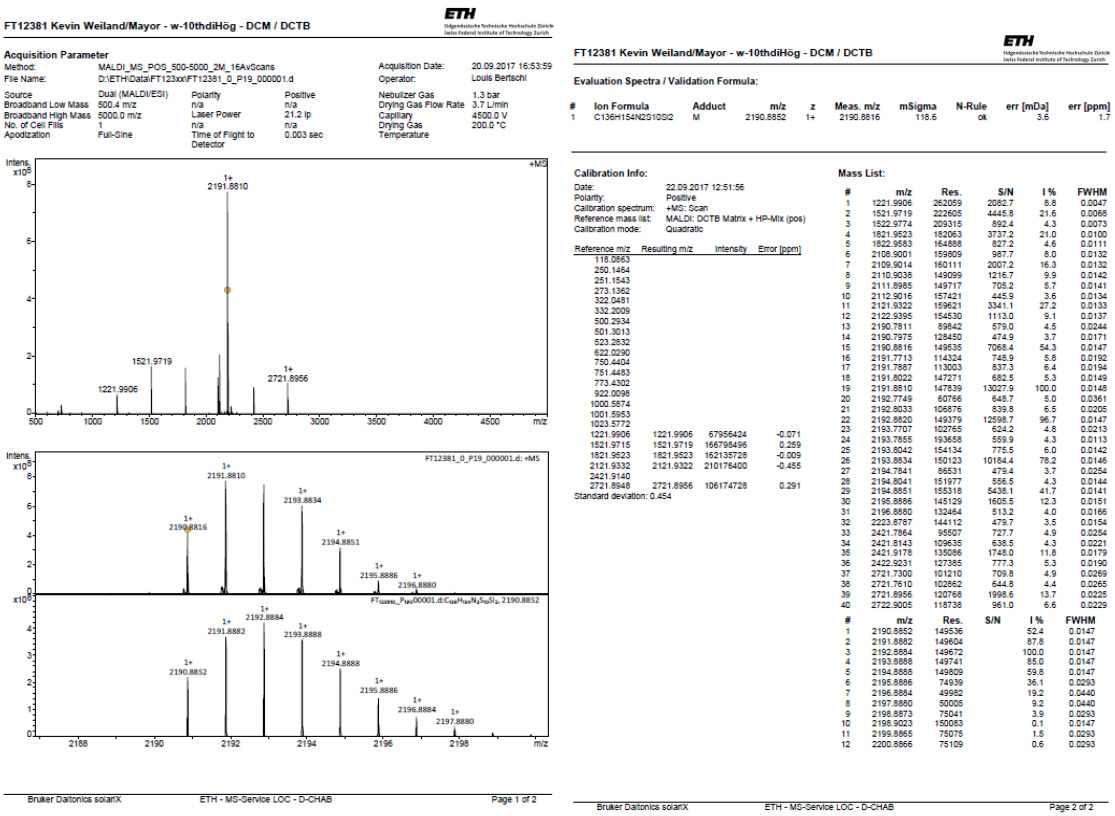

FT12381 Kevin Weiland/Mayor - w-10thdiHög - DCM / DCTB

Acquisition Parameter

| | | | | | |
|---|---|---|---|---|---|
| Method: | MALDI_MS_POS_500-5000_2M_16AvScans | | | Acquisition Date: | 20.09.2017 16:53:59 |
| File Name: | D:\ETH\Data\FT123xx\FT12381_0_P19_000001.d | | | Operator: | Louis Bertschi |
| Source | Dual (MALDI/ESI) | Polarity | Positive | Nebulizer Gas | 1.3 bar |
| Broadband Low Mass | 500.4 m/z | Laser Power | 21.2 lp | Drying Gas Flow Rate | 3.7 L/min |
| Broadband High Mass | 5000.0 m/z | Laser Repetition Rate | n/a | Capillary | 4500.0 V |
| No. of Cell Fills | 1 | Time of Flight to Detector | n/a | Drying Gas Temperature | 200.0 °C |
| Apodization | Full-Sine | | 0.003 sec | | |



Bruker Daltonics solariX ETH - MS-Service LOC - D-CHAB Page 1 of 2

FT12381 Kevin Weiland/Mayor - w-10thdiHög - DCM / DCTB

Evaluation Spectra / Validation Formula:

| # | Ion Formula | Adduct | m/z | z | Meas. m/z | mSigma | N-Rule | err [mDa] | err [ppm] |
|---|---|---|---|---|---|---|---|---|---|
| 1 | C136H154N2S10Si2 | M | 2190.8852 | 1+ | 2190.8816 | 118.6 | ok | 3.6 | 1.7 |

Calibration Info:

| | |
|---|---|
| Date: | 22.09.2017 12:51:56 |
| Polarity: | Positive |
| Calibration spectrum: | +MS: Scan |
| Reference mass list: | MALDI: DCTB Matrix + HP-Mix (pos) |
| Calibration mode: | Quadratic |

| Reference m/z | Resulting m/z | Intensity | Error [ppm] |
|---|---|---|---|
| 118.0863 | | | |
| 250.1464 | | | |
| 251.1543 | | | |
| 273.1362 | | | |
| 322.0481 | | | |
| 332.2009 | | | |
| 500.2934 | | | |
| 501.3013 | | | |
| 523.2832 | | | |
| 622.0290 | | | |
| 750.4404 | | | |
| 751.4483 | | | |
| 773.4302 | | | |
| 922.0098 | | | |
| 1000.5874 | | | |
| 1001.5953 | | | |
| 1023.5772 | | | |
| 1221.9906 | 1221.9906 | 67956424 | -0.071 |
| 1521.9715 | 1521.9719 | 166798496 | 0.259 |
| 1821.9523 | 1821.9523 | 162135728 | -0.009 |
| 2121.9332 | 2121.9322 | 210176400 | -0.455 |
| 2421.9140 | | | |
| 2721.8948 | 2721.8956 | 106174728 | 0.291 |

Standard deviation: 0.454

Mass List:

| # | m/z | Res. | S/N | I % | FWHM |
|---|---|---|---|---|---|
| 1 | 1221.9906 | 262059 | 2082.7 | 8.8 | 0.0047 |
| 2 | 1521.9719 | 222605 | 4445.8 | 21.6 | 0.0068 |
| 3 | 1522.9774 | 209315 | 892.4 | 4.3 | 0.0073 |
| 4 | 1821.9523 | 182063 | 3737.2 | 21.0 | 0.0100 |
| 5 | 1822.9583 | 164888 | 827.2 | 4.6 | 0.0111 |
| 6 | 2108.9001 | 159809 | 967.7 | 8.0 | 0.0132 |
| 7 | 2109.9014 | 160111 | 2007.2 | 16.3 | 0.0132 |
| 8 | 2110.9038 | 149099 | 1216.7 | 9.9 | 0.0142 |
| 9 | 2111.8985 | 149717 | 705.2 | 5.7 | 0.0141 |
| 10 | 2112.9016 | 157421 | 445.9 | 3.6 | 0.0134 |
| 11 | 2121.9322 | 159621 | 3341.1 | 27.2 | 0.0133 |
| 12 | 2122.9395 | 154530 | 1113.0 | 9.1 | 0.0137 |
| 13 | 2190.7811 | 89842 | 579.0 | 4.5 | 0.0244 |
| 14 | 2190.7975 | 128450 | 474.9 | 3.7 | 0.0171 |
| 15 | 2190.8816 | 149535 | 7068.4 | 54.3 | 0.0147 |
| 16 | 2191.7713 | 114324 | 748.9 | 5.8 | 0.0192 |
| 17 | 2191.7887 | 113003 | 837.3 | 6.4 | 0.0194 |
| 18 | 2191.8022 | 147271 | 682.5 | 5.3 | 0.0149 |
| 19 | 2191.8810 | 147839 | 13027.9 | 100.0 | 0.0148 |
| 20 | 2192.7749 | 60766 | 648.7 | 5.0 | 0.0361 |
| 21 | 2192.8033 | 106876 | 839.8 | 6.5 | 0.0205 |
| 22 | 2192.8920 | 149379 | 12598.7 | 96.7 | 0.0147 |
| 23 | 2193.7707 | 102755 | 624.2 | 4.8 | 0.0213 |
| 24 | 2193.7855 | 193658 | 559.9 | 4.3 | 0.0113 |
| 25 | 2193.8042 | 154134 | 775.5 | 6.0 | 0.0142 |
| 26 | 2193.8834 | 150123 | 10184.4 | 78.2 | 0.0146 |
| 27 | 2194.7841 | 86531 | 479.4 | 3.7 | 0.0254 |
| 28 | 2194.8041 | 151977 | 556.5 | 4.3 | 0.0144 |
| 29 | 2194.8851 | 155318 | 5438.1 | 41.7 | 0.0141 |
| 30 | 2195.8886 | 145129 | 1605.5 | 12.3 | 0.0151 |
| 31 | 2196.8880 | 132464 | 513.2 | 4.0 | 0.0166 |
| 32 | 2223.8787 | 144112 | 479.7 | 3.5 | 0.0154 |
| 33 | 2421.7864 | 95507 | 727.7 | 4.9 | 0.0254 |
| 34 | 2421.8143 | 109635 | 638.5 | 4.3 | 0.0221 |
| 35 | 2421.9178 | 135086 | 1748.0 | 11.8 | 0.0179 |
| 36 | 2422.9231 | 127385 | 777.3 | 5.3 | 0.0190 |
| 37 | 2721.7300 | 101210 | 709.8 | 4.9 | 0.0269 |
| 38 | 2721.7610 | 102862 | 644.8 | 4.4 | 0.0265 |
| 39 | 2721.8956 | 120768 | 1998.6 | 13.7 | 0.0225 |
| 40 | 2722.9005 | 118738 | 961.0 | 6.6 | 0.0229 |

| # | m/z | Res. | S/N | I % | FWHM |
|---|---|---|---|---|---|
| 1 | 2190.8852 | 149536 | | 52.4 | 0.0147 |
| 2 | 2191.8882 | 149604 | | 87.6 | 0.0147 |
| 3 | 2192.8884 | 149672 | | 100.0 | 0.0147 |
| 4 | 2193.8888 | 149741 | | 85.0 | 0.0147 |
| 5 | 2194.8888 | 149809 | | 59.8 | 0.0147 |
| 6 | 2195.8886 | 74939 | | 36.1 | 0.0293 |
| 7 | 2196.8884 | 49982 | | 19.2 | 0.0440 |
| 8 | 2197.8880 | 50005 | | 9.2 | 0.0440 |
| 9 | 2198.8873 | 75041 | | 3.9 | 0.0293 |
| 10 | 2198.9023 | 150083 | | 0.1 | 0.0147 |
| 11 | 2199.8865 | 75075 | | 1.5 | 0.0293 |
| 12 | 2200.8866 | 75109 | | 0.6 | 0.0293 |

Bruker Daltonics solariX ETH - MS-Service LOC - D-CHAB Page 2 of 2

**Figure S39:** High resolution MALDI ToF spectrum for compound **A**.

**Compound 11**

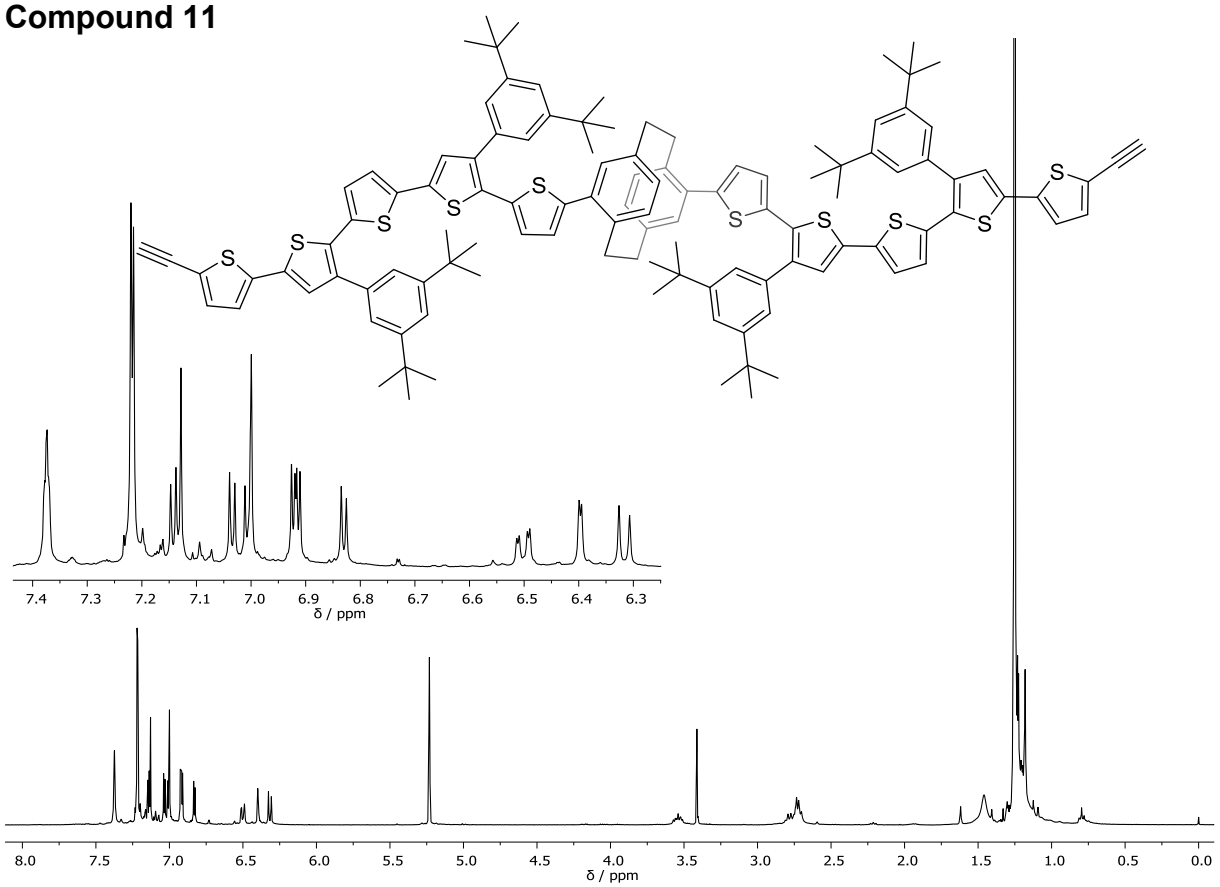


**Figure S40:** $^{1}$H NMR spectrum (400 MHz, $CD_2Cl_2$) of compound **11**.

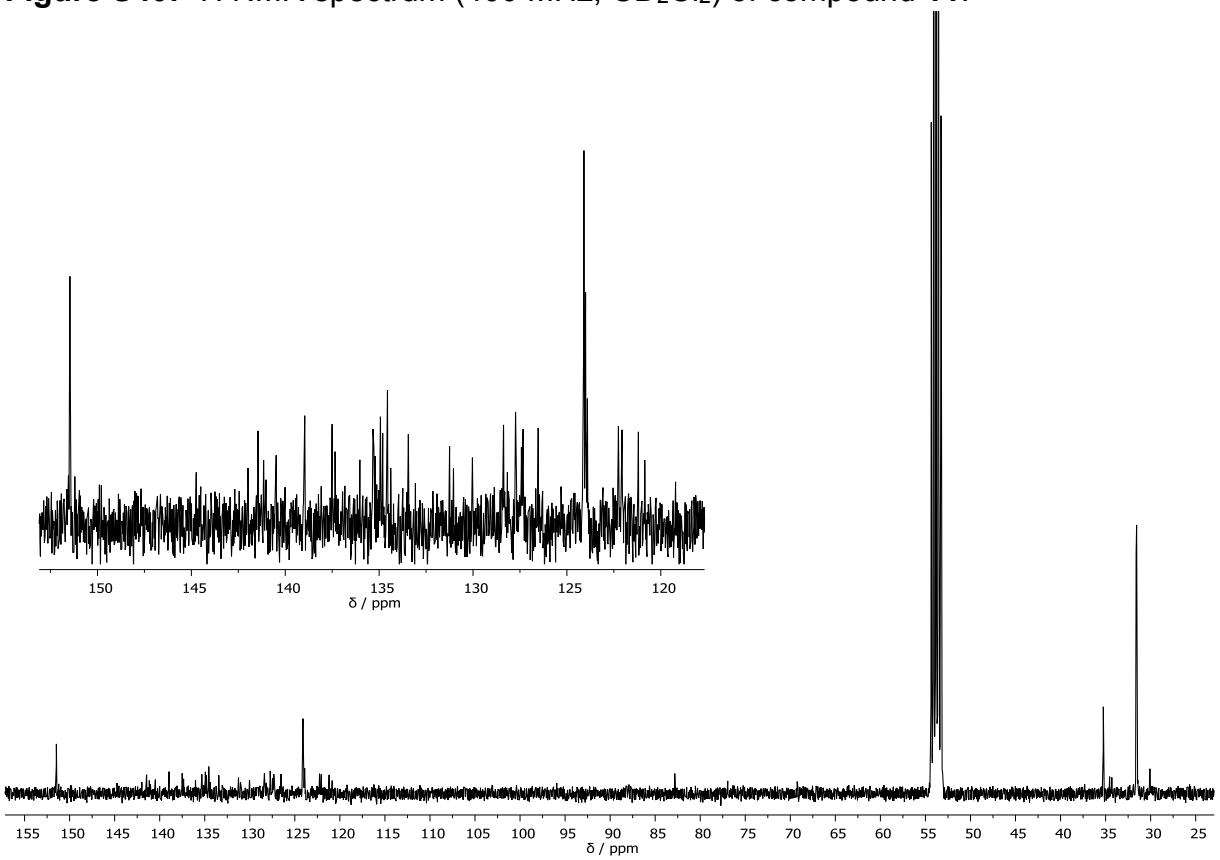


**Figure S41:** $^{13}$C NMR spectrum (101 MHz, $CD_2Cl_2$) of compound **11**.

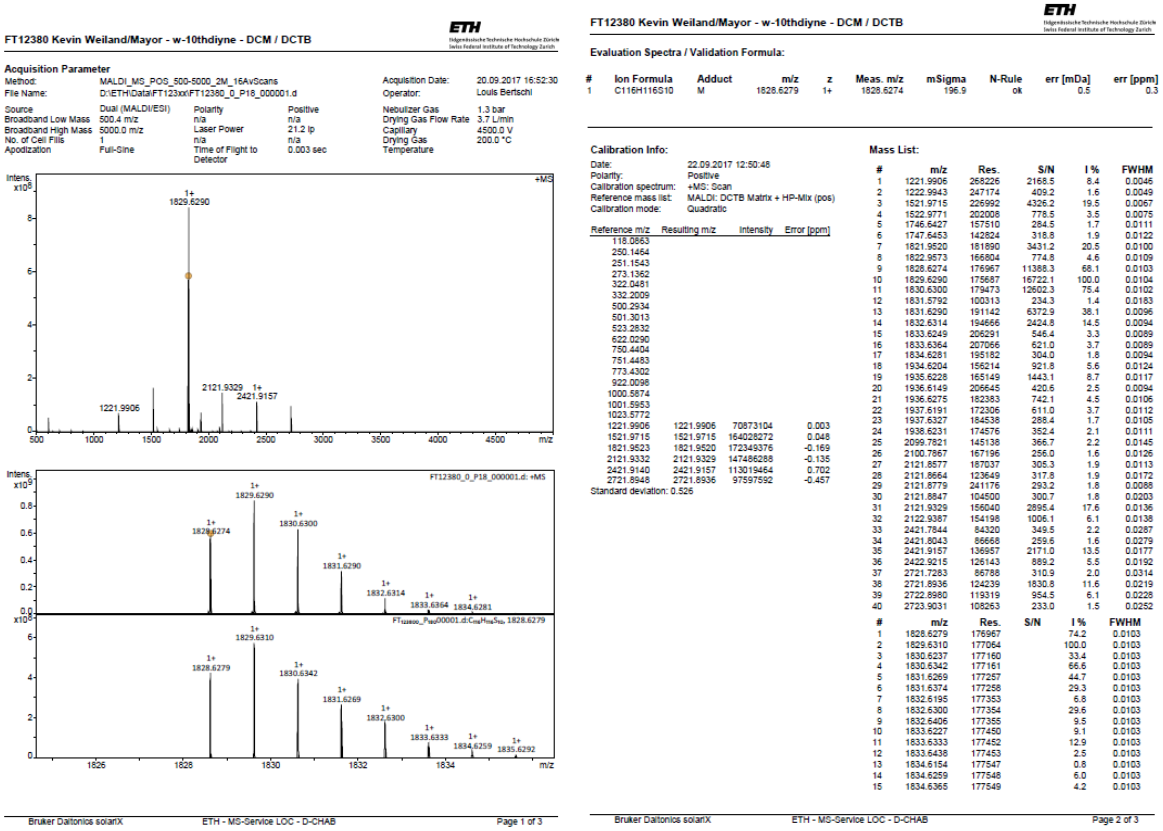

FT12380 Kevin Weiland/Mayor - w-10thdiyne - DCM / DCTB

ETH Eidgenössische Technische Hochschule Zürich Swiss Federal Institute of Technology Zurich

**Acquisition Parameter**

| | | | | | |
|---|---|---|---|---|---|
| Method: | MALDI_MS_POS_500-5000_2M_16AvScans | | | Acquisition Date: | 20.09.2017 16:52:30 |
| File Name: | D:\ETH\Data\FT123xx\FT12380_0_P18_000001.d | | | Operator: | Louis Berlschi |
| Source | Dual (MALDI/ESI) | Polarity | Positive | Nebulizer Gas | 1.3 bar |
| Broadband Low Mass | 500.4 m/z | n/a | n/a | Drying Gas Flow Rate | 3.7 L/min |
| Broadband High Mass | 5000.0 m/z | Laser Power | 21.2 lp | Capillary | 4500.0 V |
| No. of Ceil Fills | 1 | n/a | n/a | Drying Gas Temperature | 200.0 °C |
| Apodization | Full-Sine | Time of Flight to Detector | 0.003 sec | | |







Bruker Daltonics solariX ETH - MS-Service LOC - D-CHAB Page 1 of 3

FT12380 Kevin Weiland/Mayor - w-10thdiyne - DCM / DCTB

ETH Eidgenössische Technische Hochschule Zürich Swiss Federal Institute of Technology Zurich

**Evaluation Spectra / Validation Formula:**

| # | Ion Formula | Adduct | m/z | z | Meas. m/z | mSigma | N-Rule | err [mDa] | err [ppm] |
|---|---|---|---|---|---|---|---|---|---|
| 1 | C116H116S10 | M | 1828.6279 | 1+ | 1828.6274 | 196.9 | ok | 0.5 | 0.3 |

**Calibration Info:**

| | |
|---|---|
| Date: | 22.09.2017 12:50:48 |
| Polarity: | Positive |
| Calibration spectrum: | +MS: Scan |
| Reference mass list: | MALDI: DCTB Matrix + HP-Mix (pos) |
| Calibration mode: | Quadratic |

| Reference m/z | Resulting m/z | Intensity | Error [ppm] |
|---|---|---|---|
| 118.0863 | | | |
| 250.1464 | | | |
| 251.1543 | | | |
| 273.1362 | | | |
| 322.0481 | | | |
| 332.2009 | | | |
| 500.2934 | | | |
| 501.3013 | | | |
| 523.2832 | | | |
| 622.0290 | | | |
| 750.4404 | | | |
| 751.4483 | | | |
| 773.4302 | | | |
| 922.0098 | | | |
| 1000.5874 | | | |
| 1001.5953 | | | |
| 1023.5772 | | | |
| 1221.9906 | 1221.9906 | 70873104 | 0.003 |
| 1521.9715 | 1521.9715 | 164028272 | 0.048 |
| 1821.9623 | 1821.9620 | 172349376 | -0.169 |
| 2121.9332 | 2121.9329 | 147486288 | -0.135 |
| 2421.9140 | 2421.9157 | 113019464 | 0.702 |
| 2721.8948 | 2721.8936 | 97597592 | -0.457 |

Standard deviation: 0.526

**Mass List:**

| # | m/z | Res. | S/N | I % | FWHM |
|---|---|---|---|---|---|
| 1 | 1221.9906 | 268226 | 2168.5 | 8.4 | 0.0046 |
| 2 | 1222.9943 | 247174 | 409.2 | 1.6 | 0.0049 |
| 3 | 1521.9715 | 226992 | 4326.2 | 19.5 | 0.0067 |
| 4 | 1522.9771 | 202008 | 778.5 | 3.5 | 0.0075 |
| 5 | 1746.5427 | 157510 | 284.5 | 1.7 | 0.0111 |
| 6 | 1747.5453 | 142824 | 318.8 | 1.9 | 0.0122 |
| 7 | 1821.9520 | 181890 | 3431.2 | 20.5 | 0.0100 |
| 8 | 1822.9573 | 166804 | 774.8 | 4.6 | 0.0109 |
| 9 | 1828.6274 | 176967 | 11388.3 | 68.1 | 0.0103 |
| 10 | 1829.6290 | 175687 | 16722.1 | 100.0 | 0.0104 |
| 11 | 1830.6300 | 179473 | 12602.3 | 75.4 | 0.0102 |
| 12 | 1831.5792 | 100313 | 234.3 | 1.4 | 0.0183 |
| 13 | 1831.6290 | 191142 | 6372.9 | 38.1 | 0.0096 |
| 14 | 1832.6314 | 194666 | 2424.8 | 14.5 | 0.0094 |
| 15 | 1833.6249 | 206291 | 546.4 | 3.3 | 0.0089 |
| 16 | 1833.6364 | 207066 | 621.0 | 3.7 | 0.0089 |
| 17 | 1834.6281 | 195182 | 304.0 | 1.8 | 0.0094 |
| 18 | 1934.6204 | 156214 | 921.8 | 5.6 | 0.0124 |
| 19 | 1935.6228 | 165149 | 1443.1 | 8.7 | 0.0117 |
| 20 | 1936.6149 | 206645 | 420.6 | 2.5 | 0.0094 |
| 21 | 1936.6275 | 182383 | 742.1 | 4.5 | 0.0106 |
| 22 | 1937.6191 | 172306 | 611.0 | 3.7 | 0.0112 |
| 23 | 1937.6327 | 184538 | 288.4 | 1.7 | 0.0105 |
| 24 | 1938.6231 | 174576 | 352.4 | 2.1 | 0.0111 |
| 25 | 2099.7821 | 145138 | 366.7 | 2.2 | 0.0145 |
| 26 | 2100.7867 | 167196 | 286.0 | 1.6 | 0.0126 |
| 27 | 2121.8577 | 187037 | 305.3 | 1.9 | 0.0113 |
| 28 | 2121.8664 | 123649 | 317.8 | 1.9 | 0.0172 |
| 29 | 2121.8779 | 241176 | 293.2 | 1.8 | 0.0088 |
| 30 | 2121.8847 | 104500 | 300.7 | 1.8 | 0.0203 |
| 31 | 2121.9329 | 156040 | 2895.4 | 17.6 | 0.0136 |
| 32 | 2122.9387 | 154198 | 1006.1 | 6.1 | 0.0138 |
| 33 | 2421.7844 | 84320 | 349.5 | 2.2 | 0.0287 |
| 34 | 2421.8043 | 86668 | 259.6 | 1.6 | 0.0279 |
| 35 | 2421.9157 | 136957 | 2171.0 | 13.5 | 0.0177 |
| 36 | 2422.9215 | 126143 | 889.2 | 5.5 | 0.0192 |
| 37 | 2721.7283 | 86788 | 310.9 | 2.0 | 0.0314 |
| 38 | 2721.8936 | 124239 | 1830.8 | 11.6 | 0.0219 |
| 39 | 2722.8980 | 119319 | 954.5 | 6.1 | 0.0228 |
| 40 | 2723.9031 | 108263 | 233.0 | 1.5 | 0.0252 |

| # | m/z | Res. | S/N | I % | FWHM |
|---|---|---|---|---|---|
| 1 | 1828.6279 | 176967 | | 74.2 | 0.0103 |
| 2 | 1829.6310 | 177064 | | 100.0 | 0.0103 |
| 3 | 1830.6237 | 177160 | | 33.4 | 0.0103 |
| 4 | 1830.6342 | 177161 | | 66.6 | 0.0103 |
| 5 | 1831.6269 | 177257 | | 44.7 | 0.0103 |
| 6 | 1831.6374 | 177258 | | 29.3 | 0.0103 |
| 7 | 1832.6195 | 177353 | | 6.8 | 0.0103 |
| 8 | 1832.6300 | 177354 | | 29.6 | 0.0103 |
| 9 | 1832.6406 | 177355 | | 9.5 | 0.0103 |
| 10 | 1833.6227 | 177450 | | 9.1 | 0.0103 |
| 11 | 1833.6333 | 177452 | | 12.9 | 0.0103 |
| 12 | 1833.6438 | 177453 | | 2.5 | 0.0103 |
| 13 | 1834.6154 | 177547 | | 0.8 | 0.0103 |
| 14 | 1834.6259 | 177548 | | 6.0 | 0.0103 |
| 15 | 1834.6365 | 177549 | | 4.2 | 0.0103 |

Bruker Daltonics solariX ETH - MS-Service LOC - D-CHAB Page 2 of 3

FT12380 Kevin Weiland/Mayor - w-10thdiyne - DCM / DCTB

ETH Eidgenössische Technische Hochschule Zürich Swiss Federal Institute of Technology Zurich

| # | m/z | Res. | S/N | I % | FWHM |
|---|---|---|---|---|---|
| 16 | 1834.6470 | 177550 | | 0.5 | 0.0103 |
| 17 | 1835.6186 | 177644 | | 1.1 | 0.0103 |
| 18 | 1835.6292 | 177645 | | 2.6 | 0.0103 |
| 19 | 1835.6397 | 177646 | | 1.1 | 0.0103 |
| 20 | 1836.6219 | 177741 | | 0.7 | 0.0103 |
| 21 | 1836.6324 | 177742 | | 0.8 | 0.0103 |
| 22 | 1836.6431 | 177743 | | 0.2 | 0.0103 |
| 23 | 1837.6251 | 177838 | | 0.3 | 0.0103 |
| 24 | 1837.6356 | 177839 | | 0.2 | 0.0103 |
| 25 | 1838.6283 | 177935 | | 0.1 | 0.0103 |

Bruker Daltonics solariX ETH - MS-Service LOC - D-CHAB Page 3 of 3

**Figure S42:** High resolution MALDI ToF spectrum for compound **11**.

## Compound 12

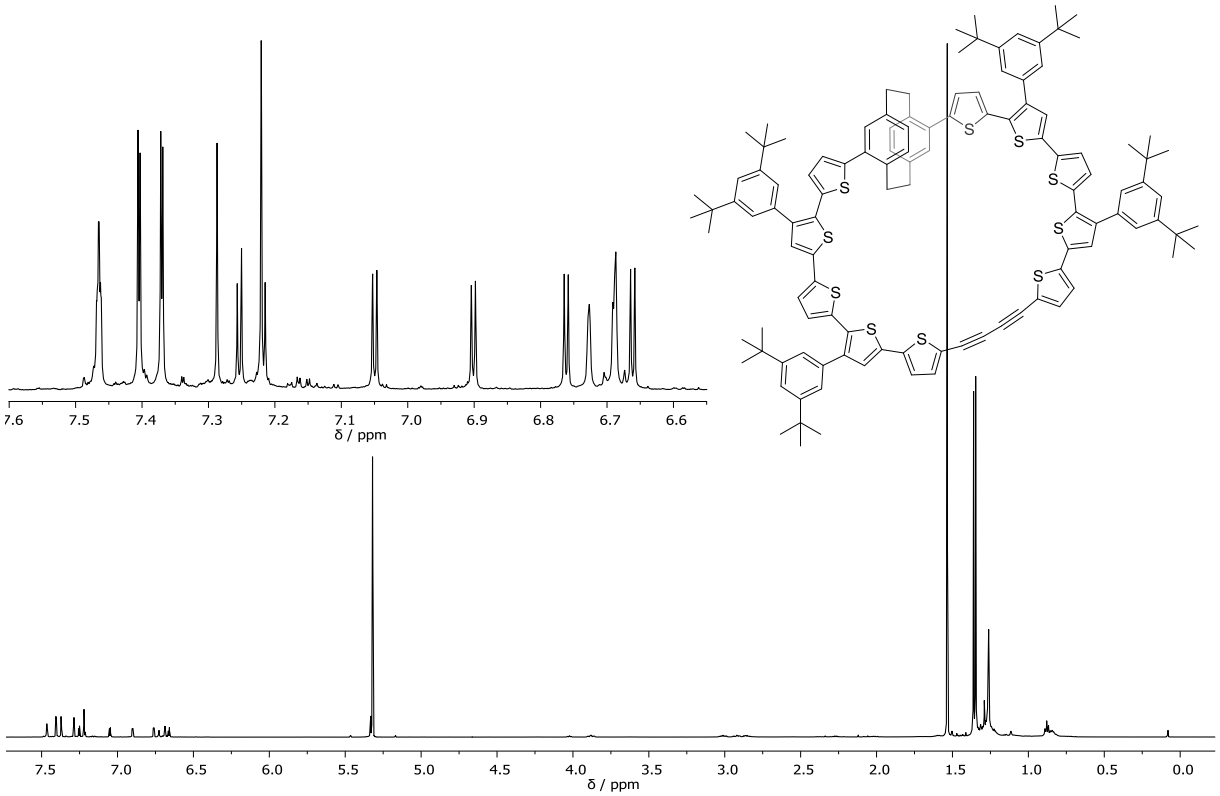


**Figure S43:** $^{1}$H NMR spectrum (600 MHz, $CD_2Cl_2$) of compound **12**.

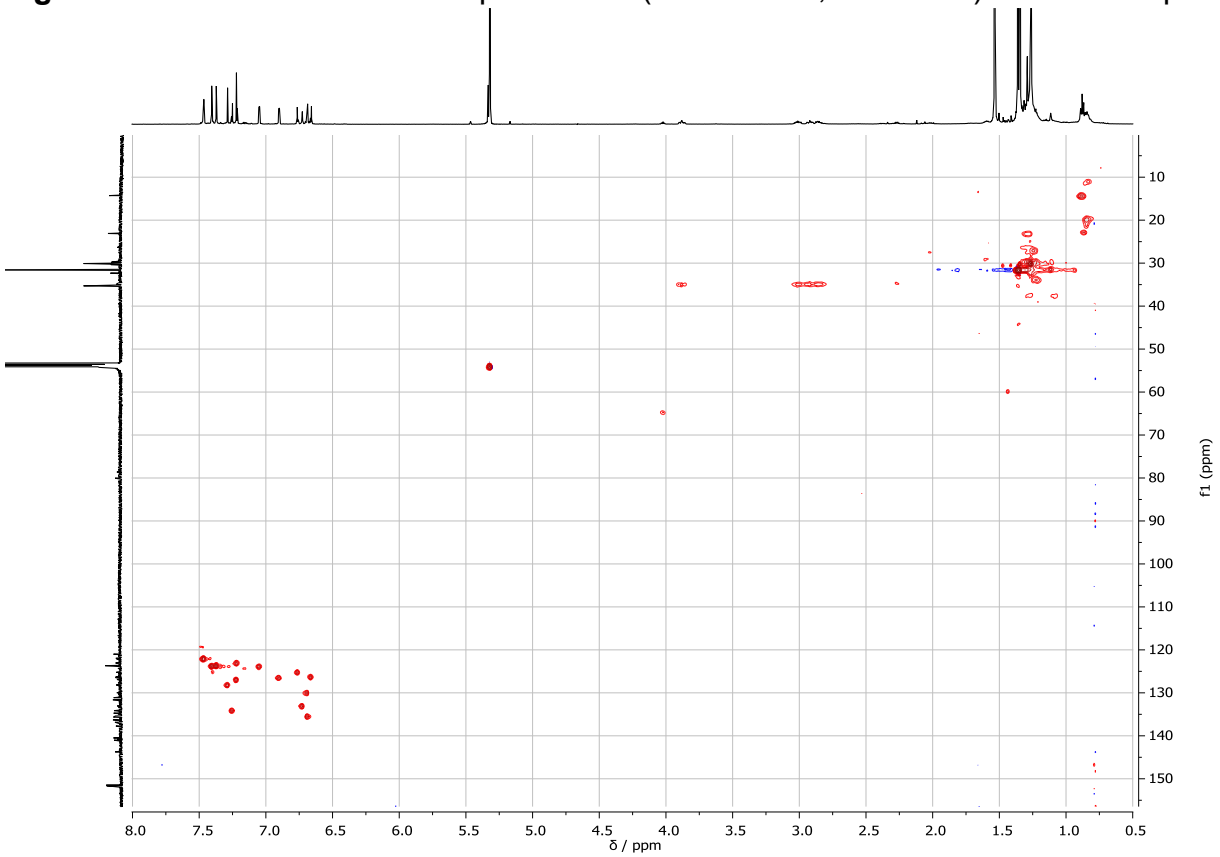


**Figure S44:** HMQC (298 K, $CD_2Cl_2$) of compound **12**.

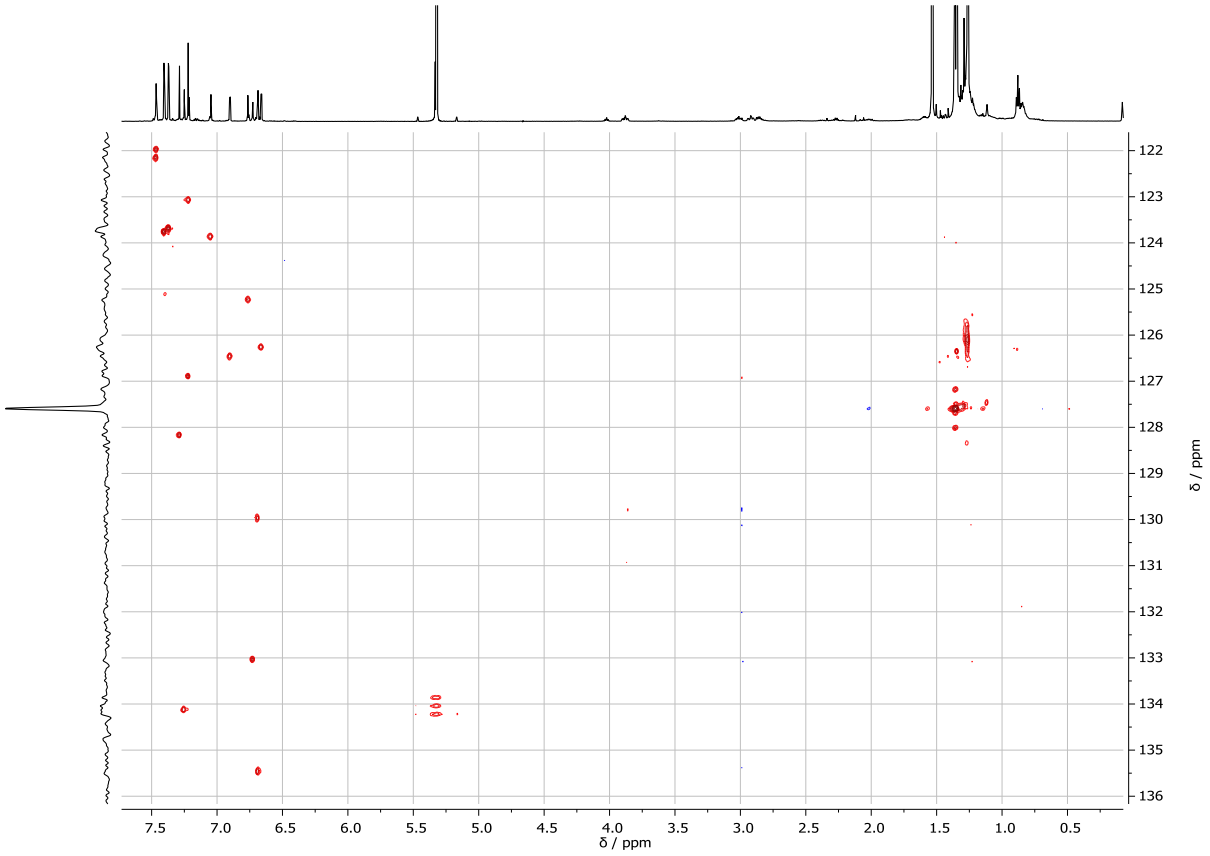


**Figure S45:** HMQC (298 K, $CD_2Cl_2$) of compound **12**.

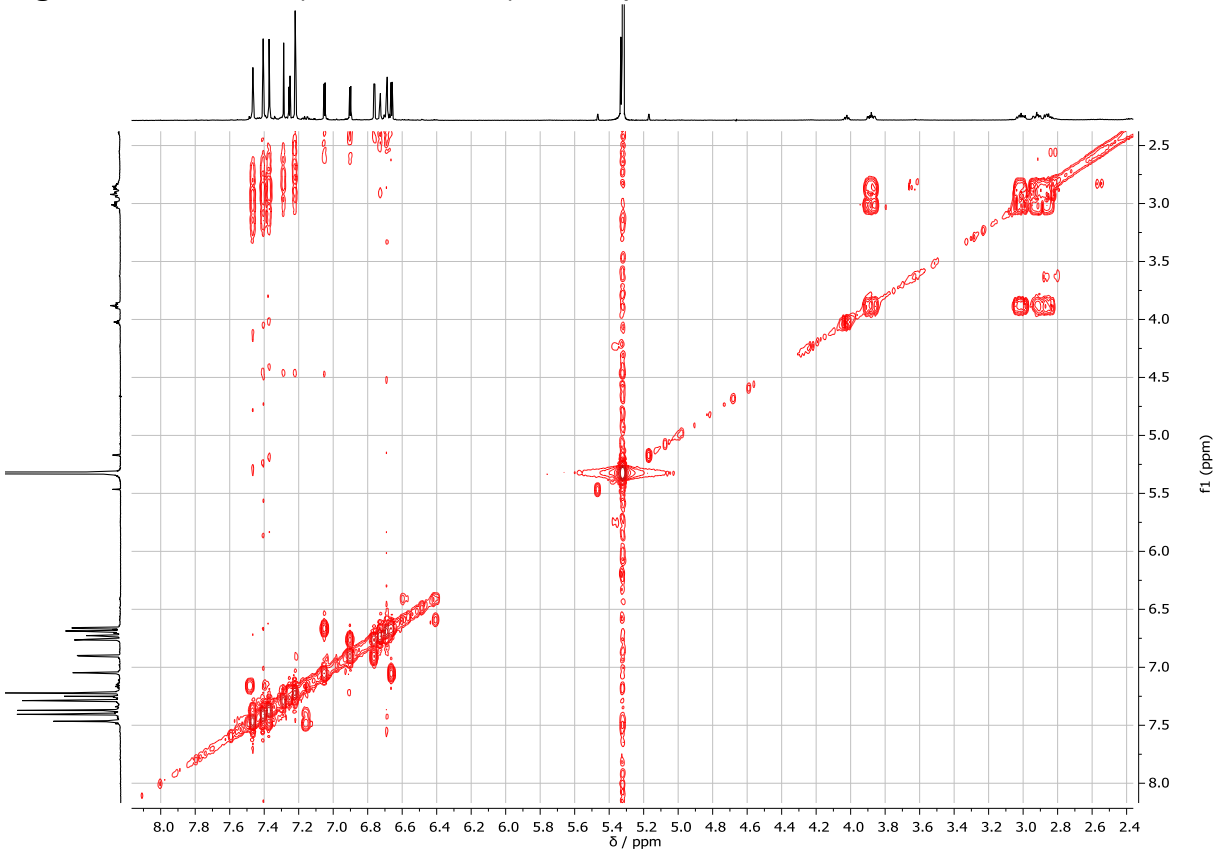


**Figure S46:** COSY (298 K, $CD_2Cl_2$) of compound **12**.

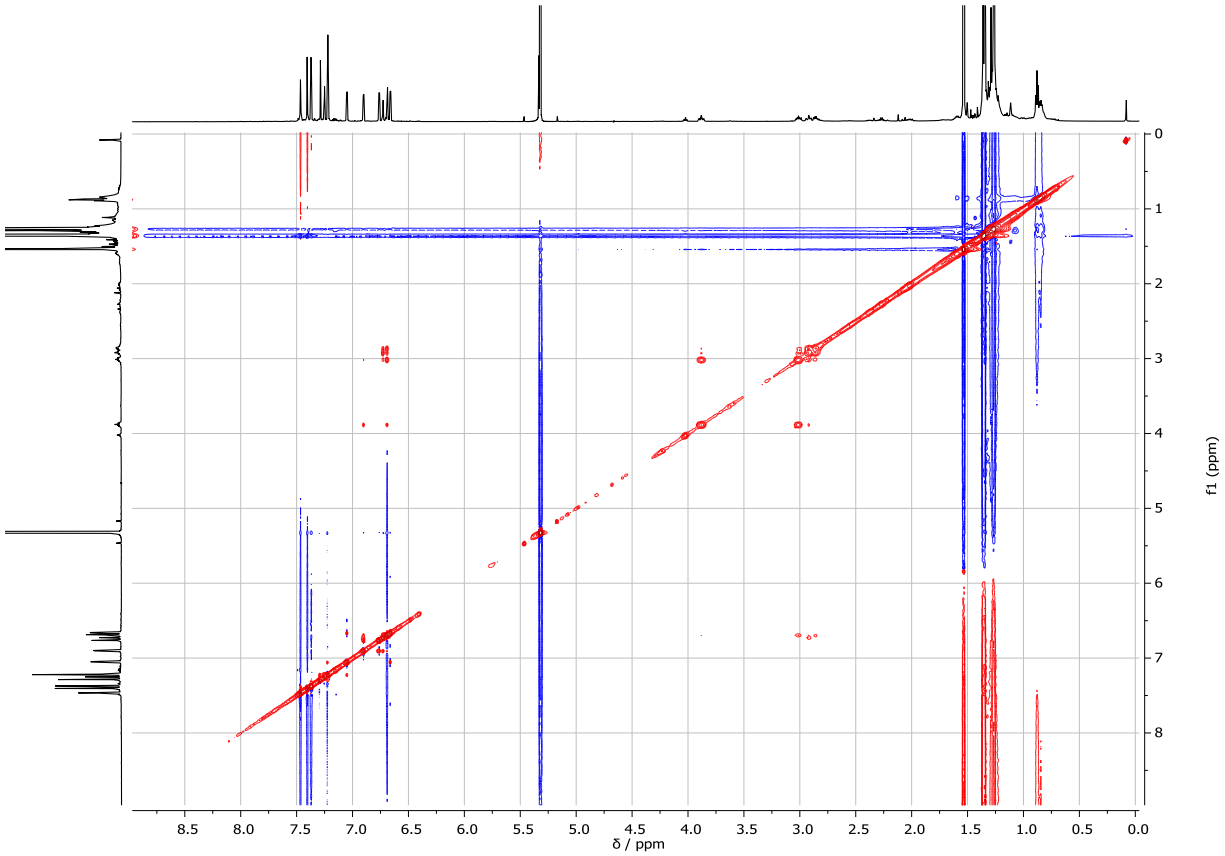


**Figure S47:** NOESY (298 K, $CD_2Cl_2$) of compound **12**.

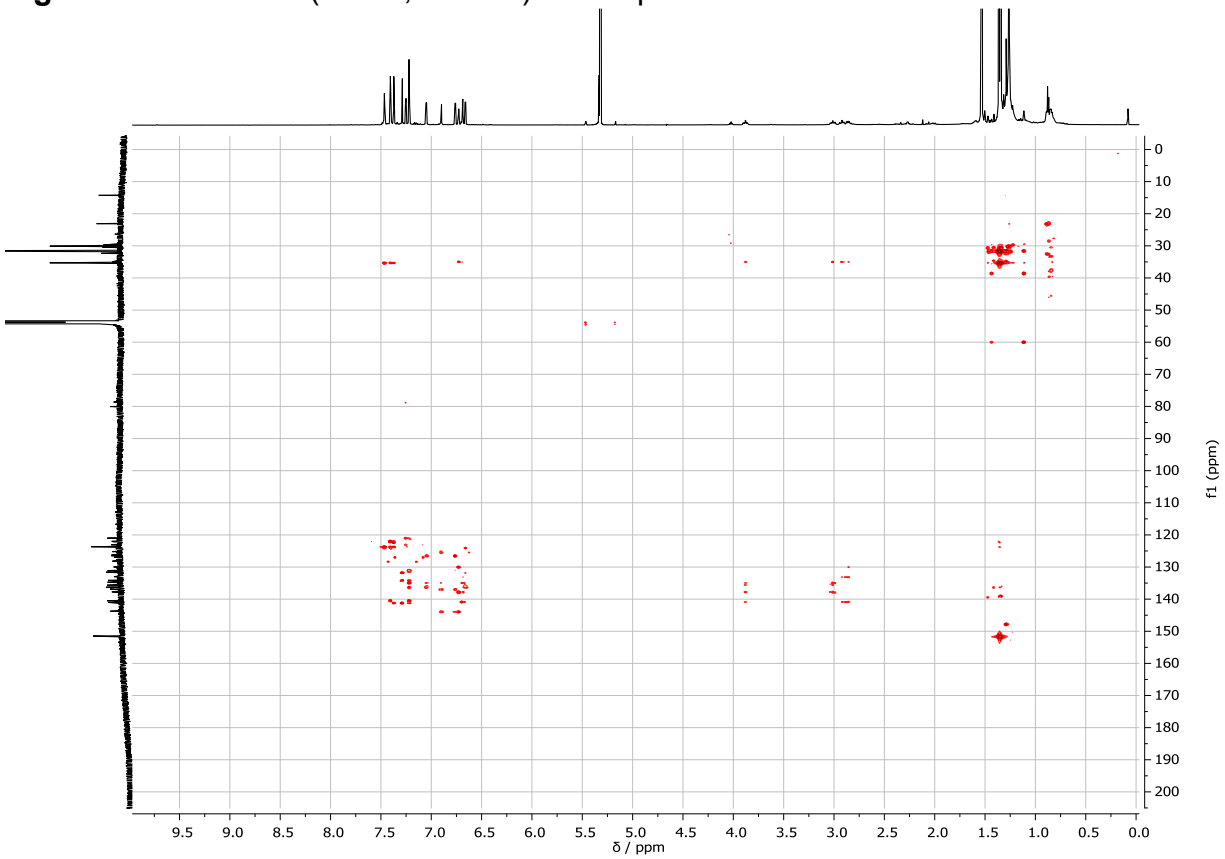


**Figure S47:** HMBC (298 K, $CD_2Cl_2$) of compound **12**.

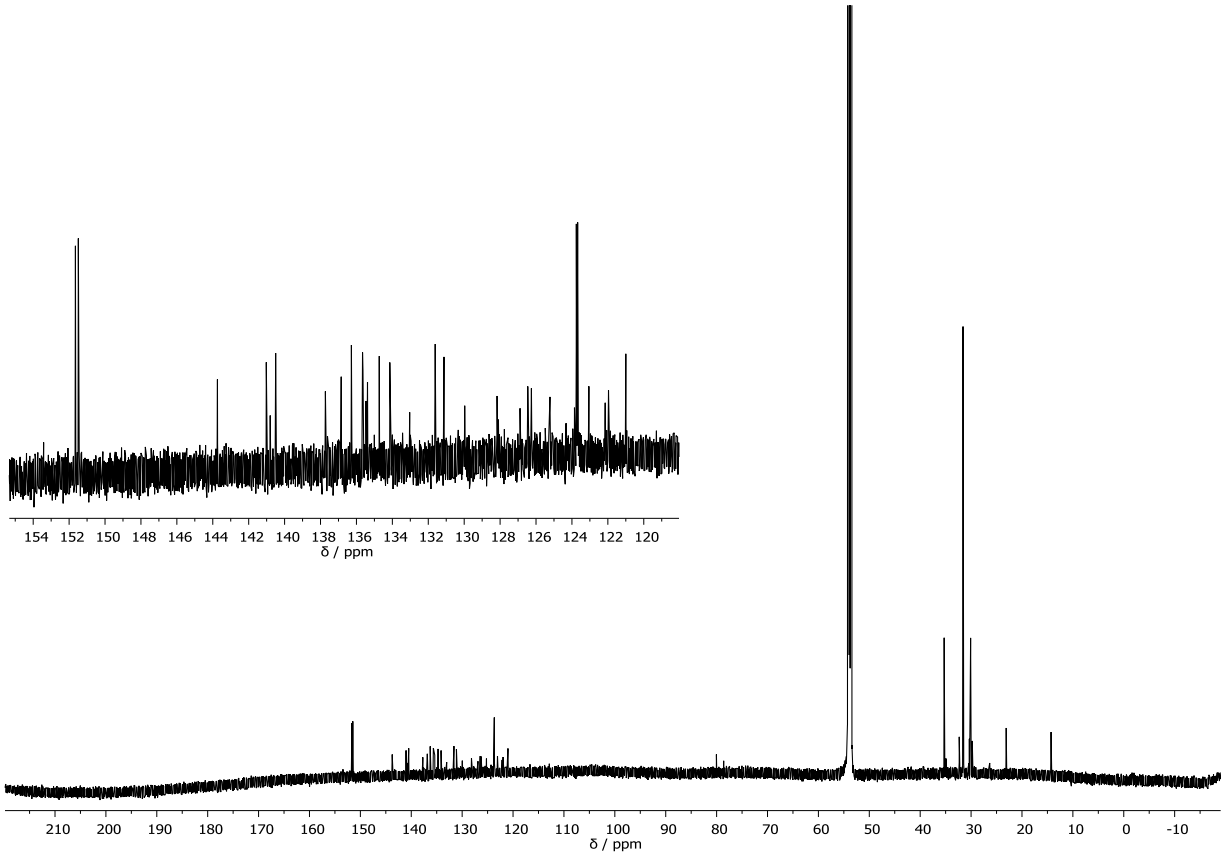


**Figure S48:** $^{13}C$ NMR spectrum (151 MHz, $CD_2Cl_2$) of compound **12**.

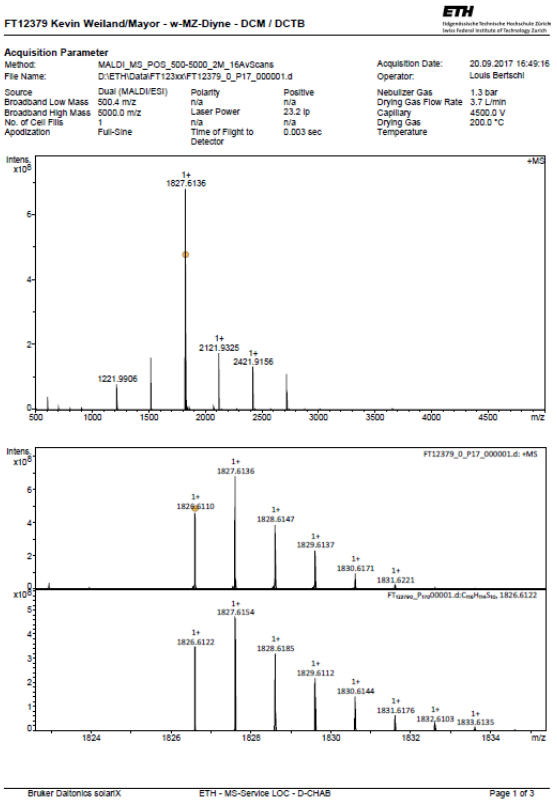

**FT12379 Kevin Weiland/Mayor - w-MZ-Diyne - DCM / DCTB**

**Acquisition Parameter**

| | | | | | |
|---|---|---|---|---|---|
| Method: | MALDI_MS_POS_500-5000_2M_16AvScans | | | Acquisition Date: | 20.09.2017 16:49:16 |
| File Name: | D:\ETH\Data\FT123xx\FT12379_0_P17_000001.d | | | Operator: | Louis Bertschi |
| Source | Dual (MALDI/ESI) | Polarity | Positive | Nebulizer Gas | 1.3 bar |
| Broadband Low Mass | 500.4 m/z | n/a | n/a | Drying Gas Flow Rate | 3.7 L/min |
| Broadband High Mass | 5000.0 m/z | Laser Power | 23.2 lp | Capillary | 4500.0 V |
| No. of Cell Fills | 1 | n/a | n/a | Drying Gas | 200.0 °C |
| Apodization | Full-Sine | Time of Flight to Detector | 0.003 sec | Temperature | |







Bruker Daltonics solarX ETH - MS-Service LOC - D-CHAB Page 1 of 3

**FT12379 Kevin Weiland/Mayor - w-MZ-Diyne - DCM / DCTB**

**Evaluation Spectra / Validation Formula:**

| # | Ion Formula | Adduct | m/z | z | Meas. m/z | mSigma | N-Rule | err [mDa] | err [ppm] |
|---|---|---|---|---|---|---|---|---|---|
| 1 | C116H114S10 | M | 1826.6122 | 1+ | 1826.6110 | 234.8 | ok | 1.2 | 0.7 |

**Calibration Info:**

| | |
|---|---|
| Date: | 22.09.2017 12:49:47 |
| Polarity: | Positive |
| Calibration spectrum: | +MS: Scan |
| Reference mass list: | MALDI: DCTB Matrix + HP-Mix (pos) |
| Calibration mode: | Quadratic |

| Reference m/z | Resulting m/z | Intensity | Error [ppm] |
|---|---|---|---|
| 118.0863 | | | |
| 250.1464 | | | |
| 251.1543 | | | |
| 273.1362 | | | |
| 322.0481 | | | |
| 332.2009 | | | |
| 500.2934 | | | |
| 501.3013 | | | |
| 523.2832 | | | |
| 622.0290 | | | |
| 750.4404 | | | |
| 751.4483 | | | |
| 773.4302 | | | |
| 922.0098 | | | |
| 1000.5674 | | | |
| 1001.5953 | | | |
| 1023.5772 | | | |
| 1221.9906 | 1221.9906 | 78790904 | -0.043 |
| 1521.9715 | 1521.9718 | 159637856 | 0.238 |
| 1821.9523 | 1821.9518 | 160126848 | -0.276 |
| 2121.9332 | 2121.9325 | 175631152 | -0.286 |
| 2421.9140 | 2421.9156 | 132007456 | 0.650 |
| 2721.8948 | 2721.8941 | 110745952 | -0.261 |

Standard deviation: 0.514

**Mass List:**

| # | m/z | Res. | S/N | I % | FWHM |
|---|---|---|---|---|---|
| 1 | 1221.9750 | 175439 | 416.7 | 2.0 | 0.0070 |
| 2 | 1221.9906 | 269271 | 2412.1 | 11.6 | 0.0045 |
| 3 | 1222.9942 | 244108 | 459.8 | 2.2 | 0.0050 |
| 4 | 1521.9718 | 229664 | 4233.5 | 23.5 | 0.0066 |
| 5 | 1522.9770 | 212777 | 862.8 | 4.8 | 0.0072 |
| 6 | 1821.9079 | 81653 | 195.9 | 1.4 | 0.0223 |
| 7 | 1821.9518 | 184112 | 3394.3 | 23.6 | 0.0099 |
| 8 | 1822.9575 | 166728 | 806.9 | 5.6 | 0.0109 |
| 9 | 1826.6110 | 179201 | 9904.9 | 68.8 | 0.0102 |
| 10 | 1827.6136 | 177735 | 14401.4 | 100.0 | 0.0103 |
| 11 | 1828.5650 | 104350 | 315.8 | 2.2 | 0.0175 |
| 12 | 1828.6147 | 175786 | 8284.9 | 57.5 | 0.0104 |
| 13 | 1829.6137 | 194952 | 4980.2 | 34.6 | 0.0094 |
| 14 | 1829.6249 | 264747 | 1154.4 | 8.0 | 0.0069 |
| 15 | 1830.6061 | 255580 | 572.9 | 4.0 | 0.0072 |
| 16 | 1830.6171 | 199077 | 2036.3 | 14.2 | 0.0092 |
| 17 | 1831.6104 | 183167 | 490.0 | 3.4 | 0.0100 |
| 18 | 1831.6221 | 199452 | 536.3 | 3.7 | 0.0092 |
| 19 | 1832.6143 | 171630 | 245.7 | 1.7 | 0.0107 |
| 20 | 1859.6076 | 148544 | 210.0 | 1.5 | 0.0125 |
| 21 | 2077.7661 | 141416 | 160.2 | 1.1 | 0.0147 |
| 22 | 2121.8545 | 73490 | 293.3 | 2.1 | 0.0289 |
| 23 | 2121.8830 | 61824 | 380.5 | 2.7 | 0.0343 |
| 24 | 2121.8926 | 134854 | 308.5 | 2.2 | 0.0157 |
| 25 | 2121.9325 | 157190 | 3662.3 | 25.9 | 0.0135 |
| 26 | 2122.8563 | 133164 | 161.9 | 1.2 | 0.0159 |
| 27 | 2122.8783 | 109858 | 217.8 | 1.6 | 0.0193 |
| 28 | 2122.9383 | 153654 | 1186.9 | 8.4 | 0.0138 |
| 29 | 2123.9437 | 139165 | 256.1 | 1.8 | 0.0153 |
| 30 | 2421.8689 | 83348 | 322.4 | 2.4 | 0.0291 |
| 31 | 2421.9156 | 136650 | 2585.1 | 19.4 | 0.0177 |
| 32 | 2422.8726 | 70023 | 177.2 | 1.3 | 0.0346 |
| 33 | 2422.9211 | 128371 | 1133.4 | 8.5 | 0.0189 |
| 34 | 2423.9258 | 121298 | 285.2 | 2.2 | 0.0200 |
| 35 | 2721.8163 | 122303 | 206.7 | 1.6 | 0.0223 |
| 36 | 2721.8276 | 108303 | 204.8 | 1.6 | 0.0251 |
| 37 | 2721.8941 | 123823 | 2104.9 | 16.3 | 0.0220 |
| 38 | 2722.8185 | 66897 | 146.4 | 1.1 | 0.0407 |
| 39 | 2722.8987 | 119033 | 1025.6 | 8.0 | 0.0229 |
| 40 | 2723.9036 | 110026 | 272.2 | 2.1 | 0.0248 |

| # | m/z | Res. | S/N | I % | FWHM |
|---|---|---|---|---|---|
| 1 | 1826.6122 | 179201 | | 74.3 | 0.0102 |
| 2 | 1827.6154 | 179300 | | 100.0 | 0.0102 |
| 3 | 1828.6080 | 179397 | | 33.4 | 0.0102 |
| 4 | 1828.6185 | 179398 | | 66.6 | 0.0102 |
| 5 | 1829.6112 | 179496 | | 44.7 | 0.0102 |
| 6 | 1829.6217 | 179497 | | 29.2 | 0.0102 |
| 7 | 1830.6039 | 179593 | | 6.8 | 0.0102 |
| 8 | 1830.6144 | 179594 | | 29.6 | 0.0102 |
| 9 | 1830.6249 | 179595 | | 9.5 | 0.0102 |
| 10 | 1831.6071 | 179691 | | 9.1 | 0.0102 |
| 11 | 1831.6176 | 179692 | | 12.9 | 0.0102 |
| 12 | 1831.6282 | 179693 | | 2.5 | 0.0102 |
| 13 | 1832.5998 | 179789 | | 0.8 | 0.0102 |
| 14 | 1832.6103 | 179790 | | 6.0 | 0.0102 |
| 15 | 1832.6208 | 179791 | | 4.2 | 0.0102 |

Bruker Daltonics solarX ETH - MS-Service LOC - D-CHAB Page 2 of 3

**FT12379 Kevin Weiland/Mayor - w-MZ-Diyne - DCM / DCTB**

| # | m/z | Res. | S/N | I % | FWHM |
|---|---|---|---|---|---|
| 16 | 1832.6314 | 179792 | | 0.5 | 0.0102 |
| 17 | 1833.6030 | 179887 | | 1.1 | 0.0102 |
| 18 | 1833.6135 | 179888 | | 2.6 | 0.0102 |
| 19 | 1833.6240 | 179889 | | 1.1 | 0.0102 |
| 20 | 1834.6062 | 179986 | | 0.7 | 0.0102 |
| 21 | 1834.6167 | 179987 | | 0.8 | 0.0102 |
| 22 | 1834.6274 | 179988 | | 0.2 | 0.0102 |
| 23 | 1835.6095 | 180084 | | 0.3 | 0.0102 |
| 24 | 1835.6200 | 180085 | | 0.2 | 0.0102 |
| 25 | 1836.6127 | 180182 | | 0.1 | 0.0102 |

Bruker Daltonics solarX ETH - MS-Service LOC - D-CHAB Page 3 of 3

**Figure S49:** High resolution MALDI ToF spectrum for compound **12**.

## Compound 1

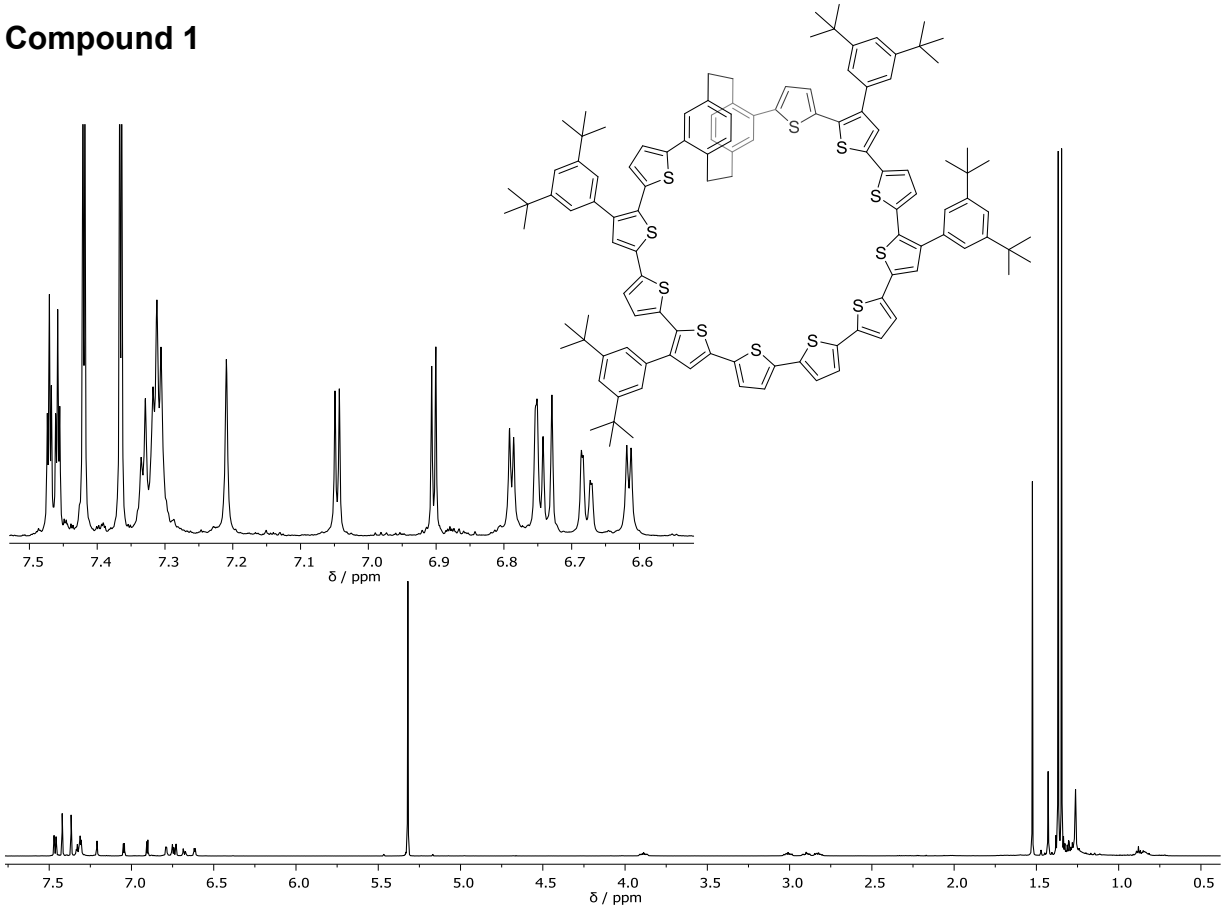


**Figure S50:** $^{1}$H NMR spectrum (600 MHz, $CD_2Cl_2$) of compound **1**.

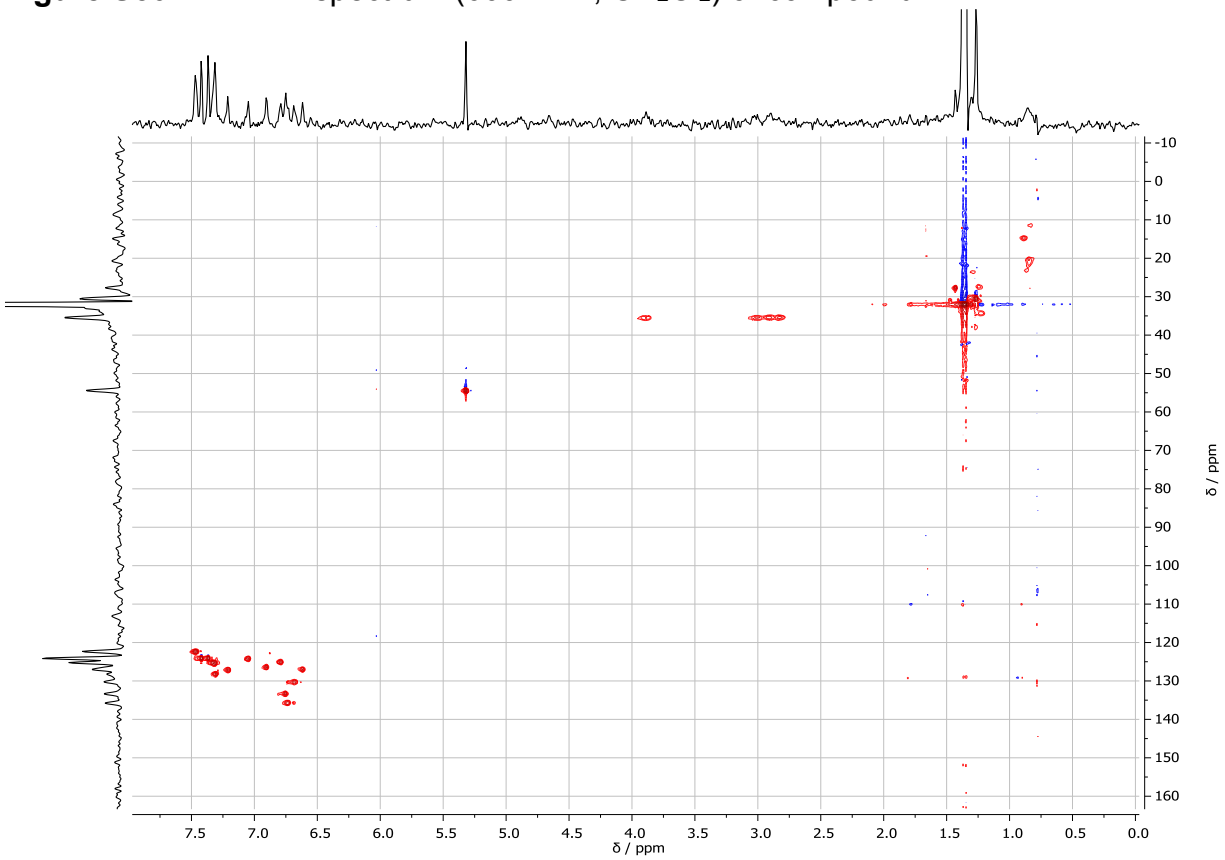


**Figure S51:** HMQC (298 K, $CD_2Cl_2$) of compound **1**.

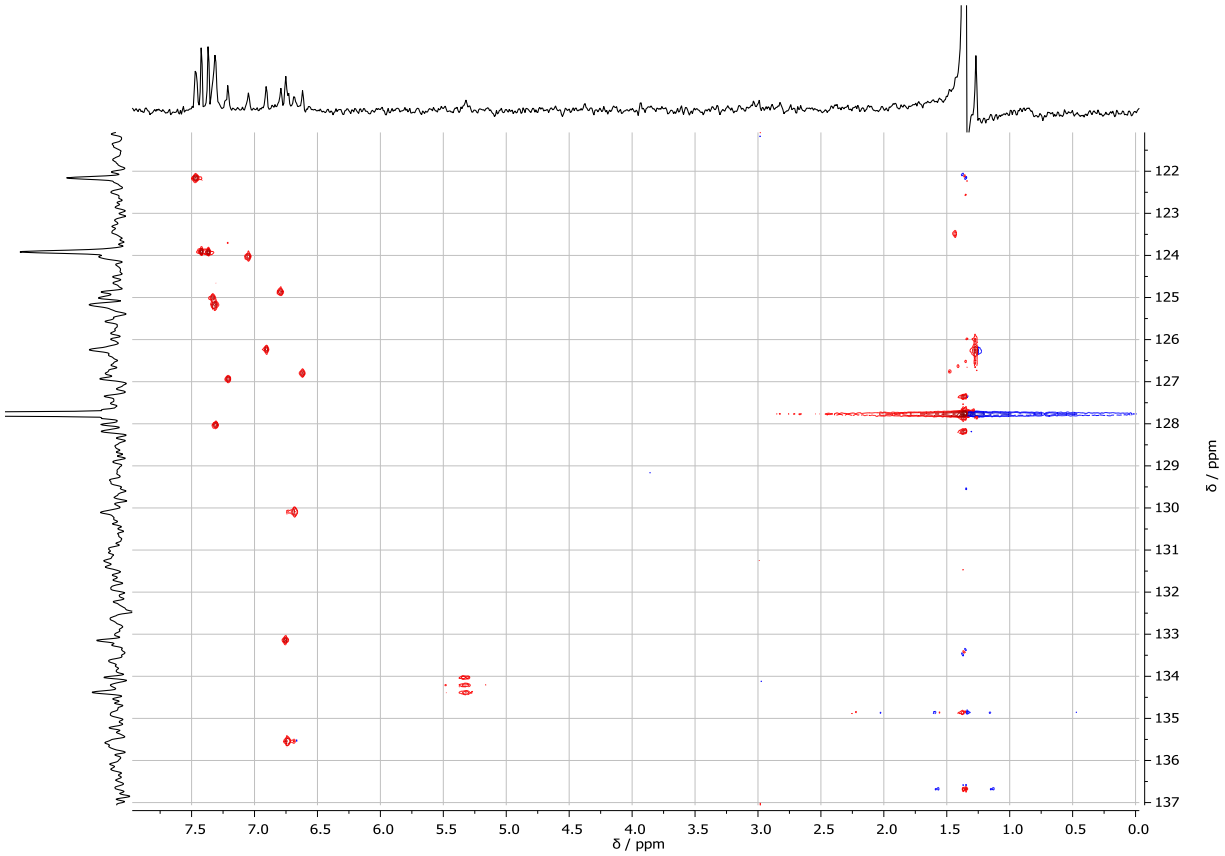


**Figure S52:** HMQC (298 K, $CD_2Cl_2$) of compound **1**.

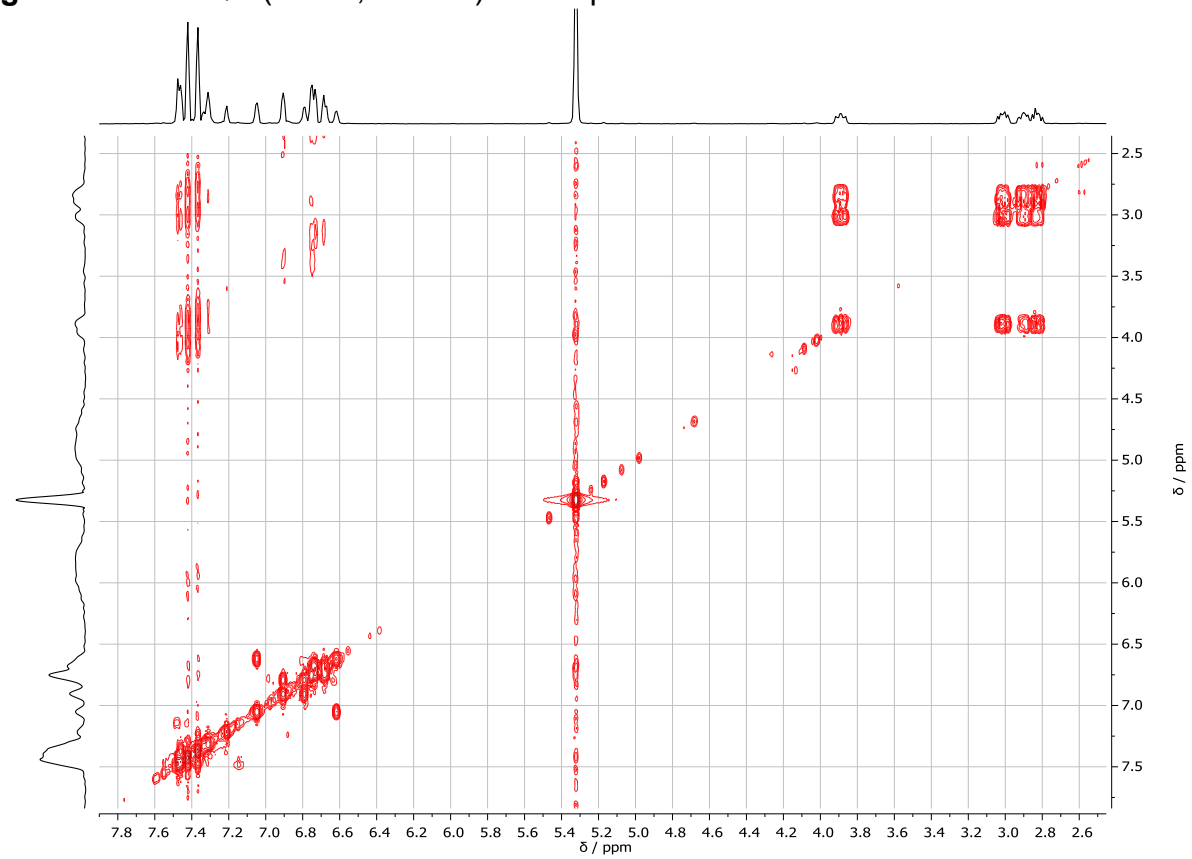


**Figure S53:** COSY (298 K, $CD_2Cl_2$) of compound **1**.

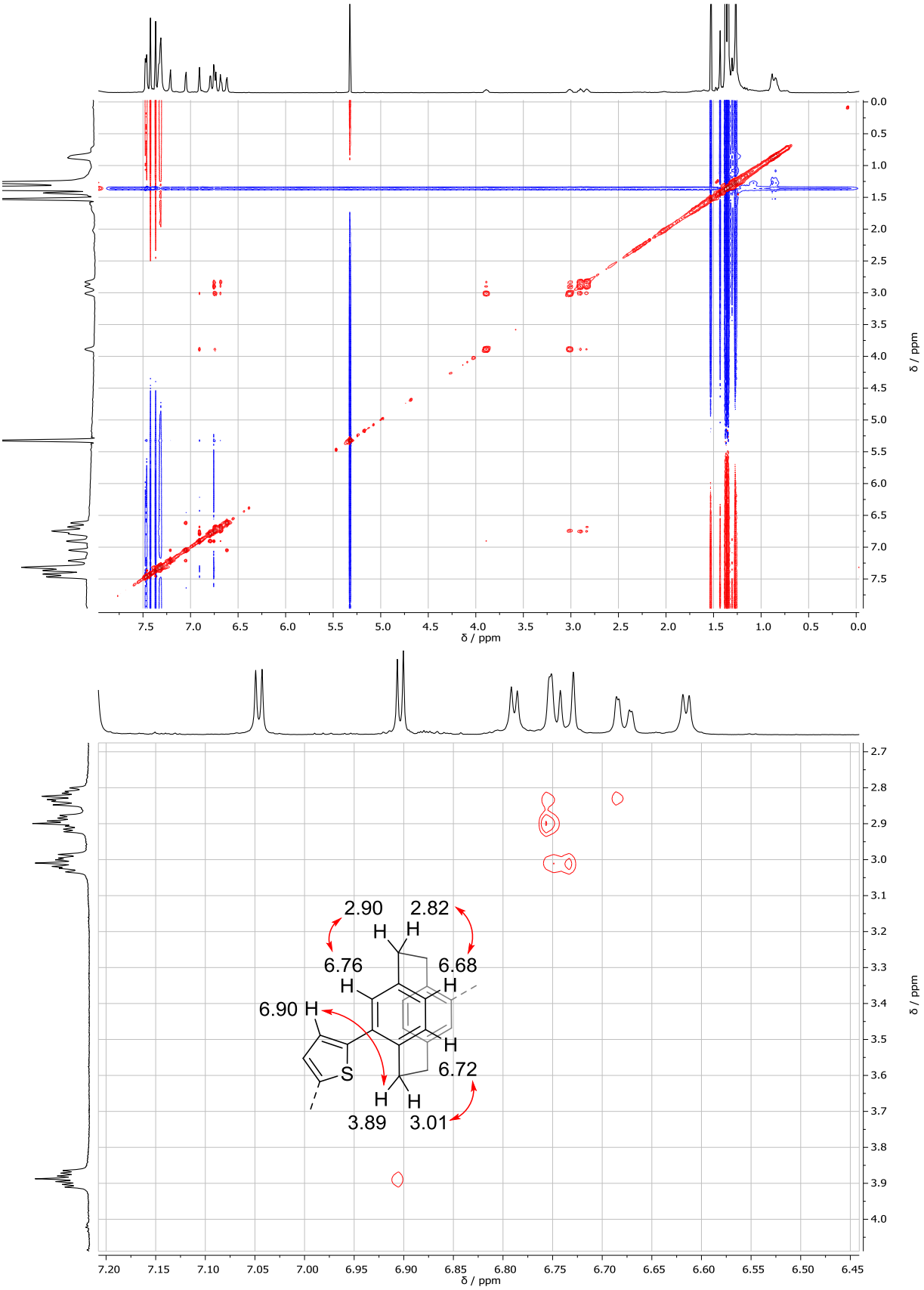


**Figure S54:** NOESY (298 K, $CD_2Cl_2$) of compound **1** with detail for the assignment of the benzylic proton resonances.

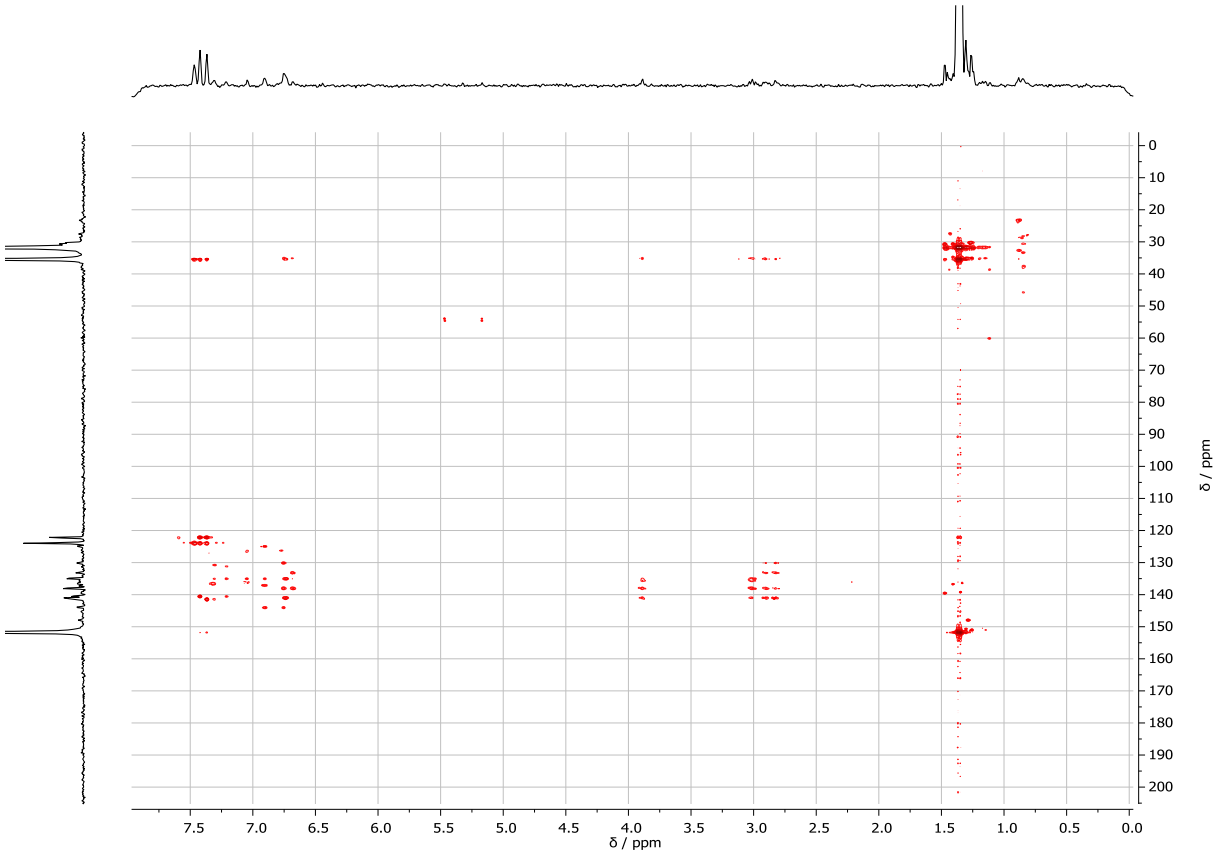


**Figure S55:** HMBC (298 K, $CD_2Cl_2$) of compound **1**.

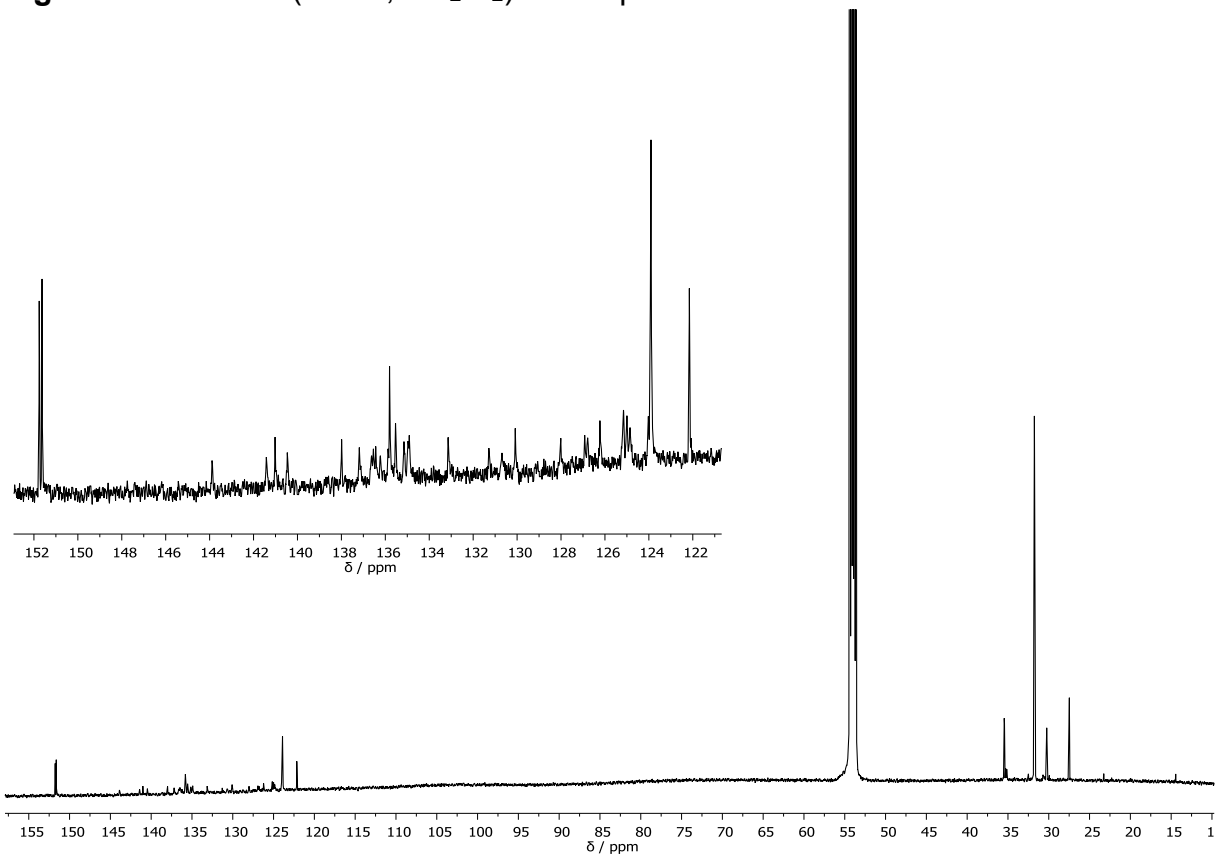


**Figure S56:** $^{13}C$ NMR spectrum (151 MHz, $CD_2Cl_2$) of compound **1**.

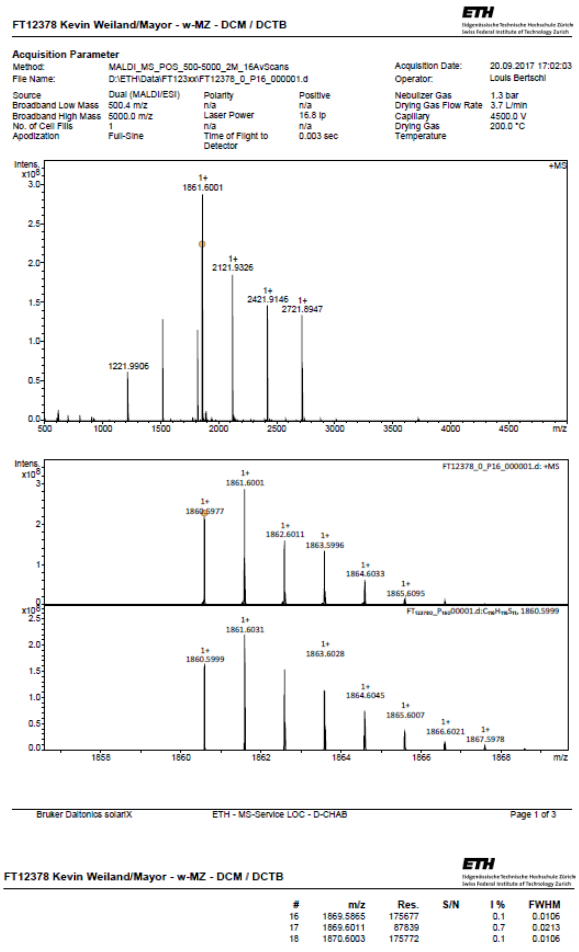

FT12378 Kevin Weiland/Mayor - w-MZ - DCM / DCTB

ETH Eidgenössische Technische Hochschule Zürich Swiss Federal Institute of Technology Zurich

**Acquisition Parameter**

| | | | | | |
|---|---|---|---|---|---|
| Method: | MALDI_MS_POS_500-5000_2M_16AvScans | | | Acquisition Date: | 20.09.2017 17:02:03 |
| File Name: | D:\ETH\Data\FT123xx\FT12378_0_P16_000001.d | | | Operator: | Louis Bertschi |
| Source | Dual (MALDI/ESI) | Polarity | Positive | Nebulizer Gas | 1.3 bar |
| Broadband Low Mass | 500.4 m/z | n/a | n/a | Drying Gas Flow Rate | 3.7 L/min |
| Broadband High Mass | 5000.0 m/z | Laser Power | 16.8 lp | Capillary | 4500.0 V |
| No. of Cell Fills | 1 | n/a | n/a | Drying Gas | 200.0 °C |
| Apodization | Full-Sine | Time of Flight to Detector | 0.003 sec | Temperature | |



Bruker Daltonics solariX | ETH - MS-Service LOC - D-CHAB | Page 1 of 3

FT12378 Kevin Weiland/Mayor - w-MZ - DCM / DCTB

**Evaluation Spectra / Validation Formula:**

| # | Ion Formula | Adduct | m/z | z | Meas. m/z | mSigma | N-Rule | err [mDa] | err [ppm] |
|---|---|---|---|---|---|---|---|---|---|
| 1 | C116H116S11 | M | 1860.5999 | 1+ | 1860.5977 | 215.0 | ok | 2.2 | 1.2 |

**Calibration Info:**

| | |
|---|---|
| Date: | 22.09.2017 11:49:07 |
| Polarity: | Positive |
| Calibration spectrum: | +MS: Scan |
| Reference mass list: | MALDI: DCTB Matrix + HP-Mix (pos) |
| Calibration mode: | Quadratic |

| Reference m/z | Resulting m/z | Intensity | Error [ppm] |
|---|---|---|---|
| 118.0863 | | | |
| 250.1464 | | | |
| 251.1543 | | | |
| 273.1362 | | | |
| 322.0481 | | | |
| 332.2009 | | | |
| 500.2934 | | | |
| 501.3013 | | | |
| 523.2832 | | | |
| 622.0290 | | | |
| 750.4404 | | | |
| 751.4483 | | | |
| 773.4302 | | | |
| 922.0098 | | | |
| 1000.5874 | | | |
| 1001.5953 | | | |
| 1023.5772 | | | |
| 1221.9906 | 1221.9906 | 62082736 | -0.018 |
| 1521.9715 | 1521.9716 | 129564504 | 0.069 |
| 1821.9523 | 1821.9523 | 114993320 | 0.018 |
| 2121.9332 | 2121.9326 | 86999040 | -0.264 |
| 2421.9140 | 2421.9146 | 147208544 | 0.251 |
| 2721.8948 | 2721.8947 | 134141216 | -0.052 |

Standard deviation: 0.228

**Mass List:**

| # | m/z | Res. | S/N | I % | FWHM |
|---|---|---|---|---|---|
| 1 | 1221.9770 | 199152 | 253.7 | 2.9 | 0.0061 |
| 2 | 1221.9857 | 371944 | 257.4 | 2.9 | 0.0033 |
| 3 | 1221.9906 | 272911 | 1917.1 | 21.5 | 0.0045 |
| 4 | 1222.9941 | 245929 | 341.2 | 3.8 | 0.0050 |
| 5 | 1521.9590 | 168670 | 472.2 | 6.1 | 0.0090 |
| 6 | 1521.9716 | 224194 | 3486.6 | 44.8 | 0.0068 |
| 7 | 1522.9764 | 206956 | 761.9 | 9.8 | 0.0074 |
| 8 | 1821.9523 | 184288 | 2600.8 | 39.8 | 0.0099 |
| 9 | 1822.9572 | 176485 | 723.2 | 11.1 | 0.0103 |
| 10 | 1823.9611 | 155627 | 126.7 | 2.0 | 0.0117 |
| 11 | 1860.5977 | 174832 | 4928.3 | 75.9 | 0.0106 |
| 12 | 1861.6001 | 173909 | 649.1 | 100.0 | 0.0107 |
| 13 | 1862.6011 | 168219 | 3624.8 | 55.9 | 0.0111 |
| 14 | 1863.5996 | 192178 | 3044.0 | 46.9 | 0.0097 |
| 15 | 1863.6111 | 309577 | 798.3 | 12.3 | 0.0060 |
| 16 | 1864.5917 | 229586 | 278.6 | 4.3 | 0.0081 |
| 17 | 1864.6033 | 193210 | 1432.1 | 22.1 | 0.0097 |
| 18 | 1865.5974 | 186487 | 353.1 | 5.5 | 0.0100 |
| 19 | 1865.6095 | 212988 | 372.5 | 5.8 | 0.0088 |
| 20 | 1866.6017 | 194548 | 213.2 | 3.3 | 0.0096 |
| 21 | 1892.5937 | 153422 | 220.3 | 3.4 | 0.0123 |
| 22 | 1893.5969 | 153339 | 286.9 | 4.4 | 0.0123 |
| 23 | 1894.6010 | 173369 | 158.3 | 2.5 | 0.0109 |
| 24 | 1895.5916 | 169456 | 136.1 | 2.1 | 0.0112 |
| 25 | 2121.9929 | 104653 | 334.2 | 5.3 | 0.0203 |
| 26 | 2121.9326 | 155397 | 4078.4 | 64.7 | 0.0137 |
| 27 | 2122.8968 | 121910 | 176.5 | 2.8 | 0.0174 |
| 28 | 2122.9377 | 154110 | 1391.8 | 22.1 | 0.0138 |
| 29 | 2123.9415 | 142977 | 282.0 | 4.5 | 0.0149 |
| 30 | 2131.7540 | 139643 | 172.1 | 2.8 | 0.0153 |
| 31 | 2132.7578 | 146418 | 116.5 | 1.9 | 0.0146 |
| 32 | 2421.8625 | 82460 | 310.7 | 5.4 | 0.0294 |
| 33 | 2421.9146 | 134687 | 2960.3 | 51.0 | 0.0180 |
| 34 | 2422.8666 | 92346 | 195.8 | 3.4 | 0.0262 |
| 35 | 2422.9200 | 131871 | 1302.2 | 22.4 | 0.0184 |
| 36 | 2423.9247 | 126531 | 310.1 | 5.4 | 0.0192 |
| 37 | 2721.8256 | 90619 | 151.2 | 2.7 | 0.0300 |
| 38 | 2721.8947 | 122326 | 2585.1 | 46.3 | 0.0223 |
| 39 | 2722.8989 | 121914 | 1301.9 | 23.3 | 0.0223 |
| 40 | 2723.9035 | 115923 | 334.1 | 6.0 | 0.0235 |

| # | m/z | Res. | S/N | I % | FWHM |
|---|---|---|---|---|---|
| 1 | 1860.5999 | 174832 | | 71.3 | 0.0106 |
| 2 | 1861.6031 | 174927 | | 96.6 | 0.0106 |
| 3 | 1862.6025 | 87510 | | 100.0 | 0.0213 |
| 4 | 1863.6028 | 87557 | | 76.1 | 0.0213 |
| 5 | 1864.5916 | 175207 | | 8.0 | 0.0106 |
| 6 | 1864.6045 | 87604 | | 41.0 | 0.0213 |
| 7 | 1865.6007 | 87651 | | 24.6 | 0.0213 |
| 8 | 1865.6158 | 175304 | | 2.4 | 0.0106 |
| 9 | 1866.5875 | 175395 | | 1.1 | 0.0106 |
| 10 | 1866.6021 | 87698 | | 11.6 | 0.0213 |
| 11 | 1866.6190 | 175398 | | 0.5 | 0.0106 |
| 12 | 1867.5978 | 87745 | | 4.6 | 0.0213 |
| 13 | 1867.6117 | 175491 | | 1.2 | 0.0106 |
| 14 | 1868.5992 | 87792 | | 2.0 | 0.0213 |
| 15 | 1868.6151 | 175585 | | 0.3 | 0.0106 |

Bruker Daltonics solariX | ETH - MS-Service LOC - D-CHAB | Page 2 of 3

FT12378 Kevin Weiland/Mayor - w-MZ - DCM / DCTB

| # | m/z | Res. | S/N | I % | FWHM |
|---|---|---|---|---|---|
| 16 | 1869.5865 | 175677 | | 0.1 | 0.0106 |
| 17 | 1869.6011 | 87639 | | 0.7 | 0.0213 |
| 18 | 1870.6003 | 175772 | | 0.1 | 0.0106 |

Bruker Daltonics solariX | ETH - MS-Service LOC - D-CHAB | Page 3 of 3

**Figure S57:** High resolution MALDI ToF spectrum for compound **1**.

**Mechanical Stabilization of Helical Chirality in a Macrocyclic Oligothiophene**

Kevin J Weiland, Thomas Brandl, Kenneth Atz, Alessandro Prescimone, Daniel Häussinger, Tomáš Šolomek and Marcel Mayor*

Supporting Information

## General Remarks

**Reagents and Solvents:** All commercially available compounds were purchased from Sigma-Aldrich, Acros, Apollo Scientific, Alfa Aesar and Fluorochem and used without further purification. Anhydrous solvents were purchased from Sigma-Aldrich and stored over molecular sieves (4 Å). Column chromatography was performed on silica gel P60 (40-63 µm) from SilicycleTM, the solvents were technical grade. TLC was performed with silica gel 60 F254 aluminium sheets with a thickness of 0.25 mm purchased from Merck.

**Synthesis:** All reactions with reagents that are easily oxidized or hydrolyzed were performed under Argon using Schlenk techniques with anhydrous solvents in glassware, which was dried prior to use.

**Analytics and Instruments:** Recycling gel permeation chromatography (GPC) was performed on a Shimadzu Prominence System equipped with SDV preparative columns from Polymer Standards Service (two Showdex columns in series, 20 x 600 mm each, exclusion limit: 30000 g/mol) with chloroform as solvent. NMR experiments were performed on Bruker Avance III NMR spectrometers operating at 400, 500 or 600 MHz proton frequencies. The instruments were equipped with a direct-observe 5 mm BBFO smart probe (400 and 600 MHz), an indirect-detection 5 mm BBI probe (500 MHz), or a five-channel cryogenic 5 mm QCI probe (600 MHz). All probes were equipped with actively shielded z-gradients (10 A). The chemical shifts are reported in ppm relative to tetramethylsilane or referenced to residual solvent peak and the J values are given in Hz (±0.1 Hz). Standard Bruker pulse sequences were used, and the data was processed on Topspin 3.2 (Bruker) using twofold zero-filling in the indirect dimension for all 2D experiments. For the macrocyclic compounds **14,15,16, and 1,** the $^{13}C$ resonances were obtained indirectly from 2D NMR spectroscopy. GC-MS was performed on a Shimadzu GC-MS-2020- SE instrument equipped with a Zebron 5 MS Inferno column, with a temperature range of up to 350 °C. MALDI-TOF mass spectra were recorded on a Bruker MicroFlex LRF spectrometer using trans-2-[3-(4-tert-Butylphenyl)-2-methyl-propenylidene]malononitrile (DCTB) as a matrix. High resolution mass spectra (HRMS) were measured on a Bruker solariX spectrometer with a MALDI source. Melting points were measured on a Büchi M-565 melting point apparatus and are uncorrected. UV/Vis absorption spectra were recorded on a Jasco V-770 Spectrophotometer. For HPLC, a Shimadzu LC-20AT HPLC was used equipped with a diodearray UV/Vis detector (SPD-M20A VP from Shimadzu, $\lambda$ = 200-600 nm) and a column oven Shimadzu CTO-20AC. The used column for separation on chiral stationary phase was a Chiralpak IG, 5 µm, 4.6 x 250 mm, Daicel Chemical Industries Ltd. CD measurements were

performed on a JASCO J-1500 CD Spectrophotometer in *n*-hexane/EtOAc 4:1 (for chiroptical experiments) or 2:1 (for determination of elution profiles for dynamic HPLC studies). The CD spectra were measured in 1 cm quartz glass cuvettes directly after chiral HPLC.

**Previously report compounds:** Dimethyl 8,13-dibromo[2.2]paracyclophane-4,15-dicarboxylate, tri*iso*propyl(thiophene-2-ylethynyl)silane and trimethyl(5-(4,4,5,5-tetramethyl-1,3,2-dioxaborolan-2-yl)thiophen-2-yl)silane were prepared following reported procedures.[1-3]

**Synthetic Procedures of structures 1-16**

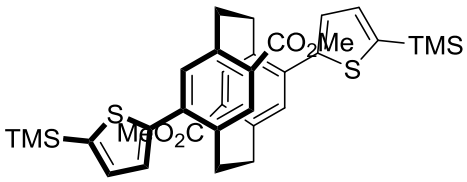


Dimethyl 8,13-dibromo[2.2]paracyclophane-4,15-dicarboxylate (2.02 g, 4.19 mmol, 1.0 eq.), trimethyl(5-(4,4,5,5-tetramethyl-1,3,2-dioxaborolan-2-yl)thiophen-2-yl)silane (4.73 g, 16.8 mmol, 4.0 eq.) and potassium phosphate (5.37 g, 25.1 mmol, 6.0 eq.) were dissolved in toluene (100 mL) and water (10 mL). The reaction mixture was degassed by bubbling a stream of Ar through the solution, $Pd(dppf)Cl_2$ (307 mg, 419 µmol, 10 mol%) was added and the reaction was heated to 110 °C for two hours. The reaction was allowed to reach room temperature, toluene was added, and the organic phase was washed with 2 M HCl and dried over $MgSO_4$. The solvent was removed under reduced pressure and the crude was purified by column chromatography (toluene), yielding **4** (2.20 g, 3.47 mmol, 83%) as a white solid.

M.p.: 174 – 176 °C.

$^1$H NMR (500 MHz, $CD_2Cl_2$): δ = 7.46 (s, 2H), 7.28 (d, $^3J_{H,H}$ = 3.5 Hz, 2H), 7.25 (d, $^3J_{H,H}$ = 3.5 Hz, 2H), 6.90 (s, 2H), 4.06 – 3.95 (m, 4H), 3.47 (s, 6H), 3.22 – 3.13 (m, 2H), 2.99 – 2.90 (m, 2H), 0.37 (s, 18H) ppm.

$^{13}$C NMR (126 MHz, $CD_2Cl_2$): δ = 166.55, 147.64, 143.43, 142.28, 138.72, 137.54, 137.29, 135.21, 134.49, 129.02, 128.20, 51.70, 35.14, 33.97, 0.17 ppm.

HRMS (MALDI TOF, DCTB): *m/z* calcd for $C_{34}H_{40}O_4S_2Si_2^+$ [$M^+$]: 632.1901, found: 632.1897.

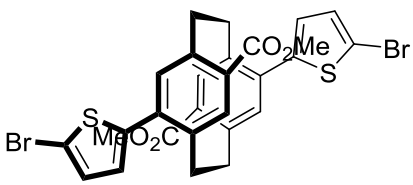


**4** (3.60 g, 5.69 mmol, 1.0 eq.) was dissolved in DMF (500 mL) and was degassed by bubbling a stream of Ar through the solution. NBS (2.43 g, 13.7 mmol, 2.4 eq.) was added and the mixture was heated to 70 °C for 18 hours. The reaction was allowed to reach room temperature and was added to 500 mL 2 M HCl. The precipitate was

filtered off and was washed with MeOH. The crude was dried under reduced pressure and **5** (3.43 g, 5.31 mmol, 93%) was obtained as an off-white solid.

M.p.: 273 – 275 °C (decomp.)

$^1$H NMR (500 MHz, $CD_2Cl_2$): δ = 7.44 (s, 2H), 7.09 (d, $^3J_{H,H}$ = 3.5 Hz, 2H), 7.00 (d, $^3J_{H,H}$ = 3.5 Hz, 2H), 6.78 (s, 1H), 4.04 (m, 1H), 3.96 – 3.88 (m, 2H), 3.59 (s, 6H), 3.13 (m, *2*H), 2.95 (m, 2H) ppm.

The solubility of **5** was not high enough to record a $^{13}$C-NMR spectrum.

HRMS (MALDI TOF, DCTB): *m/z* calcd for $C_{28}H_{22}Br_2O_4S_2^+$ [$M^+$]: 643.9321, found: 643.9319.

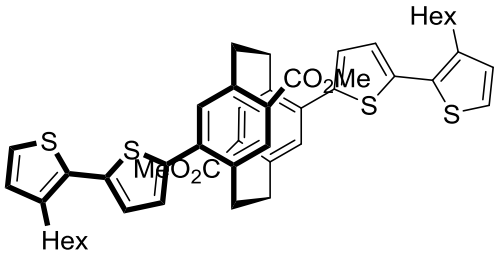


**5** (2.0 g, 3.09 mmol, 1.0 eq.), 3-hexylthiophene-2-boronic acid pinacol ester (3.70 mL, 12.4 mmol, 4.0 eq.) and $K_2CO_3$ (2.56 g, 18.5 mmol, 6.0 eq.) were suspended in toluene (15 mL) and MeOH (15 mL) and were degassed by bubbling a stream of Ar through the suspension. Pd-PEPPSI$^{TM}$-IPr (214 mg, 309 µmol, 10 mol%) was added and the reaction mixture was placed in a preheated oil bath at 70 °C for 20 minutes. The reaction mixture was allowed to reach room temperature, 2 M HCl was added, and the organic layer was dried over $MgSO_4$. The crude was purified by column chromatography (toluene), yielding **6** (2.06 g, 2.51 mmol, 81%) as a yellow solid.

M.p.: 151 – 153 °C.

$^1$H NMR (400 MHz, $CD_2Cl_2$): δ = 7.49 (s, 2H), 7.23 (m, 4H), 7.13 (d, $^3J_{H,H}$ = 3.8 Hz, 2H), 6.99 (d, $^3J_{H,H}$ = 5.2 Hz, 2H), 6.90 (s, 2H), 4.14 – 4.01 (m, 4H), 3.53 (s, 6H), 3.24 – 3.14 (m, 2H), 3.03 – 2.94 (m, 2H), 2.83 (m, 2H), 1.73 – 1.63 (m, 2H), 1.46 – 1.30 (m, 6H), 0.94 – 0.88 (m, 3H) ppm.

$^{13}$C NMR (101 MHz, $CD_2Cl_2$): δ = 166.60, 143.48, 141.96, 140.63, 138.35, 138.07, 137.63, 137.25, 134.07, 130.86, 130.78, 128.29, 128.14, 126.65, 124.51, 51.85, 34.95, 34.22, 32.26, 31.25, 29.90, 29.84, 23.23, 14.45 ppm.

HRMS (MALDI TOF, DCTB): *m/z* calcd for $C_{48}H_{52}O_4S_4^+$ [$M^+$]: 820.2743, found: 820.2740.

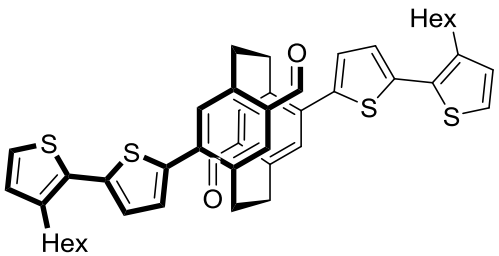


**6** (1.19 g, 1.44 mmol, 1.0 eq.) was dissolved in THF (20 mL), was degassed by bubbling through a stream of Ar, and was cooled to 0 °C. To this, DIBAL-H (1 M in toluene, 5.76 mL, 5.76 mmol, 4.0 eq.) was added and the reaction was stirred for 3 hours. To the crude reaction

mixture was added EtOAc and water. The organic layer was washed with water and dried over $MgSO_4$. The solvent was removed under reduced pressure and the crude was purified by column chromatography (gradient: $CH_2Cl_2$ to EtOAc). The solvent was removed under reduced pressure and the crude was taken up in $CH_2Cl_2$ (100 mL). To this was added Bobitt's salt (980 mg, 3.17 mmol, 2.2 eq.) and silica gel (216 mg, 3.6 mmol, 2.5 eq.) and the reaction was stirred for 18 hours. The crude was filtered through a plug of silica and the solvent was removed under reduced pressure. After purification by column chromatography (toluene), **7** (865 mg, 1.13 mmol, 79%) was obtained as a yellow solid.

M.p.: 157 – 159 °C.

$^1$H NMR (500 MHz, $CD_2Cl_2$): δ = 9.76 (s, 2H), 7.26 (d, $^3J_{H,H}$ = 5.2 Hz, 2H), 7.24 (s, 2H), 7.20 (d, $^3J_{H,H}$ = 3.8 Hz, 2H), 7.17 (d, $^3J_{H,H}$ = 3.8 Hz, 2H), 7.01 (d, $^3J_{H,H}$ = 5.2 Hz, 2H), 6.82 (s, 2H), 4.08 (m, 2H), 3.96 (m, 2H), 3.21 (m, 2H), 3.04 (m, 2H), 2.89 – 2.83 (m, 4H), 1.74 – 1.66 (m, 4H), 1.49 – 1.41 (m, 4H), 1.40 – 1.31 (m, 8H), 0.94 – 0.88 (m, 6H) ppm.

$^{13}$C NMR (126 MHz, $CD_2Cl_2$): δ = 189.27, 143.09, 140.50, 140.36, 139.21, 138.55, 137.76, 137.03, 134.79, 133.48, 130.36, 129.98, 128.76, 126.60, 124.22, 34.09, 31.70, 31.13, 30.64, 29.40, 29.27, 22.67, 13.88 ppm.

HRMS (MALDI TOF, DCTB): *m/z* calcd for $C_{46}H_{48}O_4S_4^+$ [$M^+$]: 760.2532, found: 760.2527.

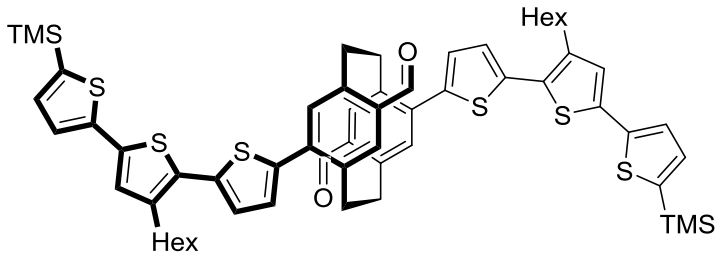


**7** (353 mg, 464 µmol, 1.0 eq.) was dissolved in $CHCl_3$ and NBS (182 mg, 1.02 mmol, 2.2 eq.) was added in the dark. The reaction was stirred for 16 hours and the solvent was removed under reduced pressure. The crude, trimethyl(5-(4,4,5,5-tetramethyl-1,3,2-dioxaborolan-2-yl)thiophen-2-yl)silane (1.05 g, 3.71 mmol, 8.0 eq.), and $K_2CO_3$ (385 mg, 2.78 mmol, 6.0 eq.) were suspended in toluene (20 mL) and MeOH (20 mL) and were degassed by bubbling through a stream of Ar. Pd-PEPPSI$^{TM}$-IPr (32.1 mg, 46.6 µmol, 10 mol%) was added and the reaction mixture was placed in a preheated oil bath at 70 °C for 30 minutes. The reaction mixture was allowed to reach room temperature, 2 M HCl was added, and the organic layer was dried over $MgSO_4$. The crude was purified by column chromatography (pentane/$CH_2Cl_2$ (1:1)), yielding **8** (441 mg, 464 µmol, 89%) as an orange amorphous solid.

$^1$H NMR (500 MHz, $CD_2Cl_2$): δ = 9.76 (s, 2H), 7.28 (d, $^3J_{H,H}$ = 3.4 Hz, 2H), 7.24 (s, 2H), 7.21 (d, $^3J_{H,H}$ = 3.9 Hz, 2H), 7.18 (m, 4H), 7.10 (s, 2H), 6.82 (s, 2H), 4.08 (m, 2H), 3.96 (m, 2H), 3.21 (m,

2H), 3.04 (m, 2H), 2.88 – 2.79 (m, 4H), 1.74 (m, 4H), 1.52 – 1.45 (m,4H), 1.38 (m, 8H), 0.97 – 0.89 (m, 6H), 0.36 (s, 18H) ppm.

$^{13}$C NMR (126 MHz, $CD_2Cl_2$): δ = 189.81, 143.66, 142.41, 141.82, 140.92, 140.88, 139.71, 138.77, 138.35, 137.60, 136.10, 135.50, 135.38, 134.05, 129.64, 129.44, 127.54, 126.99, 125.61, 54.22, 34.70, 32.30, 31.72, 30.98, 30.23, 29.87, 23.26, 14.50, 0.11 ppm.

HRMS (MALDI TOF, DCTB): *m/z* calcd for $C_{60}H_{68}O_2S_6Si_2^+$ [$M^+$]: 1068.3077, found: 1068.3067.

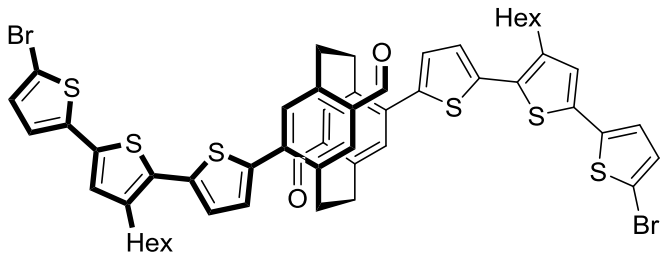

**8** (100 mg, 93.5 µmol, 1.0 eq.) was dissolved in AcOH (5 mL) and $CHCl_3$ (5 mL) and was degassed by bubbling through a stream of Ar. NBS (34.9 mmol, 196 µmol, 2.1 eq.) was added and the reaction was stirred for 16 hours. The reaction mixture was washed with $NaHCO_3$ and dried over $MgSO_4$. The solvent was removed under reduced pressure and the crude was purified by column chromatography (toluene), yielding **9** (110 mg, 93.5 µmol, 99%) as an orange amorphous solid.

$^1$H NMR (500 MHz, $CD_2Cl_2$): δ = 9.76 (s, 2H), 7.24 (s, 2H), 7.21 (d, $^3J_{H,H}$ = 3.8 Hz, 2H), 7.18 (d, $^3J_{H,H}$ = 3.8 Hz, 2H), 7.04 – 7.01 (m, 4H), 6.97 (d, $^3J_{H,H}$ = 3.8 Hz, 2H), 6.82 (s, 2H), 4.07 (m, 2H), 3.96 (m, 2H), 3.21 (m, 2H), 3.04 (m, 2H), 2.87 – 2.78 (m, 4H), 1.72 (m, 4H), 1.51 – 1.43 (m, 4H), 1.42 – 1.33 (m, 8H), 0.95 – 0.89 (m, 6H) ppm.

$^{13}$C NMR (126 MHz, $CD_2Cl_2$): δ = 189.81, 143.67, 141.84, 141.19, 139.65, 139.14, 138.41, 138.35, 137.65, 135.42, 134.95, 134.08, 131.50, 130.12, 129.45, 127.73, 127.25, 124.48, 111.58, 34.67, 32.27, 31.73, 30.98, 30.17, 29.84, 23.25, 14.48 ppm.

HRMS (MALDI TOF, DCTB): *m/z* calcd for $C_{54}H_{50}Br_2O_2S_6^+$ [$M^+$]: 1080.0496, found: 1080.0500.

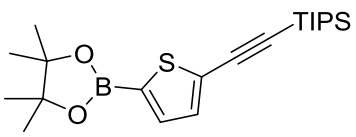

Tri*iso*propyl(thiophene-2-ylethynyl)silane (4.00 g, 15.1 mmol, 1.0 eq.) was dissolved in THF (40 mL) and was degassed by bubbling through a stream of Ar. The reaction mixture was cooled to -78 °C and *n*-BuLi (1.6 M in hexane, 9.63 mL, 15.4 mmol, 1.02 eq.) was added. It was stirred at -78 °C for one hour, allowed to reach room temperature, stirred for one hour, cooled to -78 °C and 2-*iso*propoxy-4,4,5,5-tetramethyl-1,3,2-dioxaborolane (3.39 mL, 16.6 mmol, 1.1 eq.) was added. The reaction mixture was allowed to reach room temperature overnight, and 2 M HCl was added. The organic layer was washed with 2 M HCl and dried over $MgSO_4$. The solvent was removed under reduced pressure and **10** (5.84 g, 15.0 mmol, 99%) was obtained as a brown oil.

$^1$H NMR (500 MHz, $CD_2Cl_2$): δ = 7.42 (d, $^3J_{H,H}$ = 3.6 Hz, 1H), 7.26 (d, $^3J_{H,H}$ = 3.6 Hz, 1H), 1.32 (s, 12H), 1.12 (m, 21H) ppm.

$^{13}$C NMR (126 MHz, $CD_2Cl_2$): δ = 137.17, 133.83, 130.35, 99.79, 97.85, 84.91, 25.11, 18.95, 11.87 ppm.

HRMS (MALDI TOF, DCTB): *m/z* calcd for $C_{21}H_{35}BO_2SSi+Na^+$ [$M+Na^+$]: 413.2112 found: 413.2088.

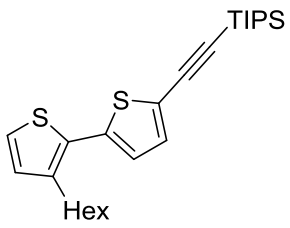


**10** (1.40 g, 3.59 mmol, 1.0 eq.), 2-bromo-3-hexylthiophene (1.33 g, 5.39 mmol, 1.5 eq.) and $K_2CO_3$ (1.49 g, 10.8 mmol, 3.0 eq.) were suspended in toluene (15 mL) and MeOH (15 mL). The reaction mixture was degassed by bubbling through a stream of Ar and Pd-PEPPSI™-IPr (122 mg, 180 μmol, 5 mol%) was added. The reaction was placed in a preheated oil bath and stirred at 70 °C for 20 minutes. The reaction was allowed to reach room temperature and 2 M HCl was added. The organic layer was washed with 2 M HCl and dried over $MgSO_4$. The solvent was removed under reduced pressure and the crude was purified via column chromatography (pentane), yielding **11** (785 mg, 1.82 mmol, 51%) as a yellow oil.

$^1$H NMR (400 MHz, $CD_2Cl_2$): δ = 7.12 (d, $^3J_{H,H}$ = 5.2 Hz, 1H), 7.10 (d, $^3J_{H,H}$ = 3.8 Hz, 1H), 6.89 (d, $^3J_{H,H}$ = 3.8 Hz, 1H), 6.87 (d, $^3J_{H,H}$ = 5.2 Hz, 1H), 2.70 – 2.64 (m, 2H), 1.58 – 1.48 (m, 2H), 1.31 – 1.17 (m, 6H), 1.05 (d, *J* = 2.2 Hz, 21H), 0.82 – 0.77 (m, 3H) ppm.

$^{13}$C NMR (101 MHz, $CD_2Cl_2$): δ = 141.06, 138.31, 133.37, 130.77, 130.34, 125.99, 124.78, 123.49, 99.66, 97.12, 32.19, 31.14, 29.77, 29.71, 23.17, 18.97, 14.40, 11.88 ppm.

HRMS (MALDI TOF, DCTB): *m/z* calcd for $C_{25}H_{38}S_2Si^+$ [$M^+$]: 430.2179 found: 430.2180.

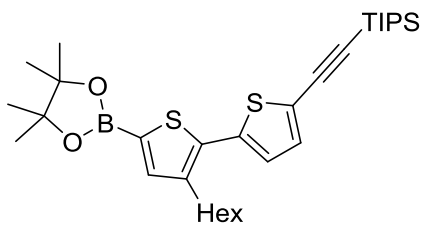


**11** (353 mg, 819 μmol, 1.0 eq.) was dissolved in THF (10 mL) and was degassed by bubbling through a stream of Ar. The reaction mixture was cooled to -78 °C and *n*-BuLi (1.6 M in hexane, 560 μL, 900 μmol, 1.1 eq.) was added. It was stirred at -78 °C for one hour, allowed to reach room temperature, stirred for one hour, cooled to -78 °C and 2-*iso*propoxy-4,4,5,5-tetramethyl-1,3,2-dioxaborolane (200 μL, 98.3 μmol, 1.2 eq.) was added. The reaction mixture was allowed to reach room temperature overnight, and 2 M HCl was added. The organic layer was washed with 2 M HCl and dried over $MgSO_4$. The solvent was removed under reduced pressure and **12** (441 mg, 792 μmol, 97%) was obtained as a green oil.

$^1$H NMR (400 MHz, $CD_2Cl_2$): δ = 7.41 (s, 1H), 7.18 (d, $^3J_{H,H}$ = 3.9 Hz, 1H), 7.03 (d, $^3J_{H,H}$ = 3.9 Hz, 1H), 2.78 – 2.71 (m, 2H), 1.68 – 1.57 (m, 2H), 1.32 (m, 18H), 1.13 (m, 21H), 0.91 – 0.85 (m, 3H) ppm.

$^{13}$C NMR (101 MHz, $CD_2Cl_2$): δ = 142.10, 140.66, 138.07, 137.28, 133.44, 126.34, 123.98, 99.57, 97.51, 84.77, 32.17, 31.08, 29.73, 25.11, 23.15, 18.96, 14.40, 11.87 ppm.

HRMS (MALDI TOF, DCTB): *m/z* calcd for $C_{31}H_{49}BO_2S_2Si^+$ [$M^+$]: 560.3031, found: 556.3029.

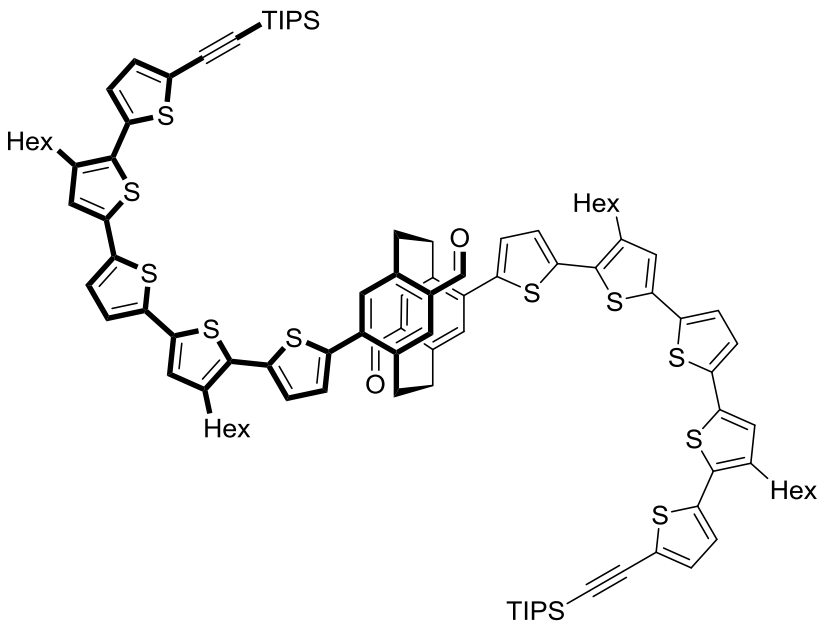


**9** (391 mg, 361 µmol, 1.0 eq.), **12** (804 mg, 1.44 mmol, 4.0 eq.), and $K_2CO_3$ (299 mg, 2.17 mmol, 6.0 eq.) were suspended in toluene (20 mL) and MeOH (20 mL). The reaction mixture was degassed by bubbling through a stream of Ar and Pd-PEPPSI™-IPr (25.0 mg, 36.1 µmol, 10 mol%) was added. The reaction mixture was placed in a preheated oil bath and was stirred at 70 °C for 30 minutes. The reaction was allowed to reach room temperature and 2 M HCl was added. The organic layer was washed with 2 M HCl and dried over $MgSO_4$. The solvent was removed under reduced pressure and the crude was purified by column chromatography (pentane/$CH_2Cl_2$ (2:1)), yielding **13** (465 mg, 261 µmol, 72%) as a red amorphous solid.

$^1$H NMR (500 MHz, $CD_2Cl_2$): δ = 9.76 (s, 2H), 7.25 (s, 2H), 7.22 – 7.18 (m, 6H), 7.14 – 7.11 (m, 4H), 7.09 (s, 2H), 7.06 (s, 2H), 7.01 (d, $^3J_{H,H}$ = 3.8 Hz, 2H), 6.82 (s, 2H), 4.08 m, 2H), 3.97 (m, 2H), 3.22 (m, 2H), 3.05 (m, 2H), 2.87 – 2.81 (m, 4H), 2.79 – 2.72 (m, 4H), 1.78 – 1.71 (m, 4H), 1.71 – 1.63 (m, 4H), 1.52 – 1.45 (m, 4H), 1.44 – 1.31 (m, 12H), 1.15 (m, 42H), 0.95 – 0.89 (m, 6H) ppm.

$^{13}$C NMR (126 MHz, $CD_2Cl_2$): δ = 189.82, 143.68, 141.91, 141.06, 139.68, 138.62, 138.36, 138.35, 137.78, 137.63, 136.52, 136.47, 135.62, 135.40, 134.07, 133.47, 129.95, 129.77, 129.75, 129.47, 127.53, 127.38, 127.11, 125.92, 125.12, 125.11, 123.64, 99.64, 97.63, 34.70, 32.30, 32.21, 31.74, 30.98, 30.93, 30.25, 30.05, 29.89, 29.75, 23.27, 23.19, 18.99, 14.50, 14.43, 11.91 ppm.

HRMS (MALDI TOF, DCTB): *m/z* calcd for $C_{104}H_{124}O_2S_{10}Si_2^+$ [$M^+$]: 1780.6344, found: 1780.6341.

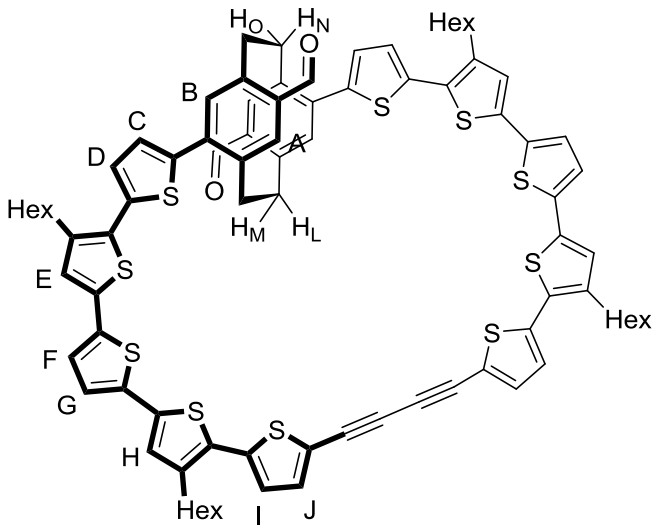


**13** (190 mg, 56.1 µmol, 1.0 eq.) was dissolved in wetted THF (50 mL) and was degassed by bubbling a stream of Ar through the solution. To the reaction mixture TBAF (1 M in THF, 320 µL, 320 µmol, 3.0 eq.) was added and the reaction was stirred for 16 hours. The completion of the reaction was confirmed by MALDI TOF MS and the reaction mixture was diluted with pyridine (50 mL). The solution was added to CuCl (318 mg, 3.21 mmol, 30.0 eq.) and $Cu(OAc)_2$ (816 mg, 4.49 mmol, 42.0 eq.) in pyridine (150 mL) at 80 °C by syringe pump over the course of 40 hours. After completion of the reaction the crude was diluted with $CH_2Cl_2$ and 2 M HCl was added. The organic layer was washed with 2 M HCl and dried over $MgSO_4$. The crude was purified by column chromatography ($CH_2Cl_2$) and **14** (134 mg, 107 µmol, 85%) was obtained as a red amorphous solid.

$^1$H NMR (600 MHz, $C_2D_2Cl_4$): $\delta$ = 9.779 (s, 2H, CHO), 7.174 (s, 2H, $H_A$), 7.131 (d, $^3J$=3.71 Hz, 2H, $H_D$), 7.049 (d, $^3J$=3.71 Hz, 2H, $H_C$), 6.996 (s, 2H, $H_{E/H}$), 6.743 (d, $^3J$=3.83 Hz, 2H, $H_I$), 6.961 (d, $^3J$=3.61 Hz, 2H, $H_{F/G}$), 6.941 (d, $^3J$=3.61 Hz, 2H, $H_{F/G}$), 6.933 (s, 2H, $H_{E/H}$), 6.917 (d, $^3J$=3.83 Hz, 2H, $H_J$), 6.705 (s, 2H, $H_B$), 4.081 (m, 2H, $H_N$), 3.805 (m, 2H, $H_L$), 2.728 (m, 4H, $H_{HexA}$), 2.796 (m, 2H, $H_M$), 2.578 (m, 4H, $H_{HexA'}$), 2.571 (m, 2H, $H_O$), 1.670 (m, 4H, $H_{HexB}$), 1.561 (m, 4H, $H_{HexB'}$) ppm.

$^{13}$C NMR (150 MHz, $C_6D_6$): $\delta$ = 191.00 (COH), 140.27, ($C_A$), 136.18 ($C_J$), 135.92 ($C_B$), 131.80 ($C_C$), 128.55 ($C_{E/H}$), 128.20 ($C_{E/H}$), 127.07 ($C_D$), 126.46 ($C_I$), 126.16 ($C_{F/G}$), 125.92 ($C_{F/G}$), 36.94 ($C_{NO}$), 34.52 ($C_{LM}$), 32.70 ($C_{HexB/B'}$), 32.65 ($C_{HexB/B'}$), 32.42 ($C_{HexA}$), 32.21 ($C_{HexA'}$). No resonances for quarternary carbon atoms could be observed due to the poor solubility of the compound.

HRMS (MALDI TOF, DCTB): *m/z* calcd for $C_{86}H_{82}O_2S_{10}^+$ [$M^+$]: 1466.3516, found: 1466.3518.

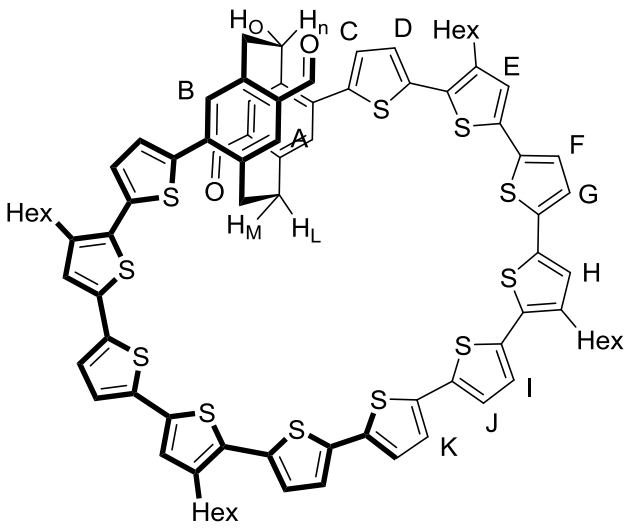


**14** (27.0 mg, 18.4 µmol, 1.0 eq.) and $Na_2S \cdot 9\ H_2O$ (133 mg, 552 µmol, 30.0 eq.) were suspended in DMF (4 mL) and 2-methoxyethanol (4 mL). The reaction mixture was degassed by bubbling through a stream of Ar and was heated to 122 °C for two hours. The reaction was followed by MALDI TOF MS and after completion of the reaction was cooled to room temperature, diluted with $CH_2Cl_2$ and 2 M HCl was added. The organic phase was washed with 2 M HCl and dried over $MgSO_4$.The solvent was removed under reduced pressure and the crude was purified by column chromatography ($CH_2Cl_2$). **15** (26.0 mg, 18.4 µmol, 94%) was obtained as a red amorphous solid.

$^1$H NMR (600 MHz, $C_6D_6$): $\delta$ = 9.784 (s, 2H, CHO), 7.235 (s, 2H, $H_A$), 7.121 (d, $^3J$=3.74 Hz, 2H, $H_D$), 7.052 (d, $^3J$=3.74 Hz, 2H, $H_C$), 7.024 (d, $^3J$=3.65 Hz, 2H, $H_I$), 7.011 (m, 2H, $H_{E/H/K}$), 7.003 (m, 2H, $H_{E/H/K}$), 6.992 (2H, $^3J$=3.65 Hz, $H_J$), 6.977 (m, 2H, $H_{F/G}$), 6.974 (m, 2H, $H_{F/G}$), 6.973 (m, 2H, $H_{E/H/K}$), 6.726 (s, 2H, $H_B$), 4.117 (m, 2H, $H_N$), 3.771 (m, 2H, $H_L$), 2.780 (m, 2H, $H_O$), 2.577 (m, 2H, $H_M$), 2.731 (m, 4H, $H_{HexA}$), 2.697 (m, 4H, $H_{HexA'}$) ppm.

$^{13}$C NMR (150 MHz, $C_6D_6$): $\delta$ = 188.72 (COH), 137.93 ($C_A$), 133.73 ($C_B$), 129.31 ($C_C$), 126.37 ($C_{E/H/K}$), 126.29 ($C_{E/H/K}$), 126.27 ($C_J$), 124.98 ($C_I$), 124.94 ($C_{E/H/K}$), 124.51 ($C_D$), 123.95 ($C_{F/G}$), 123.87 ($C_{F/G}$), 30.22 ($C_{HexA}$), 30.02 ($C_{HexA'}$). No resonances for quarternary carbon atoms and for carbon atoms from the cyclophane building block could be observed due to the poor solubility of the compound.

HRMS (MALDI TOF, DCTB): *m/z* calcd for $C_{86}H_{84}O_2S_{11}^+$ [$M^+$]: 1500.3394, found: 1500.3404.

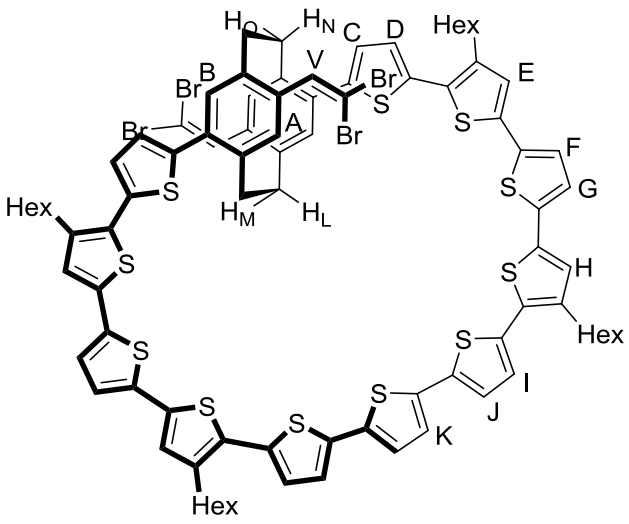


**15** (56.0 mg, 37.3 µmol, 1.0 eq.) and $PPh_3$ (396 mg, 1.50 mmol, 40.0 eq.) were suspended in $CH_2Cl_2$ and were degassed with Ar. After cooling to 0 °C, $CBr_4$ (198 mg, 598 µmol, 16.0 eq.) were added. The reaction was stirred at 0 °C for 30 minutes and at room temperature for 30 minutes. After TLC indicated completion of the reaction, the reaction mixture was filtered through a plug of silica and the solvent was removed under reduced pressure. The crude product was purified by column chromatography in (pentane/$CH_2Cl_2$ (2:1)). **16** (54.0 mg, 30.0 µmol, 80%) was obtained as a red amorphous solid.

$^1$H NMR (600 MHz, $C_6D_6$): $\delta$ = 7.359 (s, 2H, $H_A$), 7.214 (d, $^3J$ = 3.81 Hz, 2H, $H_D$), 7.065 (d, $^3J$ = 3.81 Hz, 2H, $H_C$), 7.021 (d, $^3J$ = 3.86 Hz, 2H, $H_J$), 7.002 (m, 2H, $H_G$), 6.996 (m, 2H, $H_F$), 6.988 (s, 2H, $H_V$), 6.988 (d, $^3J$ = 3.86 Hz, 2H, $H_I$), 6.969 (s, 2H, $H_K$), 6.969 (s, 2H, $H_{E/H}$), 6.969 (s, 2H, $H_{E/H}$), 6.828 (s, 2H, $H_B$), 3.941 (m, 2H, $H_N$), 3.021 (m, 2H, $H_L$), 2.816 (t, $^3J$ = 7.88 Hz, 4H, $H_{HexA}$), 2.776 (m, 2H, $H_O$), 2.693 (t, $^3J$ = 7.88 Hz, 4H, $H_{HexA'}$), 2.569 (m, 2H, $H_M$), 1.733 (tt, $^3J$ = 7.78 Hz, $^3J$ = 7.56 Hz, 4H, $H_{HexB}$), 1.632 (tt, $^3J$ = 7.78 Hz, $^3J$ = 7.56 Hz, 4H, $H_{HexB'}$) ppm.

$^{13}$C NMR (150 MHz, $C_6D_6$): $\delta$ =136.04 ($C_A$), 135.68 ($C_V$), 132.76 ($C_B$), 127.05 ($C_C$), 126.38 ($C_I$), 126.28 ($C_G$), 126.04 ($C_F$), 125.05 ($C_J$), 124.90 ($C_K$), 123.93 ($C_D$), 123.93 ($C_{E/H}$), 123.55 ($C_{E/H}$), 30.74 ($C_{HexB'}$), 30.55 ($C_{HexB}$), 30.29 ($C_{HexA}$), 30.02 ($C_{HexA'}$). No resonances for quarternary carbon atoms and for carbon atoms from the cyclophane building block could be observed due to the poor solubility of the compound.

HRMS (MALDI TOF, DCTB): *m/z* calcd for $C_{88}H_{84}Br_4S_{11}^+$ [$M^+$]: 1808.0229, found: 1808.0265.

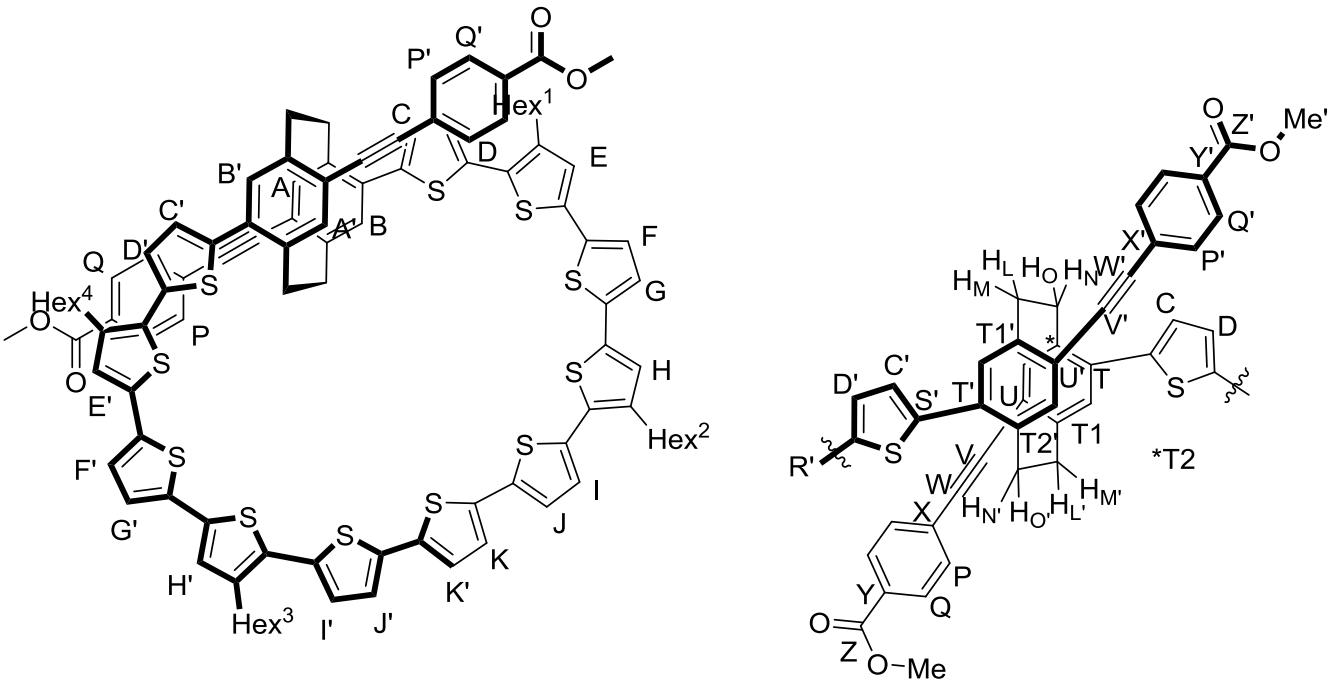

**16** (12.2 mg, 6.74 µmol, 1.0 eq.) was dissolved in THF (3 mL) and was degassed with Ar. To this was added at 0 °C an excess of freshly prepared LDA (*n*-BuLi: (2.5 M in hexane) 142 µL, 355 mmol, 52.6 eq.; and diisopropylamine: 55.0 µL, 390 mmol, 57.9 eq.; in THF (2 mL)). After warming the reaction to room temperature, the reaction was followed by MALDI TOF MS and after completion of the reaction, it was diluted with 2 M HCl and with $CH_2Cl_2$ and it was dried over $MgSO_4$. The solvent was removed under reduced pressure and the crude was dissolved in THF (3 mL). The crude was transferred to an oven dried flask, and diisopropylamine (2 mL) and methyl-4-iodobenzoate (10.5 mg, 40.2 µmol, 6.0 eq.) were added. The reaction mixture was degassed by bubbling through a stream of Ar for 20 minutes, and $Pd(PPh_3)_4$ (770 µg, 0.67 µmol, 10 mol%.) and CuI (7.00 µg, 0.34 µmol, 5 mol%) were added. The reaction was heated to 55 °C for two hours and after completion 2 M HCl was added. The crude was diluted with $CH_2Cl_2$ and washed with 2 M HCl. The crude was dried over $MgSO_4$ and the solvent was removed under reduced pressure. The crude product was purified by recycling gel permeation chromatography in $CHCl_3$. **1** (2.10 mg, 1.19 µmol, 18%) was obtained as a red amorphous solid.

$^1$H NMR (600 MHz, $C_6D_6$): $\delta$ = 8.047 (d, $^3J$=8.65, 2H, $H_{Q'}$), 7.882 (d, $^3J$=8.30, 2H, $H_Q$), 7.507 (d, $^3J$=3.75, 1H, $H_C$), 7.397 (d, $^3J$=8.65, 2H, $H_{P'}$), 7.314 (d, $^3J$=8.30, 2H, $H_P$), 7.238 (s, 1H, $H_A$), 7.179 (s, 1H, $H_{B'}$), 7.064 (s, 1H, $H_{A'}$), 7.052 (s, 1H, $H_B$), 7.034 (m, 1H, $H_{E'}$), 7.032 (m, 1H, $H_{H/H'}$), 7.013 (m, 1H, $H_{F'/G'}$), 7.009 (d, $^3J$=3.68, 1H, $H_{J/J'}$), 6.996 (m, 1H, $H_{H/H'}$), 6.989 (d, $^3J$=3.68, 1H, $H_{I/I'}$), 6.988 (m, 1H, $H_{I/I'}$), 6.976 (m, 1H, $H_{F'/G'}$), 6.973 (m, 1H, $H_{J/J'}$), 6.953 (s, 1H, $H_{K/K'}$), 6.953 (s, 1H, $H_{K/K'}$), 6.939 (m, 1H, $H_E$), 6.931 (m, 1H, $H_G$), 6.914 (m, 1H, $H_F$), 6.899 (d, $^3J$=3.65, 1H, $H_{C'}$), 6.764 (d, $^3J$=3.75, $H_D$), 6.733 (d, $^3J$=3.65, $H_{D'}$), 4.513 (m, 1H, $H_N$), 4.182 (m, 1H, $H_{N'}$), 3.732 (m, 1H, $H_L$), 3.647 (m, 1H, $H_{L'}$), 3.574 (s, 3H, OMe'), 3.550 (s, 3H, OMe), 3.059 (m, 1H, $H_{O'}$), 2.967

(m, 1H, $H_M$), 2.750 (m, 1H, $H_O$), 2.676 (m, 2H, $H_{HexA2}$), 2.676 (m, 2H, $H_{HexA3}$), 2.592 (m, 2H, $H_{HexA1}$), 2.575 (m, 1H, $H_{M'}$), 2.414 (m, 2H, $H_{HexA4}$) ppm.

$^{13}$C NMR (150 MHz, $C_6D_6$): $\delta$ =166.30 ($C_Z$), 166.19 ($C_{Z'}$), 143.57 ($C_{T1'}$), 142.93 ($C_T$), 142.93 ($C_{S'}$), 141.21 ($C_S$), 139.57 ($C_A$), 138.25 ($C_{A'}$), 138.10 ($C_R$), 138.02 ($C_{R'}$), 137.38 ($C_{T2}$), 136.95 ($C_{T2'}$), 136.58 ($C_{T'}$), 134.32 ($C_{T1}$), 133.68 ($C_{B'}$), 131.76 ($C_{P'}$), 131.31 ($C_P$), 131.15 ($C_B$), 129.90 ($C_Q$), 129.88 ($C_{X'}$), 129.75 ($C_{Y'}$), 129.55 ($C_{Q'}$), 129.30 ($C_Y$), 128.85 ($C_X$), 127.93 ($C_{C'}$), 126.96 ($C_C$), 126.95 ($C_{F'/G'}$), 126.52 ($C_{H/H'}$), 126.11 ($C_{E'}$), 126.02 ($C_{J/J'}$), 125.86 ($C_{H/H'}$), 125.82 ($C_E$), 125.21 ($C_{F'/G'}$), 125.13 ($C_{K/K'}$), 124.99 ($C_{J/J'}$), 124.77 ($C_{K/K'}$), 124.33 ($C_{I/I'}$), 124.29 ($C_{D'}$), 123.83 ($C_{I/I'}$), 123.65 ($C_G$), 123.50 ($C_{U'}$), 123.32 ($C_F$), 123.25 ($C_D$), 121.67 ($C_U$), 95.06 ($C_W$), 93.89 ($C_{W'}$), 93.46 ($C_{V'}$), 92.50 ($C_V$), 51.77 (OMe'), 51.69 (OMe), 38.77 ($C_{NO}$), 36.24 ($C_{LM'}$), 32 51 ($C_{LM}$), 31.12 ($C_{NO'}$), 30.52 ($C_{HexA4}$), 30.10 ($C_{HexA1}$), 29.91 ($C_{HexA2}$), 29.91 ($C_{HexA3}$) ppm.

HRMS (MALDI TOF, DCTB): *m/z* calcd for $C_{104}H_{96}O_4S_{11}^+$ [$M^+$]: 1760.4231, found: 1760.4248.

## $^{1}$H-, $^{13}$C-NMR ($CD_2Cl_2$, 500/126 MHz, 25 °C) and HR-MS spectra of compound 4

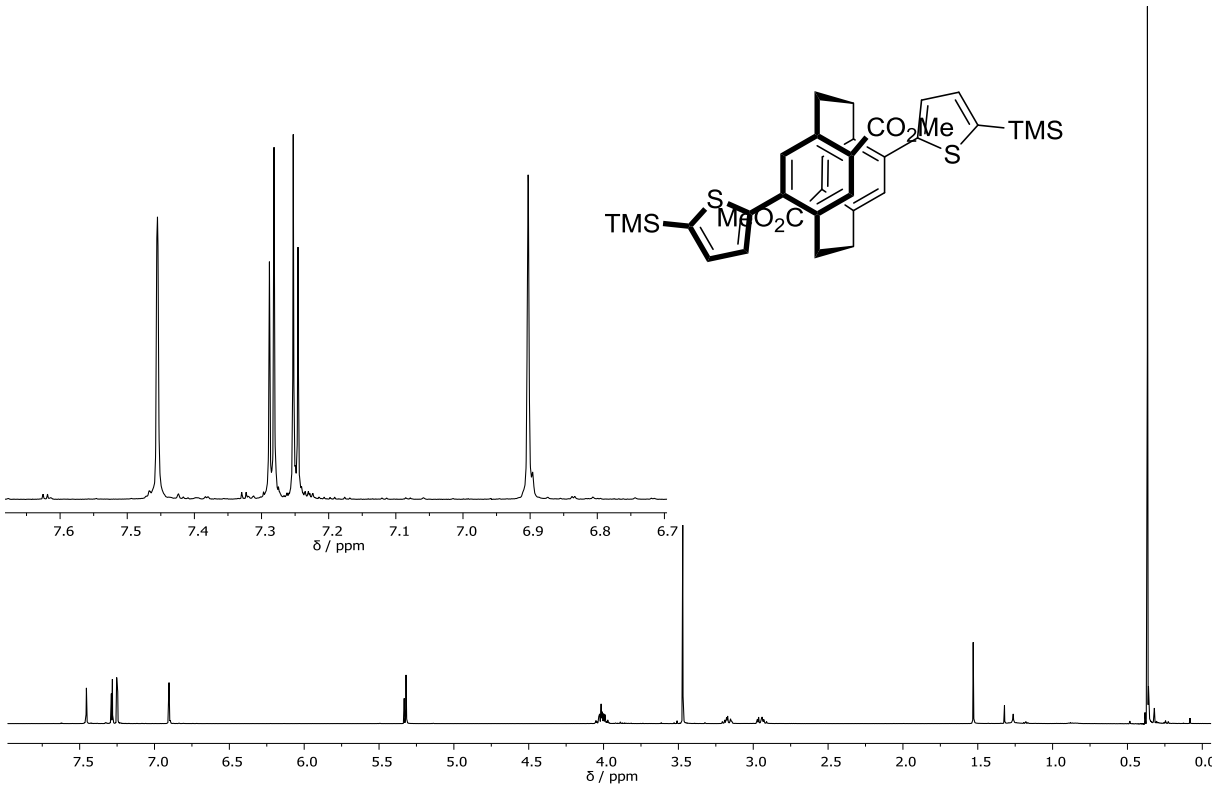


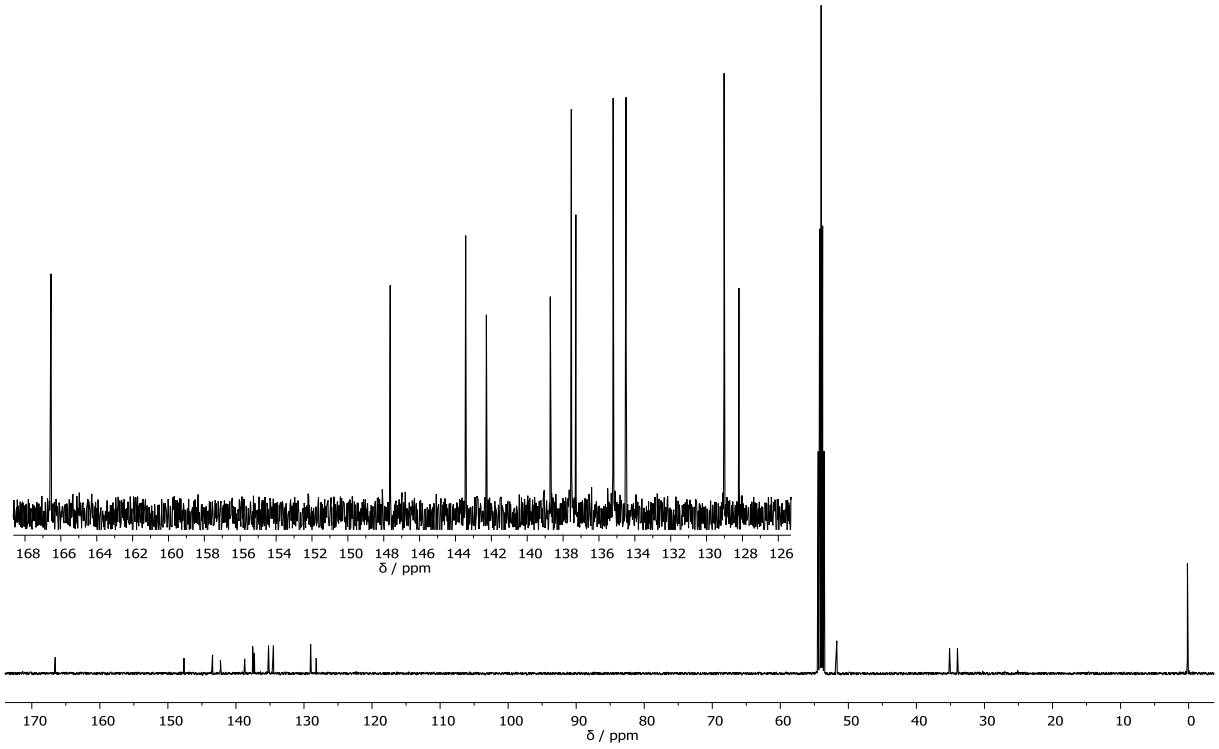

**FT13081 Kevin Weiland/Mayor - w-4 - DCM / DCTB Mix 1:10**

ETH Eidgenössische Technische Hochschule Zürich Swiss Federal Institute of Technology Zurich

**Acquisition Parameter**

| | | | | | |
|---|---|---|---|---|---|
| Method: | MALDI_MS_POS_300-2600_2M_16AvScans | | | Acquisition Date: | 08.05.2018 14:07:53 |
| File Name: | D:\ETH\Data\FT130xx\FT13081_0_A7_000001.d | | | Operator: | Louis Bertschi |
| Source | Dual (MALDI/ESI) | Polarity | Positive | Nebulizer Gas | 1.3 bar |
| Broadband Low Mass | 303.1 m/z | n/a | n/a | Drying Gas Flow Rate | 3.7 L/min |
| Broadband High Mass | 2600.0 m/z | Laser Power | 19.0 lp | Capillary | 4500.0 V |
| No. of Cell Fills | 1 | n/a | n/a | Drying Gas | 200.0 °C |
| Apodization | Full-Sine | Time of Flight to Detector | 0.001 sec | Temperature | |

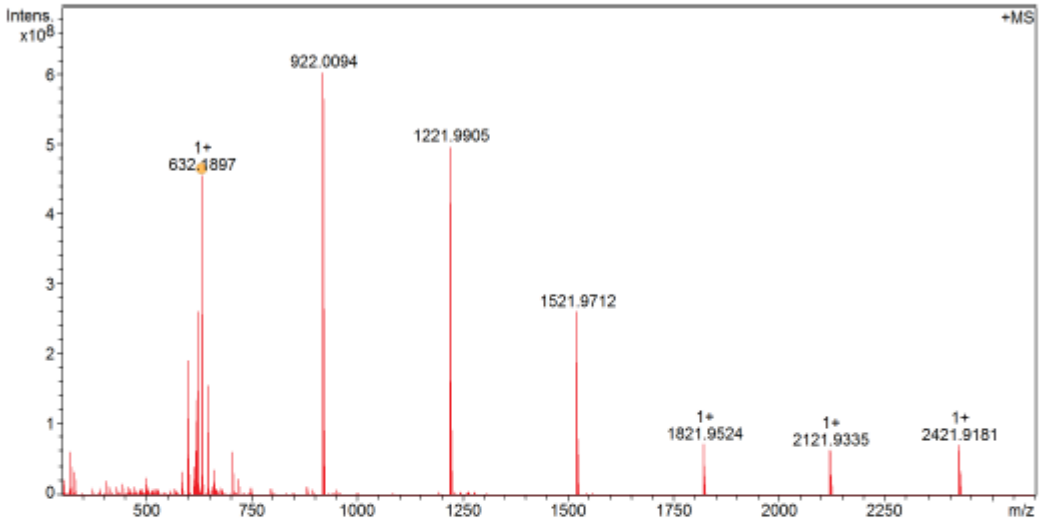


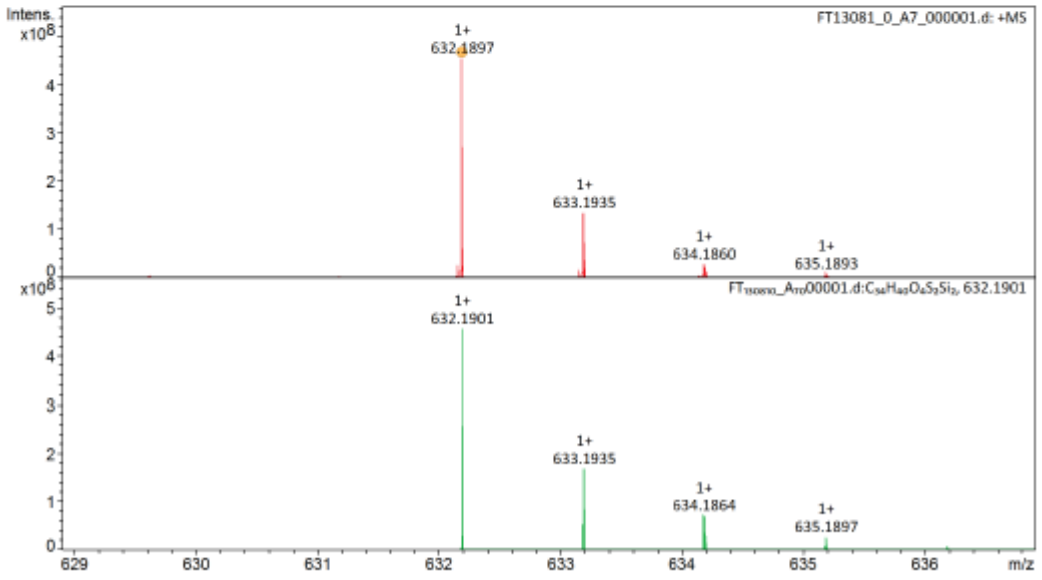

**FT13081 Kevin Weiland/Mayor - w-4 - DCM / DCTB Mix 1:10**

ETH Eidgenössische Technische Hochschule Zürich Swiss Federal Institute of Technology Zurich

**Evaluation Spectra / Validation Formula:**

| # | Ion Formula | Adduct | m/z | z | Meas. m/z | mSigma | N-Rule | err [mDa] | err [ppm] |
|---|---|---|---|---|---|---|---|---|---|
| 1 | C34H40O4S2Si2 | M | 632.1901 | 1+ | 632.1897 | 42.9 | ok | 0.4 | 0.6 |

**Calibration Info:**

Date: 08.05.2018 15:34:27
Polarity: Positive
Calibration spectrum: +MS: Scan
Reference mass list: MALDI: DCTB Matrix + HP-Mix (pos)
Calibration mode: Quadratic

| Reference m/z | Resulting m/z | Intensity | Error [ppm] |
|---|---|---|---|
| 118.0863 | | | |
| 250.1464 | | | |
| 251.1543 | | | |
| 273.1362 | | | |
| 322.0481 | | | |
| 332.2009 | 332.2009 | 34276692 | -0.017 |
| 500.2934 | 500.2935 | 25763454 | 0.116 |
| 501.3013 | | | |
| 523.2832 | 523.2833 | 8861961 | 0.076 |
| 622.0290 | 622.0288 | 261421152 | -0.248 |
| 750.4404 | 750.4405 | 10574809 | 0.031 |
| 751.4483 | | | |
| 773.4302 | | | |
| 922.0098 | 922.0094 | 604184960 | -0.478 |
| 1000.5874 | 1000.5878 | 1885966 | 0.325 |
| 1001.5953 | 1001.5956 | 2614065 | 0.361 |
| 1023.5772 | | | |
| 1221.9906 | 1221.9905 | 498322880 | -0.122 |
| 1521.9715 | 1521.9712 | 260994960 | -0.203 |
| 1821.9523 | 1821.9524 | 71425296 | 0.055 |
| 2121.9332 | 2121.9335 | 62194716 | 0.145 |
| 2421.9140 | | | |
| 2721.8948 | | | |

Standard deviation: 0.270

**Mass List:**

| # | m/z | Res. | S/N | I % | FWHM |
|---|---|---|---|---|---|
| 1 | 323.1937 | 621625 | 2361.1 | 9.8 | 0.0005 |
| 2 | 332.2009 | 590275 | 1370.6 | 5.7 | 0.0006 |
| 3 | 500.2935 | 383685 | 890.2 | 4.3 | 0.0013 |
| 4 | 586.1483 | 328000 | 1074.6 | 5.6 | 0.0018 |
| 5 | 600.1638 | 329331 | 5928.9 | 31.6 | 0.0018 |
| 6 | 601.1673 | 298541 | 1690.7 | 9.0 | 0.0020 |
| 7 | 601.1718 | 311638 | 1422.7 | 7.6 | 0.0019 |
| 8 | 614.1796 | 306285 | 1245.9 | 6.7 | 0.0020 |
| 9 | 618.1745 | 310981 | 1870.8 | 10.1 | 0.0020 |
| 10 | 619.1779 | 300049 | 598.4 | 3.2 | 0.0021 |
| 11 | 622.0267 | 403545 | 1475.0 | 8.0 | 0.0015 |
| 12 | 622.0288 | 327151 | 7947.6 | 43.3 | 0.0019 |
| 13 | 623.0324 | 310658 | 793.7 | 4.3 | 0.0020 |
| 14 | 632.1540 | 324321 | 809.7 | 4.4 | 0.0019 |
| 15 | 632.1897 | 318867 | 13867.5 | 75.5 | 0.0020 |
| 16 | 633.1896 | 271941 | 765.9 | 4.2 | 0.0023 |
| 17 | 633.1912 | 669346 | 784.4 | 4.3 | 0.0009 |
| 18 | 633.1935 | 322839 | 4042.6 | 22.3 | 0.0020 |
| 19 | 633.1981 | 329983 | 1113.3 | 6.1 | 0.0019 |
| 20 | 634.1860 | 196854 | 822.7 | 4.5 | 0.0032 |
| 21 | 634.1970 | 287851 | 638.8 | 3.5 | 0.0022 |
| 22 | 646.2058 | 325127 | 4673.9 | 26.0 | 0.0020 |
| 23 | 647.2093 | 311585 | 1607.5 | 9.0 | 0.0021 |
| 24 | 647.2139 | 316985 | 649.5 | 3.6 | 0.0020 |
| 25 | 660.2216 | 308348 | 1078.5 | 6.1 | 0.0021 |
| 26 | 705.2376 | 284253 | 1708.2 | 9.8 | 0.0025 |
| 27 | 706.2410 | 273056 | 652.6 | 3.8 | 0.0026 |
| 28 | 719.2532 | 267449 | 665.2 | 3.8 | 0.0027 |
| 29 | 922.0094 | 219005 | 16096.9 | 100.0 | 0.0042 |
| 30 | 923.0131 | 210414 | 2536.5 | 16.0 | 0.0044 |
| 31 | 1221.9905 | 160725 | 11113.5 | 82.5 | 0.0076 |
| 32 | 1222.9943 | 159762 | 2512.3 | 18.7 | 0.0077 |
| 33 | 1521.9712 | 126686 | 5368.0 | 43.2 | 0.0120 |
| 34 | 1522.9748 | 126448 | 1610.0 | 13.0 | 0.0120 |
| 35 | 1821.9524 | 104972 | 1314.7 | 11.8 | 0.0174 |
| 36 | 1822.9558 | 104752 | 518.4 | 4.7 | 0.0174 |
| 37 | 2121.9335 | 89685 | 1023.2 | 10.3 | 0.0237 |
| 38 | 2122.9368 | 89617 | 471.4 | 4.8 | 0.0237 |
| 39 | 2421.9181 | 78551 | 1106.4 | 11.5 | 0.0308 |
| 40 | 2422.9213 | 77534 | 552.3 | 5.8 | 0.0312 |

| # | m/z | Res. | S/N | I % | FWHM |
|---|---|---|---|---|---|
| 1 | 632.1901 | 318868 | | 100.0 | 0.0020 |
| 2 | 633.1897 | 319372 | | 11.7 | 0.0020 |
| 3 | 633.1935 | 319374 | | 36.9 | 0.0020 |
| 4 | 633.1964 | 319375 | | 0.5 | 0.0020 |
| 5 | 634.1864 | 319874 | | 15.7 | 0.0020 |
| 6 | 634.1892 | 319876 | | 0.4 | 0.0020 |
| 7 | 634.1932 | 319878 | | 5.2 | 0.0020 |
| 8 | 634.1968 | 319880 | | 6.7 | 0.0020 |
| 9 | 634.1997 | 319881 | | 0.2 | 0.0020 |
| 10 | 635.1858 | 320379 | | 1.4 | 0.0020 |
| 11 | 635.1897 | 320381 | | 5.8 | 0.0020 |
| 12 | 635.1930 | 320382 | | 0.3 | 0.0020 |
| 13 | 635.1967 | 320384 | | 1.1 | 0.0020 |
| 14 | 635.2002 | 320386 | | 0.8 | 0.0020 |
| 15 | 636.1826 | 320881 | | 0.9 | 0.0020 |

**FT13081 Kevin Weiland/Mayor - w-4 - DCM / DCTB Mix 1:10**

ETH
Eidgenössische Technische Hochschule Zürich
Swiss Federal Institute of Technology Zurich

| # | m/z | Res. | S/N | I % | FWHM |
|---|---|---|---|---|---|
| 16 | 636.1893 | 320885 | | 0.6 | 0.0020 |
| 17 | 636.1930 | 320887 | | 1.1 | 0.0020 |
| 18 | 636.2002 | 320890 | | 0.1 | 0.0020 |
| 19 | 637.1860 | 321387 | | 0.3 | 0.0020 |
| 20 | 637.1927 | 321391 | | 0.1 | 0.0020 |
| 21 | 637.1962 | 321393 | | 0.1 | 0.0020 |

## $^1$H-NMR ($CD_2Cl_2$, 500 MHz, 25 °C) and HR-MS spectra of compound 5

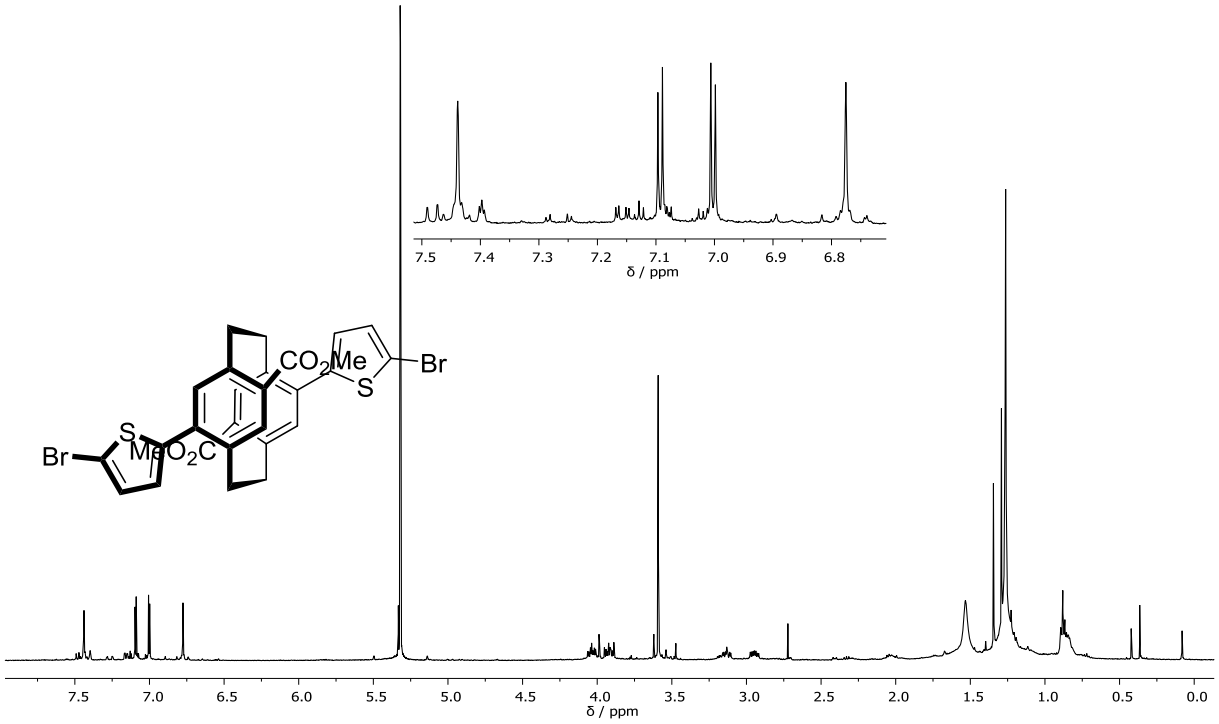

**FT13082 Kevin Weiland/Mayor - w-5 - DCM / DCTB Mix 1:10**

ETH Eidgenössische Technische Hochschule Zürich Swiss Federal Institute of Technology Zurich

**Acquisition Parameter**

| | | | | | |
|---|---|---|---|---|---|
| Method: | MALDI_MS_POS_300-2600_2M_16AvScans | | | Acquisition Date: | 08.05.2018 14:09:49 |
| File Name: | D:\ETH\Data\FT130xx\FT13082_0_A9_000001.d | | | Operator: | Louis Bertschi |
| Source | Dual (MALDI/ESI) | Polarity | Positive | Nebulizer Gas | 1.3 bar |
| Broadband Low Mass | 303.1 m/z | n/a | n/a | Drying Gas Flow Rate | 3.7 L/min |
| Broadband High Mass | 2600.0 m/z | Laser Power | 23.2 lp | Capillary | 4000.0 V |
| No. of Cell Fills | 1 | n/a | n/a | Drying Gas | 200.0 °C |
| Apodization | Full-Sine | Time of Flight to Detector | 0.001 sec | Temperature | |

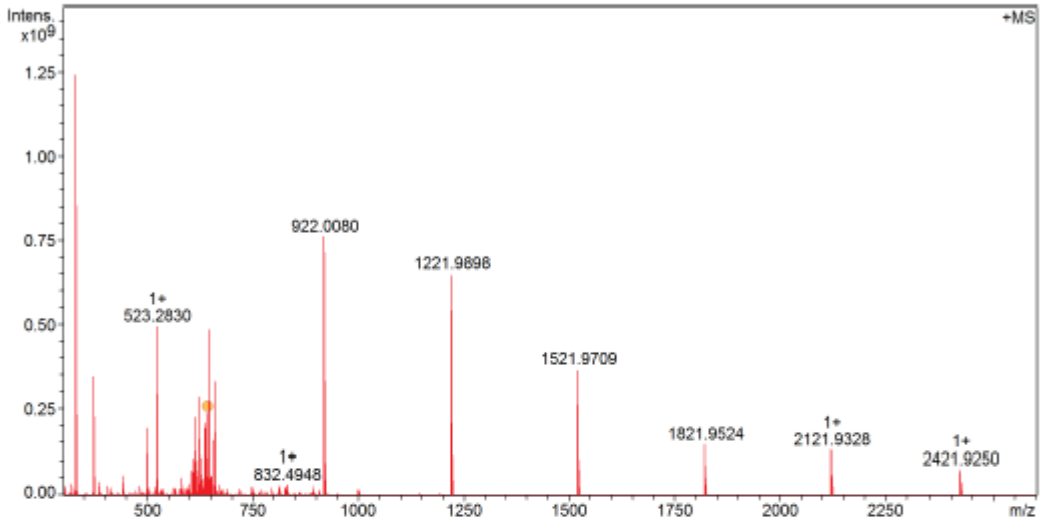


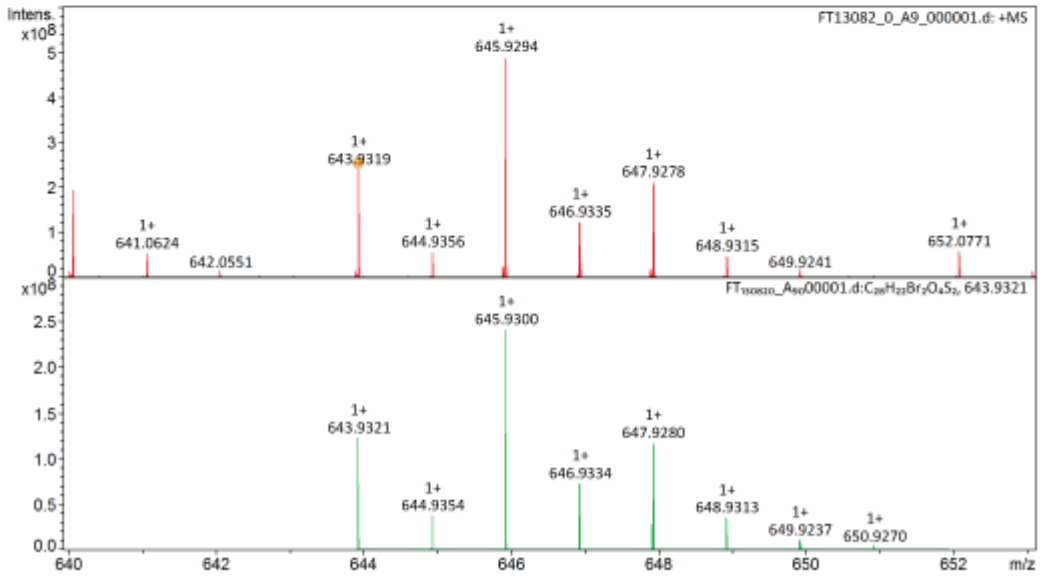

**FT13082 Kevin Weiland/Mayor - w-5 - DCM / DCTB Mix 1:10**

ETH Eidgenössische Technische Hochschule Zürich Swiss Federal Institute of Technology Zurich

**Evaluation Spectra / Validation Formula:**

| # | Ion Formula | Adduct | m/z | z | Meas. m/z | mSigma | N-Rule | err [mDa] | err [ppm] |
|---|---|---|---|---|---|---|---|---|---|
| 1 | C28H22Br2O4S2 | M | 643.9321 | 1+ | 643.9319 | 38.4 | ok | 0.1 | 0.2 |

**Calibration Info:**

Date: 08.05.2018 15:36:04
Polarity: Positive
Calibration spectrum: +MS: Scan
Reference mass list: MALDI: DCTB Matrix + HP-Mix (pos)
Calibration mode: Quadratic

| Reference m/z | Resulting m/z | Intensity | Error [ppm] |
|---|---|---|---|
| 118.0863 | | | |
| 250.1464 | | | |
| 251.1543 | | | |
| 273.1362 | | | |
| 322.0481 | | | |
| 332.2009 | 332.2009 | 1244211584 | 0.039 |
| 500.2934 | 500.2935 | 194179936 | 0.145 |
| 501.3013 | | | |
| 523.2832 | 523.2830 | 498740288 | -0.480 |
| 622.0290 | 622.0290 | 285560480 | -0.008 |
| 750.4404 | 750.4405 | 25839934 | 0.023 |
| 751.4483 | | | |
| 773.4302 | 773.4305 | 9226751 | 0.380 |
| 922.0098 | | | |
| 1000.5874 | 1000.5879 | 5495362 | 0.481 |
| 1001.5953 | 1001.5954 | 11088476 | 0.135 |
| 1023.5772 | 1023.5774 | 1079760 | 0.160 |
| 1221.9906 | 1221.9898 | 654074048 | -0.692 |
| 1521.9715 | 1521.9709 | 370540128 | -0.364 |
| 1821.9523 | 1821.9524 | 147367008 | 0.063 |
| 2121.9332 | | | |
| 2421.9140 | | | |
| 2721.8948 | | | |

Standard deviation: 0.387

**Mass List:**

| # | m/z | Res. | S/N | I % | FWHM |
|---|---|---|---|---|---|
| 1 | 332.2003 | 1275813 | 8116.7 | 16.6 | 0.0003 |
| 2 | 332.2009 | 632762 | 48780.5 | 100.0 | 0.0005 |
| 3 | 333.2045 | 598375 | 10617.8 | 21.8 | 0.0006 |
| 4 | 374.2116 | 535770 | 13758.8 | 28.2 | 0.0007 |
| 5 | 375.2152 | 524403 | 2715.9 | 5.6 | 0.0007 |
| 6 | 444.2899 | 443819 | 2038.2 | 4.7 | 0.0010 |
| 7 | 500.2935 | 394165 | 6181.8 | 15.6 | 0.0013 |
| 8 | 501.2970 | 385549 | 1942.0 | 4.9 | 0.0013 |
| 9 | 501.3014 | 388747 | 1961.8 | 5.0 | 0.0013 |
| 10 | 523.2830 | 377594 | 15347.8 | 40.1 | 0.0014 |
| 11 | 524.2866 | 374757 | 5080.8 | 13.3 | 0.0014 |
| 12 | 606.0350 | 324424 | 1883.9 | 5.9 | 0.0019 |
| 13 | 608.0331 | 326429 | 1804.0 | 5.6 | 0.0019 |
| 14 | 611.9059 | 321139 | 2720.7 | 8.7 | 0.0019 |
| 15 | 613.9038 | 321401 | 5699.9 | 18.2 | 0.0019 |
| 16 | 614.9116 | 317951 | 2160.7 | 6.9 | 0.0019 |
| 17 | 615.9019 | 323158 | 2489.4 | 7.9 | 0.0019 |
| 18 | 622.0290 | 310050 | 7040.8 | 23.0 | 0.0020 |
| 19 | 627.9196 | 311890 | 1898.7 | 6.2 | 0.0020 |
| 20 | 628.6140 | 309612 | 2769.6 | 9.0 | 0.0020 |
| 21 | 638.0609 | 305712 | 5033.8 | 16.8 | 0.0021 |
| 22 | 640.0590 | 309375 | 4733.0 | 15.8 | 0.0021 |
| 23 | 643.9319 | 300557 | 5817.1 | 19.4 | 0.0021 |
| 24 | 645.9294 | 301836 | 11566.3 | 39.4 | 0.0021 |
| 25 | 646.9335 | 301987 | 2906.9 | 9.9 | 0.0021 |
| 26 | 647.9278 | 309204 | 5012.2 | 17.1 | 0.0021 |
| 27 | 652.0771 | 303088 | 1381.9 | 4.7 | 0.0022 |
| 28 | 657.9478 | 301394 | 3673.3 | 12.8 | 0.0022 |
| 29 | 659.9451 | 297029 | 7716.1 | 26.9 | 0.0022 |
| 30 | 660.9491 | 305117 | 1792.8 | 6.3 | 0.0022 |
| 31 | 661.9436 | 314233 | 2951.5 | 10.3 | 0.0021 |
| 32 | 922.0080 | 214792 | 17675.4 | 61.2 | 0.0043 |
| 33 | 923.0125 | 216006 | 2367.7 | 8.2 | 0.0043 |
| 34 | 1221.9898 | 160033 | 13628.7 | 52.6 | 0.0076 |
| 35 | 1222.9944 | 163720 | 2917.9 | 11.3 | 0.0075 |
| 36 | 1521.9709 | 129382 | 7314.8 | 29.8 | 0.0118 |
| 37 | 1522.9747 | 129910 | 2053.4 | 8.4 | 0.0117 |
| 38 | 1821.9524 | 106122 | 2651.6 | 11.8 | 0.0172 |
| 39 | 2121.9328 | 90998 | 2148.5 | 10.5 | 0.0233 |
| 40 | 2421.9250 | 70018 | 1212.9 | 6.1 | 0.0346 |

| # | m/z | Res. | S/N | I % | FWHM |
|---|---|---|---|---|---|
| 1 | 643.9321 | 300557 | | 51.4 | 0.0021 |
| 2 | 644.9315 | 301024 | | 0.8 | 0.0021 |
| 3 | 644.9354 | 301025 | | 15.6 | 0.0021 |
| 4 | 644.9384 | 301027 | | 0.1 | 0.0021 |
| 5 | 645.9279 | 301489 | | 4.6 | 0.0021 |
| 6 | 645.9300 | 301490 | | 100.0 | 0.0021 |
| 7 | 645.9358 | 301492 | | 0.7 | 0.0021 |
| 8 | 645.9388 | 301494 | | 2.3 | 0.0021 |
| 9 | 646.9303 | 301956 | | 3.0 | 0.0021 |
| 10 | 646.9334 | 301958 | | 30.4 | 0.0021 |
| 11 | 646.9363 | 301959 | | 0.3 | 0.0021 |
| 12 | 646.9393 | 301961 | | 0.2 | 0.0021 |
| 13 | 646.9422 | 301962 | | 0.2 | 0.0021 |
| 14 | 647.9237 | 302420 | | 0.1 | 0.0021 |
| 15 | 647.9258 | 302421 | | 8.9 | 0.0021 |

**FT13082 Kevin Weiland/Mayor - w-5 - DCM / DCTB Mix 1:10**

ETH
Eidgenössische Technische Hochschule Zürich
Swiss Federal Institute of Technology Zurich

| # | m/z | Res. | S/N | I % | FWHM |
|---|---|---|---|---|---|
| 16 | 647.9280 | 302422 | | 48.6 | 0.0021 |
| 17 | 647.9338 | 151212 | | 1.6 | 0.0043 |
| 18 | 647.9367 | 302426 | | 4.5 | 0.0021 |
| 19 | 648.9288 | 302889 | | 3.5 | 0.0021 |
| 20 | 648.9313 | 302890 | | 14.8 | 0.0021 |
| 21 | 648.9343 | 302892 | | 0.1 | 0.0021 |
| 22 | 648.9373 | 302893 | | 0.3 | 0.0021 |
| 23 | 648.9401 | 302895 | | 0.4 | 0.0021 |
| 24 | 649.9237 | 303354 | | 4.6 | 0.0021 |
| 25 | 649.9319 | 151679 | | 1.1 | 0.0043 |
| 26 | 649.9347 | 303359 | | 2.2 | 0.0021 |
| 27 | 650.9270 | 303822 | | 1.4 | 0.0021 |
| 28 | 650.9357 | 303826 | | 0.2 | 0.0021 |
| 29 | 650.9381 | 303827 | | 0.2 | 0.0021 |
| 30 | 651.9305 | 304290 | | 0.2 | 0.0021 |

## $^{1}$H-, $^{13}$C-NMR ($CD_2Cl_2$, 400/101 MHz, 25 °C) and HR-MS spectra of compound 6

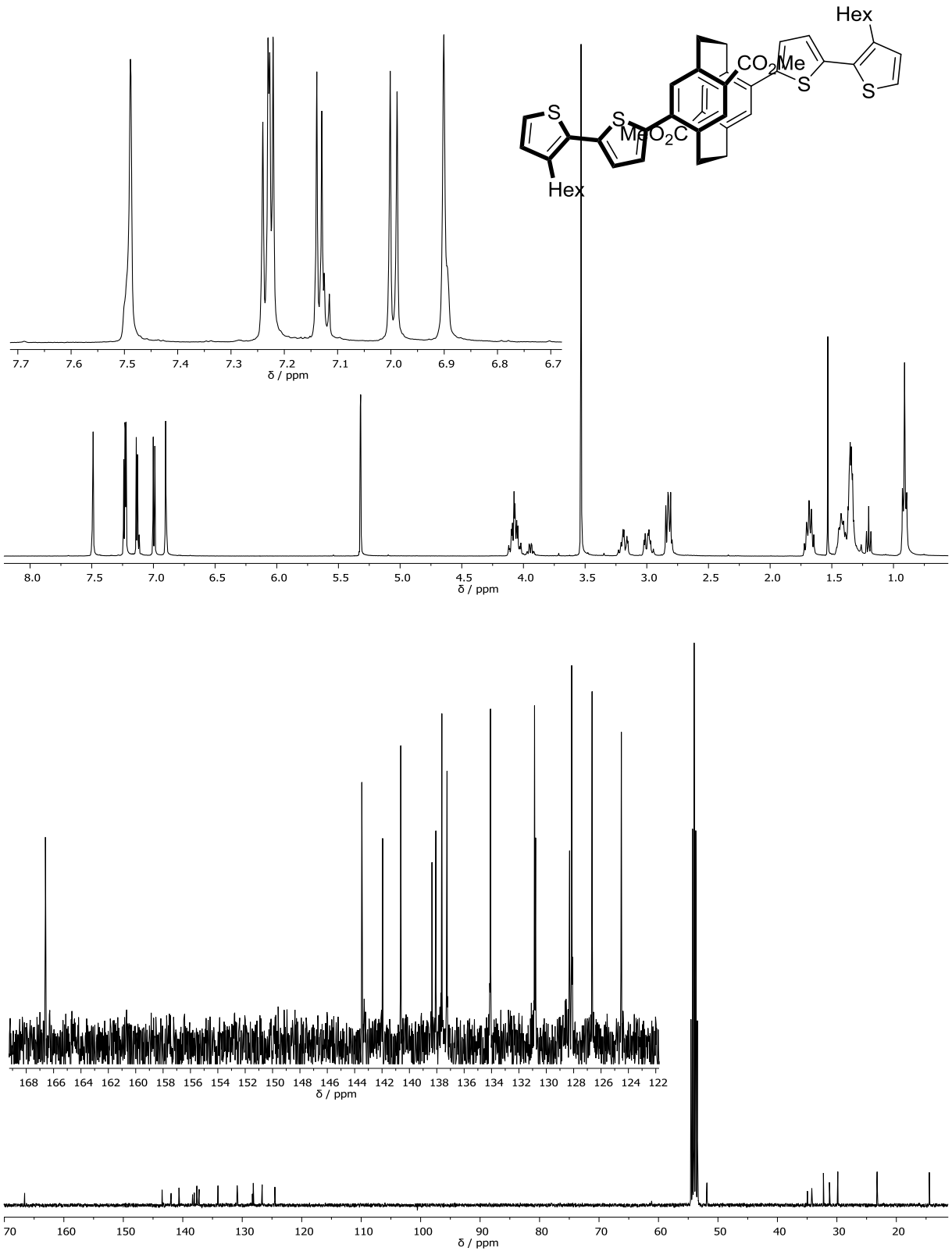

**FT13084 Kevin Weiland/Mayor - w-6 - DCM / DCTB Mix 1:10**

ETH Eidgenössische Technische Hochschule Zürich Swiss Federal Institute of Technology Zurich

**Acquisition Parameter**

| | | | | | |
|---|---|---|---|---|---|
| Method: | MALDI_MS_POS_300-2600_2M_16AvScans | | | Acquisition Date: | 08.05.2018 14:12:21 |
| File Name: | D:\ETH\Data\FT130xx\FT13084_0_A13_000001.d | | | Operator: | Louis Bertschi |
| Source | Dual (MALDI/ESI) | Polarity | Positive | Nebulizer Gas | 1.3 bar |
| Broadband Low Mass | 303.1 m/z | n/a | n/a | Drying Gas Flow Rate | 3.7 L/min |
| Broadband High Mass | 2600.0 m/z | Laser Power | 17.6 lp | Capillary | 4000.0 V |
| No. of Cell Fills | 1 | n/a | n/a | Drying Gas | 200.0 °C |
| Apodization | Full-Sine | Time of Flight to Detector | 0.001 sec | Temperature | |

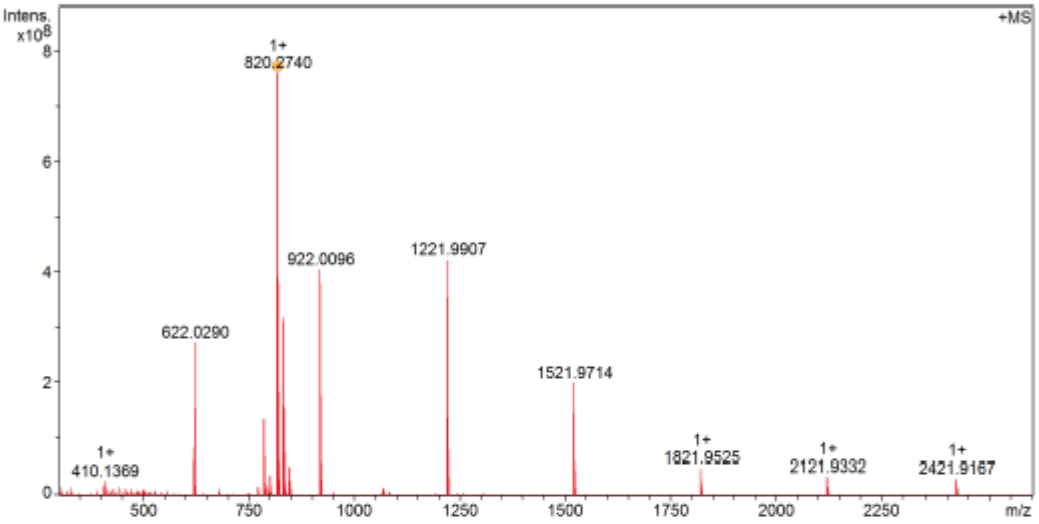


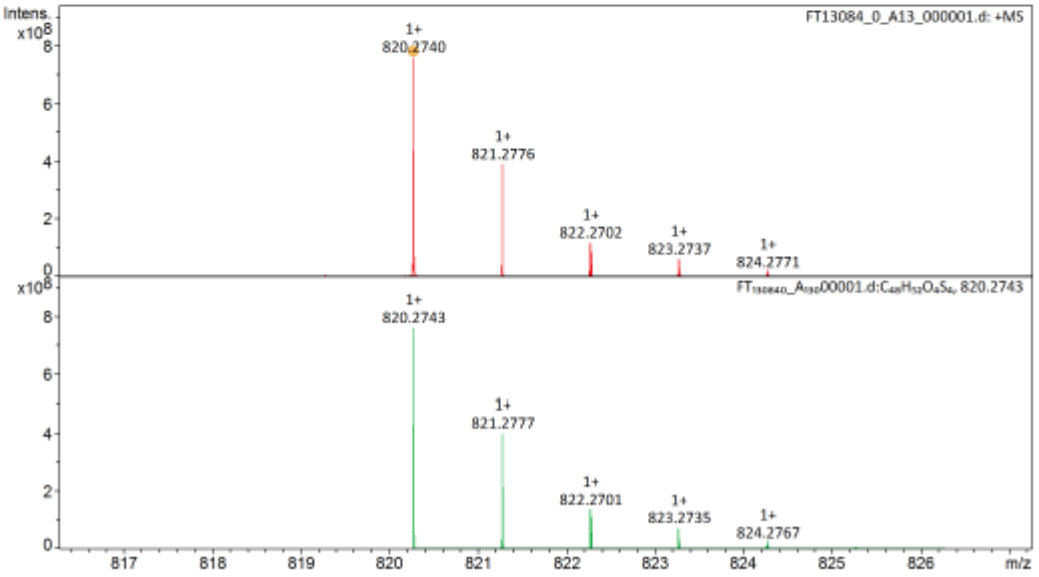


Bruker Daltonics solariX ETH - MS-Service LOC - D-CHAB Page 1 of 3

**FT13084 Kevin Weiland/Mayor - w-6 - DCM / DCTB Mix 1:10**

ETH Eidgenössische Technische Hochschule Zürich Swiss Federal Institute of Technology Zurich

**Evaluation Spectra / Validation Formula:**

| # | Ion Formula | Adduct | m/z | z | Meas. m/z | mSigma | N-Rule | err [mDa] | err [ppm] |
|---|---|---|---|---|---|---|---|---|---|
| 1 | C48H52O4S4 | M | 820.2743 | 1+ | 820.2740 | 16.9 | ok | 0.3 | 0.4 |

**Calibration Info:**

Date: 08.05.2018 15:38:12
Polarity: Positive
Calibration spectrum: +MS: Scan
Reference mass list: MALDI: DCTB Matrix + HP-Mix (pos)
Calibration mode: Quadratic

| Reference m/z | Resulting m/z | Intensity | Error [ppm] |
|---|---|---|---|
| 118.0863 | | | |
| 250.1464 | | | |
| 251.1543 | | | |
| 273.1362 | | | |
| 322.0481 | | | |
| 332.2009 | 332.2009 | 9937723 | -0.004 |
| 500.2934 | | | |
| 501.3013 | | | |
| 523.2832 | | | |
| 622.0290 | 622.0290 | 273723392 | 0.071 |
| 750.4404 | | | |
| 751.4483 | | | |
| 773.4302 | | | |
| 922.0098 | 922.0096 | 405447712 | -0.173 |
| 1000.5874 | | | |
| 1001.5953 | | | |
| 1023.5772 | | | |
| 1221.9906 | 1221.9907 | 423349664 | 0.081 |
| 1521.9715 | 1521.9714 | 200865920 | -0.059 |
| 1821.9523 | 1821.9525 | 48066432 | 0.077 |
| 2121.9332 | 2121.9332 | 32997964 | 0.038 |
| 2421.9140 | | | |
| 2721.8948 | | | |

Standard deviation: 0.119

**Mass List:**

| # | m/z | Res. | S/N | I % | FWHM |
|---|---|---|---|---|---|
| 1 | 410.1369 | 485343 | 1003.7 | 3.4 | 0.0008 |
| 2 | 445.4041 | 417491 | 571.6 | 2.0 | 0.0011 |
| 3 | 459.4197 | 429288 | 455.0 | 1.6 | 0.0011 |
| 4 | 622.0269 | 447416 | 1586.2 | 6.5 | 0.0014 |
| 5 | 622.0290 | 321979 | 8796.0 | 36.0 | 0.0019 |
| 6 | 623.0325 | 317679 | 983.2 | 4.0 | 0.0020 |
| 7 | 774.2327 | 244552 | 441.0 | 2.1 | 0.0032 |
| 8 | 788.2482 | 246320 | 3723.5 | 17.7 | 0.0032 |
| 9 | 789.2515 | 239522 | 1764.9 | 8.4 | 0.0033 |
| 10 | 790.2441 | 240307 | 637.2 | 3.0 | 0.0033 |
| 11 | 790.2550 | 234033 | 418.4 | 2.0 | 0.0034 |
| 12 | 802.2639 | 242055 | 978.3 | 4.7 | 0.0033 |
| 13 | 803.2672 | 235257 | 503.4 | 2.4 | 0.0034 |
| 14 | 820.2740 | 240210 | 20330.9 | 100.0 | 0.0034 |
| 15 | 821.2776 | 244492 | 10435.3 | 51.3 | 0.0034 |
| 16 | 822.2702 | 231972 | 3143.0 | 15.5 | 0.0035 |
| 17 | 822.2746 | 178544 | 457.2 | 2.3 | 0.0046 |
| 18 | 822.2812 | 238437 | 2258.9 | 11.1 | 0.0034 |
| 19 | 823.2737 | 231605 | 1608.1 | 7.9 | 0.0036 |
| 20 | 823.2850 | 232756 | 331.3 | 1.6 | 0.0035 |
| 21 | 824.2771 | 231709 | 391.2 | 1.9 | 0.0036 |
| 22 | 834.2899 | 236027 | 8494.7 | 41.9 | 0.0035 |
| 23 | 835.2934 | 232482 | 4200.9 | 20.7 | 0.0036 |
| 24 | 836.2861 | 218520 | 1222.0 | 6.0 | 0.0038 |
| 25 | 836.2971 | 224025 | 933.9 | 4.6 | 0.0037 |
| 26 | 837.2893 | 213897 | 623.6 | 3.1 | 0.0039 |
| 27 | 848.3059 | 219038 | 1366.3 | 6.8 | 0.0039 |
| 28 | 849.3093 | 220084 | 696.2 | 3.4 | 0.0039 |
| 29 | 922.0096 | 224145 | 10664.4 | 53.3 | 0.0041 |
| 30 | 923.0134 | 207968 | 1639.9 | 8.2 | 0.0044 |
| 31 | 1221.9907 | 161190 | 9689.3 | 55.7 | 0.0076 |
| 32 | 1222.9945 | 160878 | 2249.2 | 12.9 | 0.0076 |
| 33 | 1521.9714 | 126014 | 4081.6 | 26.4 | 0.0121 |
| 34 | 1522.9749 | 125778 | 1246.6 | 8.1 | 0.0121 |
| 35 | 1821.9525 | 105219 | 885.8 | 6.3 | 0.0173 |
| 36 | 1822.9559 | 105508 | 350.2 | 2.5 | 0.0173 |
| 37 | 2121.9332 | 90447 | 543.8 | 4.3 | 0.0235 |
| 38 | 2122.9367 | 90292 | 260.8 | 2.1 | 0.0235 |
| 39 | 2421.9167 | 78129 | 483.5 | 4.0 | 0.0310 |
| 40 | 2422.9201 | 78162 | 243.8 | 2.0 | 0.0310 |

| # | m/z | Res. | S/N | I % | FWHM |
|---|---|---|---|---|---|
| 1 | 820.2743 | 240210 | | 100.0 | 0.0034 |
| 2 | 821.2737 | 240503 | | 3.2 | 0.0034 |
| 3 | 821.2777 | 240504 | | 52.7 | 0.0034 |
| 4 | 822.2701 | 240795 | | 17.9 | 0.0034 |
| 5 | 822.2770 | 240797 | | 1.6 | 0.0034 |
| 6 | 822.2809 | 240798 | | 14.4 | 0.0034 |
| 7 | 823.2695 | 241087 | | 0.4 | 0.0034 |
| 8 | 823.2735 | 241088 | | 9.4 | 0.0034 |
| 9 | 823.2803 | 241090 | | 0.4 | 0.0034 |
| 10 | 823.2841 | 241091 | | 2.7 | 0.0034 |
| 11 | 824.2660 | 241379 | | 1.2 | 0.0034 |
| 12 | 824.2728 | 241381 | | 0.2 | 0.0034 |
| 13 | 824.2767 | 241382 | | 2.6 | 0.0034 |
| 14 | 824.2871 | 241385 | | 0.4 | 0.0034 |
| 15 | 825.2694 | 241673 | | 0.7 | 0.0034 |

**FT13084 Kevin Weiland/Mayor - w-6 - DCM / DCTB Mix 1:10**

ETH Eidgenössische Technische Hochschule Zürich Swiss Federal Institute of Technology Zurich

| # | m/z | Res. | S/N | I % | FWHM |
|---|---|---|---|---|---|
| 16 | 825.2799 | 241676 | | 0.5 | 0.0034 |
| 17 | 826.2725 | 241967 | | 0.2 | 0.0034 |

## $^{1}$H-, $^{13}$C-NMR ($CD_2Cl_2$, 500/126 MHz, 25 °C) and HR-MS spectra of compound 7

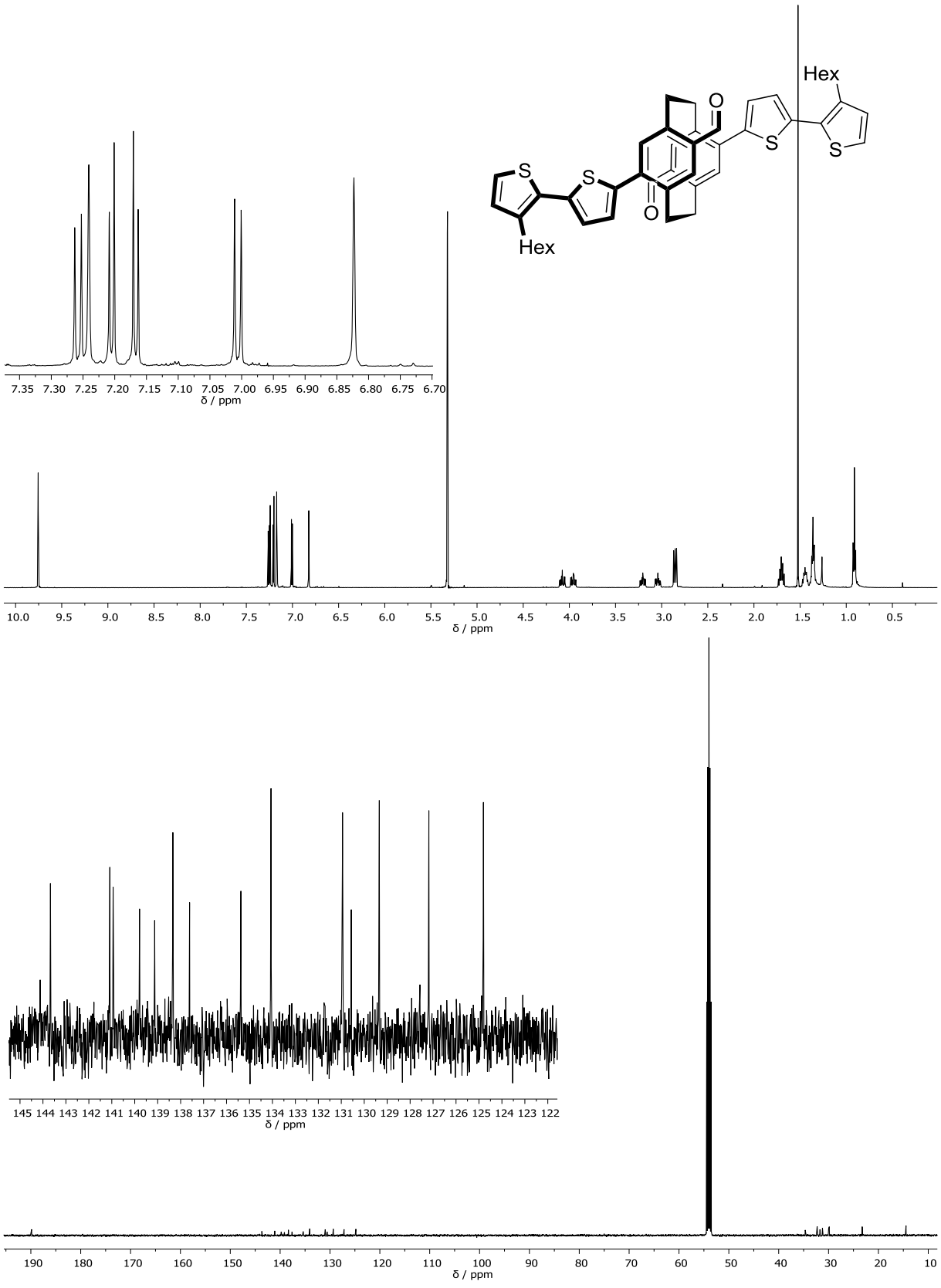

**FT13083 Kevin Weiland/Mayor - w-7 - DCM / DCTB Mix 1:10**

ETH Eidgenössische Technische Hochschule Zürich Swiss Federal Institute of Technology Zurich

**Acquisition Parameter**

| | | | | | |
|---|---|---|---|---|---|
| Method: | MALDI_MS_POS_300-2600_2M_16AvScans | | | Acquisition Date: | 08.05.2018 14:11:14 |
| File Name: | D:\ETH\Data\FT130xx\FT13083_0_A11_000001.d | | | Operator: | Louis Bertschi |
| Source | Dual (MALDI/ESI) | Polarity | Positive | Nebulizer Gas | 1.3 bar |
| Broadband Low Mass | 303.1 m/z | n/a | n/a | Drying Gas Flow Rate | 3.7 L/min |
| Broadband High Mass | 2600.0 m/z | Laser Power | 17.6 lp | Capillary | 4000.0 V |
| No. of Cell Fills | 1 | n/a | n/a | Drying Gas | 200.0 °C |
| Apodization | Full-Sine | Time of Flight to Detector | 0.001 sec | Temperature | |

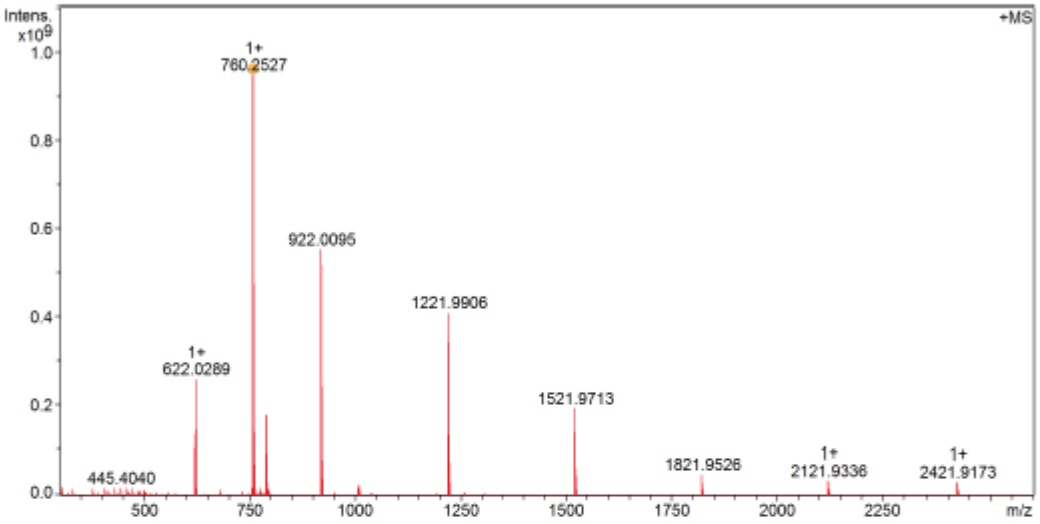


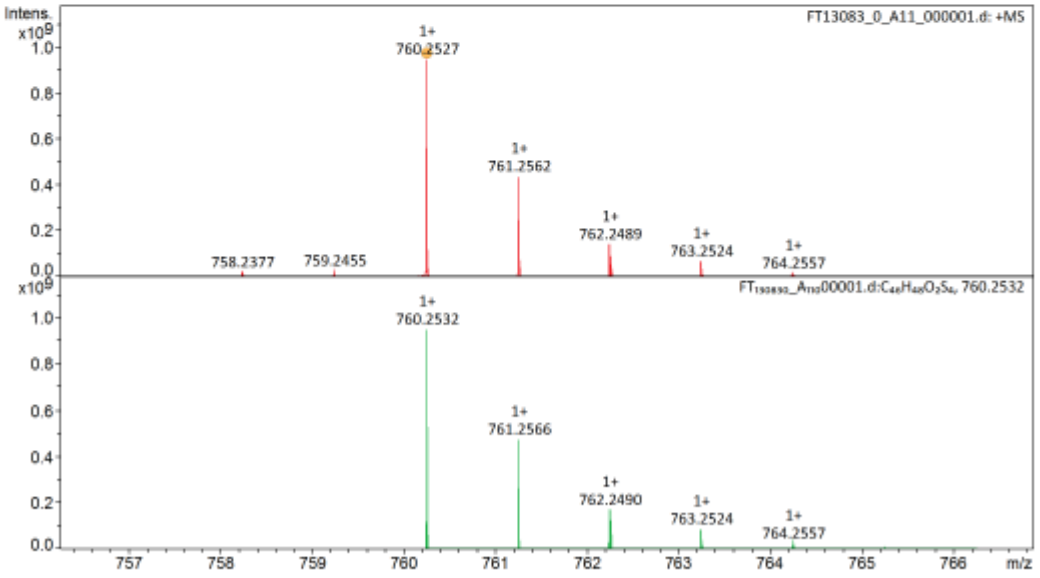

**FT13083 Kevin Weiland/Mayor - w-7 - DCM / DCTB Mix 1:10**

ETH Eidgenössische Technische Hochschule Zürich Swiss Federal Institute of Technology Zurich

**Evaluation Spectra / Validation Formula:**

| # | Ion Formula | Adduct | m/z | z | Meas. m/z | mSigma | N-Rule | err [mDa] | err [ppm] |
|---|---|---|---|---|---|---|---|---|---|
| 1 | C46H48O2S4 | M | 760.2532 | 1+ | 760.2527 | 39.5 | ok | 0.5 | 0.6 |

**Calibration Info:**

Date: 08.05.2018 15:37:19
Polarity: Positive
Calibration spectrum: +MS: Scan
Reference mass list: MALDI: DCTB Matrix + HP-Mix (pos)
Calibration mode: Quadratic

| Reference m/z | Resulting m/z | Intensity | Error [ppm] |
|---|---|---|---|
| 118.0863 | | | |
| 250.1464 | | | |
| 251.1543 | | | |
| 273.1362 | | | |
| 322.0481 | | | |
| 332.2009 | 332.2009 | 9159323 | -0.013 |
| 500.2934 | 500.2935 | 8639130 | 0.071 |
| 501.3013 | | | |
| 523.2832 | | | |
| 622.0290 | 622.0289 | 259617504 | -0.099 |
| 750.4404 | 750.4407 | 3614137 | 0.285 |
| 751.4483 | | | |
| 773.4302 | | | |
| 922.0098 | 922.0095 | 551756672 | -0.375 |
| 1000.5874 | | | |
| 1001.5953 | | | |
| 1023.5772 | | | |
| 1221.9906 | 1221.9906 | 409946464 | -0.028 |
| 1521.9715 | 1521.9713 | 193197792 | -0.112 |
| 1821.9523 | 1821.9526 | 46989968 | 0.139 |
| 2121.9332 | 2121.9336 | 32323516 | 0.217 |
| 2421.9140 | | | |
| 2721.8948 | | | |

Standard deviation: 0.237

**Mass List:**

| # | m/z | Res. | S/N | I % | FWHM |
|---|---|---|---|---|---|
| 1 | 431.3883 | 443968 | 455.6 | 1.3 | 0.0010 |
| 2 | 445.4040 | 425365 | 608.3 | 1.7 | 0.0010 |
| 3 | 459.4197 | 426506 | 478.5 | 1.4 | 0.0011 |
| 4 | 473.4353 | 406266 | 460.1 | 1.3 | 0.0012 |
| 5 | 622.0268 | 371979 | 1758.8 | 5.9 | 0.0017 |
| 6 | 622.0289 | 327393 | 8214.8 | 27.4 | 0.0019 |
| 7 | 623.0324 | 324001 | 877.6 | 2.9 | 0.0019 |
| 8 | 758.2377 | 251052 | 511.9 | 1.9 | 0.0030 |
| 9 | 759.2455 | 252093 | 746.3 | 2.7 | 0.0030 |
| 10 | 760.2527 | 255537 | 27312.0 | 100.0 | 0.0030 |
| 11 | 761.2562 | 255947 | 12613.9 | 46.2 | 0.0030 |
| 12 | 761.2611 | 263506 | 2090.2 | 7.7 | 0.0029 |
| 13 | 762.2489 | 251941 | 4021.7 | 14.7 | 0.0030 |
| 14 | 762.2598 | 244721 | 2548.6 | 9.3 | 0.0031 |
| 15 | 762.2646 | 241102 | 1006.9 | 3.7 | 0.0032 |
| 16 | 763.2524 | 245313 | 1910.1 | 7.0 | 0.0031 |
| 17 | 763.2633 | 214270 | 369.1 | 1.4 | 0.0036 |
| 18 | 764.2557 | 237681 | 421.4 | 1.5 | 0.0032 |
| 19 | 790.2562 | 198184 | 426.7 | 1.6 | 0.0040 |
| 20 | 790.2637 | 248950 | 5069.7 | 18.8 | 0.0032 |
| 21 | 791.2672 | 241007 | 2542.5 | 9.4 | 0.0033 |
| 22 | 792.2597 | 230591 | 842.3 | 3.1 | 0.0034 |
| 23 | 792.2706 | 237329 | 603.9 | 2.2 | 0.0033 |
| 24 | 793.2630 | 234767 | 420.5 | 1.6 | 0.0034 |
| 25 | 922.0095 | 217079 | 14664.5 | 58.2 | 0.0042 |
| 26 | 923.0131 | 210243 | 2256.8 | 9.1 | 0.0044 |
| 27 | 1009.3927 | 198033 | 438.2 | 1.8 | 0.0051 |
| 28 | 1010.4008 | 213228 | 589.5 | 2.5 | 0.0047 |
| 29 | 1011.4037 | 220962 | 356.6 | 1.5 | 0.0046 |
| 30 | 1221.9906 | 161125 | 9372.5 | 43.2 | 0.0076 |
| 31 | 1222.9943 | 160398 | 2155.0 | 9.9 | 0.0076 |
| 32 | 1223.9975 | 145931 | 277.4 | 1.3 | 0.0084 |
| 33 | 1521.9713 | 125584 | 3978.4 | 20.4 | 0.0121 |
| 34 | 1522.9749 | 125624 | 1255.5 | 6.4 | 0.0121 |
| 35 | 1821.9526 | 105224 | 867.5 | 5.0 | 0.0173 |
| 36 | 1822.9561 | 105673 | 318.2 | 1.8 | 0.0173 |
| 37 | 2121.9336 | 90177 | 533.0 | 3.4 | 0.0235 |
| 38 | 2122.9368 | 91096 | 239.2 | 1.5 | 0.0233 |
| 39 | 2421.9173 | 78460 | 489.9 | 3.2 | 0.0309 |
| 40 | 2422.9204 | 78081 | 245.8 | 1.6 | 0.0310 |

| # | m/z | Res. | S/N | I % | FWHM |
|---|---|---|---|---|---|
| 1 | 760.2532 | 255538 | | 100.0 | 0.0030 |
| 2 | 761.2526 | 255874 | | 3.2 | 0.0030 |
| 3 | 761.2566 | 255875 | | 50.4 | 0.0030 |
| 4 | 762.2490 | 256208 | | 17.9 | 0.0030 |
| 5 | 762.2559 | 256211 | | 1.6 | 0.0030 |
| 6 | 762.2599 | 256212 | | 12.8 | 0.0030 |
| 7 | 763.2484 | 256544 | | 0.4 | 0.0030 |
| 8 | 763.2524 | 256546 | | 9.0 | 0.0030 |
| 9 | 763.2592 | 256548 | | 0.4 | 0.0030 |
| 10 | 763.2631 | 256549 | | 2.2 | 0.0030 |
| 11 | 764.2448 | 256879 | | 1.2 | 0.0030 |
| 12 | 764.2517 | 256882 | | 0.2 | 0.0030 |
| 13 | 764.2557 | 256883 | | 2.3 | 0.0030 |
| 14 | 764.2663 | 256887 | | 0.3 | 0.0030 |
| 15 | 765.2481 | 257217 | | 0.6 | 0.0030 |

**FT13083 Kevin Weiland/Mayor - w-7 - DCM / DCTB Mix 1:10**

ETH
Eidgenössische Technische Hochschule Zürich
Swiss Federal Institute of Technology Zurich

| # | m/z | Res. | S/N | I % | FWHM |
|---|---|---|---|---|---|
| 16 | 765.2589 | 257220 | | 0.4 | 0.0030 |
| 17 | 766.2515 | 257554 | | 0.2 | 0.0030 |

## $^{1}$H-, $^{13}$C-NMR ($CD_2Cl_2$, 500/126 MHz, 25 °C) and HR-MS spectra of compound 8

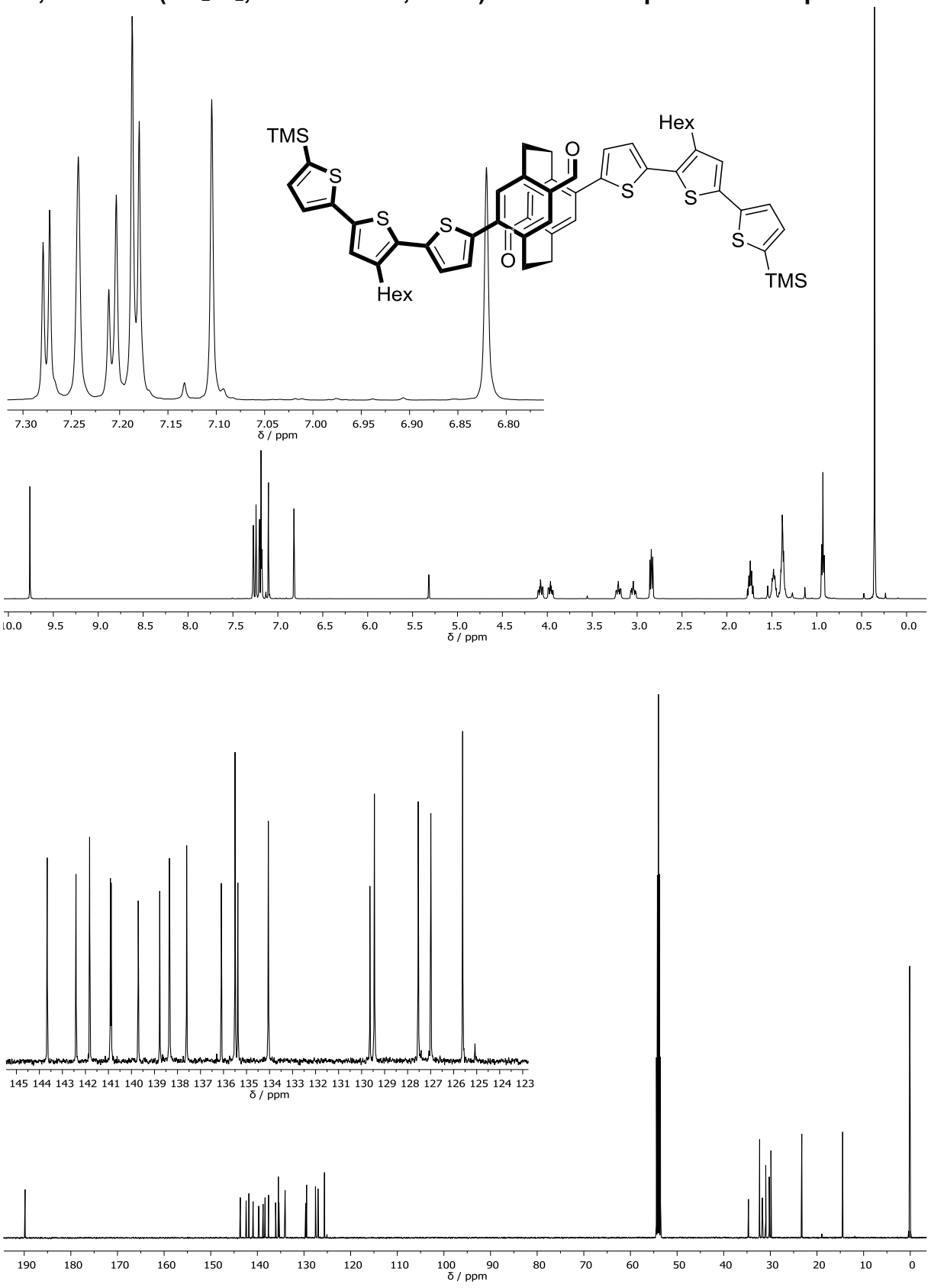

**FT13087 Kevin Weiland/Mayor - w-8 - DCM / DCTB Mix 1:10**

ETH Eidgenössische Technische Hochschule Zürich Swiss Federal Institute of Technology Zurich

**Acquisition Parameter**

| | | | | | |
|---|---|---|---|---|---|
| Method: | MALDI_MS_POS_300-2600_2M_16AvScans | | | Acquisition Date: | 08.05.2018 14:17:26 |
| File Name: | D:\ETH\Data\FT130xx\FT13087_0_A19_000001.d | | | Operator: | Louis Bertschi |
| Source | Dual (MALDI/ESI) | Polarity | Positive | Nebulizer Gas | 1.3 bar |
| Broadband Low Mass | 303.1 m/z | n/a | n/a | Drying Gas Flow Rate | 3.7 L/min |
| Broadband High Mass | 2600.0 m/z | Laser Power | 19.2 lp | Capillary | 4000.0 V |
| No. of Cell Fills | 1 | n/a | n/a | Drying Gas | 200.0 °C |
| Apodization | Full-Sine | Time of Flight to Detector | 0.001 sec | Temperature | |

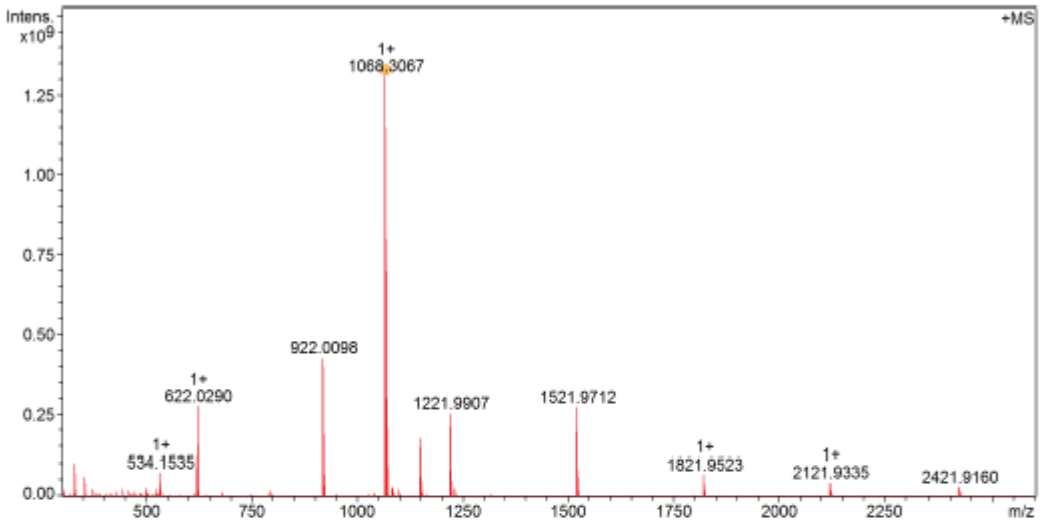


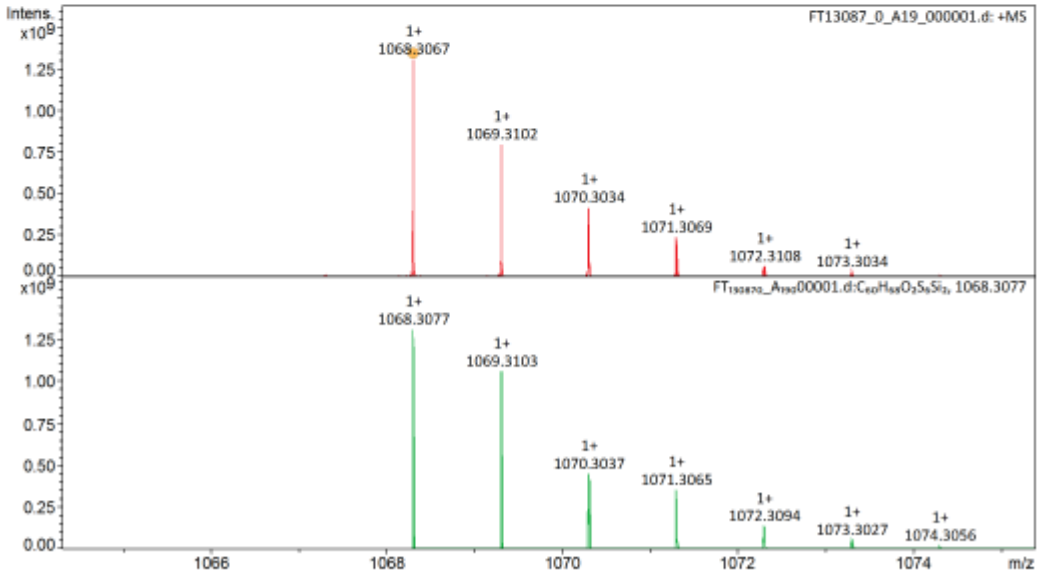

**FT13087 Kevin Weiland/Mayor - w-8 - DCM / DCTB Mix 1:10**

ETH Eidgenössische Technische Hochschule Zürich Swiss Federal Institute of Technology Zurich

**Evaluation Spectra / Validation Formula:**

| # | Ion Formula | Adduct | m/z | z | Meas. m/z | mSigma | N-Rule | err [mDa] | err [ppm] |
|---|---|---|---|---|---|---|---|---|---|
| 1 | C60H68O2S6Si2 | M | 1068.3077 | 1+ | 1068.3067 | 113.4 | ok | 0.9 | 0.9 |

**Calibration Info:**

| | |
|---|---|
| Date: | 08.05.2018 15:44:14 |
| Polarity: | Positive |
| Calibration spectrum: | +MS: Scan |
| Reference mass list: | MALDI: DCTB Matrix + HP-Mix (pos) |
| Calibration mode: | Quadratic |

| Reference m/z | Resulting m/z | Intensity | Error [ppm] |
|---|---|---|---|
| 118.0863 | | | |
| 250.1464 | | | |
| 251.1543 | | | |
| 273.1362 | | | |
| 322.0481 | | | |
| 332.2009 | | | |
| 500.2934 | | | |
| 501.3013 | | | |
| 523.2832 | | | |
| 622.0290 | 622.0290 | 277197600 | -0.008 |
| 750.4404 | | | |
| 751.4483 | | | |
| 773.4302 | | | |
| 922.0098 | 922.0098 | 428056928 | 0.043 |
| 1000.5874 | | | |
| 1001.5953 | | | |
| 1023.5772 | | | |
| 1221.9906 | 1221.9907 | 253582048 | 0.028 |
| 1521.9715 | 1521.9712 | 273841152 | -0.181 |
| 1821.9523 | 1821.9523 | 66207552 | -0.009 |
| 2121.9332 | 2121.9335 | 43442624 | 0.141 |
| 2421.9140 | | | |
| 2721.8948 | | | |

Standard deviation: 0.143

**Mass List:**

| # | m/z | Res. | S/N | I % | FWHM |
|---|---|---|---|---|---|
| 1 | 332.1993 | 414999 | 753.6 | 1.4 | 0.0008 |
| 2 | 332.2006 | 610394 | 4143.3 | 7.9 | 0.0005 |
| 3 | 333.2040 | 591322 | 808.4 | 1.5 | 0.0006 |
| 4 | 374.2113 | 537190 | 1003.5 | 1.9 | 0.0007 |
| 5 | 445.4039 | 435092 | 604.0 | 1.3 | 0.0010 |
| 6 | 500.2934 | 382764 | 973.6 | 2.1 | 0.0013 |
| 7 | 534.1535 | 382909 | 2475.3 | 5.6 | 0.0014 |
| 8 | 535.1570 | 367798 | 766.2 | 1.7 | 0.0015 |
| 9 | 622.0290 | 327025 | 8779.0 | 21.2 | 0.0019 |
| 10 | 623.0325 | 326182 | 983.3 | 2.4 | 0.0019 |
| 11 | 922.0098 | 209835 | 11287.3 | 32.7 | 0.0044 |
| 12 | 923.0134 | 207004 | 1933.5 | 5.7 | 0.0045 |
| 13 | 1068.3067 | 180485 | 28786.1 | 100.0 | 0.0059 |
| 14 | 1069.3102 | 177609 | 17538.9 | 60.9 | 0.0060 |
| 15 | 1070.3034 | 172293 | 9173.3 | 31.9 | 0.0062 |
| 16 | 1071.3069 | 183197 | 5181.3 | 18.0 | 0.0058 |
| 17 | 1071.3191 | 216167 | 789.9 | 2.8 | 0.0050 |
| 18 | 1072.2993 | 136533 | 932.2 | 3.2 | 0.0079 |
| 19 | 1072.3108 | 193228 | 1376.7 | 4.8 | 0.0055 |
| 20 | 1073.3034 | 177335 | 604.4 | 2.1 | 0.0061 |
| 21 | 1084.3030 | 180788 | 599.9 | 2.1 | 0.0060 |
| 22 | 1150.2682 | 90868 | 585.1 | 2.1 | 0.0127 |
| 23 | 1150.2959 | 178080 | 3832.5 | 13.6 | 0.0065 |
| 24 | 1151.2735 | 84527 | 451.6 | 1.6 | 0.0136 |
| 25 | 1151.2925 | 237445 | 475.1 | 1.7 | 0.0048 |
| 26 | 1151.2995 | 183303 | 2413.8 | 8.6 | 0.0063 |
| 27 | 1152.2919 | 183182 | 1204.9 | 4.3 | 0.0063 |
| 28 | 1152.3034 | 195661 | 720.6 | 2.6 | 0.0059 |
| 29 | 1153.2956 | 187249 | 798.7 | 2.8 | 0.0062 |
| 30 | 1221.9590 | 153572 | 682.2 | 2.4 | 0.0080 |
| 31 | 1221.9907 | 165662 | 5512.1 | 19.4 | 0.0074 |
| 32 | 1222.9948 | 166461 | 1246.7 | 4.4 | 0.0073 |
| 33 | 1232.2838 | 159734 | 374.6 | 1.3 | 0.0077 |
| 34 | 1521.9712 | 127613 | 5620.0 | 20.9 | 0.0119 |
| 35 | 1522.9751 | 126682 | 1669.2 | 6.2 | 0.0120 |
| 36 | 1821.9523 | 105169 | 1215.1 | 5.1 | 0.0173 |
| 37 | 1822.9557 | 105024 | 455.1 | 1.9 | 0.0174 |
| 38 | 2121.9335 | 90733 | 719.8 | 3.3 | 0.0234 |
| 39 | 2122.9368 | 91114 | 326.9 | 1.5 | 0.0233 |
| 40 | 2421.9160 | 78140 | 459.6 | 2.2 | 0.0310 |

| # | m/z | Res. | S/N | I % | FWHM |
|---|---|---|---|---|---|
| 1 | 1068.3077 | 180485 | | 100.0 | 0.0059 |
| 2 | 1069.3103 | 180654 | | 80.7 | 0.0059 |
| 3 | 1070.3037 | 180822 | | 34.4 | 0.0059 |
| 4 | 1070.3132 | 180824 | | 31.5 | 0.0059 |
| 5 | 1071.3065 | 180991 | | 27.1 | 0.0059 |
| 6 | 1071.3162 | 180993 | | 8.0 | 0.0059 |
| 7 | 1072.2998 | 181159 | | 5.2 | 0.0059 |
| 8 | 1072.3094 | 181161 | | 10.4 | 0.0059 |
| 9 | 1072.3192 | 181162 | | 1.5 | 0.0059 |
| 10 | 1073.3027 | 181329 | | 4.0 | 0.0059 |
| 11 | 1073.3123 | 181330 | | 2.6 | 0.0059 |
| 12 | 1073.3220 | 181332 | | 0.2 | 0.0059 |
| 13 | 1074.2960 | 181496 | | 0.5 | 0.0059 |
| 14 | 1074.3056 | 181498 | | 1.5 | 0.0059 |
| 15 | 1074.3153 | 181500 | | 0.5 | 0.0059 |

**FT13087 Kevin Weiland/Mayor - w-8 - DCM / DCTB Mix 1:10**

ETH
Eidgenössische Technische Hochschule Zürich
Swiss Federal Institute of Technology Zurich

| # | m/z | Res. | S/N | I % | FWHM |
|---|---|---|---|---|---|
| 16 | 1075.2989 | 181666 | | 0.3 | 0.0059 |
| 17 | 1075.3085 | 181667 | | 0.4 | 0.0059 |
| 18 | 1076.3019 | 181835 | | 0.1 | 0.0059 |

## $^{1}$H-, $^{13}$C-NMR ($CD_2Cl_2$, 500/126 MHz, 25 °C) and HR-MS spectra of compound 9

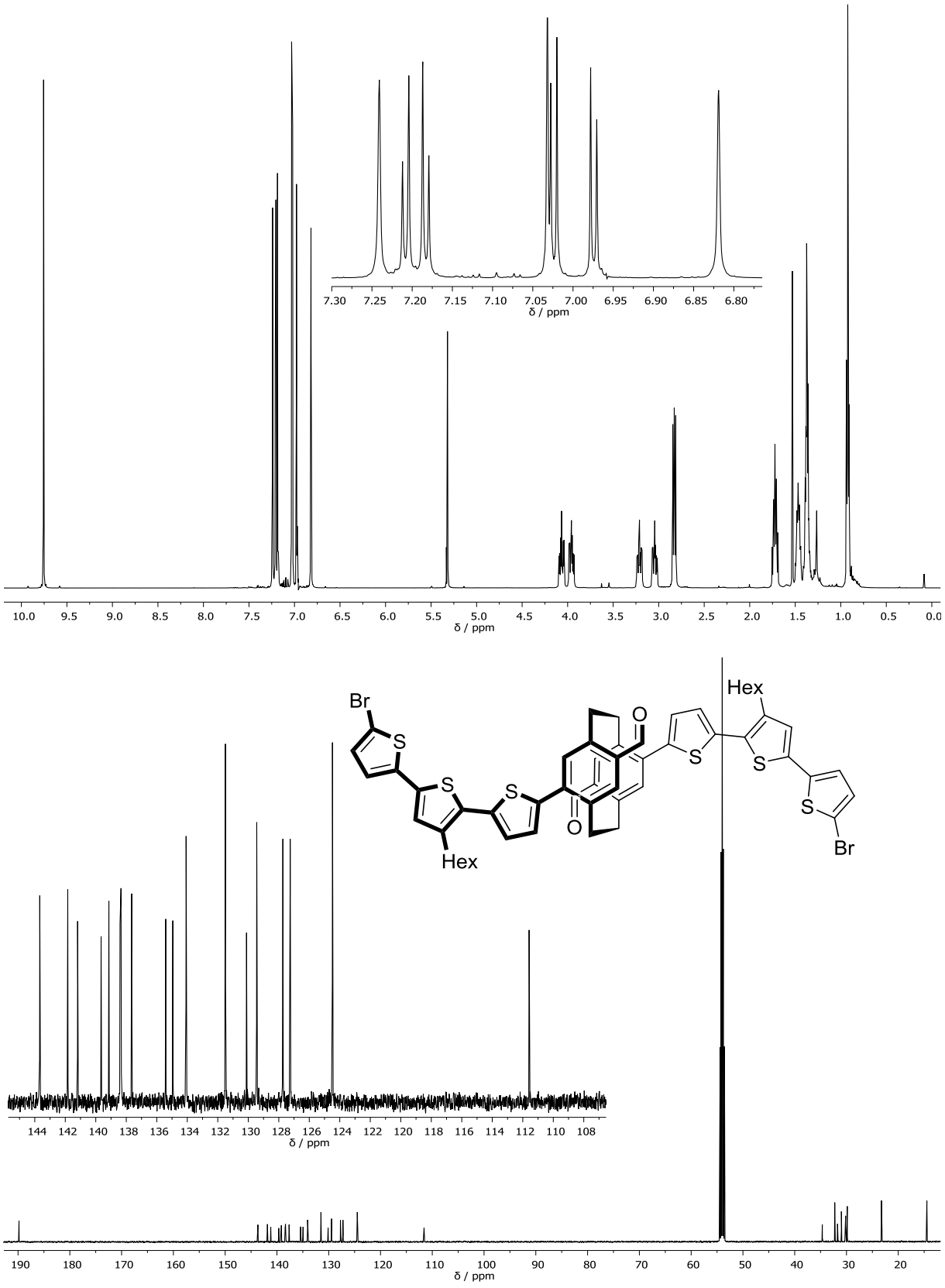

**FT13088 Kevin Weiland/Mayor - w-9 - DCM / DCTB Mix 1:10**

ETH Eidgenössische Technische Hochschule Zürich Swiss Federal Institute of Technology Zurich

**Acquisition Parameter**

| | | | | | |
|---|---|---|---|---|---|
| Method: | MALDI_MS_POS_300-2600_2M_16AvScans | | | Acquisition Date: | 08.05.2018 14:18:36 |
| File Name: | D:\ETH\Data\FT130xx\FT13088_0_A21_000001.d | | | Operator: | Louis Bertschi |
| Source | Dual (MALDI/ESI) | Polarity | Positive | Nebulizer Gas | 1.3 bar |
| Broadband Low Mass | 303.1 m/z | n/a | n/a | Drying Gas Flow Rate | 3.7 L/min |
| Broadband High Mass | 2600.0 m/z | Laser Power | 19.2 lp | Capillary | 4000.0 V |
| No. of Cell Fills | 1 | n/a | n/a | Drying Gas | 200.0 °C |
| Apodization | Full-Sine | Time of Flight to Detector | 0.001 sec | Temperature | |

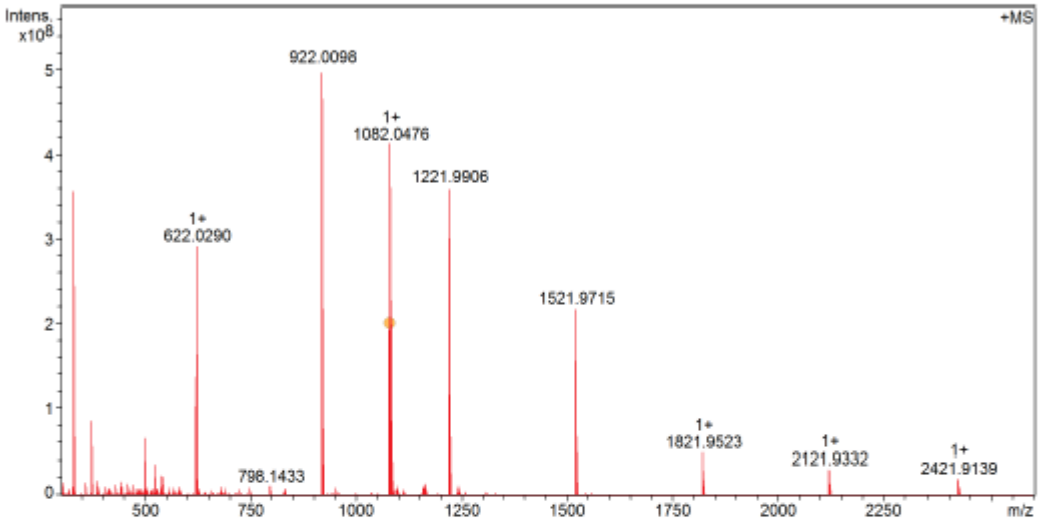


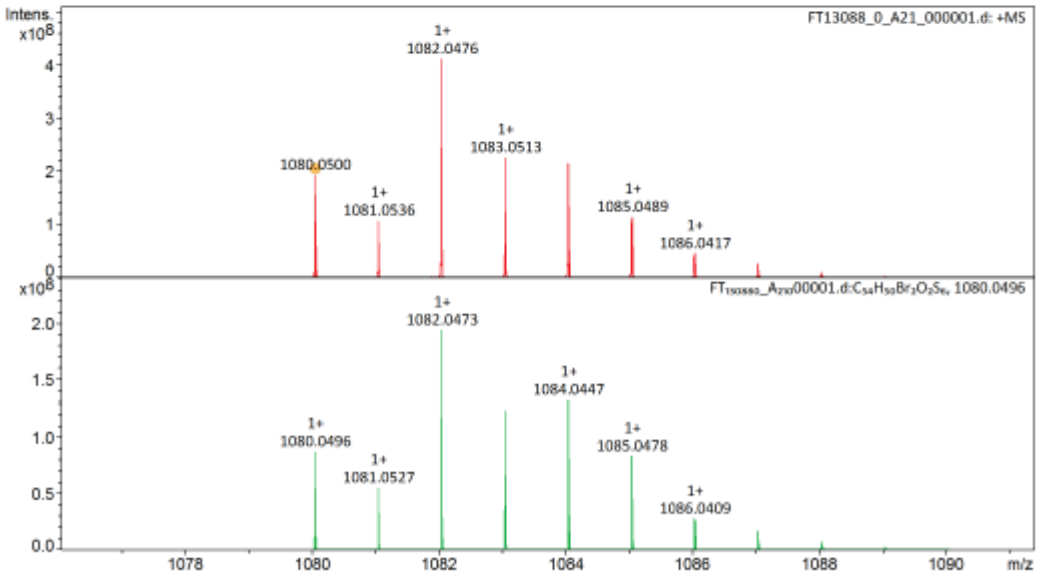

**FT13088 Kevin Weiland/Mayor - w-9 - DCM / DCTB Mix 1:10**

ETH Eidgenössische Technische Hochschule Zürich Swiss Federal Institute of Technology Zurich

**Evaluation Spectra / Validation Formula:**

| # | Ion Formula | Adduct | m/z | z | Meas. m/z | mSigma | N-Rule | err [mDa] | err [ppm] |
|---|---|---|---|---|---|---|---|---|---|
| 1 | C54H50Br2O2S6 | M | 1080.0496 | 1+ | 1080.0500 | 68.6 | ok | -0.4 | -0.3 |

**Calibration Info:**

Date: 08.05.2018 15:45:05
Polarity: Positive
Calibration spectrum: +MS: Scan
Reference mass list: MALDI: DCTB Matrix + HP-Mix (pos)
Calibration mode: Quadratic

| Reference m/z | Resulting m/z | Intensity | Error [ppm] |
|---|---|---|---|
| 118.0863 | | | |
| 250.1464 | | | |
| 251.1543 | | | |
| 273.1362 | | | |
| 322.0481 | | | |
| 332.2009 | | | |
| 500.2934 | | | |
| 501.3013 | | | |
| 523.2832 | | | |
| 622.0290 | 622.0290 | 292124000 | -0.005 |
| 750.4404 | | | |
| 751.4483 | | | |
| 773.4302 | | | |
| 922.0098 | 922.0098 | 503029984 | 0.042 |
| 1000.5874 | | | |
| 1001.5953 | | | |
| 1023.5772 | | | |
| 1221.9906 | 1221.9906 | 361715488 | -0.066 |
| 1521.9715 | 1521.9715 | 218757568 | -0.004 |
| 1821.9523 | 1821.9523 | 49181100 | 0.014 |
| 2121.9332 | 2121.9332 | 30102694 | 0.024 |
| 2421.9140 | | | |
| 2721.8948 | | | |

Standard deviation: 0.050

**Mass List:**

| # | m/z | Res. | S/N | I % | FWHM |
|---|---|---|---|---|---|
| 1 | 332.1990 | 510362 | 1829.3 | 9.1 | 0.0007 |
| 2 | 332.1993 | 1275812 | 1854.7 | 9.3 | 0.0003 |
| 3 | 332.2003 | 609958 | 14281.9 | 71.2 | 0.0005 |
| 4 | 333.2025 | 470094 | 554.2 | 2.8 | 0.0007 |
| 5 | 333.2037 | 607249 | 2735.8 | 13.6 | 0.0005 |
| 6 | 374.2095 | 378745 | 557.4 | 2.8 | 0.0010 |
| 7 | 374.2111 | 550113 | 3418.6 | 17.1 | 0.0007 |
| 8 | 375.2145 | 542962 | 857.7 | 4.3 | 0.0007 |
| 9 | 386.2839 | 514257 | 685.9 | 3.5 | 0.0008 |
| 10 | 445.4038 | 426883 | 592.0 | 3.2 | 0.0010 |
| 11 | 500.2933 | 392161 | 2274.3 | 13.1 | 0.0013 |
| 12 | 501.2967 | 382421 | 760.0 | 4.4 | 0.0013 |
| 13 | 501.3012 | 373563 | 572.5 | 3.3 | 0.0013 |
| 14 | 523.2832 | 385006 | 1227.9 | 7.3 | 0.0014 |
| 15 | 524.2866 | 373998 | 474.3 | 2.8 | 0.0014 |
| 16 | 540.0245 | 369627 | 749.6 | 4.5 | 0.0015 |
| 17 | 542.0225 | 366501 | 722.9 | 4.3 | 0.0015 |
| 18 | 622.0290 | 326034 | 9097.3 | 58.1 | 0.0019 |
| 19 | 623.0325 | 328357 | 1008.4 | 6.4 | 0.0019 |
| 20 | 922.0098 | 211527 | 13366.6 | 100.0 | 0.0044 |
| 21 | 923.0135 | 203552 | 2148.3 | 16.3 | 0.0045 |
| 22 | 1080.0500 | 185473 | 4476.2 | 38.6 | 0.0058 |
| 23 | 1081.0536 | 190646 | 2478.7 | 21.4 | 0.0057 |
| 24 | 1082.0476 | 182229 | 9508.3 | 82.0 | 0.0059 |
| 25 | 1083.0513 | 186825 | 5246.2 | 45.3 | 0.0058 |
| 26 | 1084.0453 | 175794 | 5048.3 | 43.6 | 0.0062 |
| 27 | 1084.0554 | 192087 | 1210.6 | 10.5 | 0.0056 |
| 28 | 1085.0489 | 171646 | 2643.7 | 22.8 | 0.0063 |
| 29 | 1086.0417 | 169457 | 1057.2 | 9.1 | 0.0064 |
| 30 | 1086.0529 | 166381 | 639.5 | 5.5 | 0.0065 |
| 31 | 1087.0453 | 178720 | 615.4 | 5.3 | 0.0061 |
| 32 | 1221.9906 | 162033 | 7975.9 | 71.9 | 0.0075 |
| 33 | 1222.9945 | 162686 | 1868.2 | 16.9 | 0.0075 |
| 34 | 1521.9715 | 126289 | 4452.9 | 43.5 | 0.0121 |
| 35 | 1522.9751 | 126802 | 1383.6 | 13.5 | 0.0120 |
| 36 | 1821.9523 | 105598 | 903.4 | 9.8 | 0.0173 |
| 37 | 1822.9558 | 106314 | 333.6 | 3.6 | 0.0171 |
| 38 | 2121.9332 | 90785 | 491.7 | 6.0 | 0.0234 |
| 39 | 2122.9366 | 91142 | 227.9 | 2.8 | 0.0233 |
| 40 | 2421.9139 | 77924 | 315.1 | 3.9 | 0.0311 |

| # | m/z | Res. | S/N | I % | FWHM |
|---|---|---|---|---|---|
| 1 | 1080.0496 | 185472 | | 45.1 | 0.0058 |
| 2 | 1081.0527 | 185645 | | 28.8 | 0.0058 |
| 3 | 1082.0473 | 185815 | | 100.0 | 0.0058 |
| 4 | 1082.0558 | 185817 | | 9.2 | 0.0058 |
| 5 | 1083.0504 | 185988 | | 63.7 | 0.0058 |
| 6 | 1083.0589 | 185989 | | 1.9 | 0.0058 |
| 7 | 1084.0447 | 186159 | | 68.1 | 0.0058 |
| 8 | 1084.0536 | 186160 | | 20.0 | 0.0058 |
| 9 | 1084.0620 | 186161 | | 0.3 | 0.0058 |
| 10 | 1085.0478 | 186331 | | 43.1 | 0.0058 |
| 11 | 1085.0567 | 186332 | | 4.2 | 0.0058 |
| 12 | 1086.0409 | 186501 | | 14.3 | 0.0058 |
| 13 | 1086.0509 | 186503 | | 13.6 | 0.0058 |
| 14 | 1086.0598 | 186505 | | 0.7 | 0.0058 |
| 15 | 1087.0441 | 186674 | | 9.0 | 0.0058 |

**FT13088 Kevin Weiland/Mayor - w-9 - DCM / DCTB Mix 1:10**

ETH
Eidgenössische Technische Hochschule Zürich
Swiss Federal Institute of Technology Zurich

| # | m/z | Res. | S/N | I % | FWHM |
|---|---|---|---|---|---|
| 16 | 1087.0540 | 186675 | | 2.9 | 0.0058 |
| 17 | 1088.0371 | 186844 | | 1.5 | 0.0058 |
| 18 | 1088.0473 | 186846 | | 2.8 | 0.0058 |
| 19 | 1088.0572 | 186848 | | 0.5 | 0.0058 |
| 20 | 1089.0403 | 187016 | | 0.9 | 0.0058 |
| 21 | 1089.0505 | 187018 | | 0.6 | 0.0058 |
| 22 | 1090.0434 | 187189 | | 0.3 | 0.0058 |

## $^{1}$H-, $^{13}$C-NMR ($CD_2Cl_2$, 500/126 MHz, 25 °C) and HR-MS spectra of compound 10

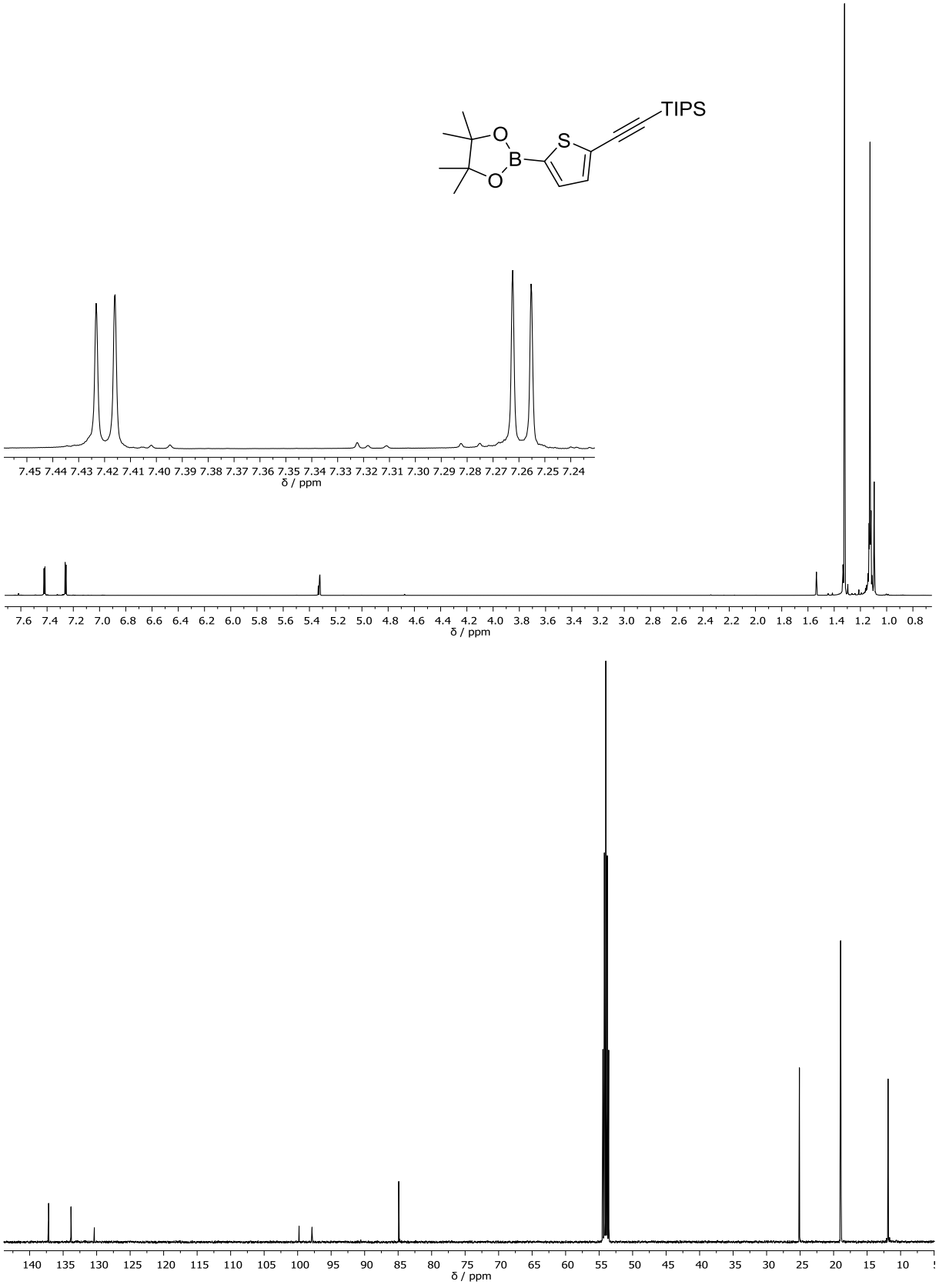

**FT13078 Kevin Weiland/Mayor - w-1 - DCM / DCTB Mix 1:10**

ETH Eidgenössische Technische Hochschule Zürich Swiss Federal Institute of Technology Zurich

**Acquisition Parameter**

| | | | | | |
|---|---|---|---|---|---|
| Method: | MALDI_MS_POS_100-1000_2M_16AvScans | | | Acquisition Date: | 08.05.2018 14:04:17 |
| File Name: | D:\ETH\Data\FT130xx\FT13078_0_A1_000001.d | | | Operator: | Louis Bertschi |
| Source | Dual (MALDI/ESI) | Polarity | Positive | Nebulizer Gas | 1.0 bar |
| Broadband Low Mass | 77.0 m/z | n/a | n/a | Drying Gas Flow Rate | 3.7 L/min |
| Broadband High Mass | 1050.0 m/z | Laser Power | 26.2 lp | Capillary | 4500.0 V |
| No. of Cell Fills | 1 | n/a | n/a | Drying Gas | 200.0 °C |
| Apodization | Full-Sine | Time of Flight to Detector | 0.000 sec | Temperature | |

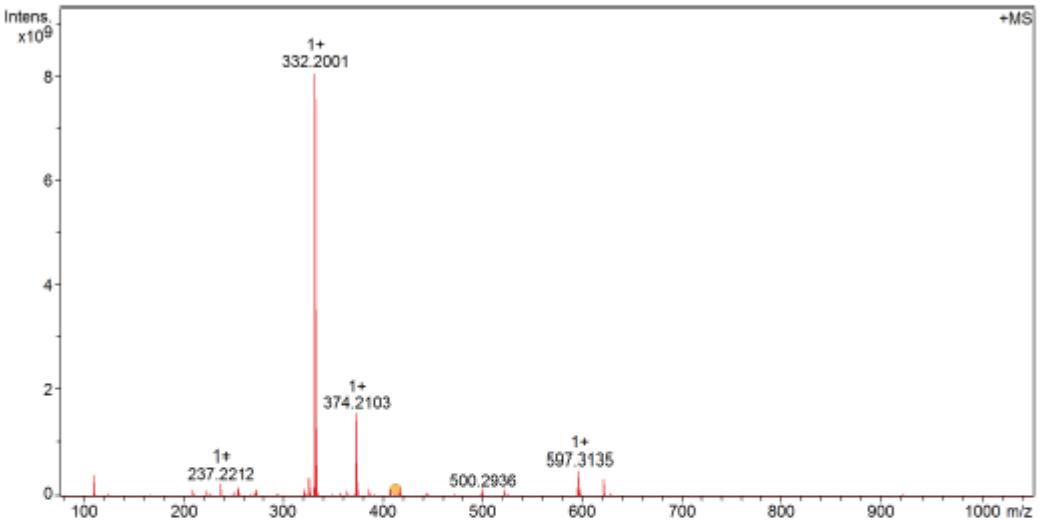


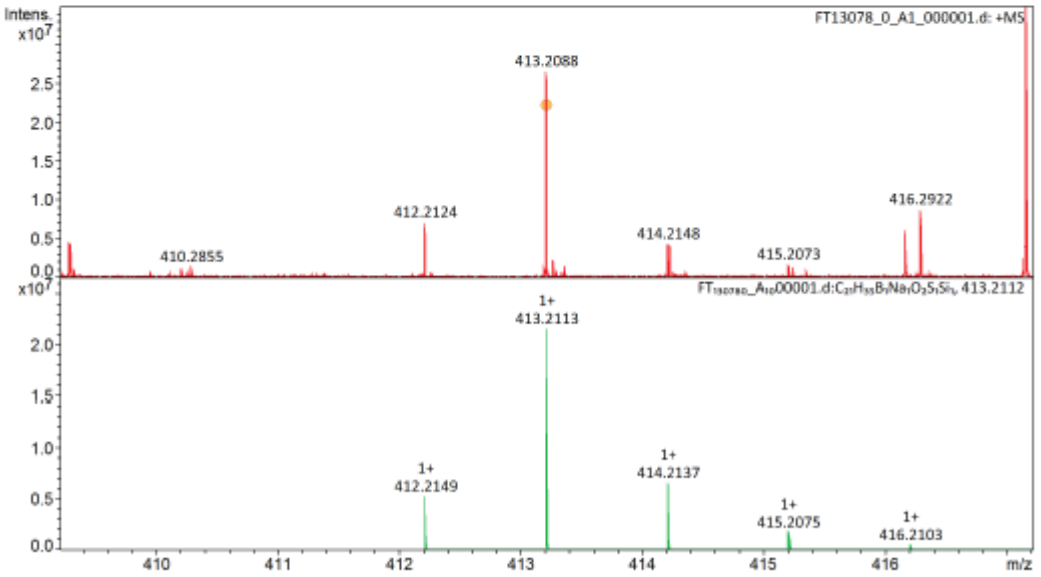

**FT13078 Kevin Weiland/Mayor - w-1 - DCM / DCTB Mix 1:10**

ETH Eidgenössische Technische Hochschule Zürich Swiss Federal Institute of Technology Zurich

**Evaluation Spectra / Validation Formula:**

| # | Ion Formula | Adduct | m/z | z | Meas. m/z | mSigma | N-Rule | err [mDa] | err [ppm] |
|---|---|---|---|---|---|---|---|---|---|
| 1 | C21H35BNaO2SSI | M+Na | 413.2112 | 1+ | 413.2112 | 56.7 | ok | 0.1 | 0.1 |

**Calibration Info:**

Date: 08.05.2018 15:25:50
Polarity: Positive
Calibration spectrum: +MS: Scan
Reference mass list: MALDI: DCTB Matrix + HP-Mix (pos)
Calibration mode: Quadratic

| Reference m/z | Resulting m/z | Intensity | Error [ppm] |
|---|---|---|---|
| 118.0863 | 118.0863 | 5148580 | -0.002 |
| 250.1464 | | | |
| 251.1543 | | | |
| 273.1362 | 273.1362 | 125165080 | 0.031 |
| 322.0481 | | | |
| 332.2009 | | | |
| 500.2934 | 500.2936 | 107561568 | 0.251 |
| 501.3013 | | | |
| 523.2832 | 523.2833 | 79611504 | 0.146 |
| 622.0290 | 622.0283 | 330525056 | -1.022 |
| 750.4404 | | | |
| 751.4483 | | | |
| 773.4302 | | | |
| 922.0098 | 922.0104 | 25530602 | 0.706 |
| 1000.5874 | | | |
| 1001.5953 | | | |
| 1023.5772 | | | |
| 1221.9906 | | | |
| 1521.9715 | | | |
| 1821.9523 | | | |
| 2121.9332 | | | |
| 2421.9140 | | | |
| 2721.8948 | | | |

Standard deviation: 0.774

**Mass List:**

| # | m/z | Res. | S/N | I % | FWHM |
|---|---|---|---|---|---|
| 1 | 110.7337 | 418858 | 1113.0 | 0.5 | 0.0003 |
| 2 | 209.1536 | 161597 | 867.7 | 0.5 | 0.0013 |
| 3 | 209.1899 | 167692 | 2754.4 | 1.5 | 0.0012 |
| 4 | 223.2056 | 172262 | 1815.9 | 1.0 | 0.0013 |
| 5 | 227.2368 | 163745 | 1137.5 | 0.6 | 0.0014 |
| 6 | 237.1848 | 152528 | 1181.8 | 0.7 | 0.0016 |
| 7 | 237.2212 | 160695 | 5089.4 | 2.9 | 0.0015 |
| 8 | 251.2369 | 159020 | 1472.8 | 0.9 | 0.0016 |
| 9 | 254.1902 | 149633 | 3729.0 | 2.3 | 0.0017 |
| 10 | 255.1936 | 138160 | 767.6 | 0.5 | 0.0018 |
| 11 | 255.2681 | 140236 | 2470.2 | 1.5 | 0.0018 |
| 12 | 273.1362 | 114163 | 2364.7 | 1.5 | 0.0024 |
| 13 | 321.3139 | 135923 | 885.4 | 0.6 | 0.0024 |
| 14 | 322.0469 | 139038 | 1331.0 | 1.0 | 0.0023 |
| 15 | 326.3767 | 141018 | 6221.0 | 4.5 | 0.0023 |
| 16 | 327.3801 | 150602 | 1405.0 | 1.0 | 0.0022 |
| 17 | 332.1871 | 119285 | 2193.0 | 1.6 | 0.0028 |
| 18 | 332.2001 | 147587 | 139700.3 | 100.0 | 0.0023 |
| 19 | 333.2030 | 123363 | 23215.5 | 16.6 | 0.0027 |
| 20 | 334.2061 | 147593 | 1526.2 | 1.1 | 0.0023 |
| 21 | 334.2075 | 127935 | 1387.4 | 1.0 | 0.0026 |
| 22 | 365.1757 | 96280 | 1115.8 | 0.8 | 0.0038 |
| 23 | 374.2103 | 108578 | 26127.9 | 19.3 | 0.0034 |
| 24 | 374.2321 | 94391 | 661.9 | 0.5 | 0.0040 |
| 25 | 375.2134 | 91347 | 4939.9 | 3.6 | 0.0041 |
| 26 | 386.2824 | 77564 | 1391.8 | 1.0 | 0.0050 |
| 27 | 407.2855 | 70250 | 2374.0 | 1.8 | 0.0058 |
| 28 | 417.1620 | 102744 | 815.9 | 0.6 | 0.0041 |
| 29 | 417.1648 | 117208 | 769.4 | 0.6 | 0.0036 |
| 30 | 418.1584 | 108524 | 1612.9 | 1.2 | 0.0039 |
| 31 | 418.1611 | 107996 | 1573.9 | 1.2 | 0.0039 |
| 32 | 444.2900 | 100178 | 788.0 | 0.6 | 0.0044 |
| 33 | 500.2936 | 98792 | 1674.4 | 1.3 | 0.0051 |
| 34 | 523.2833 | 89992 | 1215.7 | 1.0 | 0.0058 |
| 35 | 596.3173 | 79946 | 1611.3 | 1.4 | 0.0075 |
| 36 | 597.3135 | 80514 | 7423.4 | 6.1 | 0.0074 |
| 37 | 598.3172 | 82167 | 2536.0 | 2.1 | 0.0073 |
| 38 | 622.0283 | 72308 | 4971.5 | 4.1 | 0.0086 |
| 39 | 623.0321 | 74454 | 580.9 | 0.5 | 0.0084 |
| 40 | 628.6136 | 65284 | 632.1 | 0.5 | 0.0096 |

| # | m/z | Res. | S/N | I % | FWHM |
|---|---|---|---|---|---|
| 1 | 412.2149 | 99975 | | 24.5 | 0.0041 |
| 2 | 413.2113 | 100216 | | 100.0 | 0.0041 |
| 3 | 413.2183 | 100218 | | 5.7 | 0.0041 |
| 4 | 414.2137 | 100459 | | 30.6 | 0.0041 |
| 5 | 414.2203 | 100461 | | 1.0 | 0.0041 |
| 6 | 415.2075 | 100701 | | 7.8 | 0.0041 |
| 7 | 415.2164 | 100703 | | 4.7 | 0.0041 |
| 8 | 415.2231 | 100704 | | 0.1 | 0.0041 |
| 9 | 416.2103 | 100944 | | 2.1 | 0.0041 |
| 10 | 416.2187 | 50473 | | 0.5 | 0.0082 |
| 11 | 417.2040 | 101185 | | 0.2 | 0.0041 |
| 12 | 417.2131 | 101187 | | 0.3 | 0.0041 |

## $^{1}$H-, $^{13}$C-NMR ($CD_2Cl_2$, 400/101 MHz, 25 °C) and HR-MS spectra of compound 11

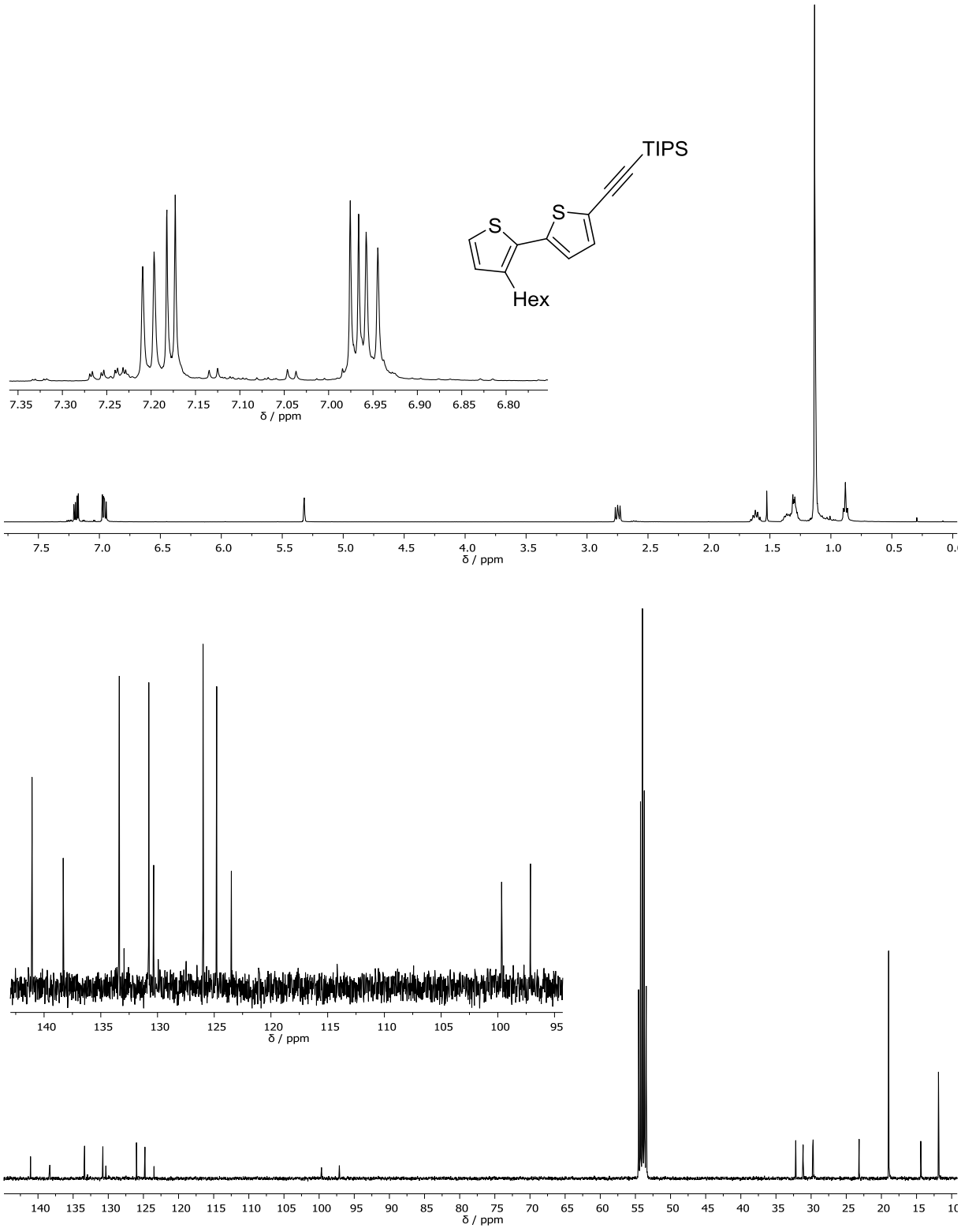

**FT13079 Kevin Weiland/Mayor - w-2 - DCM / DCTB Mix 1:10**

ETH Eidgenössische Technische Hochschule Zürich Swiss Federal Institute of Technology Zurich

**Acquisition Parameter**

| | | | | | |
|---|---|---|---|---|---|
| Method: | MALDI_MS_POS_100-1000_2M_16AvScans | | | Acquisition Date: | 09.05.2018 09:49:26 |
| File Name: | D:\ETH\Data\FT130xx\FT13079_0_A3_000002.d | | | Operator: | Louis Bertschi |
| Source | Dual (MALDI/ESI) | Polarity | Positive | Nebulizer Gas | 1.0 bar |
| Broadband Low Mass | 77.0 m/z | n/a | n/a | Drying Gas Flow Rate | 3.7 L/min |
| Broadband High Mass | 1050.0 m/z | Laser Power | 20.2 lp | Capillary | 4500.0 V |
| No. of Cell Fills | 1 | n/a | n/a | Drying Gas | 200.0 °C |
| Apodization | Full-Sine | Time of Flight to Detector | 0.000 sec | Temperature | |

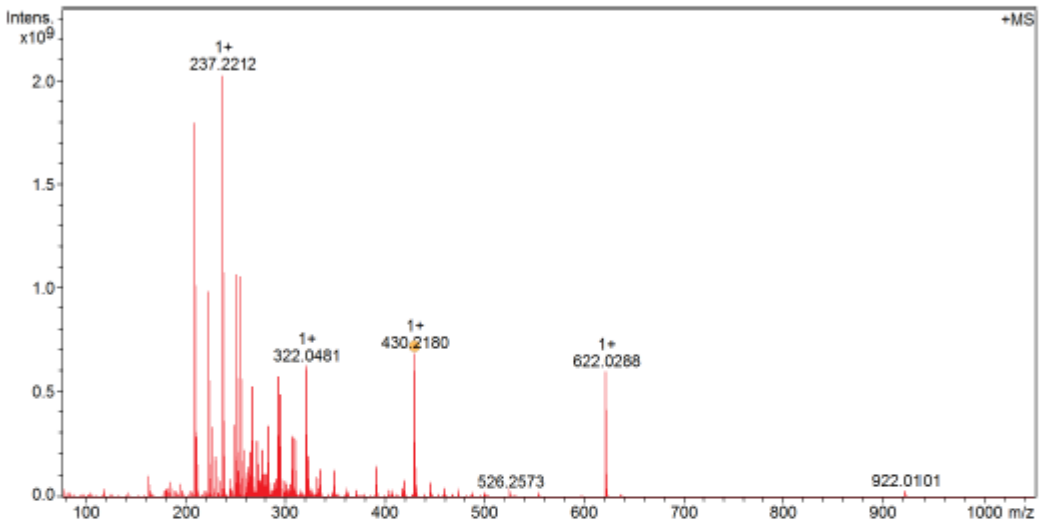


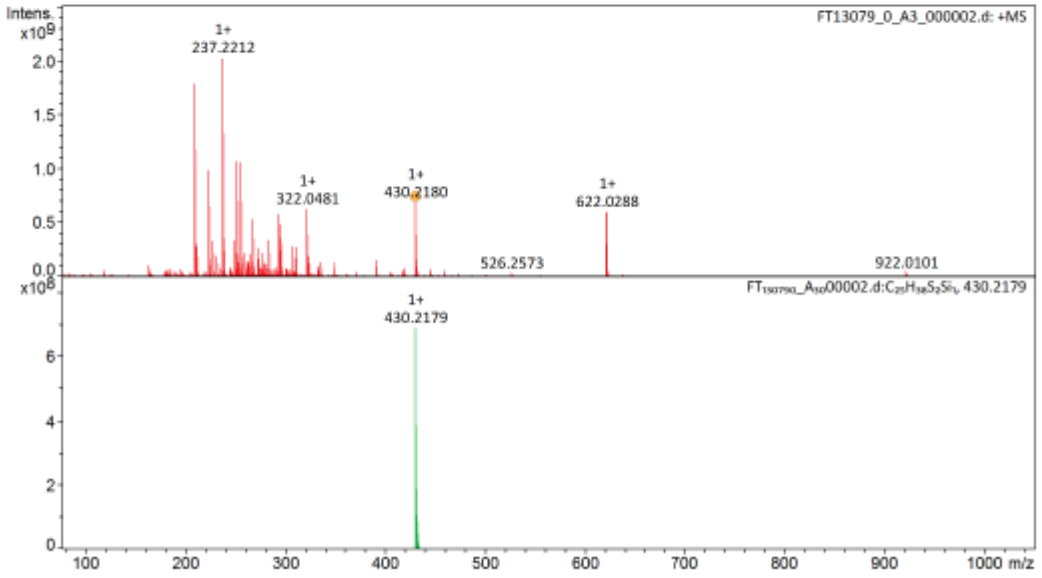

**FT13079 Kevin Weiland/Mayor - w-2 - DCM / DCTB Mix 1:10**

ETH Eidgenössische Technische Hochschule Zürich Swiss Federal Institute of Technology Zurich

**Evaluation Spectra / Validation Formula:**

| # | Ion Formula | Adduct | m/z | z | Meas. m/z | mSigma | N-Rule | err [mDa] | err [ppm] |
|---|---|---|---|---|---|---|---|---|---|
| 1 | C25H38S2Si | M | 430.2179 | 1+ | 430.2180 | 49.0 | ok | -0.1 | -0.2 |

**Calibration Info:**

Date: 09.05.2018 09:54:20
Polarity: Positive
Calibration spectrum: +MS: Scan
Reference mass list: MALDI: DCTB Matrix + HP-Mix (pos)
Calibration mode: Quadratic

| Reference m/z | Resulting m/z | Intensity | Error [ppm] |
|---|---|---|---|
| 118.0863 | 118.0863 | 42578396 | -0.001 |
| 250.1464 | | | |
| 251.1543 | | | |
| 273.1362 | | | |
| 322.0481 | 322.0481 | 626364544 | 0.052 |
| 332.2009 | | | |
| 500.2934 | | | |
| 501.3013 | | | |
| 523.2832 | | | |
| 622.0290 | 622.0288 | 601083264 | -0.304 |
| 750.4404 | | | |
| 751.4483 | | | |
| 773.4302 | | | |
| 922.0098 | 922.0101 | 32588170 | 0.311 |
| 1000.5874 | | | |
| 1001.5953 | | | |
| 1023.5772 | | | |
| 1221.9906 | | | |
| 1521.9715 | | | |
| 1821.9523 | | | |
| 2121.9332 | | | |
| 2421.9140 | | | |
| 2721.8948 | | | |

Standard deviation: 0.475

**Mass List:**

| # | m/z | Res. | S/N | I % | FWHM |
|---|---|---|---|---|---|
| 1 | 209.1538 | 235329 | 13189.1 | 34.3 | 0.0009 |
| 2 | 209.1900 | 235662 | 34029.1 | 88.5 | 0.0009 |
| 3 | 210.1934 | 233840 | 5827.2 | 15.2 | 0.0009 |
| 4 | 211.2057 | 232849 | 5344.0 | 13.9 | 0.0009 |
| 5 | 223.2057 | 221334 | 17708.1 | 48.6 | 0.0010 |
| 6 | 224.2090 | 219239 | 2884.7 | 7.9 | 0.0010 |
| 7 | 227.2369 | 216638 | 5821.6 | 16.5 | 0.0010 |
| 8 | 231.1719 | 212652 | 3271.3 | 9.2 | 0.0011 |
| 9 | 237.1849 | 207915 | 9961.6 | 28.9 | 0.0011 |
| 10 | 237.2212 | 207562 | 34443.9 | 100.0 | 0.0011 |
| 11 | 238.2246 | 206000 | 5985.1 | 17.8 | 0.0012 |
| 12 | 249.2212 | 194603 | 5500.3 | 16.8 | 0.0013 |
| 13 | 251.2370 | 196276 | 17264.9 | 52.6 | 0.0013 |
| 14 | 252.2403 | 194958 | 3393.8 | 10.4 | 0.0013 |
| 15 | 255.2683 | 192857 | 16636.6 | 52.0 | 0.0013 |
| 16 | 256.2716 | 191778 | 2812.0 | 8.8 | 0.0013 |
| 17 | 259.2032 | 188645 | 3431.3 | 10.7 | 0.0014 |
| 18 | 263.2370 | 186522 | 2256.4 | 7.3 | 0.0014 |
| 19 | 265.2526 | 185412 | 3234.1 | 10.4 | 0.0014 |
| 20 | 267.2684 | 183745 | 8110.7 | 26.1 | 0.0015 |
| 21 | 272.2948 | 180227 | 3914.5 | 12.9 | 0.0015 |
| 22 | 273.1850 | 179554 | 2391.2 | 7.9 | 0.0015 |
| 23 | 277.2504 | 141341 | 2314.9 | 7.7 | 0.0020 |
| 24 | 277.2525 | 146457 | 3290.5 | 10.9 | 0.0019 |
| 25 | 283.2995 | 173800 | 4868.1 | 16.6 | 0.0016 |
| 26 | 293.1748 | 167221 | 4359.6 | 15.3 | 0.0018 |
| 27 | 293.2839 | 167877 | 8087.3 | 28.3 | 0.0017 |
| 28 | 294.2065 | 167091 | 3465.1 | 12.1 | 0.0018 |
| 29 | 295.2997 | 166422 | 6909.1 | 24.2 | 0.0018 |
| 30 | 307.2995 | 159868 | 4129.6 | 14.1 | 0.0019 |
| 31 | 310.2013 | 158206 | 4191.8 | 13.7 | 0.0020 |
| 32 | 310.2376 | 158818 | 2863.2 | 9.4 | 0.0020 |
| 33 | 321.3153 | 152683 | 7982.4 | 25.0 | 0.0021 |
| 34 | 322.0481 | 152739 | 9848.9 | 30.9 | 0.0021 |
| 35 | 323.3309 | 152049 | 2977.0 | 9.3 | 0.0021 |
| 36 | 335.3308 | 146727 | 2278.2 | 6.8 | 0.0023 |
| 37 | 391.2843 | 125535 | 2438.0 | 7.4 | 0.0031 |
| 38 | 430.2180 | 114107 | 10762.0 | 33.9 | 0.0038 |
| 39 | 431.2213 | 114823 | 2578.3 | 8.1 | 0.0038 |
| 40 | 622.0288 | 79439 | 9766.4 | 29.6 | 0.0078 |

| # | m/z | Res. | S/N | I % | FWHM |
|---|---|---|---|---|---|
| 1 | 430.2179 | 114107 | | 100.0 | 0.0038 |
| 2 | 431.2174 | 114372 | | 6.7 | 0.0038 |
| 3 | 431.2213 | 114373 | | 27.5 | 0.0038 |
| 4 | 432.2140 | 114637 | | 12.4 | 0.0038 |
| 5 | 432.2208 | 114638 | | 1.8 | 0.0038 |
| 6 | 432.2247 | 114640 | | 3.7 | 0.0038 |
| 7 | 433.2133 | 114902 | | 0.6 | 0.0038 |
| 8 | 433.2174 | 114903 | | 3.4 | 0.0038 |
| 9 | 433.2239 | 114905 | | 0.2 | 0.0038 |
| 10 | 433.2281 | 114906 | | 0.3 | 0.0038 |
| 11 | 434.2102 | 115166 | | 0.5 | 0.0038 |
| 12 | 434.2166 | 115168 | | 0.2 | 0.0038 |
| 13 | 434.2207 | 115169 | | 0.4 | 0.0038 |
| 14 | 435.2136 | 115432 | | 0.1 | 0.0038 |

## $^{1}$H-, $^{13}$C-NMR ($CD_2Cl_2$, 400/101 MHz, 25 °C) and HR-MS spectra of compound 12

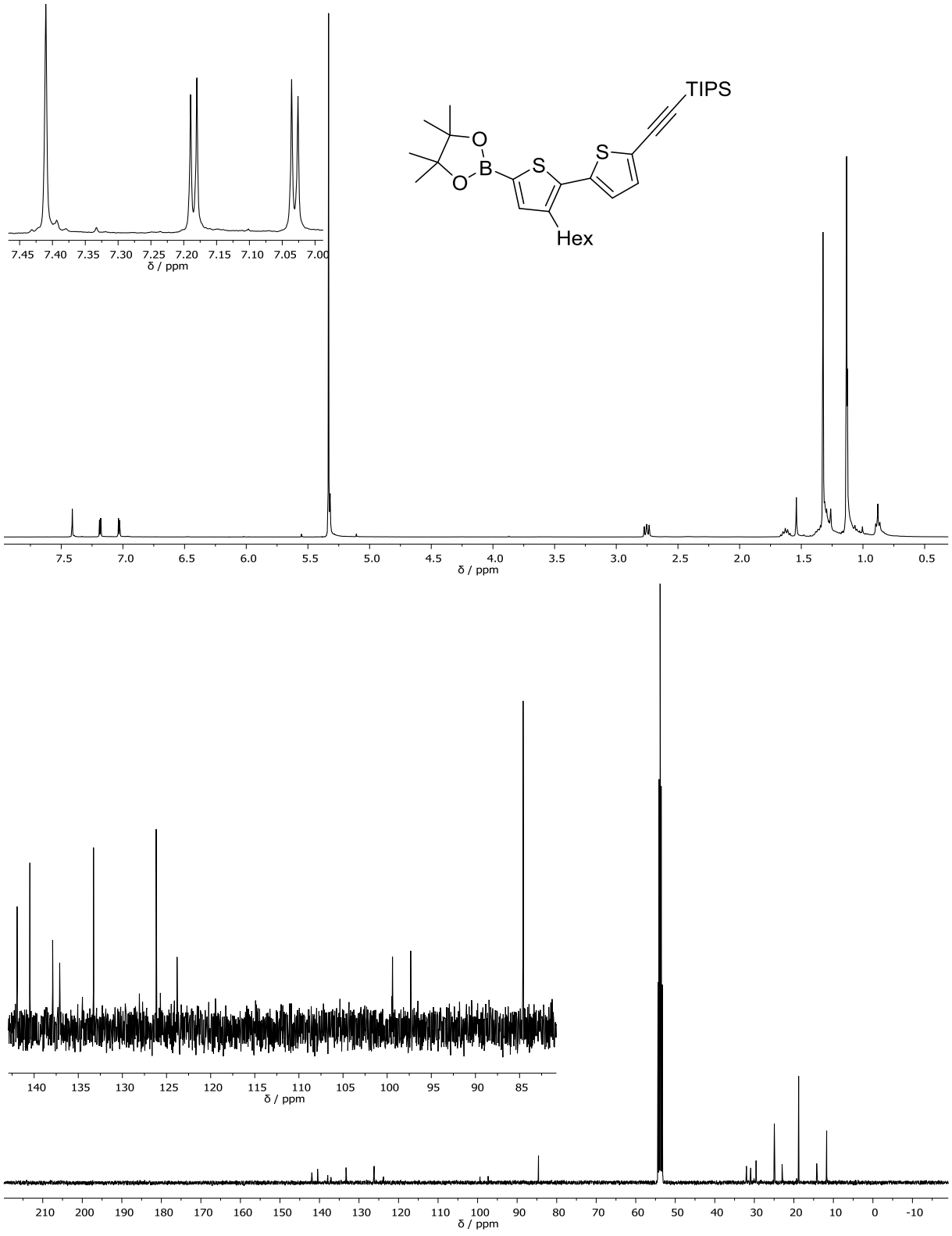

**FT13080 Kevin Weiland/Mayor - w-3 - DCM / DCTB Mix 1:10**

ETH Eidgenössische Technische Hochschule Zürich Swiss Federal Institute of Technology Zurich

**Acquisition Parameter**

| | | | | | |
|---|---|---|---|---|---|
| Method: | MALDI_MS_POS_100-1000_2M_16AvScans | | | Acquisition Date: | 08.05.2018 14:06:18 |
| File Name: | D:\ETH\Data\FT130xx\FT13080_0_A5_000001.d | | | Operator: | Louis Bertschi |
| Source | Dual (MALDI/ESI) | Polarity | Positive | Nebulizer Gas | 1.0 bar |
| Broadband Low Mass | 77.0 m/z | n/a | n/a | Drying Gas Flow Rate | 3.7 L/min |
| Broadband High Mass | 1050.0 m/z | Laser Power | 20.6 lp | Capillary | 4500.0 V |
| No. of Cell Fills | 1 | n/a | n/a | Drying Gas | 200.0 °C |
| Apodization | Full-Sine | Time of Flight to Detector | 0.000 sec | Temperature | |

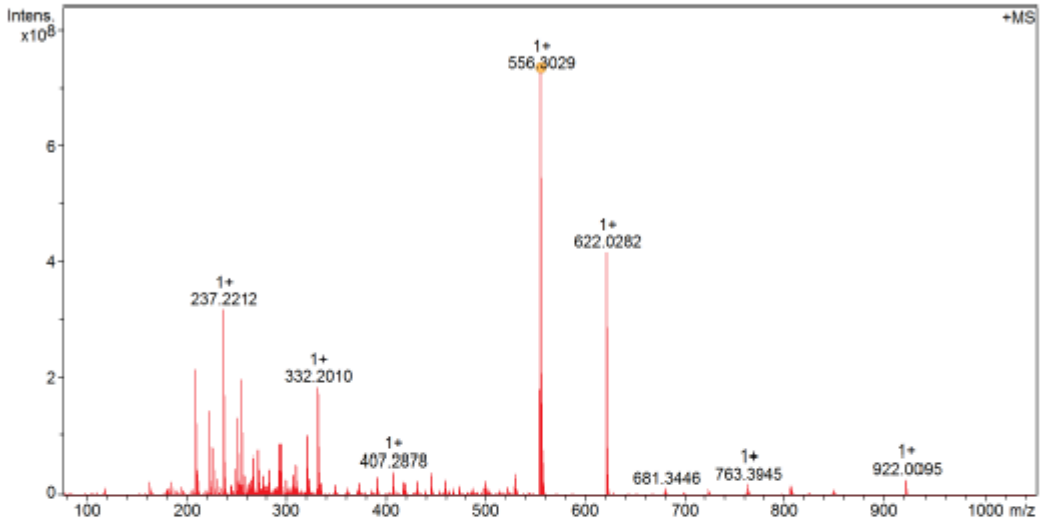


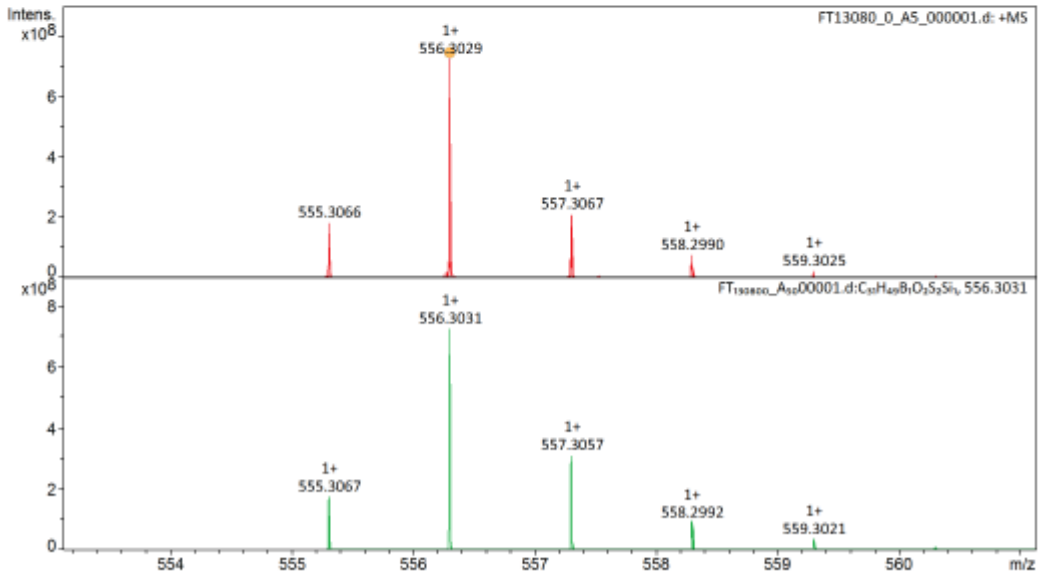


Bruker Daltonics solariX ETH - MS-Service LOC - D-CHAB Page 1 of 2

**FT13080 Kevin Weiland/Mayor - w-3 - DCM / DCTB Mix 1:10**

ETH Eidgenössische Technische Hochschule Zürich Swiss Federal Institute of Technology Zurich

**Evaluation Spectra / Validation Formula:**

| # | Ion Formula | Adduct | m/z | z | Meas. m/z | mSigma | N-Rule | err [mDa] | err [ppm] |
|---|---|---|---|---|---|---|---|---|---|
| 1 | C31H49BO2S2Si | M | 556.3031 | 1+ | 556.3029 | 64.2 | ok | 0.2 | 0.4 |

**Calibration Info:**

Date: 08.05.2018 15:32:42
Polarity: Positive
Calibration spectrum: +MS: Scan
Reference mass list: MALDI: DCTB Matrix + HP-Mix (pos)
Calibration mode: Quadratic

| Reference m/z | Resulting m/z | Intensity | Error [ppm] |
|---|---|---|---|
| 118.0863 | 118.0863 | 13323511 | 0.006 |
| 250.1464 | | | |
| 251.1543 | | | |
| 273.1362 | 273.1361 | 44396652 | -0.306 |
| 322.0481 | 322.0482 | 100212712 | 0.368 |
| 332.2009 | | | |
| 500.2934 | 500.2935 | 25036472 | 0.033 |
| 501.3013 | | | |
| 523.2832 | 523.2833 | 15440973 | 0.109 |
| 622.0290 | | | |
| 750.4404 | | | |
| 751.4483 | | | |
| 773.4302 | | | |
| 922.0098 | 922.0095 | 27624076 | -0.316 |
| 1000.5874 | | | |
| 1001.5953 | | | |
| 1023.5772 | | | |
| 1221.9906 | | | |
| 1521.9715 | | | |
| 1821.9523 | | | |
| 2121.9332 | | | |
| 2421.9140 | | | |
| 2721.8948 | | | |

Standard deviation: 0.355

**Mass List:**

| # | m/z | Res. | S/N | I % | FWHM |
|---|---|---|---|---|---|
| 1 | 209.1534 | 156234 | 1603.1 | 10.0 | 0.0013 |
| 2 | 209.1898 | 157441 | 4754.1 | 29.6 | 0.0013 |
| 3 | 210.1932 | 158827 | 807.8 | 5.0 | 0.0013 |
| 4 | 211.2055 | 157449 | 972.5 | 6.1 | 0.0013 |
| 5 | 223.2055 | 158176 | 3131.3 | 19.8 | 0.0014 |
| 6 | 227.2368 | 157948 | 1689.2 | 10.8 | 0.0014 |
| 7 | 237.1848 | 155312 | 1649.2 | 10.7 | 0.0015 |
| 8 | 237.2212 | 159438 | 6800.6 | 43.9 | 0.0015 |
| 9 | 238.2245 | 150227 | 1224.6 | 8.0 | 0.0016 |
| 10 | 249.2211 | 142980 | 963.6 | 6.4 | 0.0017 |
| 11 | 251.2369 | 143485 | 2728.6 | 18.1 | 0.0018 |
| 12 | 255.2681 | 143207 | 4044.1 | 27.2 | 0.0018 |
| 13 | 256.2715 | 138184 | 707.5 | 4.8 | 0.0019 |
| 14 | 259.2031 | 132906 | 673.1 | 4.5 | 0.0020 |
| 15 | 267.2682 | 130006 | 1321.5 | 9.0 | 0.0021 |
| 16 | 272.2947 | 128175 | 1477.8 | 10.2 | 0.0021 |
| 17 | 273.1361 | 128032 | 884.2 | 6.1 | 0.0021 |
| 18 | 277.2526 | 82036 | 665.4 | 4.6 | 0.0034 |
| 19 | 283.2996 | 121374 | 856.6 | 6.0 | 0.0023 |
| 20 | 293.1748 | 128654 | 759.1 | 5.4 | 0.0023 |
| 21 | 293.2839 | 130789 | 1669.5 | 11.9 | 0.0022 |
| 22 | 294.2065 | 131251 | 808.1 | 5.8 | 0.0022 |
| 23 | 295.2996 | 127402 | 1640.2 | 11.7 | 0.0023 |
| 24 | 307.2996 | 125452 | 680.5 | 4.9 | 0.0024 |
| 25 | 310.2014 | 123018 | 999.1 | 7.2 | 0.0025 |
| 26 | 310.2378 | 122060 | 694.3 | 5.0 | 0.0025 |
| 27 | 321.3153 | 127725 | 1405.4 | 10.1 | 0.0025 |
| 28 | 322.0482 | 128033 | 1927.4 | 13.8 | 0.0025 |
| 29 | 332.2010 | 119691 | 3566.6 | 25.6 | 0.0028 |
| 30 | 333.2045 | 120350 | 826.7 | 5.9 | 0.0028 |
| 31 | 407.2678 | 111452 | 719.3 | 5.6 | 0.0037 |
| 32 | 445.4041 | 105433 | 656.4 | 5.3 | 0.0042 |
| 33 | 531.2588 | 89789 | 583.5 | 5.2 | 0.0059 |
| 34 | 555.3066 | 87209 | 2829.4 | 25.2 | 0.0064 |
| 35 | 556.3029 | 85945 | 11217.9 | 100.0 | 0.0065 |
| 36 | 557.3000 | 115537 | 840.8 | 7.3 | 0.0048 |
| 37 | 557.3067 | 96860 | 3347.3 | 29.0 | 0.0058 |
| 38 | 558.2990 | 76763 | 1198.4 | 10.4 | 0.0073 |
| 39 | 622.0282 | 75054 | 6726.7 | 57.6 | 0.0083 |
| 40 | 623.0318 | 76940 | 857.7 | 7.4 | 0.0081 |

| # | m/z | Res. | S/N | I % | FWHM |
|---|---|---|---|---|---|
| 1 | 555.3067 | 85791 | | 24.4 | 0.0065 |
| 2 | 556.3031 | 85945 | | 100.0 | 0.0065 |
| 3 | 556.3101 | 85946 | | 8.4 | 0.0065 |
| 4 | 557.3057 | 86099 | | 43.3 | 0.0065 |
| 5 | 557.3125 | 86101 | | 1.9 | 0.0065 |
| 6 | 558.2992 | 86253 | | 12.3 | 0.0065 |
| 7 | 558.3084 | 86254 | | 9.2 | 0.0065 |
| 8 | 558.3153 | 86255 | | 0.3 | 0.0065 |
| 9 | 559.3021 | 86408 | | 4.9 | 0.0065 |
| 10 | 559.3113 | 86409 | | 1.3 | 0.0065 |
| 11 | 560.2954 | 86561 | | 0.5 | 0.0065 |
| 12 | 560.3049 | 86563 | | 1.0 | 0.0065 |
| 13 | 560.3143 | 86564 | | 0.1 | 0.0065 |
| 14 | 561.2986 | 86716 | | 0.2 | 0.0065 |
| 15 | 561.3078 | 86718 | | 0.1 | 0.0065 |

## $^{1}$H-, $^{13}$C-NMR ($CD_2Cl_2$, 500/126 MHz, 25 °C) and HR-MS spectra of compound 13

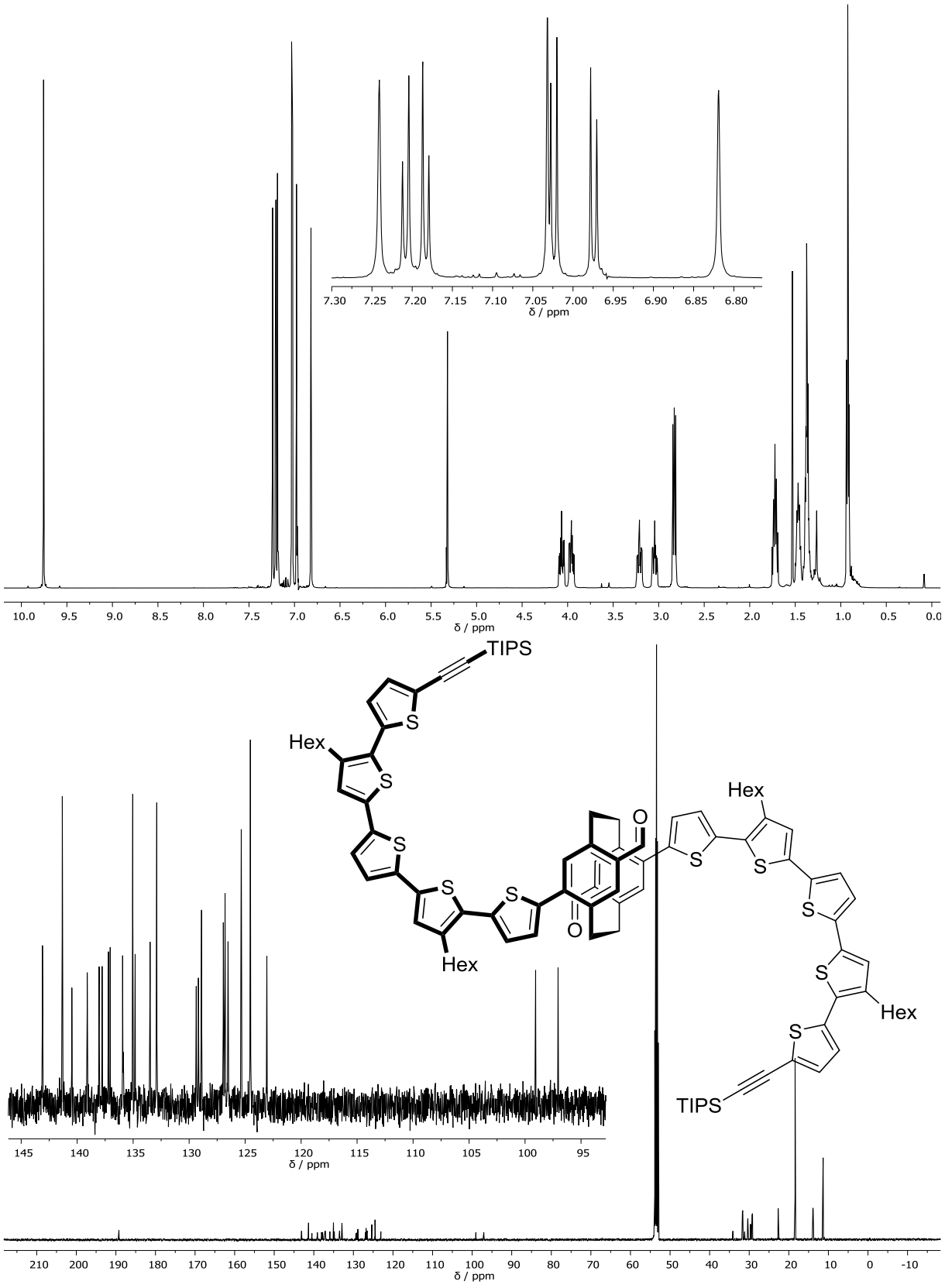

**FT13098 Kevin Weiland/Mayor - w-10 - DCM / DCTB Mix 1:10**

ETH Eidgenössische Technische Hochschule Zürich Swiss Federal Institute of Technology Zurich

**Acquisition Parameter**

| | | | | | |
|---|---|---|---|---|---|
| Method: | MALDI_MS_POS_300-2600_2M_16AvScans | | | Acquisition Date: | 08.05.2018 14:38:38 |
| File Name: | D:\ETH\Data\FT130xx\FT13098_0_B18_000001.d | | | Operator: | Louis Bertschi |
| Source | Dual (MALDI/ESI) | Polarity | Positive | Nebulizer Gas | 1.3 bar |
| Broadband Low Mass | 303.1 m/z | n/a | n/a | Drying Gas Flow Rate | 3.7 L/min |
| Broadband High Mass | 2600.0 m/z | Laser Power | 20.8 lp | Capillary | 4000.0 V |
| No. of Cell Fills | 1 | n/a | n/a | Drying Gas | 200.0 °C |
| Apodization | Full-Sine | Time of Flight to Detector | 0.002 sec | Temperature | |

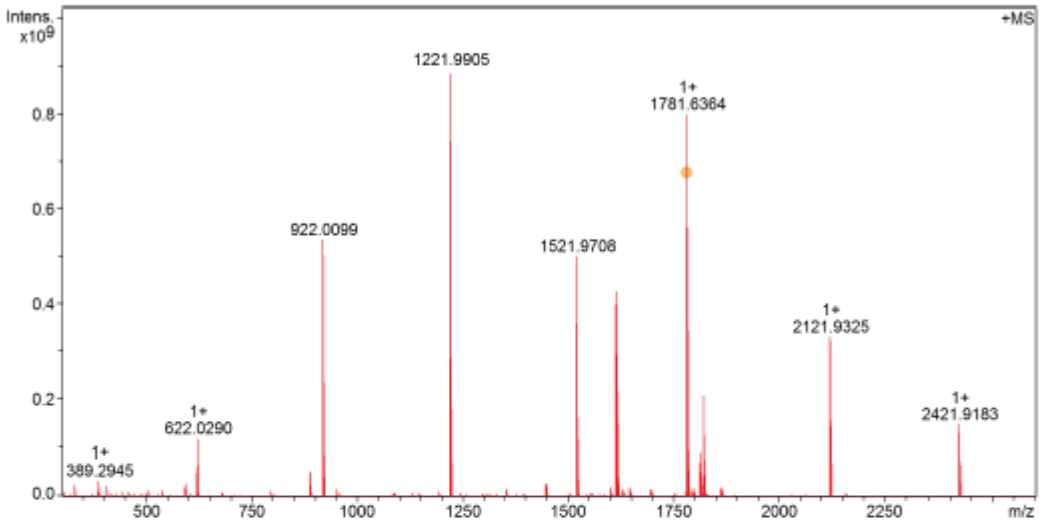


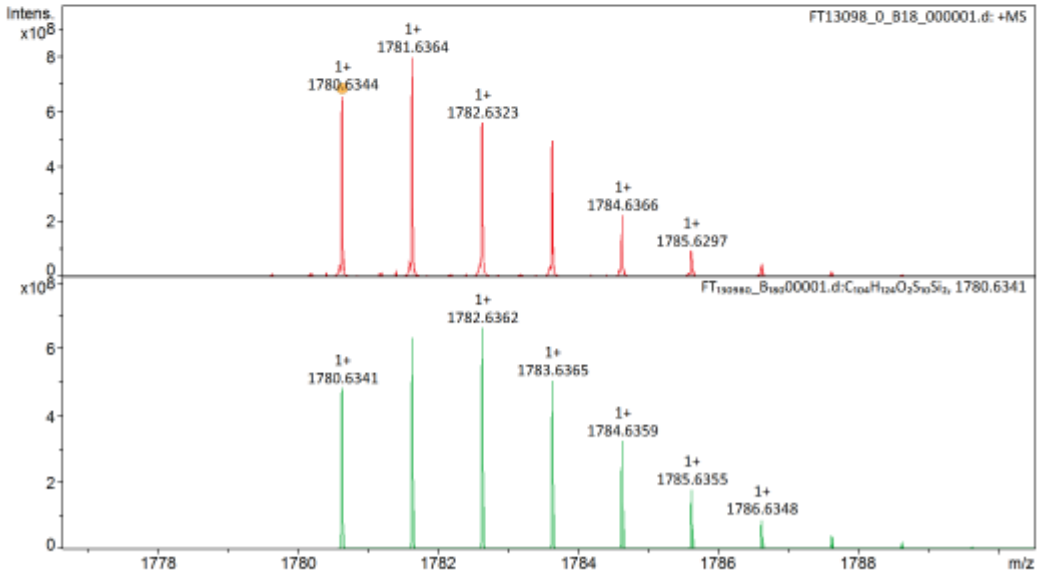

**FT13098 Kevin Weiland/Mayor - w-10 - DCM / DCTB Mix 1:10**

ETH Eidgenössische Technische Hochschule Zürich Swiss Federal Institute of Technology Zurich

**Evaluation Spectra / Validation Formula:**

| # | Ion Formula | Adduct | m/z | z | Meas. m/z | mSigma | N-Rule | err [mDa] | err [ppm] |
|---|---|---|---|---|---|---|---|---|---|
| 1 | C104H124O2S10Si2 | M | 1780.6341 | 1+ | 1780.6344 | 152.8 | ok | -0.2 | -0.1 |

**Calibration Info:**

| | |
|---|---|
| Date: | 08.05.2018 16:04:35 |
| Polarity: | Positive |
| Calibration spectrum: | +MS: Scan |
| Reference mass list: | MALDI: DCTB Matrix + HP-Mix (pos) |
| Calibration mode: | Quadratic |

| Reference m/z | Resulting m/z | Intensity | Error [ppm] |
|---|---|---|---|
| 118.0863 | | | |
| 250.1464 | | | |
| 251.1543 | | | |
| 273.1362 | | | |
| 322.0481 | | | |
| 332.2009 | | | |
| 500.2934 | | | |
| 501.3013 | | | |
| 523.2832 | | | |
| 622.0290 | 622.0290 | 117768760 | -0.012 |
| 750.4404 | | | |
| 751.4483 | | | |
| 773.4302 | | | |
| 922.0098 | 922.0099 | 535044960 | 0.096 |
| 1000.5874 | | | |
| 1001.5953 | | | |
| 1023.5772 | | | |
| 1221.9906 | 1221.9905 | 892622848 | -0.072 |
| 1521.9715 | 1521.9708 | 500600416 | -0.442 |
| 1821.9523 | 1821.9537 | 210520656 | 0.752 |
| 2121.9332 | 2121.9325 | 331274400 | -0.316 |
| 2421.9140 | | | |
| 2721.8948 | | | |

Standard deviation: 0.568

**Mass List:**

| # | m/z | Res. | S/N | I % | FWHM |
|---|---|---|---|---|---|
| 1 | 622.0290 | 304250 | 3771.4 | 13.2 | 0.0020 |
| 2 | 890.3177 | 206862 | 1384.9 | 5.8 | 0.0043 |
| 3 | 922.0099 | 197812 | 14219.8 | 59.9 | 0.0047 |
| 4 | 923.0137 | 202823 | 2279.9 | 9.8 | 0.0046 |
| 5 | 1221.9770 | 219042 | 1377.9 | 7.4 | 0.0056 |
| 6 | 1221.9905 | 156106 | 18653.9 | 100.0 | 0.0078 |
| 7 | 1222.9951 | 161335 | 4629.2 | 24.8 | 0.0076 |
| 8 | 1521.5018 | 131581 | 605.9 | 4.3 | 0.0116 |
| 9 | 1521.9708 | 126969 | 7843.0 | 56.1 | 0.0120 |
| 10 | 1522.5050 | 127805 | 597.5 | 4.3 | 0.0119 |
| 11 | 1522.9756 | 131247 | 2540.7 | 18.2 | 0.0116 |
| 12 | 1614.5529 | 121667 | 5502.0 | 44.7 | 0.0133 |
| 13 | 1615.5395 | 113407 | 721.9 | 5.9 | 0.0142 |
| 14 | 1615.5554 | 119848 | 5899.4 | 47.9 | 0.0135 |
| 15 | 1616.5366 | 196631 | 529.4 | 4.3 | 0.0082 |
| 16 | 1616.5504 | 92680 | 2961.9 | 24.1 | 0.0174 |
| 17 | 1617.5522 | 132310 | 3016.1 | 24.5 | 0.0122 |
| 18 | 1617.5666 | 214416 | 744.8 | 6.1 | 0.0075 |
| 19 | 1618.5432 | 145706 | 530.7 | 4.3 | 0.0111 |
| 20 | 1618.5563 | 138539 | 1265.8 | 10.3 | 0.0117 |
| 21 | 1780.6344 | 108823 | 9044.9 | 74.2 | 0.0164 |
| 22 | 1781.6364 | 108396 | 10906.1 | 89.5 | 0.0164 |
| 23 | 1782.6323 | 108967 | 7660.6 | 62.9 | 0.0164 |
| 24 | 1783.6335 | 115956 | 6816.8 | 55.9 | 0.0154 |
| 25 | 1783.6508 | 152412 | 1455.4 | 12.0 | 0.0117 |
| 26 | 1784.6366 | 106258 | 3033.9 | 24.9 | 0.0168 |
| 27 | 1784.6532 | 113560 | 666.1 | 5.5 | 0.0157 |
| 28 | 1785.6297 | 103752 | 1253.6 | 10.3 | 0.0172 |
| 29 | 1785.6411 | 98324 | 907.0 | 7.5 | 0.0182 |
| 30 | 1786.6333 | 118141 | 644.2 | 5.3 | 0.0151 |
| 31 | 1812.6274 | 111714 | 1123.8 | 7.9 | 0.0162 |
| 32 | 1813.6301 | 109825 | 1404.7 | 9.8 | 0.0165 |
| 33 | 1814.6350 | 104613 | 750.0 | 5.2 | 0.0173 |
| 34 | 1815.6248 | 113288 | 661.7 | 4.6 | 0.0160 |
| 35 | 1821.9537 | 109969 | 3376.0 | 23.6 | 0.0166 |
| 36 | 1822.9576 | 113184 | 1228.7 | 8.6 | 0.0161 |
| 37 | 2121.9325 | 86551 | 5232.8 | 37.1 | 0.0245 |
| 38 | 2122.9369 | 90313 | 2373.0 | 16.8 | 0.0235 |
| 39 | 2421.9183 | 76610 | 2307.7 | 16.5 | 0.0316 |
| 40 | 2422.9222 | 76423 | 1159.3 | 8.3 | 0.0317 |

| # | m/z | Res. | S/N | I % | FWHM |
|---|---|---|---|---|---|
| 1 | 1780.6341 | 108823 | | 72.4 | 0.0164 |
| 2 | 1781.6370 | 108885 | | 95.6 | 0.0164 |
| 3 | 1782.6362 | 108946 | | 100.0 | 0.0164 |
| 4 | 1783.6365 | 109007 | | 76.0 | 0.0164 |
| 5 | 1784.6359 | 109068 | | 49.4 | 0.0164 |
| 6 | 1785.6355 | 109129 | | 27.4 | 0.0164 |
| 7 | 1786.6348 | 54595 | | 13.5 | 0.0327 |
| 8 | 1787.6342 | 54626 | | 6.0 | 0.0327 |
| 9 | 1788.6336 | 36437 | | 2.4 | 0.0491 |
| 10 | 1789.6332 | 109373 | | 0.7 | 0.0164 |
| 11 | 1790.6324 | 109435 | | 0.3 | 0.0164 |

**$^1$H-, HSQC NMR ($C_2D_2Cl_4$, 600/126 MHz, 70 °C) and HR-MS spectra of compound 14**

$^1$H NMR spectrum of compound **14**

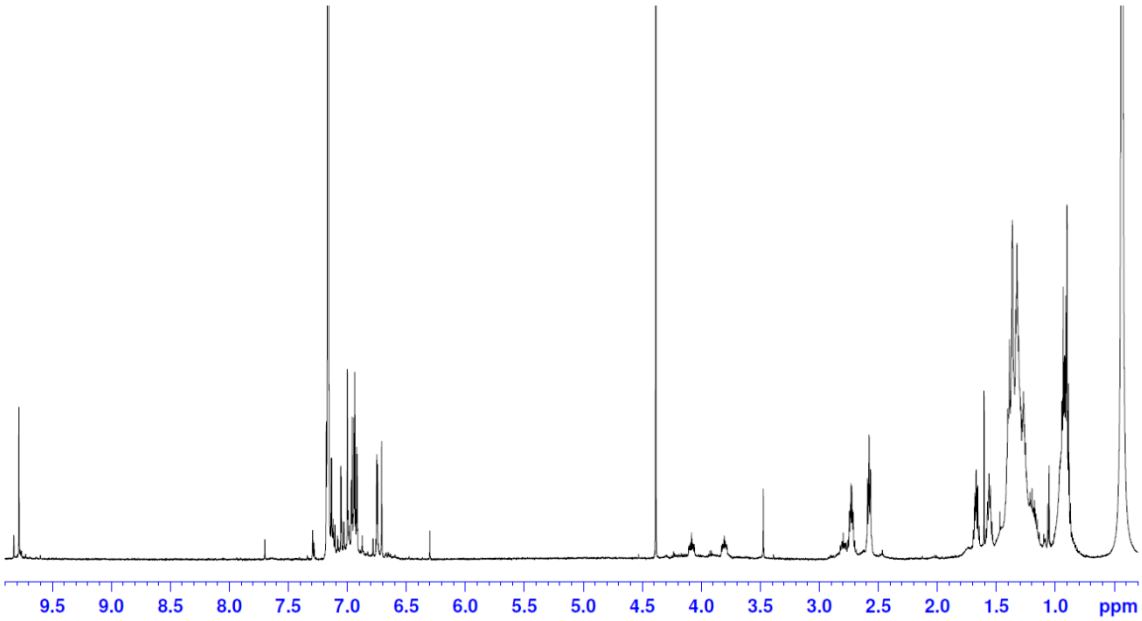


HSQC spectrum of compound **14**

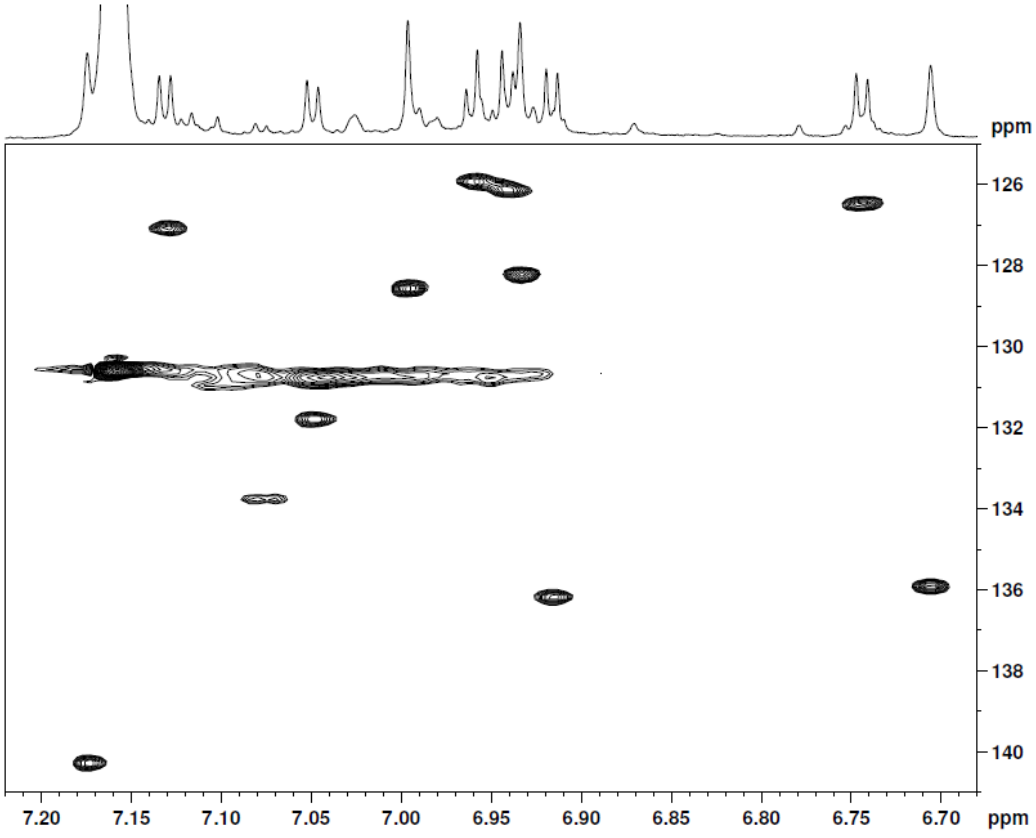

**FT13093 Kevin Weiland/Mayor - w-11 - DCM / DCTB Mix 1:10**

ETH Eidgenössische Technische Hochschule Zürich Swiss Federal Institute of Technology Zurich

**Acquisition Parameter**

| | | | | | |
|---|---|---|---|---|---|
| Method: | MALDI_MS_POS_300-2600_2M_16AvScans | | | Acquisition Date: | 08.05.2018 14:32:04 |
| File Name: | D:\ETH\Data\FT130xx\FT13093_0_B8_000001.d | | | Operator: | Louis Bertschi |
| Source | Dual (MALDI/ESI) | Polarity | Positive | Nebulizer Gas | 1.3 bar |
| Broadband Low Mass | 303.1 m/z | n/a | n/a | Drying Gas Flow Rate | 3.7 L/min |
| Broadband High Mass | 2600.0 m/z | Laser Power | 21.2 lp | Capillary | 4000.0 V |
| No. of Cell Fills | 1 | n/a | n/a | Drying Gas | 200.0 °C |
| Apodization | Full-Sine | Time of Flight to Detector | 0.002 sec | Temperature | |

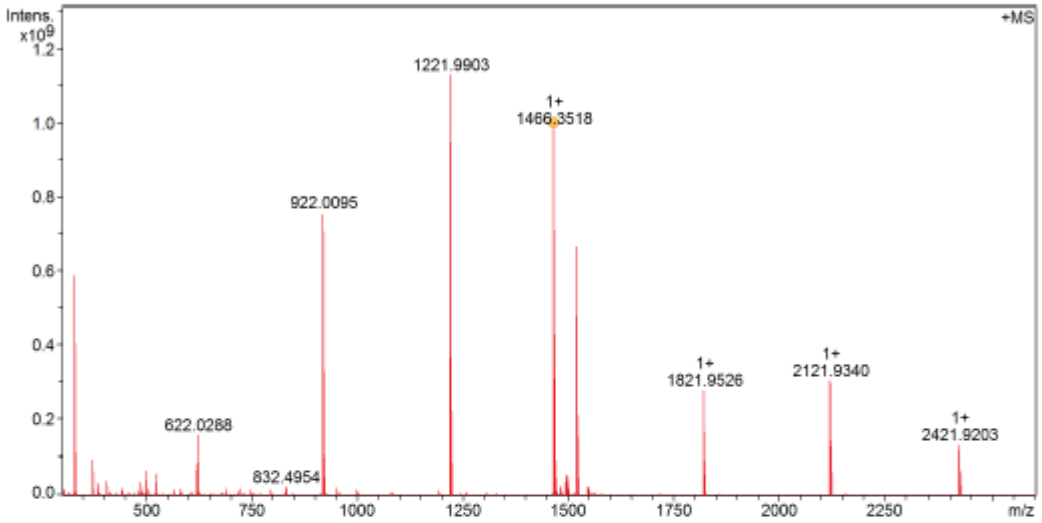


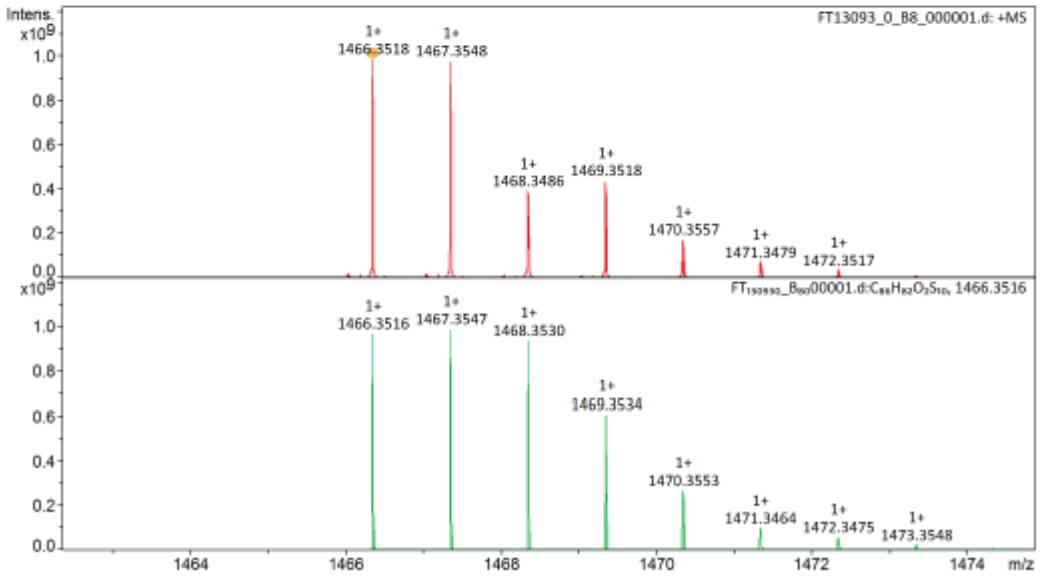

**FT13093 Kevin Weiland/Mayor - w-11 - DCM / DCTB Mix 1:10**

ETH Eidgenössische Technische Hochschule Zürich Swiss Federal Institute of Technology Zurich

**Evaluation Spectra / Validation Formula:**

| # | Ion Formula | Adduct | m/z | z | Meas. m/z | mSigma | N-Rule | err [mDa] | err [ppm] |
|---|---|---|---|---|---|---|---|---|---|
| 1 | C86H82O2S10 | M | 1466.3516 | 1+ | 1466.3518 | 218.8 | ok | -0.1 | -0.1 |

**Calibration Info:**

Date: 08.05.2018 15:57:16
Polarity: Positive
Calibration spectrum: +MS: Scan
Reference mass list: MALDI: DCTB Matrix + HP-Mix (pos)
Calibration mode: Quadratic

| Reference m/z | Resulting m/z | Intensity | Error [ppm] |
|---|---|---|---|
| 118.0863 | | | |
| 250.1464 | | | |
| 251.1543 | | | |
| 273.1362 | | | |
| 322.0481 | | | |
| 332.2009 | | | |
| 500.2934 | | | |
| 501.3013 | | | |
| 523.2832 | | | |
| 622.0290 | 622.0288 | 157456912 | -0.234 |
| 750.4404 | | | |
| 751.4483 | 751.4488 | 8722858 | 0.682 |
| 773.4302 | | | |
| 922.0098 | 922.0095 | 756691200 | -0.369 |
| 1000.5874 | | | |
| 1001.5953 | | | |
| 1023.5772 | | | |
| 1221.9906 | 1221.9903 | 1129274880 | -0.315 |
| 1521.9715 | 1521.9712 | 665952320 | -0.205 |
| 1821.9523 | 1821.9526 | 279818272 | 0.148 |
| 2121.9332 | 2121.9340 | 304924928 | 0.379 |
| 2421.9140 | | | |
| 2721.8948 | | | |

Standard deviation: 0.511

**Mass List:**

| # | m/z | Res. | S/N | I % | FWHM |
|---|---|---|---|---|---|
| 1 | 332.1988 | 551429 | 4455.0 | 9.9 | 0.0006 |
| 2 | 332.1998 | 597245 | 23475.8 | 52.1 | 0.0006 |
| 3 | 333.2019 | 369025 | 1072.3 | 2.4 | 0.0009 |
| 4 | 333.2033 | 586401 | 5414.3 | 12.0 | 0.0006 |
| 5 | 374.2107 | 520249 | 3896.0 | 8.7 | 0.0007 |
| 6 | 386.2835 | 468574 | 1315.4 | 3.0 | 0.0008 |
| 7 | 500.2931 | 369937 | 2264.6 | 5.9 | 0.0014 |
| 8 | 523.2829 | 359034 | 1978.4 | 5.2 | 0.0015 |
| 9 | 622.0288 | 312948 | 4729.7 | 13.9 | 0.0020 |
| 10 | 922.0095 | 202608 | 18611.1 | 67.0 | 0.0046 |
| 11 | 923.0135 | 201679 | 2695.5 | 9.9 | 0.0046 |
| 12 | 1221.9903 | 157581 | 23178.5 | 100.0 | 0.0078 |
| 13 | 1222.9950 | 162539 | 5610.3 | 24.2 | 0.0075 |
| 14 | 1223.9988 | 150341 | 621.5 | 2.7 | 0.0081 |
| 15 | 1466.3518 | 128697 | 15344.2 | 87.1 | 0.0114 |
| 16 | 1467.3548 | 128237 | 15229.7 | 86.5 | 0.0114 |
| 17 | 1468.3486 | 146762 | 6056.7 | 34.4 | 0.0100 |
| 18 | 1468.3604 | 137919 | 3491.5 | 19.8 | 0.0106 |
| 19 | 1469.3518 | 138639 | 6806.6 | 38.6 | 0.0106 |
| 20 | 1469.3647 | 173021 | 1313.3 | 7.5 | 0.0085 |
| 21 | 1470.3438 | 183844 | 1097.8 | 6.2 | 0.0080 |
| 22 | 1470.3557 | 150997 | 2664.1 | 15.1 | 0.0097 |
| 23 | 1471.3479 | 146623 | 1019.8 | 5.8 | 0.0100 |
| 24 | 1471.3602 | 159206 | 699.2 | 4.0 | 0.0092 |
| 25 | 1472.3517 | 147008 | 478.0 | 2.7 | 0.0100 |
| 26 | 1496.3649 | 130181 | 621.5 | 3.2 | 0.0115 |
| 27 | 1497.3682 | 126258 | 585.8 | 3.0 | 0.0119 |
| 28 | 1498.3441 | 127179 | 951.7 | 4.9 | 0.0118 |
| 29 | 1499.3474 | 126674 | 909.3 | 4.7 | 0.0118 |
| 30 | 1521.9712 | 124526 | 11433.2 | 59.0 | 0.0122 |
| 31 | 1522.9757 | 128034 | 3632.0 | 18.7 | 0.0119 |
| 32 | 1523.9796 | 125999 | 593.5 | 3.1 | 0.0121 |
| 33 | 1821.9526 | 107039 | 4934.6 | 24.8 | 0.0170 |
| 34 | 1822.9569 | 107687 | 1653.2 | 8.3 | 0.0169 |
| 35 | 2121.9105 | 599189 | 801.2 | 4.4 | 0.0035 |
| 36 | 2121.9340 | 87239 | 4883.4 | 27.0 | 0.0243 |
| 37 | 2122.9383 | 88241 | 2134.6 | 11.8 | 0.0241 |
| 38 | 2123.9424 | 93344 | 555.9 | 3.1 | 0.0228 |
| 39 | 2421.9203 | 76352 | 2073.0 | 11.7 | 0.0317 |
| 40 | 2422.9237 | 76051 | 1086.3 | 6.1 | 0.0319 |

| # | m/z | Res. | S/N | I % | FWHM |
|---|---|---|---|---|---|
| 1 | 1466.3516 | 128697 | | 98.1 | 0.0114 |
| 2 | 1467.3547 | 128785 | | 100.0 | 0.0114 |
| 3 | 1468.3530 | 128872 | | 94.7 | 0.0114 |
| 4 | 1469.3534 | 128960 | | 61.6 | 0.0114 |
| 5 | 1470.3433 | 129047 | | 9.0 | 0.0114 |
| 6 | 1470.3553 | 129048 | | 26.6 | 0.0114 |
| 7 | 1471.3464 | 129135 | | 9.1 | 0.0114 |
| 8 | 1471.3579 | 129136 | | 8.3 | 0.0114 |
| 9 | 1472.3475 | 129223 | | 5.6 | 0.0114 |
| 10 | 1472.3607 | 129224 | | 2.0 | 0.0114 |
| 11 | 1473.3424 | 129310 | | 1.1 | 0.0114 |
| 12 | 1473.3548 | 129311 | | 1.9 | 0.0114 |
| 13 | 1474.3441 | 129398 | | 0.6 | 0.0114 |
| 14 | 1474.3573 | 129399 | | 0.4 | 0.0114 |
| 15 | 1475.3399 | 129486 | | 0.1 | 0.0114 |

**FT13093 Kevin Weiland/Mayor - w-11 - DCM / DCTB Mix 1:10**

ETH Eidgenössische Technische Hochschule Zürich Swiss Federal Institute of Technology Zurich

| # | m/z | Res. | S/N | I % | FWHM |
|---|---|---|---|---|---|
| 16 | 1475.3526 | 129487 | | 0.2 | 0.0114 |

**$^{1}$H-, HSQC NMR ($C_6D_6$, 600/126 MHz, 60 °C) and HR-MS spectra of compound 15**

$^{1}$H NMR spectrum of compound **15**

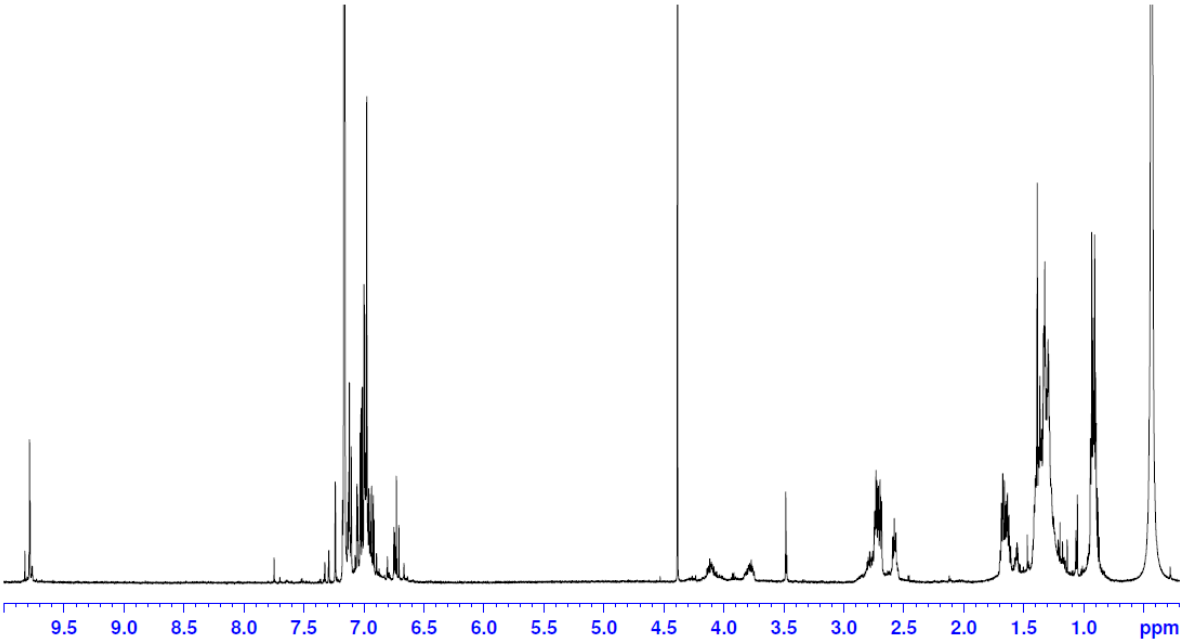


HSQC spectrum of compound **15**

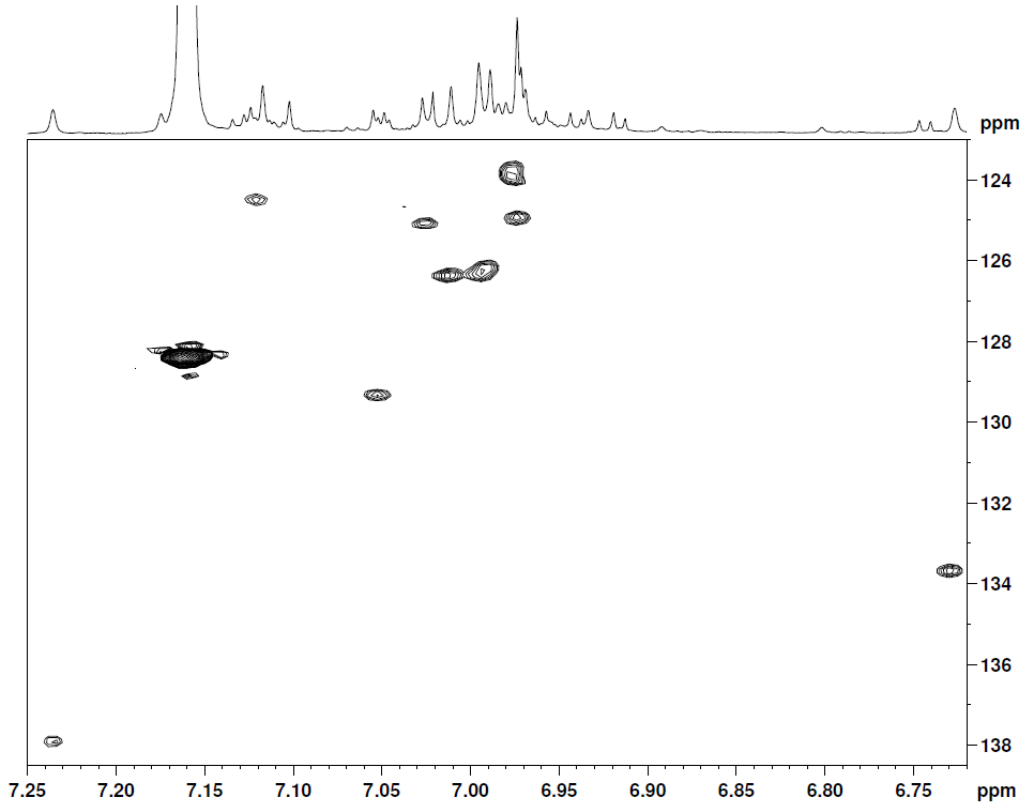

**FT13095 Kevin Weiland/Mayor - w-12 - DCM / DCTB Mix 1:10**

ETH Eidgenössische Technische Hochschule Zürich Swiss Federal Institute of Technology Zurich

**Acquisition Parameter**

| | | | | | |
|---|---|---|---|---|---|
| Method: | MALDI_MS_POS_300-2600_2M_16AvScans | | | Acquisition Date: | 08.05.2018 14:34:51 |
| File Name: | D:\ETH\Data\FT130xx\FT13095_0_B12_000001.d | | | Operator: | Louis Bertschi |
| Source | Dual (MALDI/ESI) | Polarity | Positive | Nebulizer Gas | 1.3 bar |
| Broadband Low Mass | 303.1 m/z | n/a | n/a | Drying Gas Flow Rate | 3.7 L/min |
| Broadband High Mass | 2600.0 m/z | Laser Power | 23.4 lp | Capillary | 4000.0 V |
| No. of Cell Fills | 1 | n/a | n/a | Drying Gas | 200.0 °C |
| Apodization | Full-Sine | Time of Flight to Detector | 0.002 sec | Temperature | |

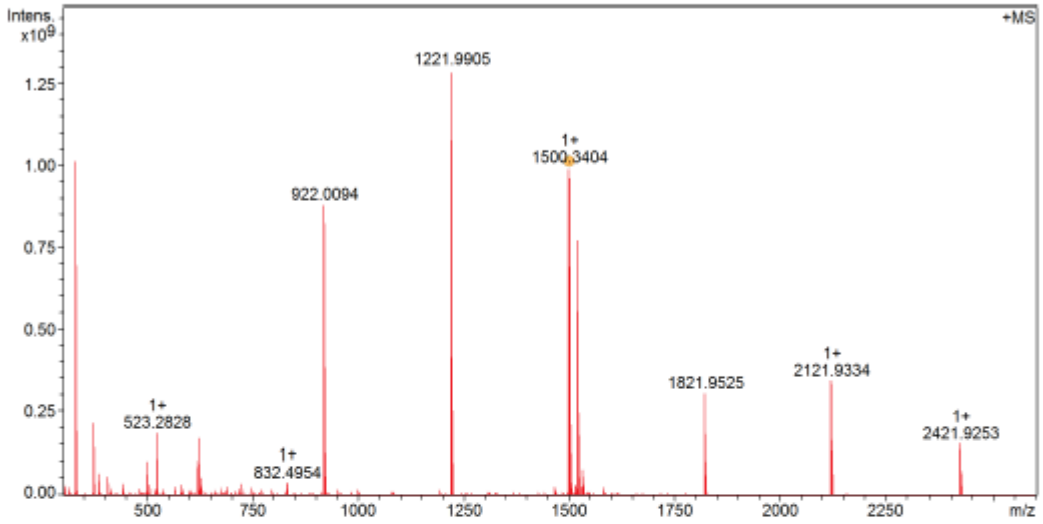


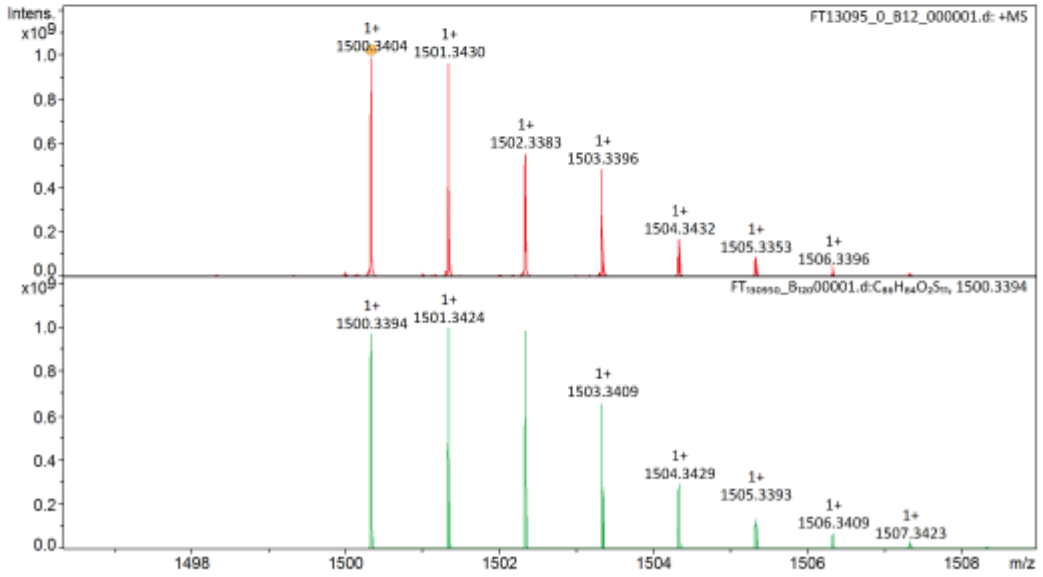

**FT13095 Kevin Weiland/Mayor - w-12 - DCM / DCTB Mix 1:10**

ETH Eidgenössische Technische Hochschule Zürich Swiss Federal Institute of Technology Zurich

**Evaluation Spectra / Validation Formula:**

| # | Ion Formula | Adduct | m/z | z | Meas. m/z | mSigma | N-Rule | err [mDa] | err [ppm] |
|---|---|---|---|---|---|---|---|---|---|
| 1 | C86H84O2S11 | M | 1500.3394 | 1+ | 1500.3404 | 189.0 | ok | -1.0 | -0.7 |

**Calibration Info:**

Date: 08.05.2018 15:59:21
Polarity: Positive
Calibration spectrum: +MS: Scan
Reference mass list: MALDI: DCTB Matrix + HP-Mix (pos)
Calibration mode: Quadratic

| Reference m/z | Resulting m/z | Intensity | Error [ppm] |
|---|---|---|---|
| 118.0863 | | | |
| 250.1464 | | | |
| 251.1543 | | | |
| 273.1362 | | | |
| 322.0481 | | | |
| 332.2009 | | | |
| 500.2934 | | | |
| 501.3013 | | | |
| 523.2832 | | | |
| 622.0290 | 622.0288 | 171417808 | -0.179 |
| 750.4404 | 750.4409 | 10226565 | 0.575 |
| 751.4483 | | | |
| 773.4302 | | | |
| 922.0098 | 922.0094 | 880950144 | -0.450 |
| 1000.5874 | | | |
| 1001.5953 | | | |
| 1023.5772 | | | |
| 1221.9906 | 1221.9905 | 1294035840 | -0.144 |
| 1521.9715 | 1521.9715 | 775205376 | 0.029 |
| 1821.9523 | 1821.9525 | 307312192 | 0.092 |
| 2121.9332 | 2121.9334 | 346476032 | 0.124 |
| 2421.9140 | | | |
| 2721.8948 | | | |

Standard deviation: 0.407

**Mass List:**

| # | m/z | Res. | S/N | I % | FWHM |
|---|---|---|---|---|---|
| 1 | 332.1989 | 300748 | 6761.7 | 13.2 | 0.0011 |
| 2 | 332.1999 | 623416 | 40018.5 | 78.2 | 0.0005 |
| 3 | 333.2022 | 320787 | 1667.5 | 3.3 | 0.0010 |
| 4 | 333.2035 | 574408 | 10091.2 | 19.7 | 0.0006 |
| 5 | 374.2091 | 321741 | 1499.4 | 2.9 | 0.0012 |
| 6 | 374.2107 | 496792 | 8525.5 | 16.7 | 0.0008 |
| 7 | 375.2143 | 506591 | 1787.8 | 3.5 | 0.0007 |
| 8 | 386.2837 | 472233 | 2594.9 | 5.2 | 0.0008 |
| 9 | 444.2893 | 430388 | 1283.2 | 2.8 | 0.0010 |
| 10 | 500.2932 | 385803 | 3394.9 | 7.9 | 0.0013 |
| 11 | 523.2828 | 368323 | 6016.8 | 14.4 | 0.0014 |
| 12 | 524.2863 | 370829 | 2023.1 | 4.8 | 0.0014 |
| 13 | 622.0288 | 323388 | 4850.8 | 13.2 | 0.0019 |
| 14 | 628.6139 | 313835 | 1528.8 | 4.2 | 0.0020 |
| 15 | 832.4954 | 224899 | 950.0 | 3.0 | 0.0037 |
| 16 | 922.0094 | 207869 | 20146.9 | 68.1 | 0.0044 |
| 17 | 923.0135 | 210050 | 2962.1 | 10.2 | 0.0044 |
| 18 | 1221.9905 | 159051 | 25227.1 | 100.0 | 0.0077 |
| 19 | 1222.9952 | 164655 | 6158.6 | 24.4 | 0.0074 |
| 20 | 1500.3404 | 128403 | 14904.8 | 76.9 | 0.0117 |
| 21 | 1501.3430 | 127190 | 14500.1 | 74.8 | 0.0118 |
| 22 | 1502.3383 | 135989 | 8390.5 | 43.3 | 0.0110 |
| 23 | 1502.3510 | 238215 | 2340.2 | 12.1 | 0.0063 |
| 24 | 1503.3396 | 135482 | 7307.0 | 37.7 | 0.0111 |
| 25 | 1504.3312 | 201303 | 1334.6 | 6.9 | 0.0075 |
| 26 | 1504.3432 | 156145 | 2544.8 | 13.1 | 0.0096 |
| 27 | 1505.3353 | 147313 | 1293.1 | 6.7 | 0.0102 |
| 28 | 1505.3480 | 168067 | 621.2 | 3.2 | 0.0090 |
| 29 | 1521.9715 | 125788 | 11617.2 | 59.9 | 0.0121 |
| 30 | 1522.9759 | 129514 | 3696.7 | 19.1 | 0.0118 |
| 31 | 1523.9802 | 126962 | 575.4 | 3.0 | 0.0120 |
| 32 | 1532.3328 | 130266 | 1175.2 | 6.1 | 0.0118 |
| 33 | 1533.3359 | 129103 | 1127.3 | 5.8 | 0.0119 |
| 34 | 1534.3274 | 153434 | 541.4 | 2.8 | 0.0100 |
| 35 | 1821.9525 | 107236 | 5246.3 | 23.7 | 0.0170 |
| 36 | 1822.9571 | 107529 | 1735.6 | 7.9 | 0.0170 |
| 37 | 2121.9334 | 82701 | 5516.8 | 26.8 | 0.0257 |
| 38 | 2122.9387 | 83536 | 2175.9 | 10.6 | 0.0254 |
| 39 | 2421.9253 | 77405 | 2423.7 | 11.8 | 0.0313 |
| 40 | 2422.9293 | 76932 | 1189.0 | 5.8 | 0.0315 |

| # | m/z | Res. | S/N | I % | FWHM |
|---|---|---|---|---|---|
| 1 | 1500.3394 | 128403 | | 97.3 | 0.0117 |
| 2 | 1501.3424 | 128489 | | 100.0 | 0.0117 |
| 3 | 1502.3405 | 128575 | | 99.1 | 0.0117 |
| 4 | 1503.3409 | 128660 | | 66.3 | 0.0117 |
| 5 | 1504.3310 | 128745 | | 11.0 | 0.0117 |
| 6 | 1504.3429 | 128746 | | 29.1 | 0.0117 |
| 7 | 1505.3393 | 64416 | | 20.2 | 0.0234 |
| 8 | 1506.3291 | 128916 | | 2.2 | 0.0117 |
| 9 | 1506.3409 | 128917 | | 7.0 | 0.0117 |
| 10 | 1507.3301 | 129002 | | 1.5 | 0.0117 |
| 11 | 1507.3423 | 129003 | | 2.3 | 0.0117 |
| 12 | 1508.3317 | 129087 | | 0.9 | 0.0117 |
| 13 | 1508.3449 | 129088 | | 0.5 | 0.0117 |
| 14 | 1509.3276 | 129173 | | 0.2 | 0.0117 |
| 15 | 1509.3401 | 129174 | | 0.3 | 0.0117 |

**$^1$H-,2D-NMR ($C_6D_6$, 600/151 MHz, 60 °C) and HR-MS spectra of compound** 16

$^1$H NMR spectrum of compound **16**

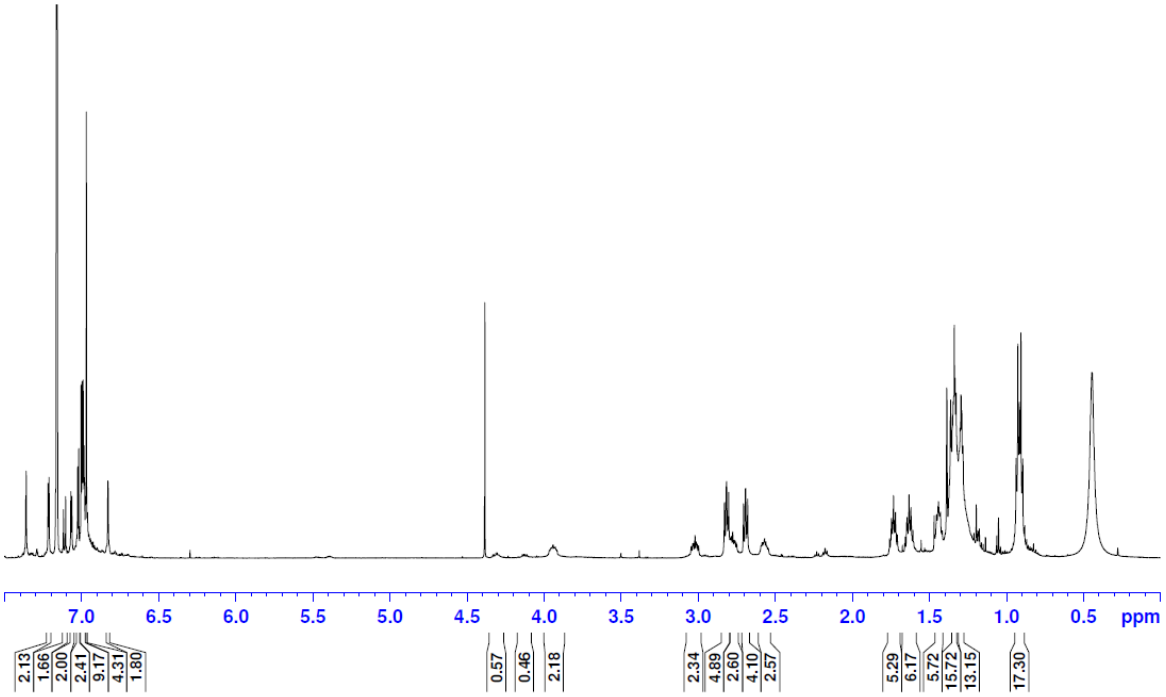


COSY spectrum of the alkyl resonances of compound **16**

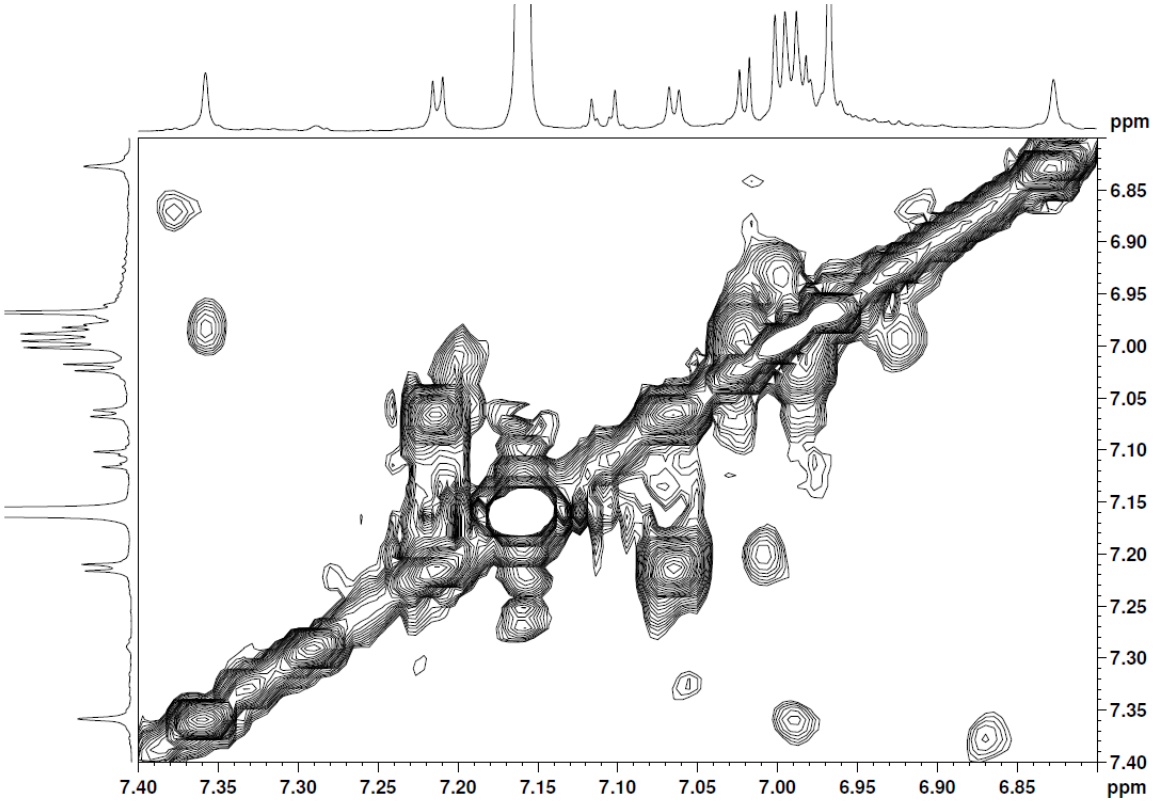


COSY spectrum of the aryl resonances of compound **16**

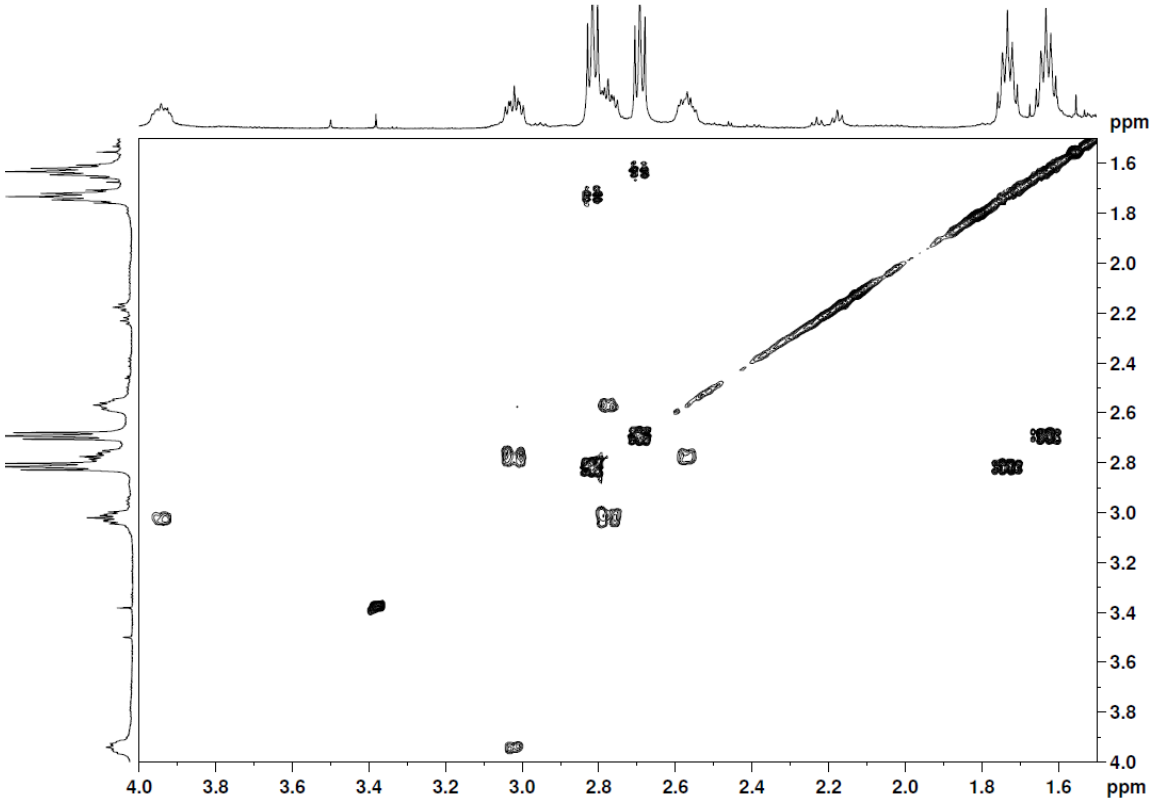


HSQC spectrum of the aryl resonances of compound **16**

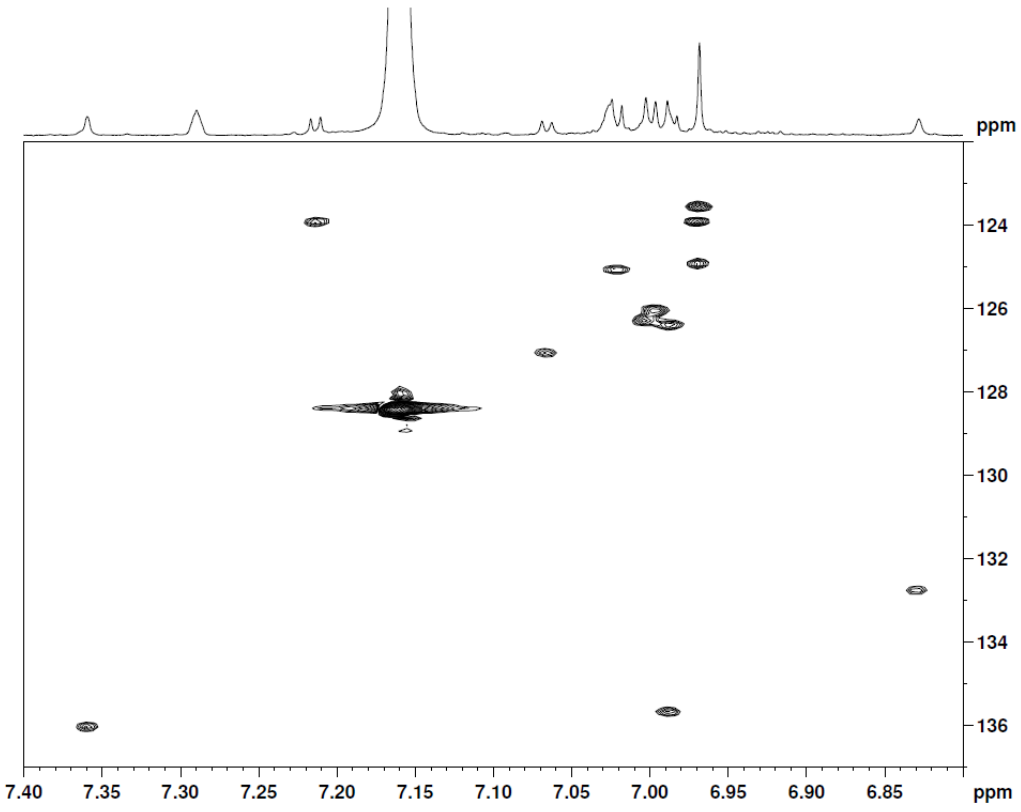

**FT13097 Kevin Weiland/Mayor - w-13 - DCM / DCTB Mix 1:10**

ETH Eidgenössische Technische Hochschule Zürich Swiss Federal Institute of Technology Zurich

**Acquisition Parameter**

| | | | | | |
|---|---|---|---|---|---|
| Method: | MALDI_MS_POS_300-2600_2M_16AvScans | | | Acquisition Date: | 08.05.2018 14:37:26 |
| File Name: | D:\ETH\Data\FT130xx\FT13097_0_B16_000001.d | | | Operator: | Louis Bertschi |
| Source | Dual (MALDI/ESI) | Polarity | Positive | Nebulizer Gas | 1.3 bar |
| Broadband Low Mass | 303.1 m/z | n/a | n/a | Drying Gas Flow Rate | 3.7 L/min |
| Broadband High Mass | 2600.0 m/z | Laser Power | 21.0 lp | Capillary | 4000.0 V |
| No. of Cell Fills | 1 | n/a | n/a | Drying Gas | 200.0 °C |
| Apodization | Full-Sine | Time of Flight to Detector | 0.002 sec | Temperature | |

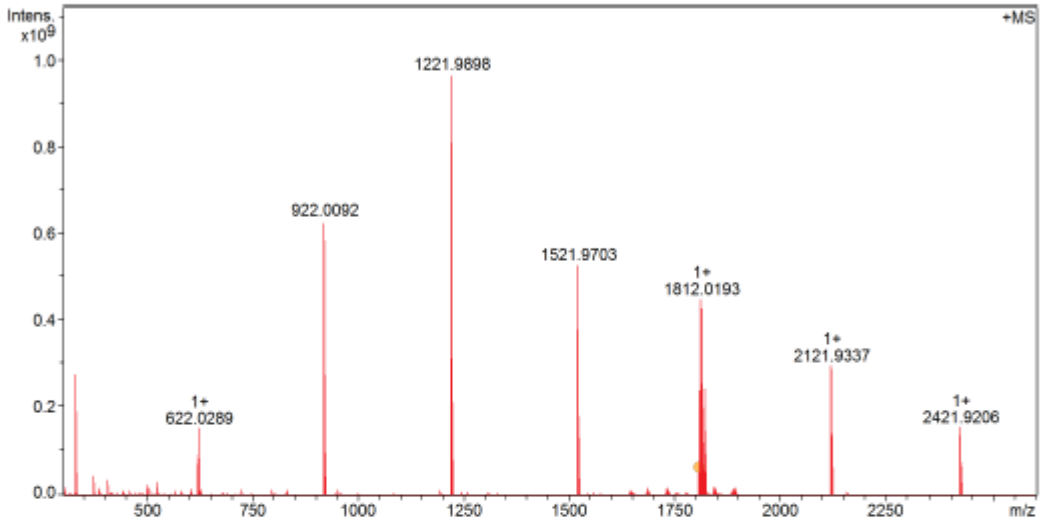


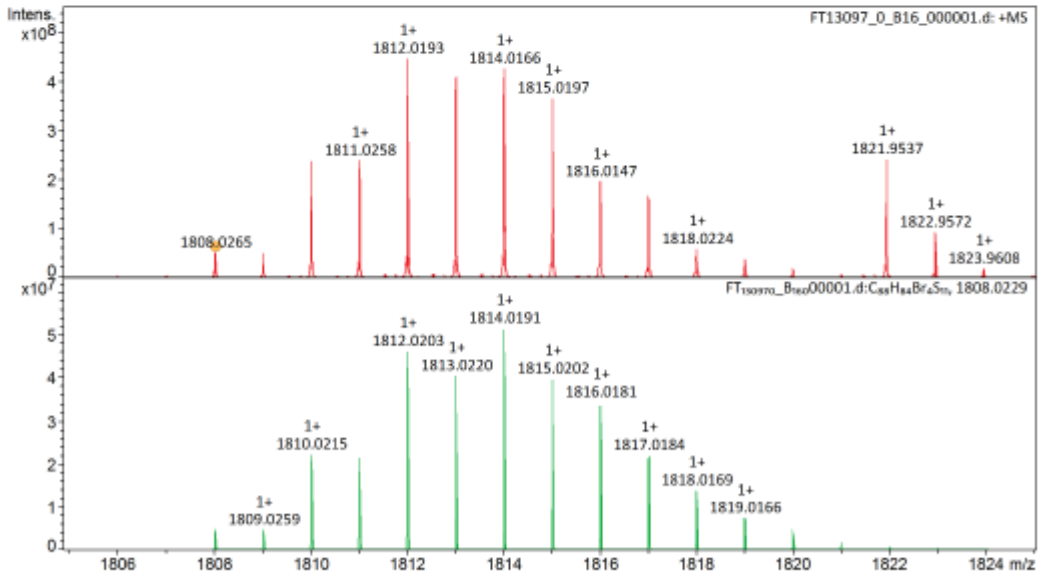

**FT13097 Kevin Weiland/Mayor - w-13 - DCM / DCTB Mix 1:10**

ETH Eidgenössische Technische Hochschule Zürich Swiss Federal Institute of Technology Zurich

**Evaluation Spectra / Validation Formula:**

| # | Ion Formula | Adduct | m/z | z | Meas. m/z | mSigma | N-Rule | err [mDa] | err [ppm] |
|---|---|---|---|---|---|---|---|---|---|
| 1 | C88H84Br4S11 | M | 1808.0229 | 1+ | 1808.0265 | 101.0 | ok | -3.6 | -2.0 |

**Calibration Info:**

Date: 08.05.2018 16:01:32
Polarity: Positive
Calibration spectrum: +MS: Scan
Reference mass list: MALDI: DCTB Matrix + HP-Mix (pos)
Calibration mode: Quadratic

| Reference m/z | Resulting m/z | Intensity | Error [ppm] |
|---|---|---|---|
| 118.0863 | | | |
| 250.1464 | | | |
| 251.1543 | | | |
| 273.1362 | | | |
| 322.0481 | | | |
| 332.2009 | | | |
| 500.2934 | | | |
| 501.3013 | | | |
| 523.2832 | | | |
| 622.0290 | 622.0289 | 150140240 | -0.176 |
| 750.4404 | | | |
| 751.4483 | 751.4486 | 2963159 | 0.470 |
| 773.4302 | | | |
| 922.0098 | 922.0092 | 630761536 | -0.619 |
| 1000.5874 | | | |
| 1001.5953 | 1001.5961 | 2311518 | 0.857 |
| 1023.5772 | | | |
| 1221.9906 | 1221.9898 | 967268032 | -0.674 |
| 1521.9715 | 1521.9703 | 527858976 | -0.781 |
| 1821.9523 | 1821.9537 | 243721840 | 0.743 |
| 2121.9332 | 2121.9337 | 295324320 | 0.277 |
| 2421.9140 | | | |
| 2721.8948 | | | |

Standard deviation: 0.811

**Mass List:**

| # | m/z | Res. | S/N | I % | FWHM |
|---|---|---|---|---|---|
| 1 | 332.1993 | 304860 | 2168.9 | 5.6 | 0.0011 |
| 2 | 332.2007 | 591681 | 11123.7 | 28.6 | 0.0006 |
| 3 | 333.2042 | 572504 | 2567.3 | 6.6 | 0.0006 |
| 4 | 374.2114 | 523565 | 1810.5 | 4.7 | 0.0007 |
| 5 | 622.0289 | 309071 | 4681.4 | 15.5 | 0.0020 |
| 6 | 922.0045 | 181078 | 1735.5 | 6.9 | 0.0051 |
| 7 | 922.0092 | 199769 | 16416.7 | 65.2 | 0.0046 |
| 8 | 923.0131 | 204450 | 2598.1 | 10.5 | 0.0045 |
| 9 | 1221.9898 | 155777 | 20965.7 | 100.0 | 0.0078 |
| 10 | 1222.9944 | 162600 | 5603.7 | 26.7 | 0.0075 |
| 11 | 1521.9564 | 115397 | 1130.7 | 6.2 | 0.0132 |
| 12 | 1521.9703 | 125575 | 9967.4 | 54.6 | 0.0121 |
| 13 | 1522.9750 | 129223 | 3364.1 | 18.4 | 0.0118 |
| 14 | 1808.0265 | 109300 | 733.6 | 5.3 | 0.0165 |
| 15 | 1809.0297 | 109436 | 712.5 | 5.2 | 0.0165 |
| 16 | 1810.0226 | 113253 | 3421.5 | 24.7 | 0.0160 |
| 17 | 1811.0258 | 111241 | 3449.6 | 24.9 | 0.0163 |
| 18 | 1811.9912 | 116947 | 635.4 | 4.6 | 0.0155 |
| 19 | 1812.0000 | 233892 | 644.0 | 4.7 | 0.0077 |
| 20 | 1812.0193 | 112490 | 6420.2 | 46.3 | 0.0161 |
| 21 | 1812.0361 | 154360 | 1104.1 | 8.0 | 0.0117 |
| 22 | 1813.0026 | 286084 | 588.8 | 4.3 | 0.0063 |
| 23 | 1813.0225 | 109765 | 5986.1 | 43.2 | 0.0165 |
| 24 | 1813.9882 | 116818 | 593.5 | 4.3 | 0.0155 |
| 25 | 1813.9981 | 350453 | 639.8 | 4.6 | 0.0052 |
| 26 | 1814.0166 | 113908 | 6129.9 | 44.2 | 0.0159 |
| 27 | 1814.0328 | 122502 | 1446.3 | 10.4 | 0.0148 |
| 28 | 1815.0197 | 110287 | 5271.2 | 38.0 | 0.0165 |
| 29 | 1816.0147 | 86687 | 2814.3 | 20.3 | 0.0209 |
| 30 | 1817.0170 | 112823 | 2322.8 | 16.8 | 0.0161 |
| 31 | 1818.0091 | 118946 | 597.1 | 4.3 | 0.0153 |
| 32 | 1818.0224 | 95859 | 840.9 | 6.1 | 0.0190 |
| 33 | 1819.0132 | 109786 | 531.8 | 3.8 | 0.0166 |
| 34 | 1821.9537 | 108963 | 3491.9 | 25.2 | 0.0167 |
| 35 | 1822.9572 | 111035 | 1333.9 | 9.6 | 0.0164 |
| 36 | 2121.9337 | 84594 | 4615.6 | 30.5 | 0.0251 |
| 37 | 2122.9381 | 87998 | 2142.3 | 14.2 | 0.0241 |
| 38 | 2123.9420 | 90173 | 547.0 | 3.6 | 0.0236 |
| 39 | 2421.9206 | 79565 | 2416.5 | 15.8 | 0.0304 |
| 40 | 2422.9239 | 79220 | 1217.2 | 8.0 | 0.0306 |

| # | m/z | Res. | S/N | I % | FWHM |
|---|---|---|---|---|---|
| 1 | 1808.0229 | 109299 | | 8.8 | 0.0165 |
| 2 | 1809.0259 | 109360 | | 9.3 | 0.0165 |
| 3 | 1810.0215 | 109420 | | 43.6 | 0.0165 |
| 4 | 1811.0240 | 109481 | | 42.3 | 0.0165 |
| 5 | 1812.0203 | 54771 | | 89.6 | 0.0331 |
| 6 | 1813.0220 | 109602 | | 78.5 | 0.0165 |
| 7 | 1814.0191 | 54831 | | 100.0 | 0.0331 |
| 8 | 1815.0202 | 54861 | | 76.9 | 0.0331 |
| 9 | 1816.0181 | 54891 | | 66.4 | 0.0331 |
| 10 | 1817.0184 | 54922 | | 43.2 | 0.0331 |
| 11 | 1818.0169 | 54952 | | 27.4 | 0.0331 |
| 12 | 1819.0166 | 54982 | | 14.7 | 0.0331 |
| 13 | 1820.0154 | 110024 | | 7.3 | 0.0165 |
| 14 | 1821.0148 | 55042 | | 3.3 | 0.0331 |
| 15 | 1822.0137 | 110145 | | 1.3 | 0.0165 |

**FT13097 Kevin Weiland/Mayor - w-13 - DCM / DCTB Mix 1:10**

ETH
Eidgenössische Technische Hochschule Zürich
Swiss Federal Institute of Technology Zurich

| # | m/z | Res. | S/N | I % | FWHM |
|---|---|---|---|---|---|
| 16 | 1823.0130 | 110206 | | 0.5 | 0.0165 |
| 17 | 1824.0125 | 110266 | | 0.2 | 0.0165 |

## $^1$H-, 2D-NMR ($C_6D_6$, 600/151 MHz, 25 °C) and HR-MS spectra of compound **1**

$^1$H NMR spectrum of compound **1**

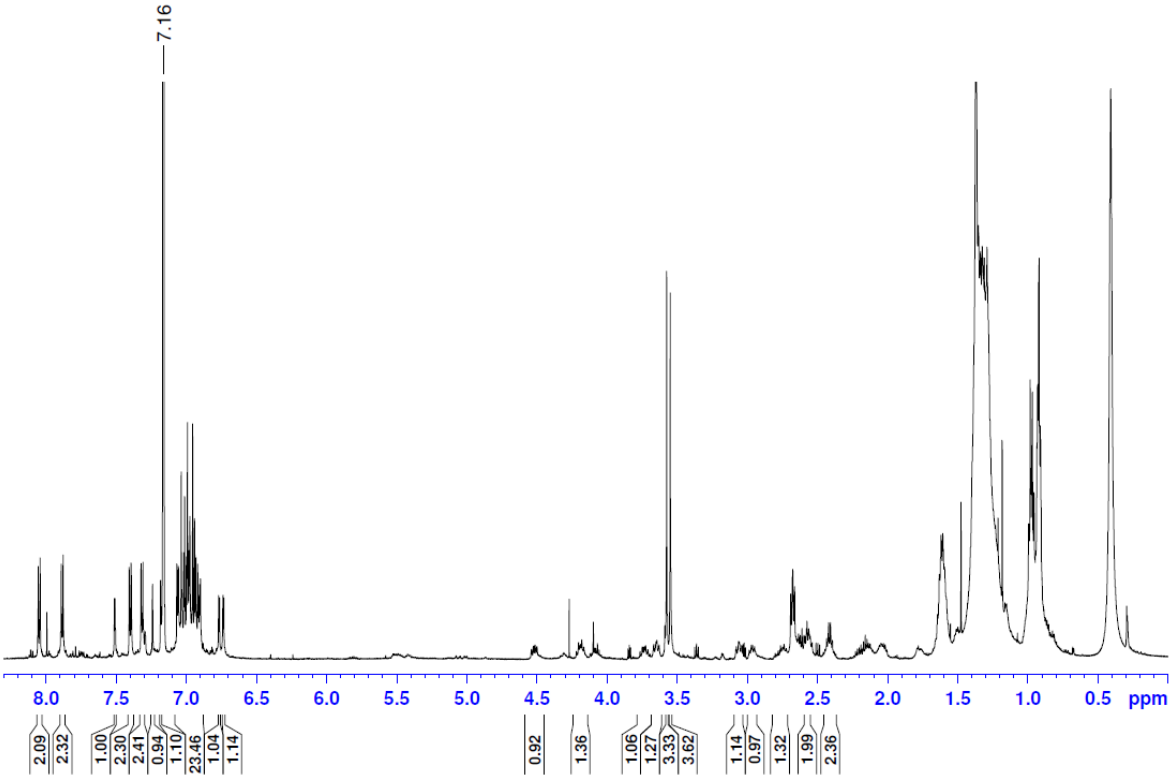


COSY spectrum of the alkyl resonances of compound **1**

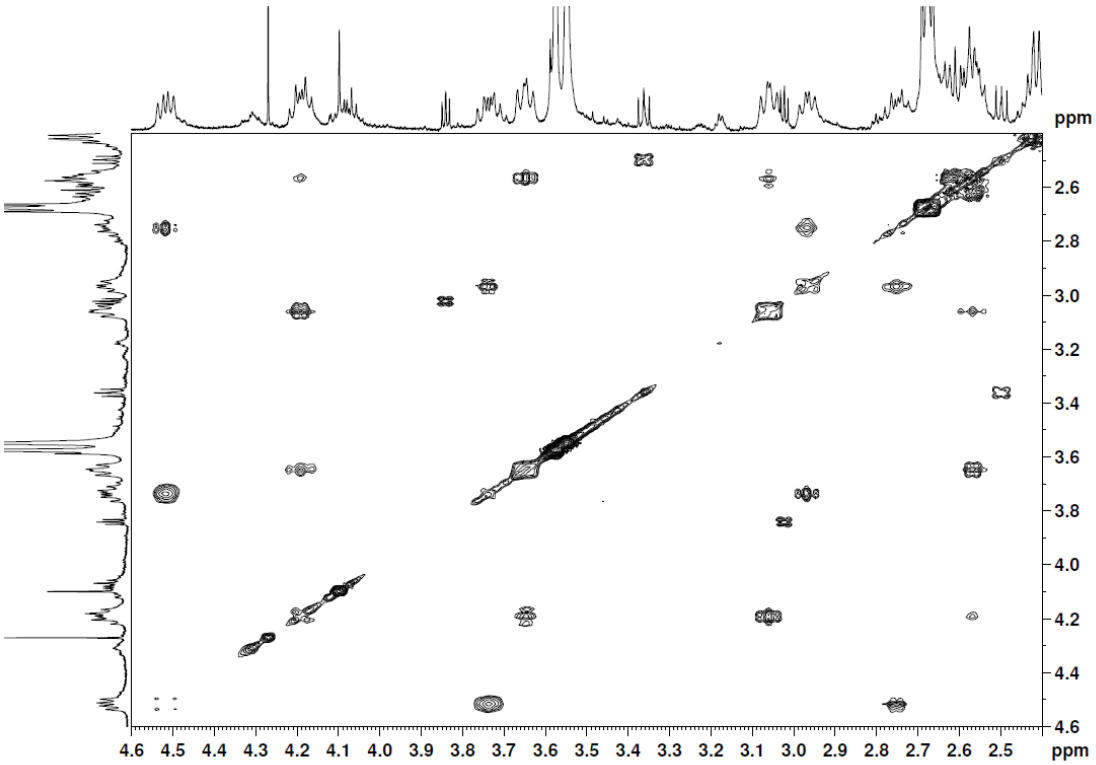

COSY spectrum of the aryl resonances of compound **1**

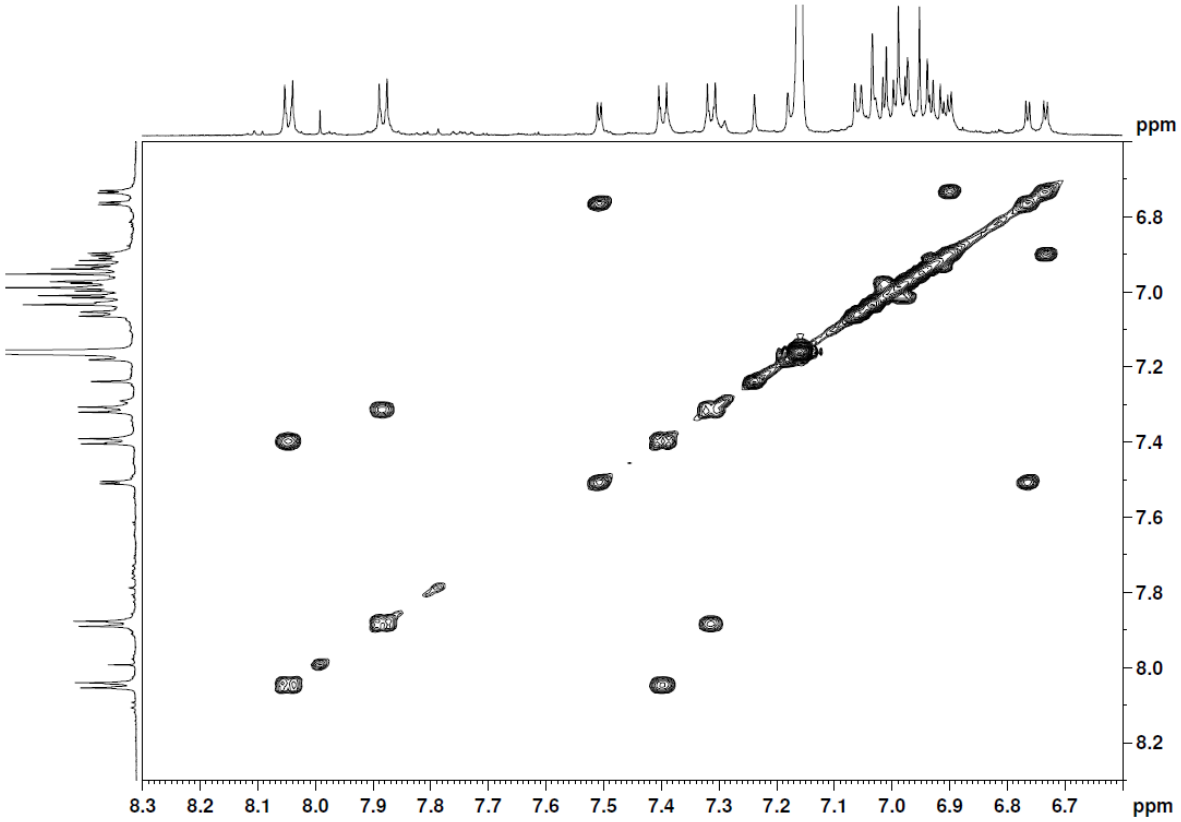


HSQC spectrum of the aryl resonances of compound **1**

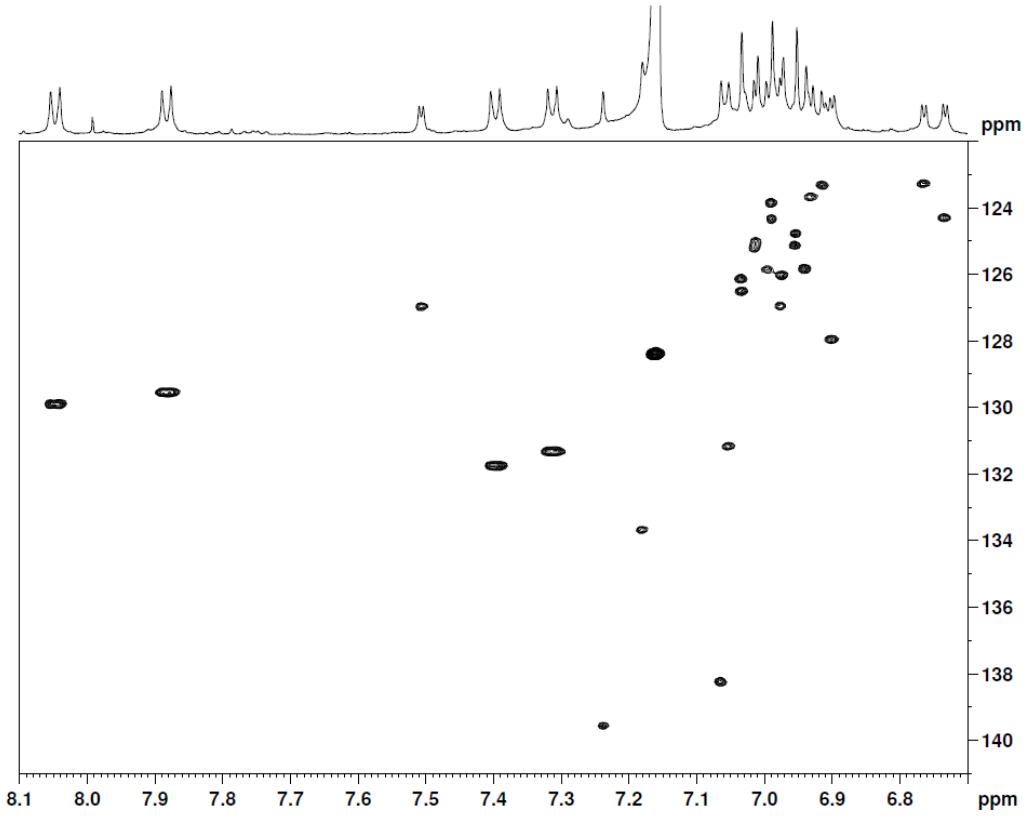

$^{1}$H-$^{1}$H NOESY spectrum of compound **1**

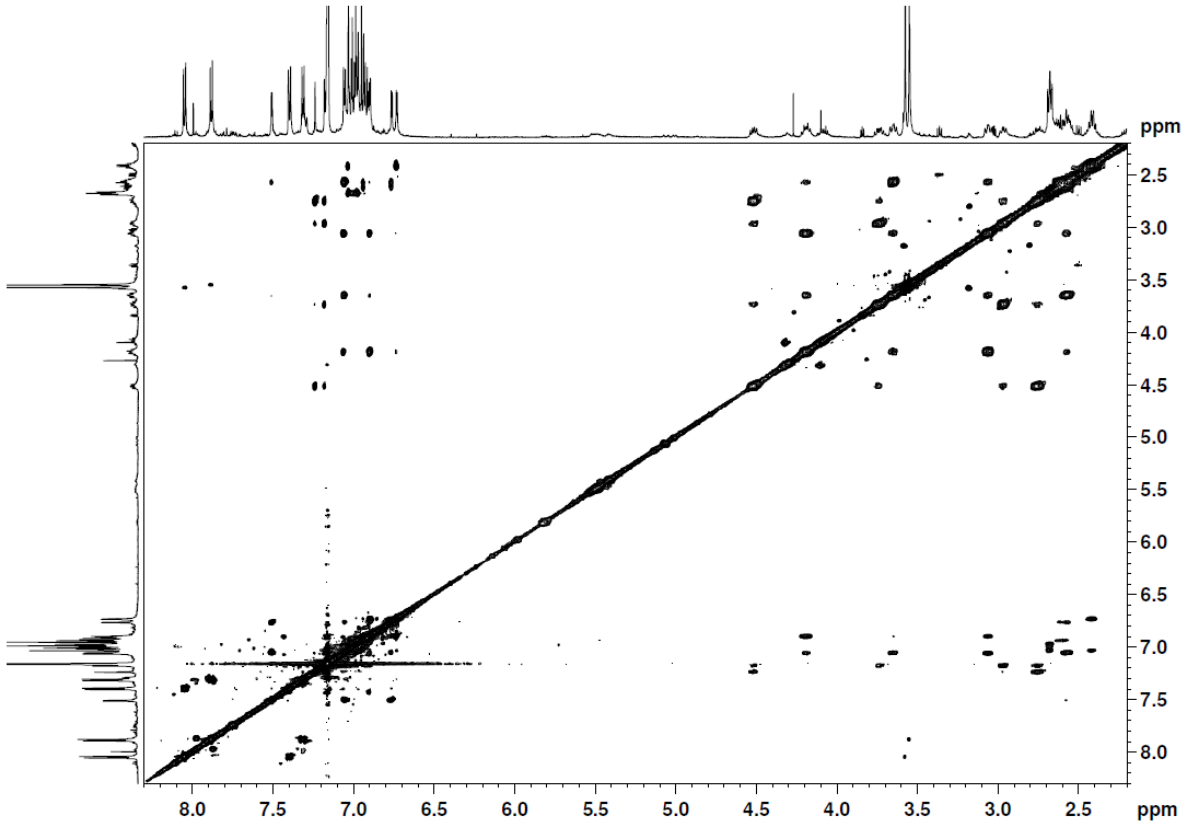

**FT13096 Kevin Weiland/Mayor - w-ME - DCM / DCTB Mix 1:10**

ETH Eidgenössische Technische Hochschule Zürich Swiss Federal Institute of Technology Zurich

**Acquisition Parameter**

| | | | | | |
|---|---|---|---|---|---|
| Method: | MALDI_MS_POS_300-2600_2M_16AvScans | | | Acquisition Date: | 08.05.2018 14:36:01 |
| File Name: | D:\ETH\Data\FT130xx\FT13096_0_B14_000001.d | | | Operator: | Louis Bertschi |
| Source | Dual (MALDI/ESI) | Polarity | Positive | Nebulizer Gas | 1.3 bar |
| Broadband Low Mass | 303.1 m/z | n/a | n/a | Drying Gas Flow Rate | 3.7 L/min |
| Broadband High Mass | 2600.0 m/z | Laser Power | 23.4 lp | Capillary | 4000.0 V |
| No. of Cell Fills | 1 | n/a | n/a | Drying Gas | 200.0 °C |
| Apodization | Full-Sine | Time of Flight to Detector | 0.002 sec | Temperature | |

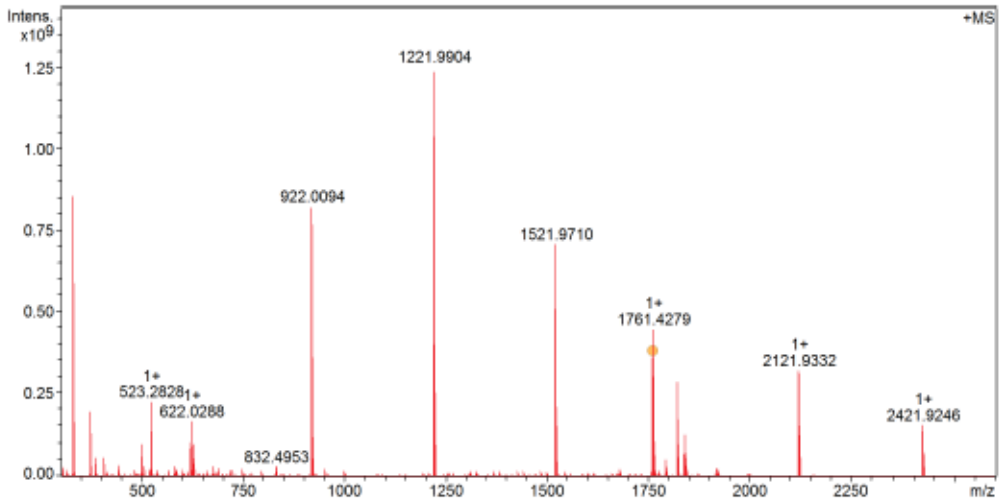


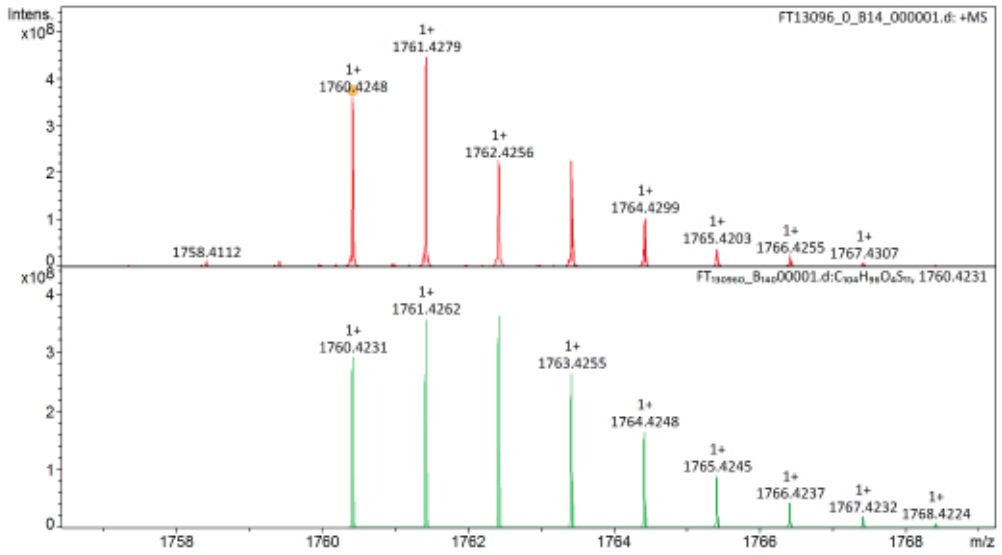

**FT13096 Kevin Weiland/Mayor - w-ME - DCM / DCTB Mix 1:10**

ETH Eidgenössische Technische Hochschule Zürich Swiss Federal Institute of Technology Zurich

**Evaluation Spectra / Validation Formula:**

| # | Ion Formula | Adduct | m/z | z | Meas. m/z | mSigma | N-Rule | err [mDa] | err [ppm] |
|---|---|---|---|---|---|---|---|---|---|
| 1 | C104H96O4S11 | M | 1760.4231 | 1+ | 1760.4248 | 206.5 | ok | -1.7 | -0.9 |

**Calibration Info:**

Date: 08.05.2018 16:00:19
Polarity: Positive
Calibration spectrum: +MS: Scan
Reference mass list: MALDI: DCTB Matrix + HP-Mix (pos)
Calibration mode: Quadratic

| Reference m/z | Resulting m/z | Intensity | Error [ppm] |
|---|---|---|---|
| 118.0863 | | | |
| 250.1464 | | | |
| 251.1543 | | | |
| 273.1362 | | | |
| 322.0481 | | | |
| 332.2009 | | | |
| 500.2934 | | | |
| 501.3013 | | | |
| 523.2832 | | | |
| 622.0290 | 622.0288 | 164536480 | -0.191 |
| 750.4404 | | | |
| 751.4483 | 751.4487 | 14035381 | 0.588 |
| 773.4302 | | | |
| 922.0098 | 922.0094 | 823344128 | -0.391 |
| 1000.5874 | | | |
| 1001.5953 | | | |
| 1023.5772 | | | |
| 1221.9906 | 1221.9904 | 1252224000 | -0.169 |
| 1521.9715 | 1521.9710 | 708022016 | -0.310 |
| 1821.9523 | 1821.9533 | 282717280 | 0.520 |
| 2121.9332 | 2121.9332 | 320923072 | 0.010 |
| 2421.9140 | | | |
| 2721.8948 | | | |

Standard deviation: 0.502

**Mass List:**

| # | m/z | Res. | S/N | I % | FWHM |
|---|---|---|---|---|---|
| 1 | 332.1989 | 534066 | 5925.5 | 11.9 | 0.0006 |
| 2 | 332.1999 | 602430 | 34251.6 | 68.9 | 0.0006 |
| 3 | 333.2035 | 570461 | 8032.1 | 16.2 | 0.0006 |
| 4 | 374.2091 | 340984 | 1566.6 | 3.2 | 0.0011 |
| 5 | 374.2107 | 499169 | 7681.8 | 15.5 | 0.0007 |
| 6 | 375.2143 | 507680 | 1601.9 | 3.2 | 0.0007 |
| 7 | 386.2837 | 473921 | 2263.6 | 4.6 | 0.0008 |
| 8 | 500.2931 | 383231 | 3294.7 | 7.9 | 0.0013 |
| 9 | 523.2828 | 369410 | 7262.6 | 17.9 | 0.0014 |
| 10 | 524.2863 | 372479 | 2363.8 | 5.8 | 0.0014 |
| 11 | 622.0288 | 322419 | 4640.1 | 13.1 | 0.0019 |
| 12 | 628.6139 | 314670 | 2780.4 | 7.9 | 0.0020 |
| 13 | 629.6173 | 307956 | 1077.6 | 3.1 | 0.0020 |
| 14 | 922.0094 | 207588 | 18983.4 | 65.8 | 0.0044 |
| 15 | 923.0135 | 208861 | 2746.8 | 9.7 | 0.0044 |
| 16 | 1221.9904 | 158859 | 24317.2 | 100.0 | 0.0077 |
| 17 | 1222.9952 | 165137 | 6085.0 | 25.0 | 0.0074 |
| 18 | 1521.9710 | 125626 | 12701.8 | 56.5 | 0.0121 |
| 19 | 1522.9758 | 130198 | 3730.7 | 16.6 | 0.0117 |
| 20 | 1760.4248 | 111665 | 4419.9 | 28.9 | 0.0158 |
| 21 | 1761.4279 | 110871 | 5459.8 | 35.7 | 0.0159 |
| 22 | 1762.4256 | 80889 | 2723.3 | 17.8 | 0.0218 |
| 23 | 1763.4250 | 124073 | 2769.9 | 18.1 | 0.0142 |
| 24 | 1764.4299 | 130636 | 1272.5 | 8.3 | 0.0135 |
| 25 | 1765.4203 | 139019 | 473.3 | 3.1 | 0.0127 |
| 26 | 1792.4163 | 112807 | 562.6 | 3.4 | 0.0159 |
| 27 | 1793.4196 | 111899 | 696.0 | 4.2 | 0.0160 |
| 28 | 1821.9533 | 106834 | 3723.2 | 22.6 | 0.0171 |
| 29 | 1822.9578 | 108982 | 1309.9 | 8.0 | 0.0167 |
| 30 | 1838.3382 | 107838 | 898.7 | 5.5 | 0.0170 |
| 31 | 1839.3416 | 107032 | 1069.9 | 6.5 | 0.0172 |
| 32 | 1840.3349 | 102238 | 1343.8 | 8.2 | 0.0180 |
| 33 | 1841.3384 | 106542 | 1605.6 | 9.7 | 0.0173 |
| 34 | 1842.3305 | 97940 | 500.6 | 3.0 | 0.0188 |
| 35 | 1842.3438 | 86430 | 745.8 | 4.5 | 0.0213 |
| 36 | 1843.3341 | 103883 | 581.5 | 3.5 | 0.0177 |
| 37 | 2121.9332 | 82618 | 4979.1 | 25.6 | 0.0257 |
| 38 | 2122.9378 | 80534 | 1941.3 | 10.0 | 0.0264 |
| 39 | 2421.9246 | 78630 | 2417.7 | 12.2 | 0.0308 |
| 40 | 2422.9284 | 77571 | 1209.2 | 6.1 | 0.0312 |

| # | m/z | Res. | S/N | I % | FWHM |
|---|---|---|---|---|---|
| 1 | 1760.4231 | 111665 | | 80.4 | 0.0158 |
| 2 | 1761.4262 | 111729 | | 98.5 | 0.0158 |
| 3 | 1762.4252 | 111792 | | 100.0 | 0.0158 |
| 4 | 1763.4255 | 111855 | | 72.9 | 0.0158 |
| 5 | 1764.4248 | 111919 | | 45.9 | 0.0158 |
| 6 | 1765.4245 | 111982 | | 24.6 | 0.0158 |
| 7 | 1766.4237 | 112046 | | 11.8 | 0.0158 |
| 8 | 1767.4232 | 112109 | | 5.1 | 0.0158 |
| 9 | 1768.4224 | 56086 | | 2.0 | 0.0315 |
| 10 | 1769.4220 | 112236 | | 0.7 | 0.0158 |
| 11 | 1770.4220 | 112299 | | 0.2 | 0.0158 |

## Size mismatch calculation

The difference in size between the ethynyl methyl benzoates and the diameter of the oligothiophenic macrocycle can be measured from geometry of (*P*)-**1** optimized by B3LYP/6-31G(d) method (see the Quantum Chemical Calculations section below). To ease to computational costs, the hexyl chains were replaced with methyl groups. The inner diameter of the macrocyclic ring is 13.485 Å, while the distance between the carbonyl oxygen atoms of the two methyl carboxylates is 21.133 Å. A representative schematic picture of the molecule is displayed in Figure S1 with the distances illustrated with green lines.

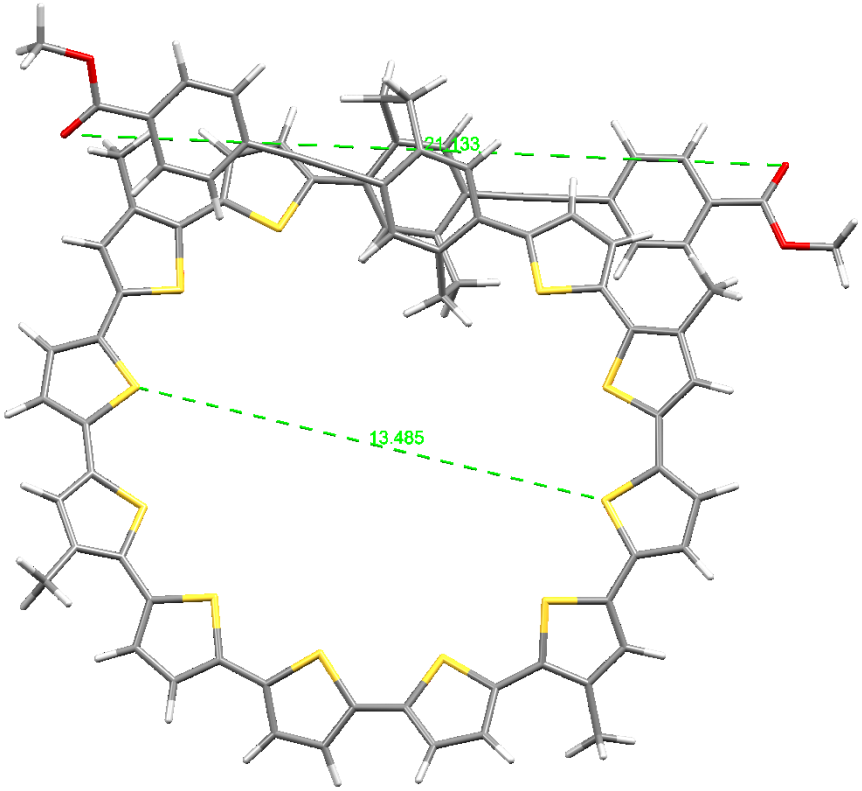


***Figure S1.*** Optimized geometry (B3LYP) for (*P*)-**1** where the hexyl chains are replaced with methyl groups.

## Dynamic HPLC elution profiles and thermodynamical analysis

Elution profiles for the dynamic HPLC experiment (ChiralpakIG, eluent ethyl acetate/*n*-hexane 2:3, 1.0 mLmin$^{-1}$, column oven: T = 18 °C). All experiments were repeated three times at each temperature, only one representative example is shown. The elution profiles were analyzed at $\lambda$ = 409 nm, where macrocycle **2** has its maximum absorption. The elution profile at 55 °C was not taken into consideration for data analysis with DCXplorer and was only used in dHPLC Y2K.

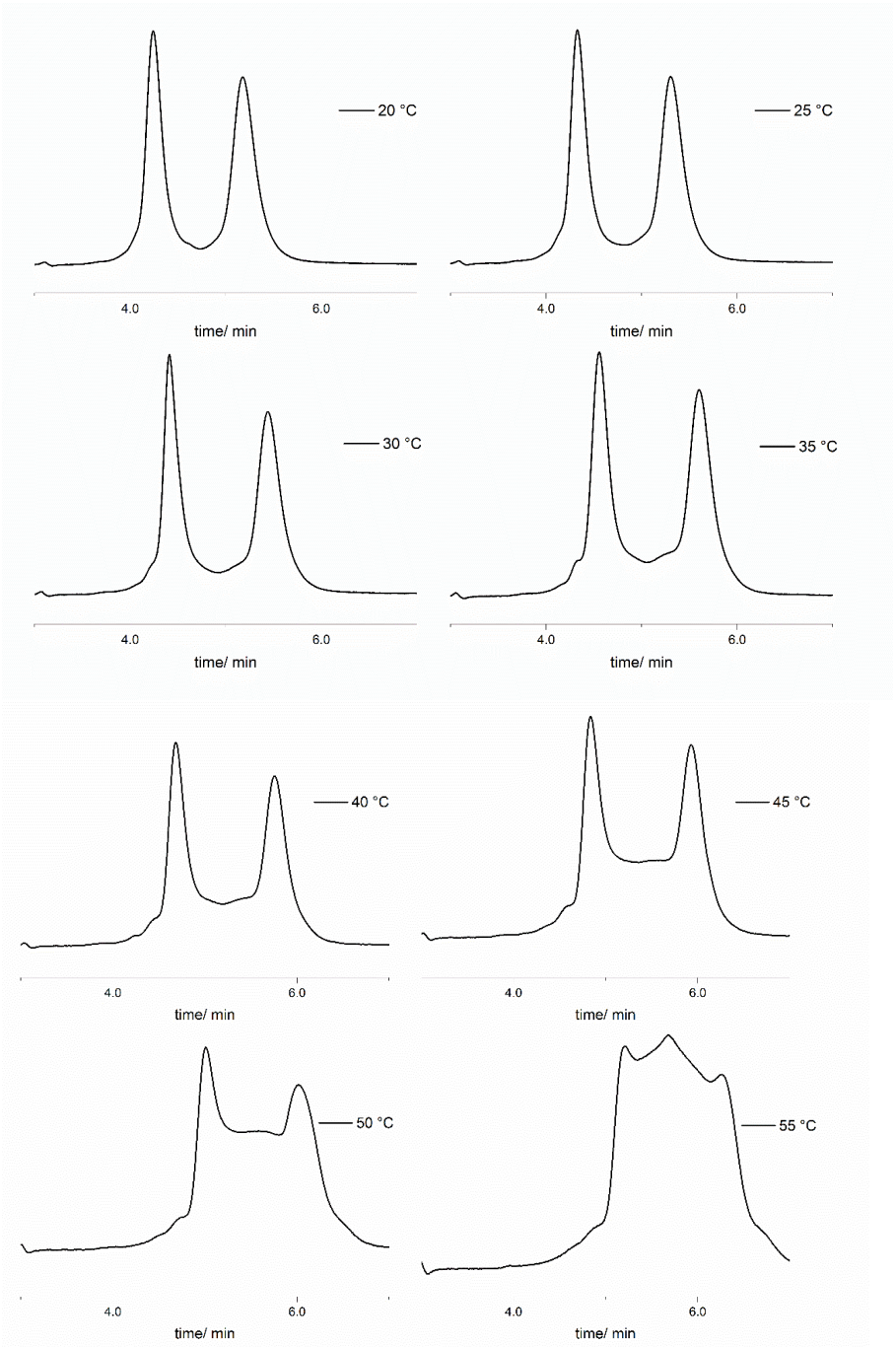


***Figure S2.*** Representative elution profiles obtained from the dynamic HPLC experiment at a temperature range from 20 – 55 °C.

## Data evaluation with DCXplorer

The rate constants are obtained directly from the parameters given, via the software DCXplorer by Trapp and coworkers and are shown in the following table, together with the key parameters that are used for the determination.

***Table S1.*** Obtained data from DCXplorer.

| | tR1 [min] | tR2 [min] | wh1 [s] | wh2 [s] | h1 [%] | hp [%] | h2 [%] | A1 | A2 | k1 [1/s] |
|---|---|---|---|---|---|---|---|---|---|---|
| **20 °C column** | | | | | | | | | | |
| First Elution | 4.241 | 5.179 | 10.1 | 17.6 | 100 | 6.75 | 80.28 | 46.61 | 53.39 | **6.13E-04** |
| Second Elution | 4.24 | 5.175 | 9.9 | 17.8 | 100 | 6.81 | 80.29 | 46.12 | 53.88 | **6.19E-04** |
| Third Elution | 4.24 | 5.176 | 9.9 | 17.8 | 100 | 6.79 | 80.37 | 46.7 | 53.3 | **6.26E-04** |
| k1 with error | | | | | | | | | | **6.19± 0.07E-04** |
| **25 °C column** | | | | | | | | | | |
| First Elution | 4.328 | 5.304 | 9.9 | 17.6 | 100 | 7.89 | 80 | 47.37 | 52.63 | **7.49E-04** |
| Second Elution | 4.328 | 5.303 | 9.9 | 17.4 | 100 | 7.64 | 79.86 | 48.24 | 51.76 | **7.39E-04** |
| Third Elution | 4.335 | 5.308 | 9.9 | 17.4 | 100 | 7.65 | 80.26 | 46.36 | 53.64 | **7.10E-04** |
| k1 with error | | | | | | | | | | **7.27± 0.22E-04** |
| **30 °C column** | | | | | | | | | | |
| First Elution | 4.411 | 5.443 | 8.3 | 17.3 | 100 | 9.04 | 76.13 | 47.97 | 52.03 | **1.04E-03** |
| Second Elution | 4.415 | 5.444 | 8.2 | 17.8 | 100 | 9.25 | 76.49 | 47.3 | 52.7 | **1.06E-03** |
| Third Elution | 4.425 | 5.455 | 8.2 | 17.6 | 100 | 9.2 | 76.23 | 47.74 | 52.26 | **1.06E-03** |
| k1 with error | | | | | | | | | | **1.05± 0.01E-03** |
| **35 °C column** | | | | | | | | | | |
| First Elution | 4.557 | 5.601 | 11 | 17.6 | 100 | 13.95 | 84.59 | 48.19 | 51.81 | **1.19E-03** |
| Second Elution | 4.556 | 5.6 | 10.9 | 17.6 | 100 | 13.95 | 84.22 | 48.2 | 51.8 | **1.21E-03** |
| Third Elution | 4.556 | 5.6 | 10.7 | 17.6 | 100 | 13.84 | 83.81 | 48.26 | 51.74 | **1.21E-03** |
| k1 with error | | | | | | | | | | **1.20± 0.01E-03** |
| **40 °C column** | | | | | | | | | | |

| | | | | | | | | | | |
|---|---|---|---|---|---|---|---|---|---|---|
| First Elution | 4.684 | 5.757 | 10.9 | 17.8 | 100 | 20.78 | 83.43 | 48.81 | 51.19 | **1.74E-03** |
| Second Elution | 4.684 | 5.756 | 10.9 | 17.6 | 100 | 20.84 | 83.62 | 48.45 | 51.55 | **1.73E-03** |
| Third Elution | 4.687 | 5.76 | 10.7 | 17.4 | 100 | 20.81 | 83.42 | 48.29 | 51.71 | **1.74E-03** |
| k1 with error | | | | | | | | | | **1.74± 0.01E-03** |
| **45 °C column** | | | | | | | | | | |
| First Elution | 4.837 | 5.929 | 11.4 | 17.9 | 100 | 34.16 | 87.24 | 49.13 | 50.87 | **2.55E-03** |
| Second Elution | 4.836 | 5.927 | 11.4 | 17.9 | 100 | 34.24 | 87.31 | 48.73 | 51.27 | **2.54E-03** |
| Third Elution | 4.836 | 5.927 | 11.4 | 17.9 | 100 | 34.24 | 87.31 | 48.73 | 51.27 | **2.54E-03** |
| k1 with error | | | | | | | | | | **2.54± 0.01E-03** |
| **50 °C column** | | | | | | | | | | |
| First Elution | 5.009 | 6.015 | 12.5 | 28.8 | 100 | 58.25 | 81.36 | 47.18 | 52.82 | **3.26E-03** |
| Second Elution | 5.011 | 6.015 | 12.5 | 28.6 | 100 | 58.78 | 81.14 | 47.2 | 52.8 | **3.29E-03** |
| Third Elution | 5.009 | 6.016 | 12.6 | 27.8 | 100 | 58.78 | 81.32 | 47.64 | 52.36 | **3.31E-03** |
| k1 with error | | | | | | | | | | **3.29± 0.03E-03** |

Through the Eyring equation, the Gibbs free energy of racemization can be calculated at 25 °C directly from the obtained elution profile:

$$\Delta G^{\ddagger}_{298} = RT\left[ln\left(\frac{k_B T}{h}\right) - ln(k_e)\right] \quad (1)$$

$$= 8.31 \cdot 10^{-3} \cdot 298 \left[ln\left(\frac{1.38 \cdot 10^{-23} \cdot 298}{6.63 \cdot 10^{-34}}\right) - \ln\left(7.27 \cdot 10^{-4}\right)\right] = 90.84 \pm 0.07\ kJ\ mol^{-1}$$

Plotting $ln(k_{eT}/T)$ against 1/*T* for all obtained elution profiles and linear regression of the obtained graph (y = ax + b) gives access to the full thermodynamic analysis.

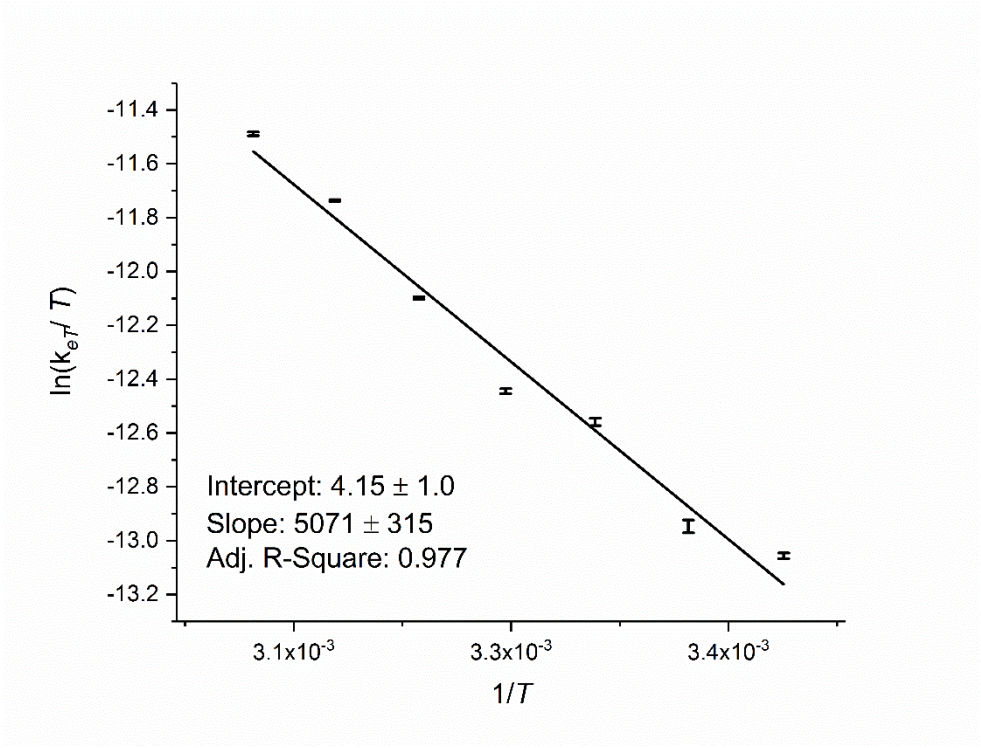


***Figure S3.*** Eyring plot of ln($k_{eT}$/*T*) against 1/*T* with linear regression (y=ax + b).

From this, the entropy and enthalpy of the enantiomerization process can be calculated through:

$$\Delta H_e^{\ddagger} = -aR = -(-5071 \cdot 8.31 \cdot 10^{-3}) = 42.14 \pm 2.57\ kJ\ mol^{-1} \quad (2)$$

$$\Delta S_e^{\ddagger} = R\left[b - \left(\frac{k_B}{h}\right)\right] = 8.31 \cdot (4.15 - 23.8) = -163.3 \pm 8.3\ J\ mol^{-1}K^{-1} \quad (3)$$

From the obtained values, the Gibbs free activation energy can be calculated for every temperature. To validate the data, the activation energy at 25 °C (298 K) is again calculated from the data obtained through the full thermodynamical analysis.

$$\Delta G_{e298}^{\ddagger} = \Delta H_e^{\ddagger} - T\Delta S_e^{\ddagger} = 42.14 - (-0.163 \cdot 298) = 90.80\ kJ\ mol^{-1} \quad (4)$$

The value obtained directly from $k_{e298\ K}$ is in good agreement with the value obtained from the full thermodynamical analysis with $\Delta\Delta G_{e298\ K}^{\ddagger}$ = 0.04 kJ mol$^{-1}$.

**Data evaluation with dHPLC Y2K**

The calculations with the software dHPLC Y2K, relying on the stochastic model implemented in the software were performed by Marco Pierini (University of Rome, Italy).[4]

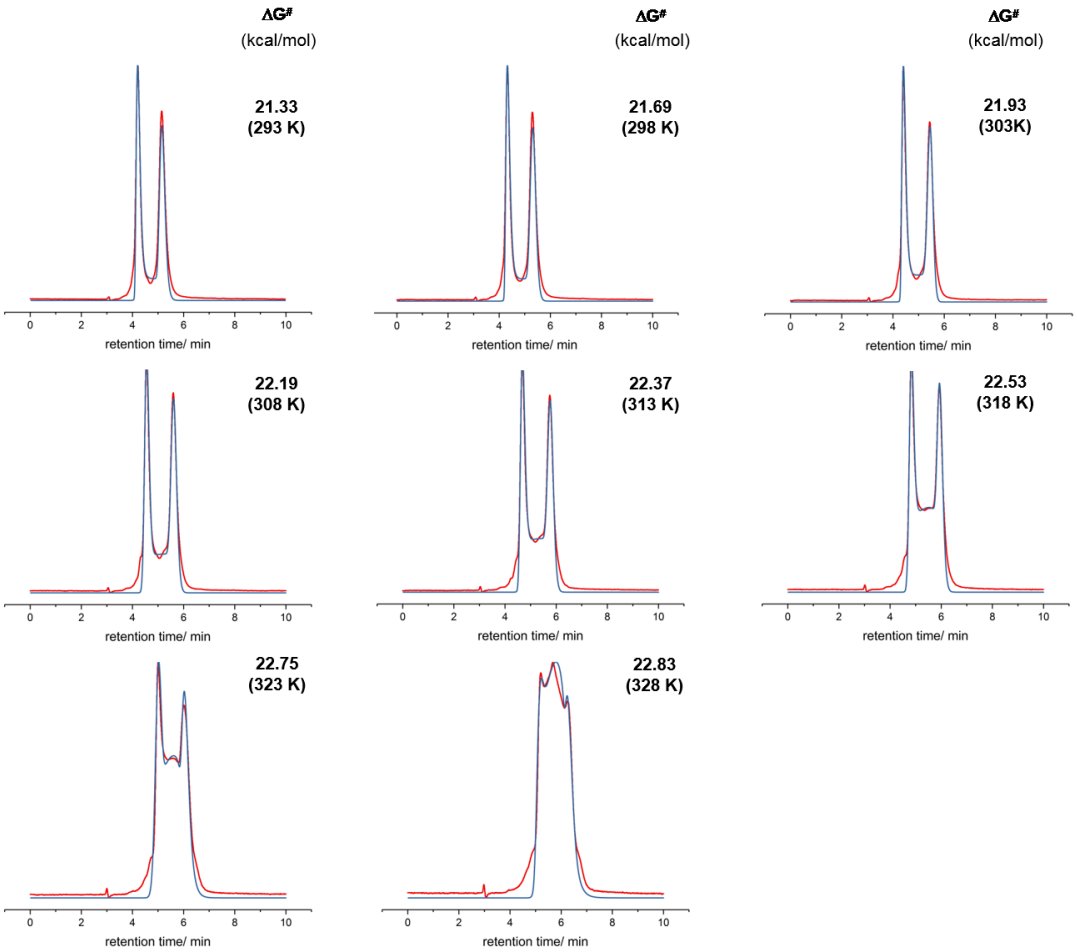


***Figure S4.*** Representative elution profiles and simulated data from the software dHPLC Y2K. Measured elution profiles (red), simulated elution profiles (blue).

The obtained values for the free energy of enantiomerization were subjected to an Eyring analysis and compared with the data obtained from DCXplorer.

## Eyring plots for DCXplorer and dHPLC Y2K

After data analysis of the elution profiles with both programs, we next performed an Eyring analysis in order to obtain the thermodynamic data of the enantiomerization.

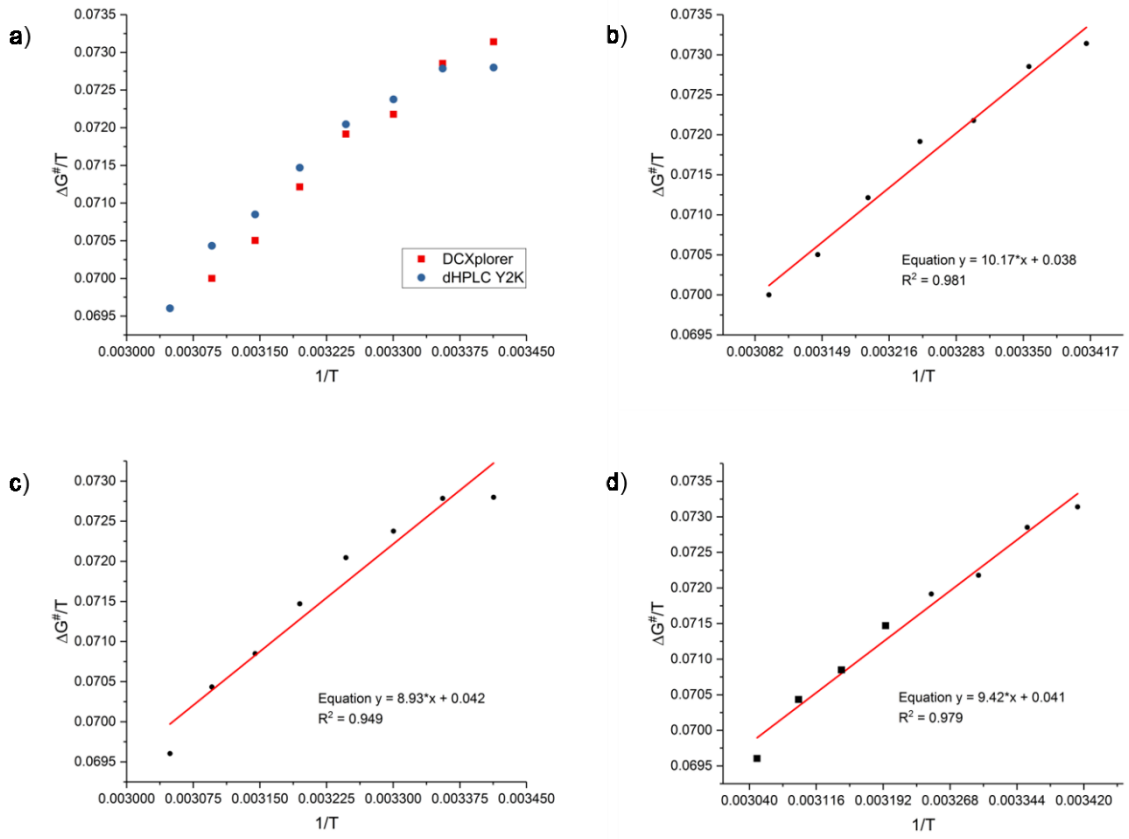


***Figure S5.*** Eyring plots of the data obtained from the elution profiles. a) all data points obtained from both programs; b) Eyring plot of the data obtained from DCXplorer; c) Eyring plot of the data obtained from dHPLC Y2K; d) Eyring plot of selected data points from both programs (Squares: dHPLC Y2K, circles: DCXplorer).

Figure S5a shows all data points obtained from DCXplorer and dHPLC Y2K. Figure S5b shows the linear regression of the data produced From DCXplorer. The enthalpy of enantiomerization is found to be $\Delta H_{DCXplorer}^{\ddagger}$ = 42.14 ± 2.57 kJ mol$^{-1}$ the value for the entropy is determined as $\Delta S_{DCXplorer}^{\ddagger}$ = -163.3 ± 8.3 J mol$^{-1}$ K$^{-1}$ . The Eyring plot for the data obtained with the software dHPLC Y2K (Figure S5c) gives an enthalpy of enantiomerization $\Delta H_{dHPLC\ Y2K}^{\ddagger}$ = 37.30 ± 3.50 kJ mol$^{-1}$, the entropy for the enantiomerization is found to be $\Delta S_{dHPLC\ Y2K}^{\ddagger}$ = -178.06 ± 8.4 J mol$^{-1}$ K$^{-1}$.

*Uray* and coworkers describe a combination of both programs, as DCXplorer excellently fits data in the low temperature range, while dHPLC Y2K is better suited for high rates of conversion.[5] Figure S5d shows an Eyring plot for the combined data. The data points represented by squares are taken from dHPLC Y2K, the data points represented by circles are taken from DCXplorer. This combined approach gives $\Delta H_{combined}^{\ddagger}$ = 39.41 ± 2.30 kJ mol$^{-1}$ and $\Delta S_{combined}^{\ddagger}$ = -172.06 ± 5.0 J mol$^{-1}$ K$^{-1}$.

**Variable Temperature Exchange Spectroscopy**

All EXSY NMR experiments were performed on a Bruker Avance III NMR spectrometer operating at 600.13 MHz proton frequency. The instrument was equipped with an indirect 5-mm BBI probe with *z*-gradient. The experiments were performed between 373 and 393 K and the temperature was calibrated using a glycerol standard showing accuracy within +/- 0.2 K. Temperature equilibration was achieved after 20 min and only then the EXSY experiments were performed.

Phase-sensitive EXSY experiments with a gradient pulse during the mixing time were performed with 2048 time points and 12 ppm sweep width in F2 and 256 time increments for 1 ppm sweep width in the indirect dimension F1, which corresponds to acquisition times of 142 ms in F2 and 213 ms in F1, the resolution was 2.3 Hz in F1 and 3.5 Hz in F2. Each increment was recorded with 8 scans and a recycling delay of 1.5 s. The mixing times were set to 1000, 500 or 250 ms and the total experiment varied between 68 and 94 min.

The data sets were processed with Bruker topspin 3 software after zero-filling to 1k data points in F1 and a shifted square sine bell apodization function in both dimensions. Manual integration of the EXSY cross peaks, normalized with the diagonal peaks yielded the rate constants which were determined applying the initial rate approximation. Eyring analysis of these rates yielded the enthalpic and entropic contributions to the activation energy.

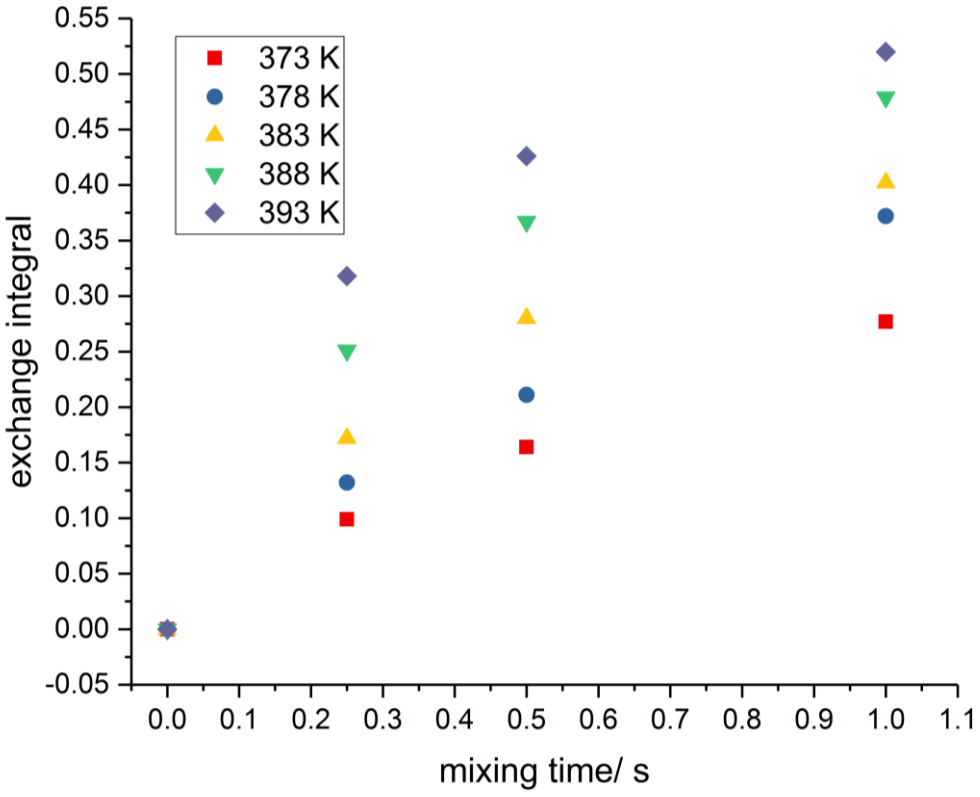


***Figure S6.*** Exchange integral versus mixing time for five temperatures of macrocycle **2** in $C_2D_2Cl_4$ from 373 – 393K.

An exponential fit was applied for all temperatures, the rate constant for each temperature was obtained at 0.05 s mixing time through linear extrapolation.

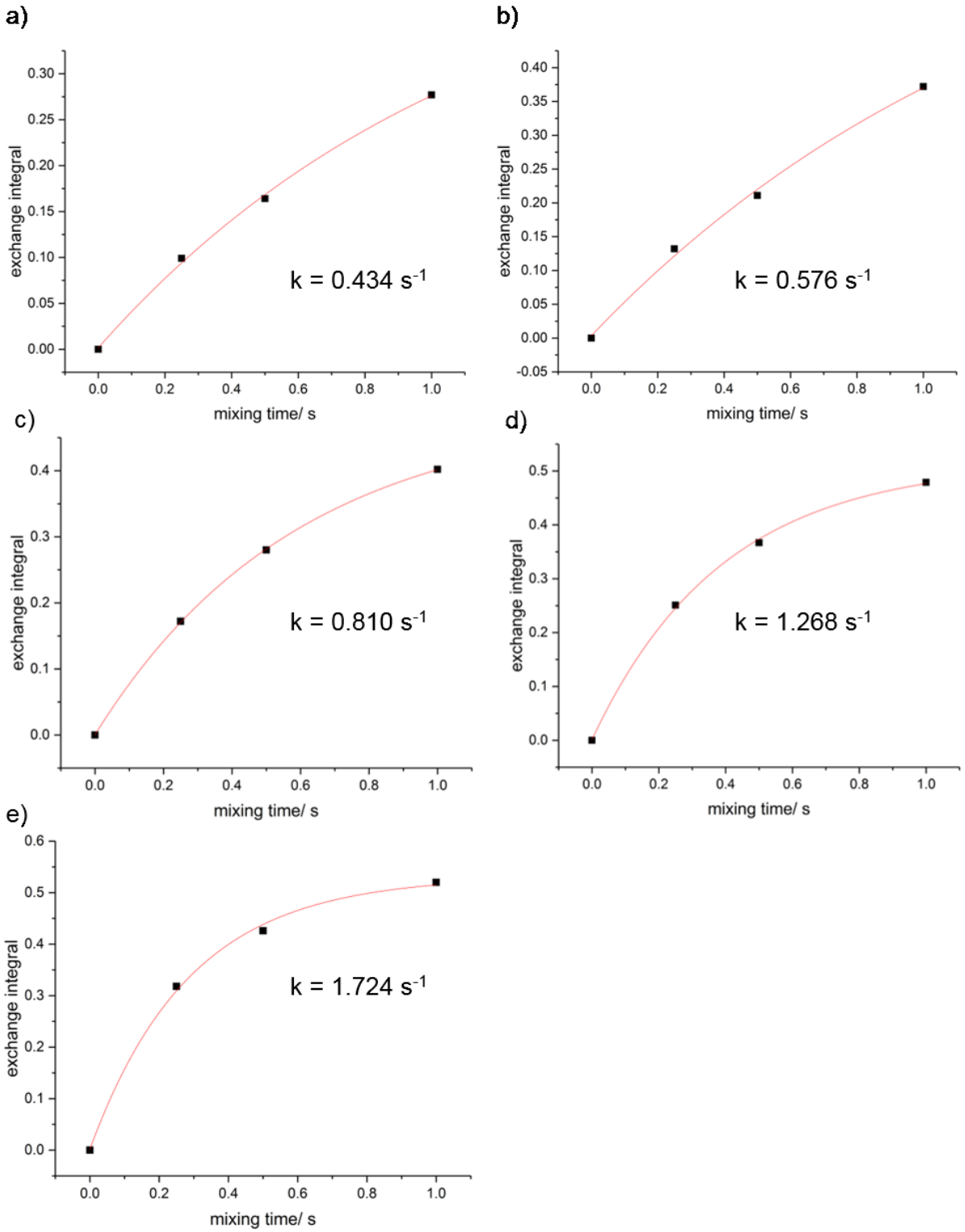


***Figure S7.*** Exponential fit for the exchange integral versus mixing time for a) 373 K, b) 378 K, c) 383 K, d) 388 K, e) 393 K. The rate constants were extrapolated at 0.05 s mixing time for all cases.

The rate constants were further used to evaluate the thermodynamic parameters of the EXSY experiment.

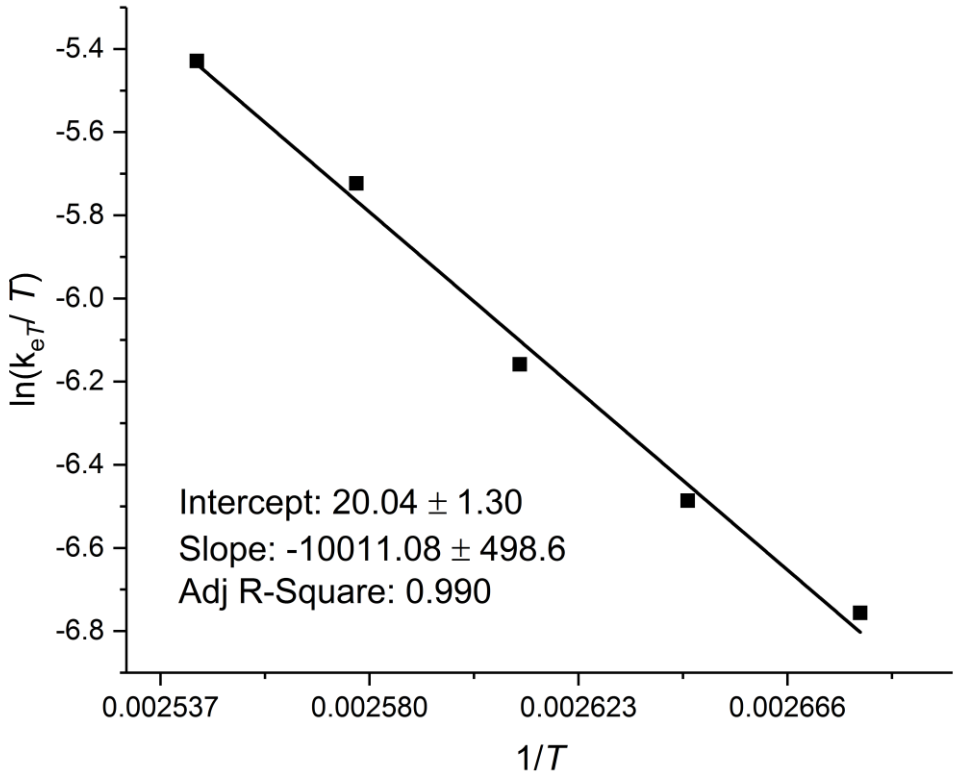


***Figure S8.*** Eyring plot of ln($k_{eT}$/*T*) against 1/*T* with linear regression (y=ax + b).

From this, the entropy and enthalpy of the enantiomerization process can be calculated through equations 2-4:

$$\Delta H_e^{\ddagger} = 83.15 \pm 4.19\ kJ\ mol^{-1} \quad (2)$$

$$\Delta S_e^{\ddagger} = -31.24 \pm 10.81\ J\ mol^{-1}K^{-1} \quad (3)$$

The activation energy at 298 K can be calculated:

$$\Delta G_{e298}^{\ddagger} = \Delta H_e^{\ddagger} - T\Delta S_e^{\ddagger} = 83.15 - (-0.031 \cdot 298) = 92.39\ kJ\ mol^{-1} \quad (4)$$

**Determination of the absolute configuration of 1**

To determine the absolute configuration of the respective enantiomers the measured electronic circular dichroism (ECD) spectra were compared to the spectra calculated by TD-DFT approach. The experimental CD spectra were measured directly after separation of the enantiomers by chiral HPLC (ChiralpakIG, eluent ethyl acetate/*n*-hexane 1:4, 1.0 mL $min^{-1}$, column oven: T = 18 °C) with the cell holder temperature in the CD spectrometer set to 10 °C. The spectra were further calculated with the TD-CAM-B3LYP method after structure optimization (see the Quantum Chemical Calculations section below).[6] The data obtained from the calculation (75 states) were analyzed with the SpecDis (v1.71) software.[7] This approach showed good agreement of the experimental and calculated data and allowed us to assign the absolute configuration of the respective enantiomers.

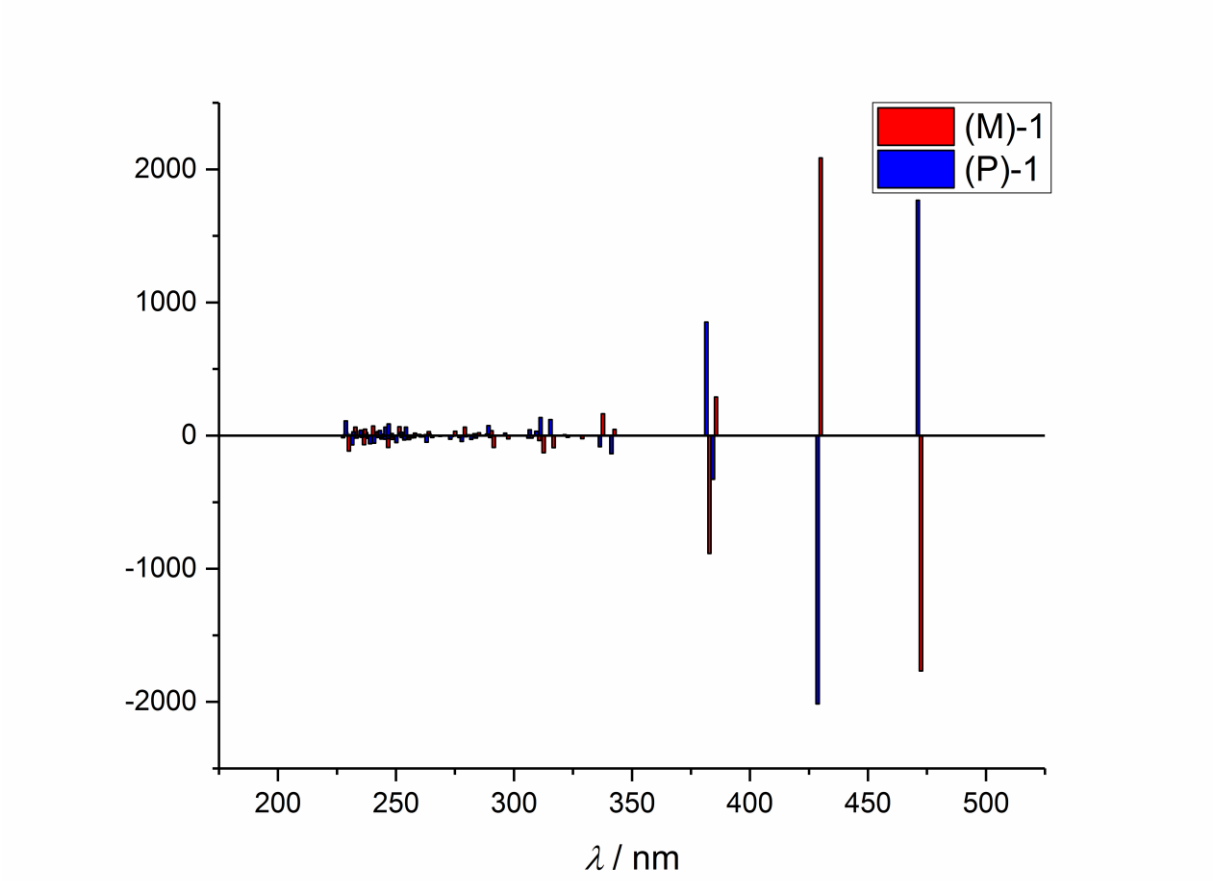


***Figure S9.*** Simulated states for the ECD calculation (CAM B3LYP).

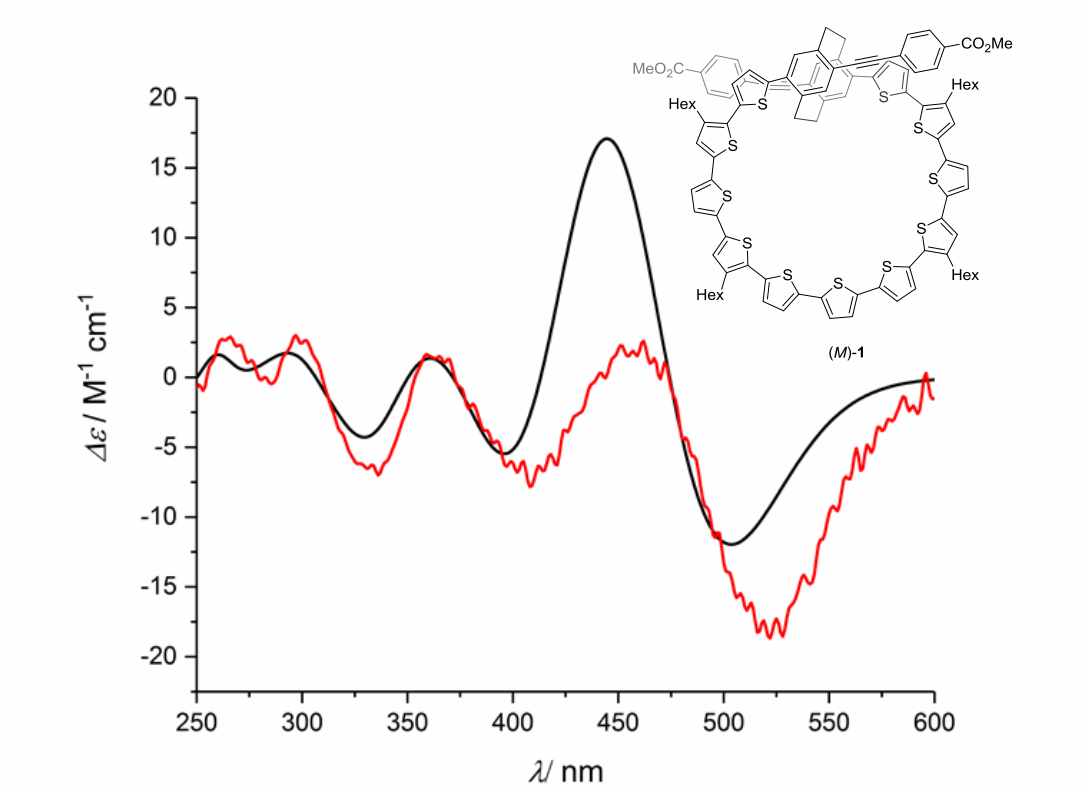


***Figure S10.*** Experimental (red) and calculated (black) ECD spectrum of (*M*)-**1**. The sigma/gamma ratio was set to 0.16 eV to simulate vibrational broadening and the spectrum was shifted by +20 nm.

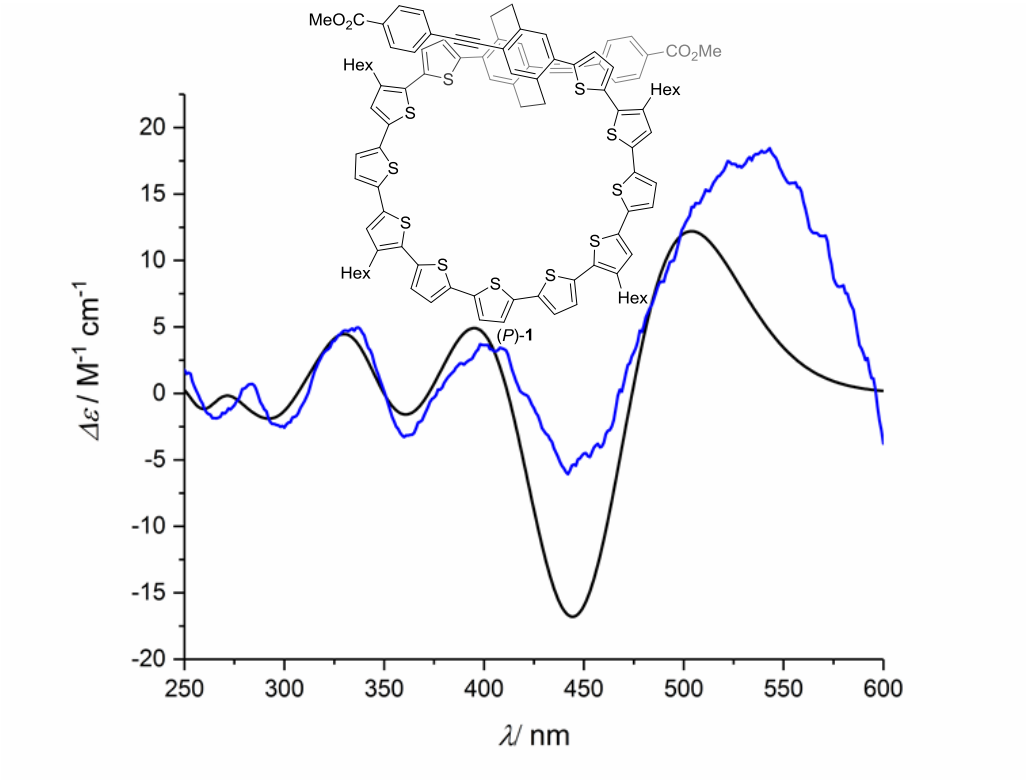


***Figure S11.*** Experimental (blue) and calculated (black) ECD spectrum of (*P*)-**1**. The sigma/gamma ratio was set to 0.16 eV to simulate vibrational broadening and the spectrum was shifted by +20 nm.

## Quantum Chemical Calculations

The Gaussian 09 (release D01) program suite was used in all calculations.[6] The potential energy surface scans were performed at either semi-empirical PM6 or B3LYP/6-31G(d) level of theories. The full gas phase geometry optimizations were done with B3LYP functional and 6-31G(d) basis set, and the character of the stationary point reached was confirmed by a subsequent frequency calculation. The zero-point vibrational energy correction obtained this way was used unscaled. The electronic circular dichroism spectra were obtained at CAM-B3LYP/cc-pVDZ level of theory calculating the first 75 electronic transitions. The velocity form of the rotatory strength was used. Empirical vibrational broadening for the electronic transitions was assumed (0.16 eV) and the position of the absorption bands was empirically shifted by +20 nm to match the energy of the first electronic transition. The ECD spectra were simulated in SpecDis (v1.71).[7]

## Detailed Theoretical Analysis of the Enantiomerization Process

First, the size of the molecule was alleviated to some extent by replacing the hexyl substituents by methyl groups. Nevertheless, the size of the used model allowed us to use only the semi-empirical PM6 method to explore the potential energy surface of the enantiomerization process. The relatively flexible nature of macrocycle **1** prevented us from locating the specific transition states. Therefore, potential energy surface (PES) scans were used to map the regions of PES where one of the arms of **1** threads through the macrocyclic ring. We assumed that this would allow us to divide the enantiomerization pathway to a set of relatively simple molecular distortions that could be treated separately to obtain a reliable estimate of the activation enthalpy for the enantiomerization process. Because **1** is chiral, one can discriminate the clockwise and anticlockwise rotation of the [2.2]paracyclophane unit because they are not identical. Also, each methyl carboxylate group can adopt a set of four distinct conformations: (i) *cis* and (ii) *trans* configuration of the full carboxylate group with respect to the benzene ring and (iii) s-*cis* and (iv) s-*trans* configuration of the methoxy group in the carboxylate. This theoretically makes for a total of 32 possible enantiomerization pathways. However, some of the conformations are not populated due to their large energy. For instance, the s-*trans* conformation of the methoxy group in 4-ethynylbenzene is 48.9 kJ $mol^{-1}$ (at 0 K, ZPVE included) less stable than the s-*cis* conformation conformations, i.e. conformations (iv) are disfavored leaving only 8 out of 32 possibilities. In addition, a number of conformations/ pathways will be comparable in energy, those that involve conformations (i) and (ii) in particular. As a result, only the clockwise and anticlockwise rotation of a single enantiomer could suffice to reveal the details of the enantiomerization process.

The rotation of the [2.2]paracyclophane (PC) unit required constraining two dihedral angles, one for each benzene (top and bottom, respectively) ring plane that it adopts with the plane defined by the adjacent thiophene unit (Figure S12).

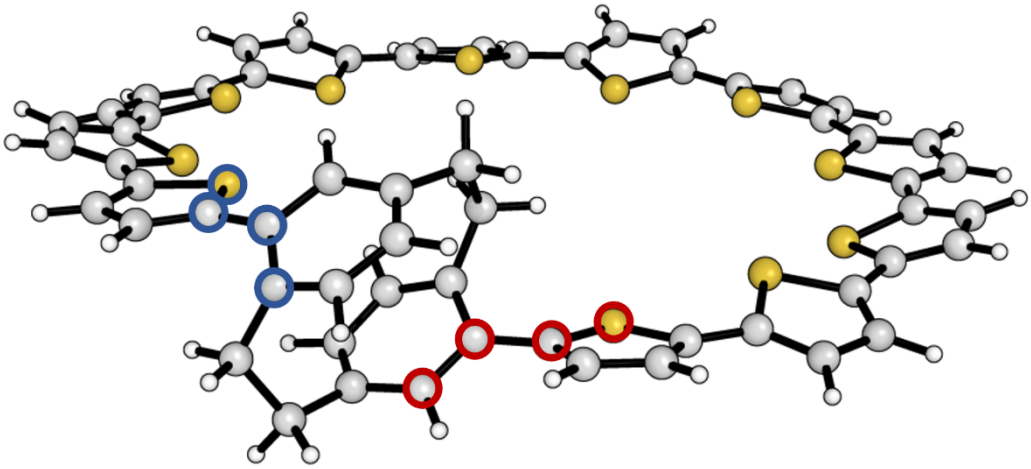

***Figure S12.*** Two dihedral angles defined by blue and red circles used as the variable *α* to explore the rotation of the [2.2]paracyclophane unit. The value of the dihedral angles in this particular picture is set to |*α*| = 140°.

If only one of the two possible dihedral angles was constrained and used as a variable to explore the PES with PM6 (or B3LYP) method, typically, the calculation resulted in the rotation of that particular thiophene ring when the dihedral angle reached larger values. To simplify our calculations these two dihedral angles were assumed to have identical value and are denoted together as dihedral angle *α* (Figure S12). The PES scans were performed in the range of *α* = 50°, close to a value found for the local energy minimum, in steps of 5° or 10° until one of the arms was observed to pass through the macrocycle during the optimization process or the energy reached very high values (> 120 kJ $mol^{-1}$) when compared to experiment, approximately ± 270° (more than a half twist theoretically required to reach the minimum of the other enantiomer) in each direction.

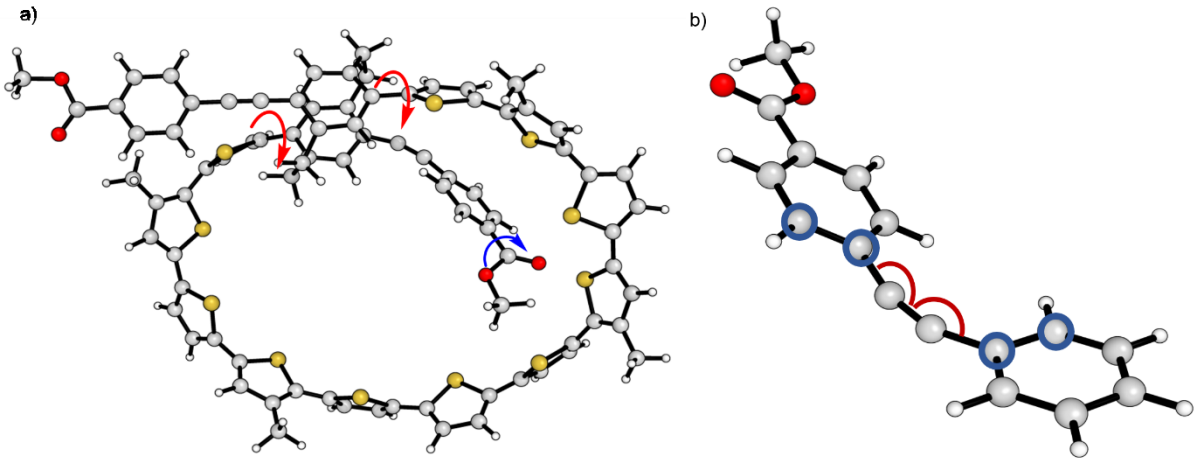


***Figure S13.*** a) Snapshot of the geometry of **1** with $\alpha$ = 220°. Increasing the angle $\alpha$ by 1° (red arrows) leads to threading of the entire arm through the macrocycle accompanied by a full 180° rotation (blue arrow) of the methyl carboxylate to avoid the steric hindrance from the thiophene units. b) A crop from the geometry of **1** in a) used to estimate the energy required to bend the arm during the rotation by B3LYP calculations with two valence (red half-circles) and one dihedral (blue circles) angles frozen during the optimization.

The arm bends the acetylenic moiety as it approaches the macrocycle due to steric hindrance of the methyl carboxylate and thiophene units in the macrocycle (see Figure S13), i.e. the arm is clearly long-enough to gear the smooth rotation of the central PC unit, which does not otherwise require a very large activation energy. The latter process was modeled by another PES scan with the same set of dihedral angles $\alpha$ as the variable for the parent macrocycle **2a** that contains no bulky arms preventing the PC rotation. This PES scan (Figure S14) was done at B3LYP/6-31G(d) level of theory and the estimated activation energy agrees excellently with the experimental activation free energy of a similar system, **2b**, determined by VT NMR spectroscopy.[8]

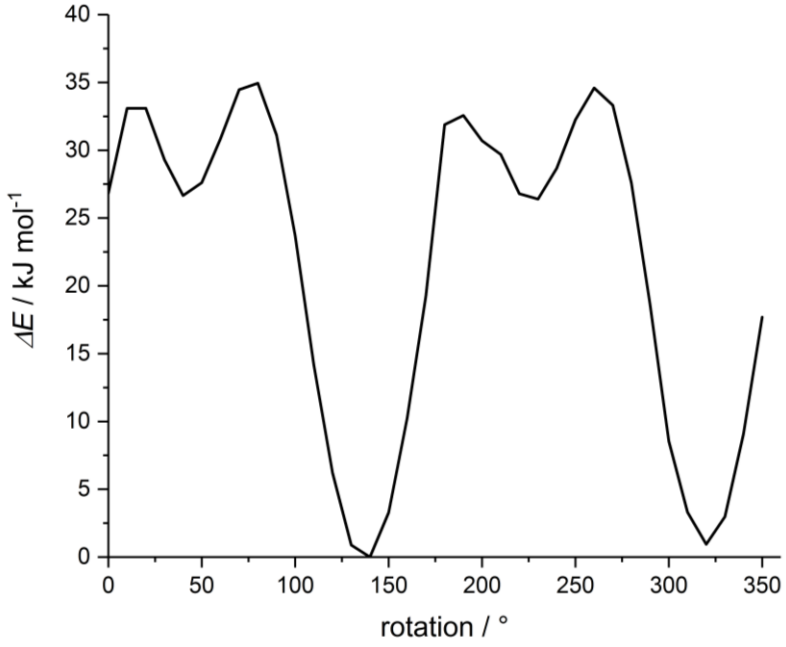


***Figure S14.*** B3LYP/6-31G(d) PES scan simulating the rotation of the PC unit in macrocycle **2b**.

Unexpectedly, we observed that the methyl carboxylate group needs to be (s-*cis* conformation of the methoxy group) rotated during the constrained optimization of **1** by nearly 180° to alleviate its steric hindrance with the thiophene units. This allows for a smooth passage through the macrocycle completing the enantiomerization when $\alpha > 220°$ in one direction of the two possible rotations (Figure S13), even when very small optimization steps were employed and the full Hessian matrix was calculated in each optimization step. The other direction of the PC rotation led to very high energies (> 120 kJ $mol^{-1}$) at high values of $\alpha$ without the arm passing through the macrocycle. Clearly, the steric hindrance of the methyl carboxylate and the sulfur atoms of the thiophene units are prohibitive to allow for its passage. However, we found that rotation of the methoxy group to its less stable s-*trans* conformation decreases the steric hindrance and, as a result, allows the arm to thread through the macrocycle (Figure S15). We therefore performed the PES scans to reveal the barrier that may lead to the desired process directly upon the methoxy group rotation, while freezing the variable $\alpha$ with values from (185°–200°, Figure S16).

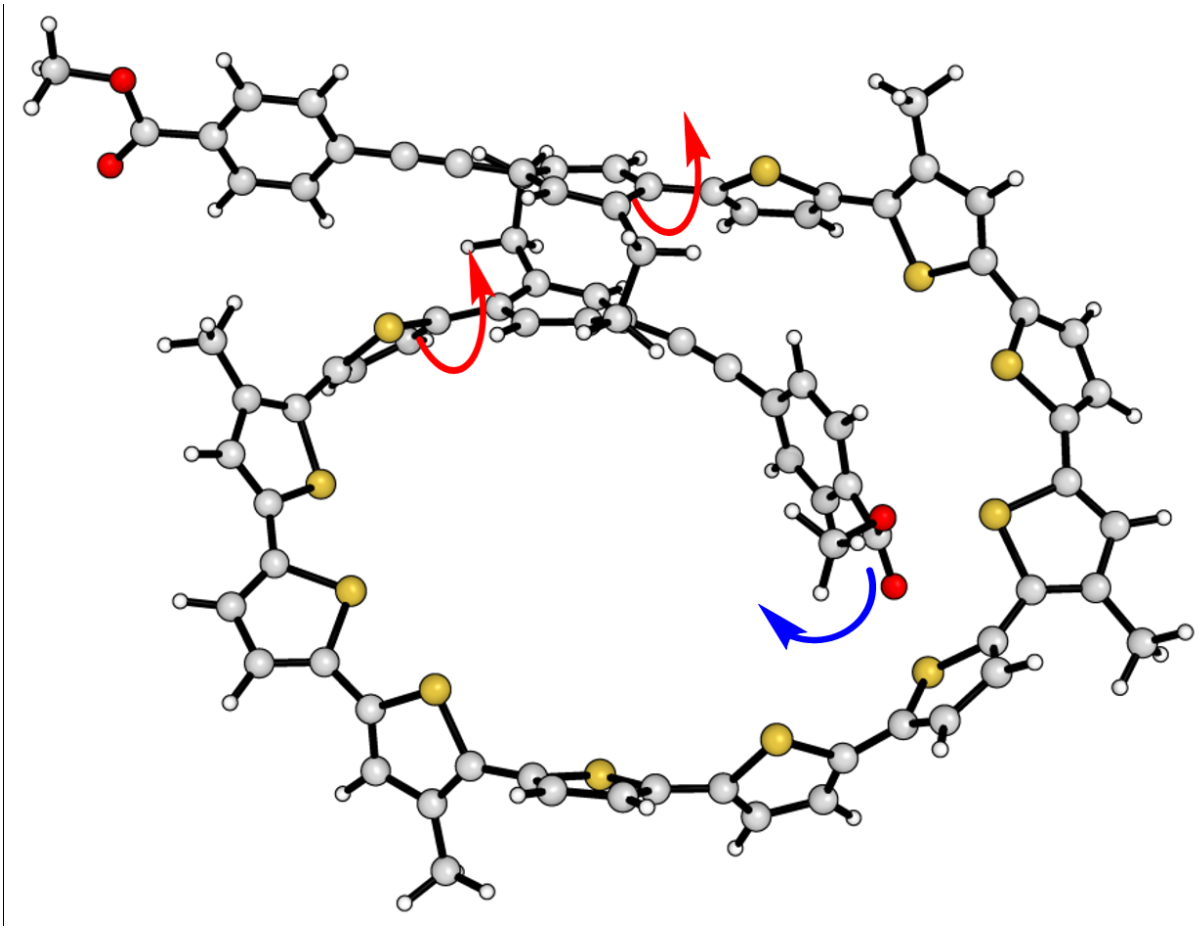

***Figure S15.*** The preconfined dihedral angles at 200°, combined with bending of the acetylene and a rotation of the methoxy group allow the system to racemize.

Again, the methoxy group can rotate in two non-equivalent directions as a consequence of the chirality of the studied system. We however found only moderate differences in energy following

any of the directions (Figures S16 and S17). At $\alpha$ = 185°, the methoxy group rotated smoothly but did not lead directly to the enantiomerization but only to the s-*trans* conformer. Increasing $\alpha$ in steps of 5° provided us with the PES profiles that are discontinuous after the energy barrier reached the maximum. The parts of the PES after this energy maximum are on the other side of the enantiomerization energy barrier. When $\alpha \geq 200°$ a smooth potential leading directly to the other enantiomer was obtained. In this case, the maximum energy on the calculated PES is the lowest found for any of the studied dihedral angle values $\alpha$ and, therefore, it represents part of the potential energy surface that can serve as a good estimate for the enantiomerization barrier of **1**.

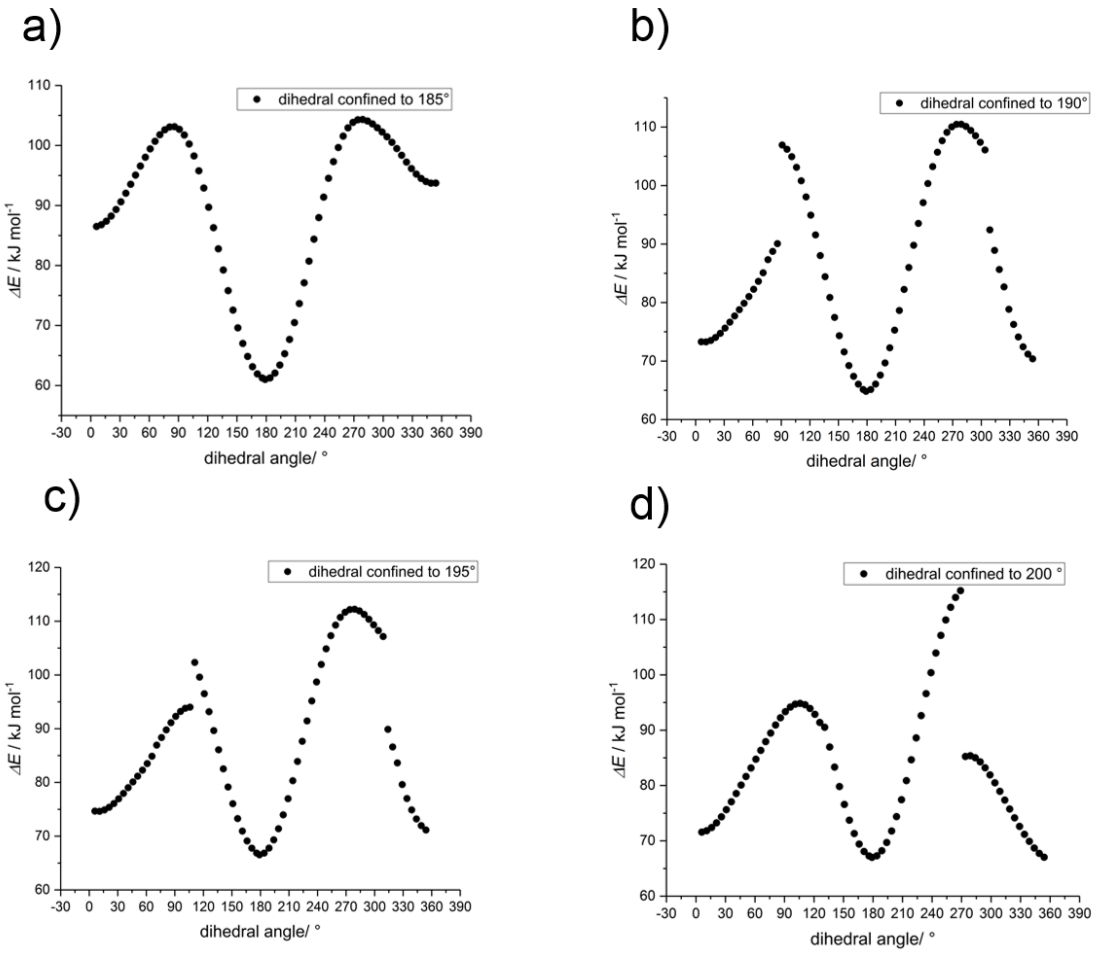


***Figure S16.*** Potential energy profiles for the rotation of the methyl ester from its s-*cis* to s-*trans* conformation with the dihedral angles $\alpha$ frozen during the PES scan (a-e, 185° - 200°, step: 5°). The energies are normalized to the energy of the equilibrium geometry. The two maxima in each profile correspond to two possible directions of the methoxy group rotation.

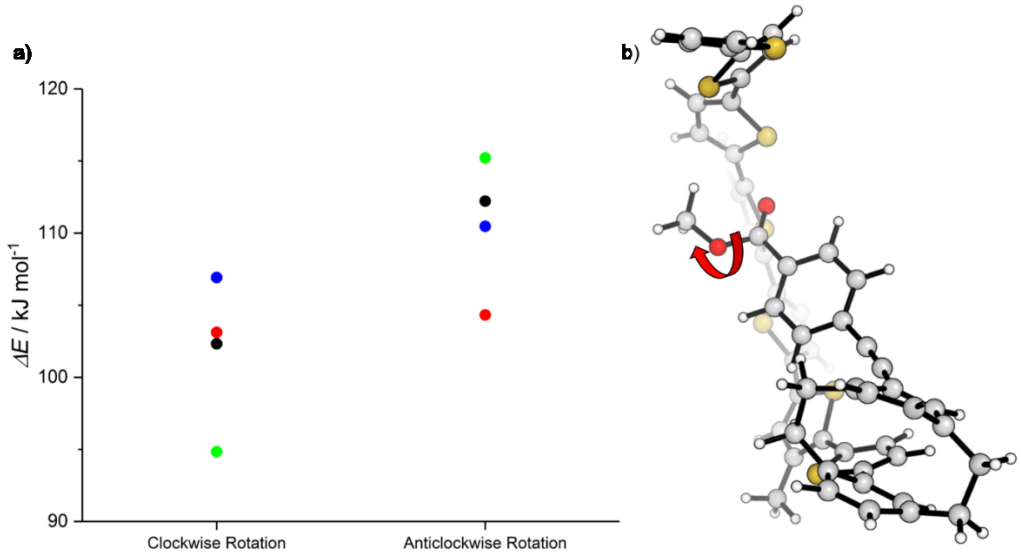


***Figure S17.*** a) Points of the highest energy on the potential energy profiles shown in Figure S16. Points of the same color correspond to a profile of the same value of *α* that was kept constant in the partial optimizations. Red: 185°, blue: 190°, black 195°, green, 200°. b) Definition of the direction of rotation. The red arrow corresponds to a clockwise rotation around the oxygen-carbonyl axis.

As a result, four distinct processes can be identified to play a crucial role in the rotation of the central PC unit that interconnects the potential energy minima of the two enantiomers: (i) a considerable turn of the PC from its energy minimum geometry, (ii) bending of the *para*-ethynyl methylbenzoate arm, and, unexpectedly, (iii) a rotation of either (a) the methyl carboxylate by ~180° or (b) the methoxy group from its more stable *s-cis* to *s-trans* conformation. Each of these processes could be studied on simplified models with the help of B3LYP/6-31G(d) optimizations followed by single point B3LYP/cc-pVTZ calculations. The process (i) has already been discussed above (Figure S14). The energy required to bend the acetylene unit (ii) in the arm of **1** was studied on a model obtained by cropping one of the PC benzene rings with the full arm from the partially optimized geometry of **1** at $\alpha$ = –220° (Figure S13). A set of valence and dihedral angles were frozen (Figure S13b) and a partial optimization on the model was performed to relax the bond lengths that differ between the PM6 (PES scans) and the B3LYP geometries. A full geometry optimization of the molecule was also performed and used as a reference. The energy difference obtained represents the energy required to bend the arm for its passage through the macrocycle in **1**. The processes (iiia) and (iiib) were explored in methyl 4-ethynylphenylbenzoate. Both the carboxylate group and methoxy group rotations were performed as PES scans at B3LYP/6-31G(d) level of theory. The obtained energies were then corrected as follows: The methyl carboxylate group rotation activation free energy has been determined experimentally by variable temperature $^{13}$C NMR in methyl benzoate to be 20.6 kJ mol$^{-1}$.[9] We performed the same PES scan for methyl benzoate and took the difference of the experimental and the theoretical (31.7 kJ mol$^{-1}$) values as the correction for the methyl 4-

ethynylphenylbenzoate model to obtain a corrected value of 20.9 kJ $mol^{-1}$. The experimental activation enthalpy of the methoxy group rotation in methyl formate has been determined experimentally by ultrasonic attenuation experiments by Bailey and North to be 32.6 kJ $mol^{-1}$.[10] Calculation of the PES of this rotation with B3LYP/6-31G(d) method provided surprisingly large energy of 58.5 kJ $mol^{-1}$, a value similar to the one obtained for the methyl 4-ethynylphenylbenzoate model. After correction, the activation energy for this process was found to be 27.8 kJ $mol^{-1}$.

Addition of the numbers for these processes (i-iii), therefore, provides a reliable semiquantitative estimate for the activation enthalpy of enantiomerization of macrocycle **1**.

**Crystal structure data for 6**

Crystal data for **6**: formula $C_{48}H_{52}O_4S_4$, M = 821.20, F(000) = 436, colourless plate, size 0.020 · 0.100 · 0.100 $mm^3$, triclinic, space group P -1 , Z = 1, a = 7.6438(6) Å, b = 7.7858(6) Å, c = 19.8762(16) Å, α = 95.895(3)°, β = 91.044(3)°, γ = 117.920(3)°, V = 1036.71(14) $Å^3$, $D_{calc.}$ = 1.315 Mg · $m^{-3}$. The crystal was measured on a Bruker Kappa Apex2 diffractometer at 123K using graphite-monochromated Cu $K_\alpha$-radiation with λ = 1.54178 Å, $\Theta_{max}$ = 70.616°. Minimal/maximal transmission 0.84/0.95, μ = 2.454 $mm^{-1}$. The Apex2 suite has been used for datacollection and integration. From a total of 12231 reflections, 3671 were independent (merging r = 0.032). From these, 3615 were considered as observed (I>2.0σ(I)) and were used to refine 253 parameters. The structure was solved by other methods using the program Superflip. Least-squares refinement against Fsqd was carried out on all non-hydrogen atoms using the program CRYSTALS. R = 0.0751 (observed data), wR = 0.0587 (all data), GOF = 1.0297. Minimal/maximal residual electron density = -0.82/0.71 e $Å^{-3}$. Chebychev polynomial weights were used to complete the refinement. Plots were produced using CAMERON. Crystallographic data (excluding structure factors) for the structure in this paper have been deposited with the Cambridge Crystallographic Data Center, the deposition number is 1866881. Copies of the data can be obtained, free of charge, on application to the CCDC, 12 Union Road, Cambridge CB2 1EZ, UK [fax: +44-1223-336033 or e-mail: deposit@ccdc.cam.ac.uk].

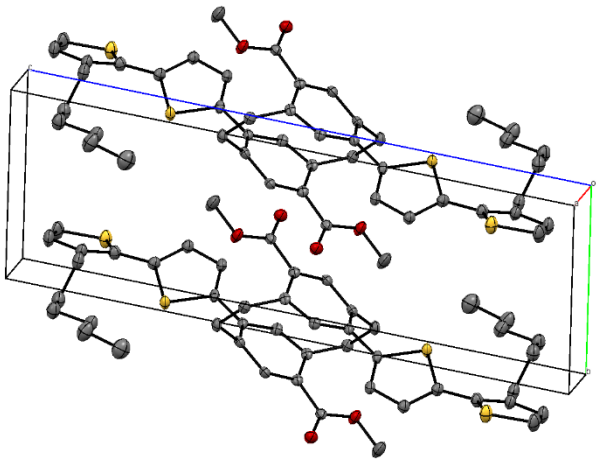

***Figure 18*** Unit cell for **6**.

## Atomic coordinates of B3LYP/6-31G(d) optimized geometry of (*M*)-1 for ECD spectra

| | | | |
|---|---|---|---|
| C | 5.090737 | 10.895990 | 0.253460 |
| C | -9.740852 | 5.960885 | -2.387189 |
| C | -9.236642 | -8.360001 | 4.368665 |
| O | -8.665281 | -6.145416 | 3.046913 |
| O | -7.877763 | -7.953609 | 4.149566 |
| C | -7.724382 | -6.801016 | 3.456120 |
| C | 12.853071 | -3.592854 | -3.321168 |
| O | 11.435890 | -3.652443 | -3.102935 |
| O | 11.602427 | -5.905693 | -3.067001 |
| C | 10.921712 | -4.900537 | -2.992818 |
| C | 8.929151 | -0.963007 | 2.825536 |
| C | -6.942399 | -6.275648 | -0.659583 |
| C | 6.002276 | -1.435082 | 1.604115 |
| S | 5.947548 | 1.285608 | 1.226542 |
| S | 4.255817 | -1.392560 | 1.749163 |
| C | 7.277855 | 2.276069 | 1.778460 |
| C | 8.280426 | 1.473585 | 2.287373 |
| C | 7.990606 | 0.078078 | 2.276612 |
| C | 6.736546 | -0.193525 | 1.749453 |
| C | 6.414248 | -2.720228 | 1.302333 |
| C | 5.342303 | -3.642014 | 1.152545 |
| C | 4.091731 | -3.081326 | 1.314741 |
| C | 2.744854 | -3.661126 | 1.262559 |
| C | -4.697314 | -4.838527 | 2.392729 |
| C | -6.007740 | -5.202272 | 2.663802 |
| C | -6.296364 | -6.446130 | 3.245483 |
| C | -5.244696 | -7.316406 | 3.571397 |
| C | -3.930956 | -6.961033 | 3.293937 |
| C | -3.635410 | -5.721124 | 2.688267 |
| C | -2.300639 | -5.366462 | 2.354850 |
| C | -1.178279 | -5.038605 | 2.012751 |
| S | -2.411152 | 8.111276 | 0.024900 |
| C | -3.939997 | 8.838811 | -0.438728 |
| C | -3.791042 | 10.205659 | -0.581830 |
| C | -2.475644 | 10.665009 | -0.342763 |
| C | -1.585427 | 9.660778 | -0.010713 |
| S | 0.946172 | 8.459322 | 0.148956 |
| C | -0.178752 | 9.796092 | 0.297564 |
| C | 0.487674 | 10.932310 | 0.716790 |
| C | 1.871680 | 10.736028 | 0.937974 |
| C | -7.428116 | 7.513758 | -0.691593 |
| C | -6.452606 | 8.511453 | -0.457925 |
| C | -5.152556 | 8.066258 | -0.600171 |
| S | -5.142201 | 6.372637 | -1.059220 |
| C | 2.299585 | 9.443168 | 0.696497 |
| C | -6.899769 | 6.277838 | -1.018024 |
| S | 3.794876 | 7.179901 | 1.278356 |
| C | 3.621713 | 8.870505 | 0.835004 |
| C | 4.866127 | 9.463176 | 0.657559 |
| C | 5.933306 | 8.544141 | 0.853618 |
| C | 5.541177 | 7.260534 | 1.176627 |
| S | 5.649639 | 4.488699 | 1.382453 |
| C | 6.359615 | 6.090217 | 1.400364 |
| C | 7.720676 | 6.001198 | 1.632757 |
| C | 8.190339 | 4.673115 | 1.779650 |
| C | -9.179285 | 3.483617 | -2.022757 |
| C | -8.843418 | 4.858227 | -1.891102 |
| C | -7.595925 | 5.041380 | -1.306512 |
| S | -6.864251 | 3.495002 | -0.901460 |
| C | -8.223843 | 2.605017 | -1.555099 |
| C | -9.069563 | -1.043027 | -1.630567 |
| C | -9.379149 | 0.337903 | -1.627963 |
| C | -8.269112 | 1.159417 | -1.555113 |
| S | -6.809159 | 0.191913 | -1.472138 |
| C | -7.716382 | -1.310250 | -1.543911 |
| C | 7.197506 | 3.716175 | 1.676693 |
| C | -6.596622 | -4.877825 | -1.098541 |
| C | -7.546253 | -3.816925 | -1.098619 |
| S | -5.355989 | -2.743211 | -1.908650 |
| C | -7.045284 | -2.589572 | -1.483381 |
| C | -5.333578 | -4.451904 | -1.491608 |
| C | -2.386267 | -6.791130 | -1.642972 |
| C | -3.776442 | -6.502339 | -1.681643 |
| C | -4.069483 | -5.158305 | -1.530068 |
| S | -2.583734 | -4.250845 | -1.325028 |
| C | -1.582081 | -5.682634 | -1.470536 |
| C | 1.005188 | -7.034467 | 1.618564 |
| C | 1.765603 | -1.942979 | -0.419616 |
| C | 1.226544 | -5.539487 | 1.729735 |
| C | 0.137454 | -4.635363 | 1.662867 |
| C | 0.368660 | -3.360645 | 1.105918 |
| C | 1.641699 | -2.927337 | 0.739724 |
| C | 2.507198 | -4.983167 | 1.682671 |
| C | 0.367644 | -7.459867 | 0.219561 |
| C | 2.277182 | -2.633674 | -1.757956 |
| C | 0.763988 | -6.518775 | -0.910361 |
| C | -0.121511 | -5.551245 | -1.464553 |
| C | 0.436228 | -4.341760 | -1.924063 |
| C | 1.797635 | -4.065667 | -1.882433 |
| C | 2.118288 | -6.379131 | -1.213567 |
| C | 7.429534 | -6.183583 | -2.429435 |
| C | 8.799985 | -6.128202 | -2.638155 |
| C | 9.450322 | -4.892627 | -2.772313 |
| C | 8.702782 | -3.707719 | -2.695454 |
| C | 7.330269 | -3.756718 | -2.487415 |
| C | 6.669242 | -4.996405 | -2.350300 |
| C | 5.265849 | -5.048566 | -2.128688 |
| C | 4.066211 | -5.084935 | -1.919187 |
| C | 2.662936 | -5.177610 | -1.710134 |
| H | 5.123914 | 11.565564 | 1.123522 |

| | | | |
|---|---|---|---|
| H | 4.293405 | 11.255228 | -0.405071 |
| H | 6.044365 | 11.003606 | -0.273772 |
| H | -9.162522 | 6.808270 | -2.769062 |
| H | -10.396436 | 6.343079 | -1.593087 |
| H | -10.387670 | 5.597458 | -3.192501 |
| H | -9.175654 | -9.291544 | 4.932274 |
| H | -9.777790 | -7.600165 | 4.938710 |
| H | -9.749372 | -8.519322 | 3.416105 |
| H | 13.094671 | -2.531270 | -3.383328 |
| H | 13.389971 | -4.062312 | -2.492446 |
| H | 13.120877 | -4.103405 | -4.250135 |
| H | 8.380587 | -1.828697 | 3.210016 |
| H | 9.623579 | -1.328834 | 2.057329 |
| H | 9.534446 | -0.552056 | 3.640541 |
| H | -6.102179 | -6.749676 | -0.143385 |
| H | -7.795476 | -6.265476 | 0.026431 |
| H | -7.209664 | -6.912572 | -1.513750 |
| H | 9.196944 | 1.876208 | 2.707473 |
| H | 7.451027 | -2.982154 | 1.124692 |
| H | 5.487615 | -4.676296 | 0.862650 |
| H | -4.476761 | -3.881041 | 1.933156 |
| H | -6.828966 | -4.537795 | 2.417311 |
| H | -5.464661 | -8.274408 | 4.029137 |
| H | -3.118571 | -7.640141 | 3.532973 |
| H | -4.605229 | 10.851539 | -0.891569 |
| H | -2.174474 | 11.701388 | -0.448776 |
| H | -0.019096 | 11.873283 | 0.900827 |
| H | 2.528529 | 11.509308 | 1.317858 |
| H | -8.490989 | 7.682686 | -0.569734 |
| H | -6.692551 | 9.523131 | -0.149587 |
| H | 6.973828 | 8.819846 | 0.714412 |
| H | 8.362656 | 6.872603 | 1.703069 |
| H | 9.232405 | 4.422931 | 1.947139 |
| H | -10.095990 | 3.148392 | -2.497266 |
| H | -9.817286 | -1.825331 | -1.701944 |
| H | -10.391621 | 0.724880 | -1.663763 |
| H | -8.570212 | -3.952440 | -0.765348 |
| H | -1.983932 | -7.787789 | -1.789829 |
| H | -4.533851 | -7.255941 | -1.860348 |
| H | 0.339901 | -7.410320 | 2.404856 |
| H | 1.968428 | -7.541649 | 1.741251 |
| H | 2.428336 | -1.098138 | -0.219786 |
| H | 0.770964 | -1.523458 | -0.605670 |
| H | -0.496785 | -2.758840 | 0.841682 |
| H | 3.364917 | -5.613951 | 1.906711 |
| H | 0.678904 | -8.492714 | 0.018689 |
| H | -0.717574 | -7.466309 | 0.329025 |
| H | 1.933167 | -2.012924 | -2.594602 |
| H | 3.370249 | -2.615251 | -1.772248 |
| H | -0.238669 | -3.540063 | -2.213469 |
| H | 2.812202 | -7.159674 | -0.911085 |
| H | 6.927961 | -7.140805 | -2.327456 |
| H | 9.391464 | -7.035613 | -2.701532 |
| H | 9.202772 | -2.751429 | -2.800195 |
| H | 6.753198 | -2.839933 | -2.424185 |
| H | -3.324259 | 12.124802 | -0.291989 |
| C | 10.818824 | 3.547826 | -2.518045 |
| H | 11.343509 | 3.044066 | -3.336548 |
| H | 11.565092 | 3.769852 | -1.743290 |
| H | 10.441231 | 4.505014 | -2.891433 |

## (*P*)-1

| | | | |
|---|---|---|---|
| C | -3.813166 | -4.448613 | -1.695855 |
| C | -5.160118 | -4.038957 | -1.895914 |
| C | -6.321967 | -3.732108 | -2.096453 |
| C | -7.679519 | -3.364664 | -2.306391 |
| C | -8.055664 | -2.005392 | -2.376941 |
| C | -9.384356 | -1.654084 | -2.568825 |
| C | -10.371527 | -2.642164 | -2.698878 |
| C | -10.005940 | -3.995144 | -2.633547 |
| C | -8.678347 | -4.353033 | -2.438373 |
| C | -3.554007 | -5.737743 | -1.187791 |
| C | -2.718025 | -3.566821 | -1.888977 |
| C | -1.456531 | -4.147862 | -1.934622 |
| C | -1.186281 | -5.446466 | -1.460107 |
| C | -2.265180 | -6.180673 | -0.890578 |
| C | -2.855148 | -2.061619 | -1.779711 |
| C | -2.085436 | -7.175550 | 0.248454 |
| C | -3.576295 | -4.255979 | 1.692377 |
| C | -2.271683 | -2.466661 | 0.713392 |
| C | -1.128024 | -3.176034 | 1.075761 |
| C | -1.189807 | -4.463131 | 1.648382 |
| C | -2.457293 | -5.091345 | 1.738668 |
| C | -2.181181 | -1.491695 | -0.456648 |
| C | -2.588110 | -6.598206 | 1.647898 |
| C | 0.206847 | -5.904118 | -1.462649 |
| S | 1.505518 | -4.732552 | -1.340637 |
| C | 2.747433 | -5.956383 | -1.511423 |
| C | 2.159353 | -7.202898 | -1.637500 |
| C | 0.740073 | -7.169178 | -1.606343 |
| C | 4.138658 | -5.555704 | -1.477498 |
| C | 6.235624 | -4.142214 | -1.497388 |
| S | 4.555979 | -3.907224 | -1.923864 |
| C | 6.438354 | -5.445357 | -1.089835 |
| C | 5.268202 | -6.255896 | -1.072058 |
| C | -6.126682 | 5.294351 | 1.652680 |
| C | 7.185267 | -3.054677 | -1.578536 |
| S | 6.653961 | -1.382711 | -1.495230 |
| C | 8.296754 | -0.781332 | -1.615321 |
| C | 9.183526 | -1.838412 | -1.707394 |
| C | 8.561079 | -3.109606 | -1.695892 |
| C | 8.588254 | 0.635413 | -1.624072 |
| S | 7.487298 | 1.817570 | -0.947424 |
| C | 8.546907 | 3.151365 | -1.381518 |
| C | 9.704147 | 2.682988 | -1.991970 |
| C | 9.709862 | 1.267564 | -2.119771 |
| C | -6.875988 | 6.454001 | 1.729947 |
| C | -6.113411 | 7.637559 | 1.577743 |
| C | -4.764700 | 7.410644 | 1.367194 |
| S | -4.439017 | 5.689222 | 1.378842 |
| C | -3.698135 | 8.360244 | 1.143736 |
| C | -3.782776 | 9.700980 | 0.825001 |
| C | -2.532287 | 10.348201 | 0.627682 |
| C | -1.458591 | 9.482744 | 0.799844 |
| S | -2.017692 | 7.876908 | 1.239251 |
| C | 8.161268 | 4.516533 | -1.090848 |
| C | -0.040290 | 9.733467 | 0.657739 |
| S | 6.473336 | 5.015840 | -1.109174 |
| C | 6.882630 | 6.663094 | -0.663957 |
| C | 8.252538 | 6.795267 | -0.542226 |
| C | 8.966652 | 5.597561 | -0.781419 |
| C | 0.676287 | 10.892677 | 0.894394 |
| C | 2.067503 | 10.762472 | 0.669660 |
| C | 2.451487 | 9.501634 | 0.252897 |
| S | 1.047078 | 8.461466 | 0.110831 |
| C | 3.787220 | 9.043499 | -0.059672 |
| C | 4.884588 | 9.813014 | -0.398834 |
| C | 6.056176 | 9.060328 | -0.642156 |
| C | 5.884385 | 7.696556 | -0.495386 |
| S | 4.231020 | 7.344933 | -0.022079 |
| C | 0.000236 | -5.152924 | 2.001868 |
| C | 1.015696 | -5.725572 | 2.356055 |
| C | 2.220028 | -6.373832 | 2.741238 |
| C | 2.196806 | -7.656328 | 3.331614 |
| C | 3.379370 | -8.286072 | 3.691532 |
| C | 4.615119 | -7.658209 | 3.474107 |
| C | 4.647066 | -6.379245 | 2.896949 |
| C | 3.466472 | -5.743803 | 2.535467 |
| C | -3.508134 | -2.920009 | 1.255430 |
| C | -4.683046 | -2.042935 | 1.313556 |
| C | -6.031367 | -2.297392 | 1.166400 |
| C | -6.857249 | -1.150094 | 1.317972 |
| C | -6.578674 | 1.384295 | 1.744716 |
| C | -7.744995 | 1.940731 | 2.250067 |
| C | -7.705043 | 3.365128 | 2.254190 |
| C | -6.536376 | 3.912107 | 1.760864 |
| S | -4.444242 | -0.360101 | 1.736474 |
| S | -5.461018 | 2.638693 | 1.234397 |
| C | -6.153810 | 0.005618 | 1.605680 |
| C | -11.778002 | -2.200685 | -2.900727 |
| O | -12.633409 | -3.242080 | -3.035147 |
| C | -14.008087 | -2.881413 | -3.235060 |
| C | 5.847557 | -8.390846 | 3.868276 |
| O | 6.977702 | -7.712268 | 3.551576 |
| C | 8.202726 | -8.360315 | 3.924081 |
| O | 5.861445 | -9.480168 | 4.409038 |
| O | -12.137123 | -1.039484 | -2.942217 |
| C | 5.272957 | -7.686297 | -0.603394 |
| C | -8.909562 | 1.147093 | 2.779149 |
| H | -7.294279 | -1.239259 | -2.273309 |
| H | -9.682332 | -0.612124 | -2.622314 |
| H | -10.766760 | -4.760692 | -2.735941 |
| H | -8.395749 | -5.399874 | -2.387853 |
| H | -4.405643 | -6.335367 | -0.871734 |

| | | | |
|---|---|---|---|
| H | -0.618559 | -3.525450 | -2.238219 |
| H | -3.915243 | -1.794152 | -1.781798 |
| H | -2.390447 | -1.545332 | -2.628900 |
| H | -2.631303 | -8.109284 | 0.063534 |
| H | -1.030695 | -7.434236 | 0.348423 |
| H | -4.553462 | -4.669702 | 1.932593 |
| H | -0.150570 | -2.790238 | 0.799296 |
| H | -1.119734 | -1.311070 | -0.658578 |
| H | -2.631695 | -0.516167 | -0.260723 |
| H | -3.640305 | -6.868560 | 1.789095 |
| H | -2.015993 | -7.108052 | 2.431923 |
| H | 2.727577 | -8.112318 | -1.790729 |
| H | 0.123792 | -8.052600 | -1.734354 |
| H | 7.404679 | -5.808292 | -0.754204 |
| H | 10.257111 | -1.697468 | -1.768617 |
| H | 9.104004 | -4.044527 | -1.782606 |
| H | 10.512222 | 0.728168 | -2.612818 |
| H | -7.950189 | 6.450236 | 1.880072 |
| H | -6.541184 | 8.633075 | 1.626069 |
| H | -4.731223 | 10.211472 | 0.691378 |
| H | 8.725163 | 7.725223 | -0.245722 |
| H | 10.041762 | 5.516173 | -0.677133 |
| H | 0.217614 | 11.798154 | 1.272997 |
| H | 2.778887 | 11.561341 | 0.848566 |
| H | 4.831396 | 10.890688 | -0.507330 |
| H | 6.996284 | 9.499022 | -0.958001 |
| H | 1.242070 | -8.144717 | 3.499608 |
| H | 3.370621 | -9.272198 | 4.144095 |
| H | 5.599336 | -5.888991 | 2.729894 |
| H | 3.492135 | -4.757709 | 2.083756 |
| H | -6.416678 | -3.271081 | 0.886707 |
| H | -7.928235 | -1.163736 | 1.151540 |
| H | -8.511912 | 3.970327 | 2.655612 |
| H | -14.547335 | -3.824826 | -3.326519 |
| H | -14.382334 | -2.305131 | -2.384581 |
| H | -14.120521 | -2.284011 | -4.143756 |
| H | 8.243453 | -8.513649 | 5.005850 |
| H | 8.292684 | -9.329910 | 3.426801 |
| H | 8.998678 | -7.687790 | 3.602321 |
| H | 6.137098 | -7.879687 | 0.040106 |
| H | 4.369237 | -7.921057 | -0.032104 |
| H | -9.641834 | 0.927297 | 1.990720 |
| H | -8.581153 | 0.189992 | 3.196939 |
| H | 5.325501 | -8.389744 | -1.445233 |
| H | -9.434936 | 1.700745 | 3.564523 |
| C | -2.419258 | 11.795660 | 0.229077 |
| H | -1.563504 | 11.962446 | -0.433074 |
| H | -2.290689 | 12.450684 | 1.101396 |
| H | -3.324259 | 12.124802 | -0.291989 |
| C | 10.818824 | 3.547826 | -2.518045 |
| H | 11.343509 | 3.044066 | -3.336548 |
| H | 11.565092 | 3.769852 | -1.743290 |
| H | 10.441231 | 4.505014 | -2.891433 |

## References

[1] N. V. Vorontsova, V. I. Rozenberg, E. V. Sergeeva, E. V. Vorontsov, Z. A. Starikova, K. A. Lyssenko, H. Hopf, Chem. - Eur. J. **2008**, *14*, 4600–4617.
[2] D. Thirion, C. Poriel, R. Métivier, J. Rault-Berthelot, F. Barrière, O. Jeannin, Chem. - Eur. J. **2011**, *17*, 10272–10287.
[3] L. Wang, H. Liu, Z. Huai, S. Yang, *ACS Appl. Mater. Interfaces* **2017**, *9*, 28828–28837.
[4] R. Cirilli, R. Costi, R. Di Santo, F. La Torre, M. Pierini, G. Siani, Anal. Chem. **2009**, *81*, 3560–3570.
[5] G. Uray, S. Jahangir, W. M. F. Fabian, J. Chromatogr. A **2010**, *1217*, 1017–1023.
[6] Gaussian: Frisch, M. J.; Trucks, G. W.; Schlegel, H. B.; Scuseria, G. E.; Robb, M. A.; Cheeseman, J. R.; Scalmani, G.; Barone, V.; Petersson, G. A.; Nakatsuji, H.; Li, X.; Caricato, M.; Marenich, A. V.; Bloino, J.; Janesko, B. G.; Gomperts, R.; Mennucci, B.; Hratchian, H. P.; Ortiz, J. V.; Izmaylov, A. F.; Sonnenberg, J. L.; Williams-Young, D.; Ding, F.; Lipparini, F.; Egidi, F.; Goings, J.; Peng, B.; Petrone, A.; Henderson, T.; Ranasinghe, D.; Zakrzewski, V. G.; Gao, J.; Rega, N.; Zheng, G.; Liang, W.; Hada, M.; Ehara, M.; Toyota, K.; Fukuda, R.; Hasegawa, J.; Ishida, M.; Nakajima, T.; Honda, Y.; Kitao, O.; Nakai, H.; Vreven, T.; Throssell, K.; Montgomery, J. A., Jr.; Peralta, J. E.; Ogliaro, F.; Bearpark, M. J.; Heyd, J. J.; Brothers, E. N.; Kudin, K. N.; Staroverov, V. N.; Keith, T. A.; Kobayashi, R.; Normand, J.; Raghavachari, K.; Rendell, A. P.; Burant, J. C.; Iyengar, S. S.; Tomasi, J.; Cossi, M.; Millam, J. M.; Klene, M.; Adamo, C.; Cammi, R.; Ochterski, J. W.; Martin, R. L.; Morokuma, K.; Farkas, O.; Foresman, J. B.; Fox, D. J. Gaussian 09, Revision D.01, Gaussian, Inc., Wallingford CT, **2009**.
[7] T. Bruhn, A. Schaumlöffel, Y. Hemberger, G. Bringmann, Chirality **2013**, *25*, 243–249.
[8] K. J. Weiland, N. Münch, W. Gschwind, D. Häussinger, M. Mayor, Helv. Chim. Acta (prepared for publication).
[9] D. M. Pawar, K. K. Wilson, E. A. Noe, J. Org. Chem. **2000**, *65*, 1552–1553.
[10] J. Bailey, A. M. North, Trans. Faraday Soc. **1968**, *64*, 1499.

## Supporting Information

# Large Conductance Variations in a Mechanosensitive Single–Molecule Junction

*Davide Stefani, Kevin J. Weiland, Maxim Skripnik, Chunwei Hsu, Mickael L. Perrin, Marcel Mayor, Fabian Pauly and Herre S. J. van der Zant*

# Supporting Section I. Synthesis and Characterisation

## 1. General remarks

All compounds, if commercially available, were used as received. 4-Acetylthioiodobenzene and 4,12-bisethynyl[2.2]paracyclophane were synthesised according to literature known procedures.[1,2] $^{1}$H- and $^{13}$C-NMR spectra were recorded on an *Oxford 400 MHz NMR* with an *Avance III 400 spectrometer*. The chemical shifts are reported in parts per million (ppm) relative to the residual solvent peak and the *J* values are given in Hz (± 0.1 Hz). Deuterated $CD_2Cl_2$ was purchased from *Sigma Aldrich*. The spectra were recorded at 298 K. High resolution ESI-TOF was performed on a *Bruker maxis$^{TM}$ 4G*. The melting point was measured on a *Büchi M-565* melting point apparatus and is uncorrected. The MS spectrum was measured in *m/z* (%). Silica gel for column chromatography (40-63 μm, 230-400 mesh) was purchased from *Silicycle Inc* and TLC was performed on TLC silica gel 60 $F_{254}$ aluminium sheets from *Merck KGaA*.

## 2. Synthetic procedure and analytical data

To a stirred solution of CuI (2.79 mg, 14.6 μmol, 0.05 eq), $Pd(PPh_3)_4$ (33.9 mg, 29.3 μmol, 0.1 eq), and 4-acetylthioiodobenzene (204 mg, 732 μmol, 2.5 eq) in 10 mL THF (7.5 mL) and diisopropylamine (2.5 mL) under Ar was added 4,12-bisethynyl[2.2]paracyclophane (75 mg, 293 μmol, 1.0 eq). The reaction mixture was heated to 55 °C overnight. Subsequently, it was cooled to room temperature, filtered through a plug of celite, and the solvent was removed under reduced pressure. The crude product was purified by column chromatography in toluene/$CH_2Cl_2$ (1:1). 4,12-bis(((4'-acetylthio)phenyl)ethynyl)[2.2]paracyclophane was isolated as a white solid (88 mg, 158 μmol, 54%). mp: 192-193 °C; $^{1}$H NMR (400 MHz, $CD_2Cl_2$): δ 7.67 – 7.62 (m, 4H), 7.48 – 7.44 (m, 4H), 7.04 (dd, *J* = 7.9, 1.9 Hz, 2H), 6.63 (d, *J* = 1.9 Hz, 2H), 6.54 (d, *J* = 7.9 Hz, 2H), 3.67 (ddd, *J* = 13.1, 10.4, 2.9 Hz, 2H), 3.23 (ddd, *J* = 12.8, 10.4, 4.6 Hz, 2H), 3.12 – 2.91 (m, 4H), 2.44 (s, 6H); $^{13}$C NMR (101 MHz, $CD_2Cl_2$) δ 193.98, 143.03, 140.32, 137.82, 135.04, 133.81, 132.47, 131.25, 128.74, 125.52, 124.83, 92.55, 91.99, 34.58, 34.41, 30.69; HRMS (ESI, +): *m/z* calcd. for $C_{36}H_{28}NaO_2S_2$ $[M+Na]^+$ 579.1429; found: 579.1423.

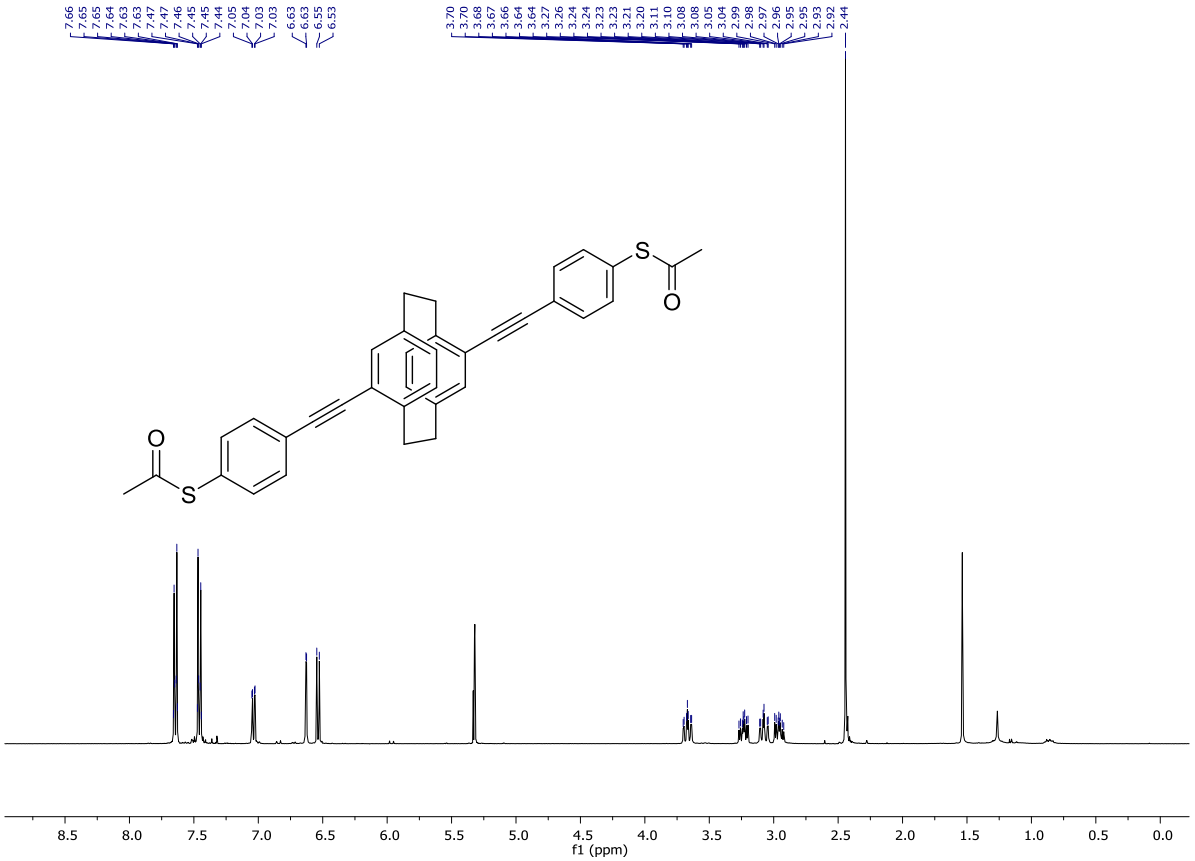


**Figure S1.** $^{1}H$ NMR spectrum (400 MHz, 298 K; $CD_2Cl_2$).

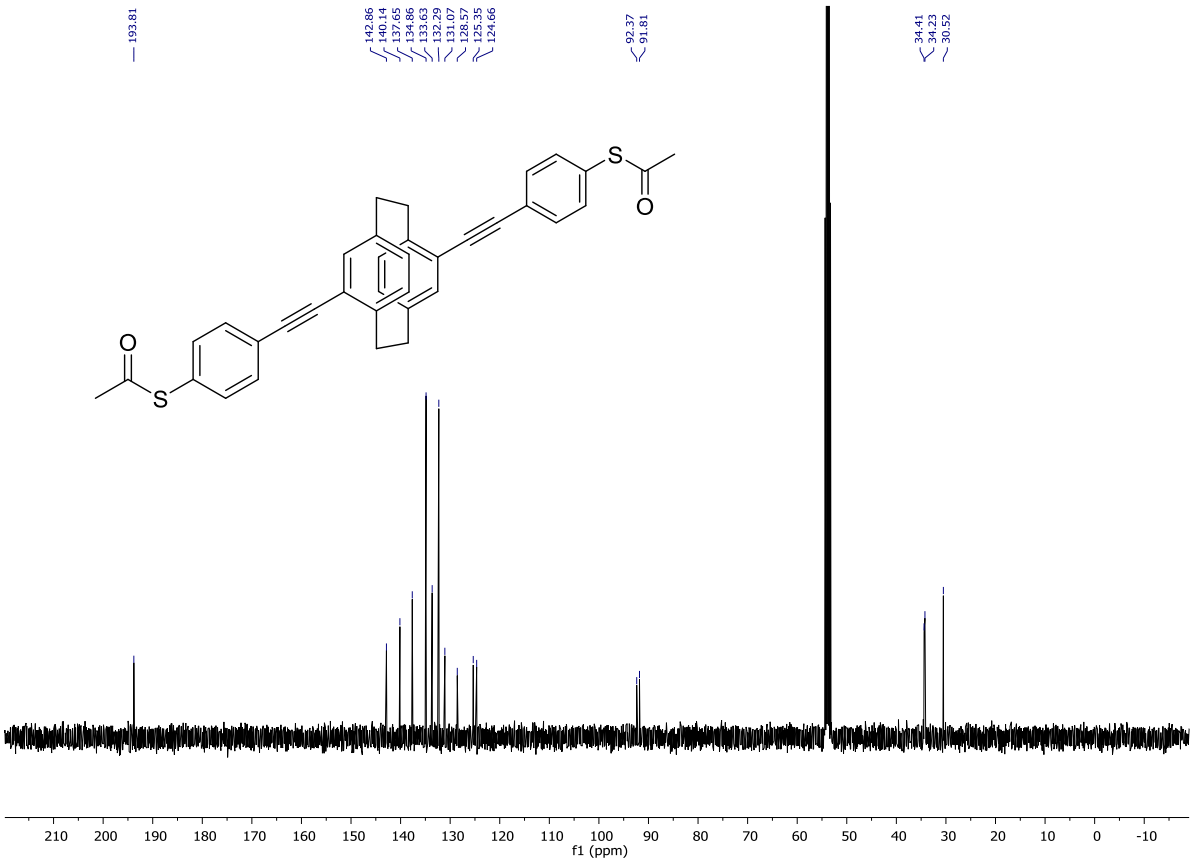


**Figure S2.** $^{13}C$ NMR spectrum (126 MHz, 298 K; $CD_2Cl_2$).

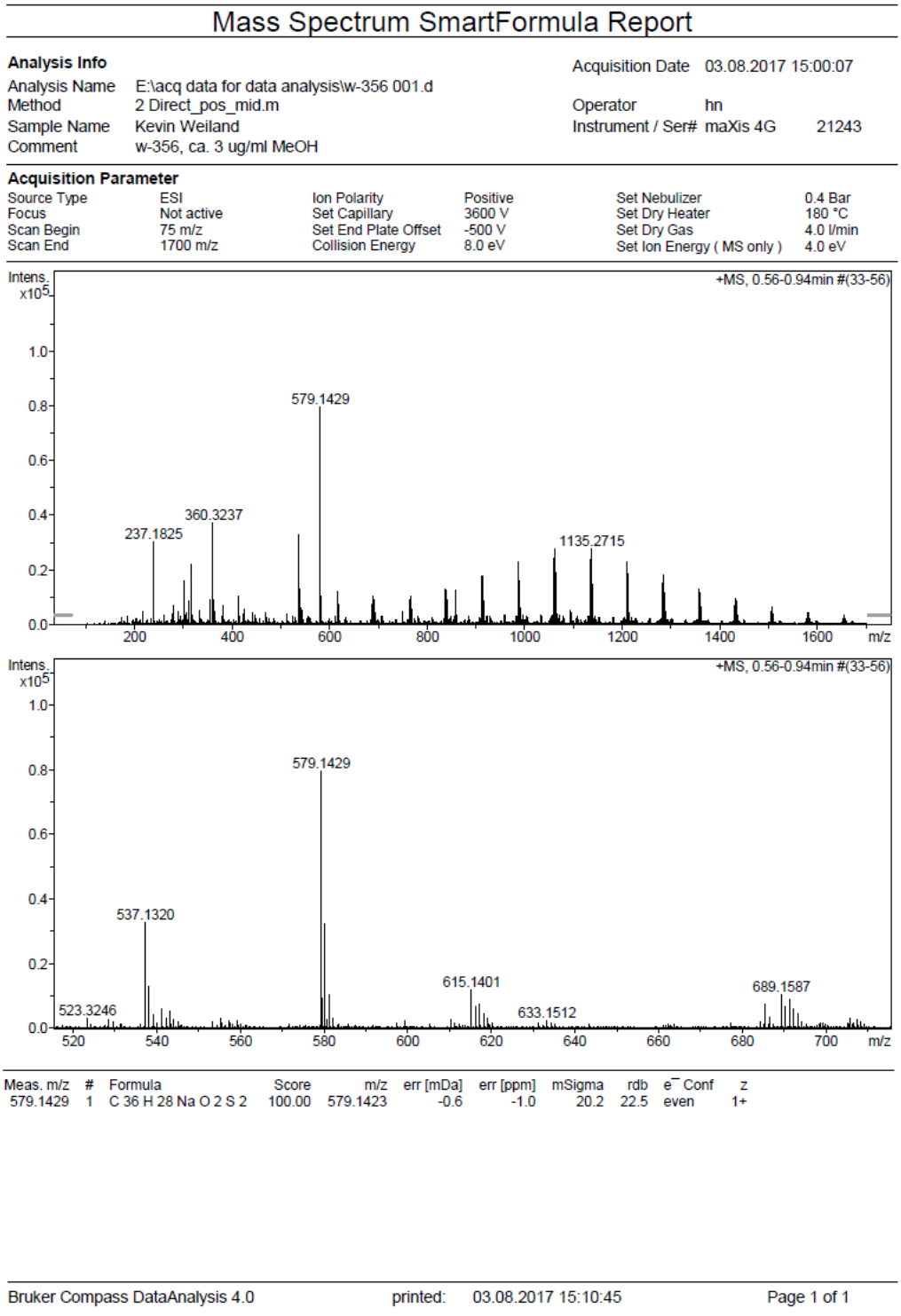


**Figure S3.** HR ESI spectrum.

## 3. Crystal data and structure refinement

**Table S1** Single crystal data

| | |
|---|---|
| Empirical Formula | $C_{36}H_{28}O_2S_2$ |
| Formula Weight | 556.75 |
| Crystal habit | colorless plates |
| Temperature/K | 123 |
| Crystal system | monoclinic |
| Space group | P $2_1$/n |
| a/Å | 6.96730(10) |
| b/Å | 10.7521(2) |
| c/Å | 18.3959(3) |
| α/° | 90 |
| β/° | 90.5290(10) |
| γ/° | 90 |
| Volume/Å$^3$ | 1378.04(4) |
| Z | 2 |
| $\rho_{calc}$/g cm$^{-3}$ | 1.342 |
| μ/mm$^{-1}$ | 1.313 |
| F(000) | 583.997 |
| Crystal size/mm$^3$ | 0.030 x 0.130 x 0.250 |
| Radiation | Ga$K_\alpha$ (λ = 1.34143 Å) |
| $\Theta_{max}$/° | 59.338 |
| Reflections collected | 27529 |
| Independent reflections | 3022 merging (r = 0.028) |
| Observed reflections | 2956 |
| Parameters | 181 |
| Goodness-of-fit on F$^2$ | 1.0848 |
| Final R indices [I≥2σ(I)] | 0.0343 |
| Final R indices [all data] | 0.0372 |
| Largest diff. peak hole/e Å$^{-3}$ | -0.31/0.28 |
| CCDC number | 1836317 |

Single crystals suitable for crystal structure determination were grown by slow evaporation of a solution of hexane and dichloromethane at room temperature. The crystal was measured on a Stoe StadiVari. Minimal/maximal transmission 0.84/0.96. The STOE X-AREA suite has been used for data collection and integration. The structure was solved by other methods using the program Superflip. Least-squares refinement against F was carried out on all non-hydrogen atoms using the program CRYSTALS. Chebychev polynomial weights were used to complete the refinement. Plots were produced using CAMERON. Crystallographic data (excluding structure factors) for the structure in this paper have been deposited with the Cambridge Crystallographic Data Center. Copies of the data can be obtained, free of

charge, on application to the CCDC, 12 Union Road, Cambridge CB2 1EZ, UK [fax: +44-1223-336033 or e-mail: deposit@ccdc.cam.ac.uk]. Molecular drawings were generated using Mercury.

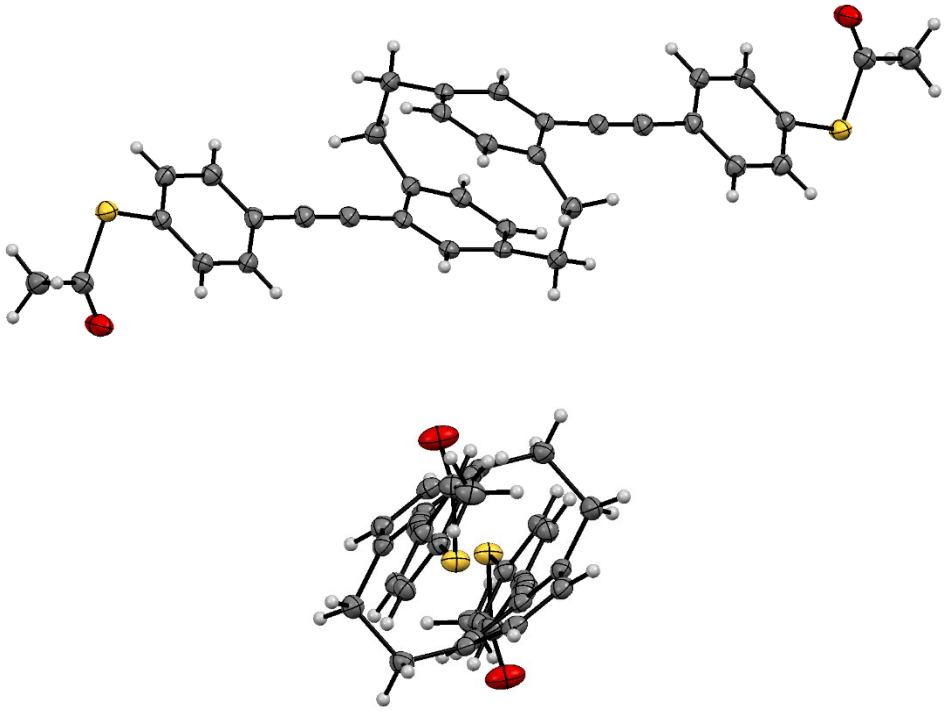

**Figure S4.** ORTEP diagrams of molecule **1**, ellipsoids shown at the 50% probability level.

# Supporting Section II. Transport Measurements

## 1. Fast-breaking measurements

The conductance histograms for fast-breaking and distance-modulation measurements are displayed in Fig. S5. The most probable conductance values ($3.7 \cdot 10^{-6}$ $G_0$ and $2.7 \cdot 10^{-6}$ $G_0$, respectively) match well despite the measurement being performed on different samples and with different techniques. Distance-modulation measurements were recorded for a maximum time of 120 s, and therefore the histogram highlights the most stable configurations, as opposed to the fast-breaking measurements, where metastable ones have a bigger impact on the conductance histogram.

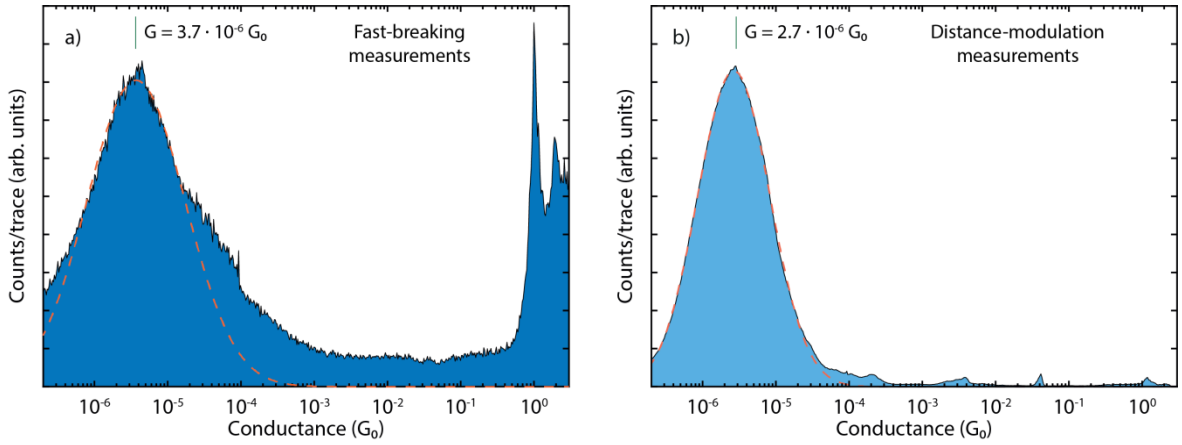


**Figure S5.** One-dimensional histogram a) of a fast-breaking measurement of sample **A** and b) of a distance-modulation measurement of sample **B**. The applied bias is 100 mV in both cases, fast-breaking measurements were recorded at 4.0 nm/s. The dashed orange line shows the fit result.

Figures S6-S9 show the two-dimensional histograms of samples **A-D**. The concentrations of the molecular solution dropcasted were 9 µM for sample **A** and **B**, 90 µM for sample **C**, and 900 µM for sample **D.** As can be seen from the histograms, no significant dependence on the concentration is observed and all samples show similar conductance oscillations.

For each measurement we perform a thorough characterisation of the bare device before dropcasting the molecular solution to ensure that the electrodes are clean and well aligned. The characterisation of the bare device used for sample **A** is shown in Fig. S10.

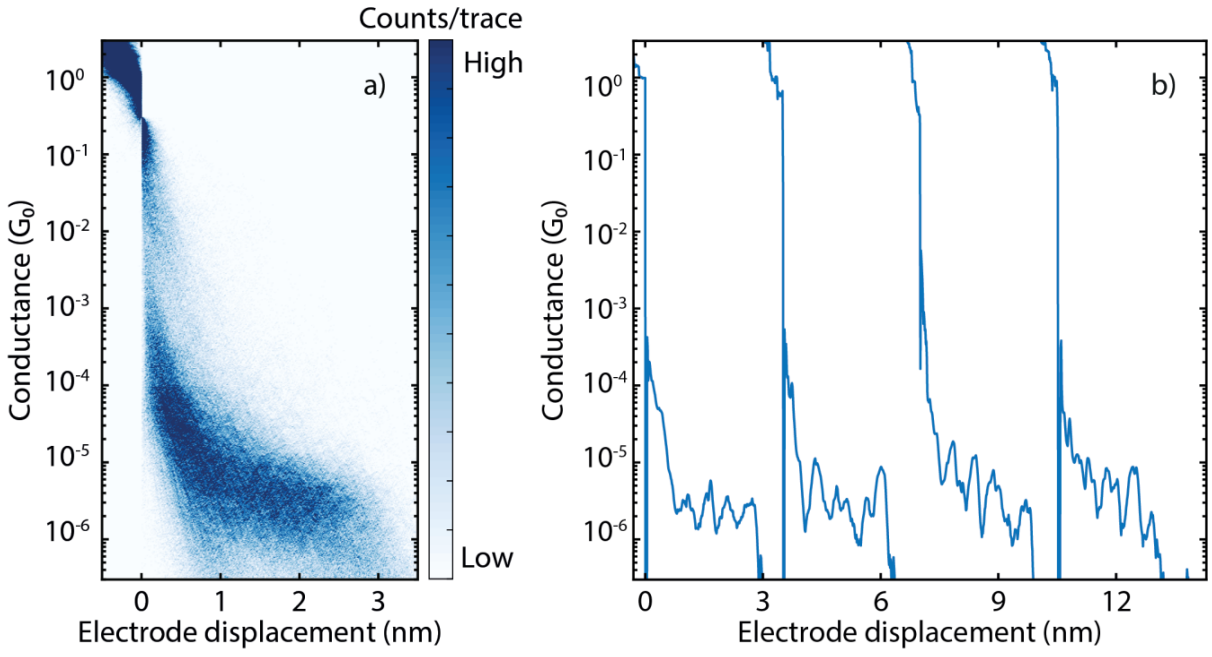


**Figure S6.**

a) Two-dimensional conductance histogram of sample **A** with no data selection. b) Examples of the 3,000 consecutive breaking traces. The applied bias is 100 mV and the electrode speed is 4.0 nm/s.

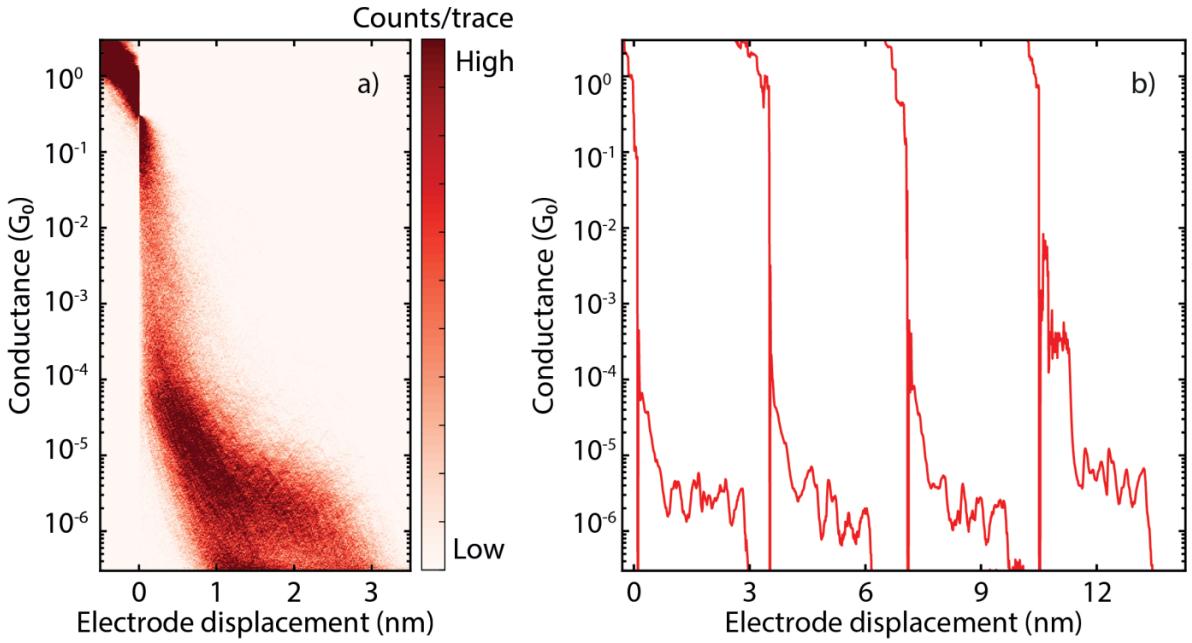


**Figure S7.** a) Two-dimensional conductance histogram of sample **B** with no data selection. b) Examples of the 3,000 consecutive breaking traces. The applied bias is 100 mV and the electrode speed is 4.0 nm/s.

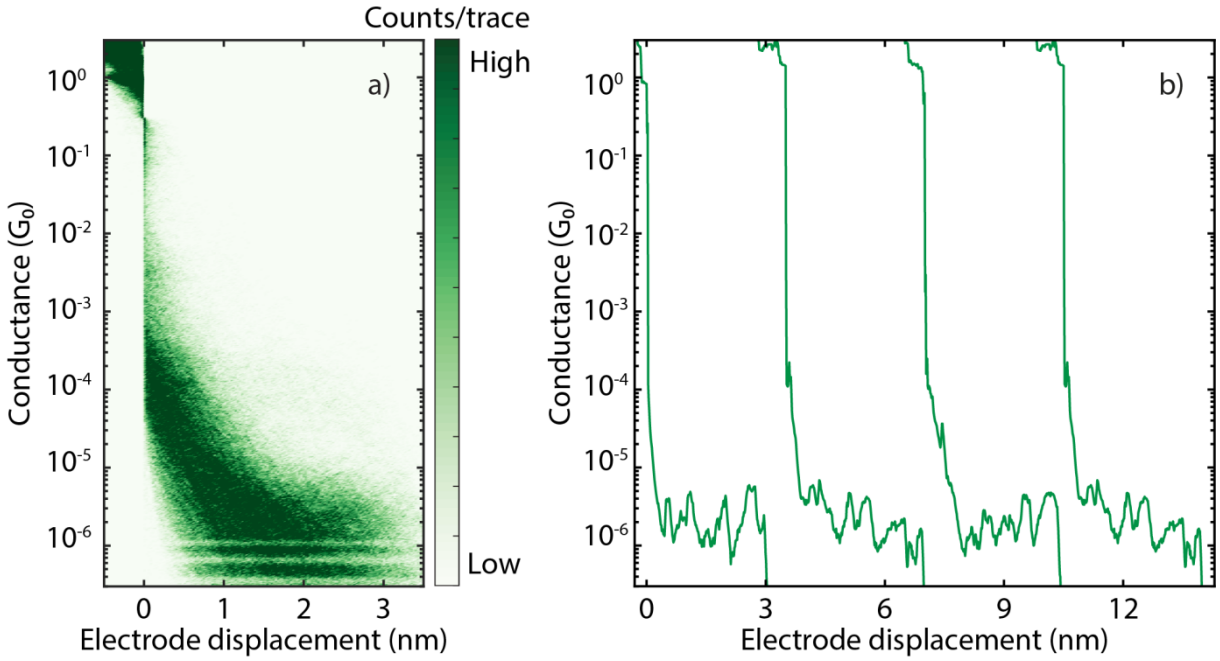


**Figure S8.** a) Two-dimensional conductance histogram of sample **C** with no data selection. b) Examples of the 3,000 consecutive breaking traces. The applied bias is 100 mV and the electrode speed is 4.0 nm/s.

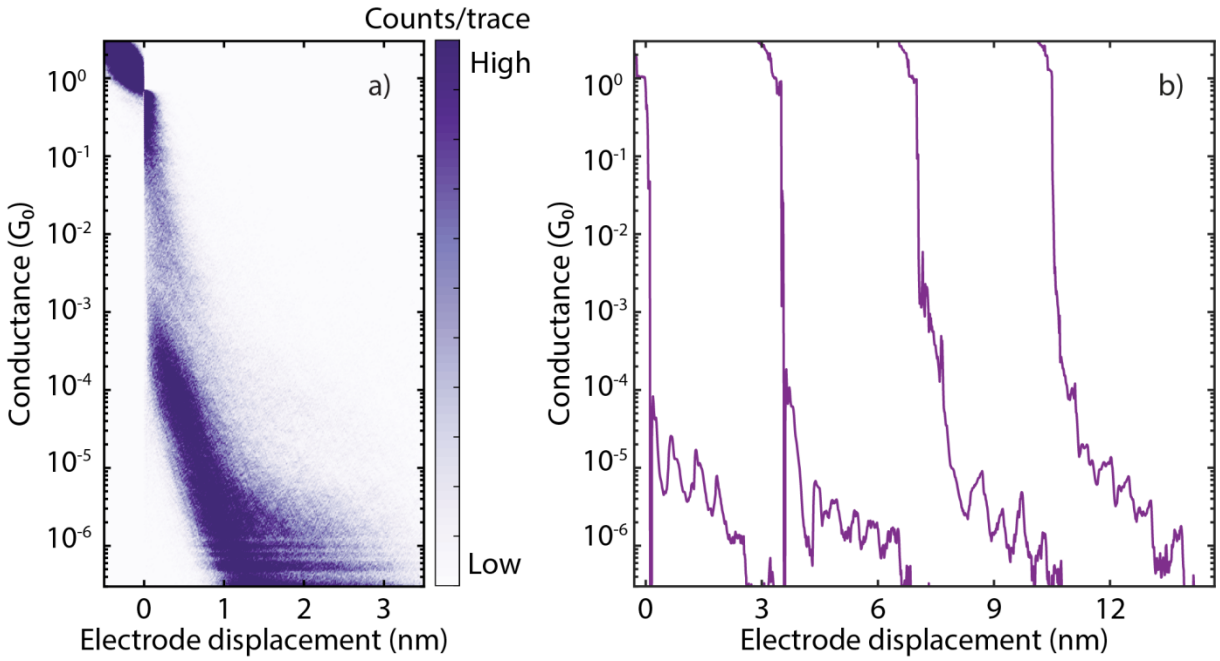


**Figure S9.** a) Two-dimensional conductance histogram of sample **D** with no data selection. b) Examples of the 5,000 consecutive breaking traces. The applied bias is 100 mV and the electrode speed is 4.0 nm/s.

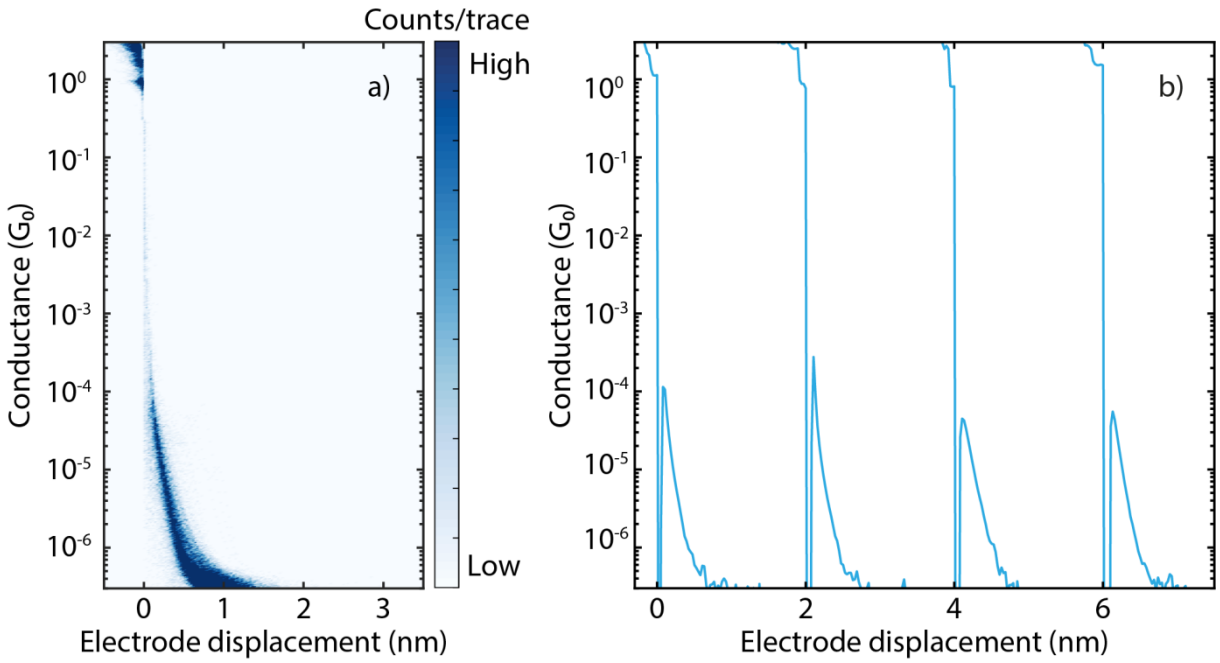


**Figure S10.** a) Two-dimensional conductance histogram and b) examples of conductance traces from the characterisation of the pristine sample used for measurements **A**. The applied bias is 100 mV and the electrode speed is 8.0 nm/s.

**Estimation of the oscillation periodicity**

To estimate the periodicity of the conductance variations, we selected 315 breaking traces from the 3,000 of sample **A** that showed particularly clear oscillations. For each trace we then identified the position of peaks with a prominence of at least 30% and calculated the distance between consecutive peaks. We fit a Gaussian to the histogram and find the parameters shown in the inset of Fig. S11.

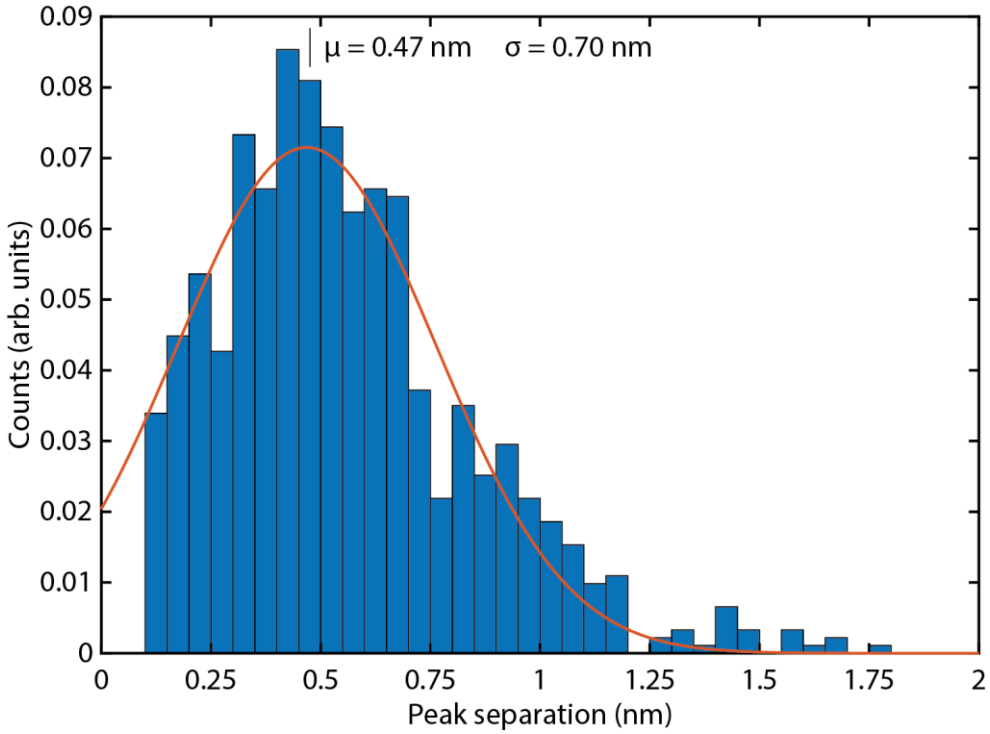


**Figure S11.** Distribution of the separation between consecutive peaks found in the selected breaking traces from sample **A**. The Gaussian fitted to it is represented as an orange line.

## 2. Distance-modulation measurements

Additional measurements of sample **B** are shown in Fig. S12. These measurements were taken with a peak-to-peak amplitude of 2.5 Å, smaller than those presented in the main text and in the following figures. Also in this case, both traces in-phase and in antiphase are observed.

More examples of traces in-phase (Fig. S13), in antiphase (Fig. S14) and with doubled frequency (Fig. S15-S16) are reported here. Figure S17 shows a trace for which the behaviour changes from antiphase to in-phase. The inset shows the moment of the transition. Figure S18 presents the Fourier Transform of the distance-modulation traces showing that it is mainly at the same frequency of the driving modulation.

Figure S19 shows another full distance-modulation trace with the initial opening of the gap, the gap size modulation, and the final breaking to the noise level.

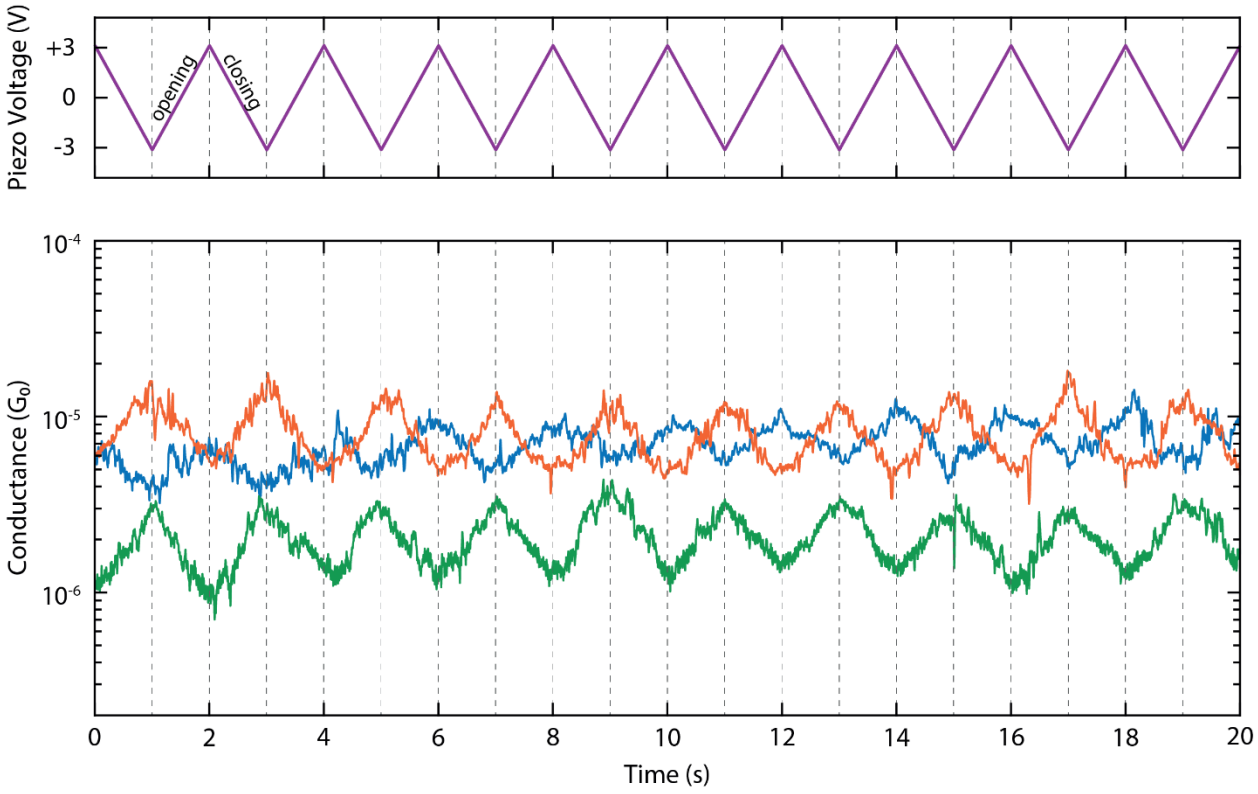


**Figure S12.** Examples of distance-modulation traces. The total modulation time is 120 s at a frequency of 0.5 Hz. The blue, green and orange lines (bottom panel) represent three different conductance measurements, whereas the purple line (top panel) represents the voltage applied to the piezoelectric stack. The applied piezo voltage translates into a **peak-to-peak distance of 2.5 Å** and a higher voltage corresponds to a larger electrode distance. The conductance responds to the electrode-separation modulation either in-phase (blue curve) or in antiphase (orange and green curves).

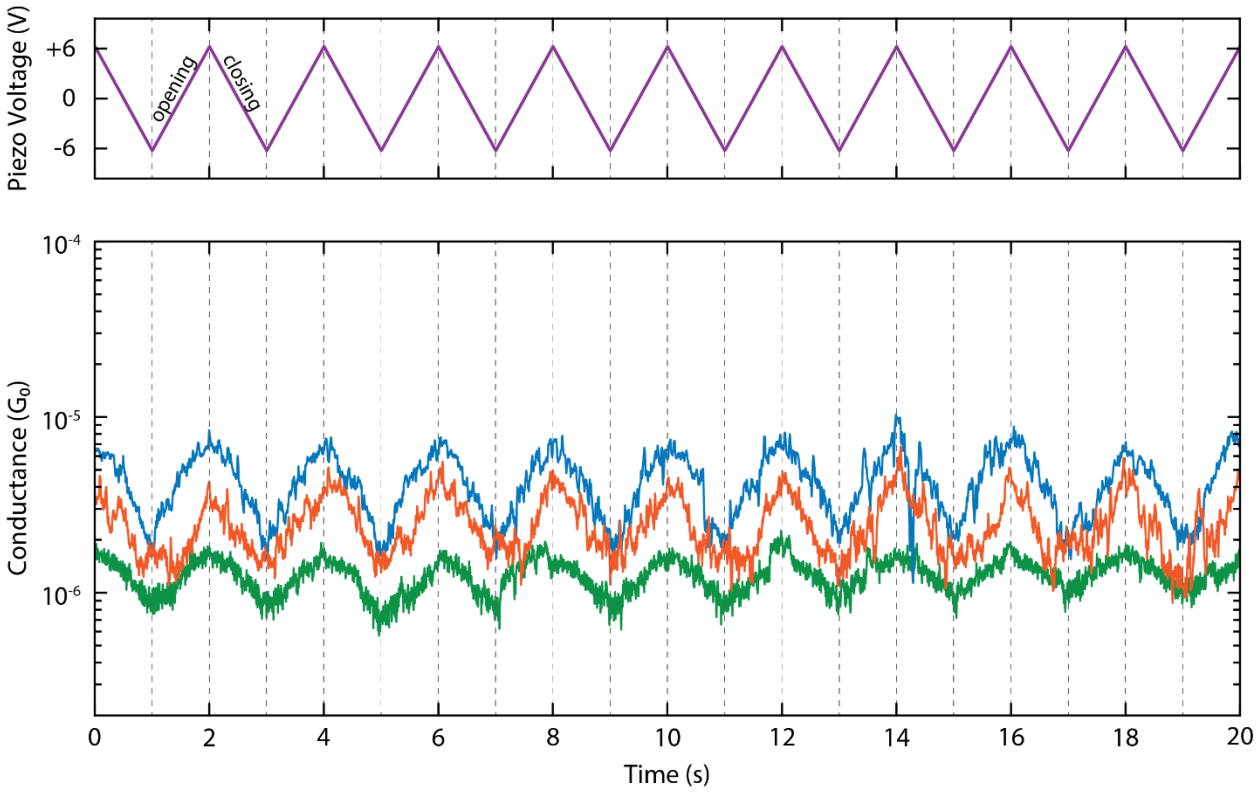


**Figure S13.** Examples of distance-modulation traces. The total modulation time is 120 s at a frequency of 0.5 Hz. The blue, green and orange lines (bottom panel) represent three different conductance measurements, whereas the purple line (top panel) represents the voltage applied to the piezoelectric stack. The applied piezo voltage translates into a peak-to-peak distance of 5.0 Å and a higher voltage corresponds to a larger electrode distance. In these cases, the conductance responds **in-phase** with the gap-size variation.

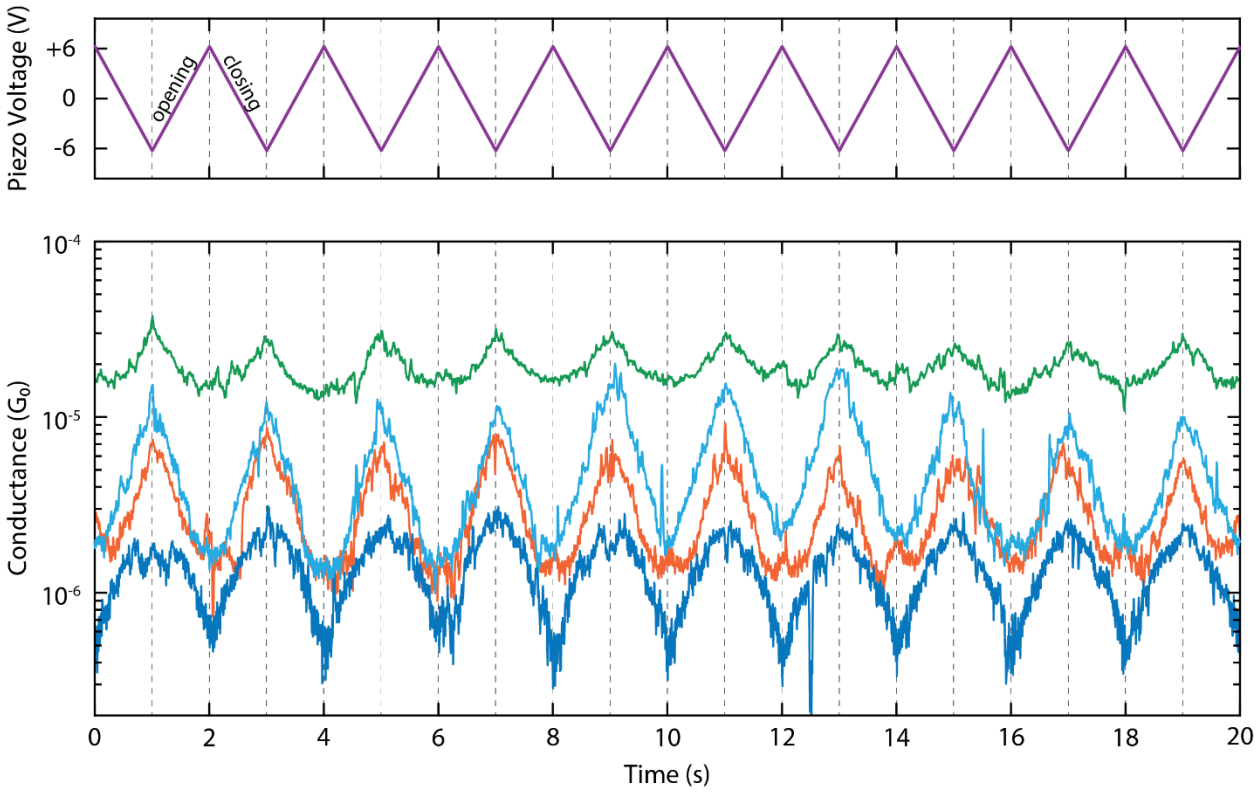


**Figure S14.** Examples of distance-modulation traces. The total modulation time is 120 s at a frequency of 0.5 Hz. The blue, green, cyan and orange lines (bottom panel) represent three different conductance measurements, whereas the purple line (top panel) represents the voltage applied to the piezoelectric stack. The applied piezo voltage translates into a peak-to-peak distance of 5.0 Å and a higher voltage corresponds to a larger electrode distance. In these cases the conductance responds **in antiphase** with the gap-size variation.

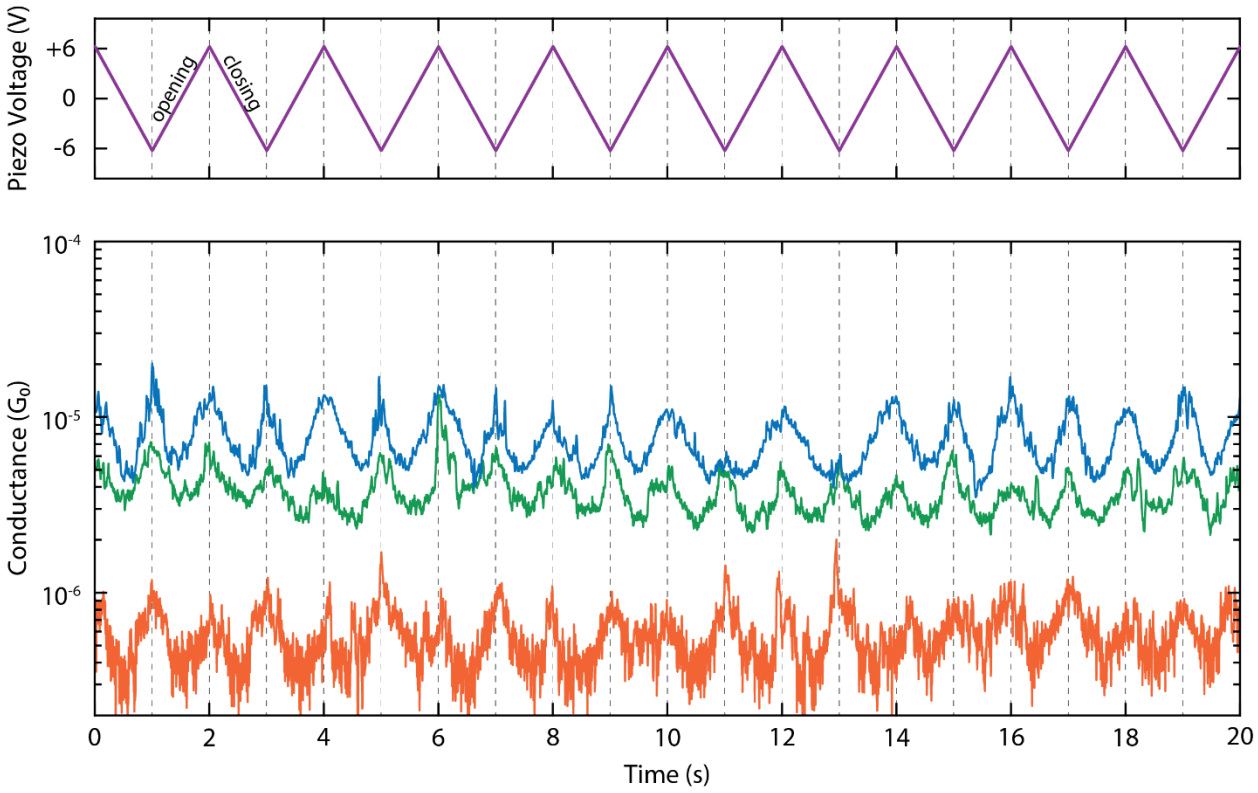


**Figure S15.** Examples of distance-modulation traces. The total modulation time is 120 s at a frequency of 0.5 Hz. The blue, green and orange lines (bottom panel) represent three different conductance measurements, whereas the purple line (top panel) represents the voltage applied to the piezoelectric stack. The applied piezo voltage translates into a peak-to-peak distance of 5.0 Å and a higher voltage corresponds to a larger electrode distance. In these cases the conductance responds with **double the frequency** of the driving modulation.

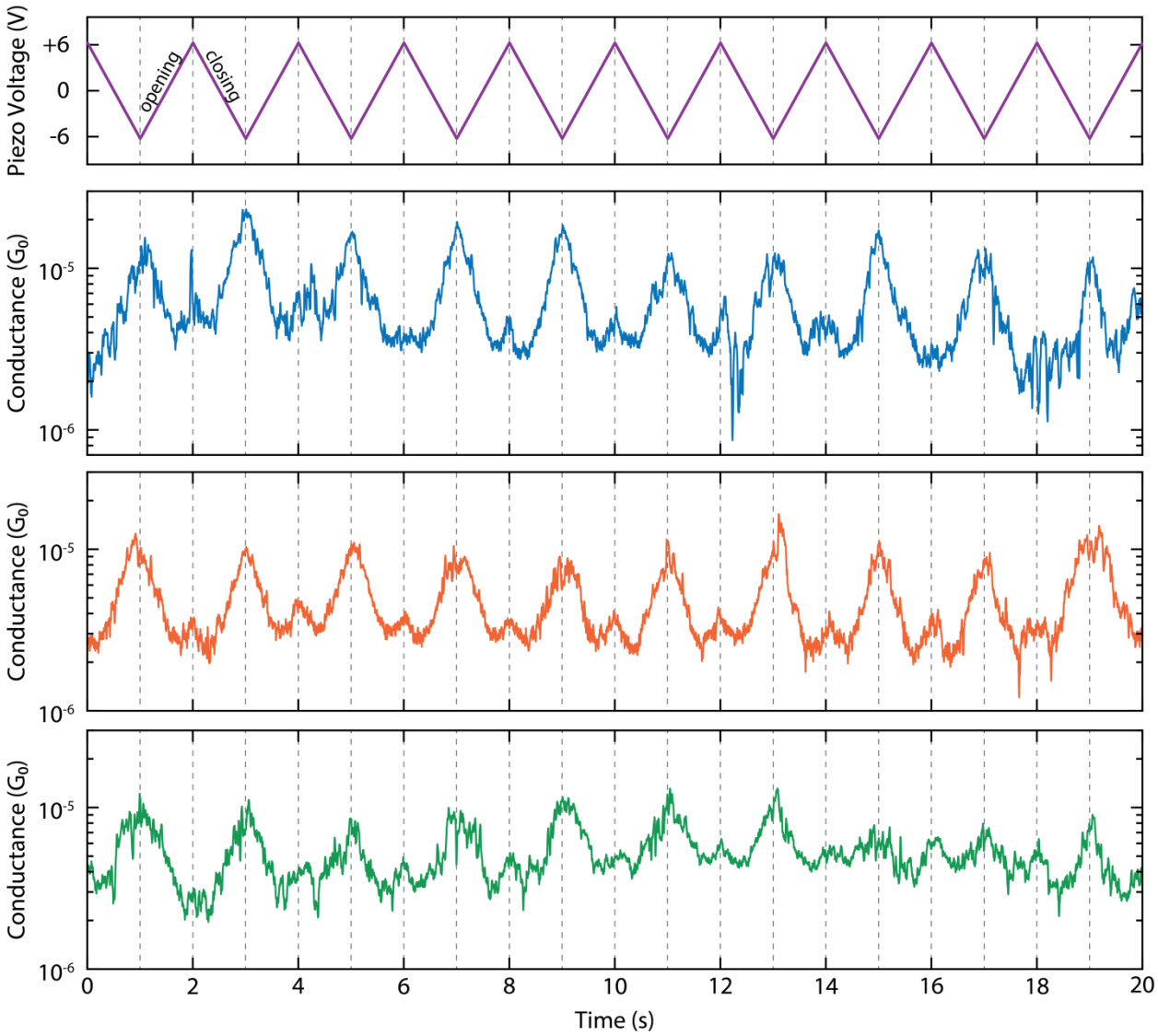


**Figure S16.** Examples of distance-modulation traces. The total modulation time is 120 s at a frequency of 0.5 Hz. The blue, green and orange lines (bottom panels) represent three different conductance measurements, whereas the purple line (top panel) represents the voltage applied to the piezoelectric stack. The applied piezo voltage translates into a peak-to-peak distance of 5.0 Å and a higher voltage corresponds to a larger electrode distance. In these cases the conductance responds with **double the frequency** of the driving modulation, with subsequent peaks having different heights.

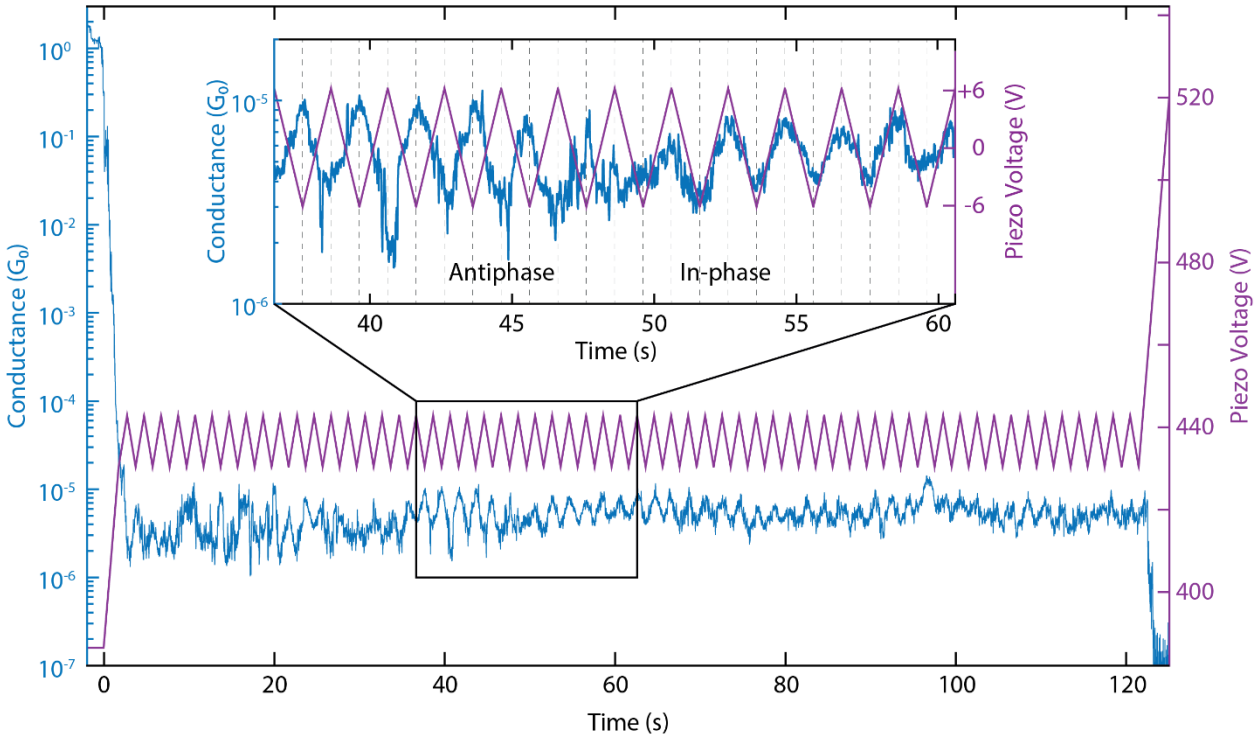


**Figure S17.** Example of a distance-modulation trace. The total modulation time is 120 s at a frequency of 0.5 Hz. The blue line represents the conductance measurement, whereas the purple line the voltage applied to the piezoelectric stack. The applied piezo voltage translates into a peak-to-peak distance of 5.0 Å, and a higher voltage corresponds to a larger electrode distance. The inset shows a portion of the trace in which a shift from antiphase to in-phase occurs.

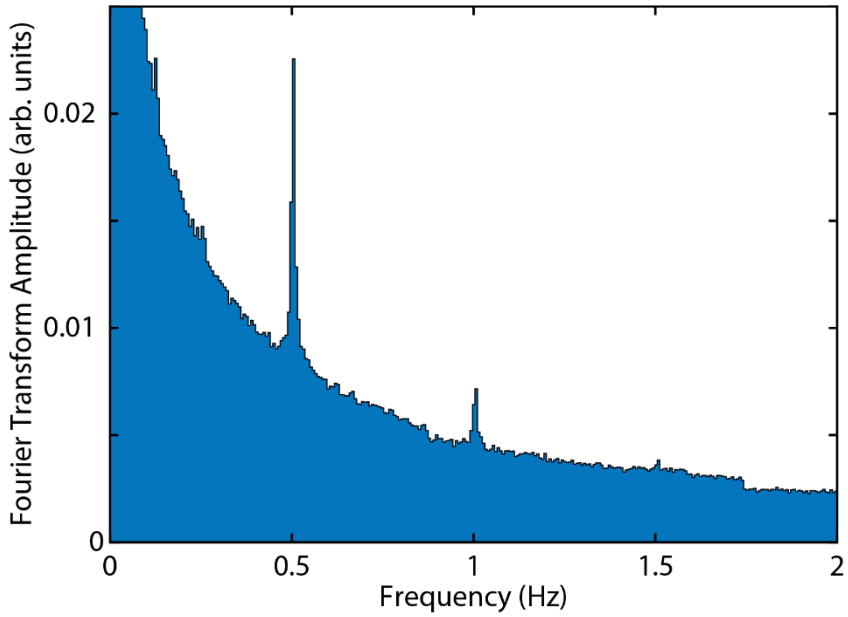


**Figure S18.** Fourier Transform of the conductance traces measured with a displacement modulation at 0.5 Hz. A pronounced peak is found at the driving frequency of the piezoelectric stack and a smaller one at the second harmonic.

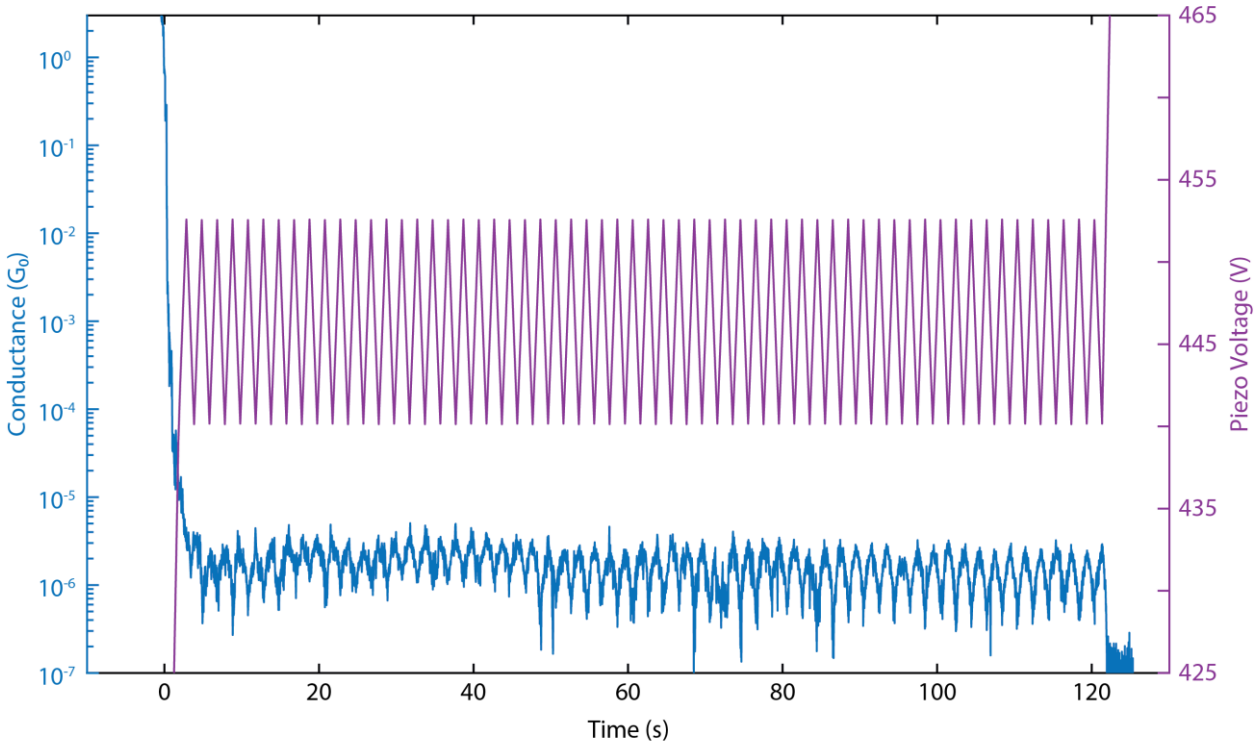


**Figure S19.** Example of a distance-modulation trace. The full trace is shown here with the initial opening of the gap, the gap size modulation at 0.5 Hz for 120 s, and the final breaking to the noise level. The blue line represents the conductance measurement, whereas the purple line represents the voltage applied to the piezoelectric stack. The applied piezo voltage translates into a peak-to-peak distance of 5.0 Å and a higher voltage corresponds to a larger electrode distance.

## 3. Statistical analysis

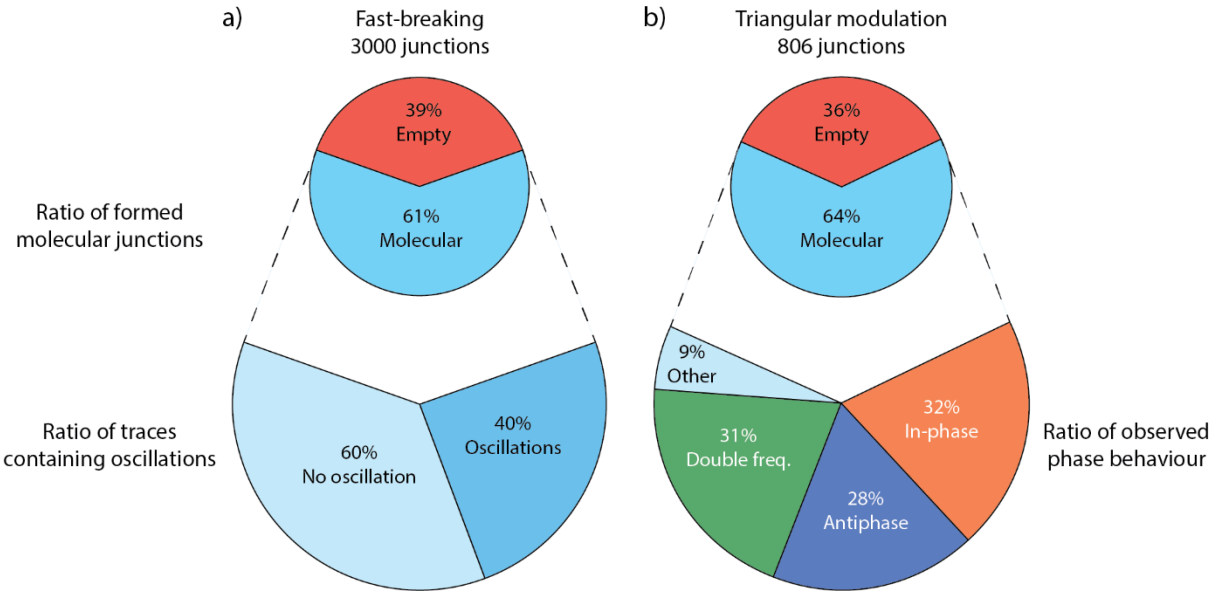


**Figure S20.** a) Junction-formation statistics and percentage of molecular junctions showing conductance oscillations for fast-breaking measurements (sample **A**). b) Junction-formation statistics and percentage of phase response behaviours of the conductance oscillations in triangular modulation measurements (sample **B**). The percentage of molecular traces is remarkably similar despite the measurements being performed on different samples and with different techniques.

## 4. Estimation of the gauge factor

The gauge factor of a strain gauge *GF* is defined as the ratio between the change in relative electrical conductance $\Delta G/G$ and the mechanical strain $\varepsilon$. From the distance modulation experiment it is possible to estimate the gauge factor of the molecule. To do so, we selected 123 traces from the 806 of sample **B** that showed particularly clear and stable oscillations. We then split each trace into semi-periods of the piezo modulation, i.e., portions in which the electrodes move in the same direction. For each of these portions we then identified the maxima and minima in conductance and their respective positions. From the former two, $\Delta G/G$ is extracted by dividing the change in conductance with the average conductance for the portion of trace considered; from the latter, $\varepsilon$ is obtained by dividing the electrode displacement ($\Delta L$) by the size of the relaxed molecule ($L$ = 1.75 nm). The *GF* is thus given by:

$$GF = \frac{\frac{\Delta G}{G}}{\varepsilon} = \frac{\frac{\Delta G}{G}}{\frac{\Delta L}{L}}$$

Since the frequency of the modulation was 0.5 Hz for a maximum time of 120 s, each trace can provide up to 120 gauge factor values.

The *GF* distribution is shown in Fig. S21. Both in-phase and antiphase traces were among the selected traces, which means that both positive and negative values in the gauge factor can be obtained: negative gauge factor values are obtained from antiphase traces. The peaks in the distribution are found at *GF* = +5 and *GF* = -7. The distribution of the absolute values is plotted in the main text (Fig. 3b).

This simple method for estimating the *GF* yielded the same qualitative result as others with more restrictive constraints in the peak selection or with preliminary smoothing of the curves, showing that noise spikes do not play an important role in the average result.

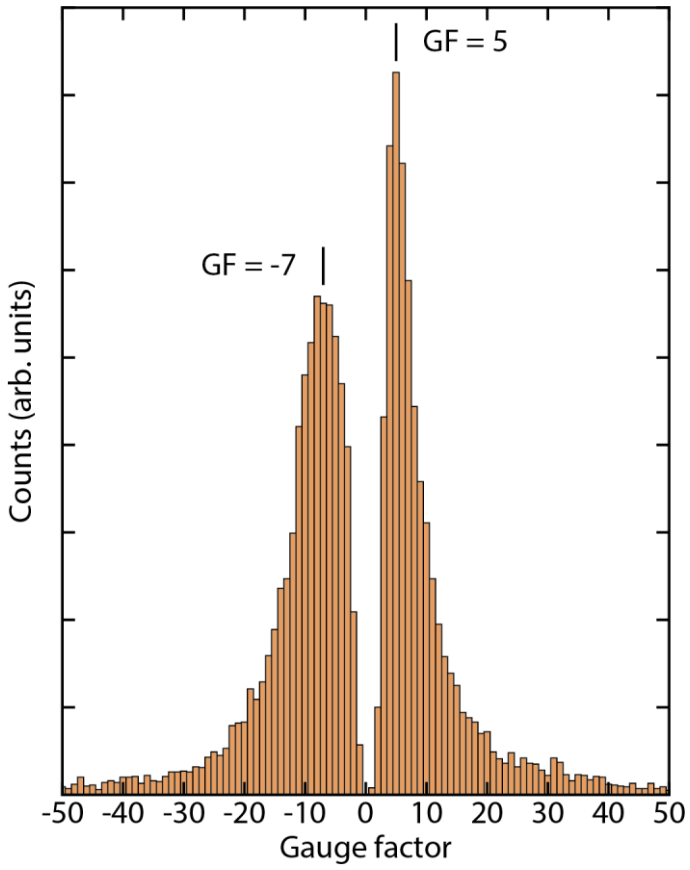


**Figure S21.** Distribution of gauge factor values obtained from 123 selected traces of the distance-modulation measurements performed on sample **B**.

# Supporting Section III. Transport Calculations

## 1. Setup of DFT simulations

Throughout all DFT calculations we used the def-SVP basis set and the PBE functional.[3,4] During structural relaxations the total energy was converged to $10^{-6}$ a.u. and the maximum norm of the Cartesian gradient to $10^{-3}$ a.u. Initial configurations of molecular junctions were obtained in the following way: The gas-phase molecule was relaxed with one gold atom at each sulfur atom. Independently, we relaxed the corresponding gold leads with a benzene ring attached through a sulfur atom. We then combined the relaxed structures to the final system, which we call extended central cluster (ECC), as described in Bürkle *et al.*[5] In short, this was done by replacing the benzene rings, attached to the leads, with the relaxed molecule. Finally, the obtained system was relaxed once again, giving the initial structure for further molecular junction simulations, in which the lead separation was varied in steps of 0.1 or 0.2 Å.

## 2. Quantum interference effects

The source of the transmission valley in Fig. 5 lies in the quantum mechanical interference of frontier orbital contributions to the transmission. Its presence can be explained solely by the gas-phase HOMO (GPH) and gas-phase LUMO (GPL). However, the shift in energy of the conductance dip as a function of the displacement can only be explained, if one also takes the GPH-1 and GPL+1 into account. The underlying theory is described in the literature.[6,7] In a toy model, the electronic transmission of our ECC can be expressed as

$$\tau(E) = \frac{(2\pi\beta^2)^2}{2} G^a(E) G^r(E) \rho_l(E) \rho_r(E) \quad (1)$$

where β is the transfer integral of the gold-sulfur bond, $G^{a/r}(E)$ are matrix elements of the energy-dependent advanced and retarded Green's functions of the molecule that connect terminal sulfur atoms, and $\rho_{l/r}(E)$ are the local densities of states of the left and right leads. The zeroth-order Green's functions, describing a molecular junction, in which the molecule does not interact with the leads, are given as

$$G^{(0)r/a}(E) = \sum_k \frac{C_{l,k} C^*_{r,k}}{E - \epsilon_k \pm i\eta} \quad (2)$$

with the expansion coefficients $C_{l/r,k}$ of the $k$-th molecular orbital at the left/right sulfur atom and the orbital energies $\epsilon_k$. Using $G^{a/r}(E) \approx G^{(0)a/r}(E)$, the transmission can be written as

$$\tau(E) \propto \left|G^{(0)r}(E)\right|^2. \tag{3}$$

A general rule for the conductance, i.e. the transmission at the Fermi energy $E_F$, can be deduced from Eq. 2: Since $E_F - \epsilon_{HOMO}$ and $E_F - \epsilon_{LUMO}$ have opposite signs, the corresponding summands in the zeroth-order Green's function $G^{(0)r}(E)$,

$$\frac{C_{l,HOMO}C^*_{r,HOMO}}{E_F-\epsilon_{HOMO}+i\eta} + \frac{C_{l,LUMO}C^*_{r,LUMO}}{E_F-\epsilon_{LUMO}+i\eta}, \tag{4}$$

will have the same (different) signs, if the products $C_{l,HOMO}C^*_{r,HOMO}$ and $C_{l,LUMO}C^*_{r,LUMO}$ have different (same) signs. The sign of each coefficient $C_{l/r,k}$ corresponds to the sign of the wave function $k$ at the particular site *l,r*, i.e. on the electrode-connecting sulfur atoms.

The HOMO and LUMO in the molecular subspace of our ECC at displacements close to the observed transmission valley (precisely, for displacements *d* with -1 Å < *d* < 2 Å) are related to the GPH and GPL, respectively (Fig. 5c). Since these molecular orbitals are centrally symmetric, the coefficients $C_{l/r,k}$ need to be of the same sign for each orbital at the left and right sites. As a consequence the products $C_{l,k}C^*_{r,k}$ yield identical signs for both orbitals, which finally leads to an antiresonance in the transmission $\tau(E)$ at an energy $\epsilon_{HOMO} < E < \epsilon_{LUMO}$.

The shift of this energy upon mechanical deformation can be explained, if we take also the HOMO-1 and LUMO+1 (attributed to GPH-1 and GPL+1) into account. To illustrate this, we calculate the conductance according to Eq. 3 for a toy model system, which has four molecular orbitals with displacement-dependent energies $\epsilon_k(d) \coloneqq a_k \arctan(b_k + \mathrm{d}) + \epsilon_k^0$, where $k \in \{\mathrm{HOMO}-1, \mathrm{HOMO}, \mathrm{LUMO}, \mathrm{LUMO}+1\}$. The coefficients $a_k, b_k$ and $\epsilon_k^0$ are chosen to mimic the energy dependence of the orbitals according to the DFT results in Fig. 5c. The products $C_{l,k}C^*_{r,k} =: c_k$ were chosen according to the symmetries of the gas-phase molecular orbitals of the studied molecule from Fig. 4a: $c_k = \pm 1$ for centrally symmetric/antisymmetric wave functions. Figure S22 shows the resulting transmission map on the left side. The map on the right side shows the transmission of an extended toy model, where we additionally

assume four more molecular orbitals (eight in total) at displacement-independent energies of -1.4, -1.2, 5 and 8 eV with products $c_k$ equal to -1, 1, 1 and -1.

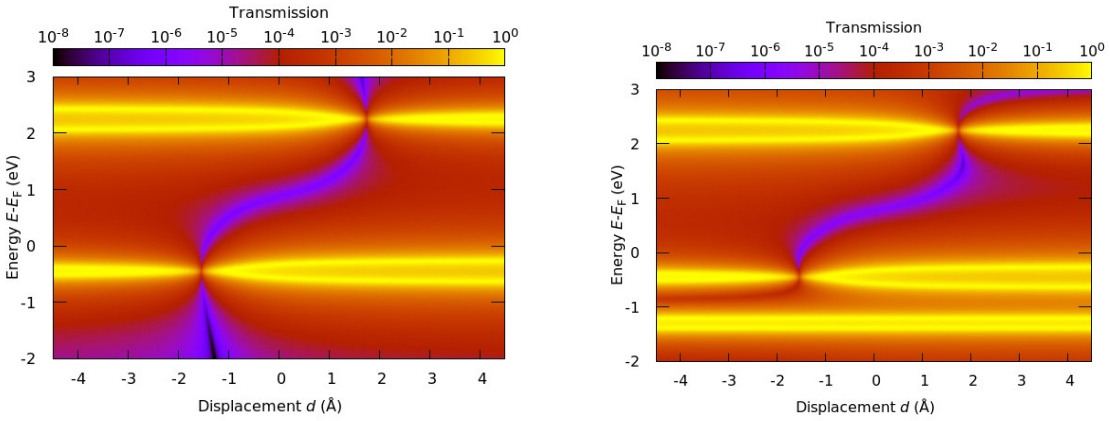


**Figure S22.** Calculated transmission of a toy model. The molecular orbital energies and their dependence on the displacement (causing the horizontal yellow traces) were modelled in such a way as to mimic the traces obtained from the DFT calculations in Fig. 5. The simpler model (left map) considers four orbitals, while the refined model (right map) additionally considers four more displacement-independent orbitals (of which only two are visible in the chosen energy range).

An antiresonance with a clear displacement dependence occurs between the frontier orbitals within this toy model. The antiresonance crosses the orbital energies, where GPH-1, GPH and GPL, GPL+1 degenerate. This exactly matches the observations made in the DFT transmission map, although the shape of the antiresonance valley is slightly different. The position of the antiresonance depends on the relative energy distances $\Delta_H \coloneqq \epsilon_{GPH} - \epsilon_{GPH-1}$ and $\Delta_L \coloneqq \epsilon_{GPL+1} - \epsilon_{GPL}$. At $d = -1.5$ Å GPH-1 and GPH degenerate and $\Delta_H = 0$. Since GPH and GPH-1 energies are equal and their coefficients are of opposite sign ($c_{GPH-1} = -1$ and $c_{GPH} = +1$) the corresponding summands in Eq. 2 cancel out. Therefore, at $d = -1.5$ Å the orbitals GPH-1 and GPH do not contribute to the total conductance. For $d < -1.5$ Å GPH-1 and GPH change their order so that $\Delta_H < 0$. Now the HOMO-1 is attributed to the GPH and the HOMO to the GPH-1. This means that HOMO and LUMO are of different symmetries, which, according to the argument above, leads to summands of the same sign and the resulting contributions to the conductance add up in a constructive manner. In this case there is no antiresonance between the HOMO and the LUMO anymore. An analogous explanation for the vanishing of the destructive interference can be given for $d >$ 1.8 Å, where GPL and GPL+1 change their energetic order ($\Delta_L < 0$).

## 3. Displacement dependence of molecular orbital energies

As stated above, the displacement dependence of the orbital energies is crucial for the theoretical explanation of the displacement-dependent transmission. The isovalue plots of the four frontier orbitals are shown in Fig. 5a. These are sufficient to understand the displacement dependence of the orbital energies. First, we consider the GPH and GPL: Starting from $d = 0$ Å (near the total energy minimum at 0.2 Å, where the molecule is closest to its gas-phase configuration) their energies increase, if the molecule is stretched (see Fig. 5c). The reason for this is the shifting of the stacked benzene rings.

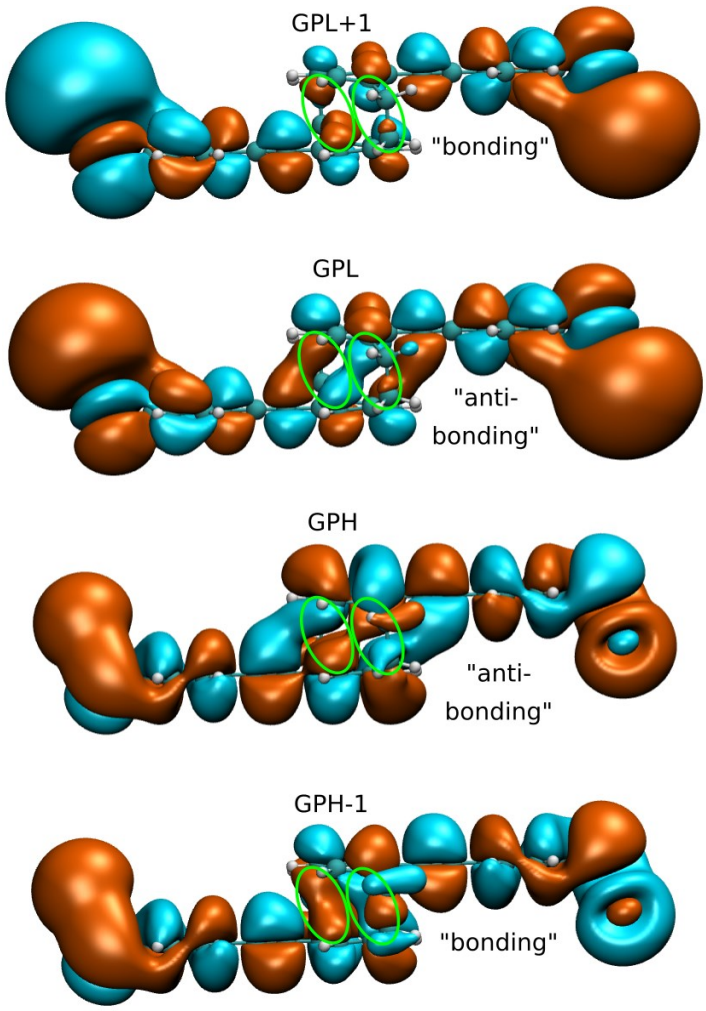


**Figure S23.** Molecular orbitals of the gas phase configuration. The sulfur atoms are terminated with one gold atom each. Green circles mark the parts of the wave function which arise from the π-orbitals of the stacked benzene rings. These parts show a sign change for GPH and GPL and no sign change for GPH-1 and GPL+1.

The wave function at the opposing stacked rings shows a sign change for GPH and GPL, marked with green circles in Fig. S23, which corresponds to an antibonding configuration. Upon stretching these π-orbitals are brought closer together, thereby increasing the energy. Additionally, the π-orbitals of each OPE unit are moved away from the orbitals arising from the ethynyl atoms of the other unit, which have the same sign and therefore correspond to a bonding configuration, which as well increases the orbital energy. We can use an analogous argumentation to justify the decrease of the orbital energy of the two other frontier orbitals, GPH-1 and GPL+1. Here, the opposing π-orbitals have the same sign and are in a

bonding configuration. If the molecule is stretched, these π-orbitals are brought closer to each other and are removed from the energetically unfavourable ethynyl-chain orbitals, which reduces the orbital energy. If the benzene rings are shifted too far, the energy change can even be reversed. This is observed, e.g., for the trace caused by GPL+1 in Fig. 5c. Starting from $d = 0$ Å at first, it moves to lower energies and from $d = 3$ Å back to higher ones. This happens because the benzene rings are shifted far enough that the π-orbitals start to feel the presence of the next neighbour orbitals of the other OPE unit, which are again of opposite sign. This corresponds to a transition from a bonding to an antibonding configuration, which results in an increase of orbital energy.

## 4. Choice of displacement scale

The conductance dip in Fig. 5b occurs when the transmission valley intersects the Fermi energy. The displacement at which this intersection takes place is affected by the energies of the frontier orbitals and their couplings to the leads (i.e. by the lead-molecule bonds). In the system presented in Fig. 5 the conductance dip and the minimum of the total energy are separated by 0.2 Å. In other simulated configurations (not presented here) with a different pair of leads, the conductance dip and total energy minimum were separated by a larger distance of around 1 Å.

Since only relative displacements are physically meaningful, we have chosen the zero displacement to coincide with the minimum of the conductance in Fig. 5. Instead, the vanishing displacement in Fig. 4 is determined by the initial geometry.

Due to well-known issues of DFT the calculated molecular orbital energies are likely to be offset compared to the real quasiparticle energies. Beyond absolute conductance values, this implies that there are uncertainties in the DFT with regard to the exact position of the conductance dip as a function of the displacement. However, the qualitative results discussed here, including the occurrence of an antiresonance feature that is sensitive to the stress in the molecule, are well explained.

## References

(1) Bondarenko, L.; Dix, I.; Hinrichs, H.; Hopf, H. *Synthesis* **2004**, *2004*, 2751–2759.
(2) Shi, Z.; Wang, L.; Wang, H.; Cao, X.; Zhang, H. *Org. Lett.* **2007**, *9*, 595–598.
(3) Schäfer, A.; Horn, H.; Ahlrichs, R. *J. Chem. Phys.* **1992**, *97*, 2571–2577.
(4) Perdew, J.; Burke, K.; Ernzerhof, M. *Phys. Rev. Lett.* **1996**, *77*, 3865–3868.
(5) Bürkle, M.; Viljas, J.; Vonlanthen, D.; Mishchenko, A.; Schön, G.; Mayor, M.; Wandlowski, T.; Pauly, F. *Phys. Rev. B* **2012**, *85*.
(6) Yoshizawa, K.; Tada, T.; Staykov, A. *J. Am. Chem. Soc.* **2008**, *130*, 9406–9413.
(7) Nozaki, D.; Lücke, A.; Schmidt, W. *J. Phys. Chem. Lett.* **2017**, *8*, 727–732.

**A Tetrasubstituted Helically Chiral Macrocycle with Anchoring Groups for Gold Electrodes**

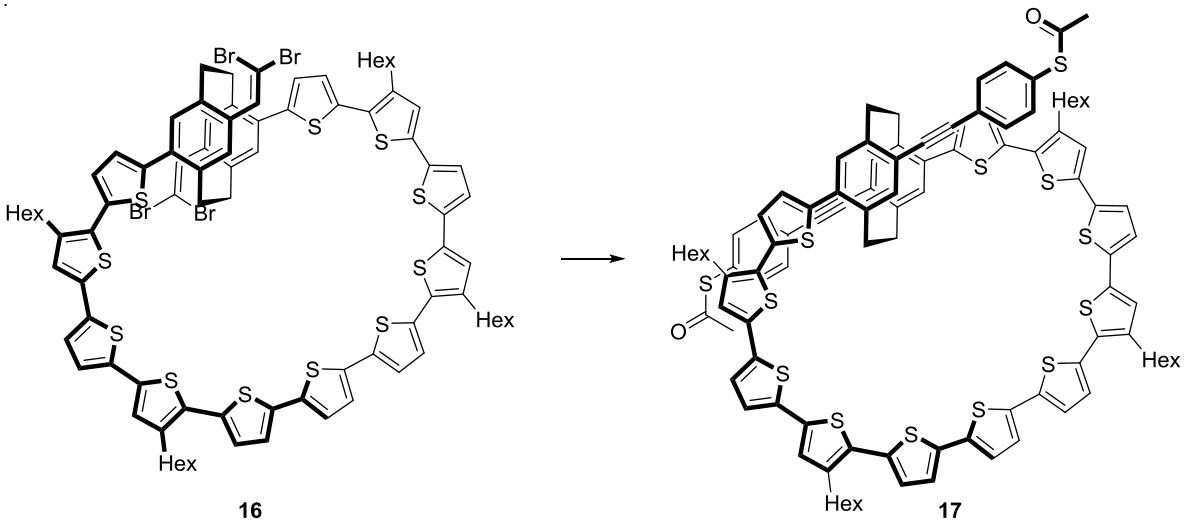


**Molecule 16** (10.0 mg, 5.51 µmol, 1.0 eq.) was dissolved in THF (3 mL) and was degassed with Ar. To this was added dropwise at 0 °C an excess of freshly prepared LDA (*n*-BuLi: (1.6 M in hexane) 116 µL, 291 mmol, 52.7 eq.; and diisopropylamine: 45.0 µL, 320 mmol, 57.9 eq.; in THF (2 mL)). After warming the reaction to room temperature, the reaction was followed by MALDI TOF MS and after completion of the reaction, it was diluted with 2 M HCl and with $CH_2Cl_2$ and it was dried over $MgSO_4$. The solvent was removed under reduced pressure and the crude was dissolved in THF (3 mL). The crude was transferred to an oven dried flask, and diisopropylamine (2 mL) and 4-acetylthioiodobenzene (22.3 mg, 80.2 µmol, 14.6 eq.) were added. The reaction mixture was degassed by bubbling through a stream of argon for 20 minutes, and $Pd(PPh_3)_4$ (1.20 mg, 1.04 µmol, 19 mol%.) and CuI (6.00 µg, 0.32 µmol, 6 mol%) were added. The reaction was heated to 55 °C for two hours and after completion 2 M HCl was added. The crude was diluted with $CH_2Cl_2$ and washed with 2 M HCl. The crude was dried over $MgSO_4$ and the solvent was removed under reduced pressure. **17** was obtained as a red amorphous solid. The poor stability of the compound did not allow for characterization by NMR experiments.

HRMS (MALDI TOF, DCTB): *m/z* calcd for $C_{104}H_{96}O_2S_{13}^+$ [$M^+$]: 1792.3774, found: 1792.3790.

**FT13099 Kevin Weiland/Mayor - w-15 - DCM / DCTB Mix 1:10**

ETH Eidgenössische Technische Hochschule Zürich Swiss Federal Institute of Technology Zurich

**Acquisition Parameter**

| | | | | | |
|---|---|---|---|---|---|
| Method: | MALDI_MS_POS_300-2600_2M_16AvScans | | | Acquisition Date: | 08.05.2018 14:40:11 |
| File Name: | D:\ETH\Data\FT130xx\FT13099_0_B20_000001.d | | | Operator: | Louis Bertschi |
| Source | Dual (MALDI/ESI) | Polarity | Positive | Nebulizer Gas | 1.3 bar |
| Broadband Low Mass | 303.1 m/z | n/a | n/a | Drying Gas Flow Rate | 3.7 L/min |
| Broadband High Mass | 2600.0 m/z | Laser Power | 23.0 lp | Capillary | 4000.0 V |
| No. of Cell Fills | 1 | n/a | n/a | Drying Gas | 200.0 °C |
| Apodization | Full-Sine | Time of Flight to Detector | 0.002 sec | Temperature | |

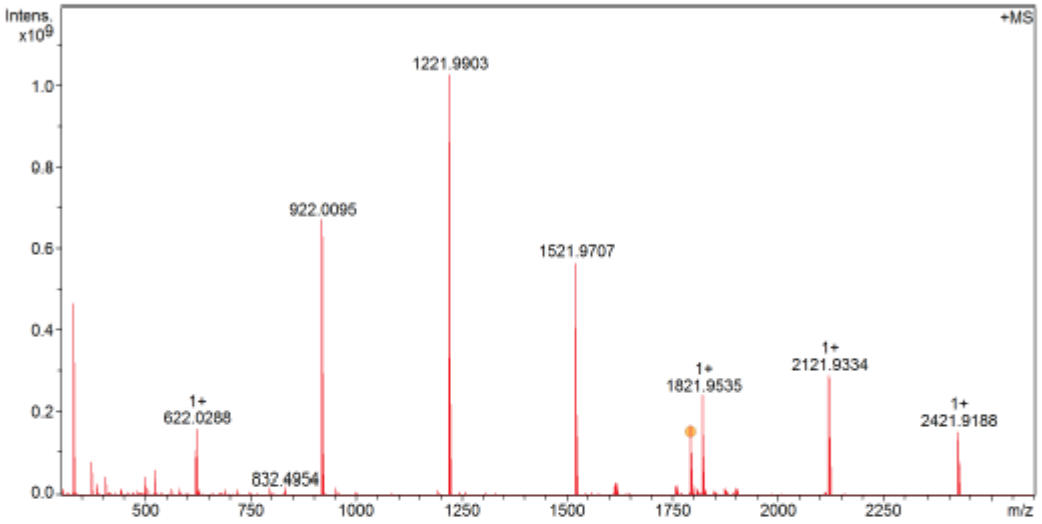


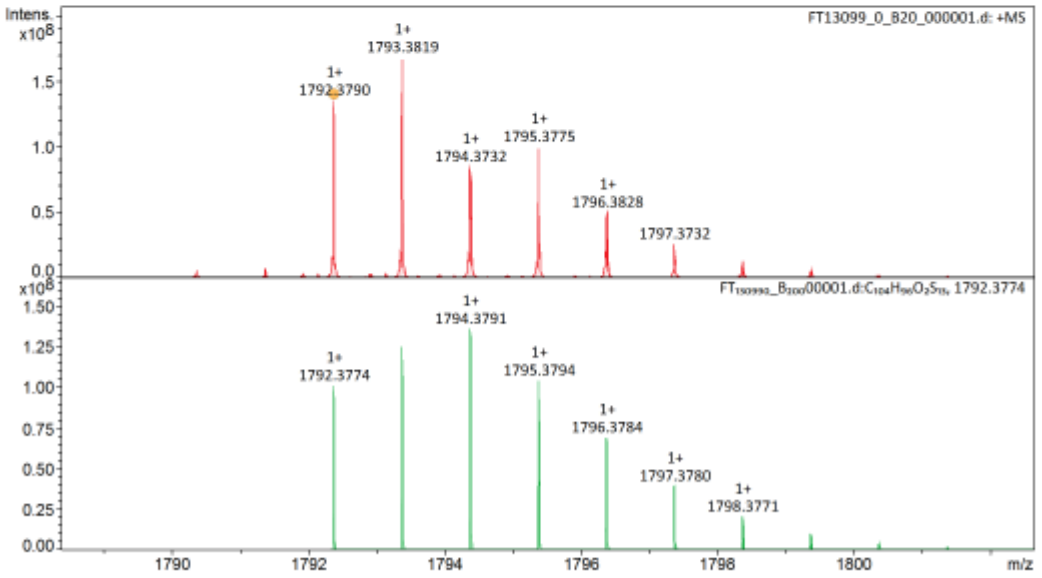

**FT13099 Kevin Weiland/Mayor - w-15 - DCM / DCTB Mix 1:10**

ETH Eidgenössische Technische Hochschule Zürich Swiss Federal Institute of Technology Zurich

**Evaluation Spectra / Validation Formula:**

| # | Ion Formula | Adduct | m/z | z | Meas. m/z | mSigma | N-Rule | err [mDa] | err [ppm] |
|---|---|---|---|---|---|---|---|---|---|
| 1 | C104H96O2S13 | M | 1792.3774 | 1+ | 1792.3790 | 200.4 | ok | -1.6 | -0.9 |

**Calibration Info:**

Date: 08.05.2018 16:05:48
Polarity: Positive
Calibration spectrum: +MS: Scan
Reference mass list: MALDI: DCTB Matrix + HP-Mix (pos)
Calibration mode: Quadratic

| Reference m/z | Resulting m/z | Intensity | Error [ppm] |
|---|---|---|---|
| 118.0863 | | | |
| 250.1464 | | | |
| 251.1543 | | | |
| 273.1362 | | | |
| 322.0481 | | | |
| 332.2009 | | | |
| 500.2934 | | | |
| 501.3013 | | | |
| 523.2832 | | | |
| 622.0290 | 622.0288 | 160373056 | -0.220 |
| 750.4404 | | | |
| 751.4483 | 751.4487 | 5937956 | 0.628 |
| 773.4302 | | | |
| 922.0098 | 922.0095 | 671198976 | -0.302 |
| 1000.5874 | | | |
| 1001.5953 | | | |
| 1023.5772 | | | |
| 1221.9906 | 1221.9903 | 1029135680 | -0.292 |
| 1521.9715 | 1521.9707 | 569543552 | -0.493 |
| 1821.9523 | 1821.9535 | 240478896 | 0.641 |
| 2121.9332 | 2121.9334 | 292087392 | 0.120 |
| 2421.9140 | | | |
| 2721.8948 | | | |

Standard deviation: 0.591

**Mass List:**

| # | m/z | Res. | S/N | I % | FWHM |
|---|---|---|---|---|---|
| 1 | 332.1986 | 432563 | 3059.5 | 7.4 | 0.0008 |
| 2 | 332.1990 | 586072 | 3469.5 | 8.4 | 0.0006 |
| 3 | 332.2000 | 584777 | 18598.9 | 45.3 | 0.0006 |
| 4 | 333.2019 | 364687 | 936.5 | 2.3 | 0.0009 |
| 5 | 333.2035 | 566361 | 4205.6 | 10.2 | 0.0006 |
| 6 | 374.2108 | 511719 | 3070.3 | 7.5 | 0.0007 |
| 7 | 386.2836 | 464441 | 1098.7 | 2.7 | 0.0008 |
| 8 | 500.2932 | 376231 | 1423.8 | 4.0 | 0.0013 |
| 9 | 523.2830 | 365391 | 1911.4 | 5.6 | 0.0014 |
| 10 | 622.0288 | 314219 | 4862.3 | 15.6 | 0.0020 |
| 11 | 922.0095 | 199587 | 16852.5 | 65.2 | 0.0046 |
| 12 | 923.0135 | 201302 | 2549.6 | 10.0 | 0.0046 |
| 13 | 1221.9903 | 156103 | 21571.6 | 100.0 | 0.0078 |
| 14 | 1222.9948 | 163788 | 5760.4 | 26.7 | 0.0075 |
| 15 | 1223.9985 | 150291 | 681.2 | 3.2 | 0.0081 |
| 16 | 1521.9566 | 80290 | 1137.2 | 6.2 | 0.0190 |
| 17 | 1521.9707 | 125230 | 10144.9 | 55.3 | 0.0122 |
| 18 | 1522.9754 | 129514 | 3447.8 | 18.8 | 0.0118 |
| 19 | 1523.9792 | 127500 | 582.5 | 3.2 | 0.0120 |
| 20 | 1616.2844 | 134730 | 472.1 | 2.9 | 0.0120 |
| 21 | 1617.2883 | 123756 | 485.8 | 3.0 | 0.0131 |
| 22 | 1759.3952 | 113575 | 329.7 | 2.5 | 0.0155 |
| 23 | 1792.3790 | 113505 | 1769.9 | 13.2 | 0.0158 |
| 24 | 1793.3819 | 111696 | 2199.2 | 16.4 | 0.0161 |
| 25 | 1794.3732 | 128916 | 1107.5 | 8.3 | 0.0139 |
| 26 | 1794.3886 | 142291 | 965.8 | 7.2 | 0.0126 |
| 27 | 1795.3775 | 124884 | 1305.6 | 9.7 | 0.0144 |
| 28 | 1795.3944 | 204345 | 396.6 | 3.0 | 0.0088 |
| 29 | 1796.3828 | 129043 | 647.8 | 4.8 | 0.0139 |
| 30 | 1797.3732 | 133153 | 332.6 | 2.5 | 0.0135 |
| 31 | 1821.9229 | 95959 | 395.5 | 3.0 | 0.0190 |
| 32 | 1821.9355 | 189568 | 324.6 | 2.4 | 0.0096 |
| 33 | 1821.9535 | 109505 | 3134.6 | 23.4 | 0.0166 |
| 34 | 1822.9573 | 111783 | 1155.7 | 8.6 | 0.0163 |
| 35 | 2121.8941 | 90300 | 551.5 | 3.5 | 0.0235 |
| 36 | 2121.9334 | 84698 | 4528.3 | 28.4 | 0.0251 |
| 37 | 2122.9378 | 89168 | 2139.4 | 13.4 | 0.0238 |
| 38 | 2123.9417 | 92490 | 541.8 | 3.4 | 0.0230 |
| 39 | 2421.9188 | 80092 | 2387.2 | 14.9 | 0.0302 |
| 40 | 2422.9224 | 79423 | 1223.5 | 7.6 | 0.0305 |

| # | m/z | Res. | S/N | I % | FWHM |
|---|---|---|---|---|---|
| 1 | 1792.3774 | 113505 | | 74.2 | 0.0158 |
| 2 | 1793.3805 | 113568 | | 92.0 | 0.0158 |
| 3 | 1794.3791 | 113632 | | 100.0 | 0.0158 |
| 4 | 1795.3794 | 113695 | | 76.5 | 0.0158 |
| 5 | 1796.3784 | 113758 | | 51.5 | 0.0158 |
| 6 | 1797.3780 | 113821 | | 29.4 | 0.0158 |
| 7 | 1798.3771 | 113885 | | 15.1 | 0.0158 |
| 8 | 1799.3764 | 113948 | | 7.0 | 0.0158 |
| 9 | 1800.3754 | 57006 | | 2.9 | 0.0316 |
| 10 | 1801.3747 | 114075 | | 1.1 | 0.0158 |
| 11 | 1802.3751 | 114138 | | 0.4 | 0.0158 |
| 12 | 1803.3764 | 114201 | | 0.1 | 0.0158 |

## PERSONAL DATA

| | |
|---|---|
| Name | Kevin Julian Weiland |
| Nationality | German |
| Date & Place of Birth | 08 Aug 1987, Friedrichshafen |
| Email | kevin.weiland@gmx.de |

## PROFESSIONAL CAREER

| | |
|---|---|
| 02/2019 – today | **Chemist Quality Control & Analytical Development**<br>Carbogen AMCIS AG, Switzerland |

## EDUCATION

| | |
|---|---|
| 03/2014 – 10/2018 | **PhD Student Chemistry (Marie Curie Fellow)**<br>University of Basel, Switzerland<br>*Molecular Loops – Mating Cyclophanes and Macrocycles.*<br>Thesis Advisor: Prof. Dr. Marcel Mayor<br>Grade: summa cum laude |
| 10/2011 – 12/2013 | **Master of Science in Chemistry**<br>Ludwig-Maximilians-University Munich, Germany<br>*Synthesis of Reactive Fluorescent Dyes Based on Perylene-3,4,9-tricarboxylic Acid.*<br>Thesis Advisor: Prof. Dr. Heinz Langhals<br>Grade: very good |
| 03/2012 – 05/2012 | **Scholarship**<br>University of Maryland, College Park, USA<br>*Spray Pyrolysis Synthesis for Energetic Nanoparticles.*<br>Advisor: Prof. Dr. Mike Zachariah |
| 10/2008 – 09/2011 | **Bachelor of Science in Chemistry and Biochemistry**<br>Ludwig-Maximilians-University Munich, Germany<br>*Synthesis and Coordination Chemistry of Sugar Amino Acids.*<br>Advisor: Prof. Dr. Peter Klüfers<br>Grade: good |

## PRACTICAL EXPERIENCE

| | |
|---|---|
| 03/2014 – 10/2018 | **Teaching Assistant**<br>University of Basel, Switzerland<br>Lab courses for beginner and advanced chemistry students, supervision of research projects and master theses. |
| 10/2011 – 02/2012 | **Teaching Assistant**<br>Ludwig-Maximilians-University Munich, Germany<br>Lab courses and lecture assistant for chemistry students |
| 11/2007 – 07/2008 | **Civil Service**<br>GSD Seniorenwohnpark Vaterstetten, Germany<br>Property management |

## SCIENTIFIC PUBLICATIONS

1.) **Nano Letters**, 2018, *18*, 5981 – 5988.
*Large Conductance Variations in a Mechanosensitive Single-Molecule Junction.*
Davide Stefani*, Kevin J. Weiland*, Maxim Skripnik*, Chunwei Hsu, Mickael L. Perrin, Marcel Mayor, Fabian Pauly and Herre S. J. van der Zant (* equal contribution)

2.) **Helvetica Chimica Acta**, 2019, *102*, e1800205.
*A Chiral Macrocyclic Oligothiophene with Broken Conjugation – Rapid Racemization through Internal Rotation.*
Kevin J. Weiland, Nathalia Münch, Wanja Gschwind, Daniel Häussinger and Marcel Mayor

3.) **Journal of the American Chemical Society**, 2019, *141*, 2104 – 2110.
*Mechanical Stabilization of Helical Chirality in a Macrocyclic Oligothiophene.*
Kevin J. Weiland, Thomas Brandl, Kenneth Atz, Alessandro Prescimone, Daniel Häussinger, Tomáš Šolomek and Marcel Mayor

4.) **European Journal of Organic Chemistry**, 2019, 3073 – 3085.
*Beyond Simple Substitution Patterns – Symmetrically Tetrasubstituted [2.2]Paracyclophanes as 3D Functional Materials.*
Kevin J. Weiland, Almudena Gallego, Marcel Mayor

## SELECTED ORAL PRESENTATIONS

09/2017 *A Molecular Macrocyclic Loop*
**Workshop on Molecular Electronics**, Muggendorf, Germany

01/2017 *[2.2]Paracyclophane – A Versatile Building Block for Molecular Electronics*
**3rd Annual Meeting and Workshop**, Granada, Spain

09/2016 *A Molecular Macrocyclic Loop*
**Joint MOLESCO-iSwitch Workshop**, Freiburg, Germany

05/2016 *A Molecular Macrocyclic Loop*
**MOLESCO Workshop**, IBM Zurich, Switzerland

09/2015 *A Molecular Macrocyclic Loop*
**Joint MOLESCO-DFG Network Workshop on Single-Molecule Electronics**, University of Regensburg, Germany

05/2015 *Towards a Perylene-Based Cyclophane with Charge Transfer Capability*
**Workshop and Training Course**, University of Oviedo, Spain

## AWARDS AND HONORS

1.) **Marie-Curie Fellow**, PhD fellow in the Marie Curie Initial Training Network “MOLESCO” under the EU FP7 program.

2.) **Helvetica Prize of the Swiss Chemical Society 2019 (runner up)**, awarded for the best published paper of PhD/Postdocs in Helvetica Chimica Acta.